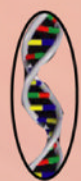




Léon N. Collignon  
Claud B. Normand  
Editors

Nova  
Biomedical



# Photobiology

Principles, Applications and Effects

NOVA

# **PHOTOBIOLOGY**

## **PRINCIPLES, APPLICATIONS AND EFFECTS**

No part of this digital document may be reproduced, stored in a retrieval system or transmitted in any form or by any means. The publisher has taken reasonable care in the preparation of this digital document, but makes no expressed or implied warranty of any kind and assumes no responsibility for any errors or omissions. No liability is assumed for incidental or consequential damages in connection with or arising out of information contained herein. This digital document is sold with the clear understanding that the publisher is not engaged in rendering legal, medical or any other professional services.



# **PHOTOBIOLOGY**

## **PRINCIPLES, APPLICATIONS AND EFFECTS**

**LÉON N. COLLIGNON**  
**AND**  
**CLAUD B. NORMAND**  
**EDITORS**

**Nova Biomedical Press, Inc.**  
*New York*

Copyright © 2010 by Nova Science Publishers, Inc.

**All rights reserved.** No part of this book may be reproduced, stored in a retrieval system or transmitted in any form or by any means: electronic, electrostatic, magnetic, tape, mechanical photocopying, recording or otherwise without the written permission of the Publisher.

For permission to use material from this book please contact us:

Telephone 631-231-7269; Fax 631-231-8175

Web Site: <http://www.novapublishers.com>

#### **NOTICE TO THE READER**

The Publisher has taken reasonable care in the preparation of this book, but makes no expressed or implied warranty of any kind and assumes no responsibility for any errors or omissions. No liability is assumed for incidental or consequential damages in connection with or arising out of information contained in this book. The Publisher shall not be liable for any special, consequential, or exemplary damages resulting, in whole or in part, from the readers' use of, or reliance upon, this material.

Independent verification should be sought for any data, advice or recommendations contained in this book. In addition, no responsibility is assumed by the publisher for any injury and/or damage to persons or property arising from any methods, products, instructions, ideas or otherwise contained in this publication.

This publication is designed to provide accurate and authoritative information with regard to the subject matter covered herein. It is sold with the clear understanding that the Publisher is not engaged in rendering legal or any other professional services. If legal or any other expert assistance is required, the services of a competent person should be sought. FROM A DECLARATION OF PARTICIPANTS JOINTLY ADOPTED BY A COMMITTEE OF THE AMERICAN BAR ASSOCIATION AND A COMMITTEE OF PUBLISHERS.

#### **LIBRARY OF CONGRESS CATALOGING-IN-PUBLICATION DATA**

Photobiology : principles, applications, and effects / editors, Lion N. Collignon and Claud B. Normand.,

p. cm.

Includes index.

ISBN 978-1-61122-881-6 (eBook)

*Published by Nova Science Publishers, Inc., 10 New York*

# CONTENTS

<b>Preface</b>		vii
<b>Chapter 1</b>	<b>On Possible Coherent Effects in Primary Visual Perception</b>	1
	<i>V. D. Svet and A.M. Khazen</i>	
<b>Chapter 2</b>	<b>Photobiology of Infant Skin</b>	39
	<i>Georgios N. Stamatas, M. Catherine Mack and Katharine M. Martin</i>	
<b>Chapter 3</b>	<b>Molecular Typing of Polymorphic Genes by Time-Resolved Fluorescence Resonance Energy Transfer</b>	69
	<i>L. Nardo, M. Bondani, G. Tosi, R. S. Accolla and A. Andreoni</i>	
<b>Chapter 4</b>	<b>Protein Photo-Oxidative Damage – Consequences, Characterisation and Control</b>	91
	<i>Jolon M. Dyer</i>	
<b>Chapter 5</b>	<b>Early Stages in Formation of Photosynthetic Pigment Apparatus</b>	115
	<i>Olga B. Belyaeva and Felix F. Litvin</i>	
<b>Chapter 6</b>	<b>Chemopreventive Action of Organic and Inorganic Materials on Phototoxic Effect</b>	137
	<i>Kazutaka Hirakawa</i>	
<b>Chapter 7</b>	<b>Pigmentation as a UV-Screening Strategy of Lichenized Fungi from the Tropical Andes and its Possible Role on Planetary Surfaces</b>	159
	<i>Vicente Marcano, José Alberto Rojas, Alirio Balza, Ricardo Díaz, Roxana Pérez and Pedro Benítez</i>	
<b>Chapter 8</b>	<b>Diversity and Evolution of Animal Rhodopsin and Phototransduction Cascade</b>	179
	<i>Akihisa Terakita</i>	

<b>Chapter 9</b>	<b>Effects of Natural Ultraviolet Radiation Exposure in Inland Water Ecosystems of Chilean Patagonia</b>	<b>195</b>
	<i>Patricio De los Ríos and Patricio Acevedo</i>	
<b>Chapter 10</b>	<b>Folic Acid - An Important Factor for Skin Homeostasis and Repair</b>	<b>209</b>
	<i>Anja Knott, Heiko Mielke, Katja Reuschlein, Sören Jaspers, Urte Koop, Franz Stäb, Horst Wenck and Stefan Gallinat</i>	
<b>Chapter 11</b>	<b>Transcriptional Changes in Energy Metabolism and Protein Synthesis Predominate in the Early Phase After Photodynamic Therapy</b>	<b>219</b>
	<i>Yuji Morimoto, Kouji Matsumura, Yoshinori Nakagishi and Satoko Kawauchi</i>	
<b>Chapter 12</b>	<b>The Oriental Hornet Vespa Orientalis (Hymenoptera: Vespinae) Cuticular Yellow Stripe as an Organic Solar Cell: A Hypothesis</b>	<b>233</b>
	<i>Marian Plotkin, Stanislav Volynchik, Reuben Hiller, David J. Bergman and Jacob S. Ishay</i>	
<b>Chapter 13</b>	<b>Commentary: Application of Imaging Mass Spectrometry to Photobiology</b>	<b>243</b>
	<i>Takahiro Hayasaka, Takayuki Naito and Mitsutoshi Setou</i>	
<b>Chapter 14</b>	<b>Coordinative and Dynamic Regulation of Translation and Transcription by Nitric Oxide and Superoxide upon Ultraviolet Light Irradiation</b>	<b>251</b>
	<i>Shiyong Wu and Oliver L. Carpenter</i>	
<b>Chapter 15</b>	<b>Photodynamic Therapy with Preserved Immune System – Expectation for Treatment for Localized Bacterial Infection</b>	<b>269</b>
	<i>Yuji Morimoto, Masamitsu Tanaka and Manabu Kinoshita</i>	
<b>Index</b>		<b>273</b>

## PREFACE

Photobiology is the scientific study of the interactions of light and living organisms. The last decades have witnessed great strides in understanding the biological effects of light from the molecular all the way up to the whole organism level. Much of the boost for advancing the science of photobiology came from the dramatic increase over this period in the incidence of melanoma and other sun-related skin diseases. In this book, current knowledge about the risks of ultraviolet radiation (UVR) on infant skin are summarized, including epidemiologic evidence regarding sun exposure in this age group. This book also explores and discusses the complex cascade of modifications induced within proteins through exposure to irradiation. Exciting new approaches to the characterization, location, tracking, and ultimately control of photooxidation within proteins are discussed as well. Moreover, the prevention for phototoxic effect is one of the important themes of photobiology. The chemopreventive action of novel organic and inorganic materials on photosensitized biomolecules damage is described in this book. Other chapters provide insights into the death and protective responses of cells treated by photodynamic therapy (PDT) as well as the relationships among gene expressions, examine the effects of natural ultraviolet radiation at zooplankton populations and communities in inland water ecosystems, and the application of folates and their role for skin homeostasis.

Chapter 1 - The modern physiology of vision has saved up many facts which contradict the accepted approach to mechanisms of primary visual perception. From H.Helmholtz time it is considered that an image of some object primarily constructed by the eye cornea and lens first unequivocally is projected to the matrix of photoreceptors (rod and cone cells), and then is exposed to processing in several layers of the nervous cells arranged behind them. Actually, at the taxonomically superior animals with developed brain including human beings, the optical image is projected to photoreceptors through the layers of nervous cells, i.e. the human retina is inverted.

The next not clear till now effect is the termination of vision at stabilization of micro oscillations of eye, so called Troxler effect. Absence of oscillations means no vision. And, at last, recently opened ultra fast reaction of photoisomerisation of rodopsine inevitably causes a question on the possible reasons and consequences of such fast reaction as time duration of the arisen potentials of photoreceptors is on 9-10 orders more.

It appears that if to consider all the specified features in common it is possible, at least at a physical level, to offer a new model of primary visual perception, which, in the first, is well

coordinated with morphological and experimental data, and secondly, eliminates the arisen contradictions.

Such model assumes, that, owing to the specified features, the eye apparatus is capable to fix the so-called "full optical field" scattered by object or optical amplitude-phase distribution of optical field, though the registered parameter is light intensity. Certainly, it is possible only at registration of scattered object fields as interferometric patterns or holograms.

Chapter 2 - The last decades have witnessed great strides in understanding the biological effects of light from the molecular all the way up to the whole organism level. Much of the boost for advancing the science of photobiology came from the dramatic increase over this period in the incidence of melanoma and other sun-related skin diseases, as well as the realization that light plays an important role in skin aging. Due to the fact that many of these conditions occur late in life, little attention has been paid to the effects of light on infant skin, with the exception of the use of violet-blue light for the treatment of jaundice in newborns. However, mounting evidence shows that a history of early sun exposure may affect the development of sun-related conditions later in life. In this chapter the authors summarize current knowledge about the risks of ultraviolet radiation (UVR) on infant skin, including epidemiologic evidence regarding sun exposure in this age group. Based on published results of studies performed using cell culture models, animal models, and human clinical trials, the authors specifically examine the effects of UVR on the biology of infant skin, as well as the known effects of blue-light phototherapy on neonatal skin. Finally, the authors identify areas for future research in this exciting field of science.

Chapter 3 - Gene polymorphism is responsible for the expression of many variants of a protein among different subjects of the same species. To be classified into polymorphism, variations of gene sequences must appear in at least 1% of the population. Such genetic variants, called alleles, though not necessarily directly pathogenic, are frequently correlated to the occurrence of diseases. For this reason, the possibility to perform wide range screening of the relevant polymorphic genes would provide a powerful tool for disease prediction.

DNA sequencing, which is the election technique to identify allelic variants, is expensive and time consuming and is not applicable to the screening of vast populations. However, if the relevant alleles are known, other molecular typing methods can offer a valuable alternative to sequencing. Several of these techniques are based on the detection of light emitted as either chemiluminescence or fluorescence. Most of them consist in ON/OFF intensity measurements, as the emission/non-emission of light is triggered by recognition of the genomic template by allele specific probes. These techniques often require preliminary purification of DNA and amplification of the polymorphic gene of interest.

In this Chapter, the authors focus on the HLA-DQB1 locus of the human major histocompatibility complex (MHC), which comprises the most polymorphic genes in the human genome. This very high degree of polymorphism dictates the tissue compatibility in organ transplants and the susceptibility to several diseases, such as insulin-dependent diabetes mellitus (IDDM).

The authors introduce a novel typing method that promises to avoid purification and amplification of DNA, and apply it to the recognition of HLA-DQB1 allelic variants. The author's method is based on time-resolved fluorescence resonance energy transfer (FRET) measurements performed on a donor-acceptor dual-labelled oligonucleotide probe, which carries the donor and the acceptor at its opposite ends. The fluorescence of the FRET donor is quenched by the acceptor in a strongly donor-acceptor distance-dependent way, which makes

the donor fluorescence decay time sensitive to the conformation of the probe-target complex. Fluorescence decay time values are measured with a time-correlated single-photon counting apparatus endowed with 30 ps resolution, which allows extremely high sensitivity on conformational differences. As the apparatus can reveal single photons, the decay time can be measured even for a single probe molecule, avoiding DNA amplification.

Target oligonucleotides with sequences equal to those of the region around codon 57 of the exon □2 allelic variants were synthesized. This region was chosen because it is the most polymorphic region of DQB1 gene and because its variability is associated with susceptibility/resistance to IDDM. An oligonucleotide corresponding to DQB1-0201 allele was used as the only dual-labelled probe. This probe forms a perfect double strand with the complementary target oligonucleotide (allele 0201), whereas for any other allelic variant, probe and target sequence are slightly mismatched at sites that differ from allele to allele. This causes the probe-target hybrid conformation to be different from allele to allele and thus the distance between the donor and the acceptor bound at the ends of the probe to change. It is shown that the donor fluorescence lifetime is correspondingly different and specific for each probe-target pair, which provides a tool for precise identification of each allele. The present results indicate that the author's method can be successfully used to molecularly type even highly polymorphic genetic systems, such as the HLA system.

Chapter 4 - UV-induced photomodification of proteins has been implicated in damage to a broad range of different protein-based substrates. Protein photo-oxidation has been linked to such diverse degenerative processes as human hair and skin damage, degradation of pharmaceuticals, reduced food quality and nutrition, discolouration of natural fibres, eye lens opacification, loss of enzymatic activity and crop damage. Ongoing ozone reduction in the stratosphere, with resultant increased exposure to UVB, has generated further impetus for advancing the understanding and controlling the complex protein degradation mechanisms and pathways underlying these damage processes.

For proteins, photo-oxidative damage is generally attributable to the generation and attack of reactive oxygen species (ROS) on amino acid residue side chains and the protein backbone. Singlet oxygen and hydroxyl radicals, in particular, play a significant role in initiating protein modification.

This chapter explores and discusses the complex cascade of modifications induced within proteins through exposure to irradiation, the effect of photo-oxidation on protein substrate properties from the protein primary level through to higher order structure, and the mechanisms underpinning protein photo-oxidation. It will also discuss exciting new approaches to the characterisation, location, tracking, and ultimately control of photo-oxidation within proteins.

Chapter 5 - Contemporary data are reviewed concerning the mechanism of terminal light-dependent stage of chlorophyll biosynthesis from the dark precursor, protochlorophyllide. The application of spectral methods provided the possibility to investigate this process immediately in plants leaves. The photochemical hydrogenation of the precursor molecule catalyzed by the photoenzyme, protochlorophyllide oxidoreductase with the involvement of hydrogen donor NADPH includes two consecutive photoreactions that give rise to a branched network of dark reactions. These reactions produce a number of chlorophyll-protein complexes of the light-harvesting antenna and minor components integrated into the structure of two photochemical systems of photosynthesis. One of the branches of the reaction pathways represents the terminal light-dependent biosynthesis of pheophytin a, which is an

immediate electron acceptor of photosystem II in green plant leaves. The features of chlorophyll biosynthesis at early stages of etiolated leaf formation and in green plant leaves are considered.

Footnote: Dedicated to the memory of the author's friend and colleague, Dr. N.V. Ignatov.

Chapter 6 - The prevention for phototoxic effect is one of the important themes of photobiology. Photosensitized damage of biomolecules including DNA, proteins, and low molecular weight compounds participates in solar carcinogenesis, photogenotoxicity, and phototoxicity. Ultraviolet radiation and visible-light induce oxidation of the above biomaterials via the electron transfer from biomolecules to an excited endogenous and/or exogenous photosensitizer or the formation of reactive oxygen species, especially singlet oxygen. Chemoprevention of photosensitized biomolecules damage is important methods against the above phototoxic effects. Organic ultraviolet B absorbers and antioxidants such as vitamins are useful ultraviolet-protector. However, the oxidized products of organic materials occasionally produce secondary reactive oxygen species to damage biomolecules. To avoid this problem, organic quenchers have been studied. For examples, xanthone derivative isolated from plant can prevent photosensitized DNA damage through quenching of the excited state of photosensitizer. These molecules may be used as the preventive drugs for an adverse side-effect of photodynamic therapy. On the other hand, inorganic sunscreen such as titanium dioxide and zinc oxide particles are effective materials to shield solar UVA. Furthermore, inorganic materials can be used as an antioxidant based of their catalytic activity for decomposition of reactive oxygen species generated from the photochemical reaction.

Chapter 7 - Photochemical analysis of secondary compounds in lichens from the Venezuelan Andean snow and glacier zones (4800-5000 m) was carried out in order to determine the absorbance capacity of UV radiation in the UVA, UVB and UVC ranges and to characterize the probable UV-protective function. Spectrotometric (UV-VIS, NIR, FTIR, MS, NMR) and chromatographic (HPTLC) standardized techniques were utilized to identify the lichen compounds. UVB irradiance in the glacier zone (5000 m) revealed a value of  $\sim 3 \text{ W m}^{-2}$  which is sufficient to produce important biochemical and cell alterations. Of a total of 25 lichen species distributed in the glacier and snow zones, 68% showed the presence of phenolic compounds having strong absorption for UVC radiation, 96% had strong absorption for UVB radiation and 100% had strong absorption for UVA radiation. The substance groups that had the highest resistance to UVA and UVB radiation were characterized by ester bonds among both phenolic units (depsides). They were the most abundant products to be found among the lichens, whereas substances having ester and ether bonds in both phenolic units (depsidones) had a higher capacity to absorb UVC radiation. Microorganisms having adaptive UV-screening responses similar to the lichens investigated can perhaps be expected to occur on Earth-like planets containing  $\text{O}_2$  levels  $\leq 10^{-2}$  PAL and orbiting around G, F, and K stars.

Chapter 8 - Many animals sense light signals for visual and non-visual functions. Light is captured by rhodopsin-like photopigments in photoreceptor cells and is transduced to cellular light-response through a G-protein-mediated phototransduction cascade. More than 2000 kinds of rhodopsin-like photopigments have been identified thus far and they are divided into eight subgroups. Accumulated evidence suggests that displacement of counterion, an essential amino acid residue for rhodopsin-like photopigment to absorb visible light, is closely related to the evolution of vertebrate visual pigments. Four kinds of phototransduction cascades have been found thus far, such as those mediated by transducin (Gt type G protein) in vertebrate

rod and cone visual cells, by Gq type G protein in insect and molluscan rhabdomeric-type visual cells, by Go type G protein in scallop and lizard ciliary-type visual cells and by Gs type G protein in Jellyfish visual cells. Since photoreception has evolved with phototransduction cascades and has diverged in different species, the study on rhodopsin-like pigment and the signaling cascade of varied animals is important for the understanding of the diversity and evolution of animal phototransduction. Here the classification of animal phototransduction cascades are reviewed. Animal photoreceptor cells are roughly divided into two types, ciliary and rhabdomeric types. In the case of the ciliary type photoreceptors, the jellyfish (pre-bilaterian) Gs-mediated, vertebrate (deuterostomes) Gt-mediated and scallop (protostome) and lizard (deuterostome) Go-mediated phototransductions exhibit partial similarity, because all involve cyclic nucleotide signaling, suggesting a monophyletic origin of ciliary phototransduction among animals. The amphioxus (deuterostome) rhabdomeric-type photoreceptor cells contain the homologue of the melanopsin, the circadian photopigment in the photosensitive retinal ganglion cells of vertebrates, and have a Gq-mediated phototransduction cascade similar to protostome rhabdomeric-type visual cells. The phototransduction of amphioxus rhabdomeric photoreceptor cells represents an evolutionary link between phototransduction of the invertebrate visual cells and the vertebrate circadian photoreceptor cells. Based on these findings, the authors discuss a functional and evolutionary classification of animal phototransduction and photoreceptor cells, the rhabdomeric photoreceptor cell containing phosphoinositol signaling mediated by Gq, and the ciliary photoreceptor cell containing cyclic nucleotide signaling mediated by Gt, Go or Gs.

Chapter 9 - Exposure to natural ultraviolet radiation has risen in southern Patagonia due to atmospheric ozone depletion. The available literature describes how natural ultraviolet radiation affects the ecosystems, and in aquatic environments ultraviolet radiation can penetrate the water column under conditions of low concentration of substances such as dissolved organic carbon which provide a screen effect by absorbing wavelengths corresponding to natural ultraviolet radiation. The present chapter is a description of literature about the effects of natural ultraviolet radiation in zooplankton populations and communities in the inland water ecosystems of Chilean Patagonia (38–51°S). At the population level, two patterns have been observed: first, the effects in species with a low tolerance to natural ultraviolet radiation exposure, which corresponds with transparent species; and second, the effects in species with photoprotective substances that are tolerant to high levels of natural ultraviolet radiation. On the community scale it has been observed that under high exposure to natural ultraviolet radiation only tolerant species are present, and under oligotrophy it was observed that few species are tolerant, mainly calanoid copepods, which are dominant in zooplankton assemblages.

Chapter 10 - For decades, it has been widely accepted that folates play a central role in cell metabolism, cell turnover and DNA repair. Despite the abundant food supply, insufficient folate status has been named one of the most frequent vitamin deficiencies in the industrialized world. Accordingly, a number of epidemiological studies correlated inadequate folate supply with an increased incidence for certain diseases.

Human skin represents the outermost barrier of the body. The epidermal compartment undergoes a life-long renewal process and the skin is constantly exposed to environmental factors, such as ultraviolet (UV) irradiation. Until recently, however, only very little was known about the effects of folates on human skin and its importance for tissue homeostasis was certainly underappreciated.

A number of both *in vitro* and *in vivo* studies were published that now help to elucidate the function folates play in the skin, particularly during the process of photo-aging. Altogether, these studies demonstrated that topically applied folic acid is bio-available for human skin, that its cellular up-take is significantly increased upon UV irradiation and that topical application improves epidermal regeneration *in vivo*, to name a few effects. Although many questions still need to be addressed the available literature appears to support the notion that folates play an important role for skin homeostasis and that this crucial vitamin serves to facilitate the cellular response following solar irradiation.

Chapter 11 - The mechanism of the cytotoxic effect of photodynamic therapy (PDT) with respect to gene profile has not been fully elucidated. The authors used DNA microarrays to analyze the time courses of transcriptional responses of lung cancer cells (RERF) at 0, 30, 60, 120 and 240 min after PDT using a water-soluble photosensitizer (ATX-S10•Na(II)). Apoptotic cell death was prominent and loss of ~ 40% of cells was seen at 120 min and 240 min after PDT using a 670-nm laser. Approximately 1300 genes in 10K tested genes responded to PDT with a more than 1.5-fold induction rate. Most of the up-regulated genes (~ 700) were revealed to be closely related to energy metabolism and protein synthesis. Immediately after PDT, genes related to activities of ATP synthase and NADH dehydrogenase were significantly up-regulated. In addition, genes related to translation in protein synthesis, ribosomal proteins and proteasome were overexpressed both at 0 min and 240 min after PDT. Expression levels of heat shock protein-related genes gradually increased over a period of 240 minutes. Further characterization of the PDT- induced gene expression profiles obtained here may lead to identification of novel biomarkers and shed light on the cytotoxic mechanism of PDT.

Chapter 12 - Many animals such as insects, reptiles, amphibians and marine vertebrates and invertebrates are endowed with bright colors and contrasting patterns intended to warn other animals that they are venomous and such is the case also insofar as the brown yellow coloration of the Oriental hornet. The present work, however, suggests that in the Oriental hornet this is not the only purpose of these bright pigments. The Oriental hornet *Vespa orientalis* (Hymenoptera, Vespinae) correlates its flight activity with the insolation. The Oriental hornet cuticle bears yellow-colored stripes composed of yellow granules. The yellow granule contains xanthopterin. This array of yellow granules maximizes the ability of the extensively conjugated xanthopterin to absorb a wide range of visible light extending up to UV light. Photovoltaic properties of yellow cuticle evince that the potential difference between darkness and UV illumination is sufficient for ATP production from ADP. This unique photovoltaic behavior of yellow cuticle suggests that it may act as an organic solar cell.

Chapter 13 - Within the field of photobiology, the mechanism of phototransduction has been a subject of intense investigation. Phototransduction is regulated by the light-sensitive interaction among visual pigment-coupled receptor proteins, such as rhodopsin, in the retina. There are some reports that the conformation of rhodopsin is influenced by the composition of phospholipids in the lipid bilayer membrane. Very recently, the authors reported the distribution of retinal phospholipids based on *in situ* analysis with vacuum type imaging mass spectrometry. However, there has been no *in situ* analysis of retinal phospholipids under natural conditions with atmospheric pressure. The authors recently developed an atmospheric pressure matrix-assisted laser desorption/ionization (AP-MALDI)-based imaging mass spectrometry (IMS) system. This system enables us to perform structural analyses using a

tandem mass spectrometer, as well as to visualize phospholipids and peptides with high spatial resolution in frozen sections. In the present study, the authors used the AP-MALDI-based IMS system to visualize and identify phospholipids in mouse retinal sections. From a spectrum obtained by raster-scanned analysis of the sections, peaks with high intensities were analyzed by tandem mass spectrometry (MS/MS) analysis. As a result, six diacyl-phosphatidylcholine (PC) species, i.e., PC (16:0/16:0), PC (16:0/18:1), PC (16:0/22:6), PC (18:0/18:0), PC (18:0/18:1), and PC (18:0/22:6), were identified. The ion images revealed different distributions on the retinal sections: PC (16:0/18:1), PC (18:0/18:0), and PC (18:0/18:1) were distributed in the inner plexiform, PC (16:0/16:0) in the inner plexiform layer, inner segment and outer segment, and both PC (16:0/22:6) and PC (18:0/22:6) in the inner and outer segments. The AP-MALDI-based IMS system demonstrated a zonal distribution of PC species on the retinal sections. Therefore, this approach may be useful for analyzing the phototransduction mechanism through phospholipids and the association of phospholipids in such diseases.

Chapter 14 - Exposure to ultraviolet light (UV) leads to a rapid elevation of nitric oxide (NO<sup>•</sup>) and superoxide (O<sub>2</sub><sup>•-</sup>) in irradiated cells. NO<sup>•</sup> competes with superoxide dismutase (SOD) for O<sub>2</sub><sup>•-</sup> to form peroxynitrite (ONOO<sup>-</sup>), which increases the oxidative stress and reduces NO<sup>•</sup> bioavailability. The balance between NO<sup>•</sup> and ONOO<sup>-</sup> plays significant roles in regulation of gene expression at both the translational and transcriptional levels. In mammalian cells, three nitric oxide synthases (NOS) – neuronal NOS (nNOS, NOS1), inducible NOS (iNOS, NOS2) and endothelial NOS (eNOS, NOS3) catalyze L-arginine (L-Arg) to generate NO<sup>•</sup> in response to UV-irradiation. Depending on the type of cells and physical properties of the irradiation, the patterns of NO<sup>•</sup> and ONOO<sup>-</sup> productions can be very dynamic. The production of NO<sup>•</sup> and ONOO<sup>-</sup> leads to the phosphorylation of the alpha subunit of the eukaryotic initiation factor 2alpha (eIF2α) by two eIF2α kinases (EIF2AK) - the dsRNA-dependent protein kinase-like endoplasmic reticulum (ER) kinase (PERK, EIF2AK3) and the general control nonderepressible protein kinase 2 (GCN2, EIF2AK4). The activation of EIF2AKs and phosphorylation of eIF2α inhibit global protein synthesis, which leads to the activation of transcription factor - nuclear factor kappa-light-chain-enhancer of activated B cells (NF-κB). Additionally, production of NO<sup>•</sup> and ONOO<sup>-</sup> generates oxidative and nitrosative stresses that induce signaling pathways that further modulate transcriptional activation. The combined effect of translational and transcriptional regulation ultimately determines aspects of cell physiology, such as growth and death.

Chapter 15 - Bacterial infections in orthopedics are resistant to conservative therapies, and patients must therefore undergo invasive treatments and prolonged administration of antibiotics, resulting in a significant decrease in quality of life. A novel strategy for overcoming the current status is therefore needed.

Photodynamic therapy (PDT), a therapeutic modality for proliferating diseases combined with tumor-seeking photosensitizers and low-powered laser irradiation, achieves a successful outcome in clinical use.



## ***Chapter 1***

# **ON POSSIBLE COHERENT EFFECTS IN PRIMARY VISUAL PERCEPTION**

***V. D. Svet<sup>1\*</sup> and A.M. Khazen<sup>2\*\*</sup>***

<sup>1</sup> Laboratory of Signal Processing & Imaging, Institute of Acoustics,  
4 Shvernik St. 117036, Moscow.

<sup>2</sup> Physics and Biophysics Consultant.

## **ABSTRACT**

The modern physiology of vision has saved up many facts which contradict the accepted approach to mechanisms of primary visual perception. From H.Helmholtz time it is considered that an image of some object primarily constructed by the eye cornea and lens first unequivocally is projected to the matrix of photoreceptors (rod and cone cells), and then is exposed to processing in several layers of the nervous cells arranged behind them. Actually, at the taxonomically superior animals with developed brain including human beings, the optical image is projected to photoreceptors through the layers of nervous cells, i.e. our retina is inverted.

The next not clear till now effect is the termination of vision at stabilization of micro oscillations of eye, so called Troxler effect. Absence of oscillations means no vision. And, at last, recently opened ultra fast reaction of photoisomerisation of rodopsine inevitably causes a question on the possible reasons and consequences of such fast reaction as time duration of the arisen potentials of photoreceptors is on 9-10 orders more.

It appears that if to consider all the specified features in common it is possible, at least at a physical level, to offer a new model of primary visual perception, which, in the first, is well coordinated with morphological and experimental data, and secondly, eliminates the arisen contradictions.

Such model assumes, that, owing to the specified features, the eye apparatus is capable to fix the so-called "full optical field" scattered by object or optical amplitude-phase distribution of optical field, though the registered parameter is light intensity.

---

\* Corresponding author: E-mail: vsvetd@mail.ru

\*\* E-mail: akhazen@yahoo.ru

Certainly, it is possible only at registration of scattered object fields as interferometric patterns or holograms.

## INTRODUCTION

The fundamentals of the theory of visual perception which were first stated in the works of T. Young and G. Helmholtz [1] are based on the following two major propositions:

- With the help of the refractive system of the visual apparatus an image of an object is projected on a photoreceptor in the retina in the form of spatial distribution of the intensity of the light field which is a reduced and *identical* copy of the examined object.
- At the moment of visual perception the image of an object in relation to the retina is stabilized or stationary.

The electric potentials from photoreceptors caused by light are initially processed in the nerve cells in the layers of the retina and then are relayed through the optic nerve to the visual cortex of the brain where the image of the object is formed.

However, numerous experimental morphological and neurophysiologic data on the retina of animals with developed brains contradict certain assumptions of the existing theory of visual perception.

*The first contradiction* is related to the “strange” morphological structure of the retina where the layers of cells are located *in front* of the photoreceptors, whose photosensitive buttends are turned to the dark opaque epithelium layer, i.e. retina is inverted [2,3]. As the cells and their components vary significantly in their refractive indices [4], the existence of inhomogeneous layers of cells in front of the photoreceptors leads to natural concerns about the existence of direct scattering. However, direct scattering would lead to distortions in the projected image, i.e. it *would not be clearly consistent* with the projected image of the object. This is the first contradiction.

*The second contradiction* relates to the condition for stabilizing the projection of an image on the retina at the time of visual perception. More than 100 years ago, it was discovered that the visual apparatus is in constant motion. Out of the six possible types of movements [5, 6] two are important for this consideration: tremor and drift. These are significantly different in amplitude and temporal parameters. They are also the least understood ones because in the absence of these the so-called “empty field” appears, i.e. vision vanished [6]. In other words, we do not see an image of a subject if it is stabilized regarding the retina. There are no convincing explanations for this phenomenon, although it clearly contradicts the existing theory.

The emergence of coherent chemistry and femtosecond laser spectroscopy revealed another intriguing fact in the visual apparatus - the tremendous speed of the photoisomeration reaction of rodopsine in a photoreceptor. As it was measured, as soon as a quantum of light falls on a molecule of rodopsine its transformation into photorodopsine takes 100-200

*femtoseconds* [7-9]. Moreover, it turned out that all the subsequent biochemical reactions which result in output membrane potential of a photoreceptor also occur *coherently*, but with a larger increase in time. As a result of all the biochemical reactions, the duration of the output potentials at synapses of the photoreceptors increases by 8-9 orders (!) or up to tens of milliseconds. Neurophysiology explains the need for quick initial reaction by minimizing energy dissipation of absorbed light quanta, though it is possible that there are other reasons.

It follows from the above that the existing theory of visual perception describes the functioning of the visual apparatus very superficially and clearly needs some adjustments and additions, especially in terms of coherent and incoherent optical interactions in the mechanisms of vision.

As will be shown below, a simultaneous examination of the optical properties of the inverted retina together with micro-oscillations and the high speed of photoisomerization reaction allows us to suggest a completely new mechanism of primary vision based on coherent and interferential effects in the registered optical field. Moreover, each of the three factors is necessary for the mechanism to function.

The authors realize that the suggested model of visual perception is radically different from the accepted one and, undoubtedly, needs to be tested experimentally. At the same time, it does not contradict much of quantitative and qualitative experimental data in neurophysiology and psychophysiology of vision, but is well corroborated by it.

## **1. DIRECT LIGHT SCATTERING IN THE LAYERS OF CELLS OF THE INVERTED RETINA**

The debate about the causes and the role of the inverted nature of the retina continued for more than 100 years [10-13]. Many experts believe that this anatomical structure, together with the capillary system supplying the photoreceptor, allows to protect them better from light overload [14, 15]. At the same time, however, this explanation assumes that possible light scattering in the layers of cells is small. Such an explanation is self-contradictory, as the layers of nerve cells are almost transparent and cannot provide protection against light overloads through absorption. It could only be provided by redistribution of intensity over a large area of photoreceptors, i.e. scattering, but this would inevitably lead to *distorted* images.

Direct scattering of light in layers of the retina is due to differences of local coefficients of light refraction in the cells and their components, the shapes and locations of which are irregular and random. Numerous experimental measurements performed on the retina and separate cell preparations indicate that the scattering may be strong enough [16-23]. In particular, several studies [21-23] have shown that the angular divergence of the laser beam passing through a photoreceptor may increase by several times. Significant direct scattering was also reported in works [17-20].

Realizing that the direct scattering impairs the quality of the projected image, some researchers have suggested that its impact may be reduced by specific optical properties of Müller glial cells [24, 25] which penetrate layers of nerve cells of the retina in the longitudinal direction like single mode fiber in a regular optic faceplate. In other words, the image is not distorted because it is projected onto the photoreceptors through a regular bio-optical-fiber structure. Despite the elegant experiments conducted by its authors [24], this

hypothesis also raises objections. The major reason for this is that the number of Müller cells is about 10-15% of the total number of cells in the retina [2] and their real anatomic form is incompatible with the ideal geometry of single mode optical fibers.

Quite another approach was made in paper [26], which contained two assumptions: a) inverted retina should create a strong direct light scattering, and b) a further visual perception is based on processing the correlation characteristics of the arising angular scattering spectra. As stated in the paper [26], “vision happens by accident, not in spite of it”. In support of this hypothesis, in paper [27] approximate calculations of the spectra of the direct scattering were conducted and some possible principles of handling the scattering spectra were carried out. In work [28] more accurate calculations which took into account the possible size of the cells and their components were carried out. And in paper [29], some algorithms of image processing were refined, taking into account a possible partial temporal coherence of light fields. Finally, it has been shown [29] that the degree of scattering significantly depends on the diameter of the pupil and the thickness of the layer, and that this can be strong enough to completely distort the form of the projected image.

It follows that the issue of the existence and degree evaluation of possible direct scattering of light is fundamental to this review. Therefore, following [27-29], we shall consider in more detail possible physical mechanisms of scattering.

## **1.1. Physical Mechanisms of Direct Light Scattering in the Retina and Computational Models**

The majority of researchers believe that the size of light scattering centers in a cell is less than 1 micron [15-17], and therefore the main scattering is caused by small-scale structures within the cell nucleus and organelles. It is considered that the mitochondria may be the main source of scattering. However, the results of phase-microscopy showed that significant scattering may be caused by the nucleus itself and by nucleolus [21]. In the formation of scattered fields practically all known optical phenomena such as reflection, refraction, absorption and diffraction of light are involved. And while not all of these phenomena are directly related to the scattering of light, at the macro level they all influence the structure of scattered fields. So, for example, in many works the coefficient of refraction is seen as a complex value where its imaginary part describes the frequency-dependent absorption.

It is worth noting that in ophthalmology only light backscattering is measured and evaluated: all the objective optical measurements are carried out only in “reflected” light because it is understandably impossible to measure the direct scattering *in vivo*. Backward and forward light scattering can be unambiguously the same (without taking into account polarization effects) only when the nerve cell layer is thin and symmetrical. However, from the anatomic structure of the nerve layer of the retina it is obvious that there is no symmetry, a layer of cells is inhomogeneous in structure and is a “thick” formation (relative to wavelength). Therefore, it could be argued a priori that the direct and backscattering in the retina cannot be identical.

Light scattering in biological tissue and cells is discussed in a large number of works, see, for example, [15-25], because the nature of scattering can be an important diagnostic sign in a variety of diseases. In the majority of works on scattering cell structures are considered as

complex dielectric objects subject to a certain law of distribution of the refractive index of light, which usually fluctuates in a fairly wide range from 1.3 to 1.7 [15,16]. Although the biological tissues of internal organs have different structures, morphological structures of cells do not differ. The components of a cell are cytoplasm (its size fluctuates from 10 to 40 *microns*) and various organelles (their sizes fluctuate from one to tens of *microns*) [16]. The largest organelle is the nucleus with the size of 3 - 10 *microns*. The sizes of smaller organelles such as mitochondria, lysosomes and others fluctuate from 0.5 microns to 1.5 microns. Volume ratio of different components in the cell can vary greatly depending on the type of tissue but on average it is believed that the cytoplasm is about 45-65% of a cell, the nucleus - about 5 - 25%, mitochondria - 5 - 15%, while all the other organelles range from 1% to 10% of the total [15-18]. Refractory indexes of light in the components of cells are determined by the concentration of protein. According to [18], any component of the cell can be considered as a solution of protein with a refractory index of

$$n = n_0 + \alpha C, \quad (1)$$

where  $n_0$  is the refraction index of the fill fluid similar to water and  $C$  is the concentration of the solution (g/100 ml). For protein  $\alpha = 0.0018$ , although there are cells where  $\alpha = 0.0016$ . Table 1 shows some published data on the indexes of refraction for various components of a cell [17]. It allows us to conclude that the layers of cells located before photoreceptors are a fairly complicated optically inhomogeneous medium with a random distribution of local refractory indexes.

Since in this consideration we are interested in the overall picture of the estimated scattering, layers of cells can be regarded as a sequential alternation of random transparent "phase" screens located in a uniform layer. Each screen consists of "N" transparent heterogeneities with certain sizes and random values of the refractory indexes of light [28]. To simplify the modeling phase heterogeneities were chosen in the form of spheroids oriented perpendicular to the plane of photoreceptors. In this case, different layers of cells have different thickness and the concentration of heterogeneities in each layer can be arbitrary. Possible absorption of light was not taken into account. Table 2 presents the characteristics of a group of simulated phase screens, and Figure 3 provides their images.

**Table 1. Characteristics of the components of a cell [17].**

Structure	Refractory index	Typical dimension, microns	Contents of a cell, %
Ambient liquid	1.35–1.6		
Cytoplasm	1.36–1.375	10 - 40	50 - 75
Nucleus	1.38–1.41	3 - 10	5 - 15
Mitochondria and organelles	1.38–1.41	0,5 - 1.5	5 - 10
Other organelles	1,37 – 1,4	0,5 - 1.5	1 - 10
Melanin	1.6–1.7		
Protein	1,5		

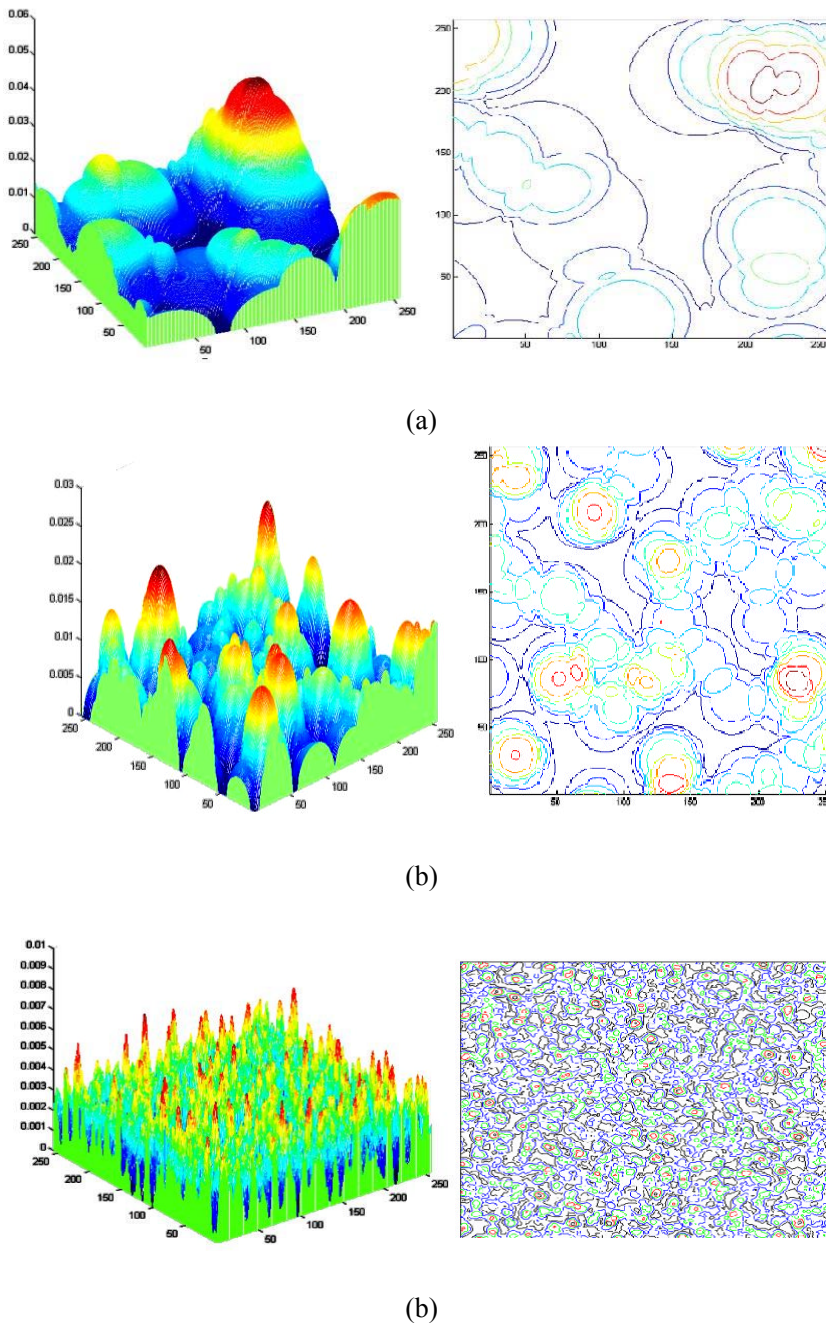


Figure 1. (a) Phase screen of the first type. Number of cells 1024, size  $0.005 * 0.005$  mm, thickness 0.06 mm, concentration  $K = 0.2$ , (b) Phase screen of the second type. Number of cells 1024, size  $0.0025 * 0.0025$  mm, thickness 0.03 mm, concentration  $K = 0.2$ , (c) Phase screen of the third type. Number of cells 1024, size  $0.0005 * 0.0005$  mm, thickness 0.01 mm, concentration  $K = 0.2$ .

Here, on three-dimensional images of cells, “height” of the phase heterogeneities is proportional to the value of phase incursion beam passing through a local non-uniformity. The values of phase shifts were calculated on the basis of the range of a random local spread

of the refractory indexes of light in the range of  $n_{\min} = 1,35$  up to  $n_{\max} = 1,5$ , and a given thickness of the layer for the chosen screen type. The combination of these screen made it possible to simulate the thickness of any layer of the nerve cells of the retina, putting them closer or apart.

Diffraction theory of constructing an image by lens with inbound aperture is based on the fact that in the focus plane the original image is reproduced by the coherent addition of complex amplitudes of waves diffracted on the diaphragm, up to a phase. Even a rough estimate of phase distortion of the wave front with a layer of cells has shown that with a difference in the refractory indexes of  $\Delta n = 0,06$  (see Table 1) phase variations  $\Delta\phi$  can reach significant values

$\Delta\phi = (2\pi / \lambda) d\Delta n \approx 22^0$  even with the layer wave thickness of  $L_{\text{sl}} = \lambda$ . Conversely, when the length of the layer  $L_{\text{sl}}$  reaches the order of several hundreds of wavelengths phase shifts will be very large.

Consider now the physical mechanism of scattering in a simplified optical model of an eye with inverted retina. According to Figure 2, the image of the constructed optical system "cornea + lens" after passing through inhomogeneous layers with a total length  $L_{\text{layer}}$  is displayed on the photoreceptors while the optical system "cornea + lens" is replaced by a single equivalent lens.

Let us assume that a photoreceptor receives light with the end turned to the layer of nerve cells, although morphologically they are addressed to the non-epithelial layer. This assumption would only increase the overall thickness of the inhomogeneous layer of cells by the length of photoreceptors. The value of the longitudinal size  $\Delta Z$  diffraction focal spots along the axis Z is critical for further consideration [30]:

$$\Delta Z \approx 3\lambda \left( \frac{F}{d_p} \right)^2 \quad (2)$$

where  $\lambda$  is wavelength of light, F is focal length lens, and  $d_{\text{vis}}$  is the size of the pupil. Note that expression (2) is true only for an ideal symmetric thin spherical lens.

An inhomogeneous layer would distort the form of an image of the point source if its length  $L_{\text{layer}}$  is several elements of  $\Delta Z$ . If the length of the layer would "accommodate" one or less than one element of the longitudinal resolution of  $\Delta Z$ , then in the first approximation distortion will be low or absent. Some of the results of evaluations with  $L_{\text{layer1}} = 220$  microns,  $F = 20$  mm, and  $\lambda = 0,5$  mm are presented in Table 3. In the last row of Table 3 a parameter  $M = L_{\text{layer}} / \Delta Z$  is introduced, which determines the rounded up number of elements  $\Delta Z$  which "fit" the length of the layer.

It is clear from these estimates that with the increase in the diameter of the pupil the value of M grows rapidly, and, hence, the degree of scattering of light should be increasing as well.

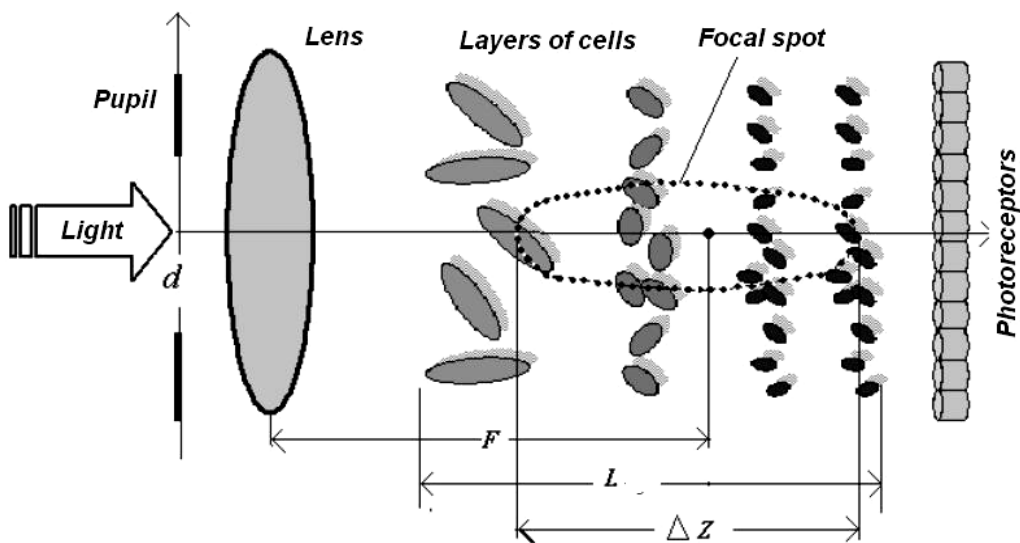


Figure 2. Calculated optical model.

**Table 2. Types of phase screens.**

Types of a phase screen	Sizes of heterogeneity, $a*b$ , microns	Thickness of the phase screen, $d$ , microns	Concentration, $K = (N/10 \text{ micron}^3)\%$
A	0,5 * 0,5	10	0,2
B	2,5 * 2,5	30	0,2
B	5*5	60	0,2

**Table 3. Longitudinal size of focal spot  $\Delta Z$  for a thin symmetrical lens.**

$D_{\text{vis}}$ , (mm)	1	2	3	4	5	6	7
$\Delta Z$ , (micron)	600	150	65	37	24	16	12
$M = L / \Delta Z$	0.4	1,6	4	7	10	15	21

In ophthalmology it is believed that the best conditions for clear distinction of an object are when the size of the pupil is between 2 and 5 mm. This is consistent with the fact that in the central region of the retina, *fovea*, the value of  $M$  can vary from 1.6 to 10 and light scattering will occur even at small pupil sizes. If we further consider that the real length of the actual thickness of the photoreceptor in the retina is higher by about 60 microns the parameter  $M$  with the same size of the pupil will vary from 2 to 13. In other words, the degree of scattering will be greater.

## 1.2. A Method for Calculating the Direct Field of Scattering

A correct analysis of an optical system that includes scattering layers is only possible with the use of wave approach. However, this is difficult because of the large wave size of the pupil's aperture, which at present makes such a calculation with use of personal computers all but impossible.

The only solution to this problem is the combination of ray and wave calculations. Thus, until the ray cone (after passing the entrance aperture of the eye's optical system) has not narrowed to a size suitable for wave calculations, the field may be calculated using the ray calculation, and after then the wave calculation. But in the case of a point source (and this, due to the superimposition principle, would include the more general case of an extended source), the ray calculation itself is complicated by the possibility of caustic surface's proximity to the entrance aperture, as it happens with the simplest eye model – the so-called Gulstrand's reduced eye model. This model of the eye's refractive system, widely accepted in ophthalmology, describes the spherical surface of the boundary between two media with different refractive indices.

In [28], we suggested one of the possible solutions to this problem – that instead of looking at the spherical surfaces of the boundary, we should concentrate on the more difficult cylindrically symmetrical surfaces, which do not exhibit this effect. In doing so, we accepted a simple model hypothesis that the accommodation of the eye's optical system to a point source in the absence of scattering also provides a point image (as far as the beams are concerned) of this source on the retina.

It is known that if in reflecting from a curvilinear surface of the boundary all the rays converge in a single point, then, according to Fermat's principle, such a surface is an ellipsoid of revolution, whose focuses are the point of emission and the focal point. In the extreme case of an infinite withdrawal of the source this surface degenerates to a paraboloid of revolution with an axis of sight to the source. The application of Fermat's principle to an optical system in the reduced eye model allows us to arrive at a description of the shape of the boundary which focuses the rays of a point source in one point. Such a surface can be described with the following parametric equations:

$$z = \frac{0,5t[(1-n^2)t + 2(nz_i - z_s)]}{(z_i - z_s)} \quad (3)$$

$$r^2 = (z - nt)(2z_i - z - nt) \quad (4)$$

In fact, the only part of the surface which is relevant and important is that which is illuminated, passes the point at  $(0; 0)$  and is a connected component that includes the corresponding parameter  $t = 0$ . Here, axis  $x$  is the symmetry axis of the surface that passes through the point of emission  $z_s < 0$  and the focal point  $z_i > 0$ . The relative index of refraction  $0 < n < 1$  is the relation of the speed of light in the medium in which the focalization takes place to the medium containing the source;  $r$  is the radial coordinate calculated from the peak of the surface that lies between the source and the focal point. In the case of an infinitely remote source this surface degenerates to an illuminated part of an oblong ellipsoid of

revolution with a long axis aimed at the source and a peak at zero point. The equation for this ellipsoid is:

$$Z = \frac{Cr^2}{\left(1 + \sqrt{1 - (K + 1)C^2 r^2}\right)} \quad (5)$$

where the curvature of surface C at its peak and the conical constant K are related to the right focal distance of the optical system  $z_i$  and the relative index of refraction n as

$$C = [z_i(1-n)] - 1, K = -n^2. \quad (6)$$

For the chosen focusing surface, a software package was designed for calculating the field of the point source. The following raw data were selected: z-coordinate of emission plane ( $z, s$ ); z-coordinate of image plane; light velocities in both the media of emission and reception; the length of emitted wave in the medium of emission; and the radial coordinates of the point source. Using these parameters, the software calculates the shape of curvature of the focusing surface, including the curvature at the peak. Such a choice of raw data corresponds to the notion that the eye changes the shape of the crystalline lens (curvature, conical constant, etc.) in order to focus the image of one point of the axis of a plane on a pre-selected surface of reception (retina).

The package consists of several programs. The first carries out an approximate calculation of the ray pattern for given data in the case of axisymmetry in order to ascertain the actual focalization of rays in a point and choose such a distance at which the ray cone narrows to an acceptable size. The narrowing should not be significant, as the simplest ray calculation does not allow calculating the wave field accurately enough due to proximity to the focus. For this reason, the raw data for the software includes the maximum and minimum lateral wave sizes chosen according to heuristic consideration.

The second program in the package consists of two parts. The first part carries out a ray calculation of the field of the point source up to that plane at which the cone is considered to be narrow enough, and onwards from which the wave calculation would be carried out. For the ray calculation, the source emits a number of rays sufficient to cover the surface of the media boundary densely. Then the trajectory of each ray is followed up to its contact with the surface, and the amplitude and phase of each ray is calculated along this trajectory. A uniform mesh with a grid size of no more than a quarter of a wave length is chosen on the same plane. For each mesh node the amplitude and the phase of the nearest ray and the number of rays (for control purposes) in the vicinity of the node are recorded, as well as the maximum deviations of their amplitudes and phases from those of the ray nearest to the node. In this way, a value set of a complex field on a rectangular mesh, which serves as the basis for the wave calculation carried out by the second part of the program, is found.

The second part of the program begins with the supplementation of the field values on the resultant mesh with zero values on a mesh elongated more than two times. As it is known, this allows decreasing aliasing in further use of the Fourier transformation in order to deduce the lateral components of the field spectrum. The deduced lateral spectrum values are multiplied by exponential factors related to the further wave transmission corresponding to the given spectrum. In this way, we obtain a set of field sections on the defined planes on z-

axis, that is, a 3D-image of the image wave field. This part of the program also includes a simple method of accounting for scattering in inhomogeneities in the focusing medium by modifying the field during sequencing of the string of phase screens. For this purpose, a separate program for the calculation of phase progressions of such screens by inputting the physical and geometrical qualities of the inhomogeneities of which such a screen consists..

The last program of the package visualizes the resultant field by plotting its longitudinal and cross-sections and to visualize the 3D image of the field.

### 1.3. Some Examples of Simulated Fields of Direct Scattering in the Retina

Below we describe some examples of simulated fields of light scattering in forward direction based on the results of [28]. Figures 3a and 3b show two images of the intensity distribution of the light field calculated for the plane of photoreceptors where the cells' nerve layers are homogenous and have the same constant index of refraction. The two-dimensional image 3a is the distribution of the intensity of a projected image of a point source along the axial coordinate Z and the transverse coordinate X. The centre of the bright spot is at 23mm with crystalline lens' focal distance  $F= 20$  mm and the size of the pupil  $d_p= 1$  mm. The three-dimensional image of the same distribution can be seen in Figure 3b. The scale is linear throughout and it can be seen that the level of the first side lobe equals 18-20%, as it should in the case of monochromatic light diffraction on a round hole in the absence of apodisation or shadowing [30]. In the case of a wide light spectrum the general picture remains the same, but the structure of the side lobe does not have the same pronounced quasi-periodic properties and is smoother.

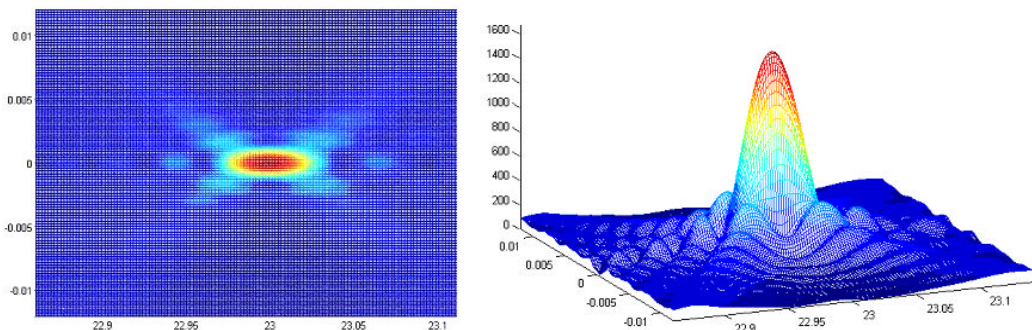


Figure 3. Image of a projected point light source where nerve layers are homogenous. 3a. Distribution of intensity on coordinates Z and X. 3b. 3D- Image.

The next images reflect the situation when the image of a point source was projected through an inhomogeneous layer of cells 50 microns thick, and the diameter of the pupil was equal to  $d_p= 1,0$  mm and  $d_p= 1,5$  mm, Figs. 4a,b and 5a,b respectively. It is worth noting that despite the small pupil diameter and a small thickness of the layer light scattering is present, though its level in general does not exceed 20%. When the diameter of the pupil increases, the scattering becomes more pronounced, although the shape of the main image of the source is

not yet distorted. However, completely different images of the point source emerge when the thickness of the inhomogeneous layer increases to about 220-250 microns and the diameter of the pupil fluctuates between 3 to 5 mm, which corresponds to vision in normal lighting conditions.

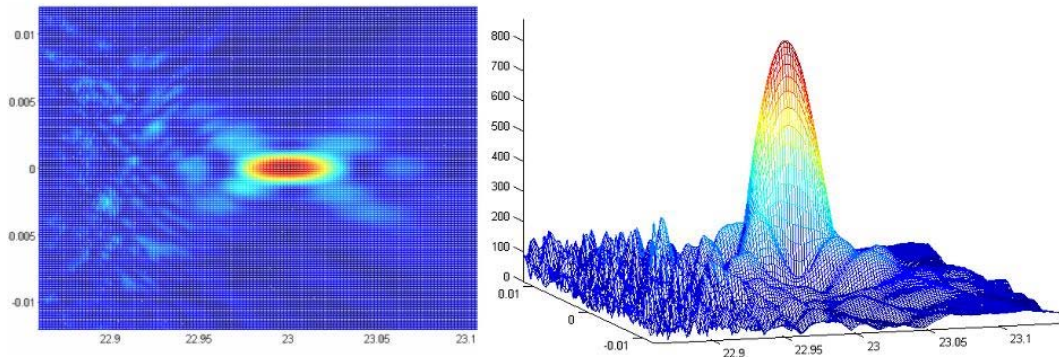


Figure 4. Image of a point source with the diameter of the pupil 1 mm, the width of an inhomogeneous layer  $L = 50$  microns and the type 3 phase screen. 4a. Distribution of intensity on coordinates Z and X. 4b. 3D-Image.

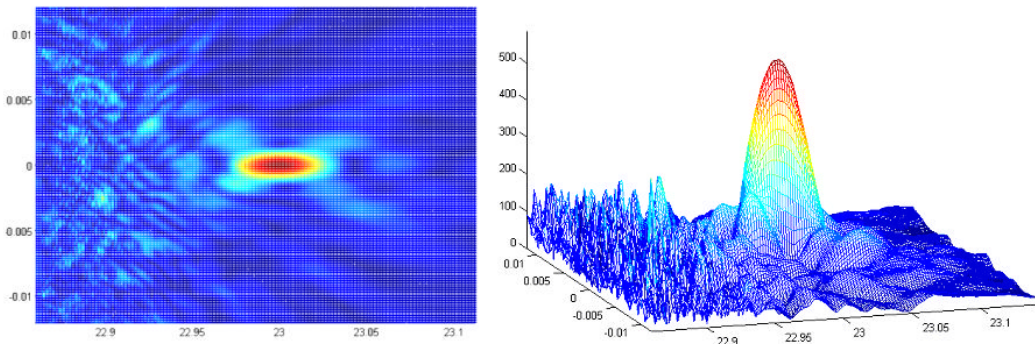


Figure 5. Image of a point source with the diameter of the pupil 1.5 mm, the width of an inhomogeneous layer  $L = 50$  microns and the type 3 phase screen. 5a. Distribution of intensity by coordinates Z and X. 5b. 3D Image.

The distribution of intensities presented here in Figure 6 has little in common with the image of a point source (in comparison to Figs. 3-5). The brightest spot in this image is not the axis, but below it and before the focus. The full image of a point source consists of several large spots of varying sizes, randomly orientated. If we further increase the size of the pupil and at the same time swap one of the type 2 screens for a type 3 phase screen (with the smallest diffusers), then the image of the third source disappears completely and an image structurally reminiscent of noise appears instead (Figure 7)

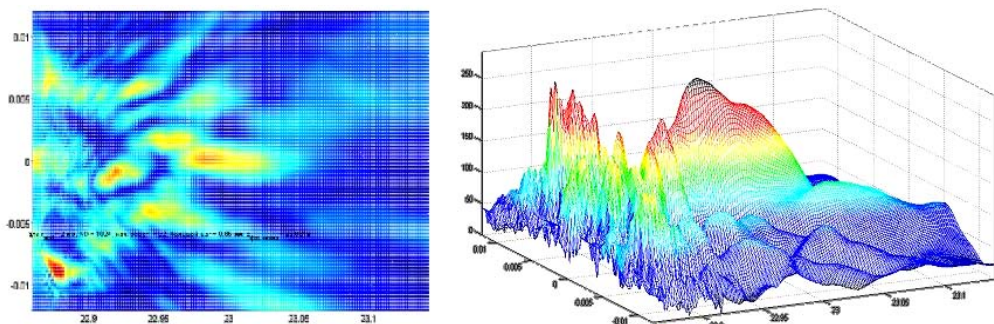


Figure 6. Image of a point source with the diameter of the pupil 3 mm, the width of the inhomogeneous layer at  $L = 200$  microns. The layer consists of three phase screens – two type 2 screens and one type 1 screen. 6a. Distribution of intensity by coordinates Z and X. 6b. 3D Image.

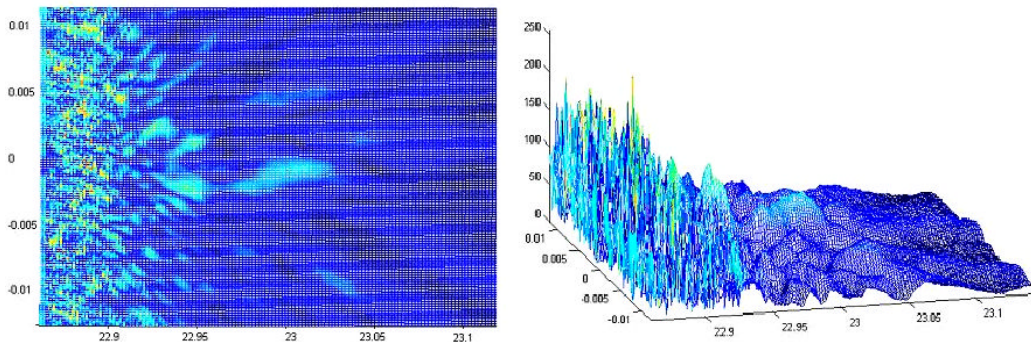


Figure 7. Image of a point source with the diameter of the pupil 5 mm, the width of the inhomogeneous layer  $L = 200$  microns. The layer consists of three phase screens of all types. 6a. Distribution of intensity by coordinates Z and X. 6b. 3D Image

As we see the image of the point source in transverse coordinates X and Y, the resultant images with different proportions of the pupil diameters and layer widths will look as shown in Figure 8. We should note that each elementary pixel on these images in terms of size is about equal to a photoreceptor (3-5 microns). The findings in the field of psychophysiology of vision show us that the effective maximum spatial frequency is not higher than (10-12) lines/mm, which corresponds to a lateral linear resolution of 80 – 100 microns.

This is why the gray-level images in Figure 8 have to undergo further low-frequency spatial filtering. If we assume that the highest spatial frequency is no more than 10 lines/mm, then after such filtering the image will be transformed into Figure 9. In this image, one pixel is equal to 50 microns. The filtering was applied with a rectangular window with no further smoothing. For this reason the edges of the “pixels” are quite sharp. It can be seen that with a large pupil size the source point images transforms into what is practically a uniformly grey background.

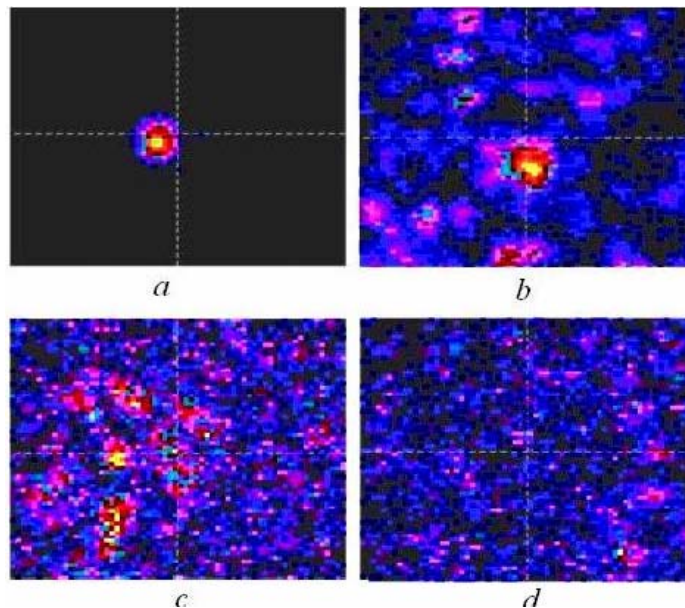


Figure 8. Images of a point source in the XY photoreceptor plane with the width of the layer 200 microns. Pupil diameters 1 mm(a), 2 mm(b), 4mm (c), 5mm (d)

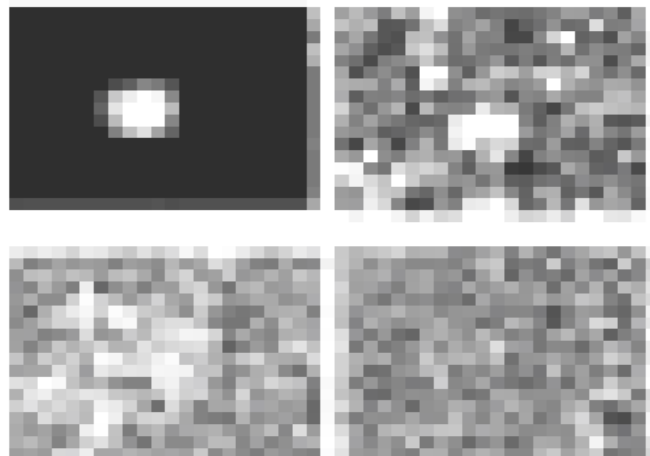


Figure 9. Monochrome images of a point source resulting from low-frequency filtration of Figure 8 with a rectangular window and a cut-off  $l$  of higher spatial frequencies at 20 lines/mm.

The results allow us to make a number of conclusions, which are important for this study:

- Cell nerve layers of the inverted retina create direct scattering of light which results from the differences in local refraction indices in the cells and their components.
- Where focal distances and widths of inhomogeneous layers are constant, the degree of scattering and its character depend on the pupil diameter.
- As the pupil diameter increases, the image of a projected point source grows distorted.

- The character of distortion is dependent on the dominant size of structural inhomogeneities in nerve cell layers. If it is comparable to or less than the length of a light wave, then the scattering is small-scale and at large pupil sizes (4-5 mm) the images of a point source transforms into an almost uniform noise image structurally similar to a grey background.
- If nerve cell layers are dominated by structural inhomogeneities significantly exceeding in size the wave length, then the small-scale scattering is minimal, but the shape of the projected image of the point source is randomly distorted.
- It is clear from the morphological composition of the retina that the formation of a direct scattered field involves inhomogeneities of all sizes, but available experimental data suggests the domination of small-scale scattering of light.

The main conclusion that can be drawn from these results is that in normal conditions (pupil diameter of 3-5 mm) the shape of the image projected onto the photoreceptor field of the inverted retina does not correspond to the shape of the initial image.

## 2. ACCIDENTAL MOVEMENTS OF THE VISUAL APPARATUS

Let us consider another phenomenon of visual perception associated with the movements of the visual apparatus. These movements have been studied for more than 100 years; however, their role and importance for visual perception are still unclear. In the early 19th century, Troxler discovered that if a motionless object was located in the field of peripheral vision and the viewer fixed their gaze on it, the image would "disappear". Only in the late 1950s Troxler's effect was reliably confirmed in laboratory conditions when the image was stabilized on the retina, and, moreover, it was discovered that a similar loss of the image occurred when other, quite small in amplitude, motions such as displacement and tremor took place. This effect of a "blank field" was also observed and most of the subjects noted that they saw "a grey background", and, sometimes, a non-uniform grey background, but none of them saw the projected images.

One particularly "intriguing" movement in this regard is tremor or physiological nystagmus - casual and high-frequency (120 Hz) random fluctuations in the ocular apparatus with angular amplitudes of no more than 25-30 arc seconds. In the first publications [32-35] it was assumed that the disappearance of an image occurred in a few seconds after these micro movements were stabilized. However, as soon as the measurement technology was improved in the late 90s, it was discovered that an image disappeared even with very short periods of stabilization (less than 80 milliseconds) [36]. This indicates that there is some other mechanism of disappearance of an image and its reconstruction when stabilization is over which is very fast.

One hypothesis was that, like in the case of the inverted retina, random motions of the visual apparatus are necessary for the adaptation of the retinal cells and neurons of the visual cortex and reducing the light load on the photoreceptor. This assumption is quite plausible for motions with large amplitudes, but it is not satisfactory for tremor because when the angular resolution of the eye is about one angular minute, an image of a point source "covers" the space of approximately  $40 \times 40$  photoreceptors. The diameters of the receptors are around 3-5

*microns*, and the occasional tremor oscillations take place with the amplitudes of about 3-15 *microns*. It follows that the central receptor sites are always “light-struck” and we therefore cannot discuss their protection against overloads.

Numerous measurements of the time-and-frequency parameters for different types of micro movements in the visual apparatus were summarized in the review [38]. It also discussed various (and sometimes conflicting) hypotheses on the role of such movements in visual perception. So far, we can be sure about one thing only: the stabilization of images on the retina leads to the inability to see and the existing theory of visual perception fails to explain this effect. There is no vision without movements.

It is curious that the observed "effect of an empty field" or the perception of a motionless image in the form of a non-uniform gray background *greatly correlates* with the images of a point source modeled above, projected on photoreceptors through a layer of nerve cells: when the size of the pupil is normal, the image of a point source by means of the direct scattering of light is transformed into an almost non-uniform gray background.

### **3. RODOPHSINE PHOTOISOMERISATION REACTION**

In recent decades, due to new developments in experimental techniques which use short-pulsed lasers, the notion of coherent chemical reactions has assumed particular importance in chemistry [7-9]. For example, photo induced electronic transitions in the photoreceptor are linked with oscillation and conformational changes in the vicinity of chromatophore. These changes ultimately can be described in terms of waves and oscillations. Hence the new term “coherent chemical reactions” emerges. It reflects the leading role of oscillations of molecules in the acts of reactions which, in certain circumstances, result in waves synchronized in time and space. Among the first results of the new methods of experimental studies, photoenergetic reactions involving bacteriorhodopsin have been described. The first stages of these reactions take place in extremely short time spans of 100-200 femtoseconds. In neurophysiology of vision experimental data were obtained that showed that the quantum of light falls on the photoreceptor and triggers photochemical reactions (rodopsine photoisomerization) in an equally short period of time [8,9].

It was shown [39, 40] that in a sufficiently wide spectral area (400-1100 nm) photo transformation of rodopsine coexists on both channels - coherent and incoherent. It is precisely the direct coherent conversion of the first intermediate (batorrhodopsine from rodopsine) which occurs in 100-200 *femtoseconds*. This revealed the coherence of all subsequent chemical reactions, i.e. a collective character of the molecular complexes, where the “initial” coherency remains in further biochemical reactions and is transferred to the products, i.e. chemical transformations of the products occur synchronously and conform by phase.

This feature of the rodopsine photoisomerization reaction inevitably raises new questions in the classical theory of vision, and, in particular, a following question: *what point of vision may the possibility of coherent chemical reactions be necessary at?*

## 4. PROPOSED MODEL OF VISUAL PERCEPTION

Let us once again list the discussed specifics of visual perception.

- Due to significant differences between the coefficients of local refractory indices, layers of inverted retinal nerve cells can cause a significant direct scattering, distorting the shape of projected images.
- With the increase of the diameter of the pupil the degree of scattering increases rapidly and the form of the projected image is distorted very quickly. With the diameter of the pupil between 3 and 6 mm the projected regular image acquires the shape of a “noise image” which is similar to the image of a uniform grey background.
- Visual perception is only possible if there are micro-oscillations of the optic apparatus. Stabilization leads to a loss of the image, to the emergence of “empty fields” (uniform grey background), and to the termination of visual perception.
- Rodopsine photoisomeration reaction is a coherent chemical reaction during which the coherent characteristics of optical radiation can be transformed into coherent transformations of products of chemical reactions.

How could this visual apparatus work?

Before suggesting a possible model let us point out another interesting feature.

We have already mentioned that the angular resolution of a normal eye is about one angular minute, although the potential angular resolution is much higher and is determined by the wave size of the pupil. If we consider that the refractive system of the eye is an ideal thin lens the diffraction angular resolution (in degrees) by the level of intensity (-3 dB) will be equal to

$$\theta_{(-3dB)} = \pm \left( \frac{29,5\lambda}{d} \right) \quad (7)$$

In (7),  $\lambda$  is the wavelength of light, and  $d$  the diameter of the pupil. In particular, if  $\lambda=0,63$  um, and  $d=3$  mm, then  $\theta \sim 22''$ , and if  $d = 6$  mm,  $\theta \sim 10''$ . Dimensions of the photoreceptor constitute 3-6 um and they in particular determine the maximum possible linear resolution. However, psychophysical measurements have shown that an average person sees objects with dimensions of no less than 100 microns (0.1 mm) [41], i.e. almost by an order of magnitude worse. However, in order to see objects with a resolution of 100 microns one does not necessarily have photoreceptors with the size of 5-7 microns. In other words, from the “technical” point of view, the number of photoreceptors in the retina is redundant - instead of the matrix of 3500\*3500 reception elements we could have 15-20 times less of these.

Why do we not use the ability to see in a much higher resolution, built in by nature itself, having all the necessary “technical” preconditions in the primary visual apparatus?

Psychophysicists of visual perception explain low angular resolution by evolutionary features of human development and the abundant number of photoreceptors by the high reliability of the retina. It is obvious that these arguments are not devoid of sense. However,

another fact should be recalled - the number of nerve fibers in the optic nerve is less than the number of photoreceptors by about two orders of magnitude, i.e. in the process of visual perception compression (and perhaps some kind of processing?) of information by 100 times occurs. In other words, the ability to distinguish details of an image at about 100 microns or more is a result of processing the input image by *the entire system of visual perception* – photoreceptors, retinal cells and visual cortex. But due to the diffraction of light on the pupil aperture, components of the light field with high spatial frequencies *must be presented* in the primary photoreceptor field and be recorded by it. In this case the question of how and at what stage these more high-frequency components are “filtered” by the primary visual apparatus in the resulting image arises.

It is clear that in the non-coherent optical methods it is not possible to answer these questions and, moreover, explain how the primary visual apparatus may work in the presence of scattering and micro oscillations.

Let us consider the phenomenological model of primary visual apparatus in the same form as in Figure 2, indicating that the entire optical system is in a high and constant chaotic movement of transverse coordinates in the absence of which the projected image is lost. However, in this scheme the following sequence of events occurs when observing a point source of light:

- The image of the source is projected by the refractive system of the eye in a certain scale through a scattering medium - the nerve cells of retinal layers
- The scattering medium transforms the original distribution of the optical field into a random distribution and it is displayed on the photoreceptor
- Photoreceptors record this spatial distribution of intensity
- Some time later (digits and tens of milliseconds after the primary photochemical reaction) the spatial distribution of electric potentials arises at the synapses of photoreceptors.
- These potentials are processed in the layers of nerve cells of the retina and then this information, processed and compressed by approximately one hundred times, enters the visual cortex through the optic nerve where a visual image of a point source is formed.
- All these transformations are carried out in the presence of oscillations of the visual apparatus.
- From the physical point of view, this issue is very similar to the issue of imaging objects through scattering media and, therefore, it is only possible to find a solution on the basis of coherent wave optics, which involves consideration of possible diffraction and interferential phenomena in the visual apparatus and determines the possibility of a full optical field that keeps all the amplitude-phase information. If conditions for registering the full field do exist in the visual apparatus, in the future a number of methods that would handle and restore the original image of an object located in a inhomogeneous scattering layer of cells can be proposed. Since the photoreceptors are quadratic receivers, the registration of the full optical field is only possible if the interference pattern of scattered fields on the photoreceptors is formed for some time, namely the time of coherence, and during this time they are able to register it. This interference pattern of optical fields can be also called a hologram.

#### 4.1. Interference and Holographic Approaches

The holographic or interference approach to visual perception is not new and it has been hotly debated in biophysics for more than 40 years. Many of these works appeared after the publication of the famous book by D. Bohm [42] on the «holonomic» principles of the universe. However, many authors have applied this approach in a very abstract way. Discussing the fact that our vision is similar to holography, none of them asked: "But, indeed, how are the holograms or interference structures formed, and how can they be extracted from visual information?" Apart from a number of speculative and often simply incorrect assumptions, in discussing "holographic eyes and brain" we can mention a number of physiologists, for example, K. Pribram [43,44], Glazer [45,46] and others, who put forward several experimentally-based holographic concepts, although they were directly related to models of visual perception as a whole. In particular, K. Pribram [44] did not even doubt that the hologram, which was originally used as a metaphor or an analogy to explain some of the abnormalities in the work of the nervous system, has become an accurate model of the natural forms of its work [44]. The inventor of holography D. Gabor also talked about the "similarity of holographic registration with the human memory" [47].

In Glazer's works [45,46], which have been largely stimulated by Hubel's and Wiesel's earlier work [42,43] on the existence of fields of neurons which respond to the specific features of images, the concept of spatial frequency of filtering visual information by the neurons of the visual cortex was proposed. Hubel's and Wiesel's work [48] showed that in the axis of any module of the visual cortex neurons can be connected to the same field of the retina, each of which gives a maximum response only to its own grid, i.e. a well-defined spatial frequency. Glazer believed that the entire space of the retina was "divided" by cortex neurons into a multitude of spatial-frequency fields, and the image is analyzed for each local field with a given value of spatial frequency or a set of spatial frequencies.

All of these hypotheses and assumptions have led researchers to the logical conclusion that in the primary visual apparatus some spatial transformations of images are implemented, which are similar to a Fourier transformation, and the visual cortex already "works" with the signals of different spatial frequencies of the resultant angular spectrum. The idea of Fourier analysis of images has become so popular among professionals in the field of physiology of vision that in many works allegations that "the human eye performs a Fourier transformation of the original image" have appeared.

The authors do not deny the possibility of analyzing the spatial frequencies, or more precisely the spatial spectrum of images in the visual apparatus, but would like to make a few comments on it.

#### 4.2. Fourier Analysis of the Images

At the outset, we note that the mathematical Fourier transformation is an integral and linear relation that converts one type of an image into another using a set of orthogonal harmonic functions. It is possible that expansion and other orthogonal functions are not harmonic. However, Fourier analysis is a very convenient mathematical method as it very

accurately describes the oscillatory processes occurring in the propagation of waves of any physical nature.

But we want to emphasize these two fundamental facts:

- The “optical refractive” visual apparatus itself consists of the cornea and lens and generally does not carry out the spatial spectral analysis. It simply projects an image of the object on a certain scale on the retinal photoreceptors, while for the mathematical description of such a projective transformation it is very convenient to use the Fourier transformation.
- Even if “the eye carries out a Fourier transformation” the further reconstruction of the image is only possible if the spatial registration of the *complex spatial spectrum* takes place, not just the intensity of the spatial spectrum.

The authors are aware that these circumstances seem trivial for opticians but the problem is that in many works on vision perception written by physicists these, unfortunately, are often ignored.

Let us turn to Figure 10 which for the purposes of this discussion shows the refractive optical system of the eye which is replaced with a single equivalent lens with a focal length  $F_l$ . Let us assume that the layer of nerve cells located in the photoreceptor in the plane  $(\xi, \eta)$  does not introduce any distortion.

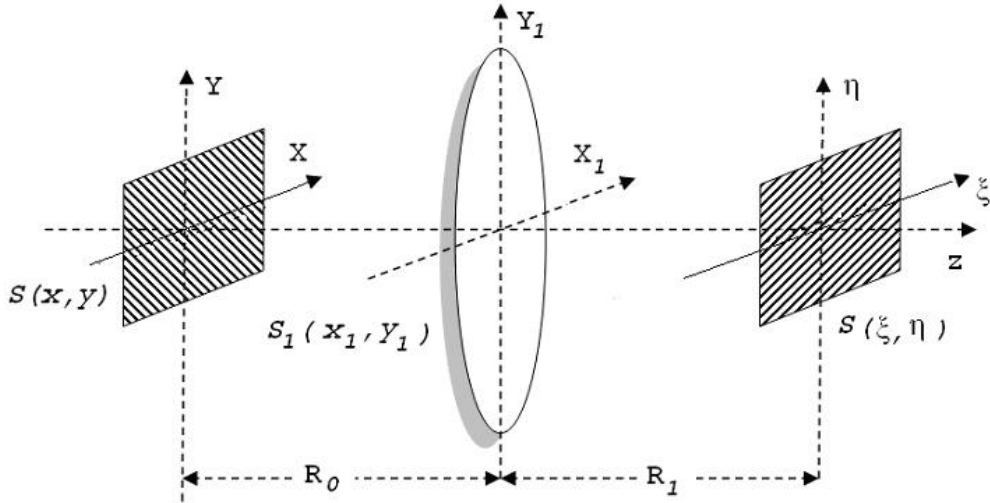


Figure 10. Basic optical system.

In line with [49] the output signal  $S(\xi, \eta)$  can be written as

$$S(\xi, \eta) = \exp[j\phi(\xi, \eta)] \iint_{XY} S(x, y) \exp\left[\frac{jk}{2R_0}(x^2 + y^2)\right] \exp\left[-\frac{jk}{2g}(x^2 + y^2)\right] dx dy \quad (8),$$

where the phase factor is

$$\exp[j\phi(\xi, \eta)] = \frac{\exp\left[\frac{jk}{2R_l}(\xi^2 + \eta^2)\right]}{\lambda g R_0 R_l}, \quad (9)$$

and the variables are related as this relation follows

$$x_n = \frac{x}{R_0} + \frac{\xi}{R_l}, \quad y_n = \frac{y}{R_0} + \frac{\eta}{R_l}, \quad g = \frac{1}{R_0} + \frac{1}{R_l} - \frac{1}{F_e} \quad (10)$$

Equation (8) allows calculating the output or form of an image at various and random positions of objects on the lens.

Let us select only two important cases. The first one - the output signal is an image of the input signal, while the second one is its Fourier spectrum.

When forming an image, as follows from the equation for a perfect lens,  $g = 0$ , i.e.

$$g = \frac{1}{R_0} + \frac{1}{R_l} - \frac{1}{F_e} = 0 \quad (11)$$

After simple transformations the expression for the output signal will then appear

$$S(\xi, \eta) = \frac{R_0}{R_l} S(-\xi \frac{R_0}{R_l}, -\eta \frac{R_0}{R_l}) \exp\left[\frac{jk}{2R_l} (\xi^2 + \eta^2)(1 + \frac{R_0}{R_l})\right] \quad (12)$$

In other words, we have received the same original image, but reversed and with the scale coefficient of  $\frac{R_0}{R_l} = \frac{1}{M}$ , as it should be, of course. If only the intensity of the signal is recorded, the phase factor in (12) can be ignored.

Now let us turn to another case where the lens actually performs the *Fourier transform*. This happens when the input image  $S(x, y)$  is *exactly* at a distance of  $R_0 = F_l$ , and the output plane is located *exactly* at a distance  $R_l = F_l$ , or, in other words, the plane of photoreceptors must be *exactly* in the focus of the lens, while

$$S(\xi, \eta) = \frac{1}{\lambda F} \iint_{xy} S(x, y) \exp\left[\frac{jk}{F} (x\xi + y\eta)\right] dx dy \quad (13)$$

Only with these conditions in the focal plane of the lens a Fourier-spectrum of image will be really established rather than its image. It is notable that the Fourier spectrum will be also formed under conditions where the object is located at an arbitrary distance from the lens, but the plane of the output signal should be located in the focus of the lens. Herewith, an additional quadratic phase factor will appear beyond the integral, and this will greatly distort the phase component of the spectrum but will not affect the amplitude spectrum [49].

A great number of ophthalmic measurements indicate that the plane of photoreceptors in the retina is always situated behind the focus of the lens, the more so as their sensitive ends are turned to the opaque epithelium. Therefore, an image of the subject is always projected on

the photoreceptor, either original or distorted by the layer of cells, and no matter of what distance from the subject it is. Therefore, the assertion that “the eye performs a Fourier transform from the original image and its angular spectrum is projected on the retina” is simply not true.

Meanwhile, primary visual perception can be actually carried out on the basis of a Fourier analysis of angular spectra, but, as the authors suggest, it happens through a different mechanism in the primary visual perception which allows recording an interference pattern of a scattered field, or a hologram.

### **4.3. Published “Holographic” Hypotheses**

Physicists have also turned their attention to a number of contradictions in the visual apparatus related to the inverted retina. However, unlike physiologists they tried to simulate possible “optical” schemes of hologram formation at the stage of primary visual perception. We should in particular mention the works of [50-52], where nerve layers of the retina were simulated as a group of regular diffractive grids following one another. This model provided satisfactory explanations for some well-known phenomena in visual perception: the Stiles-Crawford effect, the Purkinje effect, and the perception of color. The authors of [52] dubbed their retina model a “tri-chromatic four-dimensional optical correlator”, noting that apart from the determination of color it allowed to mark out the directions of emission sources. However, the authors did not describe any processing algorithms in detail.

In [53,54], it was hypothesized that a dynamic hologram may appear on the retina as a result of double refraction of light on the nerve fibers in the area of the yellow spot, as in this area of the retina the fibers are almost parallel to each other. Such a system of “thin cylinders” can be described through a model of a positive uniaxial crystal. The falling ray in this case undergoes double refraction and divides into two polarized rays – ordinary and extraordinary. As the authors of [53] estimate that the two rays diverge by about a wave length, they can form interferential structures or dynamic holograms. Moreover, in [54] the authors hypothesized that depending on accommodation the appearance of dynamic holograms can happen in different areas of the retina in the vicinity of the yellow body, which in turn suggests the possibility of extracting information about the depth of field in monocular vision.

In [55], a diffractive model of tri-chromatic vision was suggested, based on the diffraction of white light on the pupil and natural chromatic aberration in the eye’s refractive apparatus. In this model, when a “colour” diffractive pattern appears, the distinction of colour can be defined by the result of pairwise interaction of potentials of two types of photoreceptors: “rod/rod”, “cone/cone”, and “rod/cone”. In this way, as the author of [55] suggested, these three combinations form the basis of colour distinction, rather than the three types of rodopsin with maximum values of spectrum sensitivity for different wave lengths, as the accepted view is. It should be noted that the suggested diffractive mechanism of tri-chromatic vision correlates well with earlier experiments carried out in [56], although the adherents of the existing theory of tri-chromatic vision do their best to avoid discussing [56] which contradicts tri-chromatic theory.

The suggested models are plagued by a number of “inconsistencies” and even contradictions. For instance, the model of [50-52] is based on the assumption that cell layers

form regular diffractive structures, although morphologically these structures are random. The model of the retina as a positive uniaxial crystal allows constructing dynamic holograms in what practically amounts to white light, but in a very narrow field of vision; at the same time it is unclear what processes happen in the peripheral sections. In the model of [53] a mistaken view that the diffractive image of an object is its Fourier angular spectrum is expressed. The same could be said of [55].

However, as we see it, these models ignore three important factors:

- Firstly, the authors of the cited works did not consider the possible scattering of light in the layers of the retina, and in some works the inverted nature of the retina was ignored altogether.
- Secondly, the models described above did not consider micro-oscillations of the eye apparatus at all, although it is necessary to keep them in mind in capturing the field as a hologram.
- Thirdly, the use of the methods of wave coherent optics and holographic approaches by default assumes the presence of the *temporal coherence of light* in the visual apparatus, and the ability of the visual apparatus to function on the basis of coherence, particularly in the case of white light.

All of this suggests that in discussing possible interferential or holographic approaches to visual perception it is necessary to consider all these peculiarities of the visual apparatus only as a whole.

#### 4.4. Temporal Coherence of Light

The central question that arises when we attempt to use the methods of coherent optics and holography in the analysis of visual perception is the question of the coherence of light. We are so used to the fact that white light is incoherent that in the case of vision, which is after all carried out in precisely this light, the question seems all but rhetorical. However, as it was correctly noted in [57], “whether light is coherent or incoherent depends only on our ability to register that light”.

Let us formulate two questions:

- What can be the value of partial temporal coherence or the length of temporal coherence of a light field in the visual apparatus?
- Can temporal coherence remain in the electrical impulse potentials in synaptic output of photoreceptor cells if the light wave falling on them is characterized by partial temporal coherence?

The answer to the first question is defined by the possible response speed of the photoreceptors, which, as noted above, is between 100 and 200 femtoseconds. As the length of one period of optical wave-length with, for example, a wave length of  $\lambda = 0,6 \mu\text{m}$  (red light) is  $T = 2 \text{ fs}$ , in 100-200 fs a photoreceptor would register only 50-100 periods of a light wave. It is obvious that such a short signal would be coherent in time. Let us remember that

the time of radiation of one wave train of an atom is about  $10^{-8}..10^{-9}$  seconds, that is, one atom wave train contains millions of periods of a light wave.

This photoreceptors' reaction speed is what defines the maximum temporal coherence  $\tau_0$  and therefore the length of spatial temporal coherence  $l_{coh}$  and the broadband of the registered optical vibration  $\Delta\lambda$ , that is:

$$l_{coh} \leq C\tau_0 = \frac{C}{\Delta\nu} = \frac{\lambda_0^2}{\Delta\lambda} \quad (14)$$

For the specified values of  $\tau_0$  the length of temporal coherence will be within ( $30 < l_o < 60$ )  $\mu m$ . It is very important to note that the parameters  $l_{coh}$  и  $\tau_0$  refer to the so-called longitudinal coherence; that is, if two light waves traveling in the same direction “diverge in time” for a period longer than  $\tau_0$ , they will not interfere, and vice versa. So, the lateral coherence can be significantly more. It is interesting that the calculated length of space coherence of light matches by the order of magnitude the length of a photoreceptor cell.

A positive answer to the second question at a first glance seems impossible. Primary optical coherence on photoreceptor input manifests in electromagnetic processes and chemical reactions at femtosecond level, and at the photoreceptors' synapse outputs electrochemical nerve impulses originate with durations and intervals expressed in milliseconds. Therefore, the time scale changes by 8-9 orders of magnitude! The millisecond impulses are the ones which then interact with each other via chemical synapses in the nervous connections in the layers of different cells of the retina.

It would be very tempting to try to explain such an enormous deceleration by the recently discovered effect of electromagnetically induced transparency (EIT) [58], which could be used to achieve an anomalously high level of dispersion in a medium, a part of which falls not in the absorption band, but in the band of optical clarity, as the speed of light in such a medium can slow down by hundreds and thousands of times. Moreover, the effect of deceleration was achieved in the film of bacteriorodopsine, which is among the molecules which serve as the primary light detectors in the retina [59]. However, as justly noted in [60], the achievement of light deceleration has nothing in common with the effect of EIT, but can be explained by nonharmonic physical mechanisms well-known in optics and trivial in any photochromic medium with a low speed of relaxation.

At the same time, if we remember that in the retina's photoreceptors *coherent* chemical reactions take place, that is, chemical, mechanic, and electromagnetic processes that are interrelated spatially and temporally, including those with wavelike properties, then it would appear that temporal coherence may exist in the output electrical potentials.

Let us assume that a light wave falls onto the photoreceptors at an angle  $\alpha$  (Figure 11). The plane wave front is shown on Figure 11 with a dotted line, whereas the arrow shows the direction of the wave's arrival. As the wave falls onto the photoreceptors at a certain angle, they stimulated with certain delays, that is, with certain phase shifts, which for a plane electromagnetic wave are calculated linearly.

The time of optic delay can be recorded as

$$\tau_{N, opt} = \frac{d(N - 1) \sin \alpha}{C}, \quad (15)$$

where  $d$  is the distance between photoreceptors,  $N$  is the number of the photoreceptor,  $\alpha$  is the angle at which the wave falls relative to the normal line, and  $C$  is the speed of light.

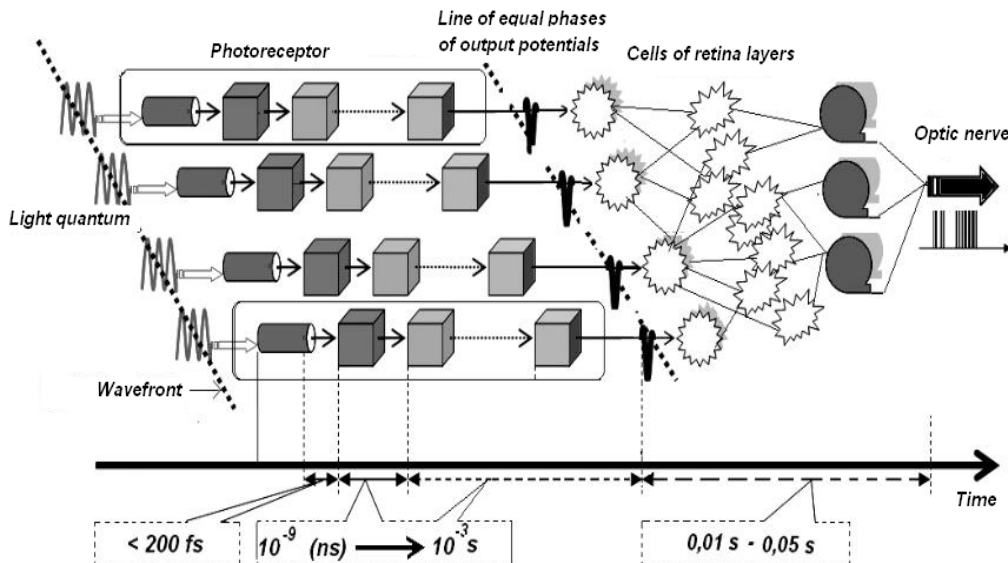


Figure 11. Retention of temporal coherence in membrane potentials of photoreceptors. The photoreceptor serves as a delay circuit with a coefficient of time transposition of  $M = 10^8-10^9$ . For the purpose of convenience, a non-inverted retina is depicted.

For example, if the wave falls at an angle of  $45^\circ$ , then the delay between adjacent photoreceptors at  $d = 5 \text{ um}$  will be about  $8 \text{ fs}$ . In this case the photoisomerization of rodopsine in the first photoreceptor will start in  $100 - 200 \text{ fs}$ , and on the adjacent photoreceptor in  $(108 - 208) \text{ fs}$ . Thereafter a sequence of various chemical reactions takes place in the photoreceptors, where each stage is characterized by increasing deceleration in the speed of product formation. As a result of such deceleration, the hyper polarization of the membrane of the first photoreceptor will take place in  $30-50 \text{ milliseconds}$ , and of the second some time later. We should also note that these times are approximately equal to the time scale of tremor and drift oscillations or their frequencies of  $10-100 \text{ GHz}$ . Despite the enormous change of time scale by 8-9 orders of magnitude, due to the coherence of all biochemical reactions the time shifts between potentials will not be *random*, but will follow a certain law, not necessarily linear as is the case in the initial plane light wave. Linear changes in delays are shown in Figure 11 for convenience of use only.

As it happens, femtosecond-long initial chemical reactions at light absorption are realized in many molecules of rodopsine in each disk. Therefore, the images of coherent shifted signals would probably look different in some ways. This, however, is all a part of the averaging of processes both inside the photoreceptor and in many adjacent ones, but this does not contradict the possibility of coherence retention in output potentials. The main thing is that temporal coherence retention in output potentials allows making a strong connection between the initial phase-amplitude field distribution in the falling light wave as an

interferential pattern to the spatio-temporal distribution of electrical output signals, and the photoreceptors' outputs can produce an “electrical” interferential pattern not unlike the initial optical one. This means the possibility of registering the full optical field in the primary visual analyzer, which can then be processed in the layers of retina nerves and then in the visual cortex.

## 5. POSSIBLE MECHANISMS FOR IMAGE RECONDTRUCTION

Preserving the spatial and temporal coherence in the output electric potentials gives an opportunity to consider the possibility of applying the existing coherent signal processing methods to reconstruct the image.

From the point of view of optical physics, this issue relates to the so-called “inverse” problems of diffraction and scattering of waves on solids situated in inhomogeneous media. In optics there are known at least three groups of techniques to reconstruct images of objects in inhomogeneous media:

- Matched filtering processing or phase conjugation of wave front;
- Nonlinear phase methods or methods of phase (correlation) speckle-interferometry;
- Methods of self-focusing in inhomogeneous media.

We should note that the method of self-focusing is hardly suitable for use in our scheme, as it requires fairly high levels of light-intensity coherent radiation.

### 5.1. Matched Filtering Processing

The method is based on the fact that the transfer characteristic of an inhomogeneous medium is accurately known (calculated or measured) for all possible positions of the light source in a three-dimensional space. If such data are available, it is possible to design a “matching” filter. Light waves passing through this filter will completely distort the balance of the wave front due to the inhomogeneous medium. Virtually synonymous with the matched filtering processing methods are the phase conjugation methods, the phase (time) inversion wave fronts, time reversal acoustics. Successful examples of using matched filtering can be found in works on astronomical adaptive optics, radio, and acoustics [61-63]. Recently, methods of adaptive optics have become widely used in ophthalmology [64, 65].

To what extent are these methods applicable in this case? On the one hand, the non-uniform layer of cells is set “morphologically” and it does not change, i.e. the condition of stability of parameters of the layer is fulfilled by default. However, certain doubts arise further on. We may record and distinguish individual images changing with the frequency of no more than 3-5 Hz. Higher speeds create twinkle effects and images do not appear. This frequency means that for several hundred milliseconds the “eye + brain” should implement matched processing with transfer functions, which are represented by a huge number of samples, about  $120 \times 10^6$ , i.e. about the number of photoreceptors. This corresponds to the speed of information processing of about 9 Gb/sec. However, it is known from

psychophysical data that the capacity of the visual channel is not more than 50 Mb/sec, i.e. almost two orders of magnitude less. Another aspect of this approach is that the question of “who calculates and stores all the measured (of course, not calculated) transfer functions?” is not considered.

But most importantly, the matched filtering processing does not offer any clues as to why the image disappears when stabilized. This leads to a serious contradiction, because the introduction of spatial oscillations (or fluctuations) significantly complicates and hinders the use of coherent processing. Indeed, compensation of the wave fronts should be carried out up to a fraction of the wavelength and amplitudes of micro oscillations are larger by orders of magnitude.

And while, of course, these comments are too simplistic, they do indicate that matched filtering processing is unlikely to be useful for our model. Although we can not completely exclude such possibility. After all, after many years of evolution nature could “remember” some of the accidents which use the principle of phase front conjugation. In particular, it may be the idea of the functioning of inverted retina as a front converter of a dynamic hologram discussed above [53, 54]. Let us note that from these models’ points of view, the ideas of ancient Greek philosophers on “visual rays emerging from the eye” do not seem that ridiculous.

## 5.2. Nonlinear Phase Methods and Speckle-Holography

Nonlinear phase methods of image reconstruction of objects via inhomogeneous media, based on the ideas of speckle-holography, do not require an *a priori* knowledge of the inhomogeneous medium’s parameters with phase precision. Moreover, at their conception they were not intended for use in image reconstruction of extended objects. They were developed for high-precision optical measurements of distance, angle of rotation, and drift of reflecting and uneven objects.

The central idea of speckle-holography or speckle-interferometry is that measurements of the parameters of object drift are made by intentionally introducing an *inhomogeneous medium (diffuser)* into an optical scheme [66, 67]. The idea, despite its paradoxical nature (after all, we are spoiling the image), is in fact crucial, and not just for optics, as it serves as the basis for a fundamentally *different* mechanism of visual perception. It can be presented as the following chain: “object – transformation of its image into a noise image – processing of noise image – image acquisition”. In speckle-interferometry, for example, such an approach allows to improve the precision of measurements by an order of magnitude in comparison to classic optical measurements. It is impossible to ignore the close connection between this approach and the ideas expressed in [26] and the results of a number of studies on the role of additive noise in the effect of stochastic resonance in visual perception [68,69].

The physical meaning of speckle-interferometry can be illustrated by the following example. Let us assume that we need to calculate the trajectory of a moving source of light (Figure 12). Let us place a diffuser between the source and the photoreceptor. At a certain point in time,  $t_1$ , we make the first exposure and in a period of time  $t_2$  a second one. Between the time between exposures  $\Delta t = t_2 - t_1$  the source will move by value  $\Delta(x,y)$ .

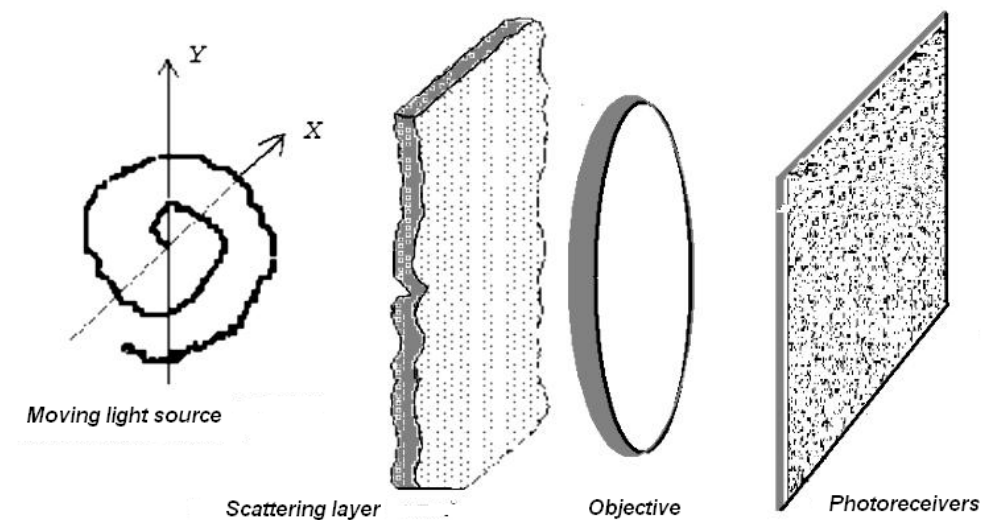


Figure 12 An optical scheme of calculating the trajectory of a point source through an inhomogeneous layer.

The inhomogeneous medium as a diffuser creates a strong scattering of light and the diffracted light waves, by interference, create a distribution of intensities on the photoreceptor in the form of a chaotic structure of spots of different sizes – speckles. Figure 13 presents two of such speckle-structures, registered with a certain time shift. Finding a difference with a naked eye is almost impossible.

As it happens, if the shift  $\Delta(x,y)$  meets certain conditions, the two speckle-structures correspond, that is they are correlated and can interfere. The result of such interference is ordinary Young bands, which can then be used to easily determine the range and direction of the shift (Figure 13). In measuring speckle-interferometry, the *scattering medium* is introduced intentionally. But the same technology can be used in observing point objects through real inhomogeneous media, for example, turbulent atmospheric slices, which can be regarded as natural diffusers.

Can the same methods be used to reconstruct images of *extended* objects viewed through inhomogeneous media? In [70-72], a few modifications of such methods of extended objects' images reconstruction when observed through an inhomogeneous medium were suggested. However, unlike in standard speckle-interferometry, where the registered value is *intensity*, image reconstruction of *extended* objects requires phase information about scattered fields. In the optical range of wave lengths such information may be acquired with the help of *interferential* recording methods. Detailed descriptions of such algorithms can be found in [71,72]; below, we will only formulate the necessary conditions in which such reconstruction is possible and explain its physical sense more fully. The conditions are as follows:

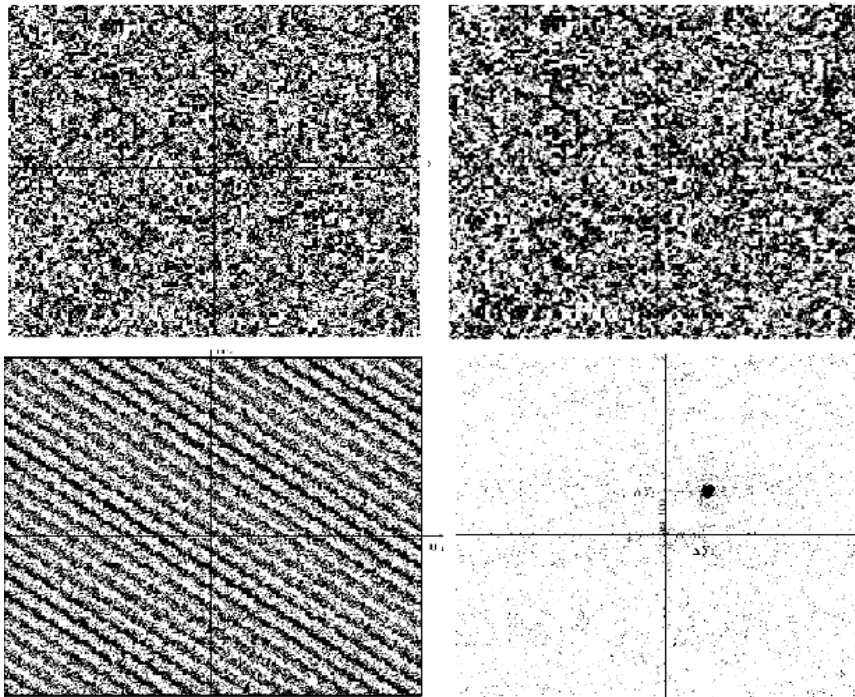


Figure 13 Two speckle structures registered at different moments in time with shifted source and the result of processing their interference pattern.

- The emitted field must be characterized by partial temporal coherence,  $\tau_c$ .
- The model of the object must be described by a system of point sources which randomly change their phases and amplitudes in time.
- Such changes may be caused both by natural physical causes and small shifts in object points or the receiving system.
- The parameters of the inhomogeneous layer must not change during each exposure.
- The time of each exposure must be less than  $\tau_c$ .

Image reconstruction can now be represented as follows. Let us assume that the crystalline lens projects an image of some object through an inhomogeneous layer.

The field of the object  $S(x, y, t)$  represented as the sum of scattered waves

$$S(x, y, t) = \sum A_i^*(x, y, t), \quad (16)$$

where  $A_i^*(x, y, t)$  are complex functions, diffracts on the phase inhomogeneities of the layer  $\Psi(x, y)$  and transforms into a random field  $P(\xi, \chi, t)$ , which can be recorded as a convolution

$$P(\xi, \chi, t) = \sum A_i^*(x, y, t) \otimes \Psi(x - \xi, y - \chi), \quad (17),$$

which describes the speckle-structure in which amplitude  $A(\xi, \chi, t)$  and phase distributions  $\psi(\xi, \chi, t)$  are random.

The light field detected by the photoreceptors can be recorded as

$$\langle |P(\xi, \chi, t)|^2 \rangle = \left\langle \sum_i A_i^*(\xi, \chi, t) \otimes \psi(x - \xi, y - \chi) \right\rangle^2 \quad (18)$$

where angle brackets denote the averaging of time. From (18) it follows that the detected field contains a multitude of combinative components. They contain all the information about phase relations in the optical field.

Although the speckle-structure appears to look like a random collection of spots, in reality its pattern is a result of a coherent combination of many waves, which form such a complicated interferential pattern. This pattern in effect constitutes a *diffusive speckle-hologram* of an object, that is, a hologram registered through a diffusive scatterer. Phase information about the light field is encoded in the angular position (inclines) and frequency of interferential bands and the amplitude in their intensity.

If we assume that the inhomogeneous cell layer of the retina is similar to an “uneven frosted glass” with a certain average diffraction index “n”, then the average difference in thickness of such a layer because of its uneven surface can be denoted by a certain value  $\delta$  and introduce a parameter of “average unevenness”:

$$\Delta G = (n - 1)\delta, \quad (19)$$

In this case the condition for choosing two speckle-structures is the following ratio:

$$\Omega = \Delta G \frac{\Delta \lambda}{\lambda_0^2} \ll 1 \quad (20)$$

It is easy to see that the second multiplier in formula (20) is a value inverse to the duration of temporal coherence.

For photoreceptors' reaction time of 100-200 fs and the parameter of unevenness of  $\Delta G = 1$  the duration of temporal coherence  $t_{coh} = 30-60 \text{ um}$ . Thus, if the maximum shifts between separate speckle structures do not exceed this value, they will remain similar or correlated. If we remember that the amplitudes of tremors are in single digits of microns, the condition (13) is fulfilled with high precision.

Let us now assume that at a certain point in time  $t_1$  we separated a single phase component from the interferential pattern as a whole

$$\Phi_1(\xi, \chi) = \arg |P_1(\xi, \chi)|^2 \quad (21)$$

and then in a time period  $t_2 = t_1 + \Delta t$  made a second measurement

$$\Phi_2(\xi, \chi) = \arg |P_2(\xi, \chi)|^2 \quad (22)$$

During this time the image shifted to a value less than  $t_{coh}$ . Now we form a diminution

$$\Delta \Phi(\xi, \chi) = \Phi_1(\xi, \chi) - \Phi_2(\xi, \chi) \quad (23)$$

and reconstruct the image by this differential hologram.

In this case the term “image reconstruction” means that we use (23) to carry out a Fourier transformation. The method for separating just the phase component and the transformation itself will be discussed a little later. Because the inhomogeneous layer introduces multiplicative noise to the spatial distribution of the signal, the operation (23) *subtracts all the constant phase shifts* acquired by the signals in passing the inhomogeneous layer.

As we use the convolution of two fields of the initial object in the reconstruction, we will not, of course, obtain its actual image. The reconstructed image will consist of separate points with random distribution and random amplitudes. The number of points will also be random. What is important, however, is that the points will be located only in the area occupied by the initial object. If we periodically repeat the calculations and average out (add) the resultant images, the pattern will be filled with new points and smoothen out; the end result will be the initial image of the object, Figure 14. Examples of images reconstructed in this way can be found in [72].

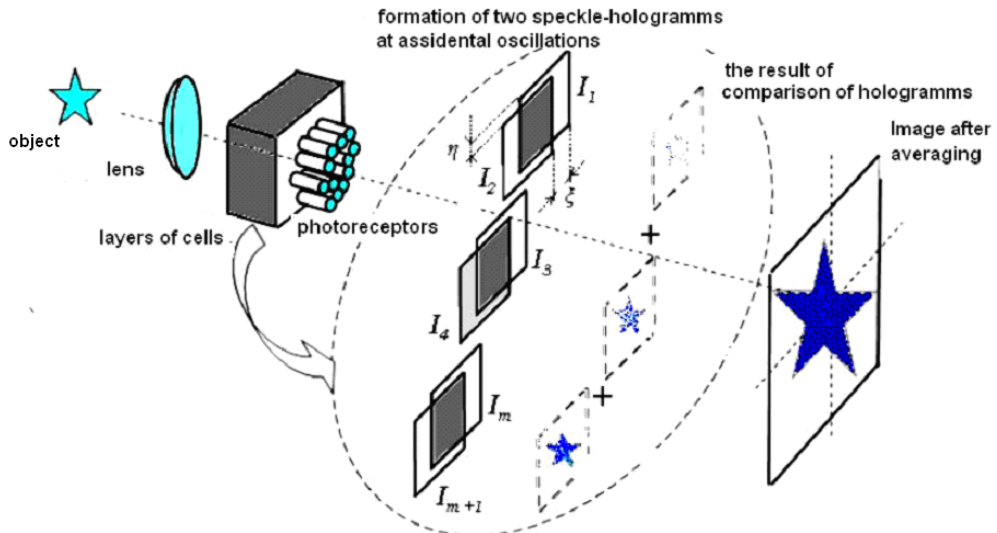


Figure 14. The principle of image reconstruction of an extended object via speckle-holograms.

The spectrum of the scattered field contains a fairly wide diapason of spatial frequencies, as the cells and their different components differ in sizes from a fraction of a light wave length to tens of wavelengths. For this reason, separating small fragments requires very small shifts, whereas large fragments require big shifts. For example, for separating an interferential structure with a spatial frequency of 100 periods/mm, shifts of less than 5 microns are required, whereas for a frequency of 5-10 period/mm the shift would have to be of about 50-200 microns. It is possible that this is the reason behind such significant differences in the shifts of oscillations of the visual apparatus. We should once again note that without such shifts it would be impossible to separate the image. Without them it looks like a noise background - “an empty field”.

Figure 15 shows the results of processing of a letter “F” projected onto an inverted retina with different values of pupil diameters and numbers of combined frames which is shown by the digits in the corner of each image.

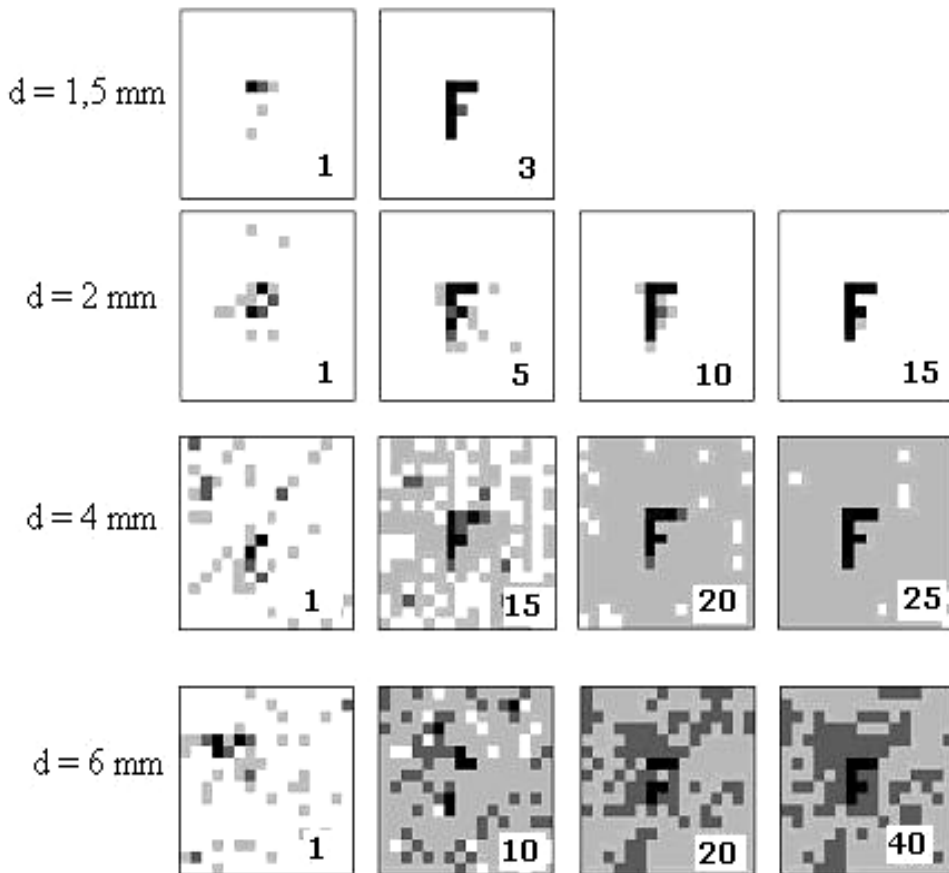


Figure 15. A reconstructed image of letter “F”.

The method of background wave generation for achieving speckle-holograms, as well as the possible types of the hologram itself, requires separate discussion. We should note that for an extended object each of its scattered waves can serve as the reference wave if its angular position is known. A background wave can also be a direct light wave not diffracted on the layer. Such a scheme of hologram registration is simply equivalent to Gabor’s hologram scheme. Finally, a reference wave can be a light wave reflected from the epithelium. Whether this wave participates in vision or, on the contrary, it is cancelled due to epithelium’s dark color to protect the retina from some excess coherent effects is an interesting question, as the cell layer is quite “thick” and the interferential pattern takes up some volume. Such a thick hologram, similar to N. Yu. Denisiuk’s hologram, would be a three-dimensional interferential filter, and can have other properties, such as the ability to distinguish color, not unlike the model of the retina as a regular diffractive grid.

How can “the visual apparatus + the brain” retrieve visual information from the speckle-holograms and perform operations like the Fourier transformation so that an image would “appear” in the initial coordinate in the visual cortex?

The described algorithm using calculations of the difference of phase distributions is not the only one possible. Another possible algorithm is a side-by-side correlative comparison of two speckle-structures in their different spatial shifts. Such a correlative algorithm would, firstly, allow to evaluate the times of group delays between electrical signals in separate photoreceptors and would therefore be able to work with broadband light waves, rather than just harmonic oscillations. Secondly, as we see it, it better corresponds to the principles by which the “*computational*” cells of the retina operate, as a correlative comparison can be carried out according to the principle of the “*concordance of signs*”, or *sign correlation*. As it is known, the sign correlator is only slightly inferior to the linear correlator in terms of noise immunity, but is much simpler in execution and is absolutely insensitive to sharp and non-stationary changes in background intensity. It, as much as the linear correlator, preserves all amplitude ratios in signals, both absolute and *relative*. We should note that mathematical descriptions of such two-level correlative circuits are very similar to descriptions of the principles of neural network functionality and the “*computational*” cells of the retina themselves.

It would also be logical to assume that the required spatial Fourier transformation or its equivalent are performed in the temporal area, as it can be expressed through the sums of temporally shifted correlative responses from many channels (cells) with pre-determined laws of addition. Such laws are simply worked-out rules of combining signals to determined addresses, while a strict link between the addresses and the object’s coordinates, as we have mentioned above, can be established by the coherence of the photoisomerization reaction. From a mathematical point of view it makes no difference whether the Fourier transformation is carried out in the initial coordinate area or in the area of its spatial frequencies. Formally, the necessary transformation can be recorded in the digital form

From (17) it follows that the time “*t*” can be changed (i.e. time delays can be introduced) and the signals can be combined after that, or the phases « $\Phi_n$ » can be changed, and signals combined afterwards. Since the signals are fairly broadband, it would be more “fair” to introduce time delays, as the phase shifts will be different for different frequencies. It would appear that in biological systems algorithms of the type “combination of signals with certain delays” are more realistic, than algorithms connected with the multiplication of initial signals by some phase functions with subsequent addition.

$$V = \sum_n^N A_n \exp(\omega_x t + \phi_n) \quad (24)$$

## CONCLUSION

A concurrent consideration of various effects in the inverted retina, namely, the direct scattering, micro-oscillations, the high speed and coherence of photochemical reactions,

offers a new mechanism of primary visual perception which is based on interference principles of image processing, and this mechanism does not contradict available experimental data.

According to this approach, it is not the identical image of an object which is projected on the retinal photoreceptors but its diffraction field of scattering in the form of an interferential structure, the formation of which is due to the partial temporal coherence of light. The coherence of photoisomerization reactions leads to the appearance of the same or similar interference structures in the form of a spatial distribution of electric potentials, but on other time scales, which is further processed in the cells of the layer and the visual cortex. The existence of oscillations in the visual apparatus, the periods of which are approximately on the same order of magnitude as the times of the electrical responses of photoreceptors, allows to propose a method of image processing based on the principles of speckle interferometry and nonlinear phase holography, i.e. on the comparison (correlation or difference) of “electrical” interference patterns. By each comparison of this sort a group of signals (correlation responses) is recorded, the coordinates of which are clearly related to the original coordinates of any areas or parts of the object. The final image of the subject can be formed in the visual cortex as a result of the addition of these signals on the given addresses and their subsequent averaging which determines the quality of the image, or rather its “recognizability”. It is obvious that such an amount of information processing through the optic nerve may be substantially less than the number of photoreceptors in the retina. In the absence of oscillations this comparison does not happen, and visual perception becomes impossible.

## REFERENCES

- [1] Helmholtz, H. L. von. (1925). *Helmholtz's Treatise on Physiological Optics*, vol. 3, translated from the third German edition but J. P. C. Southall, New York: Optical Society of America.
- [2] Cajal S. (1972). *The Structure of the Retina*, Springfield, IL, 452.
- [3] Robert, D. & Barnes, (1980). *Invertebrate Zoology* Philadelphia, PA: Saunders, 454.
- [4] Beuthan, J., Minet, O., Helfman, J. & Muller, G. (1996). The spatial variation of the refractive index in biological cells. *Physics in Medicine and Biology*, 41, 369- 382.
- [5] Carpenter, R. (1988). *Movements of the Eyes*. (2nd ed.). London: Pion. 230.
- [6] Yarbus, A. L. (1965). The role of eye movements in vision, Moscow, Nauka, 166, (in Russian).
- [7] Kandori1, H., Shichida, Y. & Yoshizawa, T. (2001). Photoisomerization in Rhodopsin, *Biochemistry*, 66, 1197-1209.
- [8] Mathies, R. A., (1995). The Phemtoseconds cis-trans Isomerization in Vision: a Classic Barrierless Photochemical Reaction, in *Ultrafast Processes in Chemistry and Photobiology*, Cambridge, Blackwell science.
- [9] El-Sayed, M. A., Tanaka, I. & Molin, Y. (1995). *Ultrafast Processes in Chemistry and Photobiology*. Blackwell Science, 306.
- [10] Dawkins, R. (1986). *The Blind Watchmaker*, New York: W. W. Norton, 96.

- [11] Goldsmith, T. (Sept. 1990). Optimization, *Constraint, and History in the Evolution of Eyes.*, The Quarterly Review of Biology, 65, 281-282.
- [12] Feynman, R., Leighton, R. & Sands, M. (1964). *The Feynman Lectures on Physics*, 3, MA: Addison-Wesley, 238.
- [13] Benson, E. (1996). Retinitis Pigmentosa: Unfolding its Mystery. *Proceedings of the National Academy of Science USA*, 93, 4526-4528.
- [14] Steinberg, R. H. & Wood, I. (1994), The Relationship of the Retinal Pigment Epithelium to the Photoreceptor Outer Segment in the *Human Retina*, chap. 2 in *The Retinal Pigment Epithelium* ed. Keith M. Zinn and Michael F. Marmor, (Cambridge; MA: Harvard University Press, 39.
- [15] Bridges, C. D. B. (1989). Distribution of Retinol Isomerase In *Vertebrate Eyes and its Emergence During Retinal Development*. Vision Research, 29, 1711-17117.
- [16] Drezek, R., Dunn, A. & Richards-Rortum, R. (1999) Light scattering from cells: finite difference time-domain simulations and goniometric measurements. *Applied Optics*, 38, 3651-3661.
- [17] Dunn, A., Smithpeter, C., Welch, A. & Richards-Rortum, R. (1997). Finite-Difference Time-Domain Simulation of Light Scattering from Single Cells. *Journal of Biomedical Optics*, 2(3), 262-266.
- [18] Sardar, D., Yow, R., Tsin. A. & Sardar, R. (September/October 2005). Optical scattering, absorption, and polarization of healthy and neovascularized human retinal tissues. *Journal of Biomedical Optics*, 10(5), 501 -512.
- [19] Yin, S., Gurder, T., Thomas, T. & Kolanda, K. (2003). Light Scatter Causes the Grayness of Detached Retina. *Arch.Ophthalmol.* 121, 1002-1008.
- [20] Hammer, H., Schweitzer, D., Thamm, E., Kolb, A. & Strobel, J. (2001). Scattering properties of the retina and the choroids determined from OCT-A-scans. *Int Ophthalmol.* 23(4-6), 291-295.
- [21] Abdallah. S. (2007). Finite-Difference Time-Domain Simulations of light scattering from Retinal Photoreceptors. University of Waterloo. Ontario, Canada, . Thesis PhD, 145.
- [22] Hoffman, K., Kreutz, W. (1976). Measurements of fast light-induced light scattering and absorption changes in outer segments of vertebrate light sensitive rod cells. *J.Biophys. Struct. Mech*, 2(1), 61-77.
- [23] William, J., Cottrell Jeremy, D., Wilson, & Thomas, H. (2007). Foster Index-of-refraction-dependent subcellular light scattering observed with organelle-specific dyes. *Journal of Biomedical Optics* 12, 35-42.
- [24] Franze, K., Grosse, J., Skatchkov, S., Schinkinger, S., Foja, C., Schild, D., Uckermann, O., Travis, K., Reichenbach, A., Guck, J. & Flechsig, P. (2007). Muller cells are living optical fibers in the vertebrate retina. *PNAS*, v.104,20, 8287-8292.
- [25] Vohnsen, B., Iglesias, I. & Artal, P. (2005). Guided light and diffraction model of human-eye photoreceptors. *J.Opt.Soc.Am. A. Opt. image sci.vis*, 22(11), 2318-2328.
- [26] Khazen, A. M. (2000). *Mind of Nature and Mind of Man*, NTTs Universitetskii, Moscow (in Russian).
- [27] Svet, V. D. (2006). About possible principles of image transformation in inverted eye retina. *Dokl.RAN, Ser.Fizika*, 409, 1, 1-5 (in Russian).

- [28] Svet, V. D., Gelfgat, V. I. (2007). About possible light scattering in the inverted eye retina. *Actual problems of modern science*, 2, Moscow, Sputnik publishing, 23-35 (in Russian).
- [29] Svet, V. D. & Khazen, A. M. (2009). About the formation of an Image in the Inverted Retina of the eye. (2009). *Biophysics*, 54,2 193-203. Pleiades Publishing, Inc.,
- [30] Born, M. & Wolf, E. (1993). Principles of optics, ed.6. Oxford: Pergamon Press,
- [31] Riggs, L. A. & Ratliff, F. (1952). The effects of counteracting the normal movements of the eye. *J.Opt. Soc. Am* 42, 872-873.
- [32] Ditchburn, R. W. & Ginsburg, B. L. (1952). Vision with a stabilized retinal image. *Nature*. 170, 36-37.
- [33] Agadjanyan G. M. (1999). Information role of tremor in the formation of vision signals. *Dokl.RAN, Ser Biology*. 3, 366-372 (in Russian).
- [34] Agadjanyan, G. M. (1999). Role of tremor and shift in a vision process, *Dokl.RAN, Ser Biology* 3b, 455-459 (in Russian).
- [35] Coppola, D. & Purves. D. (1996). The extraordinary rapid disappearance of entoptic images. *Proc Nation Acad Sci USA* 93, 8001-8004.
- [36] Martinez-Conde, S., Macknik, S. L. & H.Hubel, D. (2002) The function of bursts of spikes during the visual fixation in the awake primate lateral geniculate nucleus and primary visual cortex. *Proc Nation Acad Sci USA* 99, 13920-13925.
- [37] Martinez-Conde, S., Macknik, S. L. & Hubel, D. H. (March 2004). The role of fixation eye movements in visual perception. *Nature Reviews. Neuroscience*, 5, 229-2400.
- [38] Smitienko, O. A., Shaelaev, I. V.,Gostev, F. E.,Feldman, T. B., Nadtochenko, V. A., Sarkisov, O. M. & Ostrovsky, M. A. (2008). Coherent processes at formation of primary products of photolysis of a visual pigment rodopsine. *Dokl.RAN, Ser Biochemistry*, 421, 2. 277-281 (in Russian).
- [39] Smitienko, O. A., Shaelaev, I. V., Gostev, F. E., Feldman, T. B., Nadtochenko, V. A., Sarkisov, O. M. & Ostrovsky, M. A. (2008) Femtosecond dynamics of primary photoreaction of rodopsine in dependence on wavelength of excitation in a range 500-600nm. Proceedings of Russian Photobiology Soc., Pushino, June, 8-13, 119-124 (in Russian).
- [40] Kravkov, S. V. (1950). *Eye and its functioning. Psychophysiology of vision and hygiene of illumination*. Nauka, Moscow, 565.
- [41] Bohm, D. (1980). *Wholeness and the implicate order*. London: Routledge and Kegan Paul, 237.
- [42] Pribram, K. (1976). *Holonomy and structure in the organization of perception*. Stanford: Stanford University, 181.
- [43] Pribram, K. (1989). *Languages of the Brain*. Plenum Press, NY.
- [44] Glezer, V. D. (1985). *Vision and Thinking*, Leningrad, Nauka, 246, (in Russian).
- [45] Glezer, V. D. (1966). *Mechanisms of recognition of imaging patterns*. Leningrad,Nauka, 196, (in Russian).
- [46] Gabor, D. (1968), Holography *Nature* 217, 584.
- [47] Hubel, D. H. & Wiesel, T. N. (1965). Receptive fields and functional architecture in two non-striate visual areas (18 and 19) of the cat. *J. Neurophysiol.*28, 229-289.
- [48] Svet, V. D. (1971). *Optical signal processing*. Moscow, Energy, 146, (in Russian).
- [49] Lauinger, N. (1994). Anewinterpretation of the Stiles-Crawford effects in human vision, *J. Biol. Physics*, 19, 167-188.

- [50] Lauinger, N. (1995). The relationship between brightness, hue and saturation when the inverted human retina is interpreted as a cellular diffractive 3D chip. *SPIE Proceedings, Intelligent Robots and Computer Vision 14*. 208-232.
- [51] Lauinger, N. (1996). Inverted retina of the human eye: a trichromatic 4D space-time optical correlator *Proc. SPIE 2904, Intelligent Robots and Computer Vision XV: Algorithms, Techniques, Active Vision, and Materials Handling*. 344-360.
- [52] Titar, V. P. & Shpachenko, O. V. (2000). Holographic model of physiological optics – new approach in design of information systems. *Interdepartmental Collection on Radiotchnique, 116*, 35-39 (in Russian).
- [53] Titar, V. P., Bogdanova, T. V. & Torkatyuk, M. T. (2002) Illusions of vision: holographic interpretation models. *Optics and Spectroscopy*, 93,4, 686-694 (In Russian).
- [54] Gerald, C. & Huth, (2009). September) A New Explanation for Light Interaction with the Retina of the Eye Based on Nanostructural Geometry: Rethinking the Vision Process, [www.ghuth.com](http://www.ghuth.com).
- [55] Land, E. (1971). Lightness and retinex theory, *J. Opt. Soc. Am. 61, 1*:1-11.
- [56] Grawford, F. S. (1971). *Waves*. Berkeley Physics Course, v.3. McGraw-Hill. NY.
- [57] Harris, S. E. (1997). Electromagnetically Induced Transparency. *Physics Today*, v. 50 (7), 36 -41.
- [58] Wu, P. & Rao, D. V. G. L. N. (2005). Controllable Snail-Paced Light in Biological Bacteriorhodopsin Thin Film . *Physical Review Letters*, v. 95, 253-258.
- [59] Alexandrov, E. B. & Zapassky, V. S. (2006) In a pursuit for « slow light. *Uspekhi Physical Sciences*, 176, 10, 1093-1102 (In Russian).
- [60] Roddier, F. ssss(1999). *Adaptive optics in Astronomy*. Cambridge University press, 420,
- [61] Svet, V. D., Baykov, S. V. & Molotilov, A. M. (2003). Physical-Technical aspects of ultrasound imaging of brain structures through thick bones of the skull. Part 1. Theoretical and modeling research, *Acoustical Physics*, 3, 417-426.
- [62] Svet, V. D., Baykov, S. V. & Molotilov, A. M. (2003). Physical-Technical aspects of ultrasound imaging of brain structures through thick bones of the skull. Part 2. Experimental research, *Acoustical Physics*, 4, 613-622.
- [63] Doble, N., Yoon, G., Chen, L., Bierden, P., Oliver, S. & Williams, D. (2002). Use of a microelectromechanical mirror for adaptive optic in the human eye. *Optics Letters. Vol.27. No.17*, 156-176.
- [64] Junzhong Liang, David, R., Williams, & Donald, T. Miller, (1997). Vision and High Resolution Retinal Imaging Through Adaptive Optics, *Journal of the Optical Society of America 14*, 2884-2892.
- [65] Franson, M. (1978). *Speckle and its applications in optics*. Paris: Masson.
- [66] Jones, R. & Wykes, C. (2004) *Holographic and Speckle Interferometry*. Cambridge.
- [67] Ferri, M. & Guirao, A. (2006). Effect of optical noise on retinal image and stochastic resonance *Journal of Vision*, 6(13), 48, 48a, <http://journalofvision.org/6/13/48/>, doi:10.1167/6.13.48.
- [68] Hennig, M., Kerscher, N., Funke, K. & Worgotter. F. (2001) Stochastic resonance in visual cortical neurons: Does the eye tremor actually improve visual acuity, *Preprint submitted to Elsevier Science*, 12, October.

- [69] Svet, V. D., Kondratieva, T. V. & Zuikova, N. V. (1997). Trajectory estimation of moving target in the medium with a strong scattering. *Acoustical imaging*, 23, 555-562. Plenum Press, NY,
- [70] Svet, V. D., Kondratieva, T. V. & Zuikova, N. V. (2001). Visualization of blood flow by the method of ultrasound speckle-interferometry. *Acoustical Physics*, 47, N 5, 664-670.
- [71] Svet, V. D., Kondratieva, T. V. & Zuikova, N. V. (2002). Reconstruction of the acoustic images of dynamic objects located under a non-uniform layer. *Acoustical Physics*, 48, N 6, 779-789.

## ***Chapter 2***

# **PHOTOBIOLOGY OF INFANT SKIN**

***Georgios N. Stamatas<sup>1\*</sup>, M. Catherine Mack<sup>2</sup>  
and Katharine M. Martin<sup>2</sup>***

<sup>1</sup>Johnson & Johnson Consumer France.

<sup>2</sup>Johnson & Johnson Consumer Worldwide.

## **ABSTRACT**

The last decades have witnessed great strides in understanding the biological effects of light from the molecular all the way up to the whole organism level. Much of the boost for advancing the science of photobiology came from the dramatic increase over this period in the incidence of melanoma and other sun-related skin diseases, as well as the realization that light plays an important role in skin aging. Due to the fact that many of these conditions occur late in life, little attention has been paid to the effects of light on infant skin, with the exception of the use of violet-blue light for the treatment of jaundice in newborns. However, mounting evidence shows that a history of early sun exposure may affect the development of sun-related conditions later in life. In this chapter we summarize current knowledge about the risks of ultraviolet radiation (UVR) on infant skin, including epidemiologic evidence regarding sun exposure in this age group. Based on published results of studies performed using cell culture models, animal models, and human clinical trials, we specifically examine the effects of UVR on the biology of infant skin, as well as the known effects of blue-light phototherapy on neonatal skin. Finally, we identify areas for future research in this exciting field of science.

## **1. INTRODUCTION**

Light interacts with tissue in a plurality of ways including such phenomena as absorption, elastic and inelastic scattering, single and multi photon fluorescence, second harmonic

---

\* Corresponding author: Baby Care Science & Technology, Johnson & Johnson Consumer France, 1 rue Camille Desmoulins, 92787 – Issy les Moulineaux, France, E-mail: gstamata@its.jnj.com

generation, etc. The most probable phenomena by far are light absorption and elastic scattering.

Light absorption happens when light of a particular energy level (characterized by its wavelength) stimulates the electron clouds of specific molecules to jump to a higher energy state and then gradually fall back to baseline transforming the light energy to heat. These molecules are called chromophores and in skin the major ones are melanin and hemoglobin (both the oxygenated and the deoxygenated type). If light is delivered to the tissue at a sufficient enough intensity, the generated heat following absorption can cause damage to the molecule. Such a process can be used for beneficial purposes such as the destruction of bilirubin in jaundiced infants, but it can also be the cause of unwanted phenomena such as alterations in the DNA molecules following UVR exposure.

Elastic light scattering occurs when the direction of light propagation is changed after light interacts with molecules or agglomerations of molecules. In skin tissue major light scattering centers are keratin fibrils, organelles (including nuclei and melanocytes), cell membranes, and in the dermis collagen and elastin fibers. Whereas light absorption is the reason that skin has color, elastic scattering is the reason why skin is not transparent. Together with absorption, light scattering is an important factor of determining the penetration depth that incident light on the skin will reach before most of it will diffuse back out of the tissue. Thus they are both factors to be considered when trying to understand for example the extent of UVR-induced damage in the skin.

During the first months of life, infant skin has been known to have less constitutive pigmentation than adult skin, as well as minimal amounts of facultative pigmentation due to lack of previous exposure to the sun [1]. Moreover, recent work showing differences in papilla organization between infant and adult skin indicates differences in the vascular network at least at the capillary level. Therefore, both melanin (pigmentation) and hemoglobin (in the vasculature) concentrations and distributions differ between infant and adult, which points to differences in light absorption properties.

Light scattering properties are also expected to be different between infant and adult skin since: a) infant stratum corneum (SC) appears to be better hydrated than adult [2], b) the structure of the epidermis is different (SC and supra-papillary epidermis are thicker in adult) [3], and c) the structure of the dermal extracellular matrix are different (e.g. collagen fibers are thicker in adult skin [4]).

Taking all the above into account it is reasonable to conclude that since the optical properties between infant and adult skin are not the same, the intensity and extent of the effects following light-tissue interactions may also differ. For example, the relatively low amounts of melanin and SC scattering due to hydration in infants compared to adults suggest that infant skin may be unusually vulnerable to penetration and damage by incident UVR.

It is widely accepted that both cumulative and intermittent exposure to solar UVR are linked to a variety of deleterious outcomes such as sunburn, premature aging, and decreased immune functions. Compelling evidence has linked sun exposure in early childhood to skin cancer later in life as well [5-9]. At the same time, various environmental and cultural trends in the past few decades appear to have significantly increased exposure to UVR for children and adolescents in many parts of the world [5, 10-12]. While the projected risk of developing melanoma later in life was 1 in 1500 for newborns in 1935, recent estimates have elevated this risk to 1 in 33 for infants born [13]. Rates of all forms of skin cancer have been increasing worldwide, with an estimated 1,000,000 new cases of non-melanoma skin cancer

and 60,000 new melanomas diagnosed in the U.S. alone in 2008 [14, 15]. Rates of nonmelanoma skin cancer in younger people appear to be rising as well, particularly among young women, although further studies are required to confirm [16].

These alarming trends and statistics have fueled considerable efforts over the past few decades to investigate the biologic effects of light. They have also transformed concerns about overexposure to solar radiation, particularly early in life, into major public health efforts promoting comprehensive sun protection for infants and children. These groups are particularly vulnerable considering the relatively lower levels of protective melanin and higher surface area-to-weight ratio compared to adults.

Despite these suspicions, very few existing studies have targeted the specific effects of light, including ultraviolet light, on infant skin. This lack of attention may be due, at least in part, to the fact that many of UVR-induced effects are not seen until adulthood. Most current knowledge of the UVR-induced effects on infant skin has been derived from extrapolating studies on adult skin and reflects a limited understanding of the way infant skin develops. In fact, until recently, the bulk of research about any form of light on infant skin has involved the blue-light phototherapy used to treat neonatal jaundice.

We begin this chapter by reviewing the risks involved with UVR exposure and examine the published literature on the effects of UVR on infant skin involving cell culture models, animal models, and human clinical trials. We then examine the better studied blue-light phototherapy and propose some ideas for future research in infant skin photobiology.

## **2. RISKS ASSOCIATED WITH EXPOSURE OF SKIN TO UVR EARLY IN LIFE**

This section reviews studies concerning risks of UVR exposure during infancy and childhood, as well as epidemiologic evidence showing alarmingly high rates of sun exposure and sunburn at these ages in many parts of the world. Overexposure to either UVA (320-400 nm) or UVB (290-320 nm) radiation at any age can seriously damage human skin. UVB radiation can cause acute inflammation, including sunburn, and has been strongly linked to the development of both basal and squamous cell carcinoma [17]. Once considered innocuous, UVA is now believed to accelerate the aging process as well as promote UVB-induced cancers by suppressing processes of the cutaneous immunity [14, 18]. Importantly, evidence from case control and other epidemiologic studies has highlighted the particularly serious, long-term consequences of overexposure in infancy and childhood. This evidence includes studies linking intense exposure to UVR and sunburn during childhood to increased risks of developing cutaneous malignant melanoma (CMM) [15, 19-21] and basal cell carcinoma (BCC) [22, 23] later in life, as well as studies linking exposure to UVR over longer periods of time to the development of squamous cell carcinoma (SCC) [17, 24]. Sunlight, in fact, remains the only environmental factor definitively linked to both melanocytic nevi and cutaneous melanoma [25-28].

Concerns about long-term health effects of early sun exposure have prompted public health organizations worldwide to issue comprehensive sun protection recommendations to screen or block UVR exposure with particular emphasis on infants and children. Recommended practices include sun avoidance as a first-line strategy for infants less than six

months of age, as well as wearing hats, tightly woven clothing, and sunglasses when sun avoidance is not an option. Children and infants above six months of age are also advised to use topical sunscreen products of SPF 30 or higher, regardless of skin type [29-33].

## 2.1. Cutaneous Melanocytic Melanoma

Although malignant melanoma accounts for only 4% of all skin cancers worldwide, it is associated with approximately 75% of skin cancer-related deaths [34]. While cutaneous melanoma is rare in infants and children, prognosis and response to this malignancy in the pediatric population resembles those seen in adults [35, 36]. In addition, excessive sun exposure and/or a history of blistering sunburns in early childhood is an established risk factor for developing malignant melanoma later in life [37-39]. Fair skin, blue eyes, and red or blond hair are additional risk factors, as is a history of immunosuppression, a family or personal history of melanoma, xeroderma pigmentosum or atypical (“dysplastic”) nevi. An estimated 50-65% of all malignant melanoma arises in pre-existing nevi [40].

The exact relationship between childhood sun exposure and the lifetime risk of developing CMM remains controversial. Intermittent, or recreational, sun exposure, during childhood has been hypothesized to be the major cause of CMM, and numerous case-control studies with adults have shown an association between the number and severity of childhood sunburns and the risk of developing this skin cancer [1, 15, 35-38, 41, 42]. In a study on women, blistering sunburns at 15 to 20 years of age were significantly associated with increased risk of developing CMM (relative risk, 2.2 for >5 sunburns vs. none) [39]. However, the time-course involved, the need for retrospective analysis, and variant measures of childhood sun exposure across studies make it difficult to determine the exact relationship between childhood sun exposure and melanoma [23, 26, 43].

Ecological studies assessing ambient sun exposure appear to be more accurate and consistent than case-control studies in determining effects of exposure to sunlight during specific age periods. A systematic review of the literature using computerized bibliographic databases and article reference lists found that such studies consistently reported lower risks of melanoma among people who resided in low UVR environments in childhood than in those who resided at high UVR environments [44]. These findings are consistent with earlier studies on migrants to Israel and Australia suggesting that intense sun exposure in early childhood may be more important in increasing the risk of cutaneous melanoma in adulthood than cumulative years of sun exposure [45, 46]. Suggestions have also been made that melanocytes in early life may be more sensitive to the sun, resulting in changes in DNA that may lead to the formation of unstable and pre-malignant moles [30]. However, adult exposure to sun also appears to play a role in increasing the risk of melanoma, and whether early childhood is a critical period in which melanocytes are particularly susceptible to the biological effects of sunlight remains a subject of controversy [47, 48].

What is clear is that avoiding harmful UVR exposure in youth appears to reduce melanoma risk more than similar avoidance in adulthood [49]. This may be related to the fact that child and adolescent behavior patterns may intensify UVR exposure and blistering sunburns. Infants also have not experienced the gradual exposure to UVR that stimulates facultative pigmentation and thus may be more susceptible to the damaging effects of

excessive exposure to sunlight [1]. Several recent epidemiologic studies have suggested an association between early-life UVR exposure and specific somatic mutations at specific body sites. Intensive, intermittent UVR exposure is frequently linked to melanomas on the trunk, for example, whereas chronic UVR exposure seems more frequently linked to melanomas on the head [42, 43, 50]. Childhood exposure to UVR has also been linked to specific types of genetic damage. One population-based case study associated high exposure to ambient UVR at ages 0-20 years with *BRAF* mutations and a mean age of melanoma diagnosis of 47.3, and high UVR exposure at ages 50-60 years with *NRAS* mutations and a mean age of diagnosis of 62.1 years [51]. While these studies reflect broad population trends and require additional confirmation, they suggest significant differences between the response of infant and adult skin to UVR.

## 2.2. Melanocytic Nevi

Melanocytic nevi (MN), common skin neoplasms thought to be due to slightly altered melanocytes, can be either congenital or acquired. Most acquired MN appear after infancy, with numbers and size increasing throughout early childhood and peaking in young adulthood. MN in infants and children are primarily of concern because a small percentage of them may eventually transform into cutaneous melanoma. Strong epidemiologic evidence links the total number of benign MN on the body to the development of cutaneous melanoma [52-55] and some nevi appear to be precursor lesions to melanomas [56]. Thus, acquired MN should be closely monitored for atypical features suggestive of malignant changes.

Very few studies to date have looked at the development of nevi in the first few years of life, although there is strong evidence that risk is closely related to cumulative exposure to UVR and that density of nevi is correlated with total sun exposure [26, 29, 57-60]. A study in Queensland, Australia, where one finds the highest rate of melanoma in the world as well as the highest numbers of melanocytic nevi among children, associated both acute and chronic sun exposure in children to the development of these nevi [25]. Another study of Australian preschoolers also found that the number of lifetime sunburns and the severity of sunburns were significantly related to the presence of large acquired MN [61].

Accumulating evidence suggests that mild to moderate sun exposure, even without sunburn, is sufficient to induce MN in children, particularly in those with light skin color, blond or red hair, and blue eyes and/or whose parents had large numbers of moles. A recent cluster prevalence study in Queensland, Australia involving toddlers (ages 1-3), for example, associated the many MN that developed at a very young age with heavy sun exposure and with freckling, as well as with Caucasian ethnicity. Conversely, toddlers who were protected from the sun, whether through dark skin color, tanning ability, or the frequent application of sunscreen, showed relatively low nevi counts, and those who wore hats had lower nevi counts on the face but not on other body sites [62]. Consistent with these findings was a study of German nursery school children showing that moderate sun exposure without sunburns, such as outdoor activities during a German summer, induced nevus development. This same study found a strong association between nevus development in children and the number of moles in their parents, as well as a direct relationship between the cumulative duration of sun exposure and the risk of developing MN [63]. While all of these findings stem from studies of

toddlers rather than infants specifically, they suggest that in very young children sun exposure, even without burning, may be sufficient to increase risk of MN and, ultimately, cutaneous melanoma and that exposure to UVR below the threshold of sunburn may substantially damage DNA and precipitate malignant transformation in keratinocytes and melanocytes [58].

Sunburns on the other hand, do seem to increase the risk of large MN. Estimating the erythemally effective dose of solar UVR from questionnaire data combined with local UVR biometry, a study of preschool children in Townsville, Australia found that lifetime number of sunburns and the severity of sunburns were significantly related to the presence of large acquired MN during follow-up. The same study found that total number of hours of sun exposure and tendency to burn were independent risk factors for MN [61]. In addition, a small study recently suggested that nevi acquired on sun-exposed skin during childhood and adolescence are genetically distinct from congenital nevi. This study analyzed the mutation spectrum of congenital nevi to see if it differed from that of the MN that develop on sun-exposed skin during childhood and adolescence, which are known to harbor *BRAF* mutations more frequently than *NRAS* mutations. The congenital nevi, though indistinguishable histopathologically, showed no *BRAF* mutations, but 81% (26/32) had mutations in *NRAS* [64].

### **2.3. Nonmelanoma Skin Cancer**

Of the 1 million skin cancers diagnosed annually in the United States, approximately 75-80% are basal cell carcinomas (BCC) and 15-20% are squamous cell carcinomas (SCC) [11, 12]. BCC is a malignant neoplasm originating at the basal layer of the epidermis. While it rarely metastasizes, untreated BCC can invade local tissue and eventually lead to extensive functional and cosmetic damage. Cutaneous SCC develops in the epidermis, usually from precursor lesions called solar or actinic keratosis. Some forms of SCC are superficially invasive and can be easily treated before causing disfiguring tissue loss, while more aggressive types carry significant risk of metastasis and life-threatening complications.

BCC rarely occurs in children unless they have an underlying genetic condition [65], but intensive UVR exposure in childhood and adolescence can underlie development of BCC later in life [66]. One population-based case-control study showed a significantly increased risk of BCC in men who had relatively high levels of recreational sunlight exposure in adolescence and childhood (ages 0 to 19 years), with the relationship most pronounced among sun-sensitive subjects whose skin tended to burn rather than tan. This study found no association between cumulative sun exposure and BCC, consistent with results from a population-based, case-control study in Western Australia suggesting that a particular amount of sun exposure delivered in infrequent, intense increments increases BCC risk more than similar doses of UVR delivered more continuously over the same period of time [8, 67].

In contrast, the bulk of evidence suggests that cumulative exposure to UVR over a lifetime is a significant risk factor for SCC, regardless of age or pattern of exposure [68]. While SCC rarely develops in children without a predisposing condition such as xeroderma pigmentosum, human papilloma virus infection, or immunosuppression [40], chronic

exposures to sunlight in the first decades of life is associated with the development of SCC in adulthood [66].

Exposure to UVR in infancy and early childhood can also promote the development of solar keratoses, suggesting, by implication, that reducing exposure to sunlight in childhood may substantially reduce long-term risk of developing SCC [69]. In a study comparing Australian-born adults to Australian adults who had migrated from Great Britain at various ages (both groups of Caucasian ancestry), the proportion of persons with solar keratoses in the group who arrived as adults never reached the proportion found in Australian natives. The randomization of the 588 subjects enrolled in the study was stratified according to sex and self-rated skin type (burn only and never tan, burn first and then tan, or tan only and never burn). Younger persons in the group of immigrants who arrived in Australia between the ages of 1 and 20 years also had a lower proportion of solar keratoses than native-born Australian adults, while their older peers had the same or even higher proportion [70]. Regular sunscreen use has also been shown to prevent solar keratoses and by implication reduce the risk of developing SCC [57].

### 3. EFFECTS OF UVR ON THE BIOLOGY OF INFANT SKIN

Thus far we examined the risks associated with exposure to UVR early in life. We will now turn our attention to the possible mechanisms that could be responsible for the existence of such risks.

The effects of exposure to solar UVR on adult skin are well recognized and include erythema, hyper-pigmentation, local immunosuppression, and long-term risks of photoaging and skin cancer [71-75]. UVR has the ability to alter the skin microenvironment and has long been associated with suppression of the skin immune system (SIS) and an altered balance between epidermal proliferation and differentiation [76, 77]. In addition, it is widely recognized that exposure to UVB directly damages DNA and potentially facilitates the development of skin cancer [78-80]. However, until recently attempts to elucidate and quantify these effects in infants and children have been undermined by a number of technical limitations, namely a lack of *in vivo* methods appropriate for use in very young subjects [8, 67, 81-83]. As a result, the bulk of the current understanding of UVR effects on the biology of infant skin comes from studies using either animal models or cell cultures. However, the advent of several new non-invasive measurement techniques in the past few years has allowed for some illuminating insights from human clinical trials investigating the response of infant skin to UVR.

#### 3.1. Cell and Tissue Culture Models

##### 3.1.1. DNA repair response and cutaneous immunity

Early studies of cultured human epidermal keratinocytes showed no significant age-related differences in the rate and extent of repair or normal replication of DNA after either intense or chronic, low-level UVR exposure [84, 85]. However, considerable evidence suggests that early sun exposure may predispose cells to impaired DNA repair capacity later

in life. In a recent study, for example, cultured human keratinocytes derived from newborn, young adult, and older adult donors were exposed to a single physiologic dose of solar-simulated radiation (SSR). Effects of the exposure were analyzed on genes previously associated with UVR modulation in newborn keratinocytes, cytokines implicated in UVR immunomodulatory effects, and a recently cloned gene (*SPR2*) known to be induced during keratinocyte differentiation and by lethal UVC (100-290 nm) irradiation. Although age had relatively little effect on the response to UVR, the combination of aging and SSR exposure (“photoaging”) markedly increased the inducibility of the oncogene c-fos and decreased the baseline expression of *SPR2* and IL-1ra relative to cells from sun-protected skin of the same donors. These findings may help explain the predisposition to photocarcinogenesis in photoaged, as opposed to infant and otherwise unexposed, skin [86]. A subsequent study of DNA repair capacity of skin fibroblasts suggests that this age-related reduction in DNA repair synthesis following UVR exposure may be due to decreased expression of genes involved in nucleotide excision repair (NER) [87].

Growing evidence from proteomic studies also suggests that unique features of the skin immune system may alter the effect of UVR on infant skin. The concept of the SIS reflects current understanding of the skin’s ability to protect against penetration by external agents not just by physical means but also through cellular immunologic mechanisms. The SIS response can involve either an active immune response or an induced tolerance, both of which vary with the preexisting cellular microenvironment. Cutaneous immune reactions include responses by dendritic antigen-presenting cells such as Langerhans cells (LC), monocytes/macrophages, mast cells, lymphatic/vascular endothelial cells, and T lymphocytes, as well as humoral components such as cytokines, neuropeptides, prostaglandins, and free radicals [88]. LC are a type of immune-system-activating dendritic cells in the skin, thought to help alert the system to the presence of foreign pathogens and other foreign materials (although some evidence suggests that they may actually dampen the skin reaction to infection and inflammation) [89]. Normally neonates have a relatively small number and density of LC, and these cells have relatively short dendrites and few receptor molecules critical for immune response. LC density, distribution, morphology, and cell marker expression gradually change over time [88, 90-92].

Recent findings from proteomic studies comparing neonatal and adult murine tissue have identified numerous proteins uniquely expressed in neonatal skin that may influence the development of the skin immune system and, by implication, the impact of UVR on infant skin. These proteins include Stefin A, which appears to decrease with age and may play a role in promoting cellular proliferation in neonatal skin as well as abnormal proliferative conditions [88]. Similarly, the peroxiredoxins, which play a protective role against oxidative damage, appear to be expressed at greater levels in neonatal skin. Recent findings that peroxiredoxin-2 may be involved in inhibiting T lymphocytes and dendritic cells suggest that this protein may also be an important regulatory factor in the developing SIS [88, 93]. Such differences between the developing and the developed SIS may point in the future to differences in UVR-induced immune-modulation between infant and adult skin.

### **3.1.2. UVB-Induced vitamin D production**

Accumulating *in vitro* evidence supports the concept that UVB-induced Vitamin D production within the skin may help modulate the development of the infant SIS [88]. UVB converts 7-dehydrocholesterol in the skin to previtamin D3, which is rapidly transformed into

vitamin D3 and then hydroxylated in the liver, kidney, and other tissues, including the keratinocytes, into its biologically active form, the hormone calcitriol (1,25(OH)2D3) [94-99]. Critically important in the maintenance of healthy bones as well as in cell growth, calcitriol has well-known anti-proliferative and pro-differentiating effects and has long been known to influence the differentiation, maturation, and survival of dendritic cells. It also appears to affect the cutaneous immune response by acting directly on cells that express the vitamin D receptor such as keratinocytes, LCs,  $\gamma\delta$  T cells, mast cells, dermal dendritic cells, and macrophages [100, 101] and by indirectly altering the production of immunomodulatory cytokines and growth factors by keratinocytes [88].

Evidence from cell and tissue culture studies suggests that calcitriol may play a role in dampening the neonatal immune response by acting directly on cells within the SIS that express vitamin D receptor, as well as suppressing production of immunomodulatory cytokines and growth factors by keratinocytes [88, 100, 101]. Adding calcitriol to highly enriched LC populations from adult mice inhibits stimulation of allogeneic T cells [102, 103] and alters production of inflammatory cytokines and chemokines, stimulating production of IL-1 $\beta$ , CCL3, CCL4 and CCL5 as well as Th1-type chemokines (CXCL9, CXCL10, and CXCL11) and inhibiting production of Th2-type chemokines (CL17 and CCL22) [104]. In addition, calcitriol inhibits the maturation of LC, possibly by inhibiting the alloantigen-stimulation of naïve T cells [105].

At the same time, other *in vitro* studies suggest that calcitriol may also help protect keratinocytes from UVR-induced apoptosis, although the way these effects manifest themselves in neonatal skin specifically has not yet been explored. Consistent with findings from animal studies, calcitriol and related compounds have been shown to reduce and help repair UVB-induced cyclobutane pyrimidine dimers in cultures of irradiated human skin cells, thereby contributing to the prevention of mutations and apoptosis [106].

## 3.2. Animal Models

### 3.2.1. Modulation of the skin immune system

Numerous studies using murine models have confirmed that intense sun exposure early in life is one of many external agents that can alter the SIS. Current understanding of the UVR impact on the SIS has been built upon the pioneering studies establishing that the primary molecular event in generating the systemic immunosuppression by UVR in skin of mice is the formation of pyrimidine dimers [80]. This work demonstrated that alterations to the skin environment by either UVR or chemical carcinogens set off cellular events that ultimately suppress T cell generation that might otherwise inhibit the development of antigenic tumors [107]. These findings are consistent with retrospective, epidemiologic data showing that immunologic events in infancy can have profound effects in adulthood, and particularly those studies linking intense, intermittent exposure of skin to UVR in early childhood to CMM later in life.

SIS development and its response to UVR are little understood in humans. However, numerous studies using animal models suggest that UVR can profoundly change the neonatal immune system, including suppressing both innate and adaptive immune responses and predisposing cells to subsequent carcinogenic changes. Various studies of transgenic mice

indicate that both single high-dose and chronic exposure to SSR in early life may compromise the development of the SIS, potentially increasing the risk of developing UVR-related cancers [71, 88, 108, 109].

Although the long-term implications of neonatal exposure to UVR remain unclear, both repeated and chronic doses of SSR have been shown to reduce the number of LC in the epidermis and increase the number of dendritic cells in lymph nodes that drain irradiated skin sites [109]. Subsequent work, however, has suggested that although single, high-dose UVB exposure in neonatal mice alters the development of neonatal LC to produce a short-term reduction in their number, it enhances immune response at maturity. In one study the reduction in LC density among neonatal mice exposed to high doses (2 kJ/m<sup>2</sup>) of UVB radiation was substantially greater than in equivalently exposed older mice, although at lower doses there were no differences in susceptibility. However, at maturity, the mice irradiated as neonates showed an increased ability to respond to topically applied antigen: they transported more antigen to the lymph nodes, and their lymph node dendritic cells showed an enhanced ability to stimulate T-cell proliferation, with the response skewed towards a Th2 type response [71]. Elucidating the precise characteristics of the skin in neonatal mice that underlie this apparent sensitivity to UVR will require additional investigation.

### **3.2.2. Implications for carcinogenesis**

It has been suggested that the lack of an acute inflammatory response in neonatal mice (e.g. lack of neutrophil tissue infiltration, vascular dilatation, increased vascular permeability, and release of inflammatory mediators) may promote tolerance and limit immune development in neonatal skin, potentially increasing susceptibility of neonatal mice to carcinogenic changes [72, 73, 88]. An alternative hypothesis is that neonatal mice may be particularly susceptible to the UVR-induced melanoma due to retention of UVR-related damage by their abundant immature melanocytes [72].

Various studies suggest that melanoma antigens generated during the neonatal period are likely to generate long-lived, antigen-specific regulatory T cells that may eventually undermine effective anti-tumor immunity. Exposing the skin of neonatal mice to UVR, even with a single high dose, appears to alter the microenvironment. Mildly erythema doses of UVR in the neonatal period have been shown to alter the immune environment to favor antigen-specific immune suppression and skin tumor development, including a gradual increase in the number of regulatory T cells and B cells in the local lymph nodes that becomes significant by adulthood [71, 88]. Together with the immunosuppression linked to intense UVB exposure and the propensity of neonatal skin to develop tolerance, these changes may increase the risk of developing skin cancer, particularly melanoma later in life [88].

Although the induction of melanoma is a multi-factorial process, work by Noonan et al. using UV-irradiated HGF/SF transgenic models have provided specific experimental support for neonatal melanoma susceptibility, as well as direct evidence that neonatal UVB is responsible for inducing cutaneous melanoma [108]. Studies using a genetically engineered mouse model have shown that single high-dose exposures to UVB, but not UVA, can cause a tumor reminiscent of human melanoma in neonatal animals, but not in adults [74, 108]. In addition, several studies using transgenic mouse models have shown that a single dose of UVR is sufficient to induce melanoma in neonatal mice carrying specific mutations (*Ras* or *HGF/SF*) [75, 110-115]. Consistent with these findings are studies of young, transgenic mice

showing that UVB can promote the induction of cutaneous melanoma, as well as serve as a cofactor promoting the growth of melanoma induced by chemical agents [115].

A recent study also suggests that neonatal melanocytes exposed to UVR are unusually sensitive to UVR-induced proliferation and transformation [116]. Known to inhibit apoptosis, increase melanin production, and enhance DNA repair, the activation of melanocytes is a well-recognized protective response to sun exposure in mammals, including humans. Dendritic processes transport melanosomes from the melanocyte cell body to the dendritic tips and then to keratinocytes [117]. Melanocytes in neonatal mice, in contrast to those from older mice, migrate to the epidermal basal layer following a single dose of UVR, apparently relocating from the outer root sheath of the hair follicle, with numbers peaking 3-5 days after exposure [116, 118-120]. Moreover, in melanoma-prone mice with melanocyte-specific over-expression of *HrasG12V*, these basal layer melanocytes were larger and had more dendritic processes than those of UVR-treated wild-type mice. As the proliferation of melanocytes in response to sun damage may play a role in increasing the risk of malignant melanoma [121-123], these findings support the concept of an unusual degree of sensitivity to UVR in neonatal mouse melanocytes and may help explain the efficacy of UVR to induce melanoma in mice carrying oncogenic mutations.

### **3.2.3. UVB-induced vitamin D production**

Numerous studies using animal models suggest that UVR-induced vitamin D may serve as an immune modulator and that the direct action of calcitriol (the active form of vitamin D in the body) on the production of immunomodulatory molecules by keratinocytes may be distinctive in early life. On the one hand, topical application of a vitamin D analog to human [102] and of calcitriol to mouse skin [103] has been shown to cause significant immunosuppression to a contact sensitizer, presumably due to reduced LC function. At the same time, other studies suggest that calcitriol and related compounds may reduce UVB-induced cyclobutane pyrimidine dimers within keratinocytes [124]. They may also help promote efficient repair of UVB-induced cyclobutane pyrimidine dimers by inducing the formation of metallothionein, an antioxidant found in human skin after UVB exposure and believed necessary to prevent keratinocyte apoptosis [125, 126]. It remains unclear whether the higher levels of calcitriol produced in response to UVR by children skin [127] specifically modulate the function of dendritic cells or repair UVB-induced DNA damage associated with increased skin cancer risk. Still, preliminary data suggest that adding vitamin D<sub>3</sub> to the diet may reduce UVB-induced DNA damage in female, but not male, mice during the neonatal period [88].

## **3.3. Human Studies**

### **3.3.1. Developing barrier properties**

Recent studies confirming and elucidating differences between the barrier properties of infant and adult skin [128-133] have contributed to the notion that newborn skin may be particularly vulnerable to UVR. These findings build on existing knowledge that infant skin has a significantly thinner SC than adult, as well as relatively limited melanin production, and lack of prior facultative pigmentation and suggest that these differences continue far longer

than previous believed. Consisting of layers of flattened non-nucleated keratinized cells, the SC regulates trans-epidermal water loss (TEWL), which has been used extensively as an indicator of barrier function [128-130, 134, 135]. The natural barrier protection from the aqueous intra-uterine environment provided to the fetus by the *vernix caseosa* is wiped away at birth, leaving protection from external agents in the terrestrial environment to the SC. The contribution of the SC to the protection against UVR can be considered from the point of limiting UVR penetration due to its light scattering properties as well as absorption of UVR by SC molecules such as urocanic acid [136].

There is not a lot of information about how this physical and immunologic barrier protection develops after the first month of life. In contrast to the relatively steady state of adult skin, neonatal skin has been shown repeatedly to adjust its thickness, pH, and hydration to various environmental conditions during the first month of life [132, 137-141]. However, recent *in vivo* studies using non-invasive methodologies suggest that the skin maturation process in human continues far longer than the neonatal period [2, 3], potentially leaving the skin particularly vulnerable to the effects of UVR throughout infancy and even into toddlerhood. Ultrastructural and morphometrical evaluations of normal dermal connective tissue have established that dermal constituents such as collagen, elastin fibers, and mesenchymal cells change substantially during the perinatal period, underlying corresponding changes in the extracellular matrix during this time period as well [142]. A recent study of babies ages 3-24 months and their mothers using non-invasive microscopy tools showed significant differences in morphologic features of the SC, including glyph density and dermal papillae size, density, and distribution, as well as the ratio between visible surface papillae and glyphs [3]. The SC and total epidermis were significantly thinner in the infants. In addition, granular cells were significantly smaller and denser, and corneocytes significantly smaller, on the upper inner arms, outer forearms, and legs of the infants, indicating faster turnover rate and greater surface area for increased absorption. Also suggestive of a relatively thinner and vulnerable SC in infants are reports of *in vivo* Fourier-transform infrared spectroscopy and diffuse reflectance spectroscopy documenting significantly fewer total lipids and sebaceous lipids in infant skin, as well as relatively lower concentrations of melanin (authors' unpublished data).

These findings are consistent with new evidence suggesting that infant skin continues to develop far longer than the first month of life. One recent prospective, cohort study, for example, showed no difference in either initial skin appearance or biophysical measurements (TEWL and surface hydration) between infants who went on to develop atopic dermatitis and those who remained lesion-free, suggesting that barrier impairment found in atopic dermatitis, rather than being inherent, may be secondary to dermatitic skin changes long after the neonatal period [143]. Infants aged 8-24 months have also been shown to have significantly higher skin capacitance and pH values on both the skin of the ventral forearm and buttocks than adults [141].

Both barrier function and water handling properties of the SC also appear to continue to develop well beyond the first month of life and at least as long as the first year. These properties are influenced by a complex interplay of factors, including the presence of natural moisturizing factor (NMF), corneocyte maturity/hydrophilicity, lipid quantity and phase, density of appendages, surface microrelief, and diffusion path length [2]. Earlier evidence based primarily on TEWL measurements suggested that the SC barrier is fully functional at birth [128, 129, 132, 139, 144]. However, the conclusion that term infants are born with a

functionally mature SC, as well as the wide variations in the measured TEWL values of these earlier studies, may reflect differences in environmental acclimation times, number and age range of subjects, body site studied, or the type of measurement instruments used – particularly the use of open chamber instruments, which tend to report TEWL values in the skin of term infants lower than or equal to those reported from adults [128, 129, 144]. Our more recent work including *in vivo* Raman confocal microspectroscopy in infants gives consistently higher values for skin water concentration and water absorption-desorption rates in the SC of infants versus adults [2]. Applied for the first time on infant skin, this technique allows the acquisition of Raman spectra as a function of skin depth with a lateral resolution of 1 µm (x and y directions) and a depth resolution of 5 µm (z direction). These data can then be analyzed for water content, and water concentration profiles, calculated as a function of skin depth. Findings from this study are in agreement with some published reports from term infants [130, 145] and support the notion that although the SC may appear to be intact shortly after birth, it develops adult-like water handling properties and associated protective barrier properties only after the first year of life.

Additional studies have suggested that both water content and water concentration in the skin remain relatively high throughout at least the first year of life. Previous studies have suggested that SC hydration is low at birth and increases with postnatal age [130, 132, 133, 137, 141], with duration of the SC hydration increase ranging from two weeks postpartum [132] to 30–90 days postpartum [133]. Measurements of skin conductance and water distribution obtained using *in vivo* Raman confocal microspectroscopy indicates that this process may continue throughout the first year and that infant SC is significantly more hydrated than adult SC throughout this period [2]. In this study, infants aged 3–33 months had more water throughout most parts of the SC on the lower ventral surfaces of their arms than did adults. The epidermis of infants aged 3–12 months had a steeper water gradient and higher water concentration than that of adults within the top 20 µm. Infant skin also had a significantly lower concentration of NMF in the first 12 µm. These lower relative NMF concentrations may themselves impair barrier function and increase water desorption, since NMF plays a key role in maintaining skin hydration by absorbing and retaining water.

The signs of functional immaturity throughout the first year of life suggest increased vulnerability of infant skin to external influences, potentially including UVR. Such differences between adult and infant skin in SC water content influence skin surface morphology, the desquamation process, and epidermal expression of keratins and other proteins and thus may compromise barrier integrity [146–151]. The specific effects of this increased water content on skin optics and UVR penetration remain to be determined. In addition, the fact that dermal scatter of light is known to be greater in dry than in well-hydrated SC suggests that the increased water content found in infant skin may allow relatively more UVR to penetrate it.

### **3.3.2. Melanogenesis: developing skin response to UVR**

Preliminary *in vivo* studies using non-invasive methods suggest that skin response to solar UVR in infants may differ from that in older children and adults. A recent longitudinal study that we performed suggested that infant skin exposed to solar UVR in the first summer of life developed persistent changes in skin pigmentation [152]. In this study we compared skin changes between groups of healthy Caucasian infants and their mothers using diffuse

reflectance spectroscopy to measure changes in the apparent concentrations of skin chromophores (melanin, oxy-hemoglobin, and deoxy-hemoglobin). All groups experienced increases in apparent concentration of melanin on exposed skin sites (dorsal forearm) over the summer months, but only in the youngest group of infants (i.e. those experiencing their first summer) did these levels remain significantly elevated over the winter months. While pigmentation normally increases in the first years of life [138, 153-155] and itself plays a role in sun protection, persistent increases over the first summer raise concerns, especially given the association between rapid melanogenesis and UVR-induced DNA damage [156].

Although these findings require confirmation, they suggest that incidental UVR exposure before the physical and immunologic barrier reaches maturity, may lead to irreversible changes in the skin not seen in older children and adults.

### **3.3.3. UVB exposure and vitamin D requirements**

Mounting evidence suggests that many adults and children around the world are vitamin D deficient [157-172]. Coupled with extensive evidence linking vitamin D deficiency to a broad spectrum of diseases, including various cancers, these findings have raised concerns about recent efforts to limit UVR exposure in infants and children. Over 12% of the 380 healthy infants and toddlers recently examined in an urban primary care clinic were found to have vitamin D deficiency ( $\leq 20$  ng/mL) and 40% had levels below an accepted optimal threshold ( $\leq 30$  ng/mL) regardless of age or degree of skin pigmentation [173]. Some dermatologists have also expressed concerns that sun protective measures may restrict vitamin D<sub>3</sub> production in the skin, which is normally the body's primary source of the vitamin. As a result, there is still considerable debate among dermatologists, about the relative risks and benefits of sun exposure, oral vitamin D supplementation, and the precise amount of sunlight exposure required to balance its risks and benefits [174-176].

Complicating efforts to resolve this debate are the many factors influencing vitamin D synthesis in the skin, particularly the amount of skin pigmentation but also body mass, amount of exposed skin and unprotected skin, season, latitude, and air pollution levels [177-180]. In addition, recent evidence suggests variable responsiveness to UVB radiation among individuals, as well as low vitamin D status among some individuals despite abundant sun exposure [181]. Nonetheless, the vast majority of dermatologists and pediatricians today believe that existing evidence still supports the comprehensive sun protection measures advocated by the American Academy of Pediatrics (AAP), including sun avoidance for infants under 6 months of age and sun protection measures such as protective clothing and sunscreen when sun avoidance is impossible, together with a minimum daily vitamin D intake of 400 IU for all infants and children beginning soon after birth [30, 97].

## **4. BLUE LIGHT PHOTOTHERAPY FOR JAUNDICE**

In contrast to UVR, the effects of exposure to blue light on infant skin have been extensively investigated, largely due to the widespread use of phototherapy to treat neonatal jaundice. An estimated 60% of normal newborns develop jaundice, a yellow discoloration of the skin and sclera, within the first week of life. This condition is due to excessive conjugated bilirubin (hyperbilirubinemia) that results from excessive bilirubin formation, coupled with

the inability of the neonatal liver to clear it rapidly enough from the blood. In most infants jaundice is a normal and transient development that resolves without medical treatment, but in some infants extremely high levels of unconjugated bilirubin if left untreated can lead to bilirubin encephalopathy and subsequent kernicterus, a chronic form of bilirubin encephalopathy that can result in permanent, debilitating neurodevelopmental handicaps or even death. Consequently, newborns are routinely monitored for jaundice and treated with phototherapy when total serum levels of bilirubin exceed those specified by AAP guidelines [30]. Such treatment is designed to lower the concentration of circulating bilirubin and to keep it from increasing. The AAP also recommends prophylactic phototherapy for infants with low birth weight or early gestational age [182].

During phototherapy, absorbed light energy transformed to heat changes the shape and structure of bilirubin so that it will be excreted even without conjugation. Following phototherapy treatment the skin no longer looks jaundiced. Dermal and subcutaneous bilirubin absorb the light, inducing several different photochemical reactions that rapidly generate yellow stereoisomers of bilirubin as well as various lower molecular weight, colorless derivatives. These photoisomers have also been found in the blood of adults after sunbathing [183, 184]. Several efforts have been made to measure and characterize the photoisomers generated by intensive phototherapy, but further work must be done to elucidate their precise contributions of their specific photochemical pathway to eliminating bilirubin [183, 185, 186].

Bilirubin absorbs light most strongly in the blue region of the spectrum, and the generation rate of bilirubin photoproducts depends highly on light intensity and wavelength. In addition, tissue penetration increases greatly with increasing wavelength. As a result, the most effective wavelengths of light for treating neonatal jaundice appear to fall into the 460-490 nm range. UVR exposure is not generally a concern, since the phototherapy light sources used today do not emit significant amounts of erythemal UVR [183].

Although numerous clinical trials earlier in the 20<sup>th</sup> century established the efficacy of phototherapy in treating neonatal jaundice, ethical considerations preclude conducting any placebo-controlled trials to test the efficacy of the relatively high light doses used today, which in intensive therapy deliver irradiance of  $\geq 30 \mu\text{W}/\text{cm}^2/\text{nm}$  in the blue spectrum delivered to the maximum surface area [183]. There is considerably more evidence, however, about adverse effects of intensive phototherapy on infant skin. While reports of clinically significant toxicity are rare, the skin, serum, and urine of infants with cholestasis sometimes develop a dark, grayish-brown discoloration, a phenomenon known as “bronze baby syndrome” [187, 188]. This discoloration is thought to be due to the formation of a photo-oxidation product of bilirubin or to copper-bound porphyrins [189, 190], with possible contribution of biliverdin pigments [191] and disappears without significant sequelae once phototherapy concludes.

Phototherapy-induced erythematous and vesiculo-bullous eruptions have also been seen in newborns who were exposed to methylene blue prenatally or who are receiving agents such as furosemide or fluorescein dye for radiologic procedures [192-194]. More rarely, infants with severe cholestatic jaundice develop distinctive cutaneous complications. Several researchers, for example, have reported purpuric and bullous eruptions in neonates receiving phototherapy for hyperbilirubinemia, possibly from sensitization by accumulating porphyrins [195-197]. In fact, congenital porphyria should be considered in any infant who develops severe blistering during phototherapy. In addition, phototherapy is contraindicated for infants with congenital

porphyria or a family history of porphyria, as well as in any infant receiving photosensitizing drugs. This may include infants treated with tin-mesoporphyrin, a drug currently being used experimentally to prevent and treat hyperbilirubinemia, some of whom have shown to develop erythematous rashes when exposed to sunlight or daylight fluorescent bulbs [183, 198].

A few studies have suggested that by acutely changing the infant's thermal environment, phototherapy can increase peripheral blood flow and thus produce insensible water loss. In one study, TEWL and skin hydration were measured in seven body areas before and during phototherapy in 31 preterm infants (25-36 weeks gestation) and found a mean increase of 26.4% in TEWL during phototherapy, particularly in the cubital fossa (45.9%), groin (35.4%), and back (29%). However, this study showed no significant differences in SC hydration in six of the seven body areas, either before or during phototherapy [199, 200]. The implications of these findings for fluid replacement in infants undergoing phototherapy and their relevance to phototherapy with relative low-heat light emitting diode sources remain to be determined [183].

Finally, there is still some controversy regarding the role that blue-light phototherapy may play in increasing the risk of developing atypical nevi in childhood, widely considered to be an important risk factors for melanoma later in life. In 2002-3 Csozma *et al* studied 747 schoolchildren (14-18 years of age), nearly half of whom had received phototherapy to treat neonatal jaundice, to determine the prevalence of both common and atypical MN. They focused their study on adolescents because this is the age at which dysplastic nevi often develop. Although prevalence of common MN was similar in treated and untreated children, those who had received neonatal phototherapy were more likely to have multiple (>100) moles. In addition, neonatal blue-light phototherapy was associated with a significantly higher percentage of atypical nevi [201]. These results were consistent with a case-control prospective study that found significantly more large (2-5 mm diameter) nevi in children who had received intensive neonatal phototherapy than in a control group who had not [202]. These findings contrast with those of Bauer *et al.*, who had earlier reported no association between neonatal treatment with a blue-light lamp and an increased risk of developing MN in younger children (ages 2 to 7 years) [203]. However, in a recent multicenter study with 828 nine-year-old children, over 22% of whom had received neonatal phototherapy, no evidence was found for a major role of blue-light phototherapy on subsequent nevus count regardless of the location or size of the nevi or the phototype of the child. In contrast, nevus count correlated with a light phototype, skin and hair color, blue/green eyes, and history of sunburn [204]. Some of the apparent contradictions between these studies may be related to the ages of children studied, since common MN generally first appear in early childhood, while dysplastic nevi tend to develop around puberty [201].

## 5. CONCLUSION AND AREAS FOR FUTURE RESEARCH

Substantial epidemiologic evidence, coupled with accumulating experimental data from cell culture, animal models, and human studies, suggests that infant skin has a distinctive response to light, particularly UVR, and that this distinct response may make it particularly vulnerable to long-term photodamage. However, substantial gaps remain in the understanding

of these effects from both epidemiologic and biologic perspectives. Even our considerable knowledge of the effects of intense blue light on infant skin being treated for jaundice leaves open fundamental questions at the molecular level that await answers from studies involving infant skin cell culture and animal models.

Future experimental research will be needed to identify and quantify changes in the epidermal microenvironment and SIS during the neonatal period, as well as specifically explore the molecular events associated with the development of CMM. There is a critical need for more non-invasive studies focusing on explaining the specific optical properties of infant skin and differentiating them from those in toddlers, older children, adolescents, and adults. We also not only need to better understand the factors influencing vitamin D synthesis in the skin but will require substantially more investigation to clarify whether the higher levels of calcitriol produced in response to UVR by infant skin specifically modulate the function of dendritic cells or repair UVB-induced DNA damage associated with skin cancer risk. In addition, future efforts should be made to refine current understanding of UVB-related immunosuppression in human infants, elucidate the time course of pigmentation in sun-exposed areas, and assess the efficacy of sun protection practices in preventing some of these changes. Furthermore, substantial work remains to be done to better define the relationship between UVR and melanogenesis in early life. Particularly important will be to elucidate the precise mechanism underlying the heightened sensitivity to UVR of neonatal mouse melanocytes, as well as efforts to establish what proportion of the differences in melanogenesis observed in human infants during the first year of life are due to sun exposure as opposed to natural developmental changes.

Future studies addressing the biologic effects of UVR on infant skin will almost certainly build on efforts already underway with transgenic mouse models to identify gene loci regulating tumor suppression, apoptosis, and cell senescence. Additional work will be needed, however, to determine factors that might predispose neonatal cells to neoplastic determination, including a lack of complete differentiation, increased numbers of melanocytes in the dermis and at the dermal/epidermal junction, and/or differences in melanocytic growth factors. In addition, efforts to extend these findings to humans will be critical, as will be efforts to determine the precise initiating events in the development of melanoma in both nevus-prone individuals and in those exposed to burning doses of UVB during early life. At the same time, future efforts should be made to determine: a) the innate characteristics of neonatal melanocytes that appear to make them particularly sensitive to UVR-induced proliferation and transformation, b) which keratinocyte to melanocyte signaling pathways might be involved in inducing migration after exposure to UVR, and c) whether there might be a specific developmental window in which these effects are most pronounced. Such efforts will be key to providing potential targets for early disease diagnosis and intervention in the development of photocarcinogenesis and other UVR-related damage traceable to exposure in the first years of life.

## ABBREVIATIONS

American Academy of Pediatrics (AAP), basal cell carcinoma (BCC), cutaneous malignant melanoma (CMM), deoxyribonucleic acid (DNA), Langerhans cells (LC),

melanocytic nevi (MN), natural moisturizing factor (NMF), skin immune system (SIS), solar simulated radiation (SSR), squamous cell carcinoma (SCC), stratum corneum (SC), trans-epidermal water loss (TEWL), ultraviolet radiation (UVR)

## REFERENCES

- [1] Mancini, AJ; Lawley, L. Structure and Function of Newborn Skin. In: LFF; Eichenfield, J; Ilona, Esterly, B; Nancy, editor. *Neonatal Dermatology*. 2nd ed. Philadelphia: Saunders Elsevier; 2008.
- [2] Nikolovski, J; Stamatias, GN; Kolliaas, N; Wiegand, BC. Barrier function and water-holding and transport properties of infant stratum corneum are different from adult and continue to develop through the first year of life. *J Invest Dermatol*, 2008, 128(7), 1728-36.
- [3] Stamatias, G; Nikolovski, J; Luedtke, M; Kolliaas, N; Wiegand, B. Infant Skin Microstructure Assessed *In Vivo Differs from Adult Skin in Organization and at the Cellular Level.*, *Pediatr Dermatol* 2009 Oct 4 [Epub ahead of print].
- [4] Vitellaro-Zuccarello, L; Cappelletti, S; Dal Pozzo Rossi, V; Sari-Gorla, M. Stereological analysis of collagen and elastic fibers in the normal human dermis: variability with age, sex, and body region. *Anat Rec*, 1994, 238(2), 153-162.
- [5] Geller, AC; Colditz, G; Oliveria, S; Emmons, K; Jorgensen, C; Aweh, GN; et al. Use of sunscreen, sunburning rates, and tanning bed use among more than 10 000 US children and adolescents. *Pediatrics*, 2002, 109(6), 1009-14.
- [6] Dadlani, C; Orlow, SJ. Planning for a brighter future: a review of sun protection and barriers to behavioral change in children and adolescents. *Dermatol Online J*, 2008, 14(9), 1.
- [7] Harrison, SL; Saunders, V; Nowak, M. Baseline survey of sun-protection knowledge, practices and policy in early childhood settings in Queensland, Australia. *Health Educ Res*, 2007, 22(2), 261-71.
- [8] Thieden, E; Philipsen, PA; Sandby-Moller, J; Wulf, HC. Sunscreen use related to UV exposure, age, sex, and occupation based on personal dosimeter readings and sun-exposure behavior diaries. *Arch Dermatol*, 2005, 141(8), 967-73.
- [9] Boldeman, C; Dal, H; Wester, U. Swedish pre-school children's UVR exposure-a comparison between two outdoor environments. *Photodermatol Photoimmunol Photomed*, 2004, 20(1), 2-8.
- [10] Cokkinides, V; Weinstock, M; Glanz, K; Albano, J; Ward, E; Thun, M. Trends in sunburns, sun protection practices, and attitudes toward sun exposure protection and tanning among US adolescents, 1998-2004. *Pediatrics*, 2006, 118(3), 853-64.
- [11] Robinson, JK; Rademaker, AW; Sylvester, JA; Cook, B. Summer sun exposure: knowledge, attitudes, and behaviors of Midwest adolescents. *Prev Med*, 1997, 26(3), 364-72.
- [12] Davis, KJ; Cokkinides, VE; Weinstock, MA; O'Connell, MC; Wingo, PA. Summer sunburn and sun exposure among US youths ages 11 to 18: national prevalence and associated factors. *Pediatrics*, 2002, 110(1 Pt 1), 27-35.

- [13] Rigel, DS. Cutaneous ultraviolet exposure and its relationship to the development of skin cancer. *J Am Acad Dermatol*, 2008, 58(5 Suppl 2), S129-32.
- [14] Hebert, AA. Photoprotection in children. *Adv Dermatol*, 1993, 8, 309-24; discussion 325.
- [15] Elwood, JM; Jopson, J. Melanoma and sun exposure: an overview of published studies. *Int J Cancer*, 1997, 73(2), 198-203.
- [16] Purdue, MP; Freeman, LE; Anderson, WF; Tucker, MA. Recent trends in incidence of cutaneous melanoma among US Caucasian young adults. *J Invest Dermatol*, 2008, 128(12), 2905-8.
- [17] Stern, RS; Weinstein, MC; Baker, SG. Risk reduction for nonmelanoma skin cancer with childhood sunscreen use. *Arch Dermatol*, 1986, 122(5), 537-45.
- [18] Cole, C. Sunscreen protection in the ultraviolet A region: how to measure the effectiveness. *Photodermat Photoimmunol Photomed*, 2001, 17(1), 2-10.
- [19] Westerdahl, J; Olsson, H; Ingvar, C. At what age do sunburn episodes play a crucial role for the development of malignant melanoma. *Eur J Cancer*, 1994, 30A(11), 1647-54.
- [20] Whiteman, D; Green, A. Melanoma and sunburn. *Cancer Causes Control*, 1994, 5(6), 564-72.
- [21] Wentzell, JM. Sunscreens: the ounce of prevention. *Am Fam Physician*, 1996, 53(5), 1713-33.
- [22] Gallagher, RP; Hill, GB; Bajdik, CD; Coldman, AJ; Fincham, S; McLean, DI; et al. Sunlight exposure, pigmentation factors, and risk of nonmelanocytic skin cancer. I. Basal cell carcinoma. *Arch Dermatol*, 1995, 131(2), 157-63.
- [23] Kricker, A; Armstrong, BK; English, DR; Heenan, PJ. Does intermittent sun exposure cause basal cell carcinoma? a case-control study in Western Australia. *Int J Cancer*, 1995, 60(4), 489-94.
- [24] Balk, SJ; O'Connor, KG; Saraiya, M. Counseling parents and children on sun protection: a national survey of pediatricians. *Pediatrics*, 2004, 114(4), 1056-64.
- [25] Harrison, SL; MacLennan, R; Speare, R; Wronski, I. Sun exposure and melanocytic naevi in young Australian children. *Lancet*, 1994, 344(8936), 1529-32.
- [26] Armstrong, BK; Kricker, A. How much melanoma is caused by sun exposure? *Melanoma Res*, 1993, 3(6), 395-401.
- [27] Green, A; Siskind, V; Hansen, ME; Hanson, L; Leech, P. Melanocytic nevi in schoolchildren in Queensland. *J Am Acad Dermatol*, 1989, 20(6), 1054-60.
- [28] Luther, H; Altmeyer, P; Garbe, C; Ellwanger, U; Jahn, S; Hoffmann, K; et al. Increase of melanocytic nevus counts in children during 5 years of follow-up and analysis of associated factors. *Arch Dermatol*, 1996, 132(12), 1473-8.
- [29] Glanz, K; Saraiya, M; Wechsler, H. Guidelines for school programs to prevent skin cancer. *MMWR Recomm Rep*, 2002, 51(RR-4), 1-18.
- [30] AAP Committee on Environmental Health. Ultraviolet light: a hazard to children. American Academy of Pediatrics. Committee on Environmental Health. *Pediatrics*, 1999, 104(2 Pt 1), 328-33.
- [31] Australasian College of Dermatologists. A-Z of skin: baby and toddler protection. 2001. Available from: [http://www.dermcoll.asn.au/public/a-z\\_of\\_skin-baby\\_toddler\\_protection.asp](http://www.dermcoll.asn.au/public/a-z_of_skin-baby_toddler_protection.asp).

- [32] Cancer Council of Australia. Sun protection and infants (0-12 months). 2005. Available from: <http://www.cancer.org.au//File/PolicyPublications/PSsunprotectioninfantsMAY05.pdf>.
- [33] World Health Organization. Sunshine and Health: How to Enjoy the Sun Safely., 2006. Available from: <http://www.who.int/uv/publications/solaruvflyer2006.pdf>.
- [34] Jemal, A; Siegel, R; Ward, E; Hao, Y; Xu, J; Murray, T; et al. Cancer statistics, 2008. *CA Cancer J Clin*, 2008, 58(2), 71-96.
- [35] Osterlind, A; Tucker, MA; Stone, BJ; Jensen, OM. The Danish case-control study of cutaneous malignant melanoma. II. Importance of UV-light exposure. *Int J Cancer*, 1988, 42(3), 319-24.
- [36] Holman, CD; Armstrong, BK; Heenan, PJ. Relationship of cutaneous malignant melanoma to individual sunlight-exposure habits. *J Natl Cancer Inst*, 1986, 76(3), 403-14.
- [37] Green, A; MacLennan, R; Siskind, V. Common acquired naevi and the risk of malignant melanoma. *Int J Cancer*, 1985, 35(3), 297-300.
- [38] MacKie, RM; Aitchison, T. Severe sunburn and subsequent risk of primary cutaneous malignant melanoma in scotland. *Br J Cancer*, 1982, 46(6), 955-60.
- [39] Weinstock, MA; Colditz, GA; Willett, WC; Stampfer, MJ; Bronstein, BR; Mihm, MC, Jr.; et al. Nonfamilial cutaneous melanoma incidence in women associated with sun exposure before 20 years of age. *Pediatrics*, 1989, 84(2), 199-204.
- [40] Paller, AS; Mancini, AJ. Hurwitz Clinical Pediatric Dermatology. 3rd ed: Elsevier Saunders, 2006.
- [41] Green, A; Siskind, V; Bain, C; Alexander, J. Sunburn and malignant melanoma. *Br J Cancer*, 1985, 51(3), 393-7.
- [42] Whiteman, DC; Watt, P; Purdie, DM; Hughes, MC; Hayward, NK; Green, AC. Melanocytic nevi, solar keratoses, and divergent pathways to cutaneous melanoma. *J Natl Cancer Inst*, 2003, 95(11), 806-12.
- [43] Whiteman, DC; Stickley, M; Watt, P; Hughes, MC; Davis, MB; Green, AC. Anatomic site, sun exposure, and risk of cutaneous melanoma. *J Clin Oncol*, 2006, 24(19), 3172-7.
- [44] Whiteman, DC; Whiteman, CA; Green, AC. Childhood sun exposure as a risk factor for melanoma: a systematic review of epidemiologic studies. *Cancer Causes Control*, 2001, 12(1), 69-82.
- [45] Steinitz, R; Parkin, DM; Young, JL; Bieber, CA; Katz, L. Cancer incidence in Jewish migrants to Israel, 1961-1981. *IARC Sci Publ*, 1989, (98), 1-311.
- [46] Khlat, M; Vail, A; Parkin, M; Green, A. Mortality from melanoma in migrants to Australia: variation by age at arrival and duration of stay. *Am J Epidemiol*, 1992, 135(10), 1103-13.
- [47] Pfahlberg, A; Kolmel, KF; Gefeller, O. Timing of excessive ultraviolet radiation and melanoma: epidemiology does not support the existence of a critical period of high susceptibility to solar ultraviolet radiation- induced melanoma. *Br J Dermatol*, 2001, 144(3), 471-5.
- [48] Holland, R; Harvey, I. Adult vs childhood susceptibility to melanoma: is there a difference? *Arch Dermatol*, 2002, 138(9), 1234-5.

- [49] Autier, P; Dore, JF. Influence of sun exposures during childhood and during adulthood on melanoma risk. EPIMEL and EORTC Melanoma Cooperative Group. European Organisation for Research and Treatment of Cancer. *Int J Cancer*, 1998, 77(4), 533-7.
- [50] Whiteman, DC; Parsons, PG; Green, AC. p53 expression and risk factors for cutaneous melanoma: a case-control study. *Int J Cancer*, 1998, 77(6), 843-8.
- [51] Thomas, NE; Edmiston, SN; Alexander, A; Millikan, RC; Groben, PA; Hao, H; et al. Number of nevi and early-life ambient UV exposure are associated with BRAF-mutant melanoma. *Cancer Epidemiol Biomarkers Prev*, 2007, 16(5), 991-7.
- [52] Swerdlow, AJ; English, J; MacKie, RM; O'Doherty, CJ; Hunter, JA; Clark, J; et al. Benign melanocytic naevi as a risk factor for malignant melanoma. *Br Med J (Clin Res Ed)*, 1986, 292(6535), 1555-9.
- [53] Holly, EA; Kelly, JW; Shpall, SN; Chiu, SH. Number of melanocytic nevi as a major risk factor for malignant melanoma. *J Am Acad Dermatol*, 1987, 17(3), 459-68.
- [54] Grob, JJ; Gouvernet, J; Aymar, D; Mostaque, A; Romano, MH; Collet, AM; et al. Count of benign melanocytic nevi as a major indicator of risk for nonfamilial nodular and superficial spreading melanoma. *Cancer*, 1990, 66(2), 387-95.
- [55] Garbe, C; Buttner, P; Weiss, J; Soyer, HP; Stocker, U; Kruger, S; et al. Risk factors for developing cutaneous melanoma and criteria for identifying persons at risk: multicenter case-control study of the Central Malignant Melanoma Registry of the German Dermatological Society. *J Invest Dermatol*, 1994, 102(5), 695-9.
- [56] Crowson, AN; Magro, CM; Sanchez-Carpintero, I; Mihm, MC, Jr. The precursors of malignant melanoma. *Recent Results Cancer Res*, 2002, 160, 75-84.
- [57] Thompson, SC; Jolley, D; Marks, R. Reduction of solar keratoses by regular sunscreen use. *N Engl J Med*, 1993, 329(16), 1147-51.
- [58] Gilchrest, BA; Eller, MS; Geller, AC; Yaar, M. The pathogenesis of melanoma induced by ultraviolet radiation. *N Engl J Med*, 1999, 340(17), 1341-8.
- [59] Ortonne, JP. Photoprotective properties of skin melanin. *Br J Dermatol*, 2002, 146 Suppl 61, 7-10.
- [60] Yamaguchi, Y; Beer, J; Hearing, V. Human skin responses to UV radiation: pigment in the upper epidermis protects against DNA damage in the lower epidermis and facilitates apoptosis. *FASEB Journal*, 2006, 20(9), 1486-1488.
- [61] Harrison, SL; MacLennan, R; Buettner, PG. Sun exposure and the incidence of melanocytic nevi in young Australian children. *Cancer Epidemiol Biomarkers Prev*, 2008, 17(9), 2318-24.
- [62] Whiteman, DC; Brown, RM; Purdie, DM; Hughes, MC. Melanocytic nevi in very young children: the role of phenotype, sun exposure, and sun protection. *J Am Acad Dermatol*, 2005, 52(1), 40-7.
- [63] Wiecker, TS; Luther, H; Buettner, P; Bauer, J; Garbe, C. Moderate sun exposure and nevus counts in parents are associated with development of melanocytic nevi in childhood: a risk factor study in 1,812 kindergarten children. *Cancer*, 2003, 97(3), 628-38.
- [64] Bauer, J; Curtin, JA; Pinkel, D; Bastian, BC. Congenital melanocytic nevi frequently harbor NRAS mutations but no BRAF mutations. *J Invest Dermatol*, 2007, 127(1), 179-82.
- [65] Branstrom, R; Kristjansson, S; Dal, H; Rodvall, Y. Sun exposure and sunburn among Swedish toddlers. *Eur J Cancer*, 2006, 42(10), 1441-7.

- [66] Leiter, U; Garbe, C. Epidemiology of melanoma and nonmelanoma skin cancer--the role of sunlight. *Adv Exp Med Biol*, 2008, 624, 89-103.
- [67] Stanton, WR; Saleheen, HN; O'Riordan, D; Roy, CR. Environmental conditions and variation in levels of sun exposure among children in child care. *Int J Behav Med*, 2003, 10(4), 285-98.
- [68] Armstrong, BK; Kricker, A. The epidemiology of UV induced skin cancer. *J Photochem Photobiol B*, 2001, 63(1-3), 8-18.
- [69] Marks, R. Epidemiology of non-melanoma skin cancer and solar keratoses in Australia: a tale of self-immolation in Elysian fields. *Australas J Dermatol*, 1997, 38, Suppl 1, S26-9.
- [70] Marks, R; Jolley, D; Lectsas, S; Foley, P. The role of childhood exposure to sunlight in the development of solar keratoses and non-melanocytic skin cancer. *Med J Aust*, 1990, 152(2), 62-6.
- [71] McGee, H; Scott, DK; Woods, GM. Neonatal exposure to UV-B radiation leads to a large reduction in Langerhans cell density, but by maturity, there is an enhanced ability of dendritic cells to stimulate T cells. *Immunol Cell Biol*, 2006, 84(3), 259-66.
- [72] Wolnicka-Glubisz, A; Noonan, FP. Neonatal susceptibility to UV induced cutaneous malignant melanoma in a mouse model. *Photochem Photobiol Sci*, 2006, 5(2), 254-60.
- [73] Clydesdale, GJ; Dandie, GW; Muller, HK. Ultraviolet light induced injury: immunological and inflammatory effects. *Immunol Cell Biol*, 2001, 79(6), 547-68.
- [74] De Fabo, EC; Noonan, FP; Fears, T; Merlino, G. Ultraviolet B but not ultraviolet A radiation initiates melanoma. *Cancer Res*, 2004, 64(18), 6372-6.
- [75] Recio, JA; Noonan, FP; Takayama, H; Anver, MR; Duray, P; Rush, WL; et al. Ink4a/arf deficiency promotes ultraviolet radiation-induced melanomagenesis. *Cancer Res*, 2002, 62(22), 6724-30.
- [76] Norval, M. The mechanisms and consequences of ultraviolet-induced immunosuppression. *Prog Biophys Mol Biol*, 2006, 92(1), 108-18.
- [77] Sleijffers, A; Garssen, J; Vos, JG; Loveren, H. Ultraviolet light and resistance to infectious diseases. *J Immunotoxicol*, 2004, 1(1), 3-14.
- [78] Garssen, J; Vandebriel, RJ; van Loveren, H. Molecular aspects of UVB-induced immunosuppression. *Arch Toxicol Suppl*, 1997, 19, 97-109.
- [79] Muller, HK; Bucana, C; Kripke, ML. Antigen presentation in the skin: modulation by u.v. radiation and chemical carcinogens. *Semin Immunol*, 1992, 4(4), 205-15.
- [80] Kripke, ML; Cox, PA; Alas, LG; Yarosh, DB. Pyrimidine dimers in DNA initiate systemic immunosuppression in UV-irradiated mice. *Proc Natl Acad Sci., U S A*, 1992, 89(16), 7516-20.
- [81] Godar, DE. UV doses of American children and adolescents. *Photochem Photobiol*, 2001, 74(6), 787-93.
- [82] Stanton, WR; Chakma, B; O'Riordan, DL; Eyeson-Annan, M. Sun exposure and primary prevention of skin cancer for infants and young children during autumn/winter. *Aust NZ J Public Health*, 2000, 24(2), 178-84.
- [83] Moise, AF; Gies, HP; Harrison, SL. Estimation of the annual solar UVR exposure dose of infants and small children in tropical Queensland, Australia. *Photochem Photobiol*, 1999, 69(4), 457-63.
- [84] Liu, SC; Parsons, CS; Hanawalt, PC. DNA repair response in human epidermal keratinocytes from donors of different age. *J Invest Dermatol*, 1982, 79(5), 330-5.

- [85] Liu, SC; Parsons, S; Hanawalt, PC. DNA repair in cultured keratinocytes. *J Invest Dermatol*, 1983, 81(1 Suppl), 179s-83s.
- [86] Garmyn, M; Yaar, M; Boileau, N; Backendorf, C; Gilchrest, BA. Effect of aging and habitual sun exposure on the genetic response of cultured human keratinocytes to solar-simulated irradiation. *J Invest Dermatol*, 1992, 99(6), 743-8.
- [87] Takahashi, Y; Moriwaki, S; Sugiyama, Y; Endo, Y; Yamazaki, K; Mori, T; et al. Decreased gene expression responsible for post-ultraviolet DNA repair synthesis in aging: a possible mechanism of age-related reduction in DNA repair capacity. *J Invest Dermatol*, 2005, 124(2), 435-42.
- [88] Muller, HK; Malley, RC; McGee, HM; Scott, DK; Wozniak, T; Woods, GM. Effect of UV radiation on the neonatal skin immune system- implications for melanoma. *Photochem Photobiol*, 2008, 84(1), 47-54.
- [89] Kaplan, DH; Jenison, MC; Saeland, S; Shlomchik, WD; Shlomchik, MJ. Epidermal langerhans cell-deficient mice develop enhanced contact hypersensitivity. *Immunity*, 2005, 23(6), 611-20.
- [90] Dewar, AL; Doherty, KV; Woods, GM; Lyons, AB; Muller, HK. Acquisition of immune function during the development of the Langerhans cell network in neonatal mice. *Immunology*, 2001, 103(1), 61-9.
- [91] Simpson, CC; Woods, GM; Muller, HK. Impaired CD40-signalling in Langerhans' cells from murine neonatal draining lymph nodes: implications for neonatally induced cutaneous tolerance. *Clin Exp Immunol*, 2003, 132(2), 201-8.
- [92] Bellette, BM; Woods, GM; Wozniak, T; Doherty, KV; Muller, HK. DEC-205lo Langerinlo neonatal Langerhans' cells preferentially utilize a wortmannin-sensitive, fluid-phase pathway to internalize exogenous antigen. *Immunology*, 2003, 110(4), 466-73.
- [93] Moon, EY; Noh, YW; Han, YH; Kim, SU; Kim, JM; Yu, DY; et al. T lymphocytes and dendritic cells are activated by the deletion of peroxiredoxin II (Prx II) gene. *Immunol Lett*, 2006, 102(2), 184-90.
- [94] Lehmann, B. The vitamin D<sub>3</sub> pathway in human skin and its role for regulation of biological processes. *Photochem Photobiol*, 2005, 81(6), 1246-51.
- [95] Lehmann, B; Meurer, M. Extrarenal sites of calcitriol synthesis: the particular role of the skin. *Recent Results Cancer Res*, 2003, 164, 135-45.
- [96] Lehmann, B; Sauter, W; Knuschke, P; Dressler, S; Meurer, M. Demonstration of UVB-induced synthesis of 1 alpha,25-dihydroxyvitamin D<sub>3</sub> (calcitriol) in human skin by microdialysis. *Arch Dermatol Res*, 2003, 295(1), 24-8.
- [97] Wagner, CL; Greer, FR. Prevention of rickets and vitamin D deficiency in infants, children, and adolescents. *Pediatrics*, 2008, 122(5), 1142-52.
- [98] Reichrath, J. The challenge resulting from positive and negative effects of sunlight: how much solar UV exposure is appropriate to balance between risks of vitamin D deficiency and skin cancer? *Prog Biophys Mol Biol*, 2006, 92(1), 9-16.
- [99] Poduje, S; Sjerobabski-Masnec, I; Ozanic-Bulic, S. Vitamin D--the true and the false about vitamin D. *Coll Antropol*, 2008, 32 Suppl 2, 159-62.
- [100] Meindl, S; Rot, A; Hoetzenrecker, W; Kato, S; Cross, HS; Elbe-Burger, A. Vitamin D receptor ablation alters skin architecture and homeostasis of dendritic epidermal T cells. *Br J Dermatol*, 2005, 152(2), 231-41.

- [101] Lehmann, B; Knuschke, P; Meurer, M. UVB-induced conversion of 7-dehydrocholesterol to 1 alpha,25-dihydroxyvitamin D3 (calcitriol) in the human keratinocyte line HaCaT. *Photochem Photobiol*, 2000, 72(6), 803-9.
- [102] Hanneman, KK; Cooper, KD; Baron, ED. Ultraviolet immunosuppression: mechanisms and consequences. *Dermatol Clin*, 2006, 24(1), 19-25.
- [103] Guo, Z; Okamoto, H; Danno, K; Imamura, S. The effects of non-interval PUVA treatment on Langerhans cells and contact hypersensitivity. *J Dermatol Sci*, 1992, 3(2), 91-6.
- [104] Fujita, H; Asahina, A; Komine, M; Tamaki, K. The direct action of 1alpha, 25(OH)2-vitamin D3 on purified mouse Langerhans cells. *Cell Immunol*, 2007, 245(2), 70-9.
- [105] Kowitz, A; Greiner, M; Thieroff-Ekerdt, R. Inhibitory effect of 1alpha,25-dihydroxyvitamin D3 on allogeneic lymphocyte stimulation and Langerhans cell maturation. *Arch Dermatol Res*, 1998, 290(10), 540-6.
- [106] Wong, G; Gupta, R; Dixon, KM; Deo, SS; Choong, SM; Halliday, GM; et al. 1,25-Dihydroxyvitamin D and three low-calcemic analogs decrease UV-induced DNA damage via the rapid response pathway. *J Steroid Biochem Mol Biol*, 2004, 89-90(1-5), 567-70.
- [107] Woods, GM; Malley, RC; Muller, HK. The skin immune system and the challenge of tumour immunosurveillance. *Eur J Dermatol*, 2005, 15(2), 63-9.
- [108] Noonan, FP; Recio, JA; Takayama, H; Duray, P; Anver, MR; Rush, WL; et al. Neonatal sunburn and melanoma in mice. *Nature*, 2001, 413(6853), 271-2.
- [109] McLoone, P; Woods, GM; Norval, M. Decrease in langerhans cells and increase in lymph node dendritic cells following chronic exposure of mice to suberythemal doses of solar simulated radiation. *Photochem Photobiol*, 2005, 81(5), 1168-73.
- [110] Quelle, DE; Zindy, F; Ashmun, RA; Sherr, CJ. Alternative reading frames of the INK4a tumor suppressor gene encode two unrelated proteins capable of inducing cell cycle arrest. *Cell*, 1995, 83(6), 993-1000.
- [111] Chin, L; Pomerantz, J; DePinho, RA. The INK4a/ARF tumor suppressor: one gene--two products-two pathways. *Trends Biochem Sci*, 1998, 23(8), 291-6.
- [112] Chin, L; Merlino, G; DePinho, RA. Malignant melanoma: modern black plague and genetic black box. *Genes Dev*, 1998, 12(22), 3467-81.
- [113] Kannan, K; Sharpless, NE; Xu, J; O'Hagan, RC; Bosenberg, M; Chin, L. Components of the Rb pathway are critical targets of UV mutagenesis in a murine melanoma model. *Proc Natl Acad Sci U S A* 2003, 100(3), 1221-5.
- [114] Hacker, E; Irwin, N; Muller, HK; Powell, MB; Kay, G; Hayward, N; et al. Neonatal ultraviolet radiation exposure is critical for malignant melanoma induction in pigmented Tpras transgenic mice. *J Invest Dermatol*, 2005, 125(5), 1074-7.
- [115] Hacker, E; Muller, HK; Irwin, N; Gabrielli, B; Lincoln, D; Pavely, S; et al. Spontaneous and UV radiation-induced multiple metastatic melanomas in Cdk4R24C/R24C/TPras mice. *Cancer Res*, 2006, 66(6), 2946-52.
- [116] Walker, GJ; Kimlin, MG; Hacker, E; Ravishankar, S; Muller, HK; Beermann, F; et al. Murine neonatal melanocytes exhibit a heightened proliferative response to ultraviolet radiation and migrate to the epidermal basal layer. *J Invest Dermatol*, 2009, 129(1), 184-93.

- [117] Abdel-Malek, ZA; Knittel, J; Kadekaro, AL; Swope, VB; Starner, R. The melanocortin 1 receptor and the UV response of human melanocytes--a shift in paradigm. *Photochem Photobiol*, 2008, 84(2), 501-8.
- [118] Jimbow, K; Uesugi, T. New melanogenesis and photobiological processes in activation and proliferation of precursor melanocytes after UV-exposure: ultrastructural differentiation of precursor melanocytes from Langerhans cells. *J Invest Dermatol*, 1982, 78(2), 108-15.
- [119] Noonan, FP; Otsuka, T; Bang, S; Anver, MR; Merlino, G. Accelerated ultraviolet radiation-induced carcinogenesis in hepatocyte growth factor/scatter factor transgenic mice. *Cancer Res*, 2000, 60(14), 3738-43.
- [120] van Schanke, A; Jongsma, MJ; Bisschop, R; van Venrooij, GM; Rebel, H; de Gruijl, FR. Single UVB overexposure stimulates melanocyte proliferation in murine skin, in contrast to fractionated or UVA-1 exposure. *J Invest Dermatol*, 2005, 124(1), 241-7.
- [121] Silvers, WK; Mintz, B. Differences in latency and inducibility of mouse skin melanomas depending on the age and anatomic site of the skin. *Cancer Res*, 1998, 58(4), 630-2.
- [122] Rivers, JK. Is there more than one road to melanoma? *Lancet*, 2004, 363(9410), 728-30.
- [123] Lin, JY; Fisher, DE. Melanocyte biology and skin pigmentation. *Nature*, 2007, 445(7130), 843-50.
- [124] Dixon, KM; Deo, SS; Wong, G; Slater, M; Norman, AW; Bishop, JE; et al. Skin cancer prevention: a possible role of 1,25dihydroxyvitamin D3 and its analogs. *J Steroid Biochem Mol Biol*, 2005, 97(1-2), 137-43.
- [125] Karasawa, M; Hosoi, J; Hashiba, H; Nose, K; Tohyama, C; Abe, E; et al. Regulation of metallothionein gene expression by 1 alpha,25-dihydroxyvitamin D3 in cultured cells and in mice. *Proc Natl Acad Sci U S A*, 1987, 84(24), 8810-3.
- [126] Wang, WH; Li, LF; Zhang, BX; Lu, XY. Metallothionein-null mice exhibit reduced tolerance to ultraviolet B injury in vivo. *Clin Exp Dermatol*, 2004, 29(1), 57-61.
- [127] MacLaughlin, J; Holick, MF. Aging decreases the capacity of human skin to produce vitamin D3. *J Clin Invest*, 1985, 76(4), 1536-8.
- [128] Harpin, VA; Rutter, N. Barrier properties of the newborn infant's skin. *J Pediatr*, 1983, 102(3), 419-25.
- [129] Kalia, YN; Nonato, LB; Lund, CH; Guy, RH. Development of skin barrier function in premature infants. *J Invest Dermatol*, 1998, 111(2), 320-6.
- [130] Yosipovitch, G; Maayan-Metzger, A; Merlob, P; Sirota, L. Skin barrier properties in different body areas in neonates. *Pediatrics*, 2000, 106(1 Pt 1), 105-8.
- [131] Rutter, N; Hull, D. Water loss from the skin of term and preterm babies. *Arch Dis Child*, 1979, 54(11), 858-68.
- [132] Visscher, MO; Chatterjee, R; Munson, KA; Pickens, WL; Hoath, SB. Changes in diapered and nondiapered infant skin over the first month of life. *Pediatr Dermatol*, 2000, 17(1), 45-51.
- [133] Hoeger, PH; Enzmann, CC. Skin physiology of the neonate and young infant: a prospective study of functional skin parameters during early infancy. *Pediatr Dermatol*, 2002, 19(3), 256-62.
- [134] Menon, GK. New insights into skin structure: scratching the surface. *Adv Drug Deliv Rev*, 2002, 54 Suppl 1, S3-17.

- [135] Hoath, SB. The stickiness of newborn skin: bioadhesion and the epidermal barrier. *J Pediatr*, 1997, 131(3), 338-40.
- [136] McLoone, P; Simics, E; Barton, A; Norval, M; Gibbs, N. An action spectrum for the production of cis-urocanic acid in human skin in vivo. *Journal of Investigative Dermatology*, 2005, 124, 1071-1074.
- [137] Behne, MJ; Barry, NP; Hanson, KM; Aronchik, I; Clegg, RW; Gratton, E; et al. Neonatal development of the stratum corneum pH gradient: localization and mechanisms leading to emergence of optimal barrier function. *J Invest Dermatol*, 2003, 120(6), 998-1006.
- [138] Lock-Andersen, J; Knudstorp, ND; Wulf, HC. Facultative skin pigmentation in caucasians: an objective biological indicator of lifetime exposure to ultraviolet radiation? *Br J Dermatol*, 1998, 138(5), 826-32.
- [139] Agren, J; Sjors, G; Sedin, G. Ambient humidity influences the rate of skin barrier maturation in extremely preterm infants. *J Pediatr* 2006, 148(5), 613-7.
- [140] Chiou, YB; Blume-Peytavi, U. Stratum corneum maturation. A review of neonatal skin function. *Skin Pharmacol Physiol*, 2004, 17(2), 57-66.
- [141] Giusti, F; Martella, A; Bertoni, L; Seidenari, S. Skin barrier, hydration, and pH of the skin of infants under 2 years of age. *Pediatr Dermatol*, 2001, 18(2), 93-6.
- [142] Quaglino, D, Jr.; Bergamini, G; Boraldi, F; Pasquali Ronchetti, I. Ultrastructural and morphometrical evaluations on normal human dermal connective tissue--the influence of age, sex and body region. *Br J Dermatol*, 1996, 134(6), 1013-22.
- [143] Kikuchi, K; Kobayashi, H; O'Goshi, K; Tagami, H. Impairment of skin barrier function is not inherent in atopic dermatitis patients: a prospective study conducted in newborns. *Pediatr Dermatol*, 2006, 23(2), 109-13.
- [144] Saijo, S; Tagami, H. Dry skin of newborn infants: functional analysis of the stratum corneum. *Pediatr Dermatol*, 1991, 8(2), 155-9.
- [145] Lund, CH; Nonato, LB; Kuller, JM; Franck, LS; Cullander, C; Durand, DJ. Disruption of barrier function in neonatal skin associated with adhesive removal. *J Pediatr*, 1997, 131(3), 367-72.
- [146] Rawlings, AV; Scott, IR; Harding, CR; Bowser, PA. Stratum corneum moisturization at the molecular level. *J Invest Dermatol*, 1994, 103(5), 731-41.
- [147] Pierard, GE; Goffin, V; Hermanns-Le, T; Pierard-Franchimont, C. Corneocyte desquamation. *Int J Mol Med*, 2000, 6(2), 217-21.
- [148] Sato, J; Yanai, M; Hirao, T; Denda, M. Water content and thickness of the stratum corneum contribute to skin surface morphology. *Arch Dermatol Res*, 2000, 292(8), 412-7.
- [149] Bouwstra, JA; Honeywell-Nguyen, PL; Gooris, GS; Ponec, M. Structure of the skin barrier and its modulation by vesicular formulations. *Prog Lipid Res*, 2003, 42(1), 1-36.
- [150] Fluhr, JW; Mao-Qiang, M; Brown, BE; Hachem, JP; Moskowitz, DG; Demerjian, M; et al. Functional consequences of a neutral pH in neonatal rat stratum corneum. *J Invest Dermatol*, 2004, 123(1), 140-51.
- [151] Rawlings, AV; Matts, PJ. Stratum corneum moisturization at the molecular level: an update in relation to the dry skin cycle. *J Invest Dermatol*, 2005, 124(6), 1099-110.
- [152] Mack, M; Tierney, N; Ruvolo, E; Stamatias, G; Kollias, N; Martin, K. Yearly exposure of infant skin to solar ultraviolet radiation incurs partially irreversible changes in skin pigmentation. Abstract 855. *J Invest Dermatol*, 2009, 129(S1), S143.

- [153] Grande, R; Gutierrez, E; Latorre, E; Arguelles, F. Physiological variations in the pigmentation of newborn infants. *Hum Biol*, 1994, 66(3), 495-507.
- [154] Park, JH; Lee, MH. A study of skin color by melanin index according to site, gestational age, birth weight and season of birth in Korean neonates. *J Korean Med Sci*, 2005, 20(1), 105-8.
- [155] Watanabe, M; Ohki, Y; Yoshizawa, Y; Inoue, Y; Tokuyama, K; Morikawa, A. Maturational changes in skin color of Japanese newborn infants. *Neonatology*, 2007, 91(4), 275-80.
- [156] Gilchrest, BA; Eller, MS. DNA photodamage stimulates melanogenesis and other photoprotective responses. *J Investig Dermatol Symp Proc*, 1999, 4(1), 35-40.
- [157] Moore, C; Murphy, MM; Keast, DR; Holick, MF. Vitamin D intake in the United States. *J Am Diet Assoc*, 2004, 104(6), 980-3.
- [158] Rajakumar, K; Thomas, SB. Reemerging nutritional rickets: a historical perspective. *Arch Pediatr Adolesc Med*, 2005, 159(4), 335-41.
- [159] Pettifor, JM. Rickets and vitamin D deficiency in children and adolescents. *Endocrinol Metab Clin North Am*, 2005, 34(3), 537-53, vii.
- [160] Nesby-O'Dell, S; Scanlon, KS; Cogswell, ME; Gillespie, C; Hollis, BW; Looker, AC; et al. Hypovitaminosis D prevalence and determinants among African American and white women of reproductive age: third National Health and Nutrition Examination Survey, 1988-1994. *Am J Clin Nutr*, 2002, 76(1), 187-92.
- [161] Scanlon, KS. Vitamin D expert panel meeting, October 11-12, Atlanta, Georgia: final report. 2001. Available from: [www.cdc.gov/nccdpHP/dnpa/nutrition/pdf/Vitamin\\_D\\_Expert\\_Panel\\_Meeting.pdf](http://www.cdc.gov/nccdpHP/dnpa/nutrition/pdf/Vitamin_D_Expert_Panel_Meeting.pdf)<[http://www.cdc.gov/nccdpHP/dnpa/nutrition/pdf/Vitamin\\_D\\_Expert\\_Panel\\_Meeting.pdf](http://www.cdc.gov/nccdpHP/dnpa/nutrition/pdf/Vitamin_D_Expert_Panel_Meeting.pdf)>.
- [162] Looker, AC; Dawson-Hughes, B; Calvo, MS; Gunter, EW; Sahyoun, NR. Serum 25-hydroxyvitamin D status of adolescents and adults in two seasonal subpopulations from NHANES III. *Bone*, 2002, 30(5), 771-7.
- [163] Harkness, LS; Bonny, AE. Calcium and vitamin D status in the adolescent: key roles for bone, body weight, glucose tolerance, and estrogen biosynthesis. *J Pediatr Adolesc Gynecol*, 2005, 18(5), 305-11.
- [164] Harkness, LS; Cromer, BA. Vitamin, D. deficiency in adolescent females. *J Adolesc Health*, 2005, 37(1), 75.
- [165] Cheng, S; Tylavsky, F; Kroger, H; Karkkainen, M; Lyytikainen, A; Koistinen, A; et al. Association of low 25-hydroxyvitamin D concentrations with elevated parathyroid hormone concentrations and low cortical bone density in early pubertal and prepubertal Finnish girls. *Am J Clin Nutr*, 2003, 78(3), 485-92.
- [166] Tylavsky, FA; Ryder, KA; Lyytikainen, A; Cheng, S. Vitamin D, parathyroid hormone, and bone mass in adolescents. *J Nutr*, 2005, 135(11), 273S-8S.
- [167] DeBar, LL; Ritenbaugh, C; Aickin, M; Orwoll, E; Elliot, D; Dickerson, J; et al. Youth: a health plan-based lifestyle intervention increases bone mineral density in adolescent girls. *Arch Pediatr Adolesc Med*, 2006, 160(12), 1269-76.
- [168] El-Hajj Fuleihan, G; Nabulsi, M; Choucair, M; Salamoun, M; Hajj Shahine, C; Kizirian, A; et al. Hypovitaminosis D in healthy schoolchildren. *Pediatrics*, 2001, 107(4), E53.

- [169] Marwaha, RK; Tandon, N; Reddy, DR; Aggarwal, R; Singh, R; Sawhney, RC; et al. Vitamin D and bone mineral density status of healthy schoolchildren in northern India. *Am J Clin Nutr*, 2005, 82(2), 477-82.
- [170] Lapatsanis, D; Moulas, A; Cholevas, V; Soukakos, P; Papadopoulou, ZL; Challa, A. Vitamin D: a necessity for children and adolescents in Greece. *Calcif Tissue Int*, 2005, 77(6), 348-55.
- [171] Hill, TR; Flynn, A; Kiely, M; Cashman, KD. Prevalence of suboptimal vitamin D status in young, adult and elderly Irish subjects. *Ir Med J*, 2006, 99(2), 48-9.
- [172] Primary vitamin D deficiency in children. *Drug Ther Bull*, 2006, 44(2), 12-6.
- [173] Gordon, CM; Feldman, HA; Sinclair, L; Williams, AL; Kleinman, PK; Perez-Rossello, J; et al. Prevalence of vitamin D deficiency among healthy infants and toddlers. *Arch Pediatr Adolesc Med*, 2008, 162(6), 505-12.
- [174] Grant, WB; Garland, CF; Holick, MF. Comparisons of estimated economic burdens due to insufficient solar ultraviolet irradiance and vitamin D and excess solar UV irradiance for the United States. *Photochem Photobiol*, 2005, 81(6), 1276-86.
- [175] Wolpowitz, D; Gilchrest, BA. The vitamin D questions: how much do you need and how should you get it? *J Am Acad Dermatol*, 2006, 54(2), 301-17.
- [176] Lucas, RM; Ponsonby, AL. Considering the potential benefits as well as adverse effects of sun exposure: can all the potential benefits be provided by oral vitamin D supplementation? *Prog Biophys Mol Biol*, 2006, 92(1), 140-9.
- [177] Matsuoka, LY; Wortsman, J; Dannenberg, MJ; Hollis, BW; Lu, Z; Holick, MF. Clothing prevents ultraviolet-B radiation-dependent photosynthesis of vitamin D3. *J Clin Endocrinol Metab*, 1992, 75(4), 1099-103.
- [178] Matsuoka, LY; Wortsman, J; Haddad, JG; Kolm, P; Hollis, BW. Racial pigmentation and the cutaneous synthesis of vitamin D. *Arch Dermatol*, 1991, 127(4), 536-8.
- [179] Matsuoka, LY; Wortsman, J; Hollis, BW. Suntanning and cutaneous synthesis of vitamin D3. *J Lab Clin Med*, 1990, 116(1), 87-90.
- [180] Matsuoka, LY; Wortsman, J; Hollis, BW. Use of topical sunscreen for the evaluation of regional synthesis of vitamin D3. *J Am Acad Dermatol*, 1990, 22(5 Pt 1), 772-5.
- [181] Binkley, N; Novotny, R; Krueger, D; Kawahara, T; Daida, YG; Lensmeyer, G; et al. Low vitamin D status despite abundant sun exposure. *J Clin Endocrinol Metab*, 2007, 92(6), 2130-5.
- [182] Maisels, MJ; Watchko, JF. Treatment of jaundice in low birthweight infants. *Arch Dis Child Fetal Neonatal Ed*, 2003, 88(6), F459-63.
- [183] Maisels, MJ; McDonagh, AF. Phototherapy for neonatal jaundice. *N Engl J Med*, 2008, 358(9), 920-8.
- [184] McDonagh, AF. Sunlight-induced mutation of bilirubin in a long-distance runner. *N Engl J Med*, 1986, 314(2), 121-2.
- [185] McDonagh, AF. Ex uno plures: the concealed complexity of bilirubin species in neonatal blood samples. *Pediatrics*, 2006, 118(3), 1185-7.
- [186] Myara, A; Sender, A; Valette, V; Rostoker, C; Paumier, D; Capoulade, C; et al. Early changes in cutaneous bilirubin and serum bilirubin isomers during intensive phototherapy of jaundiced neonates with blue and green light. *Biol Neonate*, 1997, 71(2), 75-82.
- [187] Kopelman, AE; Brown, RS; Odell, GB. The "bronze" baby syndrome: a complication of phototherapy. *J Pediatr*, 1972, 81(3), 466-72.

- [188] Rubaltelli, FF; Jori, G; Reddi, E. Bronze baby syndrome: a new porphyrin-related disorder. *Pediatr Res*, 1983, 17(5), 327-30.
- [189] Onishi, S; Itoh, S; Isobe, K; Togari, H; Kitoh, H; Nishimura, Y. Mechanism of development of bronze baby syndrome in neonates treated with phototherapy. *Pediatrics*, 1982, 69(3), 273-6.
- [190] Ashley, JR; Littler, CM; Burgdorf, WH; Brann, BSt. Bronze baby syndrome. Report of a case. *J Am Acad Dermatol*, 1985, 12(2 Pt 1), 325-8.
- [191] Purcell, SM; Wians, FH, Jr.; Ackerman, NB, Jr.; Davis, BM. Hyperbiliverdinemia in the bronze baby syndrome. *J Am Acad Dermatol*, 1987, 16(1 Pt 2), 172-7.
- [192] Kearns, GL; Williams, BJ; Timmons, OD. Fluorescein phototoxicity in a premature infant. *J Pediatr*, 1985, 107(5), 796-8.
- [193] Burry, JN; Lawrence, JR. Phototoxic blisters from high frusemide dosage. *Br J Dermatol*, 1976, 94(5), 495-9.
- [194] Porat, R; Gilbert, S; Magilner, D. Methylene blue-induced phototoxicity: an unrecognized complication. *Pediatrics*, 1996, 97(5), 717-21.
- [195] Mallon, E; Wojnarowska, F; Hope, P; Elder, G. Neonatal bullous eruption as a result of transient porphyrinemia in a premature infant with hemolytic disease of the newborn. *J Am Acad Dermatol*, 1995, 33(2 Pt 2), 333-6.
- [196] Paller, AS; Eramo, LR; Farrell, EE; Millard, DD; Honig, PJ; Cunningham, BB. Purpuric phototherapy-induced eruption in transfused neonates: relation to transient porphyrinemia. *Pediatrics*, 1997, 100(3 Pt 1), 360-4.
- [197] Tonz, O; Vogt, J; Filippini, L; Simmler, F; Wachsmuth, ED; Winterhalter, KH. [Severe light dermatosis following photo therapy in a newborn infant with congenital erythropoietic urophyria]. *Helv Paediatr Acta*, 1975, 30(1), 47-56.
- [198] Valaes, T; Petmezaki, S; Henschke, C; Drummond, GS; Kappas, A. Control of jaundice in preterm newborns by an inhibitor of bilirubin production: studies with tin-mesoporphyrin. *Pediatrics*, 1994, 93(1), 1-11.
- [199] Dollberg, S; Atherton, HD; Hoath, SB. Effect of different phototherapy lights on incubator characteristics and dynamics under three modes of servocontrol. *Am J Perinatol*, 1995, 12(1), 55-60.
- [200] Maayan-Metzger, A; Yosipovitch, G; Hadad, E; Sirota, L. Transepidermal water loss and skin hydration in preterm infants during phototherapy. *Am J Perinatol*, 2001, 18(7), 393-6.
- [201] Csoma, Z; Hencz, P; Orvos, H; Kemeny, L; Dobozy, A; Dosa-Racz, E; et al. Neonatal blue-light phototherapy could increase the risk of dysplastic nevus development. *Pediatrics*, 2007, 119(6), 1269.
- [202] Matichard, E; Le Henanff, A; Sanders, A; Leguyadec, J; Crickx, B; Descamps, V. Effect of neonatal phototherapy on melanocytic nevus count in children. *Arch Dermatol*, 2006, 142(12), 1599-604.
- [203] Bauer, J; Buttner, P; Luther, H; Wiecker, TS; Mohrle, M; Garbe, C. Blue light phototherapy of neonatal jaundice does not increase the risk for melanocytic nevus development. *Arch Dermatol*, 2004, 140(4), 493-4.
- [204] Mahe, E; Beauchet, A; Aegeerter, P; Saiag, P. Neonatal blue-light phototherapy does not increase nevus count in 9-year-old children. *Pediatrics*, 2009, 123(5), e896-900.



### ***Chapter 3***

## **MOLECULAR TYPING OF POLYMORPHIC GENES BY TIME-RESOLVED FLUORESCENCE RESONANCE ENERGY TRANSFER**

***L. Nardo<sup>1</sup>, M. Bondani<sup>2</sup>, G. Tosi<sup>3</sup>, R. S. Accolla<sup>3</sup> and A. Andreoni<sup>1</sup>***

<sup>1</sup>University of Insubria, Dept. of Physics and Mathematics, and C.N.I.S.M.,  
U.d.R Como, Via Valleggio 11, 22100 Como, Italy.

<sup>2</sup>National Centre for Ultrafast and Ultraintense Lasers, C. N. R. – I. N. F. M..

<sup>3</sup>University of Insubria, Faculty of Medicine, Dept. of Clinical and Biological Sciences,  
Via O. Rossi 9, 21100 Varese, Italy.

### **ABSTRACT**

Gene polymorphism is responsible for the expression of many variants of a protein among different subjects of the same species. To be classified into polymorphism, variations of gene sequences must appear in at least 1% of the population. Such genetic variants, called alleles, though not necessarily directly pathogenic, are frequently correlated to the occurrence of diseases. For this reason, the possibility to perform wide range screening of the relevant polymorphic genes would provide a powerful tool for disease prediction.

DNA sequencing, which is the election technique to identify allelic variants, is expensive and time consuming and is not applicable to the screening of vast populations. However, if the relevant alleles are known, other molecular typing methods can offer a valuable alternative to sequencing. Several of these techniques are based on the detection of light emitted as either chemiluminescence or fluorescence. Most of them consist in ON/OFF intensity measurements, as the emission/non-emission of light is triggered by recognition of the genomic template by allele specific probes. These techniques often require preliminary purification of DNA and amplification of the polymorphic gene of interest.

In this Chapter, we focus on the HLA-DQB1 locus of the human major histocompatibility complex (MHC), which comprises the most polymorphic genes in the human genome. This very high degree of polymorphism dictates the tissue compatibility

in organ transplants and the susceptibility to several diseases, such as insulin-dependent diabetes mellitus (IDDM).

We introduce a novel typing method that promises to avoid purification and amplification of DNA, and apply it to the recognition of HLA-DQB1 allelic variants. Our method is based on time-resolved fluorescence resonance energy transfer (FRET) measurements performed on a donor-acceptor dual-labelled oligonucleotide probe, which carries the donor and the acceptor at its opposite ends. The fluorescence of the FRET donor is quenched by the acceptor in a strongly donor-acceptor distance-dependent way, which makes the donor fluorescence decay time sensitive to the conformation of the probe-target complex. Fluorescence decay time values are measured with a time-correlated single-photon counting apparatus endowed with 30 ps resolution, which allows extremely high sensitivity on conformational differences. As the apparatus can reveal single photons, the decay time can be measured even for a single probe molecule, avoiding DNA amplification.

Target oligonucleotides with sequences equal to those of the region around codon 57 of the exon  $\beta 2$  allelic variants were synthesized. This region was chosen because it is the most polymorphic region of DQB1 gene and because its variability is associated with susceptibility/resistance to IDDM. An oligonucleotide corresponding to DQB1-0201 allele was used as the only dual-labelled probe. This probe forms a perfect double strand with the complementary target oligonucleotide (allele 0201), whereas for any other allelic variant, probe and target sequence are slightly mismatched at sites that differ from allele to allele. This causes the probe-target hybrid conformation to be different from allele to allele and thus the distance between the donor and the acceptor bound at the ends of the probe to change. It is shown that the donor fluorescence lifetime is correspondingly different and specific for each probe-target pair, which provides a tool for precise identification of each allele. The present results indicate that our method can be successfully used to molecularly type even highly polymorphic genetic systems, such as the HLA system.

## I. INTRODUCTION

With the completion of the Human Genome Project, a large number of subtle variations (polymorphisms) among the genomes of different individuals of the same population have been found. The most abundant type of these variations is single nucleotide polymorphisms (SNPs): more than 9 million of single-nucleotide polymorphic variants were reported in public databases in 2006 [1]. Therefore the average overall frequency of SNPs in the human genome is approximately one per 1000 base pairs.

Most of the DNA variations detected between individuals are silent, *i.e.* they have no effect on the individual phenotype. However specific SNPs have been found to be associated with diseases or phenotypic traits. An example of such SNPs-related diseases is the well known point mutation in human  $\beta$ -globin gene that leads to sickle cell anaemia [2]. The study of SNPs is also relevant for multigene diseases such as type II diabetes [3] and for the identification of somatic mutations of genes that are pivotal in tumorigenesis. An example is the tumor suppressor gene p53 [4]. More recently, SNPs are utilized as markers in pharmacogenomics [5].

A particularly relevant, highly polymorphic locus is the MHC locus located in the short arm of human chromosome 6. It comprises many genes coding for the human leukocyte antigen (HLA) molecules that, originally discovered for their role in the rejection of

transplanted organs, play a pivotal role in the triggering of the immune response against pathogens. Indeed, they guide the development and the activation of T lymphocytes. There are two types of HLA molecules, namely class I and class II, that activate functionally distinct T cell populations, CD8+ T cells and CD4+ T cells, respectively [6]. Moreover, the expression of certain HLA molecules has been associated with the susceptibility to several autoimmune diseases, including type I IDDM [7]. Genetic markers of susceptibility to IDDM have been identified in the HLA-II region and in particular, in HLA-II DQA1 and DQB1 loci, coding for the  $\alpha$  and  $\beta$  chains of DQ heterodimer, respectively [8]. Extensive molecular studies of HLA-DQ genotype in patients with IDDM correlated the susceptibility to disease with the polymorphism of a single aminoacid in both DQ $\alpha$  and DQ $\beta$  chains [9-10]. The presence of an arginine residue in position 52 of DQ $\alpha$  chain and of a neutral residue (serine, alanine or valine) in position 57 of DQ $\beta$  chain is strongly associated with diabetes onset. On the contrary, the presence of aspartic acid in position 57 of DQ $\beta$  confers resistance to IDDM [11].

In the light of these findings, HLA-DQ typing represents an important tool for the early identification of subjects genetically predisposed to IDDM, in particular among the high risk group represented by the siblings of IDDM patients. As summarized above, the possibility to perform genotyping of clinically relevant SNPs on large sample populations is fundamental to achieve significant progresses in many fields of disease genetics, oncology and pharmacogenomics, and would be helpful in the prediction, diagnosis and possibly treatment of many severe diseases. For this reason, in search of methods allowing simple, reliable, fast and cost-benefit effective genotyping, a huge number of molecular assays have been developed in the last two decades. Most of them require high quantities of sample DNA, obtained by PCR amplification of the SNP-containing region. Common genotyping procedures include [12]: (i) digestion with restriction enzymes to test for the presence/absence of critical restriction sites; (ii) allele specific oligonucleotide (ASO) hybridization; (iii) allele specific PCR amplification (AS-PCR); (iv) oligonucleotide ligation assay; (v) primer extension in the presence of dideoxynucleotides (ddNTP).

The first method is based on the ability of special enzymes, the “restriction endonucleases”, to cleave the DNA at certain sites represented by precise base sequences. It is a very useful, but unfortunately rarely applicable way of detecting polymorphisms directly. Indeed, restriction enzymes allow discrimination among alleles only when SNPs alter the recognition site for the enzyme [13, 14].

The ASO hybridization approaches exploit differences in the thermal stability of double-stranded DNA to distinguish between perfectly matched and partially mismatched target-probe duplexes and to achieve allelic discrimination. Hence, it is critical to perform assays under controlled temperature conditions, in which hybridization occurs only between perfectly complementary probes and target alleles. Generally, the effectiveness in allele differentiation depends on the length and on the sequence of the probe, on the location of the SNP within the probe, and on the hybridization conditions. Hybridization approaches have been implemented on high-throughput platforms using microarrays because they do not require any enzymatic reaction to discriminate alleles [15, 16]. Peptide nucleic acid (PNA) probes have occasionally been used for allele-specific hybridization with surface-immobilized DNA templates [17], to attain a higher probe/target hybridization affinity.

AS-PCR involves PCR amplification of genomic DNA by using allele-specific primers encompassing the SNP, each labeled with a different fluorophore, and a common 3' reverse primer. All the allele-specific primers are added simultaneously to the reaction mixture. PCR amplification under stringent conditions is much less efficient in the presence of a mismatch between template and primer. PCR products can be separated by electrophoresis on an agarose gel and the colors of the bands determined by using a fluorimeter. The detection of a specific fluorescence color indicates successful amplification with the primer labeled with that specific fluorophore, thus, revealing the allelic specificity of the template DNA [18-19]. For applications in SNP genotyping, AS-PCR has been combined with real-time PCR and capillary array electrophoresis [19, 20].

Ligase-mediated approach for detecting SNPs exploits the fact that the ends of two single strands of DNA must be exactly aligned for DNA ligase to join them. A panel of oligoprobes, covering all the different specificities of the polymorphic region, is synthesized together with a common probe complementary to a non polymorphic region immediately next 3' to the SNP site [21]. The common probe is labeled with radioisotopes or, alternatively, with fluorescent or enzymatic labels. Each SNP-specific oligonucleotide and the common probe are hybridized to denatured DNA template. Only in the case of perfect matching, 5' and 3' oligonucleotides form a flush junction that can be sealed by the DNA ligase. After denaturation, ligated molecule can be isolated from the reaction mixture and revealed by the detection of radioactive (or fluorescent/enzymatic) signal. The allelic specificity of template DNA is then inferred by the specific 5' oligonucleotide that has allowed the ligation reaction [22-25].

The most direct way to determine whether a SNP is present is to directly sequence PCR amplified DNA by using fluorescently labeled primers and automated sequencing machines. Either allele-specific primers [19] or a common primer [26] can be used in the primer extension reactions involving allele-specific incorporation of nucleotides. Primer extension approaches involve allele-specific incorporation of nucleotides in primer extension reactions with the allelic template, utilizing enzyme specificity to achieve allelic discrimination. Primer extension assays use either allele-specific primers [19] or a common primer [26].

The recognition of the allele-specific product, a step required by any of the above-mentioned SNP genotyping methods, is most frequently pursued by means of techniques based on the detection of the light emitted by either the product itself or other components of the reaction mixture upon recognition of the genomic template. Among these techniques we mention chemiluminescence detection and monitoring of the fluorescence signal of molecular probes interacting with the allelic template.

Chemiluminescence assures high signal-to-noise ratio, rapid detection, and proneness to automation. Most of the techniques based on chemiluminescence detection apply the sequencing-by-synthesis approach and exploit generation of chemiluminescence triggered by a cascade of enzymatic reactions initiated by incorporation of a nucleotide in a duplicating DNA sequence [27]. In the sequencing-by-synthesis genotyping approach, the primer anneals to PCR-amplified template DNA upstream of the SNP site [28]. Nucleotides (dATP, dCTP, dGTP, or dTTP) are added one by one to the primer extension reaction mixture. If the added nucleotide is complementary to the nucleotide being extended, the polymerase enzyme utilizes it for primer extension, and inorganic pyrophosphate (PPi) is released. In a series of enzymatic reactions, the released PPi is used to generate light. No light signal is produced in the case of unincorporated nucleotides, which must be removed from the reaction mixture prior to addition of a new nucleotide. Therefore, by monitoring the light signals, it is possible

to verify whether a specific nucleotide has been incorporated and reconstruct the template sequence.

Techniques exploiting the monitoring of the fluorescence signal emitted by molecular probes interacting with the allelic template are widely used, because of their ease of implementation and high detection sensitivity. Currently, most of them are based on the detection of the presence/absence of a fluorescence signal (ON/OFF measurements). No quantitative intensity measurements are performed. If, on one hand, ON/OFF measurements are simple and yield real time qualitative information about the template sequence, on the other hand, renouncing to quantitative assessments limits the versatility and sensitivity of these techniques. Several fluorescence-based techniques have been devised. Among them, we mention:

- Fluorescence detection associated to capillary array electrophoresis, which has been the workhorse for the Human Genome Project and most of the initial SNP identification studies. This technique uses dideoxynucleotides labeled with different fluorescent dyes in a Sanger sequencing reaction to produce a ladder of fluorescence-tagged extension products [29]. The primer extension products are separated by electrophoresis and the specific fluorescence signal coming from each extension product reveals the base identity. The sequential arrangement of bases gives the template sequence.
- Fluorescence polarization (FP) detection that is used in combination with allele-specific primer extension methods and avoids the separation of the extended primers. When a fluorescent molecule is excited by linearly polarized light, the fluorescence light is also polarized in the direction of the molecular transition dipole moment. In solution, the fluorescence is depolarized over time as a consequence of the rotational diffusion of the fluorophore, at a rate depending on the fluorophore dimensions. In the FP detection approach, the primer extension reaction is performed on a PCR template by using ddNTPs labeled with fluorophores emitting at different wavelengths. As the rotational diffusion coefficient of the isolated ddNTPs is much larger than that of ddNTPs incorporated in the extended primer (smaller molecules rotate faster), the FP of free ddNTPs is lost more quickly with respect to incorporated ddNTPs. The base in the target sequence immediately following the primer's 3' end is complementary to that included in the ddNTP labeled with the fluorophore emitting polarized fluorescence for the longest time [30].
- Quenching of fluorescence by FRET triggered by probe-template hybridization exploits the distance-dependent non-radiative transfer of excitation energy from a fluorescent donor (D) to an acceptor (A). The FRET phenomenon occurs between closely spaced molecules (up to about 120 Angstroms) when the emission spectrum of D overlaps with the excitation spectrum of A. As a result, when D and A are in close proximity, the D fluorescence is weaker than that emitted when they are separated from each other. The excitation energy, transferred to A, can be dissipated either through non-radiative pathways, when A is a non-emitting quencher, or as fluorescence, when A is a fluorophore. Thus, the occurrence of a FRET phenomenon and its efficiency can be followed by measuring the decrease in D fluorescence or the increase in A fluorescence, depending on the kind of A molecule and on the experimental conditions. When A is a fluorophore, ideal properties to be fulfilled by

A are that it is not directly excited by the light source used for the excitation of D and that its emission spectrum is well separated from that of D. To avoid the disturbance of a noisy background when the D fluorescence is measured, the so-called black-hole quencher dyes, which do not emit fluorescence, may be used as A. Typing by means of FRET is frequently performed using molecular beacons (MBs) as allele-specific probes. MBs are palindromic oligonucleotides whose opposite ends pair up to form a stem-loop structure. The opposite ends of the MB probe carry the D and A molecules so that, due to FRET, the D fluorescence is suppressed when the probe is in its native conformation because of the vicinity of A to D [31]. Multiple allele-specific MB probes labelled with different dyes are used for querying a SNP. The loop sequence of each probe is complementary to a specific SNP. Probes are mixed all at once with the PCR-amplified template, but the high stringency of the hybridization conditions allows annealing only of perfectly matching oligonucleotide. As a result, the stem and loop structure of the matching probe is destroyed and D and A are well separated from each other, leading to enhanced fluorescence emission of D, while the non-matching probes preserve the native stem and loop conformation. The template genotype can be inferred by assessing which of the Ds is the fluorescing one. FRET has also been used in AS-PCR reactions [32] using primers with a stem and loop structure similar to MBs, and in single-base extension reactions for SNP genotyping [33].

All the methods mentioned above were optimized along years. Nevertheless, a technique allowing precise, reliable, rapid and cost-benefit effective typing of genes on vast populations is still lacking. One limitation, that is common to all the current genotyping technologies, with only a few exceptions, is that they require the PCR amplification step. In fact, preliminary PCR amplification of a SNP-containing region needs to be performed in order to obtain a number of template molecules sufficient for the actual detection.

Recently FRET methods have gained interest because, in principle, they would allow molecular typing of non PCR-amplified DNA sequences [34]. Until now such methods have been only applied to artificial systems in which the genomic template is mimicked by short oligonucleotides (20-40 bases) encompassing the polymorphic site. A further advantage of FRET is that it might produce quantitatively different fluorescence responses depending on the probe-target hybrid conformation, and, hence, makes SNP genotyping feasible by using a single probe. Pioneering attempts in this direction have been made by Gaylord and collaborators [35] and, later, by Al Attar and collaborators [36]. These authors used a cationic polymer conjugated to the targets as D and monitored the fluorescence intensity of A attached to a single peptide nucleic acid probe. As the neutral peptide backbone of the probe did not bind to D, the acceptor A received the excitation energy only upon hybridization of the probe to the targets. By applying this scheme to typing of ABL polymorphism in the BCR-ABL oncogene, Al Attar *et al.* have determined significantly different values of the FRET efficiency between D and A when the probe was hybridized to each of the possible target sequences (*i.e.* to each of the possible polymorphic variants). Thus, they demonstrated the feasibility of ABL typing by using a single probe. However, this approach has two major points of weakness. First, because a quantitative assessment of the D fluorescence intensity is required, proportional detectors need to be used. Since such detectors are normally endowed with a much reduced detection quantum efficiency, as compared to avalanche ON/OFF

detectors, the applicability of the method to unamplified genomic samples is at risk. Second, as in the cell there are many endogenous fluorophores, whose emission is superimposed with that of A, the method is not directly applicable to analyses performed with cellular lysates and its use is limited to the typing of previously purified DNA.

There exists an alternative method to measure the FRET efficiency that is based on the measurement of D fluorescence decay time,  $\tau_D$ , in the presence and in the absence of A. Recent studies [37, 38] suggest that this method offers significant advantages over intensity measurements as the  $\tau_D$  value for any fluorophore can be determined by applying the time correlated single photon counting (TCSPC) technique. TCSPC implies detection and timing of at most one photon per excitation event and subsequent reconstruction of the statistical distribution of the detection times. Thus, TCSPC is optimally implemented with ON/OFF detectors and it is sensitive to the fluorescence emitted by few/single fluorophores. Moreover, as endogenous fluorophores contained in the cellular extract most likely have decay times different from that of D, the effect of their presence in the sample is to contribute additional exponential decay components to the measured decay distribution, which can be in principle discriminated from that of D during data analysis. Thus, FRET techniques based on D decay time measurements could be suitable for typing both non-amplified and non-purified DNA samples.

Recently, we demonstrated [39] that the fluorescence decay time of the D fluorophores of D-A pairs covalently bound to synthetic DNA oligonucleotides, can be assessed with 30 ps temporal resolution on nanomolar concentrated samples by means of TCSPC measurements performed by using a state of art single-photon avalanche diode as the fluorescence detector. Such measurements allowed us to precisely assess the FRET efficiency of the pairs in solutions containing the oligonucleotides and DNA-ligands, at different ratios of the DNA base-pair to ligand concentrations. The tiny deformations induced on the oligonucleotide double stranded structure by the binding of the ligands could be revealed with sub-nanometre resolution by calculating the donor-acceptor distance as a function of the measured transfer efficiency. Ligands that bind the minor groove of DNA have been demonstrated to induce deformations qualitatively different from those induced by base intercalators. Consequently, we proposed an easy and cheap method to discriminate between the binding modes of ligands, alternative to common techniques that are based either on gel separation of restriction enzymes-digested DNA or on nuclear magnetic resonance measurements, or on the reconstruction of the bound-complex crystal-structure by X-ray diffraction.

By the same method we also quantified the (greater) D-A distance variations that occur when hybridization is impaired by single-nucleotide mismatches [37]. By hybridizing an AT oligonucleotide of 25 base pairs, carrying the same D-A pair of above, to AT oligonucleotides differing by single A→T substitutions we found definitely different  $\tau_D$  values. The same kind of analysis was performed with target oligonucleotides reproducing the polymorphic sequences of HLA-DQB1 gene between codons 52 and 57 [38]. Some of these allelic variants differ by a single nucleotide. An oligonucleotide complementary to DQB1 allele 0201, which is frequently found in IDDM patients, was used as the only dual D-A labeled probe [9]. By means of an optimized TCSPC apparatus, we measured the  $\tau_D$  values corresponding to the 0201 probe hybridized with each allele-specific oligonucleotide at very low hybrid concentration. We found a statistically different  $\tau_D$  value for each allele-probe

pair, indicating that  $\tau_D$  measurements allow distinguishing even DQB1 alleles with a single mismatch.

In this Chapter we describe the principles of TCSPC and the optimized setup that allows us to perform decay time measurements with 60% detection quantum efficiency and <30 ps temporal resolution. We report on our recent applications to SNP genotyping and discuss the pertaining results. Finally, an unpublished feasibility study performed in view of the application of our method to cellular lysates is presented. This study demonstrates that we are able to discriminate, in our time-resolved fluorescence decays, the contribution of flavines, *i.e.* the only expected endogenous fluorophores whose excitation and emission spectra are, although minimally, superimposed to that of our D-fluorophore.

## II. EXPERIMENTALS

### A. (Bio)Chemicals and Sample Preparation

#### *Oligonucleotides*

Donor-Acceptor labeled oligonucleotide probes, purified by double HPLC procedure, were purchased from Sigma-Genosys.

For the experiments on the dependence of the D fluorescence lifetime  $\tau_D$  upon the position of single base mismatches we used an AT oligonucleotide probe in which the D-fluorophore bound at the 5' end was 5-Carboxytetramethylrhodamine (TAMRA), and the A bound at the 3' end was the Sigma-Aldrich patented, non-emitting quencher Black Hole Quencher 2 (BHQ2), which is a polyaromatic azo compound that is capable of efficient quenching of many of the most widely used chromophores and does not exhibit detectable fluorescence. The formulas of TAMRA and BHQ2 are reported in Figure 1(a). Unlabeled Oligos with perfectly complementary sequence or containing single A→T substitutions at different positions, purified by DST and double RP1 procedures, were also purchased from Sigma-Genosys. The sequences of the probe and targets are reported in Figure 1(b). The probe sequence was optimized to reduce the formation of dimers and of secondary structures. The probe and the target oligos used for HLA-DQB1 typing are shown in Figure 1 (c). The probe was synthesized according to the sequence of DQB1 0201 allele between codon 52 and 57. The same codons' interval was covered by the oligonucleotides used as targets. All the oligonucleotides were dissolved in PBS at 100 µM concentration and stored at -20°C until use. The dual-labelled probe was hybridized to each target sequence by mixing the single stranded oligos in equal concentrations (50 µM), heating up to 98°C and leaving the samples cool very slowly down to room temperature. This procedure assured denaturation of secondary structures of the single strands. The annealed DNA samples were kept frozen at -20°C until use. The fluorescence decay measurements were carried out on samples diluted to 250 nM concentration.

#### *Flavine mononucleotide*

The free chromophore flavine mononucleotide (FMN) ( $\geq 97\%$  pure) was a kind gift of Prof. G. Bottioli (Institute for Molecular Genetic, Italian C. N. R., Pavia). A 5-mM stock solution of the chromophore in bidistilled water was prepared. The absorption spectrum of a

FMN sample, diluted to 100  $\mu$ M, was acquired with a spectrophotometer (Lambda 2 Perkin Elmer) in order to evaluate the FMN absorption in the TAMRA excitation spectral band. The FNM fluorescence decay was measured on a sample at 500  $\mu$ M concentration. The FMN chromophore at the same concentration value was also added as a contaminant to a SNP genotyping reaction mixture containing 250 nM of the TAMRA-(AT)-BHQ2 oligoprobe hybridized to the target sequence S0.

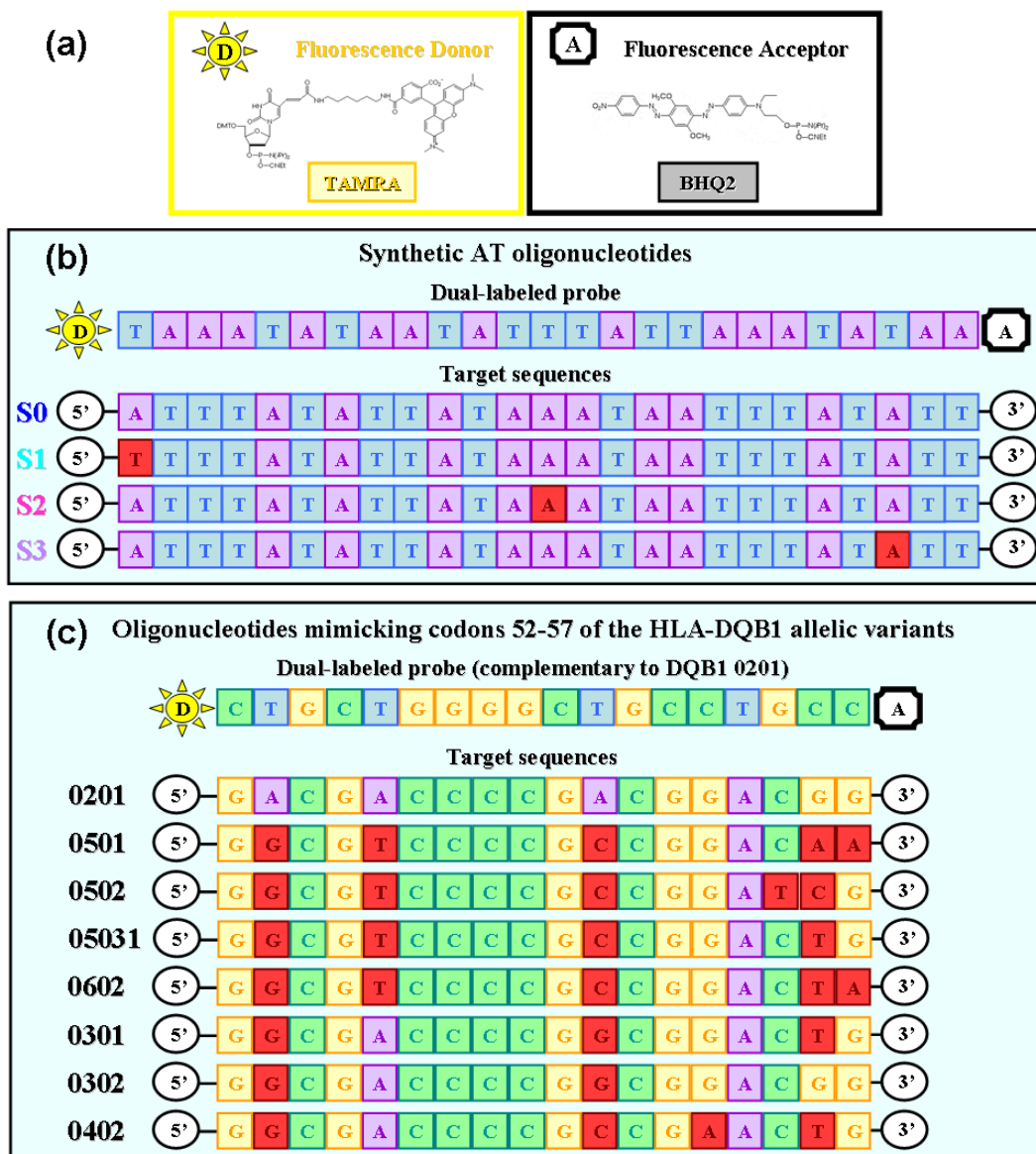


Figure 1. (a) Structures of TAMRA (donor D) and BHQ2 quencher (acceptor A). (b) Sequences of the AT synthetic oligonucleotides used as dual labeled probe (top) and as target sequences (S0: sequence perfectly matching the probe; S1-S3: sequences carrying variations, as indicated in red). (c) DQB1 0201 dual-labeled oligoprobe and target oligonucleotides corresponding to sequences, between codon 52 and 57, of the HLA-DQB1 alleles listed on the left.

## B. Principles of Time-Correlated Single-Photon Counting

In time-resolved fluorescence experiments, the fluorescent sample must be excited by a light pulse much shorter than the excited singlet-state lifetime (virtually  $\delta$ -like) and the emitted pulse must be detected with equally high temporal resolution. As the detected fluorescence pulse is subject to different sources of fluctuations, the excitation/detection event must be repeated many times and an averaging procedure must be applied to the time-resolved detector output to achieve a significant fluorescence decay measurement. When the fluorescence decay contains transients definitely faster than 1 ns, only streak cameras can be used as the detectors capable of sufficient temporal resolution. An alternative endowed with high efficacy exists if the fluorescence can be excited, at the desired excitation wavelength, by the train of equally spaced ultra-short laser pulses generated by a continuous-wave mode-locked laser. In such a case the temporal profile of the (train of) fluorescence pulses can be very effectively recovered by applying TCSPC. Namely, in TCSPC at most one fluorescence photon is detected from each pulse of the train to be analyzed. The arrival of each fluorescence pulse of the train is heralded by a signal synchronous with the excitation pulse that triggers the timing device. The latter is a device capable of measuring the time elapsing from the heralding signal to detection of the fluorescence photon (lag time) at each repetition of the excitation/detection event. The lag times over many repetitions are digitized and binned into intervals that can be as short as fractions of picosecond. The number of times that a photon has been detected within each lag interval is counted in order to record a histogram of the number of detected photons versus time analogous to those that would be ideally obtained by digitizing and averaging the output of a streak camera.

The first essential component of any TCSPC apparatus is the light source. The light source has two main functions in a TCSPC apparatus: the first is to deliver onto the sample  $\delta$ -like pulses of excitation light; the second is to provide the START signal heralding the fluorescence pulses and triggering the timing device. The light source of a TCSPC system must deliver pulses of very brief duration at a very high rate, with minimal jitter in the excitation time, in order to register the histogram of the number of detected photons versus time, that is, the fluorescence decay, in reasonable acquisition times. The second component of a TCSPC setup is the single-photon detector, which can be either a photomultiplier tube, or a reach-through mode avalanche photodiode (APD), or a single-photon avalanche diode (SPAD). SPADs are a particular class of APDs, which are not only able to detect extremely low intensity signals (down to single photons), but also to measure the time of the photon arrival very precisely, with few tens of picoseconds resolution [40]. The SPADs, like any other APD, exploit the photon-triggered avalanche current of a reverse biased p-n junction to detect an incident radiation. The fundamental difference between SPADs and APDs is that SPADs are specifically designed to operate with a reverse bias voltage well above the breakdown voltage (on the contrary APDs operate at a bias slightly below the breakdown voltage). This kind of operation is also called Geiger mode in literature. The function of the detector in the TCSPC system is to convert a photon impinging on its sensitive area into a photoelectron with almost unitary efficiency and to subsequently amplify the microscopic photoelectric current in order to obtain a macroscopic current pulse. The current pulse generated by a detected photon should be much higher than the parasitic currents intrinsic to the detector circuitry, in order to avoid “fictitious photon” detection. In other words, the

detector “operational gain” should be as high as possible. Finally, in any single photon detector there are thermal and/or electronic processes leading to dark count events. Dark counts are processed such as real photo-detection events. Detection of dark counts diminishes the signal-to-noise ratio, especially when very weak light pulses are to be analyzed. For these reason it is desirable that the detector of an efficient TCSPC system be endowed with negligible dark count rate. The properties that a detector must have in order to assure high time resolution in TCSPC measurements will be discussed after explaining the operating principles of the time to amplitude converter (TAC). Before triggering the TAC, both the START and the STOP signals are evaluated by a discriminator. The discriminator is a key element in any TCSPC system, as it is the unit that makes TCSPC essentially insensitive to the noise problems which plague the analogical methods of light analysis. A discriminator is an electronic circuit designed to discriminate between current intensity levels. If the input signal to the discriminator is below a specified threshold the signal is ignored; conversely, an input signal above threshold is recognized, causing the discriminator to produce a very neat output pulse which in turn is delivered to the TAC. By setting the discriminator threshold level to a current value substantially greater than the detector mean parasitic current level, but smaller than the detector photocurrent pulse amplitude, the detector noise can be removed from the data. More details on our discriminator, actually a constant-fraction discriminator, are given in the next section. The central element in a TCSPC system is the TAC. A TAC can be viewed as a very precise stopwatch, with the excitation pulse providing the START signal and the fluorescence pulse providing the STOP. When it receives the START signal, the TAC begins to charge the plates of a capacitor by means of a precisely controlled constant current. When it receives the STOP signal, the TAC suddenly stops the current flow through the capacitor plates, and generates an analogical voltage pulse whose amplitude is equal to the potential difference  $\Delta V$  between the capacitor plates. The latter is proportional to the time lapse between the START and the STOP signals. In other words (hence the instrument name) the TAC associates a voltage pulse of well defined amplitude to any START/STOP time lag. As the TAC current starts flowing with a fixed delay from production of the START pulse by the START discriminator, and stops flowing with a fixed delay from production of the STOP pulse by the STOP discriminator, the precision with which a fluorescence photon is timed does not depend on the actual pulse width of the detector photocurrent pulse, as would happen in any analogical technique, but rather from the time jitter between detection of a photon and emission of the corresponding photocurrent pulse. This jitter must be the smallest possible to assure good timing performances in TCSPC experiments. The timing accuracy can be up to 10 times better than the full width at half maximum of the detector pulse response. It should also be noted that TCSPC provides a differential time measurement, which is virtually unaffected by drifts and instabilities in the light source pulse period. The analog-to-digital converter (ADC) measures the amplitude of the voltage pulse coming from the TAC to determine which slot of the histogram approximating the detected photons temporal distribution a particular detected photon should be recorded into. It sends that “time slot information” to the multi-channel analyzer (MCA) in form of a digital channel number. Upon receiving the channel number, which is really just a memory address, the MCA adds one to the contents of that memory cell to record the fact that a photon was just detected with that specific START/STOP time lag. This process, which overall typically takes only a few microseconds, or even less, is then repeated over and over again until the events being recorded yield a reliable approximation of the actual temporal distribution to be studied.

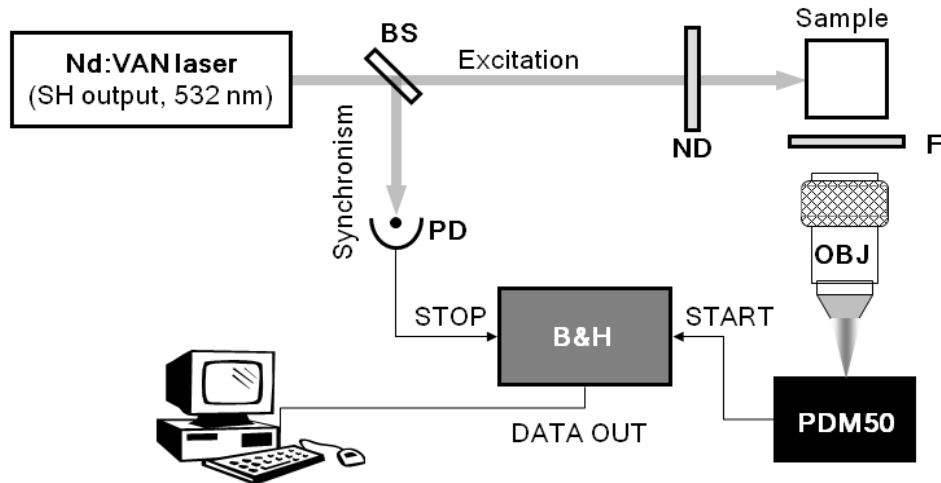


Figure 2. Experimental setup. BS, beam splitter; PD, fast photodiode; ND, neutral density filters; F, cut-off filter; OBJ, 20X microscope objective; PDM50, single-photon avalanche diode (SPAD) detector; B&H, acquisition package.

### C. Our Time-Correlated Single-Photon Counting Setup

Our TCSPC experimental setup [37, 38, 41] is sketched in Figure 2. For the measurements presented here, we used a continuous wave SESAM mode locked Nd:VAN laser (fundamental wavelength 1064 nm) as the excitation source emitting pulses at 113 MHz repetition rate, with 9 ps pulse width (GE100-SHG, Time Bandwidth Products, Zurich, CH). All samples were excited at 532 nm by the Nd:VAN built-in second harmonic output.

The emitted light is collected at 90 deg to the excitation beam through a 600 nm cut-off (long-wavelength pass) filter (LL-600, Corion, Holliston, MA), and focused by means of a 20X microscope objective on the sensitive area of the detector, a SPAD featuring 50  $\mu\text{m}$  diameter of the sensitive area, <50 Hz dark count rate and built-in active quenching circuitry (PDM50, Micro-photon-devices, Bolzano, IT), and assuring 70 ns dead-time. The TCSPC system is run in a reversed START/STOP configuration, which allows preventing the delivery to the TAC of an abnormal number of START signals when the TCSPC device is used to study very rare (single photon) events, such as fluorescence emission by low fluorescence quantum yield molecules. In these conditions, most START signals from the synchronism

branch of the timing setup would not be followed by the detection of photons on the fluorescence-detection branch within a temporal acquisition window. In the subsequent TAC dead time, any detection event would not be time-correlated. The START/STOP reversal method consists in inverting the START and STOP connections of the TAC, so that the timing process be started by the detection of a fluorescence photon by the SPAD detector. In this way, the TAC is ready to accept a START all the times a fluorescence photon is (rarely) detected. Moreover, the TAC is stopped for sure within the temporal width of the acquisition window by the laser pulse subsequent to that producing the fluorescence photon. In our

TCSPC system the STOP is given by a PIN photodiode monitoring the laser pulses. Actually the START and STOP signals are directly delivered to one board of an SPC 152 package (Becker & Hickl, Berlin, DE), integrating a constant-fraction discriminator (CFD) on both the START and the STOP channel, the TAC, the ADC and the MCA [42]. The two CFDs split their respective input pulses in two parts. One of them is anticipated/delayed by about one half of the rise time with respect to the other, reversed and attenuated by an arbitrary factor, the so called “constant fraction” (optimal values of the attenuation factor range approximately from 0.3 to 0.7). The two pulses are then subtracted one to the other, and a comparator is used to detect the instant in which the current zero-level (that is the mean dark current level) is crossed by the difference pulse. It can be demonstrated that such zero point is independent from the original pulse amplitude value. In other words, differently from threshold discriminators, a CFD builds an amplitude jitter-free reference (the zero-crossing point) to trigger the generation of the START and STOP signals to be delivered to the TAC. The SPC 152 MCA is endowed with 2.44 ps bin width in a 10 ns time window. Although the MCA operates at 12 bits, <1% differential nonlinearity is assured by a proprietary error-correction technique based on a modified dithering process [42]. Moreover, thanks to 12 bits operation, the output of the TAC can be digitalized at the very high rate of 10 MHz. The overall time resolution of our TCSPC apparatus is 30 ps (full width at half maximum of the detected laser pulses).

## D. Data Acquisition and Analysis

For each sample three independent and subsequent decay distributions were acquired. The experimental decays were processed as follows in order to determine the values of the fluorescence decay time,  $\tau_D$ , of TAMRA attached to each probe-target duplex. The  $\tau_D$  values reported in this Chapter are the average of the values determined by processing the three replica decays, and the standard deviations are assumed to represent the experimental errors.

The decays of TAMRA labeling the probe in the first line of Figure 1(b)) hybridized to any of the target sequences in the same figure, thanks to optimal labelling/purification and very low tendency to form secondary structures, displayed a two-exponential decay, with a short-lived component (decay time  $\tau_{coll} \cong 40$  ps) due to the emission of residual single stranded probe and a definitely longer component corresponding to the fluorescence emission of the hybridized probes. In order to accurately determine the decay time,  $\tau_D$ , of this second component, it has been sufficient to fit the decay patterns to a single exponential above a constant background, starting the fit 50 ps after the peak channel of the decay distribution [37].

The decay patterns detected for the fluorescence of TAMRA labeling the probe (see first line in Figure 1(c)) mimicking the complementary trait of the DQB1 0201 allele between codons 52 and 57, were much more complicated for hybridization with any of the target alleles listed in the lower part of Figure 1(c). Indeed, in all such decays, included the one pertaining to the single stranded probe, we recognized a slowly decaying component typical of unquenched TAMRA that revealed the presence of substantial amounts of either free TAMRA molecules, or TAMRA molecules carried by probe oligonucleotides missing the BHQ2 quencher or both. Moreover, even disregarding the emission of unquenched TAMRA,

the single-stranded probe decay was not a single exponential. For these reasons we devised [38] the following data acquisition/analysis protocol in order to extract, from the obtained multi-exponential decay distributions, the valuable information, that is the decay time of TAMRA molecules attached to probes correctly hybridized to their target sequences and bearing a functional BHQ. First, in all cases, we accumulated counts for the same measuring time (5,000 s). In order to reconstruct the fluorescence decays of TAMRA for the probe interacting with each of the target oligonucleotides, the corresponding decay patterns were compared to the decay pattern acquired in the same measuring time for the pure single-stranded probe at the same concentration. As in any double-stranded structure, more or less disturbed by base mismatching errors, FRET is less efficient in quenching the TAMRA fluorescence than in any possible conformation of the single stranded probe, the tail of the single-stranded probe decay should approach at best the decay of unquenched TAMRA. Thus, we fit this tail with a single exponential and preliminarily subtract this exponential from the decay pattern of the probe alone and (with the same initial amplitude) from the decays of all the hybridized samples. The resulting decay distributions are normalized to their integrals. Let us call these normalized decays  $F_{\text{probe}}$  and  $F_{201}$ ,  $F_{501}$ ,  $F_{502}$ , ..., shortly  $F_{\text{xxx}}$ . We then observe that  $F_{\text{probe}}$  is well fitted by a three-exponential decay

$$Y_{\text{probe}}(t) = A_{1p} \exp(-t/\tau_{1p}) + A_{2p} \exp(-t/\tau_{2p}) + A_{3p} \exp(-t/\tau_{3p}) \quad (1)$$

and that the  $F_{\text{xxx}}$  are well fitted by four-exponential decays

$$Y_{\text{xxx}}(t) = A_{1\text{xxx}} \exp(-t/\tau_{1\text{xxx}}) + A_{2\text{xxx}} \exp(-t/\tau_{2\text{xxx}}) + A_{3\text{xxx}} \exp(-t/\tau_{3\text{xxx}}) + A_{4\text{xxx}} \exp(-t/\tau_{4\text{xxx}}) \quad (2)$$

Of the fittings in Eq. (1) and Eq. (2) we only use the information on  $A_{1p}$ ,  $A_{2p}$ ,  $A_{3p}$  and  $A_{1\text{xxx}}$ ,  $A_{2\text{xxx}}$ ,  $A_{3\text{xxx}}$  to perform the following weighted subtraction of the fluorescence of the non-hybridized probe from the experimental  $F_{\text{xxx}}$  decays:

$$F_{\text{xxx}} - \frac{A_{1\text{xxx}} + A_{2\text{xxx}} + A_{3\text{xxx}}}{A_{1p} + A_{2p} + A_{3p}} F_{\text{probe}} \equiv D_{\text{xxx}} \quad (3)$$

Each  $D_{\text{xxx}}$  could be satisfactorily fitted by a single exponential decay, and developed over a dynamic range of two decades at least. This single exponential decay was interpreted as the decay of the fluorescence arising from the TAMRA molecules attached to probe-DQB1  $\text{xxx}$  target duplexes. Hence, the decay constant recovered from the fit of  $D_{\text{xxx}}$  is the relevant  $\tau_D$  value characterizing the degree of matching between the probe and the specific allelic target  $\text{xxx}$  (see Introduction).

Figure 3 illustrates the procedure we apply to the rough decay patterns in order to get the  $D_{\text{xxx}}$  decay distribution. In Figure 3(a) we use a logarithmic scale to plot the decay patterns recorded for the single-stranded probe (curve SS probe) and for the sample containing the probe annealed with one of the target sequences, namely DQB1 0602, thus containing probe-target hybrids (curve HYBR). The single exponential fit of the SS-probe tail, by which we determine time constant and amplitude of the decay component associated to unquenched

TAMRA emission to be subtracted from all the decay patterns, is represented by the dashed green line. Figure 3(b) shows  $F_{probe}$  and  $F_{602}$ . Although  $F_{602}$  is expected to contain a contribution with the same shape as that of  $F_{probe}$ , owing to the unavoidable presence of a non-hybridized fraction of the probe,  $F_{602}$  definitely decays more slowly than  $F_{probe}$ . This indicates that the contribution to  $F_{602}$  of fluorescence emission by TAMRA molecules labelling DQB1 0201-DQB1 0602 duplexes is sizeable. The exact fraction of non-hybridized probe can be determined and subtracted from  $F_{602}$  by applying Eq. (3). The final result, curve  $D_{602}$ , and its single exponential best fitting curve, which provides the value  $\tau_D = 877 \pm 3$  ps, are plotted in Figure 3(c).

### III. RESULTS AND DISCUSSION

We first report our results on the effects of single-nucleotide mismatches on the structures of our synthetic AT duplexes. We give particular consideration to the entity of variations in the TAMRA lifetime and to their dependence on the mismatch position. We remind that for these optimized oligonucleotides the fluorescence decays are single exponentials, provided that the first 50 ps are disregarded. The TAMRA decay distributions obtained for the probe hybridized with each of the target sequences, see Figure 1(b), are reported in Figure 4.

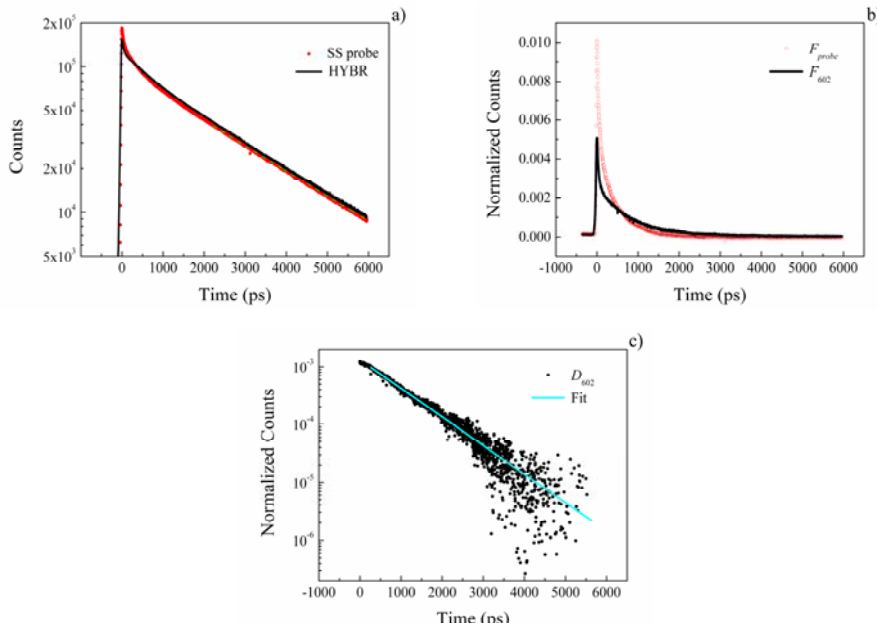


Figure 3. (a) Fluorescence decay patterns observed with the single-stranded TAMRA/BHQ2 dual-labeled DQB1 0201 probe (curve SS probe) and with the probe hybridized to the target sequence of DQB1 0602 allele (curve HYBR). Single exponential fit of the curve SS probe at long times (dashed green line). Logarithmic scale. (b) Plots of the corresponding corrected and normalized curves (see text),  $F_{probe}$  and  $F_{602}$ . (c) Fluorescence decay,  $D_{602}$ , of the 0201-probe hybridized to the target sequence 0602 and single exponential fit,  $\tau_D = 877$  ps. Logarithmic scale.

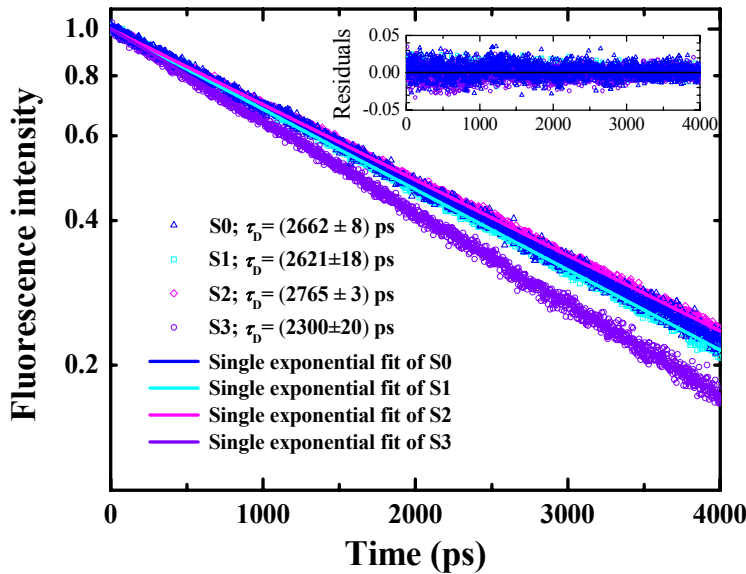


Figure 4. Experimental decay patterns of the TAMRA donor attached to the dual-labeled probe annealed with the target sequence 0 (grey dots) and with the single-nucleotide mismatched sequences 1 (black dots), 2 (crosses) and 3 (open circles). The single exponential fits are reported as solid lines of the same colors. The residuals are plotted in the inset.

Fitting triplicate data files gave the following  $\tau_D$  values ( $\pm$  standard deviation):  $\tau_D^{(0)} = 2662 \text{ ps} (\pm 8 \text{ ps})$  for the perfectly hybridized sample (sequence S0, blue in Figure 4), the smaller values  $\tau_D^{(1)} = 2621 \text{ ps} (\pm 18 \text{ ps})$  and  $\tau_D^{(2)} = 2300 \text{ ps} (\pm 20 \text{ ps})$  for hybridizations with sequences S1 and S3 (cyan and violet in Figure 4) and the greater value  $\tau_D^{(3)} = 2765 \text{ ps} (\pm 3 \text{ ps})$  for the hybridization with sequence S2 (magenta in Figure 4). The residuals of the fittings are displayed in Figure 4 inset. We thus found that sequence mismatches at positions next to either of the two ends of the oligonucleotide, as in the cases of sequences S1 and S3 in Figure 1(b), cause a shortening of the D fluorescence lifetime as compared to  $\tau_D^{(0)}$ , whereas a mismatch in a mid position, such as that in sequence S2 of Figure 1(b) yields  $\tau_D^{(3)} > \tau_D^{(0)}$ .

In the following, an explanation of the observed changes in the TAMRA lifetime, hence in the TAMRA-BHQ2 distance, upon introducing single nucleotide substitutions in the target oligonucleotides, is attempted. Namely, we believe that matching errors towards the ends of the double-stranded structure, where D and A are attached, diminish the D-A distance by preventing the rest of lateral bases to match and letting the ends of the D-5'(AT)3'-A be free to bend. This picture is supported by the fact that  $\tau_D^{(1)} > \tau_D^{(2)}$ , being the error at the first base for sequence S1 and at two bases before the end in the case of sequence S3. On the contrary a mismatch near the centre of the double-stranded structure as in the case of sequence S2 brings about an increase in the D-A distance, which can be indicative of unwinding. These situations are sketched in Figure 5.

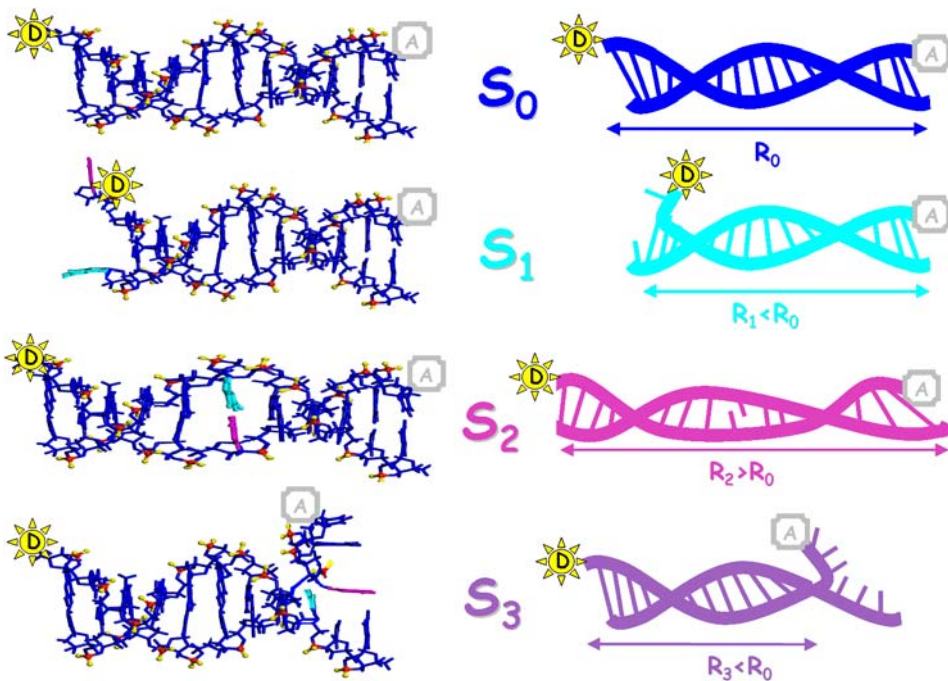


Figure 5. Matching errors towards either of the ends of the DNA duplex (see S1 and S3) diminish the D-A distance maybe by preventing the rest of lateral bases to match and letting the ends of the probe free to bend. On the contrary a mismatch near the centre of the duplex (see S2) brings about an increase in the D-A distance, which can be indicative of some unwinding.

The results of our  $\tau_d$  measurements indicate that single base mismatches in oligonucleotide duplex structures of several tens of base pairs can be safely revealed by time-resolved FRET measurements operated on donor-acceptor pairs labelling one single base mismatch in oligonucleotide duplex structures of several tens of base pairs can be safely revealed by time-resolved FRET measurements operated on donor-acceptor pairs labeling one of the sequences

forming the duplex and that the approximate position of the mismatch can also be inferred. As base mismatches at the edges and in the middle of synthetic DNA duplexes seem to induce opposite effects on the donor decay time value the question arises whether or not the time resolved FRET method is adequate to type naturally occurring allelic variants differing by more than one nucleotide. Indeed, in such an instance it is possible *a priori* that the effects of two mismatches occurring at different positions of the probe-target duplex cancel each other.

Polymorphisms constitute such a diverse ensemble with respect to both the number and position of mismatches, and the fluorogenic oligonucleotide probes can be designed in such an ample span of modes, that giving a general answer to this question is virtually impossible. A practical approach could be that of performing preliminary studies with oligos representative of the different alleles of a gene of interest in order to assess whether our time-resolved FRET method could be extended to the typing of that polymorphic genetic system. Moreover, such kind of studies should be of help in the design of optimized.

We have chosen to address, as a paradigmatic case, the complex polymorphism of the HLA DQB1 gene (see Introduction). We used a 18-nucleotide probe (Figure 1(c)), complementary to the 52-57 codon interval of 0201 allele, which presents a mismatch with all the other target oligonucleotides in correspondence to the second nucleotide of codon 52. This choice was intended to obtain hybrids with a mismatch at the D-labeled end of the probe and, thus, a shortening in the corresponding TAMRA lifetime, similarly to what was observed with our sample sequence S1. Moreover, in order to get mismatches of S3 type and to possibly reveal further shortening of  $\tau_D$ , the probe sequence was terminated in correspondence to the other highly polymorphic codon 57, in which 6 of the 7 allelic variants analysed differ from 0201 by one or more nucleotides. Few other polymorphisms with respect to allele 0201 are scattered along the target DNA sequence. One of them, common to all the other alleles, is located nearly at the center of DQB sequence at codon 55 and is in a position similar to that occurring in our sample sequence S2. This variation is expected to lead to an increase in  $\tau_D$ , though we deem that its effect alone would be minor than the combined shortening effects of polymorphisms at codons 52 and 57. The probe matched any target sequence for at least two complete codons, assuring sufficient affinity for the target recognition.

In order to quantify the relative FRET efficiency between the TAMRA donors and BHQ2 acceptors corresponding to each probe-target duplex, we applied the data analysis procedure described above (see Data acquisition and analysis).

The corresponding  $\tau_D$  values are listed in Table 1, together with their spreads for repeated measurements. The small spreads indicate that the results are accurately reproducible. The  $\tau_D$  values are significantly different for all targets and definitely different from the non-quenched fluorescence decay time of TAMRA, which is  $2519 \pm 67$  ps. Moreover, the greatest  $\tau_D$  is indeed obtained in the case of the target sequence 0201. In all other sequences the A-nucleotide of codon 52 in 0201 is substituted by a G-nucleotide. Allele 0302 differs from allele 0201 by a single additional substitution at codon 55. Interestingly, in this case the donor lifetime ( $\tau_D^{(302)} = 2083 \pm 11$  ps), although significantly different, is the most similar to that obtained for the perfectly complementary target 0201, reflecting the fact that the central mismatch at codon 55 might partially compensate the shortening effect of the lateral mismatch at codon 52. Sequence 0301 ( $\tau_D^{(301)} = 2008 \pm 15$  ps) bears another substitution in lateral position, namely at codon 57: indeed,  $\tau_D$  is significantly shorter than that measured with target allele 0302. Sequence 0402 is further substituted at codon 56, five nucleotides upstream to the 3' end.

On the contrary, alleles 0501, 0502, 05031, and 0602, have a T nucleotide instead of an A nucleotide at codon 53, 5 nucleotides downstream to the 5' end. It can be noted that substitutions at 5 nucleotides from the opposite ends, either downstream or upstream, bring about a dramatic shortening of  $\tau_D$ . Possibly, no pairing occurs between the probe and the four nucleotides that precede or follow the mismatch, respectively.

Sequence 0602 gives rise to mismatches at the same position as sequence 0501, which produces a rather similar lifetime ( $\tau_D^{(602)} = 877 \pm 3$  ps,  $\tau_D^{(501)} = 955 \pm 4$  ps). Such a similarity may suggest that the type of substitution is less important than its position in determining the efficiency of FRET in quenching the TAMRA fluorescence.

**Table 1.** Fluorescence decay times,  $\tau_D$ , measured for the double stranded samples obtained upon hybridization of the TAMRA/BHQ2-labeled probe of sequence 0201 to the different target sequences.

Target Sequence	$\tau_D$ (ps)
0201	$2241 \pm 3$
0501	$955 \pm 4$
0502	$656 \pm 10$
05031	$1189 \pm 19$
0602	$877 \pm 3$
0301	$2008 \pm 16$
0302	$2083 \pm 11$
0402	$1291 \pm 21$

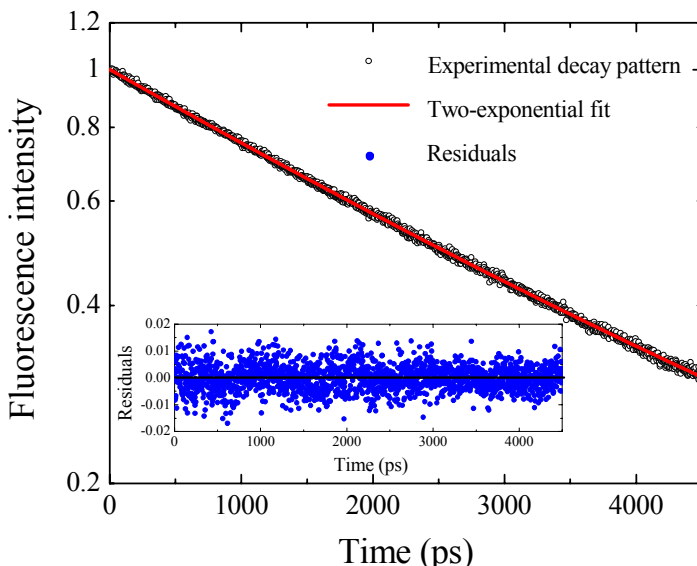


Figure 6. Fluorescence decay of the TAMRA-(AT)-BHQ2/FMN mixture (black empty circles) together with best bi-exponential fitting curve (red solid line). The residuals of the fit are reported in the figure inset (blue dots).

If the mismatch occurs at three nucleotides from the end, as in the case of sequence 0502, instead of at the final nucleotide (see 0602 and 0501), the lifetime takes a definitely shorter value, that is  $\tau_D^{(502)} = 656 \pm 10$  ps. This confirms our model, forecasting the last three bases to remain unpaired in the probe-0502 target duplex. It is also interesting to note that sequences 0402 and 05031, which bare simmetric lateral substitutions with respect to 0201, are characterized by very similar  $\tau_D$ 's ( $\tau_D^{(402)} = 1291 \pm 21$  ps,  $\tau_D^{(5031)} = 1189 \pm 19$  ps). This result indicates that the conformations of the duplexes obtained hybridizing the probe with the two "mirror image" mutated target sequences are also very similar.

In the introduction, we mentioned the interference of endogenous chromophores as a limitation of the techniques adopted in [35, 36]. To this regard, a first advantage of our

approach over that of AlAttar and coworkers is that, while the cationic conjugated polymer that these Authors use as the donor displays its absorption maximum at 380 nm, in a region of the spectrum where also the fluorescence of most endogenous fluorophores is efficiently excited, our donor is best excited by green light, which is (weakly) absorbed only by certain flavines. It is worth noting that, while we detect and analyze the donor fluorescence in order to type our samples, AlAttar and coworkers work on the relatively red shifted acceptor fluorescence signal. Moreover, the detectors featuring the highest gains, be they proportional or Geiger-mode, are best performing in the blue-green band and display much lower detection quantum efficiency at longer wavelengths. For this reason, excitation of the donor at wavelengths efficiently absorbed by many endogenous fluorophores might be an unavoidable drawback of the conjugated polymers technique, even assumed that suitable polymers absorbing at longer wavelengths exist. However, in the case we would directly apply our method to unpurified cellular extracts, the endogenous fluorophores fluorescing at the same wavelengths as TAMRA should simply add exponential decay components to the detected fluorescence decay distribution.

Such contaminant decay components can be discriminated in the decay and do not prevent precise determination of the donor lifetime. To this aim, we first accurately measured multiple fluorescence decays of flavine mononucleotide (FMN), the endogenous fluorophore having the excitation band most superimposed to that of TAMRA, with excitation with the 532 nm second harmonic of our laser. We could satisfactorily fit the FMN with single exponential decay above a constant background, and we obtained the average value ( $\pm$  standard deviation)  $\tau_{FMN} = 4126 \pm 5$  ps for the FMN fluorescence lifetime (data not shown). We then prepared a double-stranded AT sample performing the usual annealing procedure between the AT dual-labelled probe of Figure 1(b) and the perfectly complementary target oligonucleotide S0, at final TAMRA concentration 250 nm. As the absorption of FMN is very low at 532 nm, we added to the sample 500  $\mu$ M of FMN and recorded the fluorescence decay of the mixture. We fitted the obtained decay pattern with two exponential components above a constant background. The time constant of one component was fixed at  $\tau_{FMN}$ , 4126 ps. The fitting procedure yielded for the other component, representing the decay of TAMRA fluorescence, the value  $\tau_D^{(0)} = 2666$  ps ( $\pm 10$  ps), which is equal, within the experimental errors, to that obtained for the uncontaminated sample. The fluorescence decay of the mixture is plotted (black circles) in Figure 6, together with the two-exponential fit, (red solid line) and the residuals (blue dots). Considered that, in cellular extracts, no natural contaminant absorbing green light can be present in amounts as relevant as in our mixture, we believe that this result strongly supports the applicability of the method on non-purified samples.

#### IV. CONCLUSION

We have proved the potential of a time-resolved FRET technique in recognizing target oligonucleotide sequences reproducing a highly polymorphic genomic region of human DNA, whose allelic variants are associated to the development of IDDM. We demonstrated that this technique can be applied to reliably “type” each target by means of a single oligonucleotide probe. In addition, we worked with so small amounts of target DNA (few milliliters of

nanomolar-concentrated samples) that we are confident on the applicability of this technique to non-amplified genomic templates in the future. Finally, we devised a data-processing protocol that virtually allows getting rid of contributions to the fluorescence decays other than those produced by the probe when it is successfully hybridized to the target. This protocol might be relevant in view of applications to non-purified DNA samples. It is worth noting that although we adopted a sophisticated physical method, which is however routinely used in molecular fluorescence spectroscopy, the measuring apparatus is entirely made up of commercial components. The results of this preliminary study may open the possibility to perform HLA molecular typing on large populations, particularly in situations in which HLA polymorphisms is strongly associated to specific disease conditions.

## REFERENCES

- [1] Rocha, D; Gut, I; Jeffreys, AJ; Kwok, PY; Brookes, AJ; Chanock, SJ. *Hum. Genet.* 2006, 119, 451-456.
- [2] Strittmatter, WJ; Roses, AD. *Proc. Natl. Acad. Sci., USA*, 1995, 92, 4725-4727.
- [3] Altshuler, D; Hirschhorn, JN; Klannemark, M; Lindgren, CM; Vohl, MC; Nemesh, J; Lane, CR; Schaffner, SF; Bolk, S; Brewer, C; Tuomi, T; Gaudet, D; Hudson, TJ; Daly, M; Groop, L; Lander, ES. *Nat. Genet.*, 2000, 26, 76-80.
- [4] Greenblatt, MS; Bennett, WP; Hollstein, M; Harris, CC. *Cancer Res.*, 1994, 54, 4855-4878.
- [5] Marsh, S; Kwok, P; McLeod, HL. *Hum. Mutat.*, 2002, 20, 174-179.
- [6] Germain, RN. *Cell*, 1994, 76, 287-299.
- [7] Nepom, GT. *Immunol. Today*, 1990, 11, 314-315.
- [8] Todd, JA; Bell, JI; McDevitt HO. *Nature*, 1987, 329, 599-604.
- [9] Tosi, G; Mantero, G; Magalini, AR; Primi, D; Soffiati, M; Pinelli, L; Sartoris, S; Tridente, G; Accolla, RS. *Molec. Immunol.* 1993, 30, 69-76.
- [10] Tosi, G; Brunelli, S; Mantero, G; Magalini, A. R; Soffiati, M; Pinelli, L; Tridente, G, Accolla, R. S. *Molec. Immunol.*, 1994, 31, 429-437.
- [11] Tosi, G; Facchin, A; Pinelli, L; Accolla, RS. *Diabetes Care*, 1994, 17, 1045-1049.
- [12] Kim, S; Misra, A. *Ann. Rev. Biomed. Eng.*, 2007, 9, 289-320.
- [13] Lyamichev, V; Mast, AL; Hall, JG; Prudent, JR; Kaiser, MW; Takova, T; Kwiatkowski, RW; Sander, TJ; de Arruda, M; Arco, DA; Neri, BP; Brow, MAD. *Nat. Biotechnol.*, 1999, 17, 292-296.
- [14] Hall, JG; Eis, SM; Law, LP; Reynaldo, JR; Prudent, JR; Marshall, DJ; Allawi, HT; Mast, AL; Dahlberg, JE; Kwiatkowski, RW; de Arruda, M; Neri, BP; Lyamichev, VI. *Proc. Natl. Acad. Sci., USA* 2000, 97, 8272-8277.
- [15] Kennedy, GC; Matsuzaki, H; Dong, S; Liu, WM; Huang, J; Liu, G; Su, X; Cao, M; Chen, W; Zhang, J; Liu, W; Yang, G; Di, X; Ryder, T; He, Z; Surti, U; Phillips, MS; Boyce-Jacino, MT; Fodor, SPA; Jones, KW. *Nat. Biotechnol.*, 2003, 21, 1233-1237.
- [16] Matsuzaki, H; Dong, S; Loi, H; Di, X; Liu, G; Hubbell, E; Law, J; Berntsen, T; Chadha, M; Hui, H; Yang, G; Kennedy, GC; Webster, TA; Cawley, S; Walsh, PS; Jones, KW; Fodor, SPA; Mei, R. *Nat. Methods*, 2004, 1, 109-111.
- [17] Griffin, TJ; Tang, W; Smith, LM. *Nat. Biotechnol.*, 1997, 15, 1368-1372.

- [18] Saiki, RK; Bugawan, TL; Horn, GT; Mullis, KB; Erlich, HA. *Nature*, 1986, 324, 163-166.
- [19] Gibbs, RA; Nguyen, PN; Caskey, CT. *Nucleic Acids Res.*, 1989, 17, 2437-2448.
- [20] Medintz, I; Wong, WW; Berti, L; Shiow, L; Tom, J; Scherer, J; Sensabaugh, G; Mathies, RA. *Genome Res.*, 2001, 11, 413-421.
- [21] Landegren, U; Kaiser, R; Sanders, J; Hood, L. *Science*, 1998, 241, 1077-1080.
- [22] Nilsson, M; Malmgren, H; Samiotaki, M; Kwiatkowski, DJ; Chowdhary, BP; Landegren, U. *Science*, 1994, 265, 2085-2088.
- [23] Lizardi, PM; Huang, X; Zhu, Z; Bray-Ward, P; Thomas, DC; Ward, DC. *Nat. Genet.*, 1998, 19, 225-232.
- [24] Hardenbol, P; Ban'er, J; Jain, M; Nilsson, M; Namsaraev, EA; Karlin-Neumann, GA; Fakhrai-Rad, H; Ronaghi, M; Willis, TD; Landegren, U; Davis, RW. *Nat. Biotechnol.* 2003, 21, 673-678.
- [25] Hardenbol, P; Yu, F; Belmont, J; Mackenzie, J; Bruckner, C; Brundage, T; Boudreau, A; Chow, S; Eberle, J; Erbilgin, A; Falkowski, M; Fitzgerald, R; Ghose, S; Iartchouk, O; Jain, M; Karlin-Neumann, G; Lu, X; Miao, X; Moore, B; Moorhead, M; Namsaraev, E; Pasternak, S; Prakash, E; Tran, K; Wang, Z; Jones, H. B; Davis, R. W; Willis, T. D; Gibbs, R. A. *Genome Res.*, 2005, 15, 269-275.
- [26] Sokolov, BP. *Nucleic Acids Res.*, 1990, 18, 3671.
- [27] Ronaghi, M; Karamohamed, S; Pettersson, B; Uhlen, M; Nyren, P. *Anal. Biochem.*, 1996, 242, 84-89.
- [28] Langaege, T; Ronaghi, M. *Mutat. Res.*, 2005, 573, 96-102.
- [29] Sanger, F; Nicklen, S; Coulson, A. R. *Proc. Natl. Acad. Sci., USA* 1977, 74, 5463-5467.
- [30] Chen, X; Levine, L; Kwok, P. Y. *Genome Res.*, 1999, 9, 492-498.
- [31] Tyagi, S; Bratu, DP; Kramer, FR. *Nat. Biotechnol.*, 1998, 16, 49-53.
- [32] Myakishev, MV; Khripin, Y; Hu, S; Hamer, DH. *Genome Res.*, 2001, 11, 163-169.
- [33] Chen, X; Kwok, PY. *Nucleic Acids Res.*, 1997, 25, 347-353.
- [34] Chen, LH; Mc Branch, DW; Wang, HL; Helgeson, R; Wudl, F; Whitten, DG. *Proc. Natl. Acad. Sci., USA*, 1999, 96, 12287-12292.
- [35] Gaylord, BS; Massie, MR; Feinstein, SC; Bazan, GC. *Proc. Natl. Acad. Sci., USA* 2005, 102, 34-39.
- [36] Al Attar, HA; Norden, J; O'Brien, S; Monkman, AP. *Biosensors & Bioelectronics*, 2008, 23, 1466-1472.
- [37] Andreoni, A; Bondani, M; Nardo, L. *Mol. Cell. Probes*, 2009, 23, 119-121.
- [38] Andreoni, A; Bondani, M; Nardo, L. *Photochem. Photobiol. Sci.*, 2009, 8, 1202-1206.
- [39] Nardo, L; Bondani, M; Andreoni, A. *Photochem. Photobiol.*, 2008, 84, 101-110.
- [40] Rech, I; Luo, G; Ghioni, M; Yang, H; Xie, X. S; Cova, S. *IEEE j. Sel. Top. Quant.*, 2004, 10, 788-792.
- [41] Andreoni, A; Bondani, M; Nardo, L; Zhao, B; Roberts JE. *Photochem. Photobiol. Sci.*, 2009. Submitted.
- [42] Becker, W. *The bh TCSPC Handbook*; Becker & Hickl GmbH: Berlin, GE, 2006.

## ***Chapter 4***

# **PROTEIN PHOTO-OXIDATIVE DAMAGE – CONSEQUENCES, CHARACTERISATION AND CONTROL**

***Jolon M. Dyer***

Team Leader, Protein and Structure, Growth and Development Section,  
AgResearch Lincoln Research Centre, Cnr Springs Rd and Gerald St, Lincoln,  
Private Bag 4749, Christchurch 8140, New Zealand.

## **ABSTRACT**

UV-induced photomodification of proteins has been implicated in damage to a broad range of different protein-based substrates. Protein photo-oxidation has been linked to such diverse degenerative processes as human hair and skin damage, degradation of pharmaceuticals, reduced food quality and nutrition, discolouration of natural fibres, eye lens opacification, loss of enzymatic activity and crop damage. Ongoing ozone reduction in the stratosphere, with resultant increased exposure to UVB, has generated further impetus for advancing the understanding and controlling the complex protein degradation mechanisms and pathways underlying these damage processes.

For proteins, photo-oxidative damage is generally attributable to the generation and attack of reactive oxygen species (ROS) on amino acid residue side chains and the protein backbone. Singlet oxygen and hydroxyl radicals, in particular, play a significant role in initiating protein modification.

This chapter explores and discusses the complex cascade of modifications induced within proteins through exposure to irradiation, the effect of photo-oxidation on protein substrate properties from the protein primary level through to higher order structure, and the mechanisms underpinning protein photo-oxidation. It will also discuss exciting new approaches to the characterisation, location, tracking, and ultimately control of photo-oxidation within proteins.

## 1. INTRODUCTION

### 1.1. Protein Photo-Oxidative Damage

Understanding and controlling the photodegradation of complex protein-based systems represent significant goals in protein science and photobiology. These goals are also of considerable medical and commercial interest. Ultraviolet light (UV) induced photo-oxidation of proteins has been implicated in damage and degenerative processes within a diverse range of biological systems and protein-based substrates [1]. These include hair damage [2], skin carcinogenesis and ageing effects [3], loss of structural or enzymatic functionality [4, 5], deterioration in food quality [6, 7], eye lens opacification [8-10] and crop damage [11-13]. Continuing ozone depletion in the stratosphere, with a resulting increase in UVB intensity at the earth's surface [14], have added further impetus to studies aimed at elucidating the complex protein photo-oxidation processes underlying this photodamage.

### 1.2. Initiation of Damage

Tryptophan and tyrosine are the two standard amino acid residues in proteins which can absorb light at wavelengths over 290 nm [15, 16]. When oxygen is present, tryptophan excited by UVB can generate singlet oxygen and superoxide anions. Tyrosine can similarly generate ROS through photo-excitation, but this process is less efficient and often results in electron transfer to proximal cystine residues and subsequent cleavage of the disulfide bond [17].

Overall, however, proteins have low absorbance in the solar UV range. Most protein photodamage is therefore the consequence, not of direct UV absorption, but of the attack of reactive oxygen species (ROS) generated through photo-excitation of sensitisers within the proteinaceous substrate [17]. The photoproducts of protein photo-oxidation themselves, such as *N*-formylkynurenine or dityrosine, also act as photosensitisers for production of ROS, such as hydroxyl radicals, thereby promoting further degradation [18, 19]. In addition to tryptophan and tyrosine, crosslinked amino acids, such as desmosine, characteristic of proteins such as collagen and elastin, are also able to absorb UVB radiation, and it is thought that these may also act as photosensitisers [20].

### 1.3. Underpinning Oxidative Mechanisms

ROS may be generated during protein photo-oxidation through both Type I and Type II processes, with Type I reactions yielding free radicals via electron transfer and hydrogen abstraction, and Type II photo-oxidation occurring through energy transfer with molecular oxygen to yield the reactive excited state, singlet oxygen [17, 21].

Singlet oxygen is a highly reactive, electrophilic, non-radical molecule that may be formed on irradiation of triplet oxygen in the presence of photosensitisers [22]. It reacts with proteins to form hydroperoxides, which decompose and oxidise further to form a variety of photoproducts on protein residue side chains. In addition, where proteins are in proximity to

lipids, lipid hydroperoxides formed through initial ROS attack may contribute to secondary protein damage. This lipid-mediated damage is thought to occur both through the triggering of radical chains and via the by-products of free radical lipid oxidation, including electrophilic aldehydes [20].

Hydroxyl radicals are a highly reactive free radical oxygen species that form *in vitro* through initial production of superoxide and hydrogen peroxide [23]. These radicals can attack any protein residue through abstraction of the  $\alpha$ -hydrogen or direct oxidation of residue side chains, but have a particular affinity for attacking electron rich moieties, notably aromatic rings and sulfur species [24].

More recently, the characterisation of nitrated photoproducts in irradiated protein substrates has also implicated reactive nitrogen species such as peroxy nitrite in contributing to protein photo-oxidation in some systems [25, 26]. Peroxy nitrite is similar to the hydroxyl radical in its reactivity, including its affinity for aromatic species [27, 28].

## 2. PROTEIN DAMAGE HIERARCHIES

Protein oxidative damage at the primary structural level can be induced through backbone cleavage [29], scission of the residue side chain [30], modification of a terminus [31] or reaction of the side chain [32]. Within intact proteins, it has been shown that peptide  $\alpha$ - or  $\beta$ -positions are not the primary site of attack for UV-generated reactive oxygen species, which means that side-chain modification is an important component of photo-oxidative damage [33].

### 2.1. Residue Specific Modification

Although all amino acid residues are susceptible to ROS attack, the most photosensitive residues in proteins are typically aromatic and sulfur-containing amino acids [34]. Model studies on the photodegradation of free amino acids have characterised the highest levels of photo-oxidation products within solutions of tryptophan, tyrosine, histidine, phenylalanine, and cysteine. This correlates well with the observation that these residues are also those which degrade the most significantly when whole proteins are exposed to UV [35-39].

#### 2.1.1. Aromatic residues

With respect to photomodifications leading to chromophore formation in proteins, tryptophan and tyrosine photoproducts in particular have been observed to be the chief contributors [40, 41]. Hydroxyl radicals, in particular, have a characteristic affinity for aromatic ring structures [42-45]. Recent studies have revealed a wide range of photoproducts formed within intact proteins from these residues [19, 25, 46-48]. In both cases, photo-oxidation of tryptophan and tyrosine side chains results in a cascade of oxidation products forming progressively more coloured chromophores. Figures 1 and 2 outline some of the key photoproducts and pathways involved in tryptophan and tyrosine photo-oxidation respectively. The dominant photo-oxidation pathway for tryptophan is through the formation of kynurenine derivatives, while for tyrosine, dopa and topa derivatives predominate. It

should be noted that photo-oxidation of phenylalanine leads to the same general profile of products as tyrosine, through initial ring hydroxylation [49], while the most notable histidine residue photoproducts are hydroxylated derivatives and degradation to asparagines and aspartic acid [40, 50].

When tyrosine and phenylalanine residues are in close proximity to tryptophan residues, energy transfer to tryptophan can occur, with associated fluorescence quenching [51-53]. This energy transfer contributes to the preferential oxidation of tryptophan residues within proteins. In our recent studies characterising photoproducts within UVB irradiated tryptophan-free collagen, a much wider range of phenylalanine, tyrosine and histidine photoproducts was observed than is usual when tryptophan is present, including the formation of nitrated products [25].

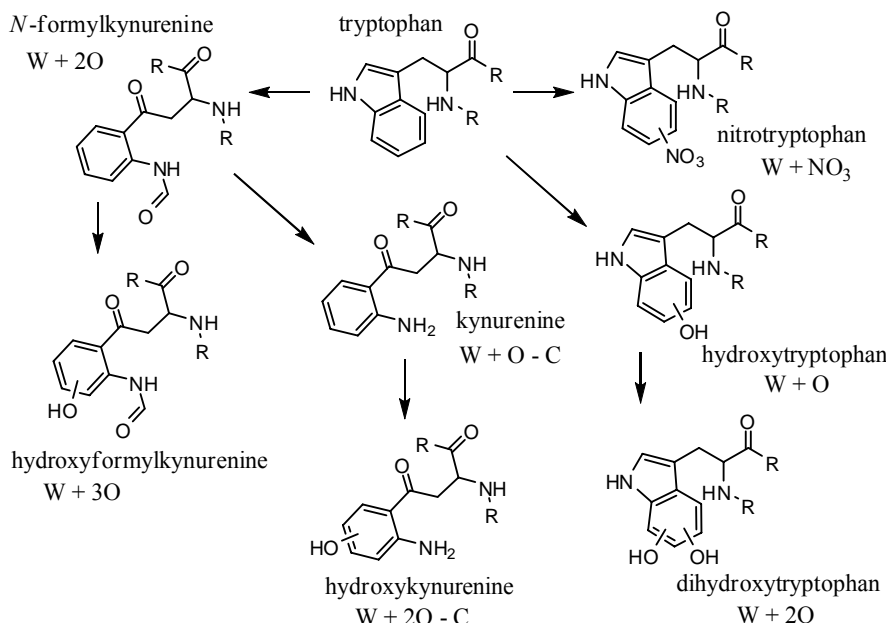


Figure 1. Key initial pathways in the photo-oxidation of the tryptophan residue side-chain, showing notable photoproducts.

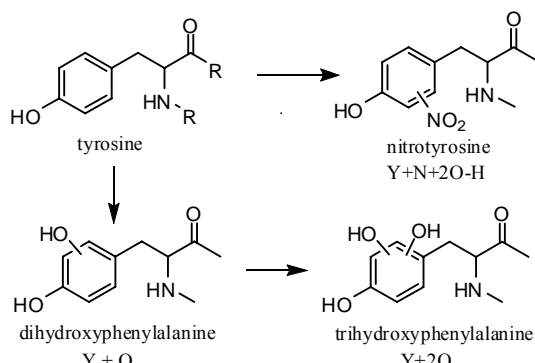


Figure 2. Key initial pathways in the photo-oxidation of the tyrosine residue side-chain, showing notable photoproducts.

### 2.1.2. Sulfur-containing residues

The sulfur-containing residues are also particularly susceptible to photodamage. Photo-oxidation of methionine leads predominantly to the formation of methionine sulfoxide, which is a reversible oxidative modification within living systems, but generally accumulates in structural proteins and other proteins particularly affected by solar radiation [54].

Cysteine residues in proteins are found as free thiols or in disulfide bonds (cystine), and are critical to the structural integrity and mechanical properties of the substrate [55-57]. These two forms are redox interconvertible and the relative ratio of these within the protein therefore has a correlation to the degree of photo-oxidative damage. High levels of disulfides can have a protective effect on other protein sites, acting as efficient quenchers [58]. Once cysteine is oxidised to sulfonic acid, the modification is irreversible. Cystine can also be photomodified to lanthionine [59, 60].

### 2.1.3. Other modifications

As a cyclic species, proline is also susceptible to photomodification through hydroxylation, with the main products being hydroxyproline and dihydroxyproline [25, 61]. These photoproducts are particularly relevant in the photodegradation of collagen, when proline residues are present in high abundance [62]. Other photodegradation products of proline include glutamic semialdehyde and pyroglutamic acid [30].

Although not residue-specific, other photomodifications of note include deamidation and decarboxylation, which are particularly abundant where photo-induced generation of ROS has initiated Fenton chemistry (hydroxyl radical production) within the protein substrate [63]. Deamidation particularly affects asparagine and glutamine residues, but also occurs at the protein or peptide *N*-terminus. Decarboxylation can occur in tandem with deamidation, and particularly affects terminal residues.

As all residue side-chains can be photo-oxidatively modified, there is a wide array of further photoproducts which have been characterised in addition to those highlighted [38, 47, 64]. However, most of these are believed to play a relatively minor role in the overall protein damage.

## 2.2. Structural Damage

### 2.2.1. Carbonylation

The level of formation of carbonyl groups in proteins is generally significantly higher than other oxidative modifications and is an irreversible modification [30]. Therefore, the formation of carbonyl groups has long been associated with protein photodamage [65, 66]. Carbonyl moieties may be generated on residue side chains, notably proline, threonine, arginine and lysine, after these residues are photo-oxidatively aldehyde or ketone derivatised [67].

### 2.2.2. Backbone cleavage and side-chain scission

ROS, in particular hydroxyl radicals, can extract  $\alpha$ -hydrogen atoms, leading to the generation of carbon-centred radicals within the protein [68]. These in turn react with molecular oxygen to form peroxy radicals, and subsequently peroxides and alkoxyl

derivatives. Peptide bond cleavage can then occur through two different pathways, namely the diamide and  $\alpha$ -amidation pathways [30]. The key difference between the two pathways is that the diamide pathways produces peptide fragments with diamide and isocyanate terminal moieties, while the  $\alpha$ -amidation pathway leads to peptide fragments with amide and  $\alpha$ -ketoacyl terminal moieties. Significantly, the  $\alpha$ -amidation pathway therefore provides another route for the introduction of carbonyl functionality.

Exposure of proteins to ionising radiation also results in residue side-chain scission, with cleavage occurring at the  $\beta$ -position [30, 40]. Side chain scission results in the formation within the protein of small carbonyl containing molecules as side-chain derivatives, including formaldehyde and acetone, from alanine and valine respectively. This can therefore lead indirectly to protein modifications such as formylation. Scission also results in the introduction of a carbon centred radical into the protein backbone.

### **2.2.3. Crosslinking**

UV irradiation of proteins also results in crosslinking between peptide chains [13, 34]. Once again, a wide and complex array of photoproducts can result, and crosslinking can be both inter- and intramolecular [30].

One key crosslinked photoproduct of tyrosine is dityrosine. Dityrosine formation is generated oxidatively in proteins through attack by ROS, such as hydroxyl or peroxy nitrite radicals, on tyrosine to form tyrosyl radicals, followed by radical-radical combination of proximal oxidised residues [46] As well as directly contributing to the coloration changes in proteins, dityrosine formation is also believed to play an important role in initiating secondary photochemical reactions in proteins [69].

Other residues with a propensity to form crosslinks on photo-oxidation include lysine, arginine and histidine [70].

## **3. EFFECT ON FUNCTIONAL ATTRIBUTES**

Accumulation of photo-oxidative modifications at the primary residue level translates to secondary, tertiary and quaternary protein level damage through denaturation, breakdown and re-ordering of the native protein conformation [40], and ultimately to the ultrastructural breakdown of the proteinaceous material. For many protein substrates, the details of these modifications behind the observed deterioration in performance, condition and quality of the protein material are not yet particularly well understood. A summary of the effects of photo-oxidation on the functional attributes of selected protein-based materials of particular interest either medically or commercially is presented.

### **3.1. Human Health and Wellbeing**

Proteins comprise a critical component of the body's external structure and defences. Photodamage to these proteins is therefore of significant concern.

### 3.1.1. Skin

Photodamage to skin is arguably the most concerning consequence of increasing UV levels around the globe. Photo-oxidation of proteins within the skin contributes directly or indirectly to photo-ageing and the development of skin disease, notably carcinogenesis [71].

Skin is composed of three major layers – the outermost epidermis, the dermis and the hypodermis [72]. The outermost sub-layer of the epidermis is the stratum corneum (SC), a highly crosslinked proteinaceous matrix which is comprised of plate-like envelopes filled with keratin. The keratin contained within the SC plays a key role in preventing moisture loss and keeping the skin hydrated. The dermis consists largely of connective tissue, with high levels of collagen [71]. Collagens are a key protein component of all the skin layers [73].

UVA, associated with erythema and carcinoma development, is primarily absorbed in the epidermis, while UVB, associated with skin photo-ageing, can pass through to the dermal layer [74]. UV exposure results in the introduction of carbonyl groups into the SC proteins, with protein oxidation levels increasing towards the outer layers [75]. Collagen and keratin photodamage contributes to the progressive loss of structural integrity and therefore cosmetic damage, including wrinkling and line formation [76]. As skin ages, it becomes thinner and more susceptible to photodamage.

There is increasing evidence for the generation of ROS in skin upon UV exposure. Chronic and acute photodamage is mediated by depleted antioxidant enzyme expression within the SC and in the epidermis, and increased levels of oxidised proteins [77]. Importantly, oxidatively modified proteins have been found to accumulate specifically within the upper dermis of photo-aged skin [77]. This correlation between overall skin photodamage and protein oxidation is considered a key pathophysiologic factor in photo-ageing and carcinogenesis.

### 3.1.2. Hair

Human hair is a proteinaceous material composed of an inner cortex of keratins enveloped in overlapping cuticle cells [78]. Intermediate filament proteins represent the major structural proteins in hair, and these are arranged into filamentous bundles within a protein matrix [79]. Hair has a high sulfur content, with extensive disulfide crosslinking within the cortex. The cuticle is also highly crosslinked, with both disulfide and isopeptide bonds [80]. Photo-oxidation of proteins within hair, therefore, can dramatically affect inherent fibre properties.

Photo-oxidation affects important perception attributes of hair such as colour, moisture retention and lustre [81, 82]. The effect of sun exposure is related to the amount of melanin present in the hair, which has a protective effect [82]. The formation of chromophores within hair proteins leads to changes in the base coloration. Manageability is also affected through changes in the physical and mechanical properties of the fibres, particularly an increase in brittleness. Photodegradation can exacerbate damage caused by cosmetic treatments, such as bleaching and dyeing. Bleaching, in particular, results in residual peroxides, which contribute to further damage with light exposure [83]. The most common protection utilised is the incorporation of UV blockers into hair-care products, however, as with UV blockers utilised in skin-care applications, these can act as photosensitisers to generate ROS and promote protein damage.

### ***3.1.3. Eyes***

The outer structures of the eye, particularly the cornea, absorb most incident UVB under typical sunlight exposure, with little reaching the lens [18]. UVA radiation, however, is strongly implicated in lens photodamage.

The proteins within the eye lens are not subject to the typical removal and replacement protective mechanisms occurring elsewhere in the body, and diffusion of the proteins becomes progressively more limited with ageing [84]. Therefore, accumulation of oxidative damage to lens crystallins is a serious concern, particularly with increasing exposure to solar UV. Cataracts result from ongoing photo-oxidation of lens proteins, which leads to loss of light transmission, sight impairment and in the worst cases blindness [38, 84].

Natural protective filters in the young lens, including kynurenone and hydroxykynurenone, absorb about 95% of light  $>300$  nm, with the remainder chiefly absorbed by tryptophan residues in the lens proteins. It has been shown the build-up of tryptophan photo-oxidation products, in particular, acts to photosensitise the lens to further damage [18, 38, 85-87]. Some photosensitisation is believed to come directly from the filter compounds, which can end up covalently bound to lens proteins through addition to nucleophilic protein sites, such as cysteine, lysine and histidine [88]. Advanced glycation endproducts have also been implicated in photosensitisation [89].

### ***3.1.4. Pharmaceuticals and cosmeceuticals***

There are many protein- and peptide-based pharmaceutical and cosmeceutical products on the market, with more constantly in further development. It is critical that protein pharmaceuticals maintain their native structure and activity during long-term storage. While photo-oxidation has been recognised as a major contributor to protein degradation in other systems, the effects of photo-induced damage have not yet been widely studied for biopharmaceuticals [21]. This is particularly important since photodegradation can lead to changes in primary, secondary, and tertiary structures of protein and these changes could lead to differences in long-term stability, bioactivity, or immunogenicity. Photostability is therefore a key issue for these products in terms of packaging, shelf-life, efficacy, and particularly with respect to the potential formation of harmful side-products [90, 91]. With pharmaceuticals, solid state photostability is often the key concern, and there is still significant work required to explore underlying photodegradation mechanisms in the absence of water [92]. With protein-based cosmetic products also, often designed for topical application, the photo-oxidative breakdown products are important with respect to efficacy and toxicity.

## **3.2. Foods**

Photo-oxidation is one means by which oxidative degradation is induced in foodstuffs during production, processing, storage, retail, and after purchase [22]. Generally speaking, the effects of photo-oxidation will be additive to other forms of oxidative degradation, but are an important consideration when determining food handling protocols. Protein photomodification is of particular concern in the following food categories.

### 3.2.1. Meat and Seafood

Flavour, colour, texture, nutritional value and functionality comprise essential quality parameters for all meat and seafood products, with direct correlation to product value and consumer perception [93]. These critical attributes are all directly or indirectly affected by protein, and associated lipid, photo-oxidation [94].

For meat and meat products, particularly, lipid oxidation must be considered in parallel to protein oxidation. Aldehyde-derived secondary products of lipid oxidation are associated with the formation of proteinaceous chromophores and fluorophores, and therefore coloration changes [95]. Oxidative degradation also leads to deterioration of the nutritional value of meat, through protein damage such as protein-protein crosslinks, protein-lipid crosslinks, protein cleavage and residue specific damage [96, 97], and is particularly important in determining meat colour [98], a characteristic to which consumers are very sensitive. The texture of meat is directly affected by the effects of photo-oxidation, with structural changes resulting from protein backbone cleavage and crosslinking [99]. These structural modifications in turn affect performance properties such as moisture retention and protein solubility [100].

Protein oxidative degradation in seafood products is generally less well studied than meat, however it is of equal concern [101-103]. Fish and seafood products are often exposed to light during retail, and photodegradation contributes to tainting and spoilage [104].

### 3.2.2. Dairy

Proteins represent a critical nutritional and functional component of dairy products. The major milk protein classes are caseins, albumins and globulins [105].

Light-induced degradation reactions in milk and dairy products create a serious problem for the dairy industry because of the development of off-flavours, the decrease in nutritional quality and functionality, and the speed and severity at which these phenomena can develop [7, 106-108]. Flavour changes are quickly noticeable in milk exposed to sunlight. In tandem with protein photodegradation, riboflavin and vitamin A gradually degrade, milk fat is photo-oxidised, oxygen dissolved in the milk is consumed, and the sensorial quality decreases significantly [106].

Off flavour development in dairy products, such as milk and cheeses, after exposure to light is thought to be mediated by the conversion of riboflavin into a highly reactive, triplet-excited state, enabling it to oxidise proteins [109]. After photo-oxidation, there is an increase in protein carbonyl content in tandem with the specific oxidation of tryptophan, histidine, and methionine residues, as well as the formation of dityrosine. Loss of tryptophan through photo-oxidation has been well-correlated with the formation of *N*-formylkynurenone and kynurenone [110]. The protein structure of all the major milk proteins changes in response to photo-oxidation [111]. Caseins are particularly susceptible to photodegradation, with photo-oxidation of tryptophan leading to observed conformational changes in the micro-environment of the residues. Formation of dityrosines is also notably high in caseins. Changes at the secondary and tertiary protein structural levels occur in the globular milk proteins, with protein unfolding noted particularly for lactalbumin and lactoglobulin. This can be accompanied by quaternary protein damage in the form of protein polymerisation [110].

Photo-oxidation also affects the hydrolysis of milk proteins. Changes are observed in the formation of peptides by chymosin after photo-oxidation, with decreased accessibility of

chymosin to oxidised proteins reflected in a lower overall level of free amino-terminal groups [112].

### **3.2.3. Crops**

Rising levels of UV exposure are becoming a concern for crop growth and yield, with increased levels of photodegradation observed [11, 113]. This affects proteins within the growing plant, due in some cases to the photo-oxidation of key enzymic tryptophan residues [12, 114]. Specific proteins appear to be particularly vulnerable to oxidative carbonylation in the matrix of plant mitochondria; these include several enzymes of the Krebs cycle, glycine decarboxylase, superoxide dismutase and heat shock proteins [113]. Photo-oxidative insults also affect the quality of high protein plant-derived foods, such as cereals. As with other foodstuffs, oxidative deterioration results in off-flavours and decreased nutritional value [115]. Increasingly, cereal and other proteinaceous plant derivatives are being utilised as additives and ingredients in formulations and processed food, and photo-oxidative stability is a key factor in the final product performance.

## **3.3. Materials**

### **3.3.1. Wool and silk textiles**

Wool and other natural animal fibres are keratinous materials with an anatomy comparable to human hair, with a central cortical region comprised largely of IFP filaments within a matrix, and an outer cuticle region with high levels of crosslinking. Animal fibres are generally >90% proteinaceous in composition. Whereas human hair typically has multiple layers of cuticle cells, many wool types, such as Merino, have only one cuticle layer [116]. Silk, on the other hand, is an extracellular fibrous material comprised mostly of fibroins [117].

Appearance retention is a critical determinant of quality and value for furnishing and apparel textile products, and is directly related to the degree and nature of protein degradation. Photodegradation correlates to several deleterious effects of commercial significance.

Firstly, coloration is severely affected through competing processes of photoyellowing and photobleaching [118]. Photoyellowing is the progressive increase in yellowness generally associated with exposure to UVB and shorter wavelength UVA. There is also an associated decrease in brightness. This phenomenon is particularly significant for apparel textiles which are exposed directly to solar radiation. UVB radiation has been shown to produce a wide range of protein-derived chromophores within wool, with ongoing exposure leading to increasingly coloured species [46, 47]. A correlation has been established between photoyellowing and the carbonyl content in silk [119]. Fluorescent whitening agents (FWA), also known as optical brightening agents (OBA), which are now commonly a component of laundry detergents, have been shown to significantly accelerate photoyellowing in wool and silk [120, 121]. These additives act as photosensitisers, generating increased ROS, hydroxyl radicals in particular, and directly cause considerable enhancement in the levels of protein photoproducts [25, 121, 122]. Bleaching is also often incorporated into fibre and textile processing, and this has also been shown to exacerbate subsequent photoyellowing.

Photobleaching is the progressive decrease in the base yellowness of the fibre generally associated with exposure to blue light or longer wavelength UVA. This is a key concern for interior textiles, where window glass filters out most UVB, and results in uneven photofading [121].

Additionally, fibre protein photo-oxidation results in phototendering, the process by which the proteins progressively lose their structural integrity. This results in increased brittleness and lowered strength, thereby leading to enhanced wear in the textile product [121].

### **3.3.2. Other**

Other protein-based materials where protein photo-oxidation is a significant issue include biomaterials, feathers and artworks/objects of historical and cultural importance, particularly those utilising paints derived from egg-based materials [123]. With an escalating move away from oil-derived materials towards biomaterials, the photostability of protein and peptide components of these is likely to take on increasing importance.

## **4. EVALUATION OF PHOTO-OXIDATION – NEW PROTEOMIC APPROACHES**

The complex array, location and interaction of modifications induced within proteins on irradiative exposure make characterisation and evaluation of photodamage very difficult in real biological systems. For this reason, holistic assessment techniques, such as fluorescence mapping and protein extractability have traditionally been used to try to study these systems.

The development and application of powerful new proteomic tools, based around mass spectrometry (MS), promise to revolutionise our understanding of protein photo-oxidation and assist significantly with the development and validation of new strategies for the control of photodamage.

### **4.1. Redox Proteomics**

Redox proteomics is an emerging discipline centred on the study of key reduction and oxidation events occurring within proteins [68]. Application and customisation of techniques adapted from classical proteomics have enabled protein oxidation to be studied and understood in far greater detail than was previously possible. This field therefore provides an ideal set of tools for evaluating the photo-oxidation of proteinaceous systems.

#### **4.1.1. Characterisation and location**

Protein MS is the underpinning tool in proteomics. The two most common modes of MS utilised for protein analysis are electrospray ionisation mass spectrometry (ESI-MS) and matrix assisted laser desorption ionisation mass spectrometry (MALDI-MS) [46, 124, 125], which differ in the means by which the sample is introduced. ESI-MS involves ionising the sample with an applied potential directly from an injected solution, while in MALDI-MS the sample is co-crystallised with a matrix on a plate and is then ionised using a laser.

With respect to studying photo-oxidation directly within proteins, two aspects, in particular, make evaluation challenging –

- Any given protein is likely to have a different pattern of damage
- Any given photomodification at a particular primary location in the protein is likely to be present in extremely low abundance within the sample as a whole

These two factors are often further complicated by extensive protein crosslinking in the substrate. In addition, any effective analytical technique must not induce any further oxidative modification. Mass spectrometry offers a significant advantage over other analytical technologies by enabling the characterisation of what is essentially an array of environmentally-induced post-translational modifications within a complex mixture without the need for complete purification. Typically, the protein sample is enzymatically digested and the generated peptides analysed. Detailed analysis of low abundance peptides within the sample is achieved through liquid chromatography (LC)-ESI or LC-MALDI, where chromatographic fractionation of the peptide mixture is performed prior to MS analysis. Where multiple chromatographic media are utilised in tandem, this approach is referred to as MudPIT (Multi-dimensional Protein Identification Technology) [126].

Through tandem mass spectrometric (MS/MS) analysis, specific peptides can be selected and fragmented through post-source decay or collision with an inert gas to generate fragment ions which provide structural information. Photomodified residues can be determined qualitatively through MS/MS comparison with native non-modified peptides. An example of this is shown in Figure 3 [47].

The location of modifications within the primary sequence of proteins is determined through bioinformatic analysis, using software such as Mascot or SEQUEST. Where unknown proteins are involved, BLAST software can be used to find homologous sequences [127]. Where extensive crosslinking inhibits complete enzymatic digestion, such as in the evaluation of hair or wool cuticle, combination chemical/enzymic digestion strategies can be employed. One example is the utilisation of 2-nitro 5-thiocyanobenzoic acid (NTCB) in tandem with trypsin. NTCB cleaves on the N-terminal side of cysteine residues to produce a characteristic terminal modification, allowing selective searching.

#### **4.1.2. Profiling and tracking**

The levels of specific photoproducts provide important information regarding the biological or commercial significance of any given photomodification. Tracking the rates of formation, and the relative levels of specific photoproducts within peptides and proteins generates a protein degradation profile: a useful tool in understanding photodegradative mechanisms, allowing the development of targeted amelioration strategies [41, 128].

Photo-oxidation typically generates a range of products in susceptible protein regions. The formation of these products may be individually detected with MS ion abundance data. MS abundance profiling gives an indication of the relative abundance of each photoproduct.

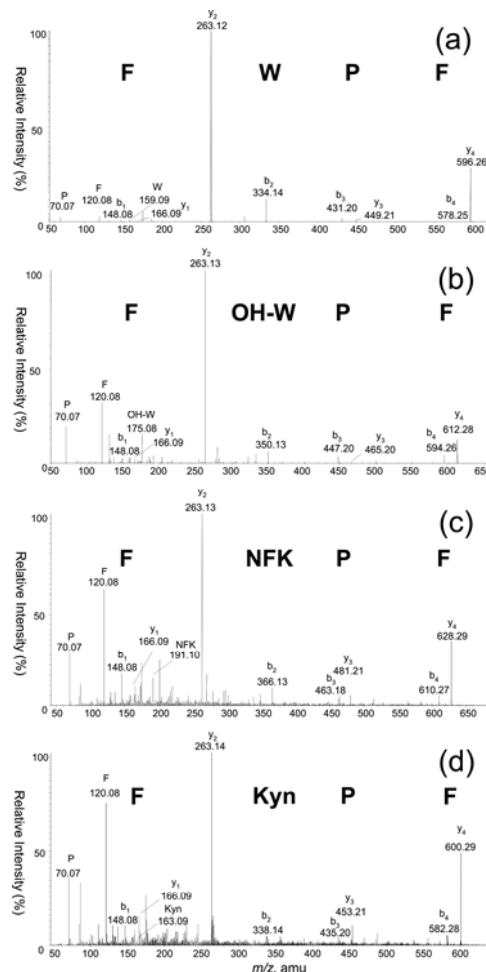


Figure 3. ESI-MS/MS spectra of the wool peptide of native sequence FWPF, (a) unmodified and with the tryptophan residue photo-oxidised to (b) hydroxykynurenine (OH-W), (c) *N*-formylkynurenine (NFK), and (d) kynurenine (Kyn) [47].

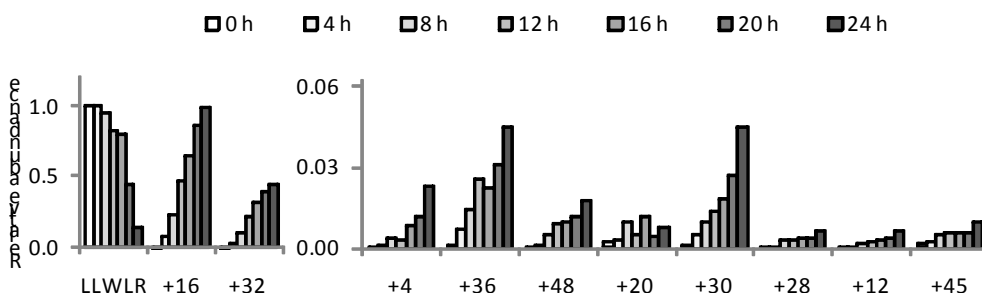


Figure 4. Relative abundance profiling of tryptophan photo-oxidation products formed during progressive UVA irradiation of the peptide, LLWLR [129].

Legend: unmodified peptide; +16) W+O modification; +32) W+2O; +4) W+O-C; +36) W+3O; +48) W+4O; +20) W+2O-C; +30) W+2O-2H; +28) W+2O-4H; +12) W+C; +45) W+N+2O-H

MS-based profiling can be further progressed to track the progressive degradation of parent peptides, and the corresponding formation of photomodifications, through the changes in their relative abundance. An example is shown in Figure 4 [129]. Tracking the variation in this profile allows the formation of specific peptide modifications to be monitored over time, or over variation in any other parameter. For instance, specific ROS can be either blocked or amplified to provide mechanistic information. This approach can be utilised to explore the relative contributions of singlet oxygen and hydroxyl radicals to the formation of specific photoproducts. The current limitations to this strategy revolve around the variation in ion abundances ratios between MS runs. Stable isotope labelling techniques, such as ICAT and iTRAQ, are currently being utilised to effectively quantitate relative protein abundance in a wide range of proteomic studies [130, 131]. We envisage the development and application of related approaches to overcome the currently limitation of MS relative abundance profiling.

A related emerging approach to evaluating protein photo-oxidation involves the characterisation and tracking of marker peptides. Marker peptides are selected through a range of criteria, including reproducible extraction and the presence of a residue which is sensitive to specific photodamage or a specific reactive species [129]. These marker peptides are then utilised to evaluate the overall profile of damage in the protein substrate. This is envisaged to be a particularly effective approach to testing and validating photoprotection treatments.

#### **4.1.3. Carbonylated proteins**

Protein carbonyl content is a good indicator of overall photo-oxidation. Traditionally, overall protein carbonylation has been evaluated through initial derivitisation with 2,4-dinitrophenylhydrazine (DNPH), and subsequent immuno- or spectrophotometric assay [126]. However, two key goals of redox proteomics, as applied to photo-oxidation, are the identification of proteins susceptible to photomodification, and the characterisation and location of specific residues where damage occurs. Recently, affinity purification has been coupled with LC-MS/MS to directly identify and locate carbonylation within a range of oxidised proteins simultaneously. This form of affinity purification involves reaction of biocytin hydrazide with the carbonyl groups in oxidatively modified proteins to induce hydrazone conjugate formation [126]. These are then affinity purified using streptavidin immobilised on agarose, and analysed using MudPIT. This approach offers promise in the evaluation of protein photo-oxidative damage

It is anticipated that as the field of redox proteomics advances, further developed technologies will be applied and customised to better understand protein photodegradation.

### **4.2. Crosslink Elucidation**

Photo-induced protein-protein crosslinks are particularly difficult to characterise and locate. Not only are any specific crosslinks likely present in very low abundance within the protein substrate, but digestion must be performed in such a way that the crosslinked peptides

remain intact during extraction and solubilisation. Novel proteomic approaches are also emerging for the elucidation of crosslinks, which offer routes to advancing progress in this area.

These approaches centre on the utilisation of partial digestion strategies, followed by isotopic labelling [132, 133].  $^{18}\text{O}$  from isotopically enriched water is incorporated into the C-termini of proteolytic peptides [134]. Since crosslinked peptides have two C-termini, two  $^{18}\text{O}$  atoms are incorporated where a crosslink is present. These are then combined with peptides from a parallel sample digested in  $^{16}\text{O}$  water. Mass spectrometric analysis of the resultant modified peptides can then distinguish and select for crosslinks through searching for a characteristic mass shift of 8 amu relative to the unlabelled peptide [133].

Application of these techniques to detecting photo-induced crosslinks is significantly more complex than for elucidation of native crosslinks, however, this approach provides a potential means to identify and locate specific crosslinked photoproducts.

## 5. DIRECTIONS

To fully understand each of the protein-based systems affected by photo-oxidation, it is critical that protein primary level information be linked and correlated to damage observed at higher orders of protein and cellular structure. Initial progress has been made in this direction, but there is substantially more progress required.

An enhanced understanding of protein photodegradative mechanisms through the characterisation and location of low abundance photomodifications, in parallel with the development of protocols to examine the pattern and relative abundance of these modifications, represent important goals in protein science. New proteomic approaches to the characterisation and understanding of protein photo-oxidation are revealing significant new levels of detail. We envisage further application and customisation of tools derived from redox proteomics to specific protein-based systems will facilitate the optimisation and validation of new targeted photoprotection treatments.

## ACKNOWLEDGMENTS

I would like to gratefully acknowledge the assistance of Anita Grosvenor for her critical review and editing of this chapter.

## REFERENCES

- [1] Kochevar, IE. Molecular and cellular effects of UV radiation relevant to chronic photodamage. In: Gilchrest, BA, editor. *Photodamage*, 1999, 51-67.
- [2] Ruetsch, SB; Yang, B; Kamath, YK. Chemical and photo-oxidative hair damage studied by dye diffusion and electrophoresis. *Journal of Cosmetic Science*, 2003, 54, 379-94.

- [3] Wondrak, GT; Roberts, MJ; Jacobson, MK, et al. 3-hydroxypyridine chromophores are endogenous sensitizers of photo-oxidative stress in human skin cells. *Journal of Biological Chemistry*, 2004, 279, 30009-20.
- [4] Sidorkina, OM; Kuznetsov, SV; Blais, JC, et al. Ultraviolet-B-induced damage to Escherichia coli Fpg protein. *Photochemistry and Photobiology*, 1999, 69, 658-63.
- [5] Dalle-Donne, I; Scaloni, A; Giustarini, D; et al. Proteins as biomarkers of oxidative/nitrosative stress in diseases: The contribution of redox proteomics. *Mass Spectrometry Reviews*, 2005, 24, 55-99.
- [6] O'Sullivan, MG; Kerry, JP. Sensory and quality properties of packaged meat. In: JP; Kerry, D; Ledward, editors. *Improving the Sensory and Nutritional Quality of Fresh Meat*. Cambridge: Woodhead Publishing Limited; 2009, 595-7.
- [7] Østdal, H; Weisbjerg, MR; Skibsted, LH; et al. Protection against photo-oxidation of milk by high urate content. *Milchwissenschaft*, 2008, 63, 119-22.
- [8] Reddy, GB; Bhat, KS. Protection against UVB inactivation (in vitro) of rat lens enzymes by natural antioxidants. *Molecular and Cellular Biochemistry*, 1999, 194, 41-5.
- [9] Kubiak, K; Kowalska, M; Nowak, W. Molecular dynamics study of early events during photo-oxidation of eye lens protein  $\gamma\beta$ -crystallin. *Journal of Molecular Structure (Theochem)*, 2003, 630, 315-25.
- [10] Fujii, N; Uchida, H; Saito, T. The damaging effect of UV-C irradiation on lens alpha-crystallin. *Molecular Vision*, 2004, 10, 814-20.
- [11] Stapleton, AE. Ultraviolet radiation and plants: Burning questions. *Plant Cell*, 1992, 4, 1353-8.
- [12] Caldwell, CR. Ultraviolet-induced photodegradation of cucumber (*Cucumis sativus* L.) microsomal and soluble protein tryptophanyl residues in vitro. *Plant Physiology*, 1993, 101, 947-53.
- [13] Gerhardt, KE; Wilson, MI; Greenberg, BM. Tryptophan photolysis leads to a UVB-induced 66 kDa photoproduct of ribulose-1,5-bisphosphate carboxylase/oxygenase (rubisco) in vitro and in vivo. *Photochemistry and Photobiology*, 1999, 70, 49-56.
- [14] Frederick, JE; Lubin, D. Possible long-term changes in biologically active ultraviolet radiation reaching the ground. *Photochemistry and Photobiology*, 1988, 47, 571-8.
- [15] Creed, D. The photophysics and photochemistry of the near-UV absorbing amino acids -II. Tyrosine and its simple derivatives. *Photochemistry and Photobiology*, 1984, 39, 563-75.
- [16] Creed, D. The photophysics and photochemistry of the near-UV absorbing amino acids-I. Tryptophan and its simple derivatives. *Photochemistry and Photobiology* 1984, 39, 537-62.
- [17] Girotti, AW; Giacomoni, PU. Lipid and protein damage provoked by ultraviolet radiation: Mechanisms of indirect photo-oxidative damage. In: Giacomoni, PU, editor. *Biophysical and Physiological Effects of Solar Radiation on Human Skin*. Cambridge, UK: RSC Publishing; 2007, 271-91.
- [18] Mizdrak, J; Hains, PG; Truscott, RJW, et al. Tryptophan-derived ultraviolet filter compounds covalently bound to lens proteins are photosensitizers of oxidative damage. *Free Radical Biology and Medicine*, 2008, 44, 1108-19.
- [19] Davies, MJ. Reactive species formed on proteins exposed to singlet oxygen. *Photochemical and Photobiological Sciences*, 2004, 3, 17-25.

- [20] Trautinger, F. Damaged proteins: Repair or removal? In: Giacomoni, PU, editor. *Biophysical and Physiological Effects of Solar Radiation on Human Skin*. Cambridge, UK: RSC Publishing; 2007, 311-9.
- [21] Kerwin, BA; Remmeli, RLJ. Protect from light: Photodegradation and protein biologics. *Journal of Pharmaceutical Sciences*, 2007, 96, 1468-79.
- [22] Min, DB; Boff, JM. Chemistry and reaction of singlet oxygen in foods. *Comprehensive Reviews in Food Science and Food Safety*, 2002, 1, 58-72.
- [23] Lee, J; Koo, N; Min, DB. Reactive oxygen species, aging, and antioxidative nutraceuticals. *Comprehensive Reviews in Food Science and Food Safety*, 2004, 3, 21-33.
- [24] Nukuna, BN; Goshe, MB; Anderson, VE. Sites of hydroxyl radical reaction with amino acids identified by  $^2\text{H}$  NMR detection of induced  $^1\text{H}/^2\text{H}$  exchange. *Journal of the American Chemical Society*, 2001, 123, 1208-14.
- [25] Dyer, J; Clerens, S; Cornellison, C, et al. Photoproducts formed in the photoyellowing of collagen in the presence of a fluorescent whitening agent. *Photochemistry and Photobiology*, 2009, In Press.
- [26] Thiagarajan, G; Lakshmanan, J; Chalasani, M, et al. Peroxynitrite reaction with eye lens proteins:  $\alpha$ -crystallin retains its activity despite modification. *Investigative Ophthalmology and Visual Science*, 2004, 45, 2115-21.
- [27] Yamakura, F; Ikeda, K. Modification of tryptophan and tryptophan residues in proteins by reactive nitrogen species. *Nitric Oxide Biology and Chemistry*, 2006, 14, 152-61.
- [28] Beckman, JS; Beckman, TW; Chen, J, et al. Apparent hydroxyl radical production by peroxynitrite: implications for endothelial injury from nitric oxide and superoxide. *Proceedings of the National Academy of Sciences of the United States of America*, 1990, 87, 1620-4.
- [29] Davies, MJ. Singlet oxygen-mediated damage to proteins and its consequences. *Biochemical and Biophysical Research Communications*, 2003, 305, 761-70.
- [30] Stadtman, ER; Levine, RL. Chemical modification of proteins by reactive oxygen species. In: I; Dalle-Donne, A; Scaloni, DA, Butterfield, editors. *Redox Proteomics - From Protein Modifications to Cellular Dysfunctions and Diseases*. Hoboken: John Wiley and Sons, Inc.; 2006, 3-23.
- [31] Gill, AC; Ritchie, MA; Hunt, LG, et al. Post-translational hydroxylation at the N-terminus of the prion protein reveals presence of PPII structure *in vivo*. *EMBO Journal*, 2000, 19, 5324-31.
- [32] Bender, DA; Barrett, GC. *Chemistry and biochemistry of the amino acids*. London: Chapman & Hall; 1985.
- [33] Goshe, MB; Chen, YH; Anderson, VE. Identification of the sites of hydroxyl radical reaction with peptides by hydrogen/deuterium exchange: prevalence of reactions with the side chains. *Biochemistry*, 2000, 39, 1761-70.
- [34] Berlett, BS; Stadtman, ER. Protein oxidation in aging, disease, and oxidative stress. *Journal of Biological Chemistry*, 1997, 272, 20313-6.
- [35] Schäfer, K; Goddinger, D; Höcker, H. Photodegradation of tryptophan in wool. *Journal of the Society of Dyers and Colourists*, 1997, 133, 350-5.
- [36] Asquith, RS; Hirst, L; Rivett, DE. *Effects of ultraviolet radiation as related to the yellowing of wool*. Applied Polymer Symposium; 1971, 333-5.

- [37] Asquith, RS; Rivett, DE. The photolysis of tyrosine and its possible relationship to the yellowing of wool. *Textile Research Journal*, 1969, 39, 633-7.
- [38] Davies, MJ; Truscott, RJW. Photo-oxidation of proteins and its role in cataractogenesis. *Journal of Photochemistry and Photobiology B: Biology*, 2001, 63, 114-25.
- [39] Boreen, AL; Edlund, BL; Cotner, JB, et al. Indirect photodegradation of dissolved free amino acids: The contribution of singlet oxygen and the differential reactivity of DOM from various sources. *Environmental Science and Technology*, 2008, 42, 5492-8.
- [40] Dean, RT; Fu, S; Stocker, R, et al. Biochemistry and pathology of radical-mediated protein oxidation. *Biochemical Journal*, 1997, 324, 1-18.
- [41] Davies, MJ; Fu, S; Wang, H, et al. Stable markers of oxidant damage to proteins and their application in the study of human disease. *Free Radical Biology and Medicine*, 1999, 27, 1151-63.
- [42] Asquith, RS; Rivett, DE. Studies on the photo-oxidation of tryptophan. *Biochimica et Biophysica Acta*, 1971, 252, 111-6.
- [43] Simat, TJ; Steinhart, H. Oxidation of free tryptophan and tryptophan residues in peptides and proteins. *Journal of Agricultural & Food Chemistry*, 1998, 46, 490-8.
- [44] Maskos, J; Rush, JD; Koppenol, WH. The hydroxylation of tryptophan. *Archives of Biochemistry and Biophysics*, 1992, 296, 514-20.
- [45] Żegota, H; Kołodziejczyk, K; Król, M, et al. o-Tyrosine hydroxylation by OH<sup>-</sup> radicals. 2-, 3-DOPA and 2,5-DOPA formation in  $\gamma$ -irradiated aqueous solution. *Radiation Physics and Chemistry*, 2005, 72, 25-33.
- [46] Dyer, JM; Bringans, S; Bryson, WG. Characterisation of photo-oxidation products within photoyellowed wool proteins: tryptophan and tyrosine derived chromophores. *Photochemical and Photobiological Sciences*, 2006, 5, 698-706.
- [47] Dyer, JM; Bringans, SD; Bryson, WG. Determination of photo-oxidation products within photoyellowed bleached wool proteins. *Photochemistry and Photobiology*, 2006, 82, 551-7.
- [48] Guedes, S; Vitorino, R; Domingues, Rr, et al. Oxidation of bovine serum albumin: identification of oxidation products and structural modifications. *Rapid Communications in Mass Spectrometry*, 2009, 23, 2307-15.
- [49] Maskos, Z; Rush, JD; Koppenol, WH. The hydroxylation of phenylalanine and tyrosine: A comparison with salicylate and tryptophan. *Archives of Biochemistry and Biophysics*, 1992, 296, 521-9.
- [50] Wei, C; Song, B; Yuan, J, et al. Luminescence and Raman spectroscopic studies on the damage of tryptophan, histidine and carnosine by singlet oxygen. *Journal of Photochemistry and Photobiology A: Chemistry*, 2007, 189, 39-45.
- [51] Teale, WWJ. The ultraviolet fluorescence of proteins in neutral solution. *Biochemical Journal*, 1960, 76, 381-8.
- [52] Chiu, HC; Bersohn, R. Electronic energy transfer between tyrosine and tryptophan in the peptides trp-(pro)<sub>n</sub>-Tyr. *Biopolymers*, 1977, 16, 277-88.
- [53] Simpson, WS. *Origins of variation in the fluorescence patterns of wool and wool proteins*. Proceedings of the 9th International Wool Textile Research Conference; 1995 1995; Biella, Italy, 1995, 429-39.
- [54] Garner, MH; Spector, A. Selective oxidation of cysteine and methionine in normal and senile cataractous lenses. *Proceedings of the National Academy of Sciences of the United States of America*, 1980, 77, 1274-7.

- [55] Hearle, JW. A critical review of the structural mechanics of wool and hair fibres. *International Journal of Biological Macromolecules*, 2000, 27, 123-38.
- [56] Parbhoo, AN; Bryson, WG; Lal, R. Disulfide bonds in the outer layer of keratin fibers confer higher mechanical rigidity: correlative nano-indentation and elasticity measurement with an AFM. *Biochemistry*, 1999, 38, 11755-61.
- [57] Katsumi, A; Tuley, EA; Bodo, I, et al. Localization of disulfide bonds in the cystine knot domain of human von Willebrand factor. *Journal of Biological Chemistry*, 2000, 275, 25585-94.
- [58] Li, Z; Bruce, A; Galley, WC. Temperature dependence of the disulfide perturbation to the triplet state of tryptophan. *Biophysical Journal*, 1992, 61, 1364-71.
- [59] Earland, C; Raven, DJ. Lanthionine formation in keratin. *Nature*, 1961, 191, 384-.
- [60] Bessems, GJ; Rennen, HJ; Hoenders, HJ. Lanthionine, a protein crosslink in cataractous human lenses. *Experimental Eye Research*, 1987, 44, 691-5.
- [61] Sionkowska, A; Kaminska, A. Thermal helix-coil transition in UV irradiated collagen from rat tail tendon. *International Journal of Biological Macromolecules*, 1999, 24, 337-40.
- [62] Kato, Y; Uchida, K; Kawakishi, S. Oxidative degradation of collagen and its model peptide by ultraviolet irradiation. *Journal of Agriculture and Food Chemistry*, 1992, 40, 373-9.
- [63] Stadtman, ER; Berlett, BS. Fenton chemistry. Amino acid oxidation. *Journal of Biological Chemistry*, 1991, 266, 17201-11.
- [64] Gieseg, S; Simpson, JA; Charlton, TS, et al. Protein-bound 3,4-dihydroxyphenylalanine is a major reductant formed during hydroxyl radical damage to proteins. *Biochemistry*, 1993, 32, 4780-6.
- [65] Holt, LA; Milligan, B. The formation of carbonyl groups during irradiation of wool and its relevance to photoyellowing. *Textile Research Journal*, 1977, 47, 620-4.
- [66] Stadtman, ER. Protein oxidation and aging. *Free Radical Research*, 2006, 40, 1250-8.
- [67] Scaloni, A. Mass spectrometry approaches for the molecular characterisation of oxidatively/nitrosatively modified proteins. In: Dalle-Donne, I; Scaloni, A; Desiderio, DM; Nibbering, NM, editors. *Redox Proteomics*, 2006.
- [68] Dalle-Donne, I; Scaloni, A; Butterfield, DA, editors. *Redox Proteomics - From Protein Modifications to Cellular Dysfunctions and Diseases*. Hoboken: John Wiley and Sons, Inc., 2006.
- [69] Vazquez, S; Aquilina, JA; Jamie, JF, et al. Novel protein modification by kynurenone in human lenses. *Journal of Biological Chemistry*, 2002, 277, 4867-73.
- [70] Taylor, CM; Wang, W. Histidinoalanine: a crosslinking amino acid. *Tetrahedron*, 2007, 63, 9033-47.
- [71] Giacomoni, PU, editor. *Biophysical and Physiological Effects of Solar Radiation on Human Skin*. Cambridge, UK: RSC Publishing; 2007.
- [72] Song, HK; Wehrli, FW; Ma, J. *In vivo* MR microscopy of the human skin. *Magnetic Resonance in Medicine*, 1997, 37, 185-91.
- [73] Epstein, EH, Jr.; Munderloh, NH. Human skin collagen. Presence of type I and type III at all levels of the dermis. *Journal of Biological Chemistry*, 1978, 253, 1336-7.
- [74] Duval, C; Regnier, M; Schmidt, R. Distinct melanogenic response of human melanocytes in mono-culture, in co-culture with keratinocytes and in reconstructed epidermis, to UV exposure. *Pigment Cell Research*, 2001, 14, 348-55.

- [75] Thiele, JJ; Schroeter, C; Hsieh, SN, et al. The antioxidant network of the stratum corneum. *Current Problems in Dermatology*, 2001, 29, 26-42.
- [76] Gilchrest, BA. A review of skin ageing and its medical therapy. *British Journal of Dermatology*, 1996, 135, 867-75.
- [77] Sander, CS; Chang, H; Salzmann, S, et al. Photoaging is associated with protein oxidation in human skin in vivo. *Journal of Investigative Dermatology*, 2002, 118, 618-25.
- [78] Hashimoto, K. The structure of human hair. *Clinics in Dermatology*, 1988, 6, 7-21.
- [79] Popescu, C; Höcker, H. Hair - the most sophisticated biological composite material. *Chemical Society Reviews*, 2007, 36, 1282-91.
- [80] Bringans, SD; Plowman, JE; Dyer, JM; et al. Characterization of the exocuticle a-layer proteins of wool. *Experimental Dermatology*, 2007, 16, 951-60.
- [81] Nogueira, ACS; Richena, M; Dicelio, LE, et al. Photo yellowing of human hair. *Journal of Photochemistry and Photobiology B: Biology*, 2007, 88, 119-25.
- [82] Nogueira, ACS; Dicelio, LE; Joekes, I. About photodamage of human hair. *Photochemical and Photobiological Sciences*, 2006, 5, 165-9.
- [83] Dawber, R. Hair: Its structure and response to cosmetic preparations. *Clinics in Dermatology*, 1996, 14, 105-12.
- [84] Williams, DL. Oxidation, antioxidants and cataract formation: a literature review. *Veterinary Ophthalmology*, 2006, 9, 292-8.
- [85] Dillon, J; Spector, A; Nakanishi, K. Identification of  $\beta$ -carbolines isolated from fluorescent human lens proteins. *Nature*, 1976, 259, 422-3.
- [86] Balasubramanian, D; Du, X; Zigler, JS. The reaction of singlet oxygen with proteins, with special reference to crystallins. *Photochemistry and Photobiology*, 1990, 52, 761-8.
- [87] Finley, EL; Dillon, J; Crouch, RK, et al. Identification of tryptophan oxidation products in bovine  $\alpha$ -crystallin. *Protein Science*, 1998, 7, 2391-7.
- [88] Parker, NR; Jamie, JF; Davies, MJ, et al. Protein-bound kynurenone is a photosensitizer of oxidative damage. *Free Radical Biology and Medicine*, 2004, 37, 1479-89.
- [89] Fuentealba, D; Friguet, B; Silva, E. Advanced glycation endproducts induce photocrosslinking and oxidation of bovine lens tissue through Type-I mechanism. *Photochemistry and Photobiology*, 2009, 85, 185-94.
- [90] Piechocki, JT; Thoma, K, editors. *Pharmaceutical Photostability and Stabilization Technology*: Informa HealthCare; 2006.
- [91] Manning, MC; Patel, K; Borchardt, RT. Stability of protein pharmaceuticals. *Journal Pharmaceutical Research*, 1989, 6, 903-18.
- [92] Byrn, SR; Xu, W; Newman, AW. Chemical reactivity in solid-state pharmaceuticals: formulation implications. *Advanced Drug Delivery Reviews*, 2001, 48, 115-36.
- [93] Kerry, JP; Ledward, D; editors. *Improving the Sensory and Nutritional Quality of Fresh Meat*. Cambridge: Woodhead Publishing Limited, 2009.
- [94] Spanier, AM; Flores, M; Toldra, F, et al. Meat flavor: contribution of proteins and peptides to the flavor of beef. In: Shahidi, F, editor. *Quality of fresh and processed foods*: Kluwer Academic/Plenum Publishers; 2004, 33-49.
- [95] Sun, Q; Faustman, C; Senecal, A; et al. Aldehyde reactivity with 2-thiobarbituric acid and TBARS in freeze-dried beef during accelerated storage. *Meat Science*, 2001, 57, 55-60.

- [96] Erickson, MC. Lipid oxidation: Flavor and nutritional quality deterioration in frozen foods. In: MP; Erickson, YC, Hung, editors. *Quality in Frozen Food*: Springer; 1997.
- [97] Love, JD; Pearson, AM. Lipid oxidation in meat and meat products - a review. *Journal of the American Oil Chemists' Society*, 1971, 48, 547-9.
- [98] Møller, JKS; Bertelsen, G; Skibsted, LH. Photo-oxidation of nitrosylmyoglobin at low oxygen pressure. Quantum yields and reaction stoichiometries. *Meat Science*, 2002, 60, 421-5.
- [99] Kan, CW; Chan, K; Yuen, CWM, et al. Wool modification. *Textile Asia*, 1997, 28, 39-45.
- [100] Xiong, YL. Protein oxidation and implications for muscle food quality. In: E; Decker, C; Faustman, CJ; Lopez-Bote, editors. *Antioxidants in Muscle Foods - Nutritional Strategies to Improve Quality*: Wiley Interscience; 2000, 85-112.
- [101] Kinoshita, Y; Sato, T. (2007). Proteomic studies on protein oxidation in bonito (*Katsuwonus pelamis*) muscle. *Food Science and Technology Research*, 13, 133-8.
- [102] Kjaersgaard, IVH; Jessen, F. Two-dimensional gel electrophoresis detection of protein oxidation in fresh and tainted rainbow trout muscle. *Journal of Agricultural and Food Chemistry*, 2004, 52, 7101-7.
- [103] Baron, CP; Kjærsgård, IVH; Jessen, F, et al. Protein and lipid oxidation during frozen storage of rainbow trout (*Oncorhynchus mykiss*). *Journal of Agricultural and Food Chemistry*, 2007, 55, 8118-25.
- [104] Tokur, B; Korkmaz, K. The effects of an iron-catalyzed oxidation system on lipids and proteins of dark muscle fish. *Food Chemistry*, 2007, 104, 754-60.
- [105] Farrell, HM; Jr; Jimenez-Flores, R; Bleck, GT; et al. Nomenclature of the proteins of cows' milk - Sixth revision. *Journal of Dairy Science*, 2004, 87, 1641-74.
- [106] Mestdagh, F; De Meulenaer, B; De Clippeleer, J, et al. Protective influence of several packaging materials on light oxidation of milk. *Journal of Dairy Science*, 2005, 88, 499-510.
- [107] Havemose, MS; Weisbjerg, MR; Bredie, WLP; et al. Influence of feeding different types of roughage on the oxidative stability of milk. *International Dairy Journal*, 2004, 14, 563-70.
- [108] Jung, MY; Yoon, SH; Lee, HO; et al. Singlet oxygen and ascorbic acid effects on dimethyl disulfide and off-flavor in skim milk exposed to light. *Journal of Food Science*, 1998, 63, 408-12.
- [109] Becker, EM; Cardoso, DR; Skibsted, LH. Deactivation of riboflavin triplet-excited state by phenolic antioxidants: mechanism behind protective effects in photo-oxidation of milk-based beverages. *European Food Research & Technology*, 2005, 221, 382-6.
- [110] Dalsgaard, TK; Otzen, D; Nielsen, J, et al. Changes in structures of milk proteins upon photo-oxidation. *Journal of Agricultural and Food Chemistry*, 2007, 55, 10968-76.
- [111] Dalsgaard, TK; Heegaard, CW; Larsen, LB. Plasmin digestion of photooxidized milk proteins. *Journal of Dairy Science*, 2008, 91, 2175-83.
- [112] Dalsgaard, TK; Larsen, LB. Effect of photo-oxidation of major milk proteins on protein structure and hydrolysis by chymosin. *International Dairy Journal*, 2009.
- [113] Møller, IM; Kristensen, BK. Protein oxidation in plant mitochondria as a stress indicator. *Photochemical and Photobiological Sciences*, 2004, 3, 730-5.

- [114] Rinalducci, S; Murgiano, L; Zolla, L. Redox proteomics: basic principles and future perspectives for the detection of protein oxidation in plants. *Journal of Experimental Botany*, 2008, 59, 3781-801.
- [115] Heinio, RL; Lehtinen, P; Oksman-Caldentey, KM; et al. Differences between sensory profiles and development of rancidity during long-term storage of native and processed oat. *Cereal Chemistry*, 2002, 79, 367.
- [116] MacKinnon, PJ; Powell, BC; Rogers, GE. Structure and expression of genes for a class of cysteine-rich proteins of the cuticle layers of differentiating wool and hair follicles. *Journal of Cell Biology*, 1990, 111, 2587-600.
- [117] Jianzhong, S; Jinqiang, L; Jinhuan, Z; et al. X-ray photoelectron spectroscopic study of silk fibroin surface. *Polymer International*, 2002, 51, 1479-83.
- [118] Duffield, PA; Lewis, DM. The yellowing and bleaching of wool. *Review of Progress in Coloration*, 1985, 15, 38-51.
- [119] Baltova, S; Vassileva, V. Photochemical behaviour of natural silk-II. Mechanism of fibroin photodestruction. *Polymer Degradation and Stability*, 1998, 60, 61-5.
- [120] Dyer, JM; Cornellison, CD; Bringans, SD, et al. The photoyellowing of stilbene-derived fluorescent whitening agents-mass spectrometric characterization of yellow photoproducts. *Photochemistry and Photobiology*, 2008, 84, 145-53.
- [121] Millington, KR. Photoyellowing of wool. Part 1: Factors affecting photoyellowing and experimental techniques. *Coloration Technology*, 2006, 122, 169-86.
- [122] Millington, KR; Maurdev, G. The generation of superoxide and hydrogen peroxide by exposure of fluorescent whitening agents to UVA radiation and its relevance to the rapid photoyellowing of whitened wool. *Journal of Photochemistry and Photobiology A: Chemistry*, 2004, 165, 177-85.
- [123] Nevin, A; Anglos, D. Assisted interpretation of laser-induced fluorescence spectra of egg-based binding media using total emission fluorescence spectroscopy. *Laser Chemistry*, 2006, Article ID 82823, 5.
- [124] Domingues, MR; Domingues, P; Reis, A, et al. Identification of oxidation products and free radicals of tryptophan by mass spectrometry. *Journal of the American Society for Mass Spectrometry*, 2003, 14, 406-16.
- [125] Abello, N; Kerstjens, HAM; Postma, DS; et al. Protein tyrosine nitration: Selectivity, physicochemical and biological consequences, denitration and proteomics methods for the identification of tyrosine-nitrated proteins. *Journal of Proteome Research*, 2009, 8, 3222-38.
- [126] Thomas, SN; Lu, BW; Nikolskaya, T; et al. MudPIT (multidimensional protein identification technology) for identification of post-translational protein modifications in complex biological mixtures. In: I; Dalle-Donne, A; Scaloni, DA; Butterfield, editors. *Redox Proteomics - From Protein Modifications to Cellular Dysfunctions and Diseases*. Hoboken: John Wiley and Sons, Inc., 2006, 233-52.
- [127] BLAST software. Available from: [http://blast.ncbi.nlm.nih.gov/Blast.cgi?PROGRAM=blastp&BLAST\\_PROGRAMS=blastp&PAGE\\_TYPE=BlastSearch&SHOW\\_DEFAULTS=on&LINK\\_LOC=blasthome](http://blast.ncbi.nlm.nih.gov/Blast.cgi?PROGRAM=blastp&BLAST_PROGRAMS=blastp&PAGE_TYPE=BlastSearch&SHOW_DEFAULTS=on&LINK_LOC=blasthome)
- [128] Gracanin, M; Hawkins, CL; Pattison, DI; et al. Singlet-oxygen-mediated amino acid and protein oxidation: Formation of tryptophan peroxides and decomposition products. *Free Radical Biology and Medicine*, 2009, 47, 92-102.

- [129] Grosvenor, AJ; Morton, JD; Dyer, JM. Profiling of residue-level photo-oxidative damage in peptides. *Amino Acids*, 2009, In Press doi: 10.1007/s00726-009-0440-7.
- [130] Wiese, S; Reidegeld, KA; Meyer, HE; et al. Protein labeling by iTRAQ: A new tool for quantitative mass spectrometry in proteome research. *Proteomics*, 2007, 7, 340-50.
- [131] Wu, WW; Wang, G; Baek, SJ, et al. Comparative study of three proteomic quantitative methods, DIGE, cICAT, and iTRAQ, using 2D gel- or LC-MALDI TOF/TOF. *Journal of Proteome Research*, 2006, 5, 651-8.
- [132] Chen, X; Chen, YH; Anderson, VE. Protein crosslinks: Universal isolation and characterization by isotopic derivatization and electrospray ionization mass spectrometry. *Analytical Biochemistry*, 1999, 273, 192-203.
- [133] Back, JW; Notenboom, V; De Koning, LJ; et al. Identification of crosslinked peptides for protein interaction studies using mass spectrometry and  $^{18}\text{O}$  labeling. *Analytical Chemistry*, 2002, 74, 4417-22.
- [134] Mirza, SP; Greene, AS; Olivier, M.  $^{18}\text{O}$  labeling over a coffee break: A rapid strategy for quantitative proteomics. *Journal of Proteome Research*, 2008, 7, 3042-8.



## ***Chapter 5***

# **EARLY STAGES IN FORMATION OF PHOTOSYNTHETIC PIGMENT APPARATUS**

***Olga B. Belyaeva\* and Felix F. Litvin***

Faculty of Biology, Lomonosov Moscow State University, Moscow, Russia.

## **ABSTRACT**

Contemporary data are reviewed concerning the mechanism of terminal light-dependent stage of chlorophyll biosynthesis from the dark precursor, protochlorophyllide. The application of spectral methods provided the possibility to investigate this process immediately in plants leaves. The photochemical hydrogenation of the precursor molecule catalyzed by the photoenzyme, protochlorophyllide oxidoreductase with the involvement of hydrogen donor NADPH includes two consecutive photoreactions that give rise to a branched network of dark reactions. These reactions produce a number of chlorophyll–protein complexes of the light-harvesting antenna and minor components integrated into the structure of two photochemical systems of photosynthesis. One of the branches of the reaction pathways represents the terminal light-dependent biosynthesis of pheophytin a, which is an immediate electron acceptor of photosystem II in green plant leaves. The features of chlorophyll biosynthesis at early stages of etiolated leaf formation and in green plant leaves are considered.

Footnote: Dedicated to the memory of our friend and colleague, Dr. N.V. Ignatov.

## **INTRODUCTION**

Chlorophyll biosynthesis in plant leaves is one of the most important biospheric processes. It enables production, renewal, and permanent maintenance of the main photosynthetic pigment required for effective photosynthesis and high productivity of plants. Annual synthesis of chlorophyll in the biosphere amounts to more than one billion metric tons of chlorophyll.

---

\* Corresponding author: Fax: +7 (495) 939-54-89; E-Mail: olgabelyaeva@mail.ru

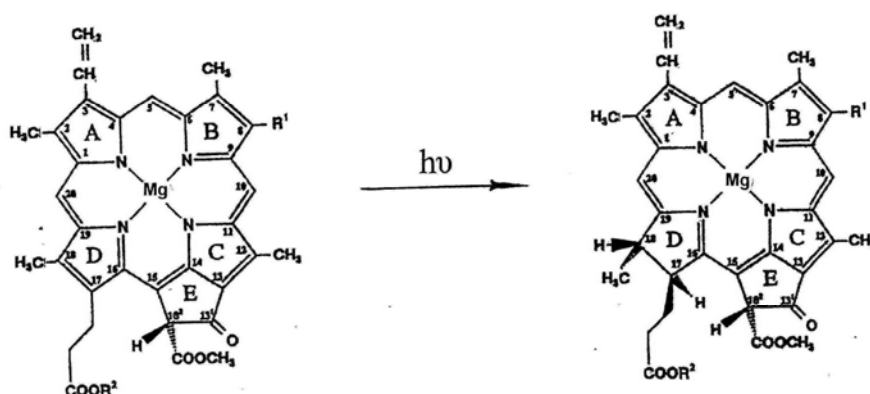


Figure 1. Structures of protochlorophyllide and chlorophyll(ide) molecules.  $R_1$  designates the  $CH_2-CH_3$  group for the monovinyl form of the pigment and  $CH=CH_2$  for the divinyl form.  $R_2$  designates  $C_{20}H_{39}$  (phytol) in the case of protochlorophyll or chlorophyll and stands for hydrogen atom in the case of protochlorophyllide and chlorophyllide.

In the absence of light chlorophyll biosynthesis ceases at the stage of protochlorophyllide accumulation in etiolated leaves. This precursor (see Figure 1) differs from chlorophyll by the absence of phytol moiety and by the presence of a double bond (rather than a single bond) in the macrocycle D-ring. The terminal light-dependent stage of chlorophyll biosynthesis begins from the fast and highly efficient photochemical reduction of the double bond, which initiates the network of dark and photochemical reactions leading to the production of several chlorophyll–protein complexes and to their incorporation into the structures that participate in the construction of photosynthetic pigment machinery.

This review deals with the studies that clarified the general sequence of photochemical and dark reactions at the terminal step of chlorophyll biosynthesis at various stages of higher plant development.

## HISTORICAL SURVEY OF RESEARCH ON THE TERMINAL LIGHT-DEPENDENT STAGE OF CHLOROPHYLL BIOSYNTHESIS

The study of chlorophyll biosynthesis as a light-dependent process began in the end of the 19th century. It was initially thought that the chlorophyll precursor is either a colorless substance “leucophyll” or a yellow pigment of etiolated leaves “etiolin.” From examining the absorption spectra, Timiryazev discovered in 1886 that the ethanolic extracts from etiolated seedlings contain a colored substance, whose absorption spectrum differs from that of chlorophyll. He termed this substance “protophylline.” Timiryazev decided that the discovered substance is a chlorophyll precursor [1,2]. Monteverde in 1894 named the chlorophyll precursor with a newly introduced term “protochlorophyll,” which became later commonly accepted [3]. Monteverde and Lyubimenko succeeded in measuring the absorption spectra of etiolated leaves directly during illumination [4]. Despite primitive technical tools available at that time (spectroscope and petroleum lamp as a light source), they were first to discover that light-induced chlorophyll formation is a multistage process, whose intermediate products can be distinguished according to the positions of absorption bands. They concluded

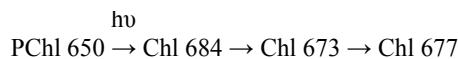
that the etiolated plant leaves produce a labile intermediate, “chlorophyllogen” or “protochlorophyll associated with protein” that converts to chlorophyll under the action of light [4]. Monteverde and Lyubimenko described the pattern of absorption spectral changes in vivo well ahead of the results obtained half a century later with the use of more sophisticated spectral methods [5,6].

Owing to the improvement of spectral and biochemical methods, new data were obtained in the middle of the 20th century, which shed some light on mechanisms of terminal stages in chlorophyll biosynthesis. The absorption spectra of protochlorophyll solutions were accurately measured [7]. The action spectrum of chlorophyll formation was found to correspond to the absorption spectrum of protochlorophyll in its natural state [8]. The kinetics of chlorophyll formation and protochlorophyll decay were compared on a quantitative basis [9]. These data taken together proved that protochlorophyll is indeed the chlorophyll precursor.

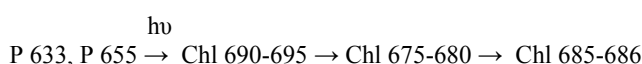
Later a notion was put forward that the protochlorophyll active form is a pigment–protein complex. Upon illumination of etiolated leaf homogenates, the transformation of precursor to chlorophyll was observed: the protochlorophyll absorption band at 635 nm disappeared from the spectrum while a new band of chlorophyll absorption at 670 nm emerged [10]. The glycerol solutions of pigment–protein complexes from etiolated leaves, termed protochlorophyllide holochromes showed a more complicated pattern of spectral changes [11–13]. Protochlorophyllide holochromes were characterized by absorption peaks at 640, 645, or 650 nm depending on plant species. The illumination led to formation of chlorophyll with the absorption maximum at 678–680 nm, which shifted later to 670–672 nm:



Owing to the development of spectral methods, the processes occurring in whole etiolated leaves were investigated in detail. Analysis of absorption spectra revealed that illumination of etiolated leaves is accompanied by the decrease in the precursor absorption band at 650 nm and by the appearance of chlorophyll(ide) absorption maximum at 684 nm, which shifts during the dark reaction first toward the short-wavelength region (the Shibata shift) and then to the long-wavelength range [5,6]:



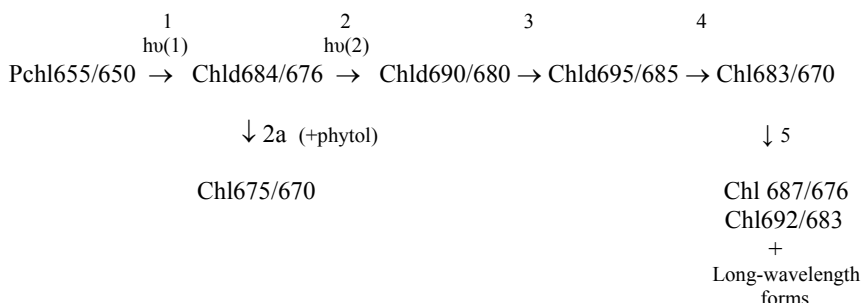
Litvin and Krasnovsky applied the method of nondestructive cryogenic fluorescence spectroscopy for studying the biosynthesis of chlorophyll from its precursor [14]. Rapid fixation of etiolated or illuminated leaves with liquid nitrogen (77 K) was used as a tool to suppress temperature-dependent stages of the light-dependent process. This approach revealed that the formation of native chlorophyll from its precursor, protochlorophyll(ide) in greening leaves includes several intermediary stages: the photochemical reaction (precursor reduction per se) and two temperature-dependent dark stages. Based on the analysis of low-temperature fluorescence spectra, the following reaction scheme was suggested:



Numbers represent the position of fluorescence maximum at 77 K. Designations P633 and P655 signify the inactive and active precursor forms, respectively.

From comparing the reaction schemes suggested by Shibata and by Litvin and Krasnovsky, one may conclude that these authors discovered by different methods the same intermediates involved in the process of native chlorophyll formation. This conclusion was supported by the results of parallel measurements of absorption and fluorescence changes [15,16]. Furthermore, the existence of one additional intermediate stage was recognized. It was found that the form Chlide690/680 produced under the action of light transforms during dark reaction into a red-shifted form Chlide695/685 [15, 17-19].

Some data pointed to even higher complexity of the process. When spectral patterns were examined as a function of light intensity, it was found out that, at low intensities of actinic light, the long-wavelength form Chl 690-695 is not the first intermediate produced. The fluorescence maximum of the earliest form observed was blue-shifted to about 675 nm. Based on this observation, a more complex scheme of light and dark reactions in chlorophyll biosynthesis with participation of two photochemical reactions was suggested [17]. The interrelations between photochemical and dark reactions were clarified by studying the process as a function of temperature, spectral composition of actinic light, as well as intensity and duration of illumination under constant dose of absorbed light energy [15, 19, 20]. The sequence of photochemical and dark reactions of chlorophyll formation from its precursor, protochlorophyllide was represented as a scheme including two consecutive photoreactions and a side-path reaction leading to the production of short-wavelength chlorophyll form:



The slash-separated numbers here and in the text below indicate the positions of spectral maxima (fluorescence/absorption) at low-temperature (77 K).

The existence of two consecutive photoreactions in the pathway of chlorophyll biosynthesis was supported by other researchers [21-23]. Mathis and Sauer [22] and later Oliver and Griffiths [23] not only confirmed the existence of two successive photoreactions but also approved the above-presented scheme of light and dark reactions, including the side-path reaction.

Remarkable advances of the last decades in studying the terminal stage of chlorophyll biosynthesis were related to identification of the hydrogen donor (NADPH) in the reaction of protochlorophyllide photoreduction [24,25] and to the discovery of protochlorophyllide-oxidoreductase (POR), the enzyme that catalyzes the photoconversion of protochlorophyllide to chlorophyllide [26-29]. It was concluded that photoreduction of protochlorophyllide is carried out in a special active complex comprising the enzyme, protochlorophyllide, and a hydrogen donor NADPH. The analysis of amino acid sequence [30,31] and secondary

structure of POR [32] led to the conclusion that this enzyme belongs to the family of short-chain alcohol dehydrogenases within the enzyme superfamily “RED” (reductases – epimerases – dehydrogenases). Two features distinguish POR from other members of short-chain dehydrogenase-reductase family: porphyrin is used as a substrate, and the enzyme activity is strictly light dependent. It was shown by gel filtration chromatography that the native enzyme POR exists predominantly in a dimeric state [33]. Presently, three POR varieties have been discovered in plant leaves: POR A, POR B, and POR C. These enzymes are encoded by different genes (*PorA*, *PorB*, *PorC*) [34,35], whose expression is differentially regulated by light [35-37].

The main active precursor of chlorophyll is the phytol-free protochlorophyllide [38,39]. At the same time, there is a minor pool of active complexes comprising the chlorophyll precursors esterified with phytol group. Both pools of chlorophyll precursor (protochlorophyllide and its esterified form) are heterogeneous, i.e., they comprise both the monovinyl and divinyl modifications of the chromophore.

## GENERAL SCHEME OF PHOTOCHEMICAL AND DARK REACTIONS AT THE TERMINAL STAGE OF CHLOROPHYLL BIOSYNTHESIS

The results obtained by many research groups including our laboratory provided new data on light-dependent biosynthesis of native photosynthetic pigment forms from protochlorophyllide as a precursor. These studies can be summarized with the scheme that presently seems the most documented and complete (Figure 2). The scheme includes a branched chain of transformations of pigment–protein complexes, which leads to the production of several native chlorophyll forms. Some of these chlorophylls are constituents of the bulk pigment (light-harvesting antenna) and others represent minor, though functionally important, pigment forms integrated in two pigment systems of photosynthesis.

### Chlorophyll Precursors

The reaction chain starts from the native forms of chlorophyll precursor, protochlorophyllide. The occurrence of several spectrally different forms of chlorophyll precursors was unveiled using the methods of low-temperature spectroscopy, including derivative spectroscopy [40-45]. Etiolated leaves contain three major spectral forms of protochlorophyllide: Pchlde633/628, Pchlde643/637, and the dominant, in most cases, form Pchlde655/650. In addition, there are five minor long-wavelength forms: Pchlde666–669/658, Pchlde680–682/668, Pchlde690–692/677, Pchlde698/686, and Pchlde728/696.

The main photoactive form Pchlde655/650 is detected only in whole etiolated leaves. Recently, direct evidence was obtained that the active protochlorophyllide Pchlde655/650 is composed of two pools: Pchlde653/648 and Pchlde657/650 [44, 46]. The photochemically active form Pchlde653 accumulates to the highest extent in very young (2–3 days) etiolated leaves, where prolamellar bodies have not yet formed [47, 48].

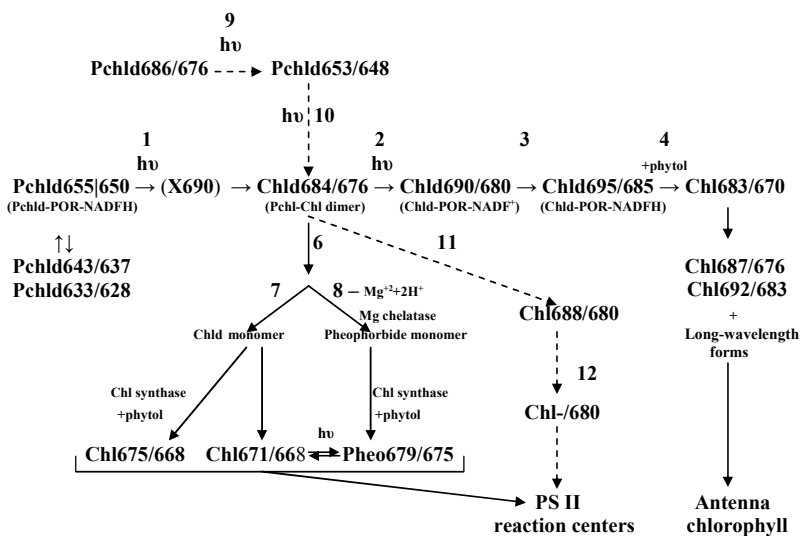


Figure 2. General scheme for conversions of the pigment chromophore at the light stage of chlorophyll biosynthesis in plant leaves. Pchlid—protochlorophyllide, Chlid—chlorophyllide, Chl—chlorophyll. Numbers indicate peak positions of fluorescence (first index) and absorption (second index) for various pigment forms. Solid line arrows designate the pathway leading to formation of native pigments in the light-harvesting complex (reactions 1–5) and the divergent pathway producing pheophytin and two short-wavelength chlorophylls of PSII reaction centers (path 6–8). Dashed line arrows denote the pathway of producing the pigment P-680 of PSII reaction centers from the long-wavelength form of protochlorophyllide (reactions 9–12). X-690 is a nonfluorescent intermediate.

Protochlorophyllide Pchlide643/637 manifests itself in absorption spectra but is practically invisible in fluorescence spectra, which is caused by highly effective energy transfer from this form to Pchlide655/650 [49–51]. Pchlide643/637 is a dominant form in etiolated leaves of some species. Measurements of absorption spectra [52] and subtracted "light–minus–dark" fluorescence spectra [44] proved that this form dominates in leaves of young plants. This form is most abundant in homogenates and reconstituted ternary complexes comprising protochlorophyllide, POR, and NADPH. The form Pchlide643/637 is photochemically active and, similarly to protochlorophyllide Pchlide655/650, transforms to chlorophyllide under the action of light at rather low temperatures. However, its photoactivity *in vivo* shows a stronger temperature dependence compared to that of the main active form Pchlide655/650 [53]. The long-wavelength position of maxima for active protochlorophyllide forms Pchlide643/637 and Pchlide655/650 is caused by the linkage of the chromophore to both the photoenzyme POR and hydrogen donor NADPH, as well as by chromophore–chromophore interactions between pigment molecules. It is supposed that protochlorophyllide molecules produce dimers [54] or tetramers [55]. Apparently, the pigment–pigment interaction is determined by aggregation of chromophore-carrying protein molecules (POR).

The form Pchlide633/628 is presumably inactive since it does not transform to chlorophyllide upon short-term illumination [43,56]. However, in plants enriched with this form, its slow conversion to chlorophyllide was observed [53,57,58] at temperatures above 5°C [53]. It was supposed that Pchlide633/628 corresponds to protochlorophyllide that is not specifically bound to POR enzyme [23,25]. The short-wavelength protochlorophyllide form is possibly attached to POR in such a way that its photochemical activity is lost [59]. The

association with protein for monomeric short-wavelength protochlorophyllide Pchlde633/628 is supported by data on fluorescence decay time for this form, which is substantially shorter (about 6 ns) [60] than the decay time for protochlorophyllide in solution (about 10 ns). According to the results of some studies, Pchlde633/628 is a precursor of photoactive forms Pchlde655/650 and P643/637 in the dark pathway of pigment synthesis [61,62]. According to Griffiths [61], the short-wavelength form Pchlde633/628 represents protochlorophyllide bound to protein but not bound to NADPH. The active short-wavelength form of protochlorophyllide is present in very young (embryonic) leaves of dicotyledonous plants [47,63,64].

The nature of native long-wavelength spectral forms is presumably related to the existence of large protochlorophyllide aggregates. This is evidenced by the presence of similar bands in spectra of aggregated protochlorophyll in model systems [65-67] and of protochlorophyll in seed coats of some plant species [68,69], where the long-wavelength protochlorophyll form resides in the crystalline state [68]. The formation of protochlorophyllide aggregates is apparently promoted by aggregation of the enzyme POR, because such aggregation facilitates the interaction of porphyrin rings of the pigment molecules.

### Linear Reaction Chain (Reactions 1-5 in the Scheme)

The linear reaction chain includes two consecutive photochemical stages (1 and 2 in the scheme) [15,19,20,22,23] and subsequent dark processes [15,18-20,22,23]. Judging from spectral changes of circular dichroism in homogenates from etiolated plant leaves exposed to illumination, one may suppose that the first photochemical reaction engages one of the two molecules composing the protochlorophyllide dimer; this reaction produces the complex of two weakly bound molecules (protochlorophyllide and chlorophyllide). The second light reaction performs the photoconversion of the second protochlorophyllide molecule [22].

The photochemical reduction of protochlorophyllide, during which two hydrogen atoms are attached to the double bond 7=8 in the pyrrole ring D, is accomplished in the ternary active pigment–enzyme complex. Based on the methods of low-temperature spectroscopy [70-76], high-resolution time-resolved spectroscopy [77-79], and EPR spectroscopy [80], it was found that the photochemical reaction comprises the production of a short-lived nonfluorescent intermediate featuring the absorption maximum at about 690–695 nm (X690) and the singlet EPR signal with g-factor of the free electron. The appearance of nonfluorescent intermediate in the course of protochlorophyllide photoreduction was also discovered in model systems, such as protochlorophyll solutions [80] and reconstituted ternary pigment–protein complexes [81-83]. The short-lived intermediate X690 is likely to be the charge-transfer complex [83-85]. The nonfluorescent intermediate is stabilized at low temperature (about 77 K). The complete reduction of the molecule occurs upon the increase in temperature and does not need light energy. The second proton is apparently donated from the tyrosine group (Tyr-275) of protochlorophyllide oxidoreductase [31]. Wilks and Timko proposed a model for the catalytic mechanism of protochlorophyllide photoreduction by oxidoreductase in the active center of the ternary complex; the model is based on comparison with the short-chain alcohol dehydrogenases whose structure is known. According to this

model, the position of porphyrin ring D is fixed against NADPH and Tyr-275, which optimizes the possibility for hydride-ion and proton transfer. The proton of tyrosine phenol group arrives at C<sub>18</sub> atom of protochlorophyllide molecule, whereas hydride-ion is transferred from NADPH to C<sub>17</sub> position [31].

The second photoreaction is followed by light-independent temperature-sensitive spectral shift to a longer wavelength: Chlide690/680 → Chlide695/685 (reaction 3 in the scheme) [18,19]. This shift corresponds tentatively to the restoration of the reduced hydrogen donor in the pigment–protein complex (reduction of NADP<sup>+</sup> produced in the primary photoreaction) [23,86,87]. On the other hand, energy transfer studies led to the suggestion that the bathochromic shift of spectral bands in this reaction can be due to shortening of intermolecular distances in the aggregated active complex [51]. It is possible that the process stage considered here is determined by simultaneous action of two factors, i.e., by structural changes of the aggregated complex and by NADPH restoration, provided that the structure of POR complex and the chromophore–chromophore interaction depend on the NADPH redox state (oxidized or reduced).

The subsequent dark reaction (reaction 4 in Figure 2) is manifested as a short-wavelength shift of the pigment spectral bands: Chlide 695/685 → Chl683/670 (the Shibata shift) [5,6]. At this stage chlorophyllide molecule is esterified in plant leaves to produce chlorophyll [88]. There is ample evidence to suggest that the Shibata shift to shorter wavelengths is related to pigment disaggregation. This is evident from the increase in chlorophyll fluorescence yield [21,89], disappearance of the double signal in circular dichroism spectra [90,91], and disturbance of energy transfer from protochlorophyllide to chlorophyll [21,89]. Based on estimated initial distance of about 25 Å between protochlorophyllide molecules in the active complex, Thorne proposed that the disruption of energy transfer implies the increase in the distance between chlorophyll and non-transformed protochlorophyllide by about 10 Å [21]. The fractionation of prolamellar bodies with isoelectric focusing gave grounds to suggest that the Shibata shift reflects disaggregation of large pigment–POR enzyme complex into smaller ones, rather than complete destruction of such complexes [92]. Disaggregation of POR may result in pigment disaggregation. The loosening of the complex is likely to facilitate the pigment esterification, i.e., the attachment of a hydrophobic alcohol to the pigment molecule.

The concluding long-wavelength shift Chl670/683 → Chl676/687; Chl683/692 (reaction 5 in the scheme) corresponds to the final integration of chlorophyll into various pigment–protein complexes of the thylakoid membrane and to formation of chlorophyll spectral forms characteristic of mature green leaf. Judging from the amount of chlorophyll synthesized by this pathway and its energy coupling (excitation energy transfer) with carotenoids and chlorophyll *b*, this chlorophyll pool is identical to the antenna chlorophyll.

## **Branching of the Biosynthetic Pathway: Side Path of Chlorophyllide Chlide684/676 Conversions (Reaction 6-8)**

The above-described direct pathway involving two successive photoreactions is manifested at sufficiently high light intensities. At low intensity light, another, light-independent side-branch pathway can be traced. The rate of the starting reaction (reaction 6) is lowered upon the decrease in temperature (this reaction actually stops at temperatures

below 273 K). Thus, the intermediate Chlide684/676 produced in the first photoreaction (reaction 1) is the point of divergence of the reaction pathways. This intermediate accumulates under suppression of both the second light reaction and the side path. The optimal condition for such accumulation is a short-term illumination with a high-intensity light at low temperature (223 K) (the second reaction is inhibited stronger under these conditions than the first one, owing to the difference in activation energies) [19,20].

As shown in our early work, the accumulated intermediate Chl684/676 transforms upon heating to the short-wavelength chlorophyll form Chl675/670 in the dark reaction (see the scheme at p.4) [19,20,22,23]. The analysis of extracts by means of thin-layer chromatography showed that the product of the side-path dark reaction is chlorophyll rather than chlorophyllide [20]. Thus, the esterification of chlorophyll molecule occurs not only during Shibata shift, as was supposed before, but it proceeds at manifold (an order of magnitude) higher rate in the reaction specified here during the dark production of Chl675/670 from the products of first photoreaction. The occurrence of two pathways for esterification of chlorophyllide in chlorophyll biosynthesis—fast and slow pathways—was demonstrated later by Domanskii et al. [93].

Considering the short-wavelength spectral shift, resistance of Chl675/670 to disaggregating treatments, comparatively high extractability of this product (compared to Chlide690/680) [19,20], and circular dichroism spectra measurements [22], it appears that the side-path reaction is accompanied by pigment disaggregation. It is reasonable to suppose that disaggregation promotes the enzymatic esterification of the pigment molecule, like it occurs at the Shibata shift stage. It turned out that the final chlorophyll form produced in the side-path reaction, designated previously as Chl675/670, is actually a composition of two chlorophyll forms, Chl671/668 and Chl675/668 [94,95] (reactions 7 in Figure 2).

## Biosynthesis of Pheophytin A

Pheophytin *a* is known to play a key role in photosynthesis: it serves as a first intermediate acceptor of electrons arriving from chlorophyll of the reaction center in photosystem II (PSII) [96,97]. However, the final stage of pheophytin biosynthesis remained unexplored.

It was found out that the terminal stage of pheophytin biosynthesis is closely related to the side-path reaction of chlorophyll biosynthesis. The active protochlorophyllide form, Pchlde655/650 is a shared precursor of both pigments. The first photoreaction producing the intermediate Chlide684/676 is also common for synthesis of both pigments (reaction 1 in Figure 2). The application of low-temperature fluorescence spectroscopy revealed that the side-path reaction sequence is divided in two branches [94,95]. In one of these paths, phytol is attached to chlorophyllide, which results in the formation of two short-wavelength chlorophyll forms: Chl671/668 and Chl675/668 (reaction 7). The parallel path (reaction 8) results in pigment pheophytinization through the replacement of central Mg atom with hydrogen, which gives rise to pheophorbide and subsequent attachment of phytol. Thus, the native pheophytin form Pheo679/675 is produced. In experiments with light action on the products of side-chain reactions, it was found that Chl671/668 is photoconverted to pheophytin and that this reaction is reversible in darkness.

Pheophytin formation represents the biosynthetic process, not the destructive reaction: it proceeds only in intact pigment–protein complexes and is not observed even in homogenates of etiolated leaves. By analogy with the results obtained for earlier dark stages of porphyrin biosynthesis, one may assume that pheophytinization is catalyzed by Mg-chelatase. This assumption is supported by several facts: the terminal stage of pheophytin biosynthesis is irreversibly inhibited upon heating above 323 K; the process is activated by the presence of ATP and is inhibited by AMP. The complex of pheophytin and chlorophyll in etiolated leaves is identical in several traits to pheophytin-containing reaction centers of PSII [94,95]. However, the high quantum yield of pheophytin fluorescence in greening leaves implies that pheophytin molecules reside in different states in these structures and the reaction centers.

## Biosynthesis of Long-Wavelength Chlorophyll as a Possible Component of PSII Reaction Centers

The reaction sequence depicted in Figure 2 with dashed lines (reactions 9–12 in the scheme) leads to the production of long-wavelength chlorophyll whose spectral characteristics are close to chlorophyll P-680, a component of PSII reaction center. This pathway was first observed upon illumination of etiolated leaves exposed to heat shock treatment [98]. Thus, a new dark reaction was revealed for Chlide 684/676, a product of protochlorophyllide photoreduction located at the point of bifurcation of the reaction sequence. This reaction is manifested in bathochromic shift of chlorophyllide spectral bands and is accompanied by chlorophyllide esterification: Chlide 684/676 → Chlide 688/680. After the completion of this reaction, fluorescence of the product was entirely quenched within 20–30 s: Chl 688/680 → Chl-/680. The authors supposed that the final product of this dark reaction chain is nonfluorescent chlorophyll Chl-680 identical to the pigment P-680 in the PSII reaction center [98].

Investigation of chlorophyll biosynthesis in young (3- to 4-day-old) etiolated leaves yielded additional data concerning the mechanism of chlorophyll P-/680 biosynthesis under natural conditions [46]. In these juvenile leaves, like in 7- to 10-day-old leaves grown under heat shock conditions, the intermediate Chlide 684/676 participated at room temperature in two dark reactions: Chlide 684/676 → Chl 675/670 (side-path reaction 6→7) and Chlide 684/676 → Chl 688/680 → Chl-/680 (reactions 11→12 in Figure 2). A specific feature of the process in young plants was accumulation of Chlide 684/676 within first 3–5 s of illumination by white light, without appreciable changes in absorption and fluorescence bands of protochlorophyllide Pchlde 655/650, even though the phototransformation of protochlorophyllide (evaluated in extracts) did occur under these conditions. Experiments with the use of monochromatic illumination in the long-wavelength region (680 nm) or white light irradiance at various temperatures led to the conclusion that this phenomenon results from the phototransformation of previously unknown weakly fluorescent long-wavelength protochlorophyllide form Pchlde 686/676 into protochlorophyllide Pchlde 653/648 (reaction 9); the latter intermediate converts to chlorophyllide Chlide 684/676 in the subsequent light reaction (reaction 10). Thus, at early stages of plant development, apart from the main branched reaction pathway, an additional branched process was found to occur, which synthesizes nonfluorescent chlorophyll Chl-/680 (possibly, the pigment of PSII reaction

center) from long-wavelength protochlorophyllide Pchlde 686/676 through the intermediate stage of producing the active protochlorophyllide form Pchlde 653/648.

Thus, the native chlorophyllide form Chlide 684/676 produced by the first photochemical reaction from Pchlde655/650 is a triple branching point of biosynthetic pathways leading to production of chlorophyll and pheophytin minor forms associated with reaction centers of PSII, as well as to formation of bulk antenna chlorophyll.

## On the “Shuttle” Mechanism of Photoenzyme POR Operation

Already in early studies of protochlorophyllide–protein complex, a suggestion was put forward about the multiple use of the carrier protein during chlorophyll biosynthesis. In a recent work [63] the authors suggested a general scheme of chlorophyll formation comprising two pathways for chlorophyll biosynthesis and regeneration of photoactive protochlorophyllide complex; i.e., two cycles of reiterative POR usage. By comparing the spectral characteristics of intermediates and reaction products, one may conclude that the two cycles in the Schoefs and Franck’s scheme correspond to the same processes that are shown in the above-presented scheme in Figure 2: the “side-path” reaction (reaction 6) and the reaction sequence leading to formation of pigment forms of the light-harvesting complex (reactions 1–4). Summing up the results of various researchers, Schoefs and Franck [63] proposed that one cycle (corresponding to the side reaction) is performed in the case when the concentration of non-photoactive protochlorophyllide is sufficiently high with respect to the concentration of produced chlorophyllide. According to the authors’ idea, in this case chlorophyllide escapes rapidly from the enzyme and is replaced by the protochlorophyllide in the POR aggregate. This cycle occurs in the etioplast membranes, embryonic leaves, isolated prolamellar bodies, and at low light intensities. The second cycle (corresponding to reactions 1–4 in Figure 2) operates when the photoconversion of protochlorophyllide pool is more complete (low ratio of inactive protochlorophyllide and the produced chlorophyllide). The authors believe that chlorophyllide in this case remains bound to the enzyme for a longer time, during which the enzyme aggregate disintegrates (at the stage of Shibata short-wavelength shift).

## Chlorophyll Photobiosynthesis in Embryonic Leaves

The pathway of chlorophyll biosynthesis in embryonic leaves of dicotyledonous plants differs from the reaction sequence described above for etiolated 3- to 8-day-old seedlings. Embryonic leaves accumulate predominantly the short-wavelength form characterized by the band of low-temperature fluorescence at about 632–635 nm [47,63,64]. In addition, there is another red-shifted form with the fluorescence band at 653–655 nm. In fluorescence spectra obtained at room temperature, the main maximum is positioned at 636–637 nm [63,64]. The short-wavelength form of embryonic leaves was found to be photoactive. Under the action of light this form converts to the short-wavelength chlorophyllide form Chl675/670. According to Dubrovskii and Litvin [64], the transformation proceeds through the production of intermediate Chlide684/676; i.e., via the side-branch reaction. In embryonic leaves the

reaction producing the short-wavelength chlorophyll is very fast and completes within 5 s [47]. It is known that proplastids of very young leaves (2–3 days) do not yet contain prolamellar bodies and possess only small-sized stromal membranes [63]. The fast rate of a short-wavelength shift Chlide684/676 → Chl675/670 in embryonic leaves at room temperature provides evidence that the pigment is rapidly released from the POR active site.

## Biosynthesis of Chlorophyll for Photosystem I Reaction Centers

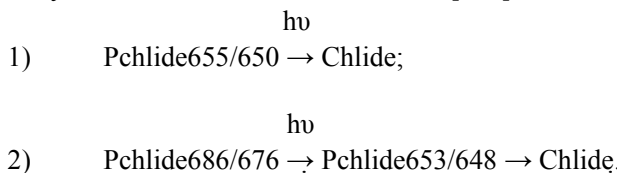
Investigation of chlorophyll formation in heterotrophic mutant cells of *Chlorella vulgaris* B-15 featuring complete genetic blockage of chlorophyll dark synthesis [99] revealed the photoactivity of a minor long-wavelength protochlorophyll form, Pchl 682/672 (esterified form) that accumulates in substantial amounts during dark culturing of mutant cells. When the mutant cells were illuminated at temperatures ranging from 26 to –70°C, two sets of photoreactions were observed. In addition to typical of greening algae photoreactions [100] involving the shorter-wavelength forms of chlorophyll precursor (Pchlde655/650 → Chlide695/684 and Pchlde640/635 → Chlide680/670), a new photoconversion was discovered that transformed the long-wavelength form of protochlorophyll Pchl682/672 to a stable (final) chlorophyll form Chl 715/696: Pchl682/672 → Chl 715/696. Based on spectral data, the authors supposed that Chl 715/696 is a pigment of the core complex of PSI. The photoactivity of PSI (photostimulated H<sub>2</sub> evolution) appeared simultaneously with the light-induced formation of Chl715/696 [101]. The efficiency of excitation energy transfer from carotenoids to Pchl682/672 and Chl715/696 remained almost unchanged during the photoreaction [99], which is only possible under constant intermolecular distances and mutual orientation of chromophores in carotenoids and porphyrins. On this basis, the authors [99] hypothesized that etiolated mutant cells already possess the core structure of PSI where protochlorophyll Pchl682/672 is present instead of chlorophyll. The formation of the core structure proceeds to completion upon the intracomplex photoreduction of protochlorophyll to chlorophyll. Since protochlorophyllide oxidoreductase exhibits specificity to the substrate and cannot reduce esterified protochlorophyll [27], one may suppose that the protochlorophyll photoreduction in this case is catalyzed by protochlorophyll reductase of previously unknown type.

## CHLOROPHYLL BIOSYNTHESIS IN GREEN PLANT LEAVES

Chlorophyll biosynthesis in green leaves ensures accumulation and maintenance of appropriate chlorophyll quantities under conditions of continuous photodegradation and dark destruction of chlorophyll. The investigation of chlorophyll synthesis in normal green leaves is strongly complicated because accumulation and transformation of minute quantities of chlorophyll precursor have to be detected on the background of already accumulated content of chlorophyll exhibiting strong absorption and high fluorescence (the chlorophyll content is several orders of magnitude higher than the concentration of its precursor).

The transformation of native protochlorophyllide forms to chlorophyll in fully developed green leaves was first tracked by studying low-temperature fluorescence spectra of leaves and

pigment extracts after temporary darkening of these samples [102]. The green leaves placed in darkness were found to accumulate the chlorophyll precursor identical in spectral features to the main active form of protochlorophyllide in etiolated leaves (fluorescence maximum at 655 nm). This spectral band disappeared rapidly upon subsequent illumination of darkened leaves. Later studies showed that leaves exposed to long darkness accumulate three protochlorophyllide forms that are characterized by the same spectral parameters as those observed in etiolated leaves (fluorescence maxima at 633, 642, and 655 nm) [103]. The intermediate Pchlde655/650 was found to be the main photoactive form. The pigment with fluorescence band at 642 nm decayed very slowly. Furthermore, the results showed that biosynthesis of chlorophyll *a* in green leaves, like in young etiolated leaves, involves the precursor form Pchlde653/648, which, in turn, originates from the photochemical reaction of another red-shifted protochlorophyllide form with an absorption maximum at about 680 nm. The authors supposed that chlorophyll biosynthesis in green leaves proceeds via two pathways, like it occurs in etiolated leaves [103]:



Thus, upon darkening of mature green leaves, chlorophyll photobiosynthesis proceeds through the same active protochlorophyllide forms as in the etiolated leaf, and the pathways of their conversions are similar to those observed during greening of etiolated leaves. The results obtained by spectral methods revealed that centers of protochlorophyllide and chlorophyll biosyntheses in green plant leaves are mainly located in the palisade mesophyll cells on the upper side of leaf blades and are almost absent in cells on the shadowed lower side of the leaf blade [104].

Our knowledge of chlorophyll biosynthesis mechanisms was substantially contributed by studies of this process in green leaves grown under natural photoperiodic conditions [44,63]. In this case the active protochlorophyllide form was characterized by the fluorescence maximum at 653–654 nm. Under intense flash illumination, the active protochlorophyllide produced the primary chlorophyllide form (reportedly, Chlide 688/678), which could further transform to either a short-wavelength product Chl675/670 or a long-wavelength form Chlide 694/682. Similarly to pigment conversions in etiolated leaves, two pathways of primary chlorophyllide transformations were observed. In very young (1-day-old) leaves, the short-wavelength form is predominantly produced (like it occurs in embryonic leaves). As the number of light–dark cycles increases, the flash illumination redirects the process along the second pathway: the long-wavelength form (fluorescence maximum at 694 nm) is initially produced and then undergoes a transformation associated with the Shibata blue spectral shift, like it occurs during greening of etiolated leaves. When the leaves were illuminated with the flash during the light period, the Shibata shift, chlorophyllide esterification, and regeneration of active protochlorophyllide form were completed an order of magnitude faster than in greening leaves. Upon illumination of leaves during the dark period (when prolamellar bodies are being formed), the short-wavelength shift proceeded at a slower rate.

Thus, in leaves of green plants grown under normal photoperiodic conditions, the light-dependent chlorophyll synthesis involves the active long-wavelength form of protochlorophyllide Pchlde653-654/648, which is spectrally similar to its main active form observed in greening etiolated leaves. In analogy to greening leaves, the green leaves possess at least two pathways of chlorophyll biosynthesis, which are recruited depending on the state and structure of biosynthetic apparatus.

## CONCLUSION

Owing to multi-year research of many laboratories, the complex reaction network for the final light-dependent stage of chlorophyll biosynthesis has been clarified. In our view, the main value of the suggested general scheme lies in the fact that it is based on spectroscopic data obtained on intact cells and tissues without any damage to native structures. The research revealed that the multistage conversion of protochlorophyllide to chlorophyll comprises two sequential photoreactions. In addition, this process proceeds in parallel with accomplishing the synthesis of pheophytin that acts as the (primary) intermediary electron acceptor in photochemical system II of photosynthesis. The other simultaneously occurring reaction utilizes a minor long-wavelength protochlorophyllide to synthesize the chlorophyll form that apparently represents the pigment P-680 in reaction centers of photosystem II. The reaction sequence producing the pigment forms of light-harvesting complex has been traced.

The suggested scheme remains phenomenological in many aspects. It mostly reflects the conversions of pigment chromophore, which are manifested in spectral changes, and contains less information on changes in protein component of the pigment–protein complex. The conclusions on the nature of such changes are hypothetical to a large degree.

The limited choice of techniques for nondestructive analysis of cell processes is often circumvented by studies on isolated subcellular and molecular structures of the cell. However, implementation of this approach for studying chlorophyll biosynthesis encounters the problem of extreme lability of pigment–protein complexes. Therefore, the results obtained with functionally active ternary complexes “protochlorophyllide–POR–NADPH” isolated from the cell or reconstituted in model systems should be considered as a remarkable advance in this research area. These investigations substantially clarified the issues related to the mechanism of the primary photoreaction. However, the subsequent secondary processes occurring in the cell have not been reproduced *in vitro* thus far. Therefore, we believe that continuation of the research using whole functional cells and tissues is justified and necessary. This approach is especially important for understanding the poorly characterized regulation of final stages in chlorophyll biosynthesis and for practical application of the pathways involved.

## REFERENCES

- [1] Timiriazeff, K. A. (1886). *Nature*, 34, 52.
- [2] Timiriazeff, K. A. (1889). La protophilline dans les plantes étiolées. *Comptes Rendus Acad Sc Paris*, 109, 414-416.

- [3] Monteverde, N. A. (1894). Über das Protochlorophyll. *Acta Horti Petropolitani*, 13, 201-217.
- [4] Monteverde, N. A. & Lubimenko, W. N. (1911). Untersuchungen über die Chlorophyllbildung bei den Pflanzen. *Biologisches Centralblatt*, 31, 481-498.
- [5] Shibata, K. (1956) Spectoscopic studies on chlorophyll formation in intact leaves. *Carn. Inst. Wash. YB*, 55, 248-250.
- [6] Shibata, K. (1957). Spectoscopic studies on chlorophyll formation in intact leaves. *J. Biochem. (Tokyo)*, 44, 147-173.
- [7] Koski, V. M. & Smith, J. H. C. (1948). The isolation and spectral absorption properties of protochlorophyll from etiolated barley seedlings. *J Amer Chem Soc*, 70, 3558-3562.
- [8] Koski, V. M., French, C. S. & Smith, J. H. C. (1951). The action spectrum for the transformation of protochlorophyll to chlorophyll a in normal and albino corn seedlings. *Arch Biochem Biophys*, 31, 1-17.
- [9] Koski, V. M. & Smith, J. H. C. (1951). Chlorophyll formation in a mutant white seedling. *Arch Biochem Biophys*, 34, 189.
- [10] Krasnovsky, A. A. & Kosobutskaya, L. M. (1952). Spectral study of chlorophyll condition during its formation in plants and in colloid solutions of etiolated leaf substances. *Doklady AN SSSR*, 85, 177-180.
- [11] Smith, J. H. C. (1952) Factore affecting the transformation of protochlorophyll to chlorophyll. *Year Book Carnegie Inst*, 51, 151-153.
- [12] Smith, J. H. C. & Kupke, D. W. (1956). Some properties of extracted protochlorophyll holochrome. *Nature*, 178, 751-752.
- [13] Smith, J. H. C., Kupke, D. W. & Giese, A. T. (1956). On the preparation, purification, and nature of the protochlorophyll-holochrome. *Carn Inst Wash YB*, 55, 243-245.
- [14] Litvin, F. F. & Krasnovsky, A. A. (1957). Study of intermediate stages of chlorophyll formation in etiolated leaves based on fluorescence spectra. *Doklady AN SSSR*, 117, 106-109.
- [15] Litvin, F. F. & Belyaeva, O. B. (1971). Sequence of photochemical and dark reactions in the terminal stage of chlorophyll biosynthesis. *Photosynthetica*, 5, 200-209.
- [16] Sironval, C. & Kuyper, P. (1972). The reduction of protochlorophyllide into chlorophyllide: IV. The nature of the intermediate P<sub>688-676</sub> species. *Photosynthetica*, 6, 254-275.
- [17] Litvin, F. F. (1958). Study of pigment state and transformations in photosynthesis (by means of nondamaging fluorescence spectroscopy). Cand. Sci. (Biology) Dissertation. Moscow.
- [18] Sironval, C., Kuyper, Y., Michel, J. M. & Brouers, M. (1967). The primary photoact in the conversion of protochlorophyll into chlorophyllide. *Stud Biophys*, 5, 43-50.
- [19] Litvin, F. F. & Belyaeva, O. B. (1968). Investigation of photochemical reactions in chlorophyll biosynthesis. *Biokhimiya*, 33, 928-936.
- [20] Litvin, F. F., Ignatov, N. V., Efimtsev, E. I. & Belyaeva, O. B. (1978). Two successive photocemical reactions in protochlorophyll(ide) reduction into chlorophyll(ide). *Photosynthetica*, 12, 375-381.
- [21] Thorne, S. W. (1971). The greening of etiolated bean leaves. II. Secondary and further photoconversion processes. *Biochem Biophys Acta*, 226, 128-134.
- [22] Mathis, P. & Sauer, K. (1973). Chlorophyll formation in greening bean leaves during the early stages. *Plant Physiol*, 51, 115-119.

- [23] Oliver, R. P. & Griffiths, W. T (1982). Pigment-protein complexes of illuminated etiolated leaves. *Plant Physiol*, *70*, 1019-1025.
- [24] Griffiths, W. T. (1974). Source of reducing equivalent for the in vitro synthesis of chlorophyll from protochlorophyll. *FEBS Lett*, *46*, 301-304.
- [25] Griffiths, W. T. (1978). Reconstitution of chlorophyllide formation by isolated etioplast membranes. *Biochem J*, *174*, 681-692.
- [26] Griffiths, W. T. & Mapleston, R. E. (1978). NADPH- protochlorophyllide oxidoreductase. In: G. Akoyunoglou and J.H.Argyroudi-Akoyunoglou (Eds), *Chloroplast Development* (99-104). Amsterdam.
- [27] Griffiths, W. T. (1980). Substrate-specificity studies on protochlorophyllide reductase in barley (*Hordeum vulgare*) etioplast membranes. *Biochem J*, *186*, 267-278.
- [28] Oliver, R. P. & Griffiths, W. T (1980). Identification of the polypeptides of NADPH: protochlorophyllide oxidoreductase. *Biochem J*, *191*, 277-280.
- [29] Apel, K., Santel, H. J., Redlinger, T. E. & Falk, H. (1980). The protochlorophyllide holochrom of barley (*Hordeum vulgare*). Isolation and characterization of the NADPH:protochlorophyllide oxidoreductase. *Eur J Biochem*, *111*, 251-258.
- [30] Baker, M. E. (1994). Protochlorophyllide reduction is homologous to human carbonil reductase and pig 20-beta-hydroxysteroid dehydrogenase. *Biochem J*, *300*, 605-607.
- [31] Wilks, H. M. & Timko, M. P. (1995). A light-dependent complexation system for analysis of NADPH:protochlorophyllide oxidoreductase identification and mutagenesis of two conserved residues that are essential for activity. *Proc Natl Acad Sci USA*, *92*, 724-728.
- [32] Birve, S., Selstam, E. & Johansson, L. (1996). Secondary structure of NADPH:protochlorophyllide oxidoreductase examined by circular dichroism and prediction methods. *Biochem J*, *317*, 549-555.
- [33] Martin, G. E. M., Timko, M. P. & Wilks, H. M. (1997). Purification and kinetic analysis of pea (*Pisum sativum L.*) NADPY: protochlorophyllide oxidoreductase expressed as fusion with maltose-binding protein in *Escherichia coli*. *Biochem J*, *325*, 139-145.
- [34] Armstrong, G., Runge, S., Frick, G., Sperling, U. & Apel, K. (1995). Identification of NADFH: protochlorophyllide oxidoreductase A and B branched pathway for light-dependent chlorophyll synthesis in *Arabidopsis thaliana*. *Plant Physiol*, *108*, 1505-1517.
- [35] Oosawa, N., Masuda, T., Awai, K., Fusada, N., Shimada, H., Ohta, H. & Takamiya, K. (2000). Identification and light-induced expression of a novel gene og NADPH-protochlorophyllide oxidoreductase isoform in *Arabidopsis thaliana*. *FEBS Lett*, *474*, 133-136.
- [36] Su, Q., Frick, G., Armstrong, G. & Apel, K. (2001). POR C of *Arabidopsis thaliana* : a third light- and NADPH-dependent protochlorophyllide oxidoreductase that is differentially regulated by light. *Plant Molecular Biology*, *47*, 805-813.
- [37] Masuda, T., Fusada, N., Oosawa, N., Takamatsu, K., Yamamoto, Y. Y., Ohta, M., Nakamura, K., Goto, K., Shibata, D., Shirano, Y., Hayashi, H., Kato, T., Tabata, S., Shimada, H., Ohta, H. & Takamiya, K. (2003). Functional analisis of Isoforms of NADPH: protochlorophyllide oxidoreductase (POR), PORB and PORC, in *Arabidopsis thaliana*. *Plant Cell Physiol*, *44*, 963-974.

- [38] Wolf, J. B. & Price, L. (1957). Terminal steps of chlorophyll a biosynthesis in higher plants. *Arch Biochem Biophys*, 72, 293-301.
- [39] Godnev, T. N. Shlyk, A. A. & Lyakhovich, Ya. P. (1957). On the reaction of protochlorophyllide to chlorophyll conversion. *Fiziologiya rastenii*, 4, 393-400.
- [40] Lang F., Vorobyeva, L. M. & Krasnovsky, A. A. (1969). Greening and bleaching processes in mutant maize leaves. In H., Metzner (Eds.), *Progress in photosynthesis research* (630-645). Tubingen.
- [41] Sironval, C., Brouers, M., Michel, J. M. & Kuyper, Y. (1968). The reduction of protochlorophyllide into chlorophyllide: I. The kinetics of the  $P_{657-647} \rightarrow P_{688-676}$  phototransformation. *Photosynthetica*, 2, 268-287.
- [42] Litvin, F. F. & Stadnichuk, I. N. (1980). Long-wavelength chlorophyll precursors in etiolated leaves and the system of native protochlorophyll forms. *Fiziologiya rastenii*, 27, 1024-1032.
- [43] Böddi, B., Ryberg, M. & Sundqvist, C. (1992). Identification of four universal protochlorophyllide forms in dark-grown leaves by analyses of the 77 K fluorescence emission spectra. *J Photochem Photobiol*, 12, 389-401.
- [44] Schoefs, B., Bertrand, M. & Franck, F. (2000). Spectroscopic properties of protochlorophyllide analized *in situ* in the course of etiolation and in illuminated leaves. *Photochem Photobiol*, 72, 85-93.
- [45] Stadnichuk, I. N., Amirjani, M. R. & Sundqvist, C. (2005). Identification of spectral forms of protochlorophyllide in the redion 670-730 nm. *Photochem Photobiol Sci*, 4, 230-238.
- [46] Ignatov, N. V. & Litvin, F. F. (2002). A new pathway of chlorophyll biosynthesis from long-wavelength protochlorophyllide Pchlde 686/676 in juvenile etiolated plants. *Photosynth Res*, 71, 195-207.
- [47] Schoefs, B. & Franck, F. (1993). Photoreduction of protochlorophyllide to chlorophyllide in 2-day old dark-grown bean leaves. Comparison with 10-day old leaves. *J Exp Bot*, 44, 1053 -1057.
- [48] Schoefs, B. & Franck, F. (2003). Protochlorophyllide reduction: mechanisms and evolution. *Photochem Photobiol*, 78, 543-557.
- [49] Kahn, A., Boardman, N. K. & Thorne, S. W. (1970). Energy transfer between protochlorophyllide molecules: evidence for multiple chromophores in the photoactive protochlorophyllide-protein complex *in vivo* and *in vitro*. *J Mol Biol*, 48, 85-101.
- [50] Litvin, F. F., Efimtsev, E. I. & Ignatov, N. V. (1976). Energy transfer in photoactive complexes of chlorophyll precursor in etiolated leaves and spectroscopic characteristics of pigment forms. *Biofizika*, 21, 307-312.
- [51] Ignatov, N. V. & Litvin, F. F. (1981). Energy transfer in pigment complexes of protochlorophyllide. *Biofizika*, 26, 664-668.
- [52] Akulovich, N. K. & Orlovskaya, K. I. (1971). Spectral characterization of protochlorophyll(ide)-holochrome during its production and transformation to chlorophyll in etiolated plants of various types. In: *Metabolism and structure of photosynthetic apparatus* (3-21). Minsk: Nauka i tekhnika.
- [53] Valter, G., Belyaeva, O. B., Ignatov, N. V., Krasnovsky, A. A. & Litvin, F. F. (1982). Photoconversions of various protochlorophyll(ide) forms in *Phaseolus coccineus*. *Biologicheskie nauki*, no. 9, 35-39.

- [54] Houssier, C. & Sauer, K. (1970). Circular dichroism and magnetic circular dichroism of the chlorophyll and protochlorophyll pigments. *J Amer Chem Soc*, 92, 779-791.
- [55] Vaugan, G. D. & Sauer, K. (1974). Energy transfer from protochlorophyllide to chlorophyllide during photoconversion of etiolated bean holochrome. *Biochem Biophys Acta*, 347, 383-394.
- [56] Bovey, F., Ogawa, T. & Shibata, K. (1974). Photoconvertible and non-photoconvertible forms of protochlorophyll(ide) in etiolated bean leaves. *Plant Cell Physiol*, 15, 1133-1137.
- [57] Shioi, Y. & Sasa, T. (1984). Chlorophyll formation in the YG-6 mutant of Chlorella vulgaris: spectral characterization of protochlorophyllide phototransformation. *Plant Cell Physiol*, 25, 131-137.
- [58] Franck, F. & Strazlka, K. (1992). Detection of the photoactive protochlorophyllide-protein complex in the light during the greening of barley. *FEBS Lett*, 309, 73-77.
- [59] Klement, H., Oster, U. & Rudiger, W. (2000). The influence of glycerol and chloroplast lipids on the spectral shifts of pigments associated with NADPH:protochlorophyllide oxidoreductase from *Avena sativa L.* *FEBS Lett*, 480, 306-310.
- [60] Mysliwa-Kurdziel, B., Amirjani, M. R., Strzalka, K. & Sundqvist, C. (2003). Fluorescence lifetime of protochlorophyllide in plants with different proportions of short-wavelength and long-wavelength protochlorophyllide spectral forms. *Photochem Photobiol*, 78, 205-212.
- [61] Griffiths, W. T. (1975). Characterization of the terminal stages of chlorophyll(ide) synthesis in etioplast membrane preparations. *Biochem J*, 152, 623-635.
- [62] Sundqvist C. & Dahlin C. (1997). With chlorophyll from prolamellar bodies to light-harvesting complexes. *Physiol Plant* V.100, 748-759.
- [63] Schoefs, B. & Franck, F. (2008). The photoenzymatic cycle of NADPH:protochlorophyllide oxidoreductase in primary bean leaves (*Phaseolus vulgaris*) during the first days of photoperiodic growth. *Photosynth Res*, 96, 15-26.
- [64] Dubrovsky, V. T. & Litvin, F. F. (2008). Detection of early photoactive forms of chlorophyll precursor in plant leaves by means of fluorescence spectroscopy at 20°C. *Biologicheskie membrany*, 25, 203-209.
- [65] Bystrova M. I., Lang F. & Krasnovsky, A. A. (1972). Spectral effects of protochlorophyllous pigment aggregation. *Molekulyarnaya Biologiya*, 6, 77-86.
- [66] Brouers, M. (1972). Optical properties of in vivo aggregates of protochlorophyllide in non-polar solvents. I. Visible and fluorescence spectra. *Photosynthetica*, 6, 415-423.
- [67] Böddi, B., Soos, J. & Lang, F. (1980). Protochlorophyll forms with different molecular arrangements. *Biochim Biophys Acta*, 593, 158-165.
- [68] Sundqvist, C., Ryberg, H., Boddi, B. & Lang, F. (1980). Spectral properties of a long-wavelength absorbing form of protochlorophyll in seeds of *Cyclantera explodens*. *Physiol Plant*, 48, 297-301.
- [69] Ignatov, N. V., Belyaeva, O. B., Timofeev, K. N. & Litvin, F. F. (1988). Photochemical reactions of protochlorophyll in the inner seed coat layers of *Cucurbita*. *Biofizika*, 33, 500-505.
- [70] Raskin, V. I. (1976). Mechanism of protochlorophyllide photoreduction in intact etiolated leaves. *Vesti AN BSSR. Ser. Biol.*, N, 5, 43-46.

- [71] Dujardin, E. & Correia, M. (1979). Long-wavelength absorbing pigment protein complexes as fluorescence quenchers in etiolated leaves illuminated in liquid nitrogen. *Photobiochem Photobiophys*, 1, 25-32.
- [72] Losev, A. P. & Lyal'kova, N. D. (1979). Study of the initial stages of protochlorophyllide photohydrogenation in etiolated leaves. *Molekulyarnaya Biologiya*, 13, 837-844.
- [73] Belyaeva, O. B. & Litvin, F. F. (1980). On the new intermediary reactions in protochlorophyllide photoreduction. *Biofizika*, 25, 617-623.
- [74] Litvin, F. F., Ignatov, N. V. & Belyaeva, O. B. (1981). Photoreversibility of transformation of protochlorophyllide into chlorophyllide. *Photobiochem Photobiophys*, 2, 233-237.
- [75] Belyaeva, O. B., Litvin, F. F. (1981). Primary reactions of protochlorophyllide into chlorophyllide phototransformation at 77 K. *Photosynthetica*, 15, 210-215.
- [76] Belyaeva, O. B., Personova, E. R. & Litvin, F. F. (1983). Photochemical reaction of chlorophyll biosynthesis at 4,2 K. *Photosynth Research*, 4, 81 - 85.
- [77] Franck, F. & Mathis, P. (1980). A short-lived intermediate in the photoenzymatic reduction of protochlorophyll(ide) into chlorophyll(ide) at a physiological temperature. *Photochem Photobiol*, 32, 799-803.
- [78] Inoue, Y., Kobayashi, T., Ogawa, T. & Shibata, K. (1981). A short intermediate in the photoconversion of protochlorophyllide to chlorophyllide *a*. *Plant Cell Physiol*, 22, 197-204.
- [79] Iwai, J., Ikeuchi, M., Inoue, Y. & Kobayashi, T. (1984). Early processes of protochlorophyllide photoreduction as measured by nanosecond and picosecond spectrophotometry. In: C., Sironval, (Eds.), Protochlorophyllide Reduction and Greening (pp. 99-112). The Hague, Martinus Nijhoff/Dr.W Junk Publisher.
- [80] Belyaeva, O. B., Timofeev, K. N. & Litvin, F. F. (1988). The primary reaction in the protochlorophyll(ide) photoreduction as investigated by optical and ESR-spectroscopy. *Photosynth Research*, 15, 247-256.
- [81] Belyaeva, O. B., Griffith, V. T., Kovalev, Yu. V., Timofeev, K. N. & Litvin, F. F. (2001). Involvement of free radicals in photoreduction of protochlorophyllide to chlorophyllide in artificial pigment-protein complexes. *Biokhimiya*, 66, 173-177.
- [82] Heyes, D. J., Hunter, C. N., van Stokkum, I. H. M., Grondelle, R. & Groot, M. L. (2003). Ultrafast enzymatic reaction dynamics in protochlorophyllide oxidoreductase. *Nature Structural Biology*, 10, 491-492.
- [83] Heyes, D. J., Heathcote, P., Rigby, S. E. J., Palacios, M. A., Grondelle, R. & Hunter, C. N. (2006). The first catalytic step of the light-driven enzyme protochlorophyllide oxidoreductase proceeds via a charge transfer complex. *J Biol Chem*, 281, 26847-26853.
- [84] Belyaeva, O.B. & Litvin, F. F. (1989). Photobiosynthesis of chlorophyll. Moscow, M.V.Lomonosov Moscow state university Publisher.
- [85] Raskin, V. I. & Schwartz, A. (2002). The charge-transfer complex between protochlorophyllide and NADPH: an intermediate in protochlorophyllide photoreduction. *Phosinh Res*, 74, 181-186.
- [86] El Hamouri, B. & Sironval, C. (1980). NADP+/NADPH control of the protochlorophyllide-chlorophyllide proteins in cucumber etioplasts. *Photobiochem Photobiophys*, 1, 219-223.

- [87] Franck, F., Bereza, B. & Boddi, B. (1999). Protochlorophyllide-NADP<sup>+</sup> and protochlorophyllide-NADPH complexes and their regeneration after flash illumination in leaves and etioplast membranes of dark-grown wheat. *Photosynth Res*, 59, 53-61.
- [88] Henningsen, K. W. & Thorne, S. W. (1974). Esterification and spectral shift of chlorophyll (ide) in wild-type and mutant seedlings development in darknes. *Physiol Plant*, 30, 82-89.
- [89] Thorne, S. W. (1971). The greening of etiolated bean leaves. III. Multiple light/dark step photoconversion processes. *Biochem Biophys Acta*, 226, 175 -183.
- [90] Henningsen, K. W., Kahn, A. & Houssier, C. (1973). Circular dichroism of protochlorophyllide and chlorophyllide holochrome subunits. *FEBS Lett*, 37, 103-109.
- [91] Schultz, A. & Sauer, K. (1972). Circular dichroism and fluorescence changes accompanying the protochlorophyllide to chlorophyllide transformation in greening leaves and holochrome preparations. *Biochem Biophys Acta*, 267, 320-340.
- [92] Wiktorsson, B., Ryberg, M., Gough, S. & Sundqvist, C. (1992). Isoelectric focusing of pigment-protein complexes solubilized from non-irradiated and irradiated prolamellar bodies. *Physiol Plant*, 85, 659-669.
- [93] Domanski, V., Rassadina, V., Gus-Mayer, S., Wanner, G., Schoch, S. & Rudiger, W. (2003). Characterization of two phases of chlorophyll formation during greening of etiolated barley leaves. *Planta*, 216, 475-483.
- [94] Ignatov, N. V. & Litvin, F. F. (1994). Photoinduced formation of pheophytin/chlorophyll-containing complexes during the greening of plant leaves. *Photosynthes Res*, 42, 27 -35.
- [95] Ignatov, N. V. & Litvin, F. F. (1995). Light-regulated pigment interconversion in pheophytin/chlorophyll-containing complexes formed during plant leaves greening. *Photosynthes Res*, 46, 445-453.
- [96] Klimov, V. V., Klevanik, A. V., Shuvalov, V. A. & Krasnovsky, A. A. (1977). Reduction of pheophytin in the primary light reaction of Photosystem II. *FEBS Lett*, 82, 183-186.
- [97] Klimov, V. V. & Krasnovsky, A. A. (1981). Pheophytin as the primary electron acceptor in photosystem II reaction center. *Photosynthetic*, 15, 592-609.
- [98] Ignatov, N. V., Satina, L. Y. & Litvin, F. F. (1999). Biosynthesis of non-fluorescent chlorophyll of photosystem II core in greening plant leaves. Effect of etiolated plants growing under heat shock conditions (38°C). *Photosynth Res*, 62, 85-195.
- [99] Ignatov, N. V. & Litvin, F. F. (1996). Photoconversion of long-wavelength protochlorophyll native form Pchl 682/672 into chlorophyll Chl 715/696 in *Chlorella vulgaris* B-15. *Photosynthes Res*, 50, 271-283.
- [100] Lebedev, N. N., Dzhelepova, I. D. & Krasnovsky, A. A. (1991). Protochlorophyllide fluorescence in cells of the green alga *Chlamydomonas reinhardtii*. *Biofizika*, 63, 1022-1030.
- [101] Boichenko, V. A. & Litvin, F. F. (1990). Light-induced modulation of hydrogenase activity upon protochlorophyll(ide) photoreduction and during biogenesis of photosystem I in greening mutants of *Chlorella*. *Biokhimiya*, 55, 1309-1318.
- [102] Litvin, F. F., Krasnovsky, A. A. & Rikhireva, G. T. (1959). Production and transformation of protochlorophyll in green plant leaves. *Doklady AN SSSR*, 127, 699-701.

- [103] Ignatov, N. V. & Litvin, F. F. (2002). Chlorophyll biosynthesis from protochlorophyllide in green plant leaves. *Biokhimiya*, 67, 1142-1150.
- [104] Ignatov, N. V. & Litvin, F. F. (2002). Localization of protochlorophyll and chlorophyll biosynthetic centers in green plant leaves and light activation of their activity. *Biologicheskie membrany*, 19, 153-159.



## ***Chapter 6***

# **CHEMOPREVENTIVE ACTION OF ORGANIC AND INORGANIC MATERIALS ON PHOTOTOXIC EFFECT**

***Kazutaka Hirakawa***

Department of Basic Engineering (Chemistry), Faculty of Engineering, Shizuoka University, Johoku 3-5-1, Naka-ku, Hamamatsu, Shizuoka 432-8561, Japan.

## **ABSTRACT**

The prevention for phototoxic effect is one of the important themes of photobiology. Photosensitized damage of biomolecules including DNA, proteins, and low molecular weight compounds participates in solar carcinogenesis, photogenotoxicity, and phototoxicity. Ultraviolet radiation and visible-light induce oxidation of the above biomaterials via the electron transfer from biomolecules to an excited endogenous and/or exogenous photosensitizer or the formation of reactive oxygen species, especially singlet oxygen. Chemoprevention of photosensitized biomolecules damage is important methods against the above phototoxic effects. Organic ultraviolet B absorbers and antioxidants such as vitamins are useful ultraviolet-protector. However, the oxidized products of organic materials occasionally produce secondary reactive oxygen species to damage biomolecules. To avoid this problem, organic quenchers have been studied. For examples, xanthone derivative isolated from plant can prevent photosensitized DNA damage through quenching of the excited state of photosensitizer. These molecules may be used as the preventive drugs for an adverse side-effect of photodynamic therapy. On the other hand, inorganic sunscreen such as titanium dioxide and zinc oxide particles are effective materials to shield solar UVA. Furthermore, inorganic materials can be used as an antioxidant based of their catalytic activity for decomposition of reactive oxygen species generated from the photochemical reaction.

## **1. INTRODUCTION**

Phototoxic effect and its protection are important themes of photobiology [1-3]. Solar radiation contributes to the control of circadian rhythm of animals including humans and acts

as the energy source of almost living things through the photosynthesis. Further, most of the population receives their nutritional vitamin D requirements through exposure to solar ultraviolet (UV) radiation, with cutaneous synthesis estimated to provide 80~100% of the vitamin D requirements of the body [4]. However, excess exposure to solar UV radiation is undoubtedly linked to skin carcinogenesis [5]. UV constitutes about 10% of the total solar radiation. There have been many reports demonstrating that the UVB (280~320 nm) component is primarily responsible for the induction of human skin cancers [5]. However, UVA (320~400 nm), which makes up 95% of natural solar UV, is also mutagenic and carcinogenic [6-9]. UVA is not filtered by standard glass and penetrates skin layer more deeply than UVB. In addition, UVA is the main cause of photoaging.

It is generally accepted that DNA damage caused by UV radiation responsible for the induction of skin cancers. The photodamage of biomolecules including DNA is induced through direct excitation of biomolecules and the indirect photosensitized reaction mediated by endogenous or exogenous photosensitizers (Figure 1) [10]. For example, pyrimidine dimer formation by UVB is caused by the direct mechanism. On the other hand, there are two categories of indirect photosensitized mechanism: the Type I (electron transfer) and the Type II (generation of reactive oxygen species (ROS)). Visible light (400~800 nm) also induces biomolecules damage through these indirect mechanism. To prevent the phototoxic effect, the clarification of the mechanism of photochemical biomolecules damage is necessary. For photoprotection, direct shielding of photo-irradiation has advantage. Anti-oxidant and quenchers are also important agents for the protection. These agents contain traditional materials, and further, novel materials have been studied. Organic and inorganic materials have specific character including advantage and disadvantage. In this chapter, the chemopreventive action of novel organic and inorganic materials on photosensitized biomolecules damage is described.

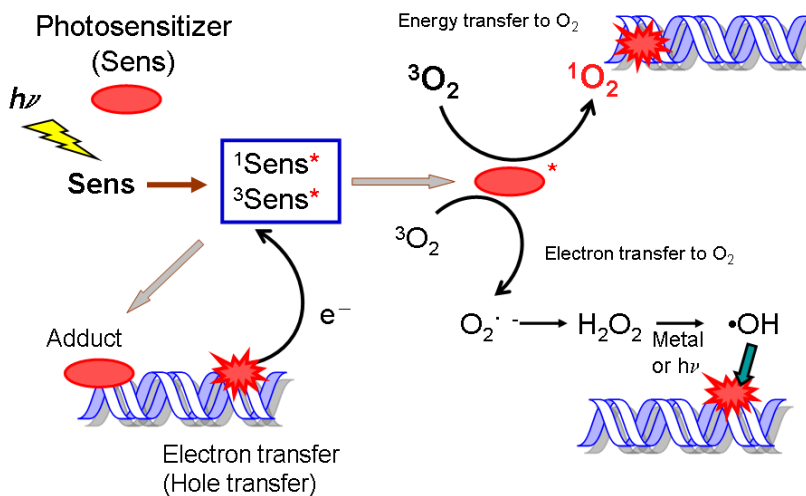


Figure 1. General mechanism of the indirect biomolecules damage through photochemical reaction.

## 2. PHOTOTOXICITY BY UV AND VISIBLE LIGHT

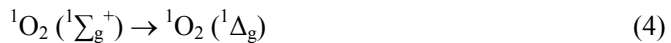
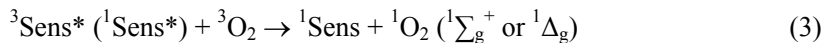
UVB radiation, which constitutes about 5% of the solar UV radiation that reaches the surface of the earth, directly activates the DNA molecule to generate dipyrimidine photoproducts such as cyclobutane pyrimidine dimers and pyrimidine (6-4) pyrimidone photoadducts, resulting in mutations and carcinogenesis. However, many studies have provided sufficient evidence that UVA radiation is also mutagenic and carcinogenic, although it is unlikely that UVA directly activates DNA bases to produce dipyrimidine photoproducts [11, 12]. It is, therefore, generally recognized that solar UV carcinogenesis involves a mechanism by which UV radiation indirectly induces DNA damage through photosensitized reactions mediated by intracellular chromophores. In addition, visible-light also cause biomolecules damage through photosensitized reaction. In this section, the general mechanisms of photodamage of biomolecules are reviewed.

### 2.1. Indirect DNA Damage by UVA Radiation

Endogenous and exogenous photosensitizers induce biomolecules damage through the Type I and the Type II mechanisms [10]. The Type I mechanism involves electron transfer from biomolecules to excited photosensitizer. This mechanism is dependent on the energy of the molecular orbital (MO) of photosensitizer (Sens), its excited state (Sens\*), and target biomolecules, namely the oxidation potential of the biomolecules and the reduction potential of the excited photosensitizer. In the case of DNA damage, guanine has the lowest oxidation potential among the four DNA bases, that is, guanine is most likely to be oxidized. Formed guanine radical cation through the electron transfer reacts with water or molecular oxygen, leading to the formation of oxidized product of guanine. These photoproducts cause mutation and cancer. Accordingly, a variety of cellular compounds have been considered to be potential endogenous photosensitizers. In addition, certain drugs may act as exogenous photosensitizers. For example, psolarens have been used for treatment of skin diseases, particularly psoriasis, in combination with UVA irradiation (PUVA therapy), and it is known that the incidence of skin tumor is increased by PUVA therapy [5].

The modification of biomacromolecules upon exposure to ROS, including hydrogen peroxide ( $H_2O_2$ ), dioxide(1-) (superoxide  $O_2^-$ ), hydroxyl radical ( $HO^\cdot$ ), and singlet oxygen ( $^1O_2$ ), is the likely initial event involved in the induction of the mutagenic and lethal effects of various oxidative stress agents [13-15]. Biomolecules damage can be induced indirectly by the excited photosensitizer via the Type II mechanism. This process can be mediated by ROS, especially  $^1O_2$ . The Type II mechanism (major Type II mechanism) involves energy transfer from an excited photosensitizer to molecular oxygen to produce  $^1O_2$ . Molecular oxygen has two low-lying singlet excited states,  $^1\Delta_g$  and  $^1\Sigma_g^+$ ,  $0.98 \text{ eV}$  ( $95 \text{ kJ mol}^{-1}$ ) and  $1.63 \text{ eV}$  ( $158 \text{ kJ mol}^{-1}$ ) above the ground triplet state ( $^3\Sigma_g^-$ ), respectively [16]. Since the lifetime of  $^1\Sigma_g^+$  is very short, the contribution of  $^1\Sigma_g^+$  to biomolecules damage is negligible and  $^1\Delta_g$  is important reactive species ( $^1O_2$  indicates  $^1\Delta_g$  in the below part of this chapter). The energy transfer reaction can be expressed as follows:





where  $^1\text{Sens}$  represents the ground state photosensitizer,  $^1\text{Sens}^*$  the excited singlet state photosensitizer, and  $^3\text{Sens}^*$  is the excited triplet state photosensitizer. The spin multiplicity of molecular oxygen (triplet state) changes into the singlet state via this energy transfer. This process must proceed through electron exchange (Dexter mechanism) [17].

On the other hand, the minor Type II mechanism has been also confirmed [2, 18]. This mechanism is mediated by the formation of  $\text{O}_2^\cdot$  by electron transfer from an excited photosensitizer to molecular oxygen. This reaction is followed by dismutation to  $\text{H}_2\text{O}_2$ . Further,  $\text{O}_2^\cdot$  can be generated by the interaction of oxygen with the sensitizer anion radical produced by the type I mechanism. Although  $\text{O}_2^\cdot$  and  $\text{H}_2\text{O}_2$  are not strong reactive species,  $\text{H}_2\text{O}_2$  can be converted into  $\text{HO}^\cdot$  through the Fenton reaction mediated by metal ions such as  $\text{Fe}^{2+}$  or UV radiation.  $\text{HO}^\cdot$  is strong reactive species and known to cause DNA damage at every nucleotide with little or no site selectivity [19].

## 2.2. Photosensitized Reaction of Visible-Light Photosensitizer and Phototoxicity

Visible light photosensitizer mainly induces biomolecules damage via the Type II mechanism (major Type II mechanism) [10, 20-22].  $^1\text{O}_2$  generation can be induced by photons with relatively small energy. Since the carcinogenicity of visible-light itself has not been demonstrated, the visible-light photosensitizers have an importance in the medical application of photochemical reaction such as the drug for photodynamic therapy (PDT) rather than their photo-carcinogenicity. PDT is a relatively new treatment for cancer and other non-malignant conditions that induces oxidative stress through the photosensitized generation of  $^1\text{O}_2$  [23-25]. The human tissue has relatively high transparency for visible-light, especially red color light, and visible-light hardly demonstrates side-effect. Because  $^1\text{O}_2$  can be easily generated by visible-light,  $^1\text{O}_2$  is considered as important reactive species of PDT. Critical sites of the generated  $^1\text{O}_2$  include mitochondria and lipid membranes [23-26]. Moreover, DNA is also an important target biomolecule of photosensitized reactions [27-30]. Adverse side effect of PDT is also serious problem in the photomedical field. The chemoprevention for this side effect is an important theme for PDT.

## 3. GENERAL CONCEPT OF CHEMOPREVENTION OF PHOTOTOXIC EFFECT

To prevent direct biomolecules damage by UV radiation, the UV filter (the physical sunscreen) is the most important method (Table 1). UVB directly activates biomacromolecules including DNA bases, resulting in the photochemical damage. Therefore,

the physical shielding is necessary for the UVB protection. The physical sunscreen is effective for UVA protection as well as UVB protection. On the other hand, to prevent the indirect mechanism of phototoxicity, other method can be used, and the clarification of indirect mechanism should be important to develop the preventive methods for UVA phototoxicity (Figure 2). Because indirect mechanisms also contribute to the photodamage of biomolecules by UVA, the quenching of the photoexcited photosensitizers and the anti-oxidation can be used for the UVA protection. In the case of the protection for visible-light induced phototoxic effect, the physical sunscreen is not appropriate, because non-color agent is required for the physical sunscreen. Therefore, the quenchers and antioxidant are advantageous for this protection. The mechanism of the quencher is deactivation of the excited photosensitizer into the ground state through electron transfer or energy transfer (Figure 3). The excitation energy is dispersed into the surroundings as heat through these processes. The antioxidant scavenges the oxidative agents such as ROS generated from the photosensitized reaction and the photoexcited drugs. In general, antioxidant itself is oxidized through this process. In the case of catalytic materials, ROS is decomposed into safety molecules, *e.g.* molecular oxygen and/or water, without the reaction of the preventive material itself.

**Table 1. Prevention methods for phototoxic effect**

Method	Wavelength dependence of the preventive effects		
	UVB	UVA	Visible-light
Physical sunscreen	+++	+++	-
Quencher	-	++	++
Antioxidant	-	+	+

+++: absolutely effective. ++: effective. +: effective but the side effect may be possible.

-: not effective (not reasonable).

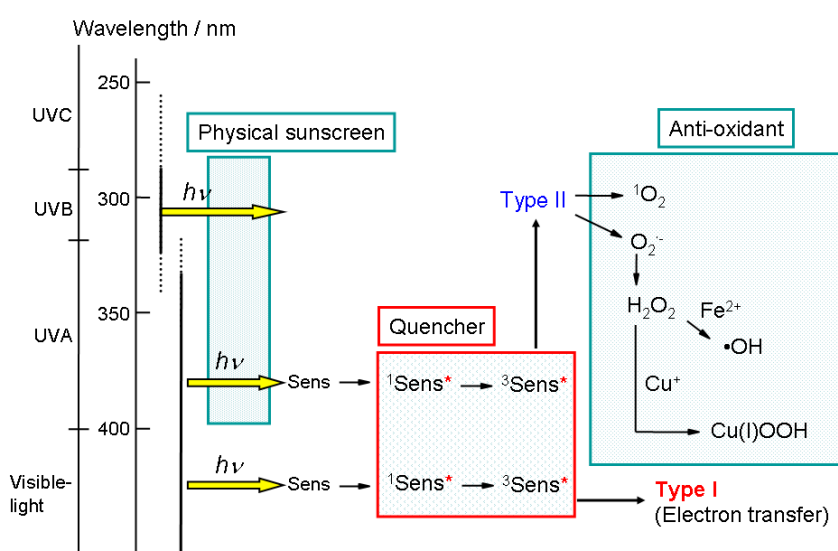


Figure 2. Patterns of chemoprevention for phototoxic effect.

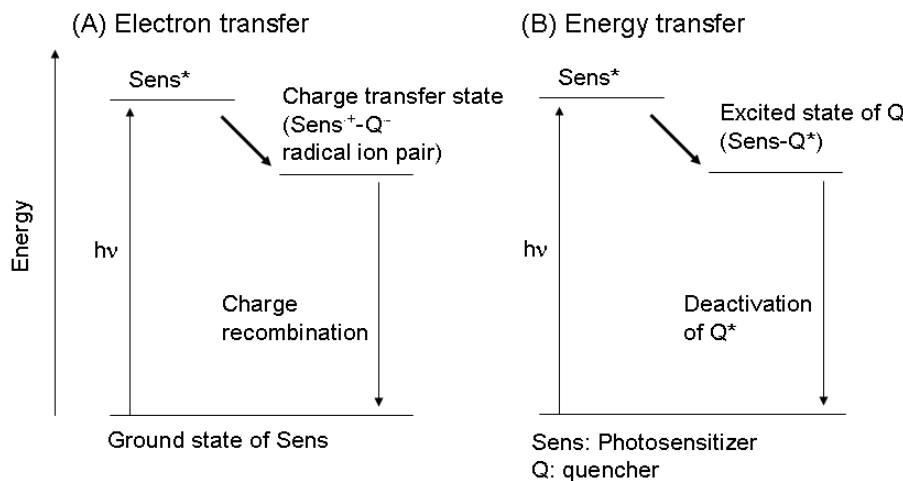


Figure 3. The mechanism of the general photo-protections.

## 4. ORGANIC MATERIALS

Many organic compounds have been studied as chemopreventive agents for phototoxicity. In this section, the study of synthesized organic sunscreen and novel protective agents is reviewed.

### 4.1. Synthesized Preventive Agent: UV Absorber

Physical shielding of UV light is one of the most important methods of the protection for phototoxic effect. Most skin care cosmetic products now include UVA filters in their formulations along with UVB filters. Especially, synthesized organic UVB absorbers have been developed to protect UVB phototoxicity. Examples of UVB absorber agents are presented in Table 2. The effectiveness of the anti-solar products is quantified using a universal indicator: the sun protection factor (SPF) for UVB and ultraviolet A protection factor (UVAPF). SPF is the ratio of the least amount of ultraviolet energy required to produce a minimal erythema on sunscreen protected skin to the amount of energy required to produce the same erythema on unprotected skin. It is measured by both *in vivo* (Colipa method) and *in vitro* methods [31]. It can be expressed by the following theoretical equation [32]:

$$\text{SPF} = \frac{\sum E_\lambda S_\lambda \Delta_\lambda}{\sum E_\lambda S_\lambda T_\lambda \Delta_\lambda} \quad (5)$$

or

$$\text{SPF} = \frac{\int E_\lambda S_\lambda d\lambda}{\int E_\lambda S_\lambda T_\lambda d\lambda} \quad (6)$$

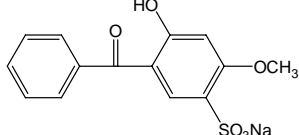
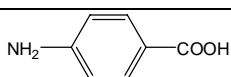
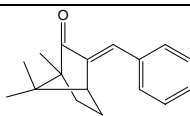
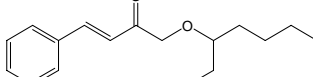
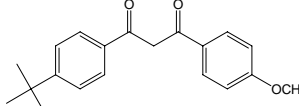
where  $E_\lambda$  is CIE (Commission Internationale de l'Éclairage) erythemal spectral efficiencies,  $S_\lambda$  is solar spectral incidence,  $T_\lambda$  is spectral transmittance of the sample, and  $d\lambda$  is the interval of wavelength. On the other hand, UVAPF is a relative effectiveness of the UVA protection [33].

On the other hand, adverse effects of UVB absorbers were reported. Sunscreens should provide and maintain their initial absorbance, hence protection, throughout the entire period of exposure to sunlight. However, not all UVA and UVB filters are sufficiently photo-stable [34]. Photoallergy and phototoxic effect by decomposed product of certain photo-protective agents should be considered. For example, *p*-aminobenzoic acid (PABA) and 2-phenylbenzimidazole-5-sulfonic acid induce both  $^1\text{O}_2$  and thymine-dimer formation, although the two have not been definitely correlated [35-39]. Solution-phase studies found that octylmethoxycinnamate, octocrylene, and PABA all produce  $^1\text{O}_2$  in phosphate-buffered saline [35, 40, 41]. In addition, benzophenones are common causes of photoallergy and are increasingly used in products other than traditional sunscreens [42]. Photoallergy occurs depending on the personal constitution. Therefore, the selection of appropriate sunscreen agent is important.

## 4.2. Self-Chemopreventive Effect of Folic Acid on Photosensitized Reaction

Naturally occurring preventive agent for phototoxicity is important to develop the photo-protection method. The photochemistry of folic acid is one of the useful topics [43]. Folic acid, which consists of the base pteridine and *p*-aminobenzoyl-*L*-glutamic acid (Figure 4), is one of the B vitamins essential for human nutrition. Pteridine moiety of folic acid analogues absorbs UVA, leading to various photochemical reactions from its excited state [43-48]. One of the most important reactions is photo-induced electron transfer. This reaction may contribute to UVA carcinogenesis. It is generally recognized that solar UVA carcinogenesis involves a mechanism by which UVA radiation indirectly induces DNA damage through photosensitized reactions mediated by intracellular chromophores. Pteridines might be important endogenous photosensitizers [18, 43, 46, 49, 50]. However, the DNA damaging activity of folic acid is very weak compared with other unconjugated pteridine compounds [43, 46]. The photoexcited state of the pteridine moiety of folic acid is effectively quenched by the aminobenzoyl moiety, resulting in the inhibition of photo-induced electron transfer from biomolecules to the pteridine moiety. The MO calculation showed that the highest occupied MO (HOMO) is located on the aminobenzoyl moiety of folic acid, suggesting that the photoexcited pteridine moiety can be quenched through intra-molecular electron transfer from the aminobenzoyl moiety (Figure 5) [43, 46, 51, 52]. It has been reported that the free energy change of the electron transfer from the aminobenzoyl moiety to the pteridine moiety is negative (-0.75 eV) [48], supporting the possibility of the photoinduced intramolecular electron transfer. Therefore, the connection of the pteridine moiety with the quencher, aminobenzoyl moiety, plays an important role in the protection for phototoxicity.

**Table 2. Examples of organic physical sunscreens.**

Compounds	$\lambda_{\text{max}} / \text{nm}$	Structure
Benzophenone-5	288	
<i>p</i> -Aminobenzoic acid	290	
4-Methylbenzylidene camphor	301	
Octylmethoxycinnamate	310	
4- <i>tert</i> -Butyl-4'-methoxydibenzoylmethane	355	

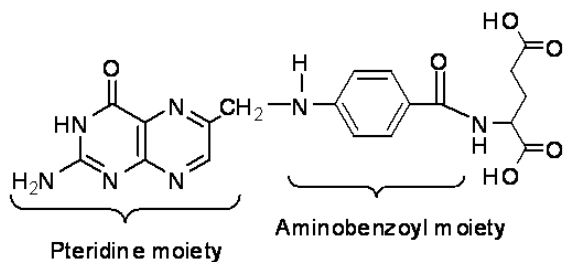


Figure 4. Structure of folic acid.

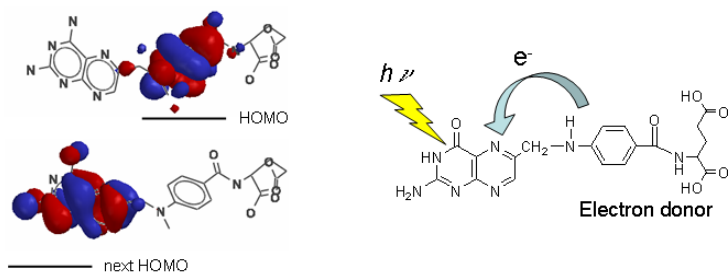


Figure 5. Calculated energy level of folic acid and the direction of the photo-induced intramolecular electron transfer.

### 4.3. Quencher Deactivates the Photoexcited Photosensitizer

As mentioned above, various endogenous molecules and natural products act as photosensitizers [53-57]. In addition, a side effect of PDT [23-25] is also caused by photosensitized biomacromolecular damage. An organic antioxidant such as vitamins can scavenge ROS generated through photosensitized reaction and protect against cancer occurrence [58]. For example,  $\beta$ -carotene is an efficient scavenger of  $^1\text{O}_2$ . However,  $\beta$ -carotene, vitamin A, and vitamin E generate ROS through their oxidation process, leading to oxidative DNA damage [59, 60]. Every antioxidant is in fact, a redox agent, protecting against ROS in some circumstances and promoting free radical or secondary ROS generation in others. Indeed, an excess amount of these antioxidants elevates cancer incidence [61-63]. A physical sunscreen itself is not necessarily oxidized through the process of the protection. But the physical protection for the phototoxicity induced by visible-light is difficult, because non-color agents are required for the physical sunscreen in the practical use.

The quenching mechanism of folic acid (section 4-2) leads us to the idea that an effective quencher can be used as a chemopreventive agent for photodamage of biomacromolecules. The naturally occurring quenchers, xanthone (XAN) derivatives, bellidifolin (BEL), gentiacaulein (GEN), norswertianin (NOR), and swerchirin (SWE), (Figure 6), show the preventive action on photosensitized DNA damage [3]. These XAN derivatives were isolated from various plants [64-68] and have no absorption in the visible-light region, *i.e.* non-color agents. DNA damage was induced by photo-irradiation in the presence of parent non-substituted XAN, whereas these substituted XAN derivatives did not induce DNA photodamage. Especially, GEN and NOR showed highly inhibitory effect on the DNA photodamage induced by riboflavin or non-substituted XAN. Although, the inhibitory effect of NOR on DNA photodamage was high, NOR induced DNA damage in the presence of Cu(II) ion without photo-irradiation. NOR is one of the derivatives of catechol, which causes oxidative DNA damage by ROS formation during the autoxidation process into the corresponding quinone form in the presence of Cu(II) ion [69]. Therefore, excess amount of NOR may exhibit a side effect. Therefore, it is suggested that GEN is the best chemopreventive agent in the XAN derivatives used in this study.

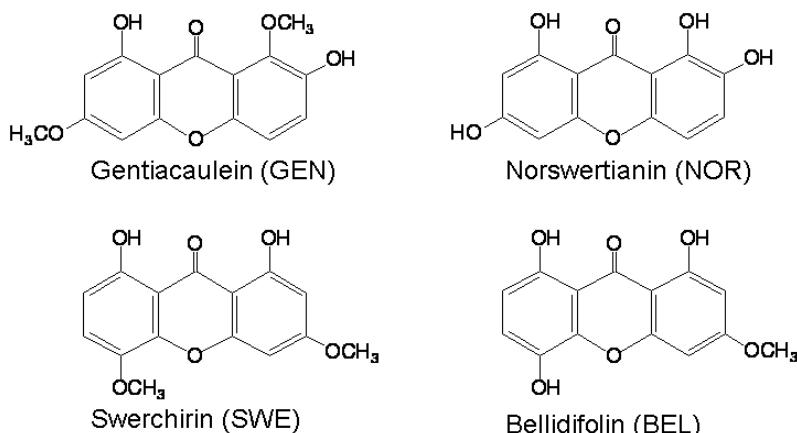


Figure 6. Structures of XAN derivatives.

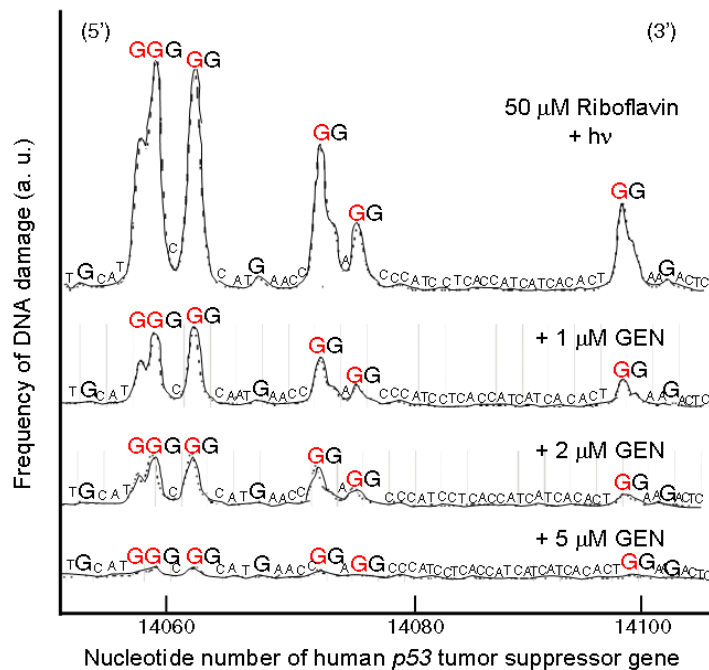


Figure 7. Effect of GEN on the sequence-specific DNA damage by photoexcited riboflavin. The reaction mixture contained the  $^{32}\text{P}$ -labeled 211-base DNA fragment, 50  $\mu\text{M}$  riboflavin, and indicated concentration of GEN in 100  $\mu\text{l}$  of 10 mM sodium phosphate buffer (pH 7.8). The reaction mixtures were exposed to  $6 \text{ J cm}^{-2}$  light ( $\lambda_{\text{max}} = 365 \text{ nm}$ ,  $1.2 \text{ mW cm}^{-2}$ ). Subsequently, the DNA fragments were treated with hot piperidine and analyzed. Horizontal axis is the nucleotide number of the *p53* tumor suppressor gene.

Photoexcited riboflavin oxidizes specifically at the underlined G of 5'-GG and 5'-GGG sequences in double-stranded DNA through photoinduced electron transfer (Figure 7). Photoexcited XAN itself, as well as riboflavin, also induces DNA damage through a Type I mechanism [57]. The underlined G in the 5'-GG and 5'-GGG sequences acts as a hole-trap [70, 71] and is finally oxidized through hole-transfer. These photosensitizers oxidize guanine into 8-oxo-7,8-dihydro-2'-deoxyguanine (8-oxo-G) and piperidine-labile products, such as imidazolone and oxazolone, at consecutive G residues [56, 57]. The piperidine-labile products can be generated via further oxidation of 8-oxo-G. These photoproducts cause mutation and/or cancer [72-77]. GEN effectively inhibited this G-specific photodamage. The preventive action of these XAN derivatives was evaluated quantitatively by the inhibitory effect of 8-oxo-G formation by photoexcited riboflavin (Figure 8). The preventive action of XAN derivatives increased in the following order: GEN > NOR >> BEL > SWE. Especially, 5  $\mu\text{M}$  GEN completely inhibited 8-oxo-G formation by 50  $\mu\text{M}$  riboflavin. The content of 8-oxo-G increased over 2  $\mu\text{M}$  of NOR, suggesting that an excess amount of NOR induces DNA damage. This DNA oxidation may be due to the ROS generated during the autoxidation of NOR by molecular oxygen. These findings have shown that GEN can act as most effective chemopreventive agent for photosensitized DNA damage among the four XAN derivatives.

Spectroscopic studies have shown that these compounds cannot act as a physical sunscreen. The fluorescence intensity of riboflavin was less affected by addition of XAN derivatives. These findings exclude the interaction between the ground state of riboflavin and

XAN derivatives and the quenching of the excited singlet state of riboflavin. The possible mechanism of the prevention of the DNA photodamage is the quenching of the excited triplet state of riboflavin. MO calculations have shown that, although the quenching through energy transfer is impossible, the mechanism through electron transfer is possible (Table 3). The electron transfer from XAN derivatives to the excited triplet state of riboflavin generates a radical ion pair, and reverse electron transfer regenerates a ground state of riboflavin and XAN derivative. The excitation energy of the photosensitizer is dispersed as thermal energy through this quenching mechanism. The lifetime of triplet excited state of riboflavin ( ${}^3\tau_0$ ) is 22  $\mu$ s in aqueous media [78]. The rate constant of quenching reaction of triplet excited state of riboflavin is required to be the magnitude at least comparable to the decay rate constant ( $1/\tau_0 = 4.5 \times 10^4 \text{ s}^{-1}$ ). The value of this rate constant is close to that of the diffusion control reaction rate constant ( $k_{\text{dif}}$ ) in this experimental condition. The value of  $k_{\text{dif}}$  can be estimated from following equation:

$$k_{\text{dif}} = 8RT[Q]/3\eta \quad (7)$$

where R, T, [Q], and  $\eta$  are gas constant, absolute temperature, concentration of XAN derivatives, and viscosity of water ( $8.91 \times 10^{-4} \text{ kg m}^{-1} \text{ s}^{-1}$ ), respectively.

The quenching mechanism of an excited photosensitizer does not lead to the formation of a secondary reactive species. Furthermore, this quencher can protect from the phototoxicity induced by visible-light, which is difficult to be shielded with a physical sunscreen. This chemopreventive mechanism is not based on anti-oxidation or the effect of sunscreen. This preventive mechanism may be used for the novel chemoprevention of phototoxicity, photogenotoxicity, and solar carcinogenesis.

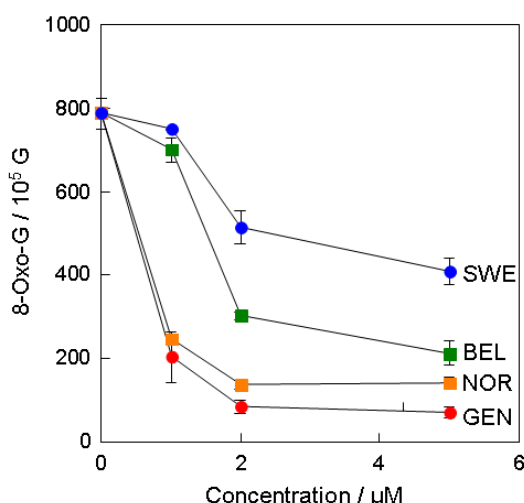


Figure 8. Effects of XAN derivatives on the formation of 8-oxo-G by photoexcited riboflavin. The reaction mixture containing 100  $\mu\text{M}$ /base calf thymus DNA, 50  $\mu\text{M}$  riboflavin, and indicated concentration of XAN derivatives in 100  $\mu\text{l}$  of 4 mM sodium phosphate buffer (pH 7.8) was exposed to 6  $\text{J cm}^{-2}$  light ( $\lambda_{\text{max}}=365 \text{ nm}$ , 1.2  $\text{mW cm}^{-2}$ ). After the reaction, DNA was digested to the nucleosides and analyzed with a high-performance liquid chromatography.

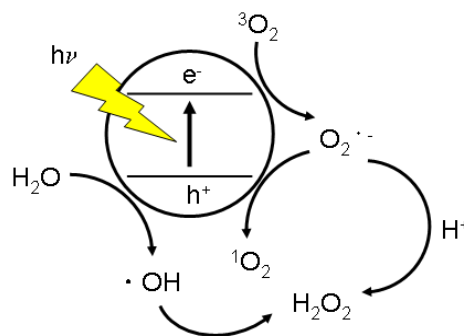


Figure 9. ROS generation through the photocatalytic reaction of semi-conductor particles.

## 5. INORGANIC MATERIALS

Organic materials are relatively unstable and tend to decay under an aerobic condition. The oxidation process of organic materials leads to the secondary ROS generation. On the other hand, certain inorganic materials such as metal oxide and noble metals are more stable than organic chemopreventive agents. Especially, inorganic sunscreen is very important for UV protection. Furthermore, the catalytic activity of stable noble metals has been studied for the anti-oxidation. In this section, application of inorganic materials for the prevention of phototoxic effect is presented.

### 5.1. Physical Sunscreen is Effective Protector for Ultraviolet Radiation

UV filter is effective method to prevent UV-mediated phototoxicity [79]. Especially, metal oxide particles such as titanium dioxide ( $\text{TiO}_2$ ) and zinc oxide ( $\text{ZnO}$ ) are important and well-known materials to shield UV radiation. The shielding mechanism is scattering of UV radiation. Since these metal oxide particles are semiconductor, a part of UV photons can be absorbed by these particles, leading to the photocatalytic reaction to generate various ROS such as  $\text{HO}^\cdot$ ,  $\text{H}_2\text{O}_2$ ,  $\text{O}_2^{\cdot-}$ , and  ${}^1\text{O}_2$  to oxidize biomolecules (Figure 9) [80-87]. UVA-irradiated  $\text{TiO}_2$  induced oxidative damage to isolated DNA at guanine, thymine, and cytosine residues [85]. Further,  $\text{TiO}_2$  can kill cancerous cells and bacteria under UVA irradiation [80-83]. However, the phototoxic effect of these materials for humans has not been reported. The action of UV protection of these materials should be more important than the ROS generation on the skin surface. In addition, the safety of nanosized particles in  $\text{TiO}_2$  and  $\text{ZnO}$  based sunscreens has been studied [88]. The risk of these metal oxide particles as nanomaterials has not been demonstrated. In general, these sunscreens consisting of  $\text{TiO}_2$  and  $\text{ZnO}$  are used for UVA protection. The metal oxide particles are considered as safety and effective UV protector.

## 5.2. Metal Nanoparticles: Platinum Nanoparticles Scavenge ROS

Inorganic materials can be used as the anti-oxidative agents other than the physical sunscreen. Various studies have demonstrated the catalytic decomposition of H<sub>2</sub>O<sub>2</sub> by noble metals such as platinum (Pt) [89-91], palladium (Pd) [90-92], silver (Ag) [93-95], and gold (Au) [92, 95]. These metals themselves are hardly oxidized by ROS, however, it is difficult to use metal powder or foils as anti-oxidative drugs. Recently, It was reported that Pt nanoparticles catalyze the decomposition of ROS [96]. These nanoparticles can be dispersed in water and used as homogenous solution. Because this removal mechanism is catalytic decomposition, no oxidized product is formed through this reaction. Platinum is used as a food additive and is not considered to be a toxic material. This result led us to the idea that inorganic materials, in particular noble metals, rather than organic antioxidants, can be used as novel chemopreventive agents against ROS-mediated photodamage of biomolecules. Colloidal dispersions of metal nanoparticles protected by water-soluble polymer such as poly-N-vinyl-2-pyrolidone (PVP) can be prepared using an alcohol reduction method [97]. The PVP-protected metal nanoparticles can form water-soluble sols. In general, the average diameters of Pt, Pd, and rhodium (Rh) nanoparticles are around 2 nm and Au and Ag tend to form relatively large particles (~ 10 nm).

Platinum nanoparticles effectively scavenged H<sub>2</sub>O<sub>2</sub> in a dose-dependent manner and showed the highest activity among the metal nanoparticles used in this report (Figure 10) [98]. A sample solution of 5 μM/atom Pt nanoparticles, among which 1 μg Pt metal is included, exhibits comparable activity for H<sub>2</sub>O<sub>2</sub> decomposition to that of 10 units of catalase. One unit of catalase can remove 1.0 μmol H<sub>2</sub>O<sub>2</sub> per min in water (pH 7.0, 25 °C). The mechanism of H<sub>2</sub>O<sub>2</sub> removal by metal nanoparticles can be explained by catalytic decomposition into water and molecular oxygen as follows:



H<sub>2</sub>O<sub>2</sub> is a long-lived ROS and plays an important role in DNA photodamage [69]. Indeed, various chemical compounds, including carcinogens, generate H<sub>2</sub>O<sub>2</sub> during the redox process [69]. Molecular oxygen is easily reduced by various compounds, leading to the formation of O<sub>2</sub><sup>·-</sup>. Formed O<sub>2</sub><sup>·-</sup> is rapidly dismutated into H<sub>2</sub>O<sub>2</sub>. Although H<sub>2</sub>O<sub>2</sub> itself is not a strong reactive species, it can generate highly reactive HO<sup>·</sup> through a Fenton reaction or a Haber-Weiss reaction. Copper ion also activates H<sub>2</sub>O<sub>2</sub> possibly due to the formation of Cu-oxygen complex such as Cu(I)OOH [59, 69]. Furthermore, H<sub>2</sub>O<sub>2</sub> can penetrate a cytoplasm membrane and be incorporated into the cell nucleus. Therefore, H<sub>2</sub>O<sub>2</sub> is considered to be one of the most important reactive species or a precursor participating in carcinogenesis. The removal of H<sub>2</sub>O<sub>2</sub> is an effective method for cancer chemoprevention. Furthermore, protective agents against H<sub>2</sub>O<sub>2</sub> are important to treat *acatalasemia*, a genetic deficiency of erythrocyte catalase inherited as an autosomal recessive trait. A catalyst consisting of an inorganic stable material is not oxidized and does not generate secondary ROS. Water-soluble nanoparticles of noble metal may become novel protective agents against ROS.

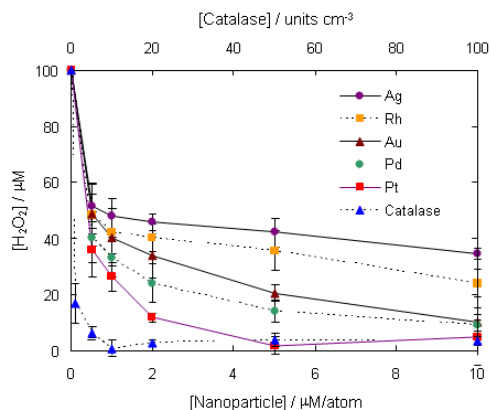


Figure 10. Removal of  $\text{H}_2\text{O}_2$  by metal nanoparticles and catalase. 100  $\mu\text{M}$   $\text{H}_2\text{O}_2$  was decomposed by metal nanoparticles or catalase.

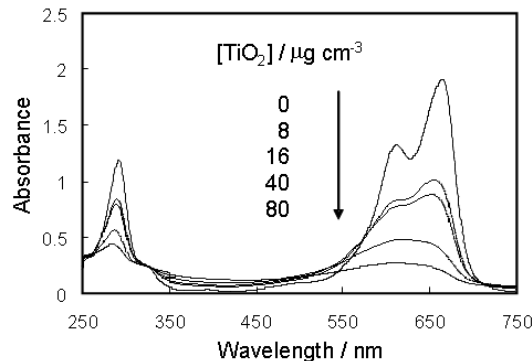


Figure 11. UV-Vis absorption spectra of methylene blue photocatalyzed by  $\text{TiO}_2$ . The sample solution containing 10  $\mu\text{M}$  methylene blue and indicated concentration of  $\text{TiO}_2$  in 10 mM sodium phosphate buffer (pH 7.6) was irradiated ( $\lambda_{\text{max}} = 365 \text{ nm}$ ,  $1 \text{ mW cm}^{-2}$ ) for 30 min.

**Table 3. Calculated triplet excited energy and ionization potentials of XAN derivatives and riboflavin**

Compounds	$E^{\text{T}}$ / kcal mol <sup>-1</sup>	$IP$ / eV
BEL	68.40	8.11
GEN	70.27	8.14
NOR	66.98	8.14
SWE	70.74	8.20
XAN	79.52	8.57
Riboflavin	57.00	8.80

$E^{\text{T}}$ : Energies of excited triplet state of the compounds.  $IP$ : Ionization energy.  $IP$  value indicates the energy level of HOMO. These values were calculated from the *ab initio* MO method at Hatree-Fock/6-31G\* level.

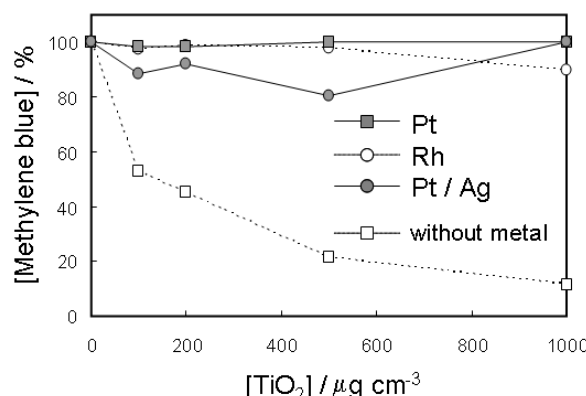


Figure 12. Inhibitory effect of metal nanoparticles on methylene blue decomposition photocatalyzed by  $\text{TiO}_2$ . The sample solution containing  $20 \mu\text{g cm}^{-3}$  metal nanoparticle, indicated concentration of  $\text{TiO}_2$ , and  $10 \mu\text{M}$  methylene blue in  $10 \text{ mM}$  sodium phosphate buffer ( $\text{pH } 7.6$ ) was irradiated ( $\lambda_{\text{max}} = 365 \text{ nm}$ ,  $1 \text{ mW cm}^{-2}$ ) for 30 min.

### 5.3. Platinum Nanoparticles Prevent the UV-Induced Phototoxicity

Photosensitized reaction by UV radiation, especially UVA radiation, is considered to cause toxic effect through oxidative biomolecules damage including DNA damage. As mentioned above, noble metal nanoparticles, especially, Pt nanoparticles effectively catalyze the decomposition of ROS. Because this removal mechanism is catalytic decomposition, no oxidized product is formed through this reaction. This result led us to the idea that inorganic materials, in particular noble metals, rather than organic antioxidants, can be used as novel chemopreventive agents against UVA-induced biomolecules damage. Therefore, the removal of ROS generated from a photocatalytic reaction of  $\text{TiO}_2$  particles using water-soluble polymer-protected Pt, Rh, and Pt/Ag bimetallic nanoparticles was examined.  $\text{TiO}_2$  (anatase) and methylene blue were used as a model of the UVA-induced reaction. The sample solution containing methylene blue and  $\text{TiO}_2$  dispersion in sodium phosphate buffer ( $\text{pH } 7.6$ ) with or without metal nanoparticle was irradiated with a UVA lamp ( $365 \text{ nm}$ ,  $1 \text{ mW cm}^{-2}$ ). The decomposition of methylene blue was evaluated by absorption measurement at  $659 \text{ nm}$ . When exposing to UVA light, the reduction-oxidation activity of  $\text{TiO}_2$  has a significant biological impact, as is exemplified by its bactericidal activity. Photo-irradiated  $\text{TiO}_2$  effectively decomposed methylene blue (Figure 11). Various ROS contribute to the photocatalytic reaction of  $\text{TiO}_2$ . Especially,  $\text{H}_2\text{O}_2$  is long-lived ROS and plays an important role in oxidative biomolecules damage. Molecular oxygen is reduced by photoexcited materials, leading to the formation of  $\text{O}_2^{\cdot-}$ . Formed  $\text{O}_2^{\cdot-}$  is rapidly dismutated into  $\text{H}_2\text{O}_2$ . Although  $\text{H}_2\text{O}_2$  itself is not a strong reactive species, it can generate highly reactive  $\text{HO}^{\cdot}$ . Therefore,  $\text{H}_2\text{O}_2$  is considered to be one of the most important ROS participating in UVA carcinogenesis and phototoxicity. Since other ROS, such as directly produced  $\text{HO}^{\cdot}$  and  ${}^1\text{O}_2$ , rapidly quenched in aqueous solution,  $\text{H}_2\text{O}_2$  should be key reactive species in this experimental condition. The  $\text{TiO}_2$  and methylene blue could be used as a simple model of UVA-induced oxidation reaction [99].

PVP-protected metal nanoparticles, in particular, the Pt nanoparticle, inhibited the methylene blue decomposition photocatalyzed by  $\text{TiO}_2$  (Figure 12) [99]. PVP itself did not

inhibit the methylene blue decomposition. This inhibitory effect can be explained by the catalytic decomposition of H<sub>2</sub>O<sub>2</sub> generated through the TiO<sub>2</sub> photocatalysis. These nanoparticles decomposed H<sub>2</sub>O<sub>2</sub> into H<sub>2</sub>O and O<sub>2</sub> similar to catalase (Section 5-2). In the case of H<sub>2</sub>O<sub>2</sub> decomposition, the Pt nanoparticle showed the highest catalytic activity per unit atom. The activity of a 1 µg Pt nanoparticle was comparable to that of 10 units of catalase. Unexpectedly, the bimetallic with Ag did not show improvement effect and rather decreased the inhibitory effect of Pt nanoparticle on the decomposition of methylene blue.

The UV-Vis absorption spectra of these metal nanoparticles were hardly changed by the photocatalytic reaction, suggesting that the noble metal nanoparticles are stable for ROS and UVA irradiation. Organic antioxidant undergoes oxidation in the removal process of ROS, leading to the formation of various oxidized products and may produce secondary ROS. In the case of noble metal catalyst, these effects are negligible.

Pt, Rh, and Pt/Ag nanoparticles effectively inhibited the methylene blue decomposition photocatalyzed by TiO<sub>2</sub>. TiO<sub>2</sub> photocatalytic system was used as a UVA-induced ROS generation. The most important ROS in this photocatalytic reaction is H<sub>2</sub>O<sub>2</sub>, because of its long lifetime in aqueous solution. This inhibitory effect of metal nanoparticle can be explained by the removal of H<sub>2</sub>O<sub>2</sub>. Unexpectedly, the activity of Pt nanoparticle was not improved by the bimetallic with Ag. Platinum is a very stable metal against various chemical compounds and is used as food additive. A PVP-protected Pt nanoparticle may be used as a novel preventive agent for UVA-induced biomolecules damage through ROS generation.

## 6. CONCLUSION

Phototoxic effect of UV and visible light is caused through direct and/or indirect mechanisms. UVB directly activates biomolecules including DNA bases to induce photochemical damage. UVA and visible-light mainly damage biomolecules through indirect mechanism such as photo-induced electron transfer and ROS generation. Especially, <sup>1</sup>O<sub>2</sub> is the important ROS to damage biomolecules through visible-light photosensitized reaction. To prevent the phototoxicity, the physical shielding of UV radiation is effective method. Organic UVB absorber and inorganic UVA sunscreen such as TiO<sub>2</sub> and ZnO are important materials. In the case of the use of UVB absorbers, the side effect caused by the decomposed product of the drugs should be considered. Organic anti-oxidant can also induce the generation of the secondary ROS through their oxidation process. Other than these traditional materials, novel materials have been studied. The quenchers and the anti-oxidative catalyst of noble metal nanoparticles are developing. For example, the quencher from plants such as XAN derivatives, which are non-color agents, effectively deactivates the photoexcited photosensitizers. These quenchers may be applied to prevent the phototoxic effect by the visible-light photosensitizer. The stable noble metal nano-catalysts can be used as scavenger for ROS generated via UV sensitized reactions.

## REFERENCES

- [1] Taylor, C. R., Stern, R. S., Leyden, J. J. & Gilchrest, B. A. (1990). Photoaging/photodamage and photoprotection. *J. Am. Acad. Dermatol.*, *22*, 1-15.
- [2] Hiraku, Y., Ito, K., Hirakawa, K. & Kawanishi, S. (2007). Photosensitized DNA damage and its protection via a novel mechanism. *Photochem. Photobiol.*, *83*, 205-212.
- [3] Hirakawa, K., Yoshida, M., Nagatsu, A., Mizukami, H., Rana, V., Rawat, M. S. M., Oikawa, S. & Kawanishi, S. (2005). Chemopreventive action of xanthone derivatives on photosensitized DNA damage. *Photochem. Photobiol.*, *81*, 314-319.
- [4] Kimlin, M. G.. (2008). Geographic location and vitamin D synthesis. *Mol. Asp. Med.*, *29*, 453-461.
- [5] IARC Working Group (1992). IARC Monographs on the *Evaluation of the Carcinogenic Risk of Chemicals to Humans*, Vol. 55, IARC, Lyon.
- [6] Strickland, P. T. (1986). Photocarcinogenesis by near-ultraviolet (UVA) radiation in Sencar mice. *J. Invest. Dermatol.*, *87*, 272-275.
- [7] van Weelden, H., de Gruji, F. R., van der Putte, S. C. J., Toonstra, J. & van der Leun, J. C. (1988). The carcinogenic risks of modern tanning equipment: is UV-A safer than UV-B? *Arch. Dermatol. Res.*, *280*, 300-307.
- [8] Tyrrell, R. M. & Keyse, S. M. (1990). The interaction of UVA radiation with cultured cells. *J. Photochem. Photobiol. B: Biol.*, *4*, 349-361.
- [9] Setlow, R. B., Grist, E., Thompson, K. & Woodhead, A. D. (1993). Wavelength effective in induction of malignant melanoma. *Proc. Natl. Acad. Sci. USA*, *90*, 6666-6670.
- [10] Hirakawa, K. (2008). DNA damage through photo-induced electron transfer and photosensitized generation of reactive oxygen species. In: Kimura, H. & Suzuki, A. (ed.) *New research on DNA damage*, Nova Science Publishers Inc. New York, 197-219.
- [11] Drobetsky, E. A., Turcotte, J. & Chateauneuf, A. (1995). A role for ultraviolet A in solar mutagenesis. *Proc. Natl. Acad. Sci. USA*, *92*, 2350-2354.
- [12] Besaratinia, A., Synold, T. W., Chen, H. H., Chang, C., Xi, B., Riggs, A. D. & Pfeifer, G. P. (2005). DNA lesions induced by UV A1 and B radiation in human cells: comparative analyses in the overall genome and in the *p53* tumor suppressor gene. *Proc. Natl. Acad. Sci. USA*, *102*, 10058-10063.
- [13] Cadet, J., Douki, T., Gasparutto, D. & Ravanat, J. L. (2003). Oxidative damage to DNA: formation, measurement and biochemical features. *Mutat. Res.*, *531*, 5-23.
- [14] Kawanishi, S., Hiraku, Y. & Oikawa, S. (2001). Mechanism of guanine-specific DNA damage by oxidative stress and its role in carcinogenesis and aging. *Mutat. Res.*, *488*, 65-76.
- [15] Drechsel, D. A. & Patel, M. (2008). Corrigendum to role of reactive oxygen species in the neurotoxicity of environmental agents implicated in Parkinson's disease. *Free Radic. Biol. Med.*, *44*, 1873-1886.
- [16] DeRosa, M. C. & Crutchley, R. J. (2002). Photosensitized singlet oxygen and its applications. *Coord. Chem. Rev.*, *233-234*, 351-371.
- [17] Dexter, D. L. (1953). A theory of sensitized luminescence in solids. *J. Chem. Phys.*, *21*, 836-850.

- [18] Kawanishi, S., Hiraku, Y. & Oikawa, S. (2001). Sequence-specific DNA damage induced by UVA radiation in the presence of endogenous and exogenous photosensitizers. *Curr. Probl. Dermatol.*, 29, 74-82.
- [19] Yamamoto, K. & Kawanishi, S. (1989). Hydroxyl free radical is not the main active species in site-specific DNA damage induced by copper (II) ion and hydrogen peroxide. *J. Biol. Chem.*, 264, 15435-15440.
- [20] Hirakawa, K., Kawanishi, S. & Hirano, T. (2005). The mechanism of guanine specific photo-oxidation in the presence of berberine and palmatine: activation of photosensitized singlet oxygen generation through DNA-binding interaction. *Chem. Res. Toxicol.*, 18, 1545-1552.
- [21] Hirakawa, K., Kawanishi, S., Matsumoto, J., Shiragami, T. & Yasuda, M. (2006). Guanine-specific DNA damage photosensitized by the dihydroxo(tetraphenylporphyrinato)antimony(V) complex. *J. Photochem. Photobiol. B: Biol.*, 82, 37-44.
- [22] Hirakawa, K., Kawanishi, S., Hirano, T. & Segawa, H. (2007). Guanine-specific DNA oxidation photosensitized by the tetraphenylporphyrin phosphorus(V) complex via singlet oxygen generation and electron transfer. *J. Photochem. Photobiol. B: Biol.*, 87, 209-217.
- [23] Dolmans, D. E. J. G. J., Fukumura, D. & Jain, R. K. (2003). Photodynamic therapy for cancer. *Nat. Rev. Cancer*, 3, 380-387.
- [24] Ackroyd, R., Kelty, C., Brown, N. & Reed, M. (2001). The history of photodetection and photodynamic therapy. *Photochem. Photobiol.*, 74, 656-669.
- [25] Moan, J. & Peng, Q. (2003). An outline of the hundred-year history of PDT. *Anticancer Res.*, 23, 3591-3600.
- [26] Ji, Z., Yang, G., Vasovic, V., Cunderlikova, B., Suo, Z., Nesland, J. M. & Peng, Q. (2006). Subcellular localization pattern of protoporphyrin IX is an important determinant for its photodynamic efficiency of human carcinoma and normal cell lines. *J. Photochem. Photobiol. B: Biol.*, 84, 213-224.
- [27] Ravanat, J. L., Sauvage, S., Caillat, S., Martinez, G. R., Medeiros, M. H., Di Mascio, P., Favier, A. & Cadet, J. (2004). Singlet oxygen-mediated damage to cellular DNA determined by the comet assay associated with DNA repair enzymes. *Biol. Chem.*, 385, 17-20.
- [28] Cadet, J., Ravanat, J. L., Martinez, G. R., Medeiros, M. H. & Di Mascio, P. (2006). Singlet oxygen oxidation of isolated and cellular DNA: product formation and mechanistic insights. *Photochem. Photobiol.*, 82, 219-225.
- [29] Kawai, K., Osakada, Y., Fujitsuka, M. & Majima, T. (2006). Effects of reaction rate of radical anion of a photosensitizer with molecular oxygen on the photosensitized DNA damage. *Chem. Commun.*, 3918-3920.
- [30] Kawai, K., Osakada, Y., Fujitsuka, M. & Majima, T. (2007). Hole transfer in DNA and photosensitized DNA damage: importance of adenine oxidation. *J. Phys. Chem. B*, 111, 2322-2326.
- [31] Groves, G. A., Agin, P. P. & Sayre, R. M. (1979). In vitro and in vivo methods to define sunscreen protection. *Aust. J. Dermatol.*, 20, 112-119.
- [32] El-Boury, S., Couteau, C., Boulande, L., Paparis, E. & Coiffard, L. J. M. (2007). Effect of the combination of organic and inorganic filters on the Sun Protection Factor (SPF) determined by *in vitro* method. *Int. J. Pharmaceutics*, 340, 1-5.

- [33] Wang, S. Q., Stanfield, J. W. & Osterwalder, U. (2008). In vitro assessments of UVA protection by popular sunscreens available in the United States. *J. Am. Acad. Dermatol.*, *59*, 934-942.
- [34] Damiani, E., Rosati, L., Castagna, R., Carloni, P. & Greci, L. (2006). Changes in ultraviolet absorbance and hence in protective efficacy against lipid peroxidation of organic sunscreens after UVA irradiation. *J. Photochem. Photobiol. B: Biol.*, *82*, 204-213.
- [35] Allen, J. M., Gossett, C. J. & Allen, S. K. (1996). Photochemical formation of singlet molecular oxygen in illuminated aqueous solutions of PABA. *J. Photochem. Photobiol.*, *32*, 33-37.
- [36] Allen, J. M., Gossett, C. J. & Allen, S. K. (1996). Photochemical formation of singlet molecular oxygen in illuminated aqueous solutions of several commercially available sunscreen active ingredients. *Chem. Res. Toxicol.*, *9*, 605-609.
- [37] Aliwell, S. R., Martineigh, B. S. & Salter, L. F. (1994). Photoproducts formed by near-UV irradiation of thymine in the presence of PABA. *J. Photochem. Photobiol. A: Chem.*, *83*, 223-228.
- [38] Sutherland, B. M. (1982). PABA acid-sunlamp sensitization of pyrimidine dimer formation and transformation in human cells. *Photochem. Photobiol.*, *36*, 95-97.
- [39] Hu, M.-L., Chen, Y.-K., Chen, L.-C. & Sano, M. (1995) PABA scavenges reactive oxygen species and protects DNA against UV and free radical damage. *J. Nutr. Biochem.*, *6*, 504-508.
- [40] Cantrell, A., McGarver, D. J. & Truscott, T. G. (2001). Photochemical and photophysical properties of sunscreens. In: Giacomoni P. U. (ed.), *Sun protection in man*, Elsevier, Amsterdam, pp. 495-519.
- [41] Hanson, K. M., Gratton, E. & Bardeen, C. J. (2006). Sunscreen enhancement of UV-induced reactive oxygen species in the skin. *Free Radic. Biol. Med.*, *41*, 1205-1212.
- [42] Nedostro, S. T. (2003). Facial erythema as a result of benzophenone allergy. *J. Am. Acad. Dermatol.*, *49*, 259-261.
- [43] Hirakawa, K. (2009). Photochemistry and photobiology of folic acid analogues. *Res. Adv. Photochem. Photobiol.*, *1*, 1-16.
- [44] Akhtar, M. J., Khan, M. A. & Ahmad, I. (1999). Photodegradation of folic acid in aqueous solution, *J. Pharm. Biomed. Anal.*, *19*, 269-275.
- [45] Akhtar, M. J., Khan, M. A. & Ahmad, I. (2000). Effect of riboflavin on the photolysis of folic acid in aqueous solution, *J. Pharm. Biomed. Anal.*, *23*, 1039-1044.
- [46] Hirakawa, K., Suzuki, H., Oikawa, S. & Kawanishi, S. (2003). Sequence-specific DNA damage induced ultraviolet A-irradiated folic acid via its photolysis product. *Arch. Biochem. Biophys.*, *410*, 261-268.
- [47] Off, M. K., Steindal, A. E., Porojnicu, A. C., Juzeniene, A., Vorobey, A., Johnsson, A. & Moan, J. (2005). Ultraviolet photodegradation of folic acid, *J. Photochem. Photobiol. B: Biol.*, *80*, 47-55.
- [48] Song, Q.-H. & Hwang, K. C. (2007). Direct observation for photophysical and photochemical processes of folic acid in DMSO solution, *J. Photochem. Photobiol. A: Chem.*, *185*, 51-56.
- [49] Ito, K. & Kawanishi, S. (1997). Photoinduced hydroxylation of deoxyguanosine in DNA by pterins: sequence specificity and mechanism, *Biochemistry*, *36*, 1774-1781.

- [50] Hirakawa, K., Aoshima, M., Hiraku, Y. & Kawanishi, S. (2002). Photohydrolysis of methotrexate produces pteridine, which induces poly-G-specific DNA damage through photoinduced electron transfer. *Photochem. Photobiol.*, **76**, 467-472.
- [51] Hirakawa, K. (2006). Fluorometry of hydrogen peroxide using oxidative decomposition of folic acid, *Anal. Bioanal. Chem.*, **386**, 244-248.
- [52] Hirakawa, K. (2009). Fluorometry of singlet oxygen generated via a photosensitized reaction using folic acid and methotrexate. *Anal. Bioanal. Chem.*, **393**, 999-1005.
- [53] Burrows, C. J. & Muller J. G. (1998). Oxidative nucleobase modifications leading to strand scission. *Chem. Rev.*, **98**, 1109-1151.
- [54] Klecak, G., Urbach, F. & Urwyler, H. (1997). Fluoroquinolone antibacterials enhance UVA-induced skin tumors. *J. Photochem. Photobiol. B: Biol.*, **37**, 174-181.
- [55] Makinen, M., Forbes, P. D. & Stenback, F. (1997). Quinolone antibacterials: a new class of photochemical carcinogens. *J. Photochem. Photobiol. B: Biol.*, **37**, 182-187.
- [56] Ito, K., Inoue, S., Yamamoto, K. & Kawanishi, S. (1993). 8-Hydroxydeoxyguanosine formation at the 5' site of 5'-GG-3' sequences in double-stranded DNA by UV radiation with riboflavin. *J. Biol. Chem.*, **268**, 13221-13227.
- [57] Hirakawa, K., Yoshida, M., Oikawa, S. & Kawanishi, S. (2003). Base oxidation at 5' site of GG sequence in double-stranded DNA induced by UVA in the presence of xanthone analogues: relationship between the DNA-damaging abilities of photosensitizers and their HOMO energies. *Photochem. Photobiol.*, **77**, 349-355.
- [58] Slaga, T. J. (1995). Inhibition of the induction of cancer by antioxidants. In: Longenecker, J. B., Kritchevsky, D. & Drezner, M. K. (ed.) *Nutrition and biotechnology in heart disease and cancer*, Plenum Publishing Corp. New York, pp. 167-174.
- [59] Yamashita, N., Murata, M., Inoue, S., Burkitt, M. J., Milne, L. & Kawanishi, S. (1998).  $\alpha$ -Tocopherol induces oxidative damage to DNA in the presence of copper(II) ions. *Chem. Res. Toxicol.*, **11**, 855-862.
- [60] Murata, M. & Kawanishi, S. (2000). Oxidative DNA damage by vitamin A and its derivative via superoxide generation. *J. Biol. Chem.*, **275**, 2003-2008.
- [61] Nitta, Y., Kamiya, K., Tanimoto, M., Kagimoto, O., Niwa, O. & Yokoro, K. (1991). Effects of administration natural vitamin E on spontaneous hepatocarcinogenesis and N-nitrosoamine initiated tumors in mice. *J. Toxicol. Pathol.*, **4**, 55-61.
- [62] The alpha-tocopherol, beta carotene cancer prevention study group (1994). The effect of vitamin E and beta carotene on the incidence of lung cancer and other cancers in male smokers. *N. Engl. J. Med.*, **330**, 1029-1035.
- [63] Omenn, G. S., Goodman, G. E., Thornquist, M. D., Balmes, J., Cullen, M. R., Glass, A., Keogh, J. P., Meyskens, F. L. Jr., Valanis, B., Williams, J. H. Jr., Barnhart, S., Cherniack, M. G., Brodkin, C. A. & Hammar, S. (1996). Risk factors for lung cancer and for intervention effects in CARET, the beta-carotene and retinol efficacy trial. *J. Natl. Cancer Inst.*, **88**, 1550-1559.
- [64] Menkovic, N., Savikin-Fodulovic, K., Bulatovic, V., Aljancic, I., Juranic, N., Macura, S., Vajs, V. & Milosavljevic, S. (2002). Xanthones from Swertia punctata. *Phytochemistry*, **61**, 415-420.
- [65] Ya, B. Q., Nian, L. C., Li, C. & Gen, X. P. (1999). Protective effect of swerchirin on hematopoiesis in  $^{60}\text{Co}$ -irradiated mice. *Phytomedicine*, **6**, 85-88.

- [66] Bajpai, M. B., Asthana, R. K., Sharma, N. K., Chatterjee, S. K. & Mukherjee, S. K. (1991). Hypoglycemic effect of swerchirin from the hexane fraction of Swertia chirayita. *Planta Med.*, *57*, 102-104.
- [67] Basnet, P., Kadota, S., Shimizu, M., Takata, Y., Kobayashi, M. & Namba, T. (1995). Bellidifolin stimulates glucose uptake in rat 1 fibroblasts and ameliorates hyperglycemia in streptozotocin (STZ)-induced diabetic rats. *Planta Med.*, *61*, 402-405.
- [68] Basnet, P., Kadota, S., Shimizu, M. & Namba, T. (1994). Bellidifolin: a potent hypoglycemic agent in streptozotocin (STZ)-induced diabetic rats from Swertia japonica. *Planta Med.*, *60*, 507-511.
- [69] Hirakawa, K., Oikawa, S., Hiraku, Y., Hirosawa, I. & Kawanishi, S. (2002). Catechol and hydroquinone have different redox properties responsible for their differential DNA-damaging ability. *Chem. Res. Toxicol.*, *15*, 76-82.
- [70] Sugiyama, H. & Saito, I. (1996). Theoretical studies of GG-specific photocleavage of DNA via electron transfer: significant lowering of ionization potential and 5'-localization of HOMO of stacked GG bases in B-form DNA. *J. Am. Chem. Soc.*, *118*, 7063-7068.
- [71] Yoshioka, Y., Kitagawa, Y., Takano, Y., Yamaguchi, K., Nakamura, T. & Saito, I. (1999). Experimental and theoretical studies on the selectivity of GGG triplets toward one-electron oxidation in B-form DNA. *J. Am. Chem. Soc.*, *121*, 8712-8719.
- [72] Bruner, S. D., Norman, D. P. G. & Verdine, G. L. (2000). Structural basis for recognition and repair of the endogenous mutagen 8-oxoguanine in DNA. *Nature*, *403*, 859-866.
- [73] Shibutani, S., Takeshita, M. & Grollman, A. P. (1991). Insertion of specific bases during DNA synthesis past the oxidation-damaged base 8-oxodG. *Nature*, *349*, 431-434.
- [74] Kino, K., Saito, I. & Sugiyama, H. (1998). Product analysis of GG-specific photooxidation of DNA via electron transfer: 2-aminoimidazolone as a major guanine oxidation product. *J. Am. Chem. Soc.*, *120*, 7373-7374.
- [75] Kino, K. & Sugiyama, H. (2001). Possible cause of G-C-->C-G transversion mutation by guanine oxidation product, imidazolone. *Chem. Biol.*, *8*, 369-378.
- [76] McBride, T. J., Schneider, J. E., Floyd, R. A. & Loeb, L. A. (1992). Mutations induced by methylene blue plus light in single-stranded M13mp2. *Proc. Natl. Acad. Sci. USA*, *89*, 6866-6870.
- [77] Negishi, K. & Hao, W. (1992). Spectrum of mutations in single-stranded DNA phage M13mp2 exposed to sunlight: predominance of G-to-C transversion. *Carcinogenesis*, *13*, 1615-1618.
- [78] Massad, W., Criado, S., Bertolotti, S., Pajares, A., Gianotti, J., Escalada, J. P., Amat-Guerri, F. & García, N. A. (2004). Photodegradation of the herbicide norflurazon sensitised by riboflavin, A kinetic and mechanistic study. *Chemosphere*, *57*, 455-461.
- [79] Salvador, A. & Chisvert, A. (2005). Sunscreen analysis: A critical survey on UV filters determination. *Analytica Chimica Acta*, *537*, 1-14.
- [80] Fujishima, A., Rao, T. N. & Tryk, D. A. (2000). Titanium dioxide photocatalyst. *J. Photochem. Photobiol. C: Photochemistry Rev.*, *1*, 1-21.
- [81] Fujishima, A., Zhang, X. & Tryk, D. A. (2008). TiO<sub>2</sub> photocatalysis and related surface phenomena. *Surface Sci. Rep.*, *63*, 515-582.

- [82] Cai, R., Hashimoto, K., Ito, K., Kubota, Y. & Fujishima, A. (1991). Photokilling of malignant cells with ultrafine TiO<sub>2</sub> powder. *Bull. Chem. Soc. Jpn.*, **64**, 1268-1273.
- [83] Cai, R., Kubota, Y., Shuin, T., Sakai, H., Hashimoto, K. & Fujishima, A. (1992). Induction of cytotoxicity by photoexcited TiO<sub>2</sub> particles. *Cancer Res.*, **52**, 2346-2348.
- [84] Tachikawa, T., Fujitsuka, M. & Majima, T. (2007). Mechanistic insight into the TiO<sub>2</sub> photocatalytic reactions: design of new photocatalysts. *J. Phys. Chem. C*, **111**, 5259-5275.
- [85] Hirakawa, K., Mori, M., Yoshida, M., Oikawa, S. & Kawanishi, S. (2004). Photo-irradiate titanium dioxide catalyzes site specific DNA damage via generation of hydrogen peroxide. *Free Radic. Res.*, **38**, 439-447.
- [86] Nosaka, Y., Daimon, T., Nosaka, A. Y. & Murakami, Y. (2004). Singlet oxygen formation in photocatalytic TiO<sub>2</sub> aqueous suspension. *Phys. Chem. Chem. Phys.*, **6**, 2917-2918.
- [87] Hirakawa, K. & Hirano, T. (2006). Singlet oxygen generation photocatalyzed by TiO<sub>2</sub> particles and its contribution to biomolecule damage. *Chem. Lett.*, **35**, 832-833.
- [88] Newman, M. D., Stotland, M. & Ellis, J. I. (2009). The safety of nanosized particles in titanium dioxide- and zinc oxide-based sunscreens. *J. Am. Acad. Dermatol.*, **61**, 685-692.
- [89] Keating, K. B., Rozner, A. G. & Youngblood, J. L. (1965). The effect of deformation on catalytic activity of platinum in the decomposition of hydrogen peroxide. *J. Catalysis*, **4**, 608-619.
- [90] McKee, D. W. (1969). Catalytic decomposition of hydrogen peroxide by metals and alloys of the platinum group. *J. Catalysis*, **14**, 355-364.
- [91] Bianchi, G., Mazza, F. & Mussini, T. (1962). Catalytic decomposition of acid hydrogen peroxide solutions on platinum, iridium, palladium, and gold surfaces. *Electrochimica Acta*, **7**, 457-473.
- [92] Eley, D. D. & Macmahon, D. M. (1972). Decomposition of hydrogen peroxide catalyzed by palladium-gold alloy wires. *J. Colloid Interface Sci.*, **38**, 502-510.
- [93] Goszner, K., Körner, D. & Hite, R. (1972). Catalytic activity of silver. I. Activity, poisoning, and regeneration during the decomposition of hydrogen peroxide. *J. Catalysis*, **25**, 245-253.
- [94] Baumgartner, H. J., Hood, G. C., Monger, J. M., Roberts, R. M. & Sanborn, C. E. (1963). Decomposition of concentrated hydrogen peroxide on silver. I. Low temperature reaction and kinetics. *J. Catalysis*, **2**, 405-414.
- [95] Goszner, K. & Bischof, H. (1974). Decomposition of hydrogen peroxide on silver-gold alloys. *J. Catalysis*, **32**, 175-182.
- [96] Kajita, M., Hikosaka, K., Itsuka, M., Kanayama, A., Toshima, N. & Miyamoto, Y. (2007). Platinum nanoparticle is a useful scavenger of superoxide anion and hydrogen peroxide. *Free Radic. Res.*, **41**, 615-626.
- [97] Hirai, H., Nakao, Y. & Toshima, N. (1979). Preparation of colloidal transition metals in polymers by reduction with alcohols or ethers. *J. Macromol. Sci. Chem.*, **A13**, 727-750.
- [98] Hirakawa, K. & Sano, S. (2009). Platinum nanoparticle catalyst scavenges hydrogen peroxide generated from hydroquinone. *Bull. Chem. Soc. Jpn.*, **82**, 1299-1303.
- [99] Hirakawa, K., Shiota, K. & Sano, S. (2008). Preventive action of metal nanoparticles on UVA-sensitized oxidation through hydrogen peroxide formation. *Photomed. Photobiol.*, **30**, 27-28.

## ***Chapter 7***

# **PIGMENTATION AS A UV-SCREENING STRATEGY OF LICHENIZED FUNGI FROM THE TROPICAL ANDES AND ITS POSSIBLE ROLE ON PLANETARY SURFACES**

***Vicente Marcano<sup>1\*</sup>, José Alberto Rojas<sup>2</sup>, Alirio Balza<sup>2</sup>,  
Ricardo Díaz<sup>1</sup>, Roxana Pérez<sup>1</sup> and Pedro Benítez<sup>1</sup>***

<sup>1</sup>Group of Atmospheric and Space Sciences, Faculty of Science,

University of the Andes, Mérida 5101, Venezuela.

<sup>2</sup>Electron Microscopy Center, University of the Andes, Mérida, Venezuela.,  
Pigmentation as a Uv-Screening Strategy of Lichens.

## **ABSTRACT**

Photochemical analysis of secondary compounds in lichens from the Venezuelan Andean snow and glacier zones (4800-5000 m) was carried out in order to determine the absorbance capacity of UV radiation in the UVA, UVB and UVC ranges and to characterize the probable UV-protective function. Spectrotometric (UV-VIS, NIR, FTIR, MS, NMR) and chromatographic (HPTLC) standardized techniques were utilized to identify the lichen compounds. UVB irradiance in the glacier zone (5000 m) revealed a value of  $\sim 3 \text{ W m}^{-2}$  which is sufficient to produce important biochemical and cell alterations. Of a total of 25 lichen species distributed in the glacier and snow zones, 68% showed the presence of phenolic compounds having strong absorption for UVC radiation, 96% had strong absorption for UVB radiation and 100% had strong absorption for UVA radiation. The substance groups that had the highest resistance to UVA and UVB radiation were characterized by ester bonds among both phenolic units (depsides). They were the most abundant products to be found among the lichens, whereas substances having ester and ether bonds in both phenolic units (depsidones) had a higher capacity to absorb UVC radiation. Microorganisms having adaptive UV-screening responses similar to the lichens investigated can perhaps be expected to occur on Earth-like planets containing  $\text{O}_2$  levels  $\leq 10^{-2}$  PAL and orbiting around G, F, and K stars.

---

\* Corresponding author: E-mail: vicente.marcano@gmail.com, marcvin@ula.ve, Tef: 58-274-2401424, Fax: 58-274-2401424.

**Keywords:** Venezuelan Andes, Snow and Glacier Zones, Cryoextremophile Lichens, UV radiation, UV-Screening Compounds, Habitable Zone.

## 1. INTRODUCTION

Earth-like planets occupying the habitable zone (HZ) and orbiting around G, F or K stars could present ozone abundances but not sufficient to cause a reduction in biologically effective irradiances (Kasting, 1987; Kasting, 1997; Kasting *et al.*, 1997; Cockell, 1999; Franck *et al.*, 2000a, b; Cockell, 2000a, b, 2002; Segura *et al.*, 2003). Hence, organisms exposed to intense UV radiation at surface habitats could have synthesized UV screening and energy quenching pigments in order to avoid damages in the biochemical machinery (Vishniac, 1996; Garcia-Pichel, 1998; Garcia-Pichel and Castenholz, 1991; Quesada and Vincent, 1997; Cockell and Knowland, 1999; Cockell and Horneck, 2001; Wynn-Williams and Edwards, 2000; Wynn-Williams *et al.*, 2002; Onofri *et al.*, 2003; De Vera *et al.*, 2003; Marcano *et al.*, 2001, 2002a, b, 2006).

The development of UV-screening strategies in heterotrophic-photosynthetic organisms similar to lichens could have allowed their occurrence in surface habitats before 1 Gyr ago when the ozone shield was not formed fully. Although the oldest certain fossil lichen is Early Devonian (Taylor *et al.*, 1995), there is strong evidence about the occurrence of lichen-like associations from Witwatersrand, South Africa, dated between 2.2 and 2.7 billion years old (Hallbauer and van Warmelo, 1974). Lichens are able to synthesize secondary compounds by mevalonic acid, acetate-polymalonate and shikimic pathways. These compounds are generally extracellular and concentrate in the external tissues of lichen (e.g. cortical layer). Likewise, these compounds are found in the internal tissues (e.g. medulla). The most common fate of acetate-polymalonate-derived phenolic acids is intermolecular esterification of two or three similar units. For instance, the carboxylic acid of one unit is joined to the hydroxyl *para* to the carboxylic acid of the second unit. Such esterifications lead to the *para*-depsides. If an ester linkage joins the first unit to a position *meta* to the carboxylic acid of the second ring, a *meta*-depside results (Culberson, 1969). The compounds synthesized by the mevalonic acid and acetate-polymalonate pathways such as phenolic carboxylic acid derivatives (e.g. *para*- and *meta*-depsides, and depsidones), xanthones, dibenzofurane derivatives (e.g. usnic acid) (Marcano *et al.*, 1999) and anthraquinones, show absorbances ranging between 200 and 400 nm which offer a protection to lichen before the lethal effect that UV radiation could cause at the molecule level (Harborne, 1968; Rundel, 1978; Solhaug and Gauslaa, 1996; Bacherau and Asta, 1997; Wynn-Williams and Edwards, 2000; Wynn-Williams *et al.*, 1999, 2002; Bjerke *et al.*, 2002). For instance, the high absorbance between 280-320 nm exhibited by these compounds suggests a protective effect for aromatic amino acids, proteins, purines, pyrimidines or nucleic acids of the UVB (280-315 nm) radiation fluxes. UVA (315-400 nm) radiation is less damaging than UVC (200-280 nm), but it can mediate photooxidative damage through reactive oxygen species as H<sub>2</sub>O<sub>2</sub> within cells (Jagger, 1985; Mancinelli and White, 2000). Although these pigments can also absorb UVC radiation (Harborne, 1968; Towers, 1968) such function is irrelevant today because the atmosphere of modern Earth screens out all UVC before it reaches the biosphere. However, this capability would have been vital on early Earth.

Our interest with this paper is to determine the capacity of the secondary compounds synthesized by lichens occurring in the Tropical Andean glacier and snow zones to absorb UV radiation in the UVA, UVB and UVC wavelength ranges, and therefore to infer its possible UV-protective function to the lethal effects of this radiation on the cell components and functions of the lichen. Thus, it is expected that the results obtained in this work may contribute with a better understand about the characteristics and limits of the adaptations exhibited by the organisms at the tropical high mountain regions, and thereby may increase the knowledge about adaptative responses developed by microorganisms in ages when the ozone shield would have not screened fully UV radiation (Cockell, 2000a, b, 2002). Likewise, the study of the UV-screening role of the lichen compounds may constitute an important contribution in the exobiology of planetary environments occupying the HZ exposed to intense UV radiation.

## 2. EXPERIMENTAL SECTION

### 2.1. Study Area

The study area was located at the Venezuelan Andean glacier and snow zones, forming part of the *Sierra Nevada de Mérida* National Park ( $8^{\circ}32.5'N$ ,  $71^{\circ}035'W$ ), and comprises the Pico Espejo ( $\geq 4765$  m, periglacier desert) and Pico Bolívar ( $\sim 5000$  m, glacier desert) sectors (Monasterio and Reyes, 1980; Diaz *et al.*, 1997). Both glacier and snow zones show mean annual temperatures  $\leq 2^{\circ}C$ , wide daily surface thermal oscillations ( $\geq 20^{\circ}C$ ), daily cycles of freezing and thawing, intense UVB, UVA and PAR (400-700 nm) radiation, and low O<sub>2</sub> (120 ~ mbars), N<sub>2</sub> (410 ~ mbars) and CO<sub>2</sub> ( $\sim 16 \times 10^{-2}$  mbars) partial pressures. Mean values of atmospheric pressure in the glacier and snow zones were near 50% sea level ( $\sim 561$  mbar; sea level, 1014 mbar) (Marcano *et al.*, 2003). An increment of the mean soil temperature ( $> 3^{\circ}C$ ) with the increment of the depth (10, 20 and 40 cm) may allow the microbial activity concerning to the nitrogen fixation (Azócar and Monasterio, 1980; Diaz *et al.*, 1997; Marcano *et al.*, 2003). Because of the extreme climatic conditions occurring in the glacier and snow zones, the dominant species were some grasses having anthocyanin pigments (*Agrostis*, *Calamagrostis*), mosses, epilithic and endolithic microlichens, cyanobacteria (*Oscillatoria*, *Nostoc*), chromobacteria, and diazotroph and heterotrophic soil microorganisms (Marcano and Morales, 1994a, 1995; Marcano *et al.*, 1996, 1997).

High UV and PAR radiation and low temperatures in the glacier and snow zones determine the existence of lichens having specialized adaptations in order to avoid an enzymatic inactivation and possible damages in membranes and biomolecules (Jagger, 1985; Mancinelli and White, 2000; Rothschild and Mancinelli, 2002). Although such adaptations are not well known in the glacier and snow zones, it is expected that microorganisms exhibit the following features:

1. Production of UV-screening secondary metabolites such as polyketides, xanthones, anthraquinones and usnic acids (Quesada and Vincent, 1997; Garcia-Pichel, 1998; Wynn-Williams *et al.*, 1999, 2002);

2. Capacity to colonize cracks in rock formations as permanent habitat and subsoil in order to resist freezing (Friedmann, 1982);
3. Synthesis of antifreeze substances such as proteins, sugars and phenolic acids (Kappen, 1973; Morita, 1975; Rothschild and Mancinelli, 2001);
4. Production of higher amounts of carotenoids in comparison to the amounts of chlorophyll (*chl a*) in photobionts in order to compensate the oxidizing effects of UV radiation (Cockell and Knowland, 1999; George *et al.*, 2001).

## 2.2. Climatic Measurements

Climatic data were obtained from several climatic stations placed among the Pico Espejo and Pico Bolívar sectors. These climatic stations belong to the Bioclimatic Scientific Program of the Sierra Nevada de Mérida National Park, which is supported by the University of the Andes, NASA Ames Research Center, USA, and Institute of Nuclear Sciences of the UNAM, México. Thermal sensors (mod. HOBO H8 4-channel logger, Onset Computer Corporation) provided with 4 thermocouples (TMC6-HA) were placed beneath the soil surface at 10, 20 and 40 cm. One thermocouple was placed on the soil surface. Humidity and precipitation data were registered at 2 m above the surface utilizing HOBO loggers. The error in the temperature measurement is  $\pm 0.5^{\circ}\text{C}$  whereas in the relative humidity measurement the error is  $\pm 3\%$ . Recorded data were retrieved by a field computer using BOXCAR 3.6. The stations were emplaced on 15 March 2001 and they are operating continuously. The complete dataset as well as climate data from other years are available at the website: <http://www.ing.ula.ve/~cme/red>. UVB and UVA radiation records were obtained utilizing UV sensors Thies (data loggers). On the other hand, values about the altitudinal distribution of the UVB and UVA radiation at the Andean tropical high mountain were also modeled for average conditions of total ozone  $O_3$  ( $D = 260$  ( $7^{\circ}$  N)), solar zenith angle  $\theta = 30^{\circ}$ , and cloudiness ( $F = 0.6$ ), according to Feister (1994), Piazena (1996) and Dvorkin and Steinberger (1999).

## 2.3. Statistical Analyses

Plot analysis of the climatic and chemical data was carried out using MATLAB 5.3. Other statistical analyses were conducted using Graphpad Instat 2.4a and SPSS 7.5.

## 2.4. Chemical Analysis of Pigments

Separation of lichen compounds was carried out utilizing HPTLC or nano-TLC standardized methods (Culberson, 1972; Culberson and Johnson, 1976; Culberson *et al.*, 1981; White and James, 1985; Arup *et al.*, 1993). In a first HPTLC analysis, acetone extracts of the lichen thalli were separated on silica gel Merck 60 F<sub>254</sub> (10 x 10 cm) plates which had been cleaned prior to use with repetitive solvent elutions and were activated at 120°C for 2 hours. After application of the extract and elution standards, the HPTLC plates were developed with a mixture of toluene/dioxane/acetic acid (180:45:5), and toluene/acetic acid

(170:30). The dried plates were sprayed with  $\text{H}_2\text{SO}_4$  10 % v/v and then exposed to UV ( $\lambda$  354 nm) light to display the bands. Rf values were analyzed using blanks and the Wintabolites 3.2 software (Mietzsch *et al.*, 1994). On the other hand, a second HPTLC analysis was carried out in plates not sprayed with  $\text{H}_2\text{SO}_4$ . This analysis was made by running large samples as bands that were detected with the help of a short wave UV-lamp, cut from the chromatogram, scraped off, eluted with methanol, and analyzed by UV spectrophotometry at 322 and 212 nm against blanks. Lichen compounds utilized as blanks were characterized previously by Fourier transform infrared (FTIR), mass (MS), and nuclear magnetic resonance (RMN) spectroscopy (Morales and Marcano, 1992; Marcano and Morales 1994b; Marcano *et al.*, 1999).

Additionally, a collection of spectra at the 200-400 nm region corresponding to lichen methanolic and ethanol extracts were obtained in order to infer the absorbance capacity in the UV-spectrum region of the lichen compounds. Likewise, molar extinction coefficients ( $\varepsilon$ ) of the extracted and separated lichen compounds were determined for each wavelength of the full UV spectrum. Ultraviolet spectra of the lichen compounds were obtained utilizing a Shimadzu spectrophotometer.

## 2.5. Microscopical Analysis

The cell morphology was evaluated by fluorescence microscopy (FM). Particularly, this technique allowed the location at the lichen tissues (e.g. epicortex, cortex or medulla) of the synthesized metabolites due to the color of the fluorescence response emitted by such substances (Kauppi and Verseghy-Patay, 1990). Specimens were examined in a Zeiss fluorescence microscope.

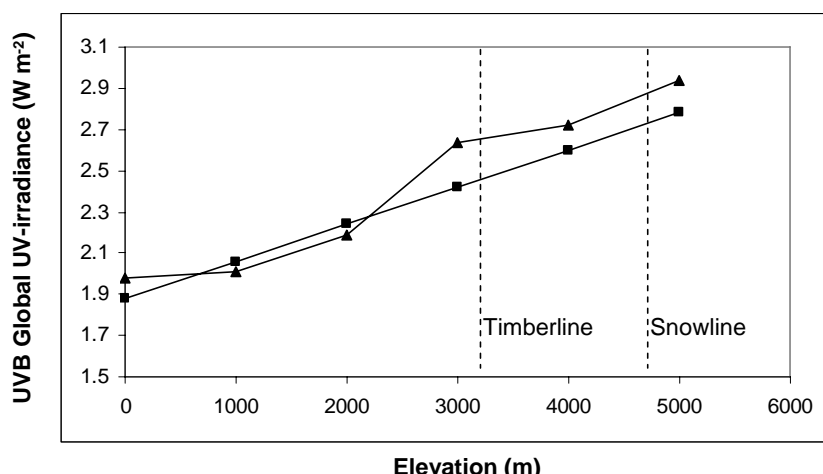


Figure 1. Altitudinal distribution of effective UVB (280-320 nm) irradiance reaching the ground from the Sierra Nevada de Mérida, Venezuelan Andes. A. Mean values obtained *in situ* using UV sensors (▲). B. Modeled for average conditions of total ozone  $\text{O}_3$  (D) = 260 ( $7^\circ \text{ N}$ ), solar zenith angle  $\theta = 30^\circ$ , and cloudiness (■), according to Feister (1994), Piazzena (1996) and Dvorkin and Steinberger (1999).

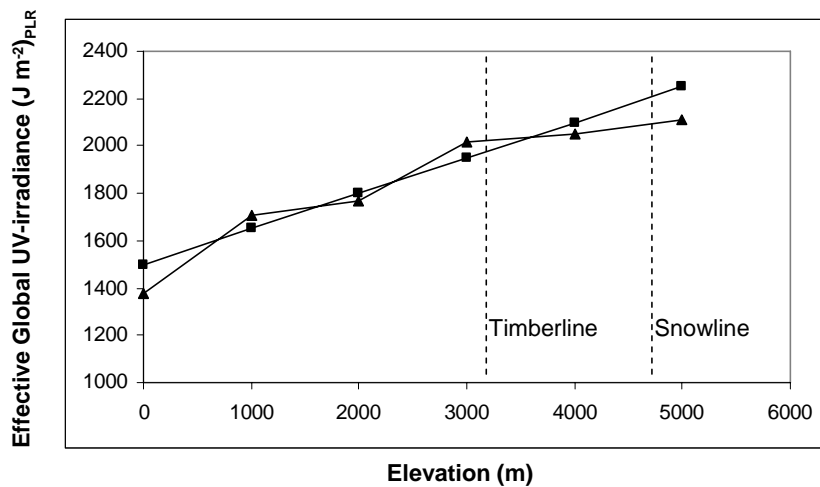


Figure 2. Altitudinal distribution of effective global UV-irradiance producing responses in plants from the Sierra Nevada de Mérida, Venezuelan Andes. A. Mean values obtained *in situ* using UV sensors (▲). B. Modeled for average conditions of total ozone  $O_3$  (D) = 260 ( $7^\circ N$ ), solar zenith angle  $\theta = 30^\circ$ , and cloudiness (■), according to Feister (1994), Piazena (1996) and Dvorkin and Steinberger (1999).

### 3. RESULTS

Altitudinal distribution of effective UVB radiation ( $W\ m^{-2}$ ) at the Andean tropical high mountain revealed an increase estimated at  $\sim 18\ mW\ m^{-2}$  per 100 m, corresponding to  $\sim 3\ W\ m^{-2}$  in the region placed in the glacier and snow zones (Figure 1). On the other hand, the altitudinal distribution of the UV effective global irradiance ( $J\ m^{-2}$ )<sub>plr</sub> producing responses in plants from the Andean tropical high mountain showed an increment of  $\sim 150\ J\ m^{-2}$  per 100 m and a value of  $\sim 2.25\ kJ\ m^{-2}$  for the region placed in the glacier and snow zones (Figure 2).

**Table I.** Lichen species collected in the glacier and snow zones of the Sierra Nevada de Mérida National Park, Pico Bolívar and Pico Espejo sectors (4800–5000 m), Venezuelan Andes.

Alectoria ochroleuca	Physcia sp.
Arthrorhapis citrinella	Protoblastenia sp.
Candellariella vitellina	Rhizocarpon geographicum
Candellariella sp.	Siphula fastigiata
Cladonia coccifera	Stereocaulon strictum
Dictyonema zahlbrucknerii	Tephromela aglaea
Hypotrachyna sp.	Tephromela atra
Lecanora sp.	Umbilicaria polyphylla
Lecidea sp.	Umbilicaria polyyrhiza
Lecidella sp.	Verrucaria sp.
Leprocaulon congestum	Xanthoparmelia conspersa
Peltigera sp.	Xanthoria elegans
Pertusaria pertusa	

**Table II. Lichen species vulnerable potentially\* to damage effects of UV radiation from the glacier and snow zones of the Sierra Nevada de Mérida National Park, Pico Bolívar and Pico Espejo sectors (4800-5000 m), Venezuelan Andes**

Lichen Species	Ultraviolet radiation		
	UVC	UVB	UVA
<i>Candellariella</i> sp.	++		
<i>Lecanora</i> sp.	+++	+	
<i>Leprocaulon congestum</i>	+		
<i>Physcia</i> sp.	++		
<i>Umbilicaria polyphylla</i>	+		
<i>Umbilicaria polyyrrhiza</i>	+		
<i>Verrucaria</i> sp	+++		
<i>Xanthoparmelia conspersa</i>	+		
Number of species	8(32%)	1(4%)	0(0%)

\* Qualitative estimation of the vulnerability to the damage effects of UV radiation based on molar extinction coefficients and absorbance values at the UV spectrum region for total extracts of lichen compounds.

A total of 25 lichen species were registered in the glacier and nival zones (Table I). The more abundant and frequent species were *Candelariella vitellina*, *Rhizocarpon geographicum*, *Stereocaulon strictum*, *Tephromela atra*, *Umbilicaria polyyrrhiza*, *U. polyphylla*, *Xanthoparmelia conspersa* and *Xanthoria elegans*. Particularly, *Xanthoria elegans* has been reported previously in the Antarctic revealing the presence of the anthraquinone parietin as an UV-screening compound (Solhaug and Gauslaa, 1996; Wynn-Williams and Edwards, 2000; Wynn-Williams *et al.*, 1999, 2002; Edwards, 2004). Likewise, *Rhizocarpon geographicum* having rhizocarpic (product from the shikimic acid pathway) and barbatic acids ( $\beta$ -orcinol para-depside), and *Tephromela atra* containing atranorin ( $\beta$ -orcinol para-depside) have been reported for the Antarctic continent (Olech, 2001; Østestedal and Lewis-Smith, 2001). However, several lichen genera and species occurring in the Andean glacier and nival zones are also known from the Antarctic (Friedmann, 1982; Kappen, 1993; Wynn-Williams *et al.*, 1999; Østestedal and Lewis-Smith, 2001). This continent exhibits large ozone changes during the year and thereby increases at UVB irradiance (Madronich *et al.*, 1996). Spectrophotometric analysis of the total extracts revealed that 32% of the species found in the glacier and snow zones showed vulnerability to biochemical damages produced by UVC radiation, 4% were vulnerable to such damages at the UVB region, and no species showed evidences of vulnerability at the UVA region (Table II). On the other hand, 68% of the species showed a potential resistance to effect of biochemical damages of UVC radiation, 96% to UVB and 100% to UVA radiation damage effects (Table III).

Particularly, analyses of the absorption spectra corresponding to total extracts revealed that *Lecanora* sp. shows a total vulnerability to the damage effects of UVC radiation, indicated by the low absorbance in the 220 and 280 nm wavelengths. Likewise, *Candellariella* sp., *Umbilicaria polyphylla* and *U. polyyrrhiza* showed a remarkable vulnerability at the UVC region (Figure 3). On the other hand, *Hypotrachyna* sp., *Candelariella vitellina* and *Dictyonema zahlbrucknerii* exhibited the higher potential resistance to the damage effects of the UVB and UVA radiation (Figure 4). *Pertusaria pertusa*, *Rhizocarpon geographicum*,

*Stereocaulon strictum* and *Tephromela atra* showed also a high absorbance at the UVB and UVA spectrum range. In *D. zahlbrucknerii* were not detected lichen compounds but due to the occurrence of cyanobacterial symbionts it is thought that their high absorbance at the UVC region could be a consequence of the presence of cyanobacterial pigments such as scytonemin and mycosporine-like amino acid derivatives (Garcia-Pichel and Castenholz, 1991; Budel *et al.*, 1997; Wynn-Williams *et al.*, 1999). Analysis by fluorescence microscopy and HPTLC revealed the frequent occurrence of  $\beta$ -orcinol depsidones and orcinol and  $\beta$ -orcinol depsides at the medullar tissue of lichen whereas than dibenzofurane derivatives and atranorin ( $\beta$ -orcinol *para*-depside) were located at the cortical tissue.

**Tabla III. Lichen species resistant potentially\* to damage effects of UV radiation from the glacier and snow zones of the Sierra Nevada de Mérida National Park, Pico Bolívar and Pico Espejo sectors (4800-5000 m), Venezuelan Andes**

Lichen	Ultraviolet radiation		
Species			
	UVC	UVB	UVA
<i>Alectoria ochroleuca</i>	**	***	***
<i>Arthrorhapis citrinella</i>	*	***	***
<i>Candellariella</i> sp.	***	**	
<i>Candellariella vitellina</i>	***	***	***
<i>Cladonia coccifera</i>	*	***	***
<i>Dictyonema zahlbrucknerii</i>	***	***	***
<i>Hypotrachyna</i> sp.	***	***	***
<i>Lecanora</i> sp.	**		
<i>Lecidea</i> sp.	*	**	***
<i>Lecidella</i> sp.	***	***	***
<i>Leprocaulon congestum</i>	***	***	
<i>Peltigera</i> sp.	***	***	***
<i>Pertusaria pertusa</i>	*	***	***
<i>Physcia</i> sp.	***	**	
<i>Protoblastenia</i> sp.	*	***	*
<i>Rhizocarpon geographicum</i>	*	***	***
<i>Siphula fastigiata</i>	**	***	***
<i>Stereocaulon strictum</i>	***	***	***
<i>Tephromela aglaea</i>	***	***	***
<i>Tephromela atra</i>	**	***	**
<i>Umbillicaria polyphylla</i>	**	***	
<i>Umbillicaria polyyrrhiza</i>	**	**	
<i>Verrucaria</i> sp.	***	***	
<i>Xanthoparmelia conspersa</i>	***	***	
<i>Xanthoria elegans</i>	***	***	***
Number of species	17(68%)	24(96%)	25(100%)

\* Qualitative estimation of the vulnerability to the damage effects of UV radiation based on molar extinction coefficients and absorbance values at the UV spectrum region for total extracts of lichen compounds.

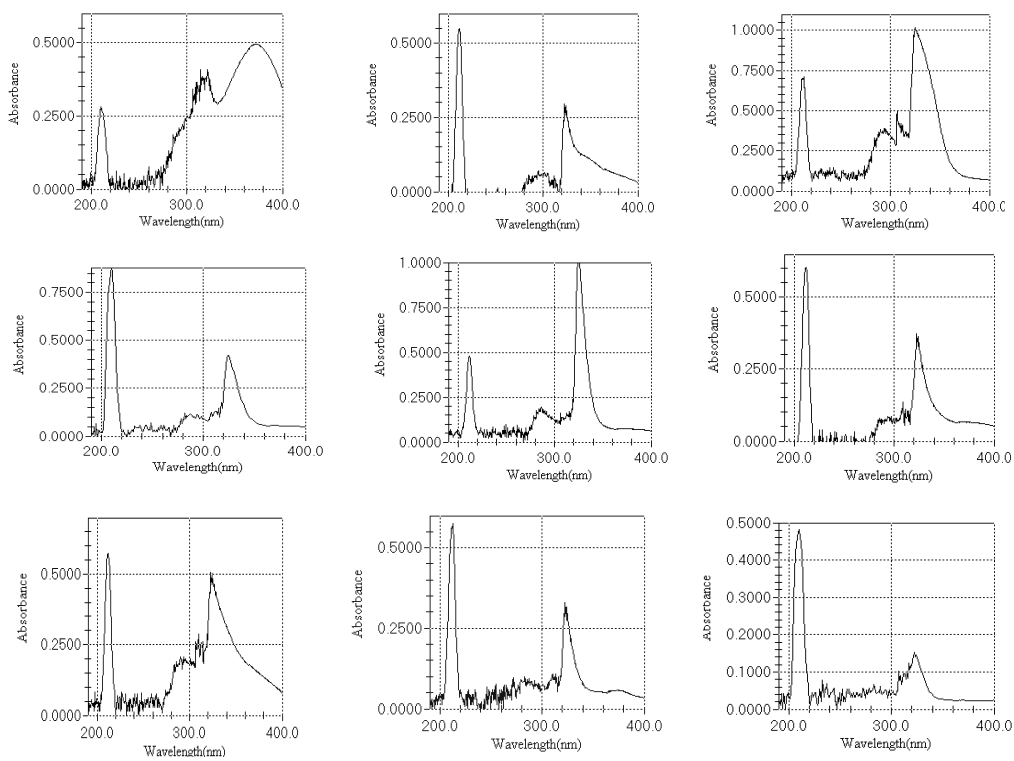


Figure 3. Absorption spectra of total extracts corresponding to vulnerable potentially lichens to UVC and UVB radiation from the glacier and snow zones of the Sierra Nevada de Mérida National Park, Venezuelan Andes. I, *Candelariella* sp.; II, *Lecanora* sp.; III, *Leprocaulon congestum*; IV, *Physcia* sp.; V, *Umbilicaria polyphylla*; VI, *Verrucaria* sp.; VII, *Xanthoparmelia conspersa*; VIII, *Umbilicaria polyrrhiza*, and IX, *Protoblastenia* sp.

Analyses of the lichen compounds separated by HPTLC utilizing blanks identified by FTIR, MS and NMR spectrometry revealed the presence of 11 major compounds. Comparisons of the molar extinction coefficients ( $\epsilon$ ) of lichen compounds showed that the  $\beta$ -orcinol depsidones have the higher absorbance at the UVC region whereas that the orcinol and  $\beta$ -orcinol depsides (*para*- or *meta*-) exhibited the lower absorbance (Figure 5). At the UVB region the depsides exhibited the higher absorbance (Figure 6) whereas at the UVA region thamnolic acid ( $\beta$ -orcinol *meta*-depside) and usnic acid (dibenzofuran derivative) showed the higher absorbance in comparison to the depsidones and other depsides that exhibited the lower absorbance (Figure 7). At the biochemical importance wavelengths (220, 260 and 280 nm), usnic, didimic (dibenzofuran derivatives), sequicaic (orcinol *meta*-depside), thamnolic ( $\beta$ -orcinol *meta*-depside), and lecanoric acids (orcinol *para*-depside) showed the lower  $\epsilon$  values whereas salazinic, protocetraric, and stictic acids ( $\beta$ -orcinol depsidones) exhibited the higher  $\epsilon$  values at the 220 and 260 nm wavelengths, and barbatic acid ( $\beta$ -orcinol *para*-depside) at 280 nm (Table IV). At the full UV spectrum, the lichen compounds showed the higher absorbance only at the 211, 306 and 324 nm (Table V).

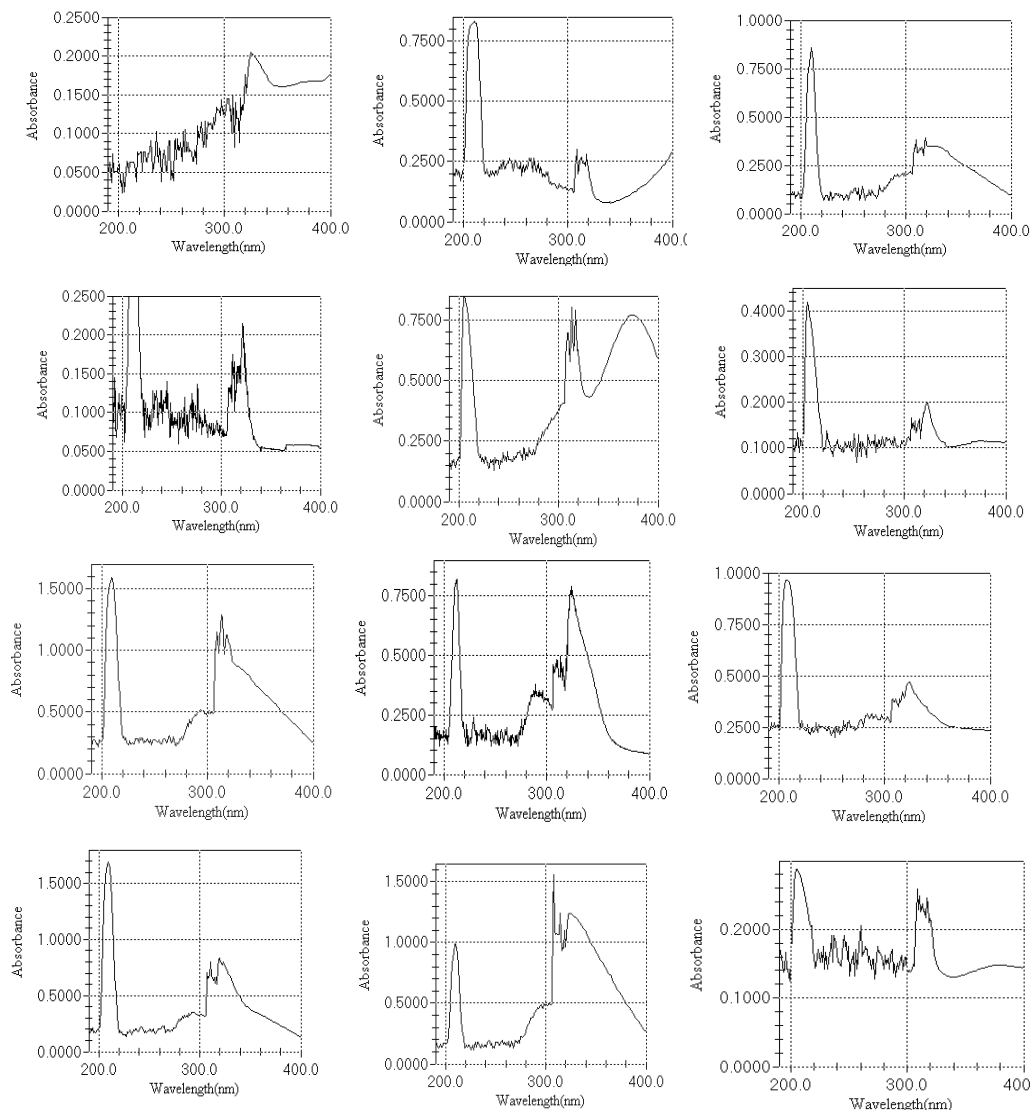


Figure 4. Absorption spectra of total extracts corresponding to resistant potentially lichens to UVC, UVB and UVA radiation from Pico Espejo and Pico Bolívar, Venezuelan Andes. I, *Hypotrachyna* sp.; II, *Xanthoria elegans*; III, *Lecidea* sp.; IV, *Lecidella* sp.; V, *Candelariella vitellina*; VI, *Peltigera* sp.; VII, *Siphula fastigiata*; VIII, *Stereocaulon strictum*; IX, *Tephromela atra*; X, *Alectoria ochroleuca*; XI, *Cladonia coccifera*, and XII, *Dictyonema zahlbrucknerii*.

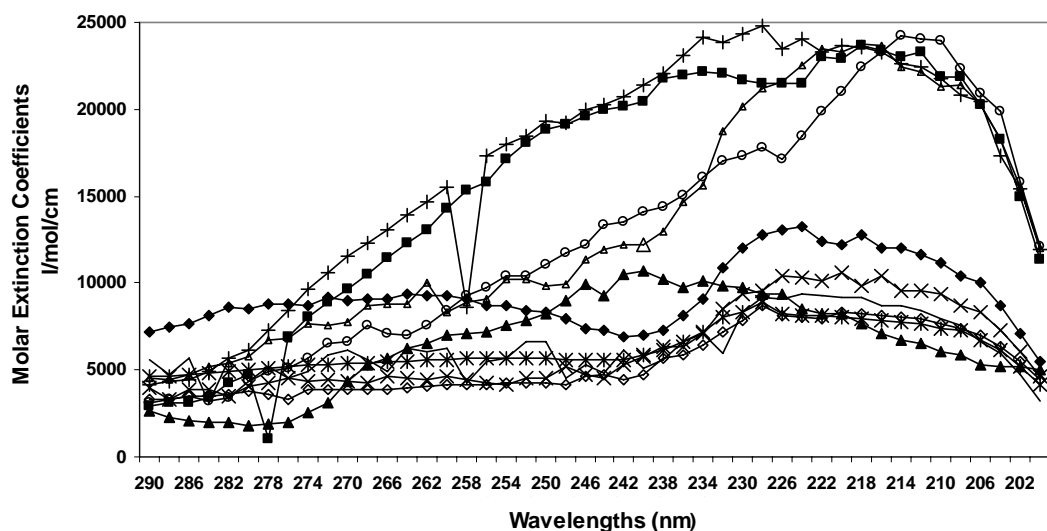


Figure 5. Molar extinction coefficients ( $\epsilon$ ) at the UVC region estimated for secondary metabolites separated of lichen species from the glacier and snow zones of the Sierra Nevada de Mérida, Venezuelan Andes.  $\diamond$  Usnic acid,  $\triangle$  stictic acid, — sequicaic acid, + salazinic acid, ■ protocetraric acid, \* lecanoric acid, ○ fumarprotocetraric acid, ▲ didimic acid, ♦ barbatic acid, and  $\times$  atranorin.

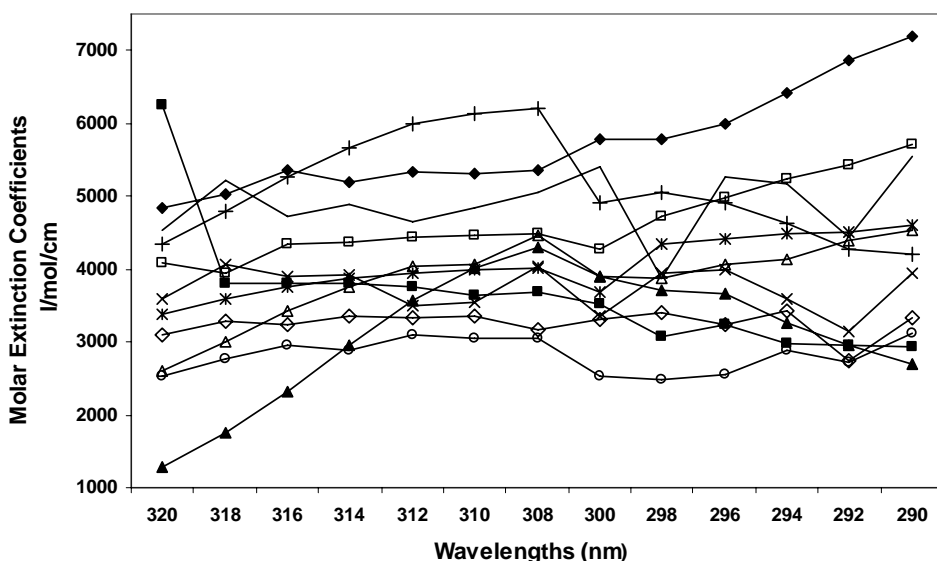


Figure 6. Molar extinction coefficients ( $\epsilon$ ) at the UVB region estimated for secondary metabolites separated of lichen species from the glacier and snow zones of the Sierra Nevada de Mérida, Venezuelan Andes.  $\diamond$  Usnic acid,  $\square$  thamnolic acid,  $\triangle$  stictic acid, — sequicaic acid, + salazinic acid, ■ protocetraric acid, \* lecanoric acid, ○ fumarprotocetraric acid, ▲ didimic acid, ♦ barbatic acid, and  $\times$  atranorin.

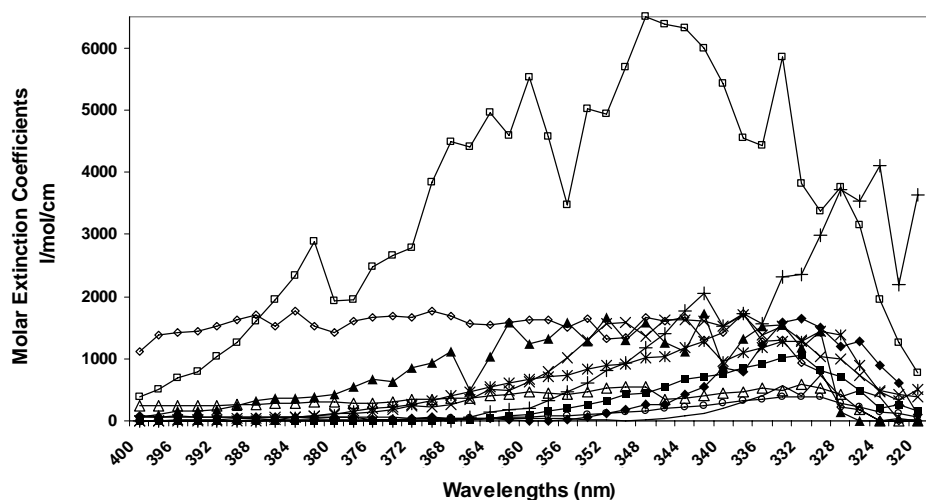


Figure 7. Molar extinction coefficients ( $\epsilon$ ) at the UVA region estimated for secondary metabolites separated of lichen species from the glacier and snow zones of the Sierra Nevada de Mérida, Venezuelan Andes.  $\diamond$  Usnic acid,  $\square$  thamnolic acid,  $\triangle$  stictic acid, – sequicaic acid, + salazinic acid, ■ protocetraric acid, \* lecanoric acid,  $\circ$  fumarprotocetraric acid,  $\blacktriangle$  didimic acid,  $\blacklozenge$  barbatic acid, and  $\times$  atranorin.

**Table IV. Molar extinction coefficients ( $\epsilon$ )\* of lichen substances (depsides, depsidones and dibenzofuran derivatives) occurring in lichens from the glacier and snow zones of Pico Espejo and Pico Bolívar, Venezuelan Andes, for biochemical importance wavelengths**

Lichen compounds	$\epsilon$ 220	$\epsilon$ 260	$\epsilon$ 280		
<b>Depsides</b>					
Atranorin	10569.6	4624.6	4032.7		
Barbatic acid	12252.7	9271.3	8512.8		
Lecanoric acid		8026.3	5625.7	5026.1	
Sequicaic acid		9203.8	6267.1	4356.1	
Thamnolic acid	8746.5	6696.4	5998.1		
<b>Depsidones</b>					
Fumarprotocetraric acid	20986.2	8382.7	4354.1		
Protocetraric acid	22935.3	14299.7	4758.9		
Salazinic acid		23659.4	15549.1	6133.6	
Stictic acid	23326.1	8332.1	5816.3		
<b>Dibenzofuran derivatives</b>					
Didimic acid	8254.4	7009.9	1776.0		
Usnic acid	8300.3	4140.3	3744.7 * 1 mol-1 cm-1		

**Table V. Maximum absorbance peaks at the UV spectrum region corresponding to secondary metabolites (depsides, depsidones and dibenzofuran derivatives) occurring in lichens from the glacier and snow zones of Pico Espejo and Pico Bolívar, Sierra Nevada de Mérida National Park, Venezuelan Andes**

Lichen compounds	UV λ max	UVC λ max (200-280 nm)	UVB λ max (290-315 nm)	UVA λ max (320-415 nm)	
<b>Depsides</b>					
	Atranorin	324.5	212	308	324.5
	Barbatic acid	325.5	212	296	325.5
	Lecanoric acid	325	210	308	325
	Sequicaic acid	322.5	212	307.6	322.5
	Thamnolic acid	324.5	211	306.6	324.5
<b>Depsidones</b>					
	Fumarprotocetraric acid	324.5	212.5	300	324.5
	Protocetraric acid	212	212	307.5	322.5
	Salazinic acid	211.5	211.5	315	324.5
	Stictic acid	211.5	211.5	307	322.5
<b>Dibenzofuran derivatives</b>					
	Didimic acid	324.5	280	309.3	324.5
	Usnic acid	321	212	312	321

#### 4. DISCUSSION

Both effective UVB irradiance and effective global UV irradiance producing responses in plants revealed values ~ 1.6 times higher in the glacier and snow zones in comparison to that registered at the sea level (Figures 1 and 2). This intensity would be sufficient to produce important biochemical and cell alterations (Jagger, 1985; Feister, 1994). Because the Sierra Nevada de Mérida is located at the tropical region ( $8^{\circ}32' N$ ), it is expected that the effective UV irradiance reaching the ground would be two and four times higher during all the year than at latitudes from subtropical regions (Caldwell *et al.*, 1980; Feister, 1994). UVB fluxes reaching the ground in the glacier and snow zones (Figure 1) were similar to those UVB fluxes reaching the ground estimated for planets with low O<sub>2</sub> levels orbiting around G, F and K stars, according to Segura *et al.* (2003), viz. G2V,  $\sim 10^{-2}$  PAL; F2V,  $\sim 10^{-2}$  PAL, and K2V,  $\sim 10^{-3}$  PAL. Likewise, UVB fluxes of  $\sim 3$  W m<sup>-2</sup> are thought occurred in Mid-Proterozoic atmosphere containing  $\sim 10^{-2}$  PAL of O<sub>2</sub> (Segura *et al.*, 2003), and in the early Mars atmosphere (Cockell, 2000a).

On the Earth's surface, unless 4% of the UVB and 96% of the UVA radiation would penetrate. Although DNA absorption spectrum shows major absorbance as located at 260 nm, an important absorption is also observed at the UVB region. UVB irradiance at the Andean high mountain could be sufficient to generate damages in the lipoproteins of cell membranes and organelles and deleterious mutations in DNA, viz. thymine dimers (Jagger, 1985; Cockell and Knowland, 1999) if organisms have not efficient UV-screening strategies. Amino acids as

tryptophan, tyrosine and cystine have also an important absorbance at the UVC and UVB regions (Jagger, 1985). Thus, proteins constituted by aromatic residues or having disulphur bonds could be susceptible to structural and functional changes when are exposed to intense UV radiation in tropical mountain environments above 4000 m (Caldwell *et al.*, 1980).

However, lichen species exposed to high UV irradiance at tropical high mountain have UV-screening strategies based on the synthesis of phenolic secondary metabolites generated probably during millions years of evolution. According to Cockell (1998) and Cockell and Knowland (1999), all the studied lichen-substance groups would have showed absorption maxima at the UV region depending upon the presence of conjugates structures having  $\pi$ -electron systems and causing energetic transitions of  $\pi$ -electrons to anti-bonding  $\pi^*$ -electron orbitals when are exposed to UV radiation. The remarkable capacity of absorbance at the UVB and UVA regions that have the lichen compounds from the Andean glacier and snow zones and further the high frequency of occurrence of these substances in the studied lichens (96%), suggest an adequate adaptation to such environment. On the other hand, the fact that only 68% of the species are resistant to the UVC radiation would be expected, because the penetration of this radiation is avoid by the ozone shield before reaching the ground. This effective UV-screening capacity that show the lichen compounds would explain the UV-resistance exhibited by lichens in extreme conditions of outer space or even in simulated Martian surface conditions including vacuum-UV to UVA ranges and up to doses of about 160 kJ m<sup>-2</sup> (De Vera *et al.*, 2003).

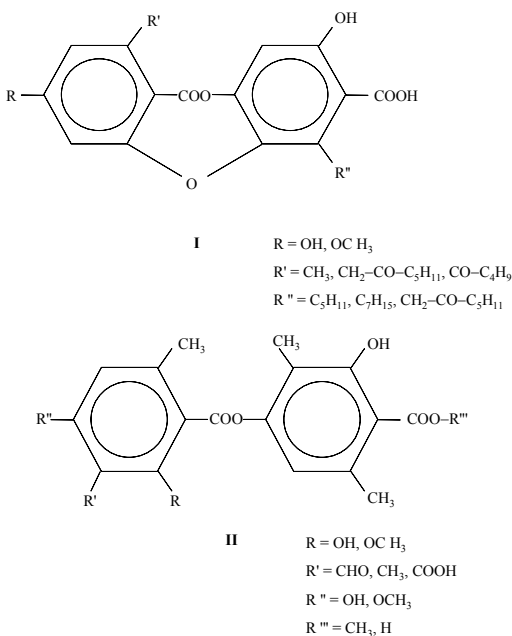


Figure 8. Phenolic structure assigned to the UV-screening pigments present in lichens from the Sierra Nevada de Mérida National Park, Pico Espejo and Pico Bolívar sectors, Venezuelan Andes. I. Depsidones. II. Depsides.

Molar extinction coefficients ( $\epsilon$ ) of the analyzed compounds revealed that the  $\beta$ -orcinol depsidones have the higher absorbance at the UVC region whereas that the orcinol and  $\beta$ -

orcinol depsides and dibenzofurane derivatives showed the lower absorbance in that UV spectrum region (Figures 5-7). Depsidones are constituted by two acetate-polymalonate-derived phenolic acid units linked by an ester bond among the 4' and 1 positions of both phenolic units and by an ether bond among the 2 and 5' positions generally, whereas that the depsides have only the same ester bond among the 4' and 1 positions of both phenolic units (Culberson, 1969) (Figure 8). Both depsides and depsidones are considered products of orsellinic acid-type cyclization unique to lichens (Marcano, 1994; Huneck and Yoshimura, 1996). On the other hand, dibenzofurane derivatives are constituted by two such acetate-polymalonate-derived phenolic acid units linked by an ether bond and a carbon-carbon bond and are considered products either of orsellinic acid-type cyclization (didimic acid) or phloroglucinol-type cyclization (usnic acid). These compounds are unknown in non-lichen-forming fungi and appear to be extremely rare in all living systems (Culberson, 1969).

According to Sala and Sargent (1981) and Rogers (1989), there strong evidence that  $\beta$ -orcinol depsidones were derived not from *para*-depsides by oxidation, but by acylation of one orsellinic acid with another, followed by intramolecular rearrangements. Thus, this substance group could be considered so old or older than depsides. The presence of ether bond in esterified compounds as  $\beta$ -orcinol depsidones is related to the capacity to absorb significantly UVC radiation. These substances could have been originated  $\sim$  2 billions years ago before to the formation of the ozone shield (Kasting, 1987; Cockell, 2000a). On the other hand, there is evidence about the existence of phenolic carboxylic acid and dibenzofurane derivatives in carbonaceous meteorites (e.g. Murchison) similar to those occurring in lichens (Hayatsu *et al.*, 1980). These substances would be synthesized abiogenically by Fischer-Tropsch-type reactions during the solar nebula formation or by other processes (Pizzarello, 2004). However, both observations could suggest the huge old of these compounds and the possibility about the occurrence of life shapes based on similar UV-screening strategies in planetary environments having  $pO_2 \leq 10^{-2}$  PAL and occupying habitable zones around high-UV, G, F, K or T-Tauri and  $\beta$  Pictoris Vega-like stars (Canuto *et al.*, 1982, 1983; Kasting *et al.*, 1997; Koerner, 1997; Cockell, 1999; Segura *et al.*, 2003).

## 5. CONCLUSIONS

In this work, we have attempted to demonstrate that phenolic carboxylic acid derivatives have the capacity to screen out UV radiation and thereby to avoid the lethal effects that such radiation could cause in organisms exposed at high elevations. Among the studied species, 96-100% showed a high absorbance to UVB and UVA radiation whereas 68% showed a high absorbance to UVC radiation. Lichen capacity to synthesize phenolic compounds having electronic transitions  $\pi$  a  $\pi^*$  could be considered a success in colonizing the high-UV, tropical high mountain glacier and snow zones.

Phenolic substances presenting a high resistance to UVA radiation are characterized by ester bonds among both phenolic units (depsides). These substances constitute the more abundant products to find in lichens. Compounds presenting both ester and ether bonds among both phenolic units (depsidones) and absorbing UVC radiation could have been originated probably before Proterozoic and Phanerozoic when the ozone shield was not formed fully. The relative low frequency of depsidones in lichens could suggest a reduced

UV-screening role in nowadays due to the existence of ozone shield. Finally, it is important to point out that the data obtained in this study are from an Earth's region having "very extreme" bioclimatic conditions due to the effects of the latitude on the daily surface thermal oscillations, and to the altitude effects on the O<sub>2</sub>, CO<sub>2</sub> and N<sub>2</sub> partial pressures, and surface temperatures. Therefore, the exobiological importance of the data obtained in this study should not be underestimated.

## ACKNOWLEDGMENTS

The authors wish to thank Cable Railway System of Mérida for their assistance to access Pico Espejo Station during several years. This work was supported by a Grant-in-Aid from CDCHT (M-790-04) of the University of the Andes, NASA Ames Research Center, USA, and Institute of Nuclear Sciences of the UNAM, México.

## REFERENCES

- Arup, U., Ekman, S., Lindblom, L. & Mattson, J. E. (1993). High performance thin layer chromatography, HPTLC, an advanced method for screening lichen substances. *Lichenologist*, 25, 61-71.
- Azócar, A. & Monasterio, M. (1980). Caracterización ecológica del clima en el páramo de Mucubají. In: M., Monasterio (Eds.), *Estudios Ecológicos en los Páramos Andinos*, Ediciones de la Universidad de Los Andes, Mérida, 207-223.
- Bacherau, F. & Asta, J. (1997). Effects of solar ultraviolet radiation at high altitude on the physiology and the biochemistry of a terricolous lichen (*Cetraria islandica* L.). *Symbiosis*, 23, 197-217.
- Bjerke, J. W., Lerfall, K. & Elvebakk, A. (2002). Effects of ultraviolet radiation and PAR on the content of usnic and divaricatic acids in two arctic-alpine lichens. *Photochem. Photobiol. Sci.*, 1(9), 678-685.
- Blumthaler, M. & Ambach, W. (1990). Indication of increasing solar Ultraviolet-B radiation flux in alpine regions. *Science*, 248, 206-208.
- Budel, B., Karsten, U. & Garcia-Pichel, F. (1997). Ultraviolet-absorbing scytonemin and mycosporine-like amino acid derivatives in exposed, rock-inhabiting cyanobacterial lichens. *Oecologia*, 112, 165-172.
- Caldwell, M. M., Robberecht, R. & Billings, W. (1980). A steep latitudinal gradient of solar ultraviolet-B radiation in the arctic-alpine life zone. *Ecology*, 61, 600-611.
- Canuto, V. M., Levine, J. S., Augustsson, T. R. & Imhoff, C. L. (1982). UV radiation from the young sun and oxygen and ozone level in the prebiological palaeoatmosphere. *Nature*, 296, 816-820.
- Canuto, V. M., Levine, J. S., Augustsson, T. R., Imhoff, C. L. & Giampapa, M. S. (1983). The young sun and the atmosphere and photochemistry of the early earth. *Nature*, 305, 281-286.
- Cockell, C. S. (1998). UV radiation, evolution and  $\pi$ -electron system. *Biological Journal of the Linnean Society*, 63, 449-457.

- Cockell, C. S. (1999). Carbon biochemistry and the ultraviolet radiation environment of F, G and K main sequence stars. *Icarus*, 141, 399-407.
- Cockell, C. S. (2000a). The ultraviolet history of the terrestrial planets: Implications for biological evolution. *Planetary and Space Science*, 48, 203-214.
- Cockell, C. S. (2000b). Ultraviolet radiation and the photobiology of Earth's early oceans. *Origins of Life Evol. Biosphere*, 30, 467-499.
- Cockell, C. S. (2002). Photobiology uncertainties in the Archean and post-Archean world. *International Journal of Astrobiology*, 1, 31-38.
- Cockell, C. S. & Horneck, G. (2001). The history of the UV radiation climate of the Earth – theoretical and space-based observations. *Photochem. Photobiol.*, 73, 447-451.
- Cockell, C. S. & Knowland, J. K. (1999). Ultraviolet radiation screening compounds. *Biological Reviews*, 74, 311-345.
- Crittenden, P. D., Kalucka, I. & Oliver, E. (1994). Does nitrogen supply limit the growth of lichens? *Cryptogamic Botany*, 4, 193-155.
- Crutzen, P. J. & Bruhl, C. (1996). Mass extinctions and supernova explosions. *Proceedings of the National Academy of Sciences*, 93, 1582-1584.
- Culberson, C. (1969). *Chemical and Botanical Guide to Lichen Products*. University of North Carolina Pres, Chape Hill, USA.
- Culberson, C. F. (1972). Improved conditions and new data for the identification of lichen products by a standard thin-layer chromatographic method. *Journal of Chromatography*, 72, 113-377.
- Culberson, C. F. & Johnson, A. (1976). A standardized two-dimensional thin-layer chromatographic method for lichen products. *Journal of Chromatography*, 128, 253-259.
- Culberson, C. F., Culberson, W. L. & Johnson, A. (1981). A standardized TLC analysis of β-orcinol depsidones. *Bryologist*, 84, 16-29.
- De Vera, J. P., Horneck, G., Rettberg, P. & Ott, S. (2003). The potential of the lichen symbiosis to cope with extreme conditions of outer space-I. Influence of UV radiation and space vacuum on the vitality of lichen symbiosis and germination capacity. *International Journal of Astrobiology*, 1, 234-242.
- Diaz, A., Péfaur, J. & Durant, P. (1997). *Ecology of South American páramos with emphasis on the fauna of the Venezuelan páramos*. In: F. E. Wielgolaski (ed.), *Polar and Alpine Tundra, Ecosystem of the World*, Elsevier, Amsterdam, 263-310.
- Dvorkin, A. Y. & Steinberger, E. H. (1999). Modeling the altitude effect on solar UV radiation. *Solar Energy*, 65, 181-187.
- Edwards, H. G. M. (2004). Raman spectroscopic protocol for the molecular recognition of key biomarkers in astrobiological recognition. *Origins of Life Evol. Biosphere*, 34, 3-11.
- Feister, U. (1994). Model calculations and measurements of chemically and biologically effective UV radiation reaching the ground. *Ber. Dt. Wetterd.*, 190, 1-79.
- Franck, S., Block, A., von Bloh, W., Bounama, C., Schellnhuber, H. J. & Svirezhev, Y. (2000a). Habitable zone for Earth-like planets in the solar system. *Planetary and Space Science*, 48, 1099-1105.
- Franck, S., von Bloh, A., Bounama, W., Steffen, C., Schönberner, M. & Schellnhuber, D. (2000b). Determination of habitable zones in extrasolar planetary systems: Where are Gaia's sisters. *J. Geophys. Res.*, 105, 1651-1658.
- Ellis, J. & Schramm, D. N. (1995). Could a nearby supernova explosion have caused a mass extinction. *Proceedings of the National Academy of Sciences*, 92, 235-238.

- Friedmann, E. I. (1982). Endolithic microorganisms in the Antarctic cold desert. *Science*, 215, 1045-1053.
- Garcia-Pichel, F. (1998). Solar ultraviolet and the evolutionary history of cyanobacteria. *Origins of Life Evol. Biosphere*, 28, 321-347.
- Garcia-Pichel, F. & Castenholz, R. W. (1991). Occurrence of UV-absorbing, mycosporine-like compounds among cyanobacterial isolates and an estimate of their screening capacity. *Appl. Environ. Microbiol.*, 59, 163-169.
- George, A. L., Murray, A. W. & Montiel, P. (2001). Tolerance of Antarctic cyanobacterial mats to enhanced UV radiation. *FEMS Microbiology Ecology*, 37, 91-101.
- Hallbauer, D. K. & van Warmelo, K. T. (1974). Fossilized plants in thucholite from Precambrian rocks of the Witwatersrand, South Africa. *Precambrian Research*, 1, 199-212.
- Harborne, J. B. (1968). *Biochemistry of phenolic compounds*, Academic Press, New York.
- Hayatsu, R., Winans, R. E., Scott, R., McBeth, R. L., Moore, L. P. & Studier, M. H. (1980). Phenolic ethers in the organic polymer of the Murchison meteorite. *Science*, 207, 1202-1204.
- Hertel, H. (1971). Ueber holarktische Krustenflechten aus den venezuelanischen Anden. *Willdenowia*, 6, 225-272.
- Huneck, S. & Yoshimura, I. (1996). *Identification of lichen substances*. Springer-Verlag, Berlin.
- Jagger, J. (1985). *Solar-UV actions on living cells*. Praeger Scientific, New York.
- Kappen, L. (1973). Response to extreme environments. In: *The Lichens* (V. Ahmadjian and M. E. Hale, Eds.), 311-380. Academic Press, London.
- Kappen, L. (1993). Lichens in the Antarctic region. In: *Antarctic Microbiology* (Friedmann, E. I. Editor), 433-490. Wiley-Liss, New York.
- Kasting, J. F. (1987). Theoretical constraints on oxygen and carbon dioxide concentrations in the Precambrian atmosphere. *Precambrian Research*, 34, 205-229.
- Kasting, J. F. (1997). Habitable zones around low mass stars and the search for extraterrestrial life. *Origins of Life Evol. Biosphere*, 27, 291-307.
- Kasting, J. F., Whittet, D. C. B. & Sheldon, W. R. (1997). Ultraviolet radiation from F and K stars and implications for planetary habitability. *Origins Life Evol. Biosphere*, 27, 413-420.
- Kauppi, M. & Verseghy-Patay, K. (1990). Determination of the distribution of lichen substances in the thallus by fluorescence microscopy. *Annales Botanici Fennici*, 27, 189-202.
- Koerner, D. W. (1997). Analogs of the early solar system. *Origins Life Evol. Biosphere*, 27, 157-184.
- Madronich, S., Weatherhead, E. & Flocke, S. J. (1996). Trends in UV radiation. In: *Special Issue on Stratospheric Ozone Depletion* (Kenneth Bowman and Sayed El-Sayed, Eds.). Intera. J. Environmental Studies, 51, 183-198.
- Mancinelli, R. L. & White, M. R. (2000). Inhibition of denitrification by ultraviolet radiation. *Adv. Space Res.*, 26, 2041-2046.
- Manny, B. A. (1969). The relationship between organic nitrogen and the carotenoid to chlorophyll *a* ratio in five freshwater phytoplankton species. *Limnol. Oceanogr.*, 14, 69-79.

- Marcano, V. (1994). *Introduction to Study of Venezuelan Andean Lichens*, Vol I, Koeltz Scientific Books, Stuttgart, Germany, 1-338.
- Marcano, V. & Morales, A. (1994a). The *Alectoria* Ach. genus (Lichenized Ascomycetes) in the Venezuelan Andes. *Ernstia*, 4, 89-100.
- Marcano, V. & Morales, A. (1994b). New species of *Ramalina* from Venezuela. *Bryologist*, 97, 26-33.
- Marcano, V. & Morales, A. (1995). Revision of *Umbilicaria* genus (Lichenized Ascomycetes) in the Venezuelan Andes. *Ernstia*, 4, 21-35.
- Marcano, V., Morales, A., Sipman, H. & Calderón, L. (1996). A first checklist of the lichen-forming fungi of the Venezuelan Andes. *Tropical Bryology*, 12, 193-235.
- Marcano, V., Galiz, L., Mohali, S., Morales, A. & Palacios, E. (1997). Revision of *Leprocaulon* Nyl. ex Lamy genus (Lichenes Imperfecti) in Venezuela. *Tropical Bryology*, 13, 47-56.
- Marcano, V., Morales, A. & Rodríguez, V. (1999). Occurrence of usnic acid in *Usnea laevis* Nylander (Lichenized Ascomycetes) from the Venezuelan Andes. *Journal of Ethnopharmacology*, 66, 343-346.
- Marcano, V., Benitez, P. & Palacios-Prü, E. (2001). Adaptative response of a fungus species to hydrocarbon environments: Results from experiments in laboratory, in *First Steps in the Origin of Life in the Universe*, J. Chela-Flores, T. Owen, F. Raulin (eds.), Kluwer Academic Publishing, Dordrecht, The Netherlands, 247-250.
- Marcano, V., Benitez, P. & Palacios-Prü, E. (2002a). Growth of a lower eukaryote in non-aromatic hydrocarbon media  $\geq C_{12}$  and its exobiological significance. *Planetary and Space Science*, 50, 693-709.
- Marcano, V., Benitez, P. & Palacios-Prü, E. (2002b). Ecophysiological responses of a *Fusarium* species grown in non-hydrocarbon media  $\geq C_{12}$ . *Rev. Ecol. Latinoamer.*, 8, 25-43.
- Marcano, V., Matheus, P., Balza, A., Durán, F. J., McKay, C. P., Navarro-González, R., Davila, D., Davis, W. & Palacios-Pru, E. (2003). Tropical Andean ecosystems as models for extrasolar and solar planetary habitats. *Origins of Life and Evolution of the Biosphere*, 32, 503-505.
- Marcano, V., Benitez, P. & Palacios-Prü, E. (2006). UV-screening strategies of a lower eukaryote grown in hydrocarbon media. *Origins of Life and Evolution of the Biospheres*, 36, 65-84.
- Mietzsch, E., Lumbsch, T. & Elix, J. (1994). *Wintabolites* (Mactabolites for Windows)-Users Manual, Essen, 1-54.
- Monasterio, M. & Reyes, S. (1980). Diversidad ambiental y variación de la vegetación en los páramos de los Andes Venezolanos. In: M., Monasterio, (Eds.), *Estudios Ecológicos en los Páramos Andinos*, Ediciones de la Universidad de Los Andes, Mérida, 47-91.
- Morales, A. & Marcano, V. (1992). Chemical compounds of *Ramalina* from Western Venezuela. Second *International Lichenological Symposium* IAL 2, Båstad, Sweden, Abstracts, 61-62.
- Morita, R. (1975). Psychrophilic Bacteria. *Bacteriological Reviews*, 39, 144-167.
- Onofri, S., Selbmann, L., Zucconi, L. & Pagano, S. (2003). Antarctic microfungi as models for exobiology. *Planetary and Space Science*, 52, 229-237.

- Piazena, H. (1996). The effect of altitude upon solar UV-B and UV-A irradiance in the tropical Chilean Andes. *Solar Energy*, 57, 133-140.
- Quesada, A., Vincent, W. F. (1997). Strategies of adaptation by Antarctic cyanobacteria to ultraviolet radiation. *Eur. J. Phycology*, 32, 335-342.
- Pizzarello, S. (2004). Chemical evolution and meteorites: an update. *Origins of Life and Evolution of the Biosphere*, 34, 25-34.
- Olech, M. (2001). *Annotated checklist of Antarctic lichens and lichenicolous fungi*. The Institute of Botany of the Jagiellonian University, Kraków, 145.
- Østestedal, D. O. & Lewis-Smith, R. I. (2001). *Lichens of Antarctica and South Georgia. A guide to their identification and ecology*. Cambridge University Press, 411.
- Rogers, R. W. (1989). Chemical variation and the species concept in lichenized ascomycetes. *Botanical Journal of the Linnean Society*, 101, 229-339.
- Rothschild, L. J. & Mancinelli, R. L. (2002). Life in extreme environments. *Nature*, 409, 1092-1101.
- Rundel, P. W. (1978). The ecological role of secondary lichen substances. *Biochemical Systematic and Ecology*, 6, 157-170.
- Rundel, P. W. (1994). Tropical alpine environments. In: P. W., Rundel, A. P., Smith, F. C., Meinzer (Eds.), *Tropical Alpine Environments: Plant form and function*, Cambridge University Press, Cambridge, 21-44.
- Sala, T., Sargent, M. V. (1981). Depsidone synthesis. Part 16. Benzophenone-ris-3<sup>1</sup>, 5<sup>1</sup>-diene-2<sup>1</sup>, 3<sup>1</sup>-dione-Depsidone interconversion: a new theory of Depsidone biosynthesis. *Journal of the Chemical Society, Perkin Transactions*, 1, 855-869.
- Segura, A., Krelove, K., Kasting, J. F., Sommerlatt, D., Meadows, V., Crisp, D., Cohen, M. & Mlawer, E. (2003). Ozone concentrations and ultraviolet fluxes on Earth-like planets around other stars. *Astrobiology*, 3, 689-708.
- Solhaug, K. A. & Gauslaa, Y. (1996). Parietin, a photoprotective secondary product of the lichen *Xanthoria parietina*. *Oecologia*, 108, 412-418.
- Taylor, T. N., Hass, H., Remy, W. & Kerp, H. (1995). The oldest fossil lichen. *Nature*, 378, 244.
- Towers, G. H. N. (1968). Metabolism of phenolics in higher plants and microorganisms. In: J. B., Harborne (Eds.), *Biochemistry of phenolic compounds*, Academic Press, New York, 249-294.
- Vishniac, H. S. (1996). Biodiversity of yeasts and filamentous microfungi in terrestrial Antarctic ecosystems. *Biodivers. Conserv.*, 5, 1365-1378.
- White, F. J. & James, P. W. (1985). A new guide to microchemical techniques for the identification of lichen substances. *British Lichen Society*, 57, (Suppl.), 1-41.
- Wynn-Williams, D. D., Edwards, H. G. M. & Garcia-Pichel, F. (1999). Functional biomolecules of Antarctic stromatolitic and endolithic cyanobacterial communities. *Eur. J. Phycol.*, 34, 381-391.
- Wynn-Williams, D. D. & Edwards, H. G. M. (2000). Antarctic ecosystems as models for extraterrestrial surface habitats. *Planetary and Space Science*, 48, 1965-1075.
- Wynn-Williams, D. D., Edwards, H. G. M., Newton, E. M. & Holden, J. M. (2002). Pigmentation as a survival strategy for ancient and modern photosynthetic microbes under high ultraviolet stress on planetary surfaces. *International Journal of Astrobiology*, 1, 39-49.

## ***Chapter 8***

# **DIVERSITY AND EVOLUTION OF ANIMAL RHODOPSIN AND PHOTOTRANSDUCTION CASCADE**

***Akihisa Terakita\****

Department of Biology and Geosciences, Graduate School of Science,  
Osaka City University, Osaka 558-8585, Japan.

## **ABSTRACT**

Many animals sense light signals for visual and non-visual functions. Light is captured by rhodopsin-like photopigments in photoreceptor cells and is transduced to cellular light-response through a G-protein-mediated phototransduction cascade. More than 2000 kinds of rhodopsin-like photopigments have been identified thus far and they are divided into eight subgroups. Accumulated evidence suggests that displacement of counterion, an essential amino acid residue for rhodopsin-like photopigment to absorb visible light, is closely related to the evolution of vertebrate visual pigments. Four kinds of phototransduction cascades have been found thus far, such as those mediated by transducin (Gt type G protein) in vertebrate rod and cone visual cells, by Gq type G protein in insect and molluscan rhabdomeric-type visual cells, by Go type G protein in scallop and lizard ciliary-type visual cells and by Gs type G protein in Jellyfish visual cells. Since photoreception has evolved with phototransduction cascades and has diverged in different species, the study on rhodopsin-like pigment and the signaling cascade of varied animals is important for the understanding of the diversity and evolution of animal phototransduction. Here the classification of animal phototransduction cascades are reviewed. Animal photoreceptor cells are roughly divided into two types, ciliary and rhabdomeric types. In the case of the ciliary type photoreceptors, the jellyfish (pre-bilaterian) Gs-mediated, vertebrate (deuterostomes) Gt-mediated and scallop (protostome) and lizard (deuterostome) Go-mediated phototransductions exhibit partial similarity, because all involve cyclic nucleotide signaling, suggesting a monophyletic origin of ciliary phototransduction among animals. The amphioxus (deuterostome) rhabdomeric-type photoreceptor cells contain the

---

\* Corresponding author: Department of Biology and Geosciences, Graduate school of Science, Osaka City University, Osaka 558-8585, Japan., E-mail: terakita@sci.osaka-cu.ac.jp, Phone: +81-6-6605-3144, Fax: +81-6-6605-3171.

homologue of the melanopsin, the circadian photopigment in the photosensitive retinal ganglion cells of vertebrates, and have a Gq-mediated phototransduction cascade similar to protostome rhabdomeric-type visual cells. The phototransduction of amphioxus rhabdomeric photoreceptor cells represents an evolutionary link between phototransduction of the invertebrate visual cells and the vertebrate circadian photoreceptor cells. Based on these findings, we discuss a functional and evolutionary classification of animal phototransduction and photoreceptor cells, the rhabdomeric photoreceptor cell containing phosphoinositol signaling mediated by Gq, and the ciliary photoreceptor cell containing cyclic nucleotide signaling mediated by Gt, Go or Gs.

## 1. INTRODUCTION

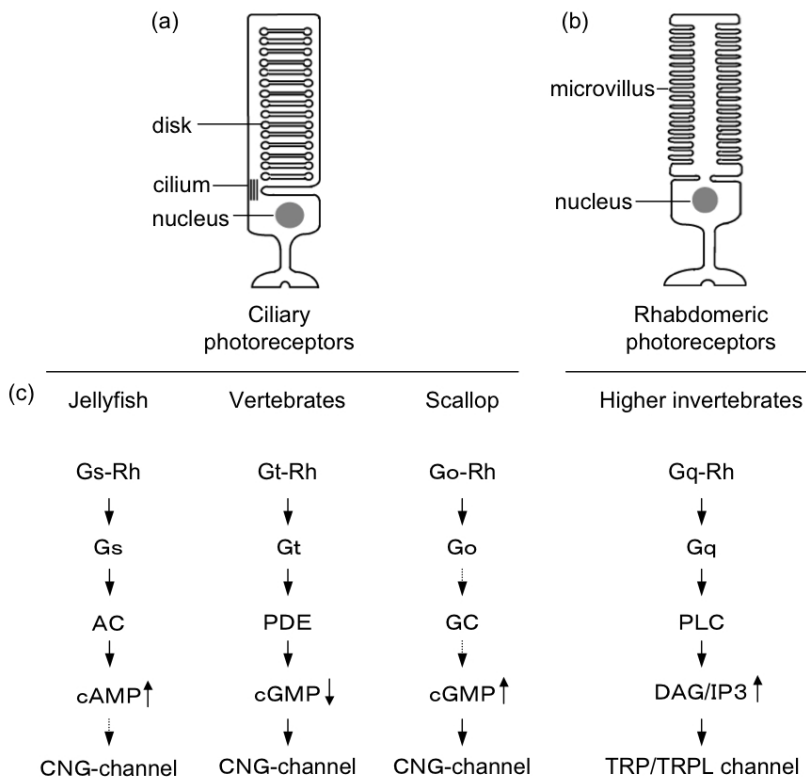
Most animals capture light information through opsin-based photopigments, specialized molecules for photoreception such as rhodopsin and utilize it for visual and non-visual functions. The opsin-based pigments are situated at the “entrance” of not only the phototransduction cascade but also cellular or physiological functions of “photoreception” [1]. Thus opsin-based pigments and phototransduction cascades could be good targets for the investigation of the evolution and diversity of photoreceptive functions. Here the diversity and evolution of animal rhodopsin and phototransduction cascade are discussed.

## 2. PHOTORECEPTOR CELLS

A vertebrate eye is a typical camera-type eye with a well-developed lens, whereas most insects have compound eyes composed of a number of ommatidia [2]. In spite of the morphological difference, both types of eyes contain photoreceptor cells specialized for capturing light [3]. Most vertebrate retinas contain two kinds of photoreceptor cells for visual function, rod and cone visual cells. Each of the cells has a portion specialized for light reception, called the “outer segment”, which develops from cilia structures (Figure 1a). The visual cell and photoreceptor cell that contain ciliary structures are called a ciliary visual cell and a ciliary photoreceptor cell, respectively. On the other hand, most higher invertebrates (protostomes), such as molluscs and arthropods possess photoreceptor cells that have a photoreceptive portion structurally different from rod and cone outer segments. The photoreceptive portion of the invertebrate photoreceptor cells contains a large number of microvilli, which develop from cell membranes and is called a “rhabdomere” (Figure 1b). Thus the photoreceptor cells containing a rhabdomere and related visual cells are called as rhabdomeric photoreceptor cells and rhabdomeric visual cells, respectively.

Eakin has proposed a noteworthy hypothesis, that is, most photoreceptor cells found in a wide variety of animals can be classified into two types, a ciliary photoreceptor cell and a rhabdomeric photoreceptor cell [3]. Furthermore, he hypothesized that most protostomes and deuterostomes possess rhabdomeric and ciliary types, respectively.

In any case, the photoreceptive portions of both types of the photoreceptor cells contain a large amount of photosensitive pigments, which capture light and drive phototransduction cascade in the cells.

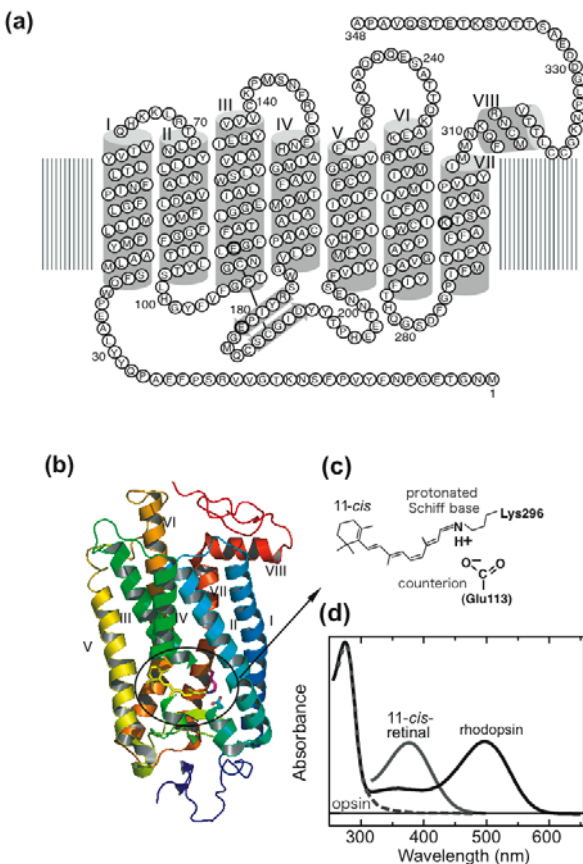


Schematic presentation of two distinct types of animal photoreceptor cells, ciliary type (a) and rhabdromeric type (b) photoreceptor cells. (c) There are four kinds of G-protein-mediated phototransduction cascades in animals, namely Gs-mediated, transducin (Gt)-mediated, Go-mediated and Gq-mediated phototransduction cascades. Phylogenetically different rhodopsins are respectively involved in each of the phototransduction cascades. It should be noted that ciliary photoreceptor cells and rhabdromeric photoreceptor cells employ cyclic nucleotide and phosphoinositol as second messengers, respectively.

Figure 1. Animal photoreceptor cells and possible phototransduction cascades.

### 3. RHODOPSINS

Vertebrate rhodopsin, which is a rod visual pigment and acts as the light-sensor of rod visual cells, is one of the best-understood photopigments [4, 5]. It consists of the protein moiety opsin and the chromophore 11-*cis*-retinal. Mammalian rhodopsin (opsin) is composed of 348 amino acids and has a seven-transmembrane helical structure (Figure 2). The 11-*cis*-retinal chromophore binds to the lysine residue at position 296 (Lys296) in the seventh helix through Schiff base linkage. Vertebrate rhodopsin absorbs visible light and its absorption maximum is at ~500nm (Figure 2). The Schiff base is protonated for visible light absorption of rhodopsin and a negatively charged amino acid residue, called a counterion, is required to stabilize the proton on the Schiff base, because the proton on the Schiff base is not stable within the protein. In vertebrate rhodopsin, a glutamic acid at position 113 (Glu113) serves as the counterion [6-8].



Secondary (a) and crystal structures (b) of bovine rhodopsin. (c) Schematic presentation of 11-cis-retinal which binds to lysine residue at position 296 (Lys296) through the protonated Schiff base linkage. Glutamic acid at position 113 serves as the counterion to stabilize protonated Schiff base in bovine rhodopsin. (d) Absorption spectra of bovine rhodopsin (solid black curve), 11-cis-retinal (gray solid curve) and bovine opsin (gray broken curve).

Figure 2. Structures and absorption spectra of bovine rhodopsin.

More than 2000 kinds of rhodopsin and related photosensitive proteins have been identified so far in a wide variety of vertebrates and invertebrates, and they are hereafter referred to as *rhodopsins*. There are similarities in the primary to tertiary structures of *rhodopsins* and many non-photoreceptive/ ligand-binding G protein coupled receptors (GPCRs) [9, 10]. It is therefore widely accepted that rhodopsins have evolved from a GPCR that binds a chemical ligand.

#### 4. EVOLUTION AND DIVERSITY OF RHODOPSINS

The diverged *rhodopsins* are divided into eight groups in the phylogenetic tree (Figure 3). Accumulated evidence indicates that the members belonging to four of the eight groups couple with four different types of G proteins, namely, Gt-coupled, Gq-coupled, Go-coupled and Gs-coupled *rhodopsins*, respectively [11-17]. The members of the four groups also bind

to 11-*cis*-retinal as a chromophore whereas the members of the retinochrome/RGR, photoisomerase and peropsin groups contain all-*trans*-retinal as a chromophore. See other reviews for details [1].

In most *rhodopsins* such as Gt-coupled, Gq-coupled, Go-coupled, and Gs-coupled *rhodopsins*, light isomerizes 11-*cis*-retinal chromophore to the all-*trans* form, and the isomerization triggers structural changes of the protein moiety opsin to activate G protein [1, 4]. Simply, the *rhodopsins* convert to a photoproduct which activates G protein by light.

Structural changes from the dark state to the photoproduct result in the spectral changes of *rhodopsins*. Many textbooks describe that reddish rhodopsin bleaches or becomes colorless upon light absorption. The color changes are spectroscopically shown in Figure 4a. Irradiation of bovine rhodopsin shifts its absorption maximum from ~500 nm to ~380nm. The photoproduct is thermally unstable, and its chromophore all-*trans*-retinal dissociates from the protein moiety [18-20] (Figure 4c). *Rhodopsins* having the bleaching photoproduct are called “bleaching *rhodopsins*”. Among diverged *rhodopsins*, Gt-coupled visual pigments, namely vertebrate rod and cone visual pigments, exhibit a nature of bleaching *rhodopsins* [19]. On the other hand, spectroscopic analyses on varied *rhodopsins* revealed that *rhodopsins* other than vertebrate visual pigments, such as the members of Gq-coupled *rhodopsin* and Go-coupled *rhodopsin* groups, have a stable photoproduct, which can revert to the original dark state by subsequent light absorption, showing photoregeneration ability [21-23] (Figure 4d). In the squid rhodopsin, light-irradiation results in a mixture of dark and irradiated states, both of which form photoequilibrium because of reversible photoreaction between dark state and photoproduct (Figure 4b, d). *Rhodopsins* that are unbleached upon irradiation and have photoregeneration ability as well as two stable states, dark and irradiated, are called bistable *rhodopsins* (pigments). Comparative analyses using mutant proteins of varied *rhodopsins* have demonstrated difference in position of the counterion, an essential amino acid residue for visible light absorption (Figure 2c), between bleaching and bistable *rhodopsins*; Glu113 in the third helix serves as a counterion in the bleaching rhodopsin, whereas Glu181 in the connecting loop between the fourth and fifth helices acts as a counterion in most *rhodopsins* (bistable *rhodopsins*) other than bleaching *rhodopsins* [24] (see Figure 2a). Interestingly, a vertebrate pineal photopigment parapinopsin [25], which belongs to the vertebrate non-visual pigment subgroup and is close to vertebrate bleaching visual pigments (Figure 3), still possesses a Glu181 counterion and exhibits a bistable nature [24, 26]. The difference in counterion position suggests that counterion displacement from Glu181 to Glu113 occurred and led to acquisition of bleaching *rhodopsin* during molecular evolution of vertebrate rhodopsin [24].

The most remarkable functional difference between bleaching and bistable *rhodopsins* has been found in G protein activation ability. Interestingly vertebrate bovine rhodopsin (bleaching rhodopsin) has ~50-fold more G protein activation ability than invertebrate Go-coupled rhodopsin (bistable rhodopsin) and ~20-fold more than parapinopsin (bistable rhodopsin) [24]. In order to elucidate a molecular mechanism related to this difference, we recently compared conformational changes between bovine rhodopsin and parapinopsin by analyzing the amplitude of structural changes using a site-directed fluorescence labeling technique. The results demonstrated that the amplitude of conformational change underlying G protein activation is larger for bovine rhodopsin and smaller for parapinopsin [27].

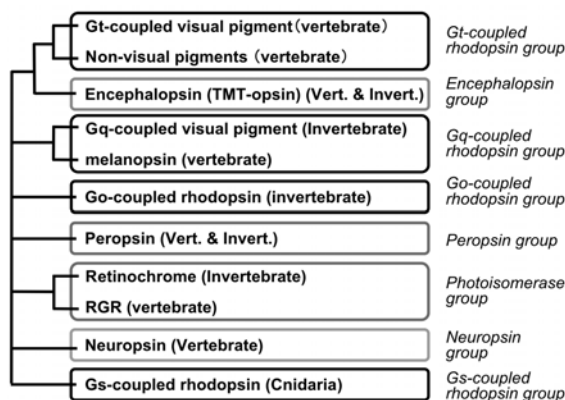
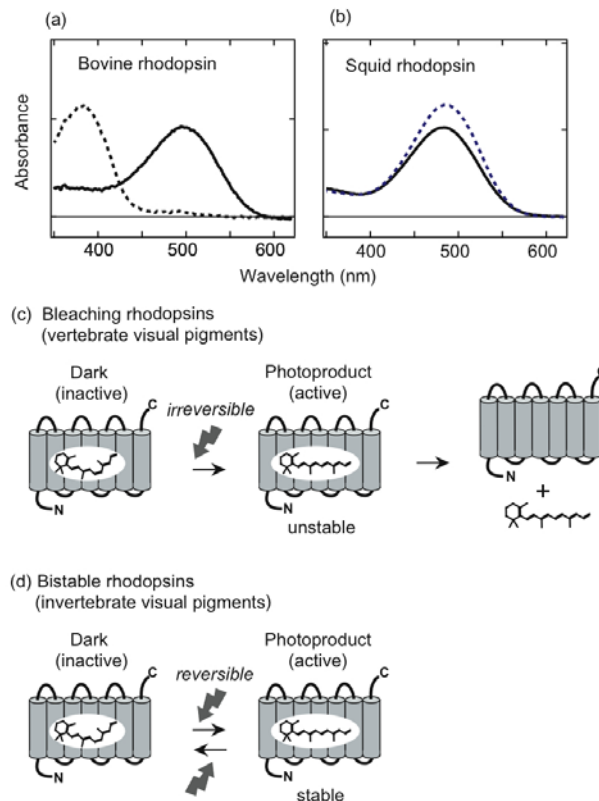


Figure 3. Schematic presentation of phylogenetic relationship of *rhodopsins* (opsins). *Rhodopsins* are divided into eight groups; seven groups of bilaterian *rhodopsins* (Gt-coupled rhodopsin, Encephalopsin, Gq-coupled rhodopsin, Go-coupled rhodopsin, peropsin, photoisomerase, neuropsin groups) and one cnidarian rhodopsin group (Gs-coupled rhodopsin group). Molecular properties of the members belonging to each *rhodopsin* group, except for those of encephalopsin and neuropsin groups have been reported. See text for detail.



Absorption spectra of dark (solid curve) and irradiated (broken curve) bovine (a) and squid rhodopsins (b). Schematic presentation of photoreaction of bleaching (c) and bistable rhodopsins (d), which convert to unstable and stable/photoregeneratable photoproducts by light absorption, respectively. Only vertebrate visual pigments in rods and cones exhibit bleaching property.

Figure 4. Photoreaction of rhodopsins.

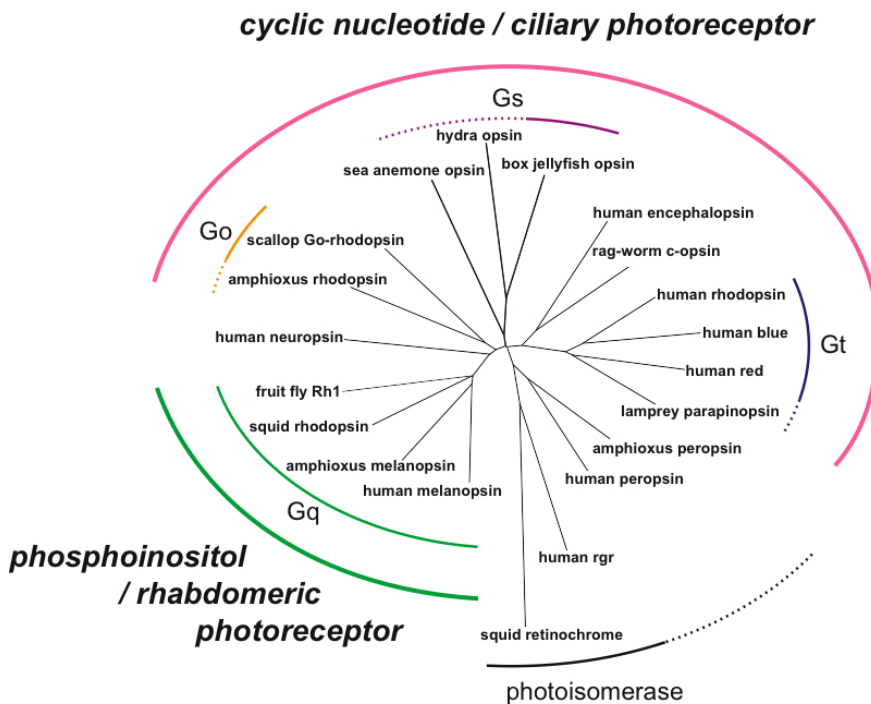


Figure 5. Phylogenetic relationship of animal *rhodopsins* and animal phototransduction cascades. The amino acid sequences of opsins that were revealed to function as photopigments and their apparent homologues are included. The G-protein subtypes that the *rhodopsins* are coupled with and the second messengers in the phototransduction cascades, as well as the photoreceptor cell types, are indicated.

The difference in the “amplitude” of the light-induced conformational change may also be related to another difference between the two rhodopsins, namely the difference in their photoreversibility. The large conformational change observed in bovine rhodopsin might enable so much internal rearrangement within the protein that it cannot be converted back to a dark state structure by further light-induced photoisomerization of retinal. Therefore it is tempting to speculate that during molecular evolution of *rhodopsins*, vertebrate visual pigments including bovine rhodopsin acquired higher G protein activation ability through acquisition of the larger conformational change, a by-product of which also resulted in abolishment of photoreversibility in the rhodopsins at the same time [27].

## 5. PHOTOTRANSDUCTION CASCADES

In the photoreceptor cells, a light signal captured by *rhodopsins* is transmitted to biochemical reactions composed of a G protein, an effector enzyme and an ion channel to generate electrophysiological responses of the cells. Namely, the phototransduction cascade from rhodopsin to the ion channel converts a light signal into a biochemical signal followed by an electrical one. Among the various phototransduction cascades, the system in vertebrate visual cells is most well studied and the details are described in other excellent reviews [4, 28, 29]. Here just a brief introduction is given.

Hetero trimeric G proteins, which consist of alpha, beta and gamma subunits, are roughly divided into four subfamilies, Gs, Gi, Gq and G12, on the basis of amino acid sequence identity of the alpha subunits [30-32]. The vertebrate visual pigments in rods and cones activate one of the Gi type G proteins, transducin (Gt), which in turn activates phosphodiesterase that hydrolyzes cGMP to GMP [11, 33]. Decrease of cGMP concentration in the photoreceptor cells results in closure of the cGMP-gated cation channel and leads to a hyperpolarizing response of the cells [34] (Figure 1c). On the other hand, in the molluscan and arthropod visual cells, light-absorbed visual pigment activates Gq, which in turn stimulates phospholipase C, which hydrolyzes phosphatidylinositol 4,5-bisphosphate (PIP2) into diacylglycerol (DG) and inositol 1,4,5-triphosphate (IP3) to start the phosphoinositol cascade, leading to a depolarizing response of the photoreceptor cells [12-15]. In *Drosophila*, it was suggested that a DG-related unsaturated fatty acid opens the transient receptor potential (TRP)-channel/transient receptor potential-like (TRPL)-channel to generate a depolarizing response [35].

## 6. RHODOPSINS AND PHOTOTRANSDUCTION IN CILIARY PHOTORECEPTOR CELLS

As mentioned above, distinct *rhodopsins* and G proteins underlie the generation of electrophysiological photoresponses of vertebrate and invertebrate photoreceptor cells. In other words, from the viewpoint of cell morphology, the two types of photoreceptor cells, ciliary and rhabdomeric, have different *rhodopsins* and different phototransduction cascades, Gt-mediated and Gq-mediated, respectively. As described, Eakin has hypothesized that diverged photoreceptor cells are divided into two types, namely rhabdomeric and ciliary photoreceptors, and also has suggested that most protostomes and deuterostomes contain rhabdomeric and ciliary photoreceptors, respectively [3]. Interestingly, the scallop has both types and therefore it is of interest to elucidate what kind of *rhodopsin* and phototransduction cascade function in the protostome ciliary photoreceptor cell. Comparative investigations on *rhodopsins* and phototransduction cascades in the two cell types of scallop revealed that the Gq-mediated phototransduction cascade identical to other protostome functions in rhabdomeric cells, whereas a different rhodopsin and a different phototransduction cascade have been found in the ciliary cells; that is, a new rhodopsin couples to Go [16]. The new rhodopsin and its homologues are called Go-coupled *rhodopsins* (Figure 3). Taken together with electrophysiological studies on scallop ciliary photoreceptor cells [36], the novel rhodopsin light-dependently activates Go, which possibly stimulates guanylyl cyclase to elevate cellular cGMP concentration in the ciliary cells. This cascade is different from that in vertebrate rod and cone visual cells where Gt and PDE are involved in the light-dependent decrease of cGMP, showing that distinct phototransduction cascades underlie the photoresponse of ciliary photoreceptors in protostomes and deuterostomes.

Cnidarian is a pre-bilaterian and phylogenetically branches from the basal position of protostomes and deuterostomes. Among cnidarians, box jellyfish are known to have well-developed camera eyes which contain ciliary photoreceptors [37-39]. Thus it is interesting to investigate the phototransduction cascade of cnidarian photoreceptor cells and to compare phototransduction cascades among ciliary photoreceptor cells of varied animals. The

identified box jellyfish opsin clusters with other cnidarian opsins [40-42] (Figure 5). We heterologously expressed a box jellyfish opsin in the cultured mammalian cells (HEK293) and successfully purified the functional opsin-based pigment that possesses 11-*cis*-retinal as a chromophore [17]. The opsin-based pigment has its absorption maximum at ~ 500nm and irradiation causes a blue shift of the spectrum to form a photoproduct which contains all-*trans*-retinal as a chromophore, like other visual pigments. Notably, immunohistochemical analyses revealed that a Gs type G protein is colocalized to photoreceptive regions with the opsin and adenylyl cyclase, suggesting that opsin-based pigment drives the Gs/adenylyl cyclase cascade which is similar to that of mammals. In fact, several lines of biochemical evidence demonstrated that the novel opsin-based pigment activates the Gs/adenylyl cyclase cascade to elevate cAMP in a light dependent manner [17]. These facts suggest that the Gs-mediated phototransduction cascade in box jellyfish photoreceptor cells is distinct from those of both rod/cone visual cells of vertebrates and scallop ciliary visual cells (Figure 1). Furthermore, parietopsin, which belongs to the vertebrate non-visual pigment subgroup and is closely related to vertebrate Gt-coupled visual pigments (Figure 3), was shown to couple with Go in the ciliary photoreceptor cells of lizard parietal eyes [43]. Taken together, judging from the G-protein subtype which mediates light information, the ciliary-type photoreceptor cells seem to have polyphyletic origins. However, in spite of these differences, all of these cells employ cyclic nucleotides (cGMP or cAMP) as the second messenger in the phototransduction signaling cascade (Figure 1). In the Gt-mediated phototransduction of vertebrate rods and cones, cyclic nucleotide-gated (CNG) channels are used to achieve light-dependent cellular responses [34, 44]. In addition, in the Go-mediated phototransduction of scallop ciliary photoreceptor cells, the role of CNG channels in generating cellular responses was also suggested from pharmacological and electrophysiological experiments [36, 45]. Interestingly, a cDNA encoding a channel, which clustered the CNG channel subfamily including vertebrate rod, cone and olfactory CNG channels, was isolated from the box jellyfish lens eyes [17]. These findings, together with the fact that CNG channels are gated by both cAMP and cGMP [44], suggest a monophyletic group of phototransduction cascades in ciliary photoreceptor cells, that is, the ciliary phototransduction cascades are characterized by employing cyclic nucleotides in phototransduction signaling, presenting an evolutionary linkage from pre-bilaterian phototransduction to vertebrate phototransduction. Notably, the similarity in phototransduction cascade among cnidarian, protostome and deutrostome ciliary photoreceptor cells also highlighted evolutionary linkage of ciliary photoreceptor cells among a wide variety of animals [17].

## 7. RHODOPSINS AND PHOTOTRANSDUCTION CASCADES IN RABDOMERIC PHOTORECEPTOR CELLS

As mentioned above, rhabdomeric photoreceptor cells in protostomes such as arthropods and molluscs employ the Gq-mediated phototransduction cascade [12-15] (Figure 1). On the other hand, some deuterostomes also contain rhabdomeric photoreceptor cells but it was unknown if the deuterostome rhabdomeric photoreceptors also contain Gq-mediated phototransduction cascade. It is also interesting to compare phototransduction cascades in protostome and deuterostome rhabdomeric cells in order to obtain a clue for evolutionary

linkage between their phototransduction systems. In higher deuterostomes, chordate lineage, rhabdomeric photoreceptors have never been found in the vertebrates, but it is known that cephalochordate, amphioxus which is one of the closest invertebrates to vertebrates has two kinds of rhabdomeric photoreceptor cells, the Joseph cells and the photoreceptor cells of the dorsal ocelli in a neural tube [46]. The type of opsin that functions in the rhabdomeric cells was then investigated by cDNA cloning, *in situ* hybridization and immunohistochemistry. Interestingly, an amphioxus homologue of melanopsin (Figure 3), which is found in a wide variety of vertebrates and is involved in circadian photoentrainment and pupillary light response in photosensitive retinal ganglion cells of mammals [47-49], is localized to both rhabdomeric photoreceptor cells [50]. Phylogenetic analysis shows that vertebrate melanopsin and invertebrate Gq-coupled visual pigment are orthologous genes [51] (Figure 3) and therefore it is important to compare their molecular properties.

Interestingly, the amphioxus melanopsin converted to a thermally stable photoproduct by light absorption and the stable photoproduct reverts to the dark state by subsequent light absorption, showing the bistable nature, like protostome Gq-coupled visual pigments in rhabdomeric photoreceptors and unlike vertebrate visual pigments [50] (Figure 4). In addition, immunohistochemical analyses revealed that the melanopsin is colocalized with Gq in the two kinds of rhabdomeric cells, and also *in vitro* biochemical studies showed that the amphioxus melanopsin activates Gq as efficiently as squid and insect visual pigments in a light-dependent manner [52]. These observations show that visual pigments in protostome rhabdomeric photoreceptor cells and melanopsin in deuterostome rhabdomeric photoreceptor cells possess almost the same molecular properties and drive the Gq-mediated cascade. Taken together with a recent electrophysiological study [53], therefore, the protostome and deuterostome rhabdomeric photoreceptor cells employ the evolutionary equivalent rhodopsin and phototransduction cascade.

Arendt has reported that some molecules involved in cell differentiation are common between the invertebrate (protostome) rhabdomeric photoreceptor cells and the mammalian photosensitive ganglion cells where melanopsin functions for the circadian photoentrainment, suggesting that these two photoreceptor cells share a common origin [54]. The finding that the deuterostome rhabdomeric photoreceptor cells employ melanopsin/Gq system like mammalian photosensitive retinal ganglion cells [55-58], together with the fact that the deuterostome and protostome rhabdomeric photoreceptor cells contain the evolutionary equivalent rhodopsin and phototransduction cascade [50], also provides evolutionary linkage between vertebrate photosensitive retinal ganglion cells and the deuterostome rhabdomeric photoreceptor cells as well as the protostome rhabdomeric photoreceptor cells.

## 8. CLASSIFICATION OF ANIMAL PHOTOTRANSDUCTION AND PHOTORECEPTOR CELLS

As mentioned, cnidarian, molluscan and vertebrate photoreceptor cells contain different sets of rhodopsin, G-proteins and effector enzymes but they employ the same type of second messenger, cyclic nucleotide (cAMP and cGMP) and possibly the CNG channel. Furthermore, the protostome rhabdomeric photoreceptors and deuterostome ones including vertebrate photoreceptive retinal ganglion cells share orthologous rhodopsins and almost the

same Gq-mediated phototransduction cascades. These findings clearly support the hypothesis of photoreceptor classification, that is, two morphologically distinct photoreceptor cell-types, ciliary type cells and rhabdomeric type cells, exist in animals. We here proposed a novel classification of animal phototransduction and photoreceptor cells, including the previous reports [3, 16, 50, 59]. The rhabdomeric photoreceptor cell containing phosphoinositol signaling is mediated by Gq, and the ciliary photoreceptor cell containing cyclic nucleotide signaling is mediated by Gt, Go or Gs (Figure 5).

## 9. CONCLUSION

More than 2000 kinds of rhodopsin-like photopigments have been identified thus far and they are divided into eight subgroups. Comparison of two distinct types of *rhodopsins*, each of which converts to unstable or stable/photoregeneratable photoproducts by light absorption highlights the evolution of vertebrate visual pigments. Mutational studies of varied *rhodopsins* suggest that displacement of counterion, an essential amino acid residue for rhodopsins to absorb visible light, during molecular evolution is closely related to evolution of vertebrate visual pigments. Interestingly vertebrate visual pigments have more efficient G protein activation ability than bistable *rhodopsins*, probably due to larger amplitude of conformational change in vertebrate rhodopsin upon light absorption.

Four kinds of phototransduction cascades have been found thus far, such as those mediated by transducin in vertebrate rod and cone visual cells, by Gq type G protein in insect and molluscan rhabdomeric-type visual cells, by Go type G protein in scallop and lizard ciliary-type visual cells and by Gs type G protein in jellyfish visual cells. Animal photoreceptor cells are roughly divided into two types, ciliary and rhabdomeric. In the case of the ciliary type photoreceptors, the jellyfish (pre-bilaterian) Gs-mediated, vertebrate (deuterostomes) Gt-mediated and scallop (protostome)/lizard (deuterostome) Go-mediated phototransductions exhibit partial similarity, because all involve cyclic nucleotide signaling, suggesting a monophyletic origin of ciliary phototransduction among animals. The amphioxus (deuterostome) rhabdomeric-type photoreceptor cells contain the homologue of the melanopsin, the circadian photopigment in the photosensitive retinal ganglion cells of vertebrates, and Gq-mediated phototransduction cascade as protostome rhabdomeric-type visual cells do. The phototransduction of amphioxus rhabdomeric photoreceptor cell represents an evolutionary link between phototransductions of the invertebrate visual cells and the vertebrate circadian photoreceptor cells. Based on these findings, we proposed a new classification of animal phototransduction and photoreceptor cells, the rhabdomeric photoreceptor cell containing phosphoinositol signaling mediated by Gq and the ciliary photoreceptor cell containing cyclic nucleotide signaling mediated by transducin, Go or Gs.

Surprisingly, the Gs-mediated phototransduction cascade in jellyfish visual cells exhibits overall similarities with the vertebrate olfactory signaling cascade, which is composed of Golf (a kind of Gs) and adenylyl cyclase type III and elicits increases in cAMP and activation of CNG channels [60]. Thus, it may be an intriguing hypothesis that the vertebrate olfactory sensory neuron, which also has ciliary morphology, shares an evolutionarily common origin with the ciliary photoreceptor cells [17].

## ACKNOWLEDGMENTS

We thank Drs M. Koyanagi and H. Tsukamoto for valuable comments on this manuscript. This work was supported in part by grants-in-aid for Scientific Research from the Japanese Ministry of Education, Science, Sports and Culture the Yamada and the Naito Foundation.

## REFERENCES

- [1] Terakita, A. (2005). The opsins. *Genome Biol*, *6*, 213.
- [2] Land, M. F. & Nilsson, D. E. (2002). *Animal eyes* Oxford, Oxford University Press.
- [3] Eakin, R. M. (1965). Evolution of photoreceptors. *Cold Spring Harb Symp Quant Biol*, *30*, 363-370.
- [4] Shichida, Y. & Imai, H. (1998). Visual pigment: G-protein-coupled receptor for light signals. *Cell Mol Life Sci*, *54*, 1299-1315.
- [5] Menon, S. T., Han, M. & Sakmar, T. P. (2001). Rhodopsin: structural basis of molecular physiology. *Physiol Rev*, *81*, 1659-1688.
- [6] Zhukovsky, E. A. & Oprian, D. D. (1989). Effect of carboxylic acid side chains on the absorption maximum of visual pigments. *Science*, *246*, 928-930.
- [7] Sakmar, T. P., Franke, R. R. & Khorana, H. G. (1989). Glutamic acid-113 serves as the retinylidene Schiff base counterion in bovine rhodopsin. *Proc Natl Acad Sci, U S A* *86*, 8309-8313.
- [8] Nathans, J. (1990). Determinants of visual pigment absorbance: role of charged amino acids in the putative transmembrane segments. *Biochemistry*, *29*, 937-942.
- [9] Lefkowitz, R. J., Sun, J. P. & Shukla, A. K. (2008). A crystal clear view of the beta2-adrenergic receptor. *Nat Biotechnol*, *26*, 189-191.
- [10] Rosenbaum, D. M., Rasmussen, S. G. & Kobilka, B. K. (2009). The structure and function of G-protein-coupled receptors. *Nature*, *459*, 356-363.
- [11] Kuhn, H. (1980). Light- and GTP-regulated interaction of GTPase and other proteins with bovine photoreceptor membranes. *Nature*, *283*, 587-589.
- [12] Terakita, A., Hariyama, T., Tsukahara, Y., Katsukura, Y. & Tashiro, H. (1993). Interaction of GTP-binding protein Gq with photoactivated rhodopsin in the photoreceptor membranes of crayfish. *FEBS Lett*, *330*, 197-200.
- [13] Lee, Y. J., Shah, S., Suzuki, E., Zars, T., O'Day, P. M. & Hyde, D. R. (1994). The *Drosophila* dgq gene encodes a G alpha protein that mediates phototransduction. *Neuron*, *13*, 1143-1157.
- [14] Yarfitz, S. & Hurley, J. B. (1994). Transduction mechanisms of vertebrate and invertebrate photoreceptors. *J Biol Chem*, *269*, 14329-14332.
- [15] Kikkawa, S., Tominaga, K., Nakagawa, M., Iwasa, T. & Tsuda, M. (1996). Simple purification and functional reconstitution of octopus photoreceptor Gq, which couples rhodopsin to phospholipase C. *Biochemistry*, *35*, 15857-15864.
- [16] Kojima, D., Terakita, A., Ishikawa, T., Tsukahara, Y., Maeda, A. & Shichida, Y. (1997). A novel Go-mediated phototransduction cascade in scallop visual cells. *J Biol Chem*, *272*, 22979-22982.

- [17] Koyanagi, M., Takano, K., Tsukamoto, H., Ohtsu, K., Tokunaga, F. & Terakita, A. (2008). Jellyfish vision starts with cAMP signaling mediated by opsin-G(s) cascade. *Proc Natl Acad Sci, U S A*, *105*, 15576-15580.
- [18] Matthews, R. G., Hubbard, R., Brown, P. K. & Wald, G. (1963). Tautomeric Forms of Metarhodopsin. *J Gen Physiol*, *47*, 215-240.
- [19] Wald, G. (1968). Molecular basis of visual excitation. *Science*, *162*, 230-239.
- [20] Farrens, D. L. & Khorana, H. G. (1995). Structure and function in rhodopsin. Measurement of the rate of metarhodopsin II decay by fluorescence spectroscopy. *J Biol Chem*, *270*, 5073-5076.
- [21] Hubbard, R. & St George, R. C. (1958). The rhodopsin system of the squid. *J Gen Physiol*, *41*, 501-528.
- [22] Tsukamoto, H., Terakita, A. & Shichida, Y. (2005). A rhodopsin exhibiting binding ability to agonist all-trans-retinal. *Proc Natl Acad Sci, USA*, *102*, 6303-6308.
- [23] Koyanagi, M. & Terakita, A. (2008). Gq-coupled rhodopsin subfamily composed of invertebrate visual pigment and melanopsin. *Photochem Photobiol*, *84*, 1024-1030.
- [24] Terakita, A., Koyanagi, M., Tsukamoto, H., Yamashita, T., Miyata, T. & Shichida, Y. (2004). Counterion displacement in the molecular evolution of the rhodopsin family. *Nat Struct Mol Biol*, *11*, 284-289.
- [25] Blackshaw, S. & Snyder, S. H. (1997). Parapinopsin, a novel catfish opsin localized to the parapineal organ, defines a new gene family. *J Neurosci.*, *17*, 8083-8092.
- [26] Koyanagi, M., Kawano, E., Kinugawa, Y., Oishi, T., Shichida, Y., Tamotsu, S. & Terakita, A. (2004). Bistable UV pigment in the lamprey pineal. *Proc Natl Acad Sci, USA*, *101*, 6687-6691.
- [27] Tsukamoto, H., Farrens, D. L., Koyanagi, M. & Terakita, A. (2009). The magnitude of the light-induced conformational change in different rhodopsins correlates with their ability to activate G proteins. *J Biol Chem*, *284*, 20676-20683.
- [28] Ebrey, T. & Koutalos, Y. (2001). Vertebrate photoreceptors. *Prog Retin Eye Res*, *20*, 49-94.
- [29] Yau, J. M., Pasupathy, A., Fitzgerald, P. J., Hsiao, S. S. & Connor, C. E. (2009). Analogous intermediate shape coding in vision and touch. *Proc Natl Acad Sci, U S A*, *106*, 16457-16462.
- [30] Hepler, J. R. & Gilman, A. G. (1992). G proteins. *Trends Biochem Sci*, *17*, 383-387.
- [31] Simon, M. I., Strathmann, M. P. & Gautam, N. (1991). Diversity of G proteins in signal transduction. *Science*, *252*, 802-808.
- [32] Suga, H., Koyanagi, M., Hoshiyama, D., Ono, K., Iwabe, N., Kuma, K. & Miyata, T. (1999). Extensive gene duplication in the early evolution of animals before the parazoan-eumetazoan split demonstrated by G proteins and protein tyrosine kinases from sponge and hydra. *J Mol Evol*, *48*, 646-653.
- [33] Stryer, L. (1986). Cyclic GMP cascade of vision. *Annu Rev Neurosci*, *9*, 87-119.
- [34] Yau, K. W. & Baylor, D. A. (1989). Cyclic GMP-activated conductance of retinal photoreceptor cells. *Annu Rev Neurosci*, *12*, 289-327.
- [35] Hardie, R. C. & Raghu, P. (2001). Visual transduction in *Drosophila*. *Nature*, *413*, 186-193.
- [36] Gomez, M. P. & Nasi, E. (1997). Antagonists of the cGMP-gated conductance of vertebrate rods block the photocurrent in scallop ciliary photoreceptors. *J Physiol*, *500*, 367-378.

- [37] Berger, E. W. (1898). The histological structure of the eyes of cubomedusae. *J Comp Neurol*, 8, 223-230.
- [38] Martin, V. J. (2002). Photoreceptors of Cnidarians. *Can J Zool*, 80, 1703-1722.
- [39] Piatigorsky, J. & Kozmik, Z. (2004). Cubozoan jellyfish: an Evo/Devo model for eyes and other sensory systems. *Int J Dev Biol*, 48, 719-729.
- [40] Plachetzki, D. C., Degnan, B. M. & Oakley, T. H. (2007). The origins of novel protein interactions during animal opsin evolution. *PLoS ONE*, 2, e1054.
- [41] Suga, H., Schmid, V. & Gehring, W. J. (2008). Evolution and functional diversity of jellyfish opsins. *Curr Biol*, 18, 51-55.
- [42] Kozmik, Z., Ruzickova, J., Jonasova, K., Matsumoto, Y., Vopalensky, P., Kozmikova, I., Strnad, H., Kawamura, S., Piatigorsky, J., Paces, V. & Vlcek, C. (2008). Assembly of the cnidarian camera-type eye from vertebrate-like components. *Proc Natl Acad Sci, U S A*, 105, 8989-8993.
- [43] Su, C. Y., Luo, D. G., Terakita, A., Shichida, Y., Liao, H. W., Kazmi, M. A., Sakmar, T. P. & Yau, K. W. (2006). Parietal-eye phototransduction components and their potential evolutionary implications. *Science*, 311, 1617-1621.
- [44] Kaupp, U. B. & Seifert, R. (2002). Cyclic nucleotide-gated ion channels. *Physiol Rev*, 82, 769-824.
- [45] Gotow, T., Nishi, T. & Kijima, H. (1994). Single K<sup>+</sup> channels closed by light and opened by cyclic GMP in molluscan extra-ocular photoreceptor cells. *Brain Res*, 662, 268-272.
- [46] Lacalli, T. C. (2004). Sensory systems in amphioxus: a window on the ancestral chordate condition. *Brain Behav Evol*, 64, 148-162.
- [47] Panda, S., Provencio, I., Tu, D. C., Pires, S. S., Rollag, M. D., Castrucci, A. M., Pletcher, M. T., Sato, T. K., Wiltshire, T., Andahazy, M., Kay, S. A., Van Gelder, R. N. & Hogenesch, J. B. (2003). Melanopsin is required for non-image-forming photic responses in blind mice. *Science*, 301, 525-527.
- [48] Hattar, S., Lucas, R. J., Mrosovsky, N., Thompson, S., Douglas, R. H., Hankins, M. W., Lem, J., Biel, M., Hofmann, F., Foster, R. G. & Yau, K. W. (2003). Melanopsin and rod-cone photoreceptive systems account for all major accessory visual functions in mice. *Nature*, 424, 76-81.
- [49] Lucas, R. J., Hattar, S., Takao, M., Berson, D. M., Foster, R. G. & Yau, K. W. (2003). Diminished pupillary light reflex at high irradiances in melanopsin-knockout mice. *Science*, 299, 245-247.
- [50] Koyanagi, M., Kubokawa, K., Tsukamoto, H., Shichida, Y. & Terakita, A. (2005). Cephalochordate melanopsin: evolutionary linkage between invertebrate visual cells and vertebrate photosensitive retinal ganglion cells. *Curr Biol*, 15, 1065-1069.
- [51] Provencio, I., Jiang, G., De Grip, W. J., Hayes, W. P. & Rollag, M. D. (1998). Melanopsin: An opsin in melanophores, brain, and eye. *Proc Natl Acad Sci, USA*, 95, 340-345.
- [52] Terakita, A., Tsukamoto, H., Koyanagi, M., Sugahara, M., Yamashita, T. & Shichida, Y. (2008). Expression and comparative characterization of Gq-coupled invertebrate visual pigments and melanopsin. *J Neurochem*, 105, 883-890.
- [53] Gomez Mdel, P., Angueyra, J. M. & Nasi, E. (2009) Light-transduction in melanopsin-expressing photoreceptors of Amphioxus. *Proc Natl Acad Sci, U S A*, 106, 9081-9086.

- [54] Arendt, D. (2003). Evolution of eyes and photoreceptor cell types. *Int J Dev Biol*, *47*, 563-571.
- [55] Panda, S., Nayak, S. K., Campo, B., Walker, J. R., Hogenesch, J. B. & Jegla, T. (2005). Illumination of the Melanopsin Signaling Pathway. *Science*, *307*, 600-604.
- [56] Qiu, X., Kumbalasiri, T., Carlson, S. M., Wong, K. Y., Krishna, V., Provencio, I. & Berson, D. M. (2005). Induction of photosensitivity by heterologous expression of melanopsin. *Nature*, *433*, 745-749.
- [57] Melyan, Z., Tarttelin, E. E., Bellingham, J., Lucas, R. J. & Hankins, M. W. (2005). Addition of human melanopsin renders mammalian cells photoresponsive. *Nature*, *433*, 741-745.
- [58] Isoldi, M. C., Rollag, M. D., Castrucci, A. M. & Provencio, I. (2005). Rhabdomeric phototransduction initiated by the vertebrate photopigment melanopsin. *Proc Natl Acad Sci U S A*, *102*, 1217-1221.
- [59] Arendt, D., Tessmar-Raible, K., Snyman, H., Dorresteijn, A. W. & Wittbrodt, J. (2004). Ciliary photoreceptors with a vertebrate-type opsin in an invertebrate brain. *Science*, *306*, 869-871.
- [60] Firestein, S. (2001). How the olfactory system makes sense of scents. *Nature*, *413*, 211-218.



***Chapter 9***

## **EFFECTS OF NATURAL ULTRAVIOLET RADIATION EXPOSURE IN INLAND WATER ECOSYSTEMS OF CHILEAN PATAGONIA**

***Patricio De los Ríos<sup>1\*</sup> and Patricio Acevedo<sup>2\*\*</sup>***

<sup>1</sup>Universidad Católica de Temuco, Facultad de Recursos Naturales,  
Escuela de Ciencias Ambientales, Casilla 15-D, Temuco, Chile  
<sup>2</sup>Universidad de la Frontera, Facultad de Ingeniería, Ciencias y Administración,  
Departamento de Ciencias Físicas, Casilla 54-D, Temuco, Chile

### **ABSTRACT**

Exposure to natural ultraviolet radiation has risen in southern Patagonia due to atmospheric ozone depletion. The available literature describes how natural ultraviolet radiation affects the ecosystems, and in aquatic environments ultraviolet radiation can penetrate the water column under conditions of low concentration of substances such as dissolved organic carbon which provide a screen effect by absorbing wavelengths corresponding to natural ultraviolet radiation. The present chapter is a description of literature about the effects of natural ultraviolet radiation in zooplankton populations and communities in the inland water ecosystems of Chilean Patagonia (38–51°S). At the population level, two patterns have been observed: first, the effects in species with a low tolerance to natural ultraviolet radiation exposure, which corresponds with transparent species; and second, the effects in species with photoprotective substances that are tolerant to high levels of natural ultraviolet radiation. On the community scale it has been observed that under high exposure to natural ultraviolet radiation only tolerant species are present, and under oligotrophy it was observed that few species are tolerant, mainly calanoid copepods, which are dominant in zooplankton assemblages.

**Keywords:** ultraviolet radiation, dissolved organic carbon, zooplankton, copepods, cladocerans, Patagonia

---

\* Corresponding authors: E-mail prios@uct.cl; E-mail(2) patorios@msn.com.

\*\* E-mail: pacevedo@ufro.cl

## INTRODUCTION

During the last decades, in polar and subpolar latitudes an increase in the penetration of natural ultraviolet radiation due to ozone depletion has been observed (Rautio & Korhola, 2002; Díaz et al., 2006). This scenario implies mainly an increase of ultraviolet-B radiation, which is harmful for live organisms (Tartarotti et al., 2000; Marinone et al., 2006; De los Ríos et al., 2007). The available literature describes the presence of natural ultraviolet radiation in high levels in southern Patagonia during the southern summer, which corresponds to the months from December to March (Villafañe et al., 2001; Díaz et al., 2006). The Chilean Meteorological Direction continuously monitors natural ultraviolet radiation for Chile. Unfortunately, there is no continuous information for many countries due to the lack of monitoring stations (Table 1); therefore, we have no continuous available information for Temuco (38°S; Table 2, Figures 1 and 2) in comparison with other cities that have joined the ultraviolet network of the Chilean Meteorological Direction. Natural ultraviolet radiation can penetrate into the water column in conditions of high transparency due mainly to low levels of dissolved organic carbon concentration or other inorganic substances that can absorb the wavelengths corresponding to natural ultraviolet radiation, generating a screen protector effect for biotic organisms (Morris et al., 1995; Villafañe et al., 2001; Marinone et al., 2006).

Ultraviolet radiation is a mutagen for organisms that has with lethal consequences if the organisms have no protective strategies (Friedberg & Friedberg, 2003). In aquatic environments there are two photoprotective strategies. One involves negative phototaxis against natural ultraviolet radiation that is expressed in migrations to deep zones without natural ultraviolet radiation exposure (Villafañe et al., 2001; Alonso et al., 2003). The second photoprotective option is the synthesis of photoprotective substances such as ascorbic acid, carotenoids, melanine or mycosporine-like amino acids. These substances can also generate a protective effect due to their antioxidant effects against peroxide formation as a consequence of interactions between natural ultraviolet radiation with dissolved organic substances (Villafañe et al., 2001; Tartarotti et al., 2004). In these scenarios, the organism exposed to natural ultraviolet radiation requires an additional energy expenditure due to the photoprotective strategies against natural ultraviolet radiation damage (Zellmer, 1996, 1999). This additional energy expenditure can generate an effect on the population that is expressed in the mortality of individuals exposed to a wide natural ultraviolet radiation gradient (Tartarotti et al., 2001). Other consequences can occur at the community level because the vulnerable would not tolerate the low energy resource availability (De los Ríos & Soto, 2005; Marinone et al., 2006).

## OPTICAL PROPERTIES IN PATAGONIAN LAKES

The large and deep Patagonian lakes are characterized by their oligotrophy and high transparency which are associated with the oligotrophy observed for these ecosystems (Campos et al., 1982, 1983, 1987a,b, 1988, 1990, 1992a,b, 1994a,b; Soto & Zúñiga, 1991; Pedrozo et al., 1993; Lovengreen et al., 1994; Soto et al., 1994; Wölfel, 1996; Modenutti et al., 1998; Quiros & Drago, 1999; Villalobos, 1999; Villalobos et al., 2003a; Soto & Campos, 1995; Soto & Stockner, 1996; Morris et al., 1995; Marinone et al., 2006; Woelfl & Geller,

2002; Woelfl, 2007; Kamjunke et al., 2009). This high transparency is due to the low humic acids concentration observed because the vegetation present in the surrounding basin absorbs nutrients, avoiding the inputs of dissolved organic compounds (Soto & Campos, 1995; De los Ríos et al., 2007a). Nevertheless, there are exceptions that correspond to small lakes that are located in coastal zones at 41°S with a high concentration of dissolved organic carbon (De los Ríos, 2003), Chiloé Island (Villalobos et al., 2003) and southern Patagonian plains (51°S, Magallanes region; De los Ríos, 2003).

These results are similar to descriptions of Argentinean Patagonian lakes and ponds (Morris et al., 1995; Marinone et al., 2006). On the basis of these descriptions, the natural ultraviolet radiation penetrates under low concentrations of dissolved organic carbon, and the wavelength corresponding to ultraviolet-B radiation penetrates to 10 m depth (Morris et al., 1995; Villafaña et al., 2001). This condition is enhanced also by the oligotrophy of large and deep lakes, a scenario in which a high transparency was observed (Soto & Campos, 1995; De los Ríos et al., 2007a) because at low concentrations of particulate materials there are no substances that generate a screen effect against natural ultraviolet radiation penetration (Laurion et al., 2000). A different situation occurs in conditions of high levels of dissolved organic carbon concentration, which absorbs the wavelength corresponding to natural ultraviolet radiation practically at the surface (Morris et al., 1995). The studies for shallow Patagonian ponds revealed that these water bodies are exposed to strong winds that generate a mix of the entire water column, which generates a physical effect that exposes the materials located at deep zones to natural ultraviolet radiation when the wind mixes the water column (Zagarese et al., 1998).

## EFFECTS AT POPULATION LEVELS IN CRUSTACEAN ZOOPLANKTON

The studies of zooplankton crustaceans of southern Patagonian inland waters revealed the existence of two different scenarios, a first scenario that corresponds to vulnerable species that are characterized by their nonpigmented body, and a second scenario that corresponds to pigmented species. Both cases correspond to different scenarios that occur in different environments considering biotic and abiotic characteristics (Villafaña et al., 2001; De los Ríos, 2003).

As a first scenario, the nonpigmented species are observed in deep lakes with fish (De los Ríos, 2003), where the nonpigmented body is a protection against visual predation by zooplanktivorous fish, but this condition generates vulnerability in conditions of natural ultraviolet radiation exposure (Winder, 2003). Examples of these species are calanoid copepods such as *Boeckella gracilipes* (Daday, 1902), *B. michaelseni* (Mrázek, 1901) and *Tumeodiaptomus diabolicus* (Brehm, 1936); cyclopoid copepods such as *Mesocyclops longisetus* (Thiebaud, 1914), *M. araucanus* (Campos et al., 1974) and *Tropocyclops prasinus* (Kiefer, 1907); and cladocerans such as *Daphnia ambigua*, *D. pulex*, *Ceriodaphnia dubia* and *Neobosmina chilensis* (Daday, 1902). These species are widespread in large and deep Patagonian lakes (Araya & Zúñiga, 1985; Modenutti et al., 1998; De los Ríos & Soto, 2007; De los Ríos, 2008). On the basis of observations for similar species in northern hemisphere lakes, the nonpigmented species have vertical migrations following a negative phototatism

against natural ultraviolet radiation exposure (Rhode et al., 2001; Vareschi & Wübbens, 2001), which is denoted in migration to deep zones without exposure to natural ultraviolet radiation (Villafañe et al., 2001; Alonso et al., 2003). The results observed for nonpigmented species revealed the vulnerability of these species in conditions of natural ultraviolet radiation exposure, which is expressed with high mortality at high ultraviolet radiation doses (Zagarese et al., 1997a; Tartarotti et al., 2000). The experimental evidence is based on experiences with *B. gracilipes* (Zagarese et al., 1997a; Tartarotti et al., 2000), *Neobosmina chilensis* (De los Ríos, 2004) and *Ceriodaphnia dubia* (Table 3; De los Ríos et al., 2007b).

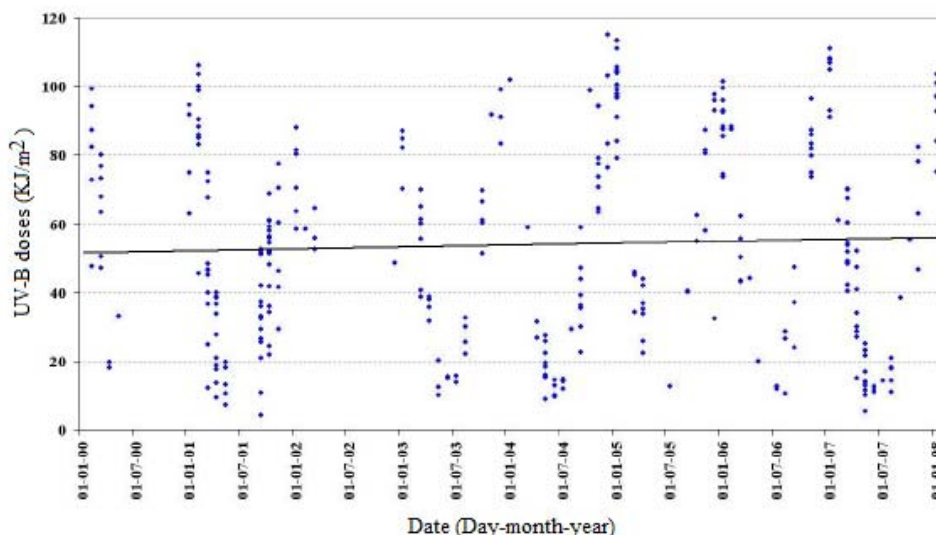


Figure 1. Variation of ultraviolet-B radiation doses for Temuco between 2000 and 2008 (cf.: De los Ríos et al., 2008, p. 214).

**Table 1. Average values of maximum UV-B radiation (in  $\text{W}/\text{m}^2$ ) for four different Chilean localities during southern summer between 2003 to 2004  
(source: Chilean Meteorological Direction)**

2003			
	January	February	December
Valdivia ( $39^\circ 48' \text{ S}$ ; $73^\circ 14' \text{ W}$ )	3.7	3.2	3.4
Puerto Montt ( $41^\circ 25' \text{ S}$ ; $73^\circ 05' \text{ W}$ )	2.9	2.9	3.1
Coyhaique ( $45^\circ 35' \text{ S}$ ; $72^\circ 06' \text{ W}$ )	3.1	2.8	3.3
Punta Arenas ( $53^\circ 00' \text{ S}$ ; $70^\circ 58' \text{ W}$ )	2.5	2.3	2.6
2004			
	January	February	December
Valdivia ( $39^\circ 48' \text{ S}$ ; $73^\circ 14' \text{ W}$ )	3.5	3.2	3.4
Puerto Montt ( $41^\circ 25' \text{ S}$ ; $73^\circ 05' \text{ W}$ )	3.4	2.8	3.2
Coyhaique ( $45^\circ 35' \text{ S}$ ; $72^\circ 06' \text{ W}$ )	3.3	2.8	3.3
Punta Arenas ( $53^\circ 00' \text{ S}$ ; $70^\circ 58' \text{ W}$ )	2.7	2.2	2.7

A second scenario occurs with pigmented species, which have photoprotective substances that generate protection against ultraviolet radiation damage; these substances are melanine, carotenoids, ascorbic acid or micosporine-like amino acids that protect from direct damage caused by natural ultraviolet radiation and indirect damage caused by oxidant damage associated with ultraviolet radiation (Borgeraas & Hessen, 2000, Hansson et al., 2007, Hylander, 2009). In this scenario the zooplankton species are also larger in size in comparison with nonpigmented species, because these are present in fishless water bodies, for example, in central and southern Patagonia (Villafaña et al., 2001; De los Ríos, 2003). In this scenario, the photoprotective substances such as carotenoids, ascorbic acids and micosporine-like amino acids are present in calanoids including *Boeckella antiqua*, *B. gibbosa*, *B. gracilipes*, *B. gracilis*, *B. poppei* and *Parabroteas sarsi* (Zagarese et al., 1997a,b; Villafaña et al., 2001; Rocco et al., 2002; Tartarotti et al., 2004; García et al., 2008), whereas the melanine is restricted to daphnid cladocerans such as *Daphnia dadayana* (De los Ríos, 2005) and probably *Daphniopsis chilensis* (Bayly, 1993). These species in southern Patagonia live in shallow water bodies that are exposed to strong winds that generate a mixing of the entire water column, which causes exposure to natural ultraviolet radiation of all planktonic species (Zagarese et al., 1998), whereas in mountain lakes in northern Patagonia and the northern Andes there are shallow water bodies that would receive ultraviolet radiation in the entire water column (De los Ríos et al., 2007a, 2008).

**Table 2. UV-B radiation, daily maximum (W/m<sup>2</sup>) and doses (kJ/m<sup>2</sup>) for Temuco (38° 41'S; 72° 35' W) (cf.: De los Ríos et al., 2007a, p. 407)**

Date	Maximum (W/m <sup>2</sup> )	Doses (kJ/m <sup>2</sup> )
28 Dec 2005	4.3	107.6
29 Dec 2006	3.5	86.8
03 Jan 2006	3.4	73.8
10 Jan 2006	4.0	91.4
25 Jan 2006	4.2	100.8
26 Jan 2006	4.2	97.6
01 Feb 2006	4.1	99.4
13 Feb 2006	4.2	101.9
02 Mar 2006	3.0	69.5
03 Mar 2006	3.2	59.4
17 Mar 2006	2.5	46.4
24 Mar 2006	2.0	43.2

**Table 3. Mortality of *Ceriodaphnia dubia* exposed to different intensities of natural UV radiation (source: De los Ríos et al., 2007b, p. 482)**

Maximum UV 280–400 nm (W/m <sup>2</sup> )	Maximum UVB 280–320 nm (W/m <sup>2</sup> )	% Mortality
57.0	3.7	100 ± 0
46.2	2.9	100 ± 0
4.0	0.3	50 ± 12
9.7	0.6	50 ± 6
58.2	3.9	100 ± 0
4.1	0.3	17 ± 3
9.9	0.6	40 ± 15

Independently of photoprotective strategies at the population level, there are notorious differences in populations of the same species. For example, for *B. gracilipes* it is possible to find specimens in large and deep lakes with fish that are characterized by nonpigmented water bodies (Villafañe et al., 2001; De los Ríos, 2003), whereas there are populations of this species that inhabit shallow water bodies in the mountain zones of central Chile and Altiplano that have a pigmented body as a photoprotective strategy against high ultraviolet radiation exposure in high mountain and tropical zones (Cabrera et al., 1997; Villafañe et al., 2001; Helbling et al., 2002). A similar situation is successful in *B. michaelseni*, which is a nonpigmented species in large and deep Patagonian lakes, whereas it is possible find this species or *P. sarsi* (De los Ríos, 2008) in shallow water bodies (De los Ríos, 2003).

**Table 4. Results of two-way ANOVA of mortality for two zooplanktonic crustacean species under exposure (+UVR) and protection (-UVR) against natural ultraviolet radiation, and low (-Chl *a*) and high chlorophyll (+Chl *a*) concentration**  
 (cf.: De los Ríos & Soto, 2005, p. 166)

	-UVR -Chl <i>a</i>	+UVR -Chl <i>a</i>	-UVR +Chl <i>a</i>	+UVR +Chl <i>a</i>		F ratio	P
Replicates	3	3	3	3	Variable		
<i>Boeckella gracilipes</i>	47 ± 1	91 ± 25	11 ± 2	69 ± 13	UVR	12.579	0.008*
					Chl <i>a</i>	3.882	0.084
					UVR- Chl <i>a</i>	0.237	0.639
<i>Daphnia pulex</i>	127 ± 11	137 ± 10	68 ± 7	133 ± 10	UVR	108.300	0.000*
					Chl <i>a</i>	56.033	0.000*
					UVR- Chl <i>a</i>	76.633	0.000*

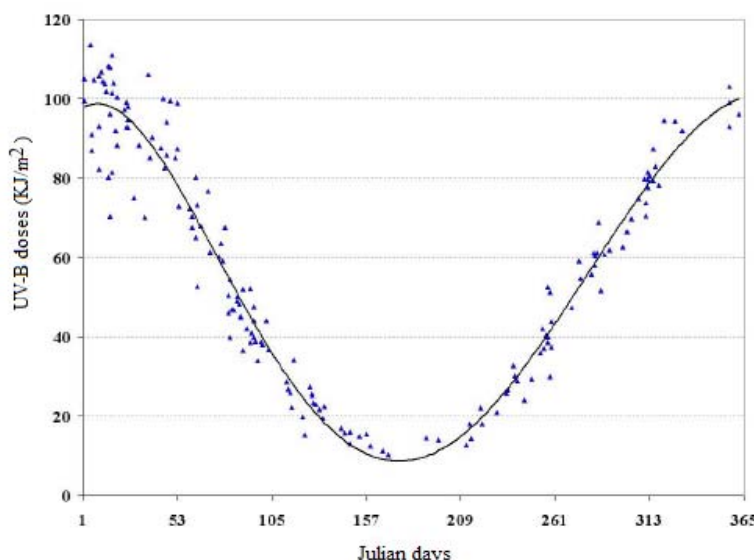


Figure 2. Seasonal variation of ultraviolet-B doses for sunny days in Temuco between 2000 and 2008 (cf.: De los Ríos et al., 2008, p. 214).

**Table 5. Results of Kruskall Wallis test for comparison of mortality of two pigmented zooplanktonic species exposed to artificial ultraviolet radiation with low and high concentrations of dissolved organic carbon that acts as natural screen against ultraviolet radiation (De los Ríos, 2005, p. 115)**

	P	Low DOC	High DOC
<i>Daphnia dadayana</i>	< 0.01	7.33 ± 2.4	0.33 ± 0.33
<i>Boeckella antiqua</i>	< 0.05	0.00 ± 0.00	1.67 ± 0.33
<i>Parabroteas sarsi</i>		0.00 ± 0.00	0.00 ± 0.00

## EFFECTS AT COMMUNITY LEVELS IN CRUSTACEAN ZOOPLANKTON

On the basis of studies at species levels, it is possible to find that exposure to natural ultraviolet radiation has effects on communities because each species has a different tolerance to ultraviolet radiation exposure (Zagarese et al., 1997a,b; De los Ríos, 2005; De los Ríos & Soto, 2005). In fact, it was found that some cladocerans are vulnerable to natural ultraviolet radiation under oligotrophic status (Table 4; Zellmer, 1996, 1999; De los Ríos, 2005; De los Ríos & Soto, 2005). In this scenario, if we observe the status of Chilean Patagonian lakes, it is possible to find that under oligotrophic status calanoid copepods are practically predominant, whereas the cladocerans are present in low abundance or absent (De los Ríos & Soto, 2006). A similar situation would happen in Argentinean Patagonian lakes, which have similarities in zooplankton assemblages and exposure to natural ultraviolet radiation (Modenutti et al., 1998; Alonso et al., 2003), whereas a different situation would be successful in Chilean Nord Patagonian lakes (39–41°S) that currently have a transition from oligotrophy to mesotrophy (Woelfl et al., 2003; De los Ríos & Soto, 2007b). In this scenario, the zooplankton assemblages are characterized by an increase in species number (De los Ríos & Soto, 2007a) and abundance of daphnids (De los Ríos & Soto, 2006; Marinone et al., 2006). Although it was not studied in Chilean lakes, the daphnids are abundant under mesotrophic status (Villalobos, 1994, 2002; Villalobos & Geller, 1997) because these have as photoprotective strategies a negative phototaxis against natural ultraviolet radiation that generates migration to depth zones without natural ultraviolet radiation (Villafañe et al., 2001; Alonso et al., 2004; De los Ríos & Soto, 2006, 2007b).

A different situation occurs in shallow water bodies. If we consider that daphnids are vulnerable to exposure to natural ultraviolet radiation under oligotrophic status (Zellmer, 1996, 1999; De los Ríos, 2005; De los Ríos & Soto, 2005), this would explain the low tolerance to natural ultraviolet radiation of *D. dadayana* in comparison with coexisting calanoids such as *B. antiqua* and *P. sarsi* that are representative of northern Argentinean Patagonia (Table 5; De los Ríos, 2005; García et al., 2008). Under this viewpoint, the exposure to natural ultraviolet radiation would be an important regulating factor that would explain the fluctuations of daphnid abundance and species number in shallow southern Patagonian inland waters (51°S; De los Ríos, 2003; Soto & De los Ríos, 2006). If we consider that southern Patagonia is exposed to natural ultraviolet radiation (Villafañe et al., 2001, 2004; Díaz et al., 2006; Marinone et al., 2006), these water bodies also have a high concentration of dissolved organic carbon, which is a natural screen against natural ultraviolet

radiation (De los Ríos, 2003). In this scenario, it would be possible that the daphnid abundance that is related to mesotrophic status and low conductivity (Soto & De los Ríos, 2006), and it also would be possible that protection against natural ultraviolet radiation is another regulating factor of species assemblages (De los Ríos, 2003).

There is a similar situation in the mountain lakes of northern Patagonia (38–42°S) because these lakes are ultraoligotrophic (Steinhart et al., 1999, 2002; De los Ríos & Roa, in press), and there are oligotrophic and mesotrophic permanent and ephemeral shallow ponds (De los Ríos et al., 2007). These differences in mountain water bodies involve different kinds of penetration of natural ultraviolet radiation into the water column (Villafañe et al., 2001). In these scenario, it would observed that the species number is directly related to chlorophyll and humic acid concentrations; this last element provides a natural screen against natural ultraviolet radiation exposure (De los Ríos et al., 2007a, 2008). In these water bodies a similar pattern of calanoid dominance and low species number in oligotrophic status ws observed (De los Ríos & Soto, 2006, 2007).

## POTENTIAL FUTURE TRENDS IN ZOOPLANKTON PHOTOBIOLOGY

The available literature is based on basic experiments with adult specimens of calanoids and cladocerans collected in Argentinean and Chilean southern Patagonian water bodies (Zagarese et al., 1997, 1998; Tartarotti et al., 2000; De los Ríos, 2005, 2007; De los Ríos & Soto, 2005; De los Ríos et al., 2007a) and central Chile (Cabrera et al., 1997), although in northern Chile (18–27°S) there are high levels of natural ultraviolet radiation (Díaz et al., 2006). Unfortunately, there are no studies on photobiology. Also, the available studies have been done with adults specimens, but there are no published studies about the effects of ultraviolet radiation on different life cycle stages, physiological activities, and the effects on individual and population growth. Also, it is necessary to study the sensibility of photoprotective behavior such as migrations (Leech & Williamson, 2001; Alonso et al., 2004) or synthesis of photoprotective substances (Tartarotti et al., 2004). Independently of these kinds of studies, it is necessary undertake uniform protocols and do comparative studies to broaden the understanding of different responses to ultraviolet radiation exposure. On a community level, the literature proposes that natural ultraviolet radiation would be a regulator of zooplankton assemblages in term of species number if we consider that under natural ultraviolet radiation only the tolerant species would be present (Marinone et al., 2006). This would explain the zooplankton assemblages (De los Ríos & Soto, 2006, 2007). In this scenario, it would be necessary to study the zooplankton community structure under different doses of natural ultraviolet radiation; this scenario would require field observations and experimental evidence using short-term and long-term studies.

## ACKNOWLEDGMENTS

The authors express their gratitude to the projects DGI-DCA-01 and DIUFRO 120614, the Chilean Meteorological Direction, and the Research Direction of the Catholic University of Temuco. A portion of this information corresponds to the doctoral thesis of the main

author, which was funded by projects DID-UACH D2001-11, CONICYT-Chile and an IAI project.

## REFERENCES

- Alonso, C., Ricci, V., Barriga, J. P., Battini, M. A. & Zagarese, H. (2004). Surface avoidance by freshwater zooplankton: field evidence on the role of ultraviolet radiation. *Limnology & Oceanography*, 49, 225-232.
- Araya, J. M. & Zúñiga, L. R. (1985). Manual taxonómico del zooplancton lacustre de Chile. *Boletín Limnológico, Universidad Austral de Chile*, 8, 1-110.
- Borgeraas, J. & Hessen, D. O. (2000). UV-B induced mortality and antioxidant enzyme activities in *Daphnia magna* at different oxygen concentrations and temperatures. *Journal of Plankton Research*, 22, 1167-1183
- Bayly, I. A. E. (1993). The fauna of athalassic saline waters in Australia and the Altiplano of South America: comparison and historical perspectives. *Hydrobiologia*, 267, 225-231
- Cabrera, S., López, M. & Tartarotti, B. (1997). Phytoplankton response to ultraviolet radiation in a high altitude Andean lake: short- versus long-term effects. *Journal of Plankton Research*, 19, 1565-1582.
- Campos, H. (1984). Limnological study of Araucanian lakes (Chile). *Verhandlungen International Vereinung für Theoretische und Applied Limnologie*, 22, 1319-1327.
- Campos, H., Arenas, J., Steffen, W., Román, C. & Agüero, G. (1982). Limnological study of lake Ranco (Chile): morphometry, physics and plankton. *Archiv für Hydrobiologie*, 94, 137-171.
- Campos, H., Soto, D., Steffen, W., Agüero, G., Parra, O. & Zúñiga, L. (1994a). Limnological studies in lake del Toro, Chilean Patagonia. *Archiv für Hydrobiologie (Supplement)*, 99, 199-215.
- Campos, H., Soto, D., Steffen, W., Agüero, G., Parra, O. & Zúñiga, L. (1994b). Limnological studies in lake Sarmiento, a subsaline lake from Chilean Patagonia. *Archiv für Hydrobiologie (Supplement)*, 99, 217-234.
- Campos, H., Steffen, W., Agüero, G., Parra, O. & Zúñiga, L. (1983). Limnological studies in lake Villarrica. Morphometry, physics, chemistry and primary productivity. *Archiv für Hydrobiologie (Supplement)*, 71, 37-67.
- Campos, H., Steffen, W., Agüero, G., Parra, O. & Zúñiga, L. (1987a). Limnology of lake Riñihue. *Limnologica*, 18, 339-357.
- Campos, H., Steffen, W., Agüero, G., Parra, O. & Zúñiga, L. (1987b). Estudios limnológicos en el lago Caburgua (Chile). *Gayana Botánica*, 44, 61-84.
- Campos, H., Steffen, W., Agüero, G., Parra, O. & Zúñiga, L. (1988). Limnological study of lake Llanquihue (Chile): morphometry, physics, chemistry and primary productivity. *Archiv für Hydrobiologie (Supplement)* 81, 37-67.
- Campos, H., Steffen, W., Agüero, G., Parra, O. & Zúñiga, L. (1989). Estudios limnológicos en el lago Puyehue (Chile): morfometría, factores físicos y químicos, plancton y productividad primaria. *Medio Ambiente*, 10, 36-53.

- Campos, H., Steffen, W., Agüero, G., Parra, O. & Zúñiga, L. (1990). Limnological study of lake Todos los Santos (Chile): morphometry, physics, chemistry and primary productivity. *Archiv für Hydrobiologie (Supplement)*, 117, 453-484.
- Campos, H., Steffen, W., Agüero, G., Parra, O. & Zúñiga, L. (1992a). Limnological study of lake Ranco (Chile). *Limnología*, 22, 337-353.
- Campos, H., Steffen, W., Agüero, G., Parra, O. & Zúñiga, L. (1992b). Limnological studies of lake Rupanco (Chile): Morphometry, physics, chemistry and primary productivity. *Archiv für Hydrobiologie (Supplement)*, 90, 85-113.
- De los Ríos, P. (2003). *Efectos de las disponibilidades de recursos energéticos, estructurales y de protección sobre la distribución y abundancia de crustáceos zooplanktónicos lacustres chilenos*: Doctoral Thesis, Austral University of Chile, Science Faculty. 1-163.
- De los Ríos P (2004). Lethal effects of ultraviolet radiation on *Neobosmina chilensis* (Cladocera, Bosminidae) exposed to ultraviolet radiation. *Crustaceana*, 77, 989-996.
- De los Ríos, P. (2005). Survival of pigmented freshwater zooplankton exposed to artificial ultraviolet radiation and two levels of dissolved organic carbon. *Polish Journal of Ecology*, 53, 113-116.
- De los Ríos P. (2007). Short term effects of exposition to artificial ultraviolet radiation on *Parabroteas sarsi* (Copepoda, Calanoida). *Biología, Bratislava*, 62, 210-213.
- De los Ríos, P., Acevedo, P., Rivera, R. & Roa, G. (2008). Comunidades de crustáceos litorales de humedales del norte de la Patagonia chilena (38° S): rol potencial de la exposición a la radiación ultravioleta. In: A.V. Volpedo & Fernández L. (Eds.), *Efecto de los cambios globales sobre la biodiversidad*: 209-218. CYTED Programa Iberoamericano de Ciencia y Tecnología para el Desarrollo Red 406RT0285.
- De los Ríos, P., E., Hauenstein, Acevedo, P. & Jaque, X. (2007a). Littoral crustaceans in mountain lakes of Huerquehue National Park (38°S, Araucania Region, Chile). *Crustaceana*, 80, 401-410.
- De los Ríos, P., Acevedo, P. & Verdugo, K. (2007). Survival of *Ceriodaphnia dubia* (Crustacea, Cladocera) exposed to different screens against natural ultraviolet radiation. *Polish Journal of Environmental Studies*, 16, 481-485.
- De los Ríos, P. & Romero-Mieres, M. (2009). Littoral crustaceans in lakes of Conguillío National Park (38°S), Araucania region, Chile. *Crustaceana*, 82, 117-119.
- De los Ríos, P. & Soto, D. (2005). Survival of two species of crustacean zooplankton under to two chlorophyll concentrations and protection or exposure to natural ultraviolet radiation. *Crustaceana*, 78, 163-169.
- De los Ríos, P. & Soto, D. (2006). Effects of the availability of energetic and protective resources on the abundance of daphniids (Cladocera, Daphniidae) in Chilean Patagonian lakes (39°-51°S). *Crustaceana*, 79, 23-32.
- De los Ríos, P. & Soto, D. (2007). Crustacean (Copepoda and Cladocera) zooplankton richness in Chilean Patagonian lakes. *Crustaceana*, 80, 285-296.
- Diaz, S., Camillón, C., Deferrari, G., Fuenzalida, H., Armstrong, R., Booth, C., Paladani, A., Cabrera, S., Casiccia, C., Lovengreen, C., Pedroni, J., Rosales, A., Zagarese, H. & Vernet, M. (2006). Ozone and UV radiation over southern South America: Climatology and Anomalies. *Photochemistry & Photobiology*, 82, 834-843.
- García, P. E., Pérez, A. P., Diéguez, M. C., Ferraro, M. A. & Zagarese, H. E. (2008). Dual control of the levels of photoprotective compounds by ultraviolet radiation and

- temperature in the freshwater copepod *Boeckella antiqua*. *Journal of Plankton Research*, 30, 817-827.
- Hann, B. J. (1986). Revision of the genus *Daphniopsis* Sars 1903 (Cladocera-Daphnidae) and a description of *Daphniopsis chilensis*, new species, from South America. *Journal of Crustacean Biology*, 6, 246-263.
- Hansson, L. A., Hylander, S. & Sommaruga, R. (2009). Escape from UV threats in zooplankton: a cocktail of behavior and protective pigmentation. *Ecology*, 88, 1932-1939.
- Helbling, E. W., Zaratti, F., Sala, L. O., Palenque, E. R., Menchim, C. F. & Villafañe, V. E. (2002). Mycosporine-like aminoacids protect the copepod *Boeckella titicacae* (Harding) against high levels of solar UVR. *Journal of Plankton Research*, 24, 225-234.
- Hylander, S. (2009). Zooplankton responses to threats from UV and predation. PhD Thesis, Department of Ecology, Limnology, University of Lund, Sweden. 1-115.
- Kamjunke, N., Vogt, B. & Wölfl, S. (2009). Trophic interactions of the pelagic ciliate *Stentor* spp. in North Patagonian lakes. *Limnologica*, 39, 107-114.
- Laurion, I., Ventura, M., Catalán, J., Psenner, R. & Sommaruga, R. (2000). Attenuation of ultraviolet radiation in mountain lakes: factors controlling the among and within lake variability. *Limnology & Oceanography*, 45, 1274-1268.
- Leech, D. M. & Williamson, C. E. (2001). In situ exposure to ultraviolet radiation alters the depth distribution in *Daphnia*. *Limnology & Oceanography*, 46, 416-420.
- Lowengreen, C., Ojeda, F. & Montecino, V. (1994). Spectral composition of the aquatic lightfield of the Lakes Rinihue, Todos los Santos, Laguna Negra and El Yeso Reservoir. *Archiv für Hydrobiologie*, 129, 497-509.
- Marinone, M. C., Menu-Marque, S., Añón Suárez, D., Dieguez, M. C., Pérez, A. P., De los Ríos, P., Soto, D. & Zagarese, H. E. (2006). UV radiation as a potential driving force for zooplankton community structure in Patagonian lakes. *Photochemistry & Photobiology*, 82, 962-971.
- Modenutti, B. E., Balseiro, E. G., Queimaliños, C. P., Añón Suárez, D. A., Dieguez, M. C. & Albariño, R. J. (1998). Structure and dynamics of food webs in Andean lakes. *Lakes Reservoirs, Research and its Management*, 3, 179-189.
- Morris, D. P., Zagarese, H. E., Williamson, C. E., Balseiro, E. G., Hargreaves, B. R., Modenutti, B. E., Moeller, R. E. & Queimaliños, C. P. (1995). The attenuation of solar UV radiation in lakes and the role of dissolved organic carbon. *Limnology & Oceanography*, 40, 1381-1391.
- Pedrozo, F., Chillrud, S., Temporetti, P. & Díaz, M. (1993) Chemical composition and nutrient limitation in river and lakes of northern Patagonian Andes (39.5–42°S, 71°W) (Rep. Argentina). *Verhandlungen International Vereinigung für Theoretische und Applied Limnologie*, 25, 207-214.
- Quiros, R. & Drago, E. (1999) The environmental state of Argentinean lakes: an overview. *Lakes Reservoirs, Research and its Management*, 4, 55-64.
- Rautio, M. & Korkhola, A. (2002a). UV-Induced pigmentation in subarctic *Daphnia*. *Limnology & Oceanography*, 47, 295-299.
- Rautio, M. & Korkhola, A. (2002b). Impacts of UV radiation on the survival of some key subarctic crustaceans. *Polar Biology*, 25, 460-468.
- Rhode, S. C., Pawlowski, M. & Tollrian, R. (2001). The impact of ultraviolet radiation on the vertical distribution of zooplankton of the genus *Daphnia*. *Nature, London*, 412, 69-72.

- Rocco, V. E., Opezzo, O., Pizarro, R., Sommaruga, R., Ferraro, M. & Zagarese, H. E. (2002). Ultraviolet damage and counteracting mechanisms in the freshwater copepod *Boeckella poppei* in the Antarctic Peninsula. *Limnology & Oceanography*, 47, 829-836.
- Soto, D. & Campos, H. (1995). Los lagos oligotróficos del bosque templado húmedo del sur de Chile. In: J. Armesto, M. Khalin, & M Villagrán (Eds.), *Ecología del Bosque Chileno*: 134-148. Editorial Universitaria, Santiago de Chile.
- Soto D., Campos, H., Steffen, W., Parra, O. & Zúñiga, L. (1994). The Torres del Paine lake district (Chilean Patagonia): a case of potentially N-limited lakes and ponds. *Archiv für Hydrobiologie*, 99, 181-197.
- Soto, D. & De los Ríos, P. (2006). Trophic status and conductivity as regulators of daphniids dominance and zooplankton assemblages in lakes and ponds of Torres del Paine National Park. *Biologia, Bratislava*, 61, 541-546.
- Soto, D. & Stockner, J. G. (1996). The temperate rain forest lakes of Chile and Canada: comparative ecology and sensitivity to anthropogenic change. In: R. Lawford, P. Alaback & E. Fuentes (eds.), *High latitude rain forest of the west coast of the Americas. Climate, hydrology, ecology and conservation*: 266-280. Springer-New York, USA.
- Soto, D. & Zúñiga, L. R. (1991). Zooplankton assemblages of Chilean temperate lakes: a comparison with North American counterparts. *Revista Chilena de Historia Natural*, 64, 569-581.
- Steinhart, G. S., Likens, G. E. & Soto, D. (1999). Nutrient limitation in Lago Chaiquenes (Parque Nacional Alerce Andino, Chile): evidence from nutrient experiments and physiological assays. *Revista Chilena de Historia Natural*, 72, 559-568.
- Steinhart, G. S., Likens, G. E. & Soto, D. (2002) Physiological indicators of nutrient deficiency in phytoplankton of southern Chilean lakes. *Hydrobiologia*, 489, 21-27.
- Storz, U. C. & Paul, R. J. (1998). Phototaxis in water fleas (*Daphnia magna*) is differently influenced by visible and UV light. *Journal of Compared Physiology (A)*, 183, 709-717.
- Tartarotti, B., Baffico, G., Temporetti, P. & Zagarese, H. (2004). Mycosporine-like amino acids in planktonic organisms living under different UV exposure conditions in Patagonian lakes. *Journal of Plankton Research*, 26, 753-762.
- Vareschi, E. & Wubbens, D., (2001). Vertical migration of *Daphnia pulex* in response to UV radiation. *Verhandlungen International Vereinung für Theoretische und Applied Limnologie*, 27, 3349-3353.
- Villafañe, V. E., Barbieri, E. S. & Helbling, W. E. (2004). Annual patterns of ultraviolet radiation effects on temperate marine phytoplankton of Patagonia Argentina. *Journal of Plankton Research*, 26, 167-174.
- Villafañe, V. E., Helbling, E. W. & Zagarese, H. E. (2001). Solar ultraviolet radiation and its impact on aquatic ecosystems of Patagonia, South America. *Ambio*, 30, 112-117.
- Villalobos, L. (1994). Distribution of *Daphnia* in high mountain and temperate lakes of South America. *Verhandlungen International Vereinung für Theoretische und Applied Limnologie*, 25, 2400-2404.
- Villalobos, L. (1999). Determinación de capacidad de carga y balance de fósforo y nitrógeno de los lagos Riesco, Los Palos, y Laguna Escondida en la XI región. Technical Report Fisheries Research Foundation-Chile, FIP-IT/97-39.
- Villalobos, L. (2002). Comparison of the filtration structures in South American *Daphnia*. *Archiv für Hydrobiologie*, 154, 647-663.

- Villalobos, L. & Geller, W. (1997). Setular bosses: Report of a new ultrafine structure on the filter appendages of *Daphnia*. *Archiv für Hydrobiologie*, 140, 565-575.
- Villalobos, L., Parra, O., Grandjean, M., Jaque, E., Wölfl, S. & Campos, H. (2003). River basin and limnological study in five humic lakes of the Chiloé Island. *Revista Chilena de Historia Natural*, 76, 10-15.
- Villalobos, L., Wölfl, S., Parra, O. & Campos, H. (2003). Lake Chapo: a baseline of a deep, oligotrophic North Patagonian lake prior to its use for hydroelectricity generation: II. Biological properties. *Hydrobiologia*, 510, 225-237.
- Villafañe, V. E., Helbling, E. W. & Zagarese, H. E. (2001). Solar ultraviolet radiation and its impact on aquatic ecosystems of Patagonia, South America. *Ambio*, 30, 112-117.
- Winder, M. (2001). Zooplankton ecology in high mountain lakes: 1-157. Doctoral Thesis submitted to the Swiss Federal Institute of Technology, Zürich, Switzerland.
- Wölfl, S. (1996). Untersuchungen zur Zooplanktonstruktur einschliesslich der mikrobiellen Gruppen unter besonderer Berücksichtigung der mixotrophen Ciliaten in zwei Südchilenischen Andenfußseen: 1-242. (Doctoral Thesis, Universität Konstanz).
- Woelfl, S. (2007). The distribution of large mixotrophic ciliates (*Stentor*) in deep North Patagonian lakes (Chile): First results. *Limnologica*, 37, 28-36.
- Woelfl, S. & Geller, W. (2002). Chlorella-bearing ciliates dominant in an oligotrophic North Patagonian lake (Pirihueico lake, Chile): abundance, biomass and symbiotic photosynthesis. *Freshwater Biology*, 47, 231-242.
- Wölfl, S., Villalobos L. & Parra, O. (2003). Trophic parameters and method validation in a Lake Riñihue (North Patagonia, Chile) from 1978 to 1997. *Revista Chilena de Historia Natural*, 76, 459-474.
- Zagarese, H. E., Feldman, M. & Williamson, C. E. (1997a). UV-B induced damage and photoreactivation in three species of *Boeckella* (Copepoda, Calanoida). *Journal of Plankton Research*, 19, 357-367.
- Zagarese, H. E., Williamson, C. E., Vail, T. L., Olsen, O. & Queimaliños, C. P. (1997b). Long term exposure of *Boeckella gibbosa* (Copepoda, Calanoida) to in situ levels of solar UVB radiation. *Freshwater Biology*, 37, 99-106.
- Zagarese, H. E., Tartarotti, B., Cravero, W. & González, P. (1998). UV damage in shallow lakes: the implications of water mixing. *Journal of Plankton Research*, 20, 1423-1433.
- Zellmer, I. D. (1996). The impact on UV-B tolerance and recovery from UV-B damage in *Daphnia pulex*. *Hydrobiologia*, 319, 87-92.
- Zellmer, I. D. (1999). The effects of natural UVA and UVB on subarctic *Daphnia pulicaria* in its natural habitat. *Hydrobiologia*, 379, 55-62.



## ***Chapter 10***

# **FOLIC ACID - AN IMPORTANT FACTOR FOR SKIN HOMEOSTASIS AND REPAIR**

***Anja Knott, Heiko Mielke, Katja Reuschlein, Sören Jaspers,  
Urte Koop, Franz Stäb, Horst Wenck and Stefan Gallinat*** \*

Research & Development, Beiersdorf AG, Unnastrasse 48, 20245 Hamburg, Germany.

## **ABSTRACT**

For decades, it has been widely accepted that folates play a central role in cell metabolism, cell turnover and DNA repair. Despite the abundant food supply, insufficient folate status has been named one of the most frequent vitamin deficiencies in the industrialized world. Accordingly, a number of epidemiological studies correlated inadequate folate supply with an increased incidence for certain diseases.

Human skin represents the outermost barrier of the body. The epidermal compartment undergoes a life-long renewal process and the skin is constantly exposed to environmental factors, such as ultraviolet (UV) irradiation. Until recently, however, only very little was known about the effects of folates on human skin and its importance for tissue homeostasis was certainly underappreciated.

A number of both *in vitro* and *in vivo* studies were published that now help to elucidate the function folates play in the skin, particularly during the process of photoaging. Altogether, these studies demonstrated that topically applied folic acid is bioavailable for human skin, that its cellular up-take is significantly increased upon UV irradiation and that topical application improves epidermal regeneration *in vivo*, to name a few effects. Although many questions still need to be addressed the available literature appears to support the notion that folates play an important role for skin homeostasis and that this crucial vitamin serves to facilitate the cellular response following solar irradiation.

---

\* Corresponding author: Beiersdorf AG, Research & Development, Department of Skin Research & Skin Structure, Bf. 519, Unnastrasse 48, 20245 Hamburg, Germany, Phone: ++49-40-4909-5829, Fax: ++49-40-4909-6770, Email: stefan.gallinat@beiersdorf.com

## INTRODUCTION

Human skin represents the outermost barrier of the body and is as such constantly affected by internal and external influences. As a consequence, age-associated changes develop that contribute to the phenotypical changes that are clinically evident. The relevant intrinsic factors contributing to skin aging comprise the genetic background and hormonal changes, to name two main factors. However, cutaneous aging is influenced to a much larger extent by extrinsic stimuli which mainly consist of the exposure to solar ultraviolet (UV)A and (UV)B irradiation. Sun exposure induces both short- and long-term effects. The acute effects include well-known phenomena such as suntan, vitamin D synthesis but also sunburn. On the other hand, long-term effects of chronic UV irradiation contribute to accelerated skin aging (coined photo-aging) but can also lead to actinic keratosis and even carcinogenesis. These features are ultimately the result of damages to subcellular compartments, cells and macromolecules [Grether-Beck et al., 2005].

The damage inflicted by UV irradiation occurs in both epidermis and dermis and comprises many facets, depending on the type of UV irradiation [Scharffetter-Kochanek et al., 1997]. These alterations contribute substantially to the biomechanical changes which manifest themselves in variable epidermal thickness, dermal elastosis, decreased/fragmented collagen, increased matrix-degrading metalloproteinases, inflammatory infiltrates and vessel ectasia [Yaar and Gilchrest, 2007]. The resulting visible skin changes include loss of firmness and elasticity as well as wrinkle formation [Kligman, 1989].

For obvious reasons, several cutaneous mechanisms exist that serve to effectively protect the skin from internal and external harm. Besides its powerful antioxidant systems, skin coloration as a result of melanogenesis is a means that reduces the detrimental effects of solar irradiation. By absorbing harmful UV light melanin acts as a shield for skin cells as well as the extracellular compartments and serves as a natural sun protection system. This protective mechanism is also of major relevance for protecting the water-soluble vitamin folic acid from degradation. Interestingly, this particular mechanism has been suggested to play a role in the evolution of human skin color [Jablonski and Chaplin, 2000]. The fact that folates are sensitive to UV irradiation led to the hypothesis that a highly melanized skin protects against UV-induced photolysis of folates [Roe, 1987; Suh et al., 2001]. Accordingly, the degree of skin color might be a compromise regulating the extent of UV light that reaches the viable layers of the skin [Branda and Eaton, 1978; Jablonski and Chaplin, 2000]. As hominids migrated outside of the tropics, varying degrees of de-pigmentation developed in order to permit adequate UVB-induced synthesis of vitamin D<sub>3</sub>. On the contrary, skin pigmentation needs to be dark enough to protect cutaneous folate levels.

Folates are not only essential for normal cell growth and metabolism, but they are also involved in DNA synthesis and repair. Recent dermatological studies indicate that folates play an important role also in skin homeostasis. Here, we discuss the latest scientific findings with a special focus on the role of folates during the process of photo-aging. First, relevant facts about folates are given, followed by an overview presenting *in vitro* and *in vivo* studies elucidating the current knowledge with respect to folate function in the skin.

## Folic Acid – Discovery and Biochemical Function

In the early nineteen thirties, a scientist named Dr. Lucy Wills observed that yeast extract was effective in treating anemia in pregnant women. In the late 1930s, folate was identified as the corrective substance in yeast extract and was later extracted as a pure compound from spinach leaves in 1941 [Mitchell et al.]. The term ‘folate’ originates from the Latin word ‘folium’ for leaf. This vitamin, also named vitamin B9, exists in a number of different forms, which occur naturally in different food sources such as leafy green vegetables, citrus fruits and juices, and dried beans and peas [U.S. Department of Agriculture, 2003; Rampersaud et al., 2003]. To maintain an adequate folate status, however, folates have to be taken up with the diet since mammals do not have the ability to synthesize this vitamin.

The entire human body contains between 5-10 mg of folic acid with approx. 50% being present in the liver [Thamm et al., 1998]. As reported by the Institute of Medicine in the U.S., the recommended dietary allowance (RDA) for adults  $\geq 19$  years is 400  $\mu\text{g}/\text{day}$  [Bailey, 2004]. However, women in the childbearing age, pregnant and lactating women do require substantially higher amounts of folic acid since an optimal maternal folate status reduces the risk of neural tube defects in the offspring. Also, a number of common medications, including certain anti-tumor agents, increase the requirements for dietary folate [Bailey, 1990]. Importantly, folate status is negatively affected by several dietary factors and lifestyle (e.g. smoking).

An insufficient folate status has been named by several authors as the most frequent vitamin deficiency in the industrialized world [Senti and Pilch, 1985; Rasmussen et al., 2000]. In 1996, the U.S. Food and Drug Administration (FDA) published regulations to prevent folate deficiencies requiring the addition of folic acid to a variety of food sources including enriched breads, cereals and other grain products [Oakley et al., 1996; Malinow et al., 1998; Daly et al., 1997; Crandall et al., 1998]. Since cereals and grains are widely consumed in the U.S., these products have become a very important contributor of folic acid to the American diet.

Folates function as a carbon donor for the synthesis of purines and thymidine and are involved in cell turnover. Folate is also essential for the metabolism of homocysteine, and helps maintain normal levels of this amino acid. The discovery of the link between insufficient folic acid intake and the incidence of neural tube defects [Bailey et al., 2003] emphasizes that an adequate folate status is essential throughout gestation to guarantee normal development and growth.

In dermatology, it was shown that folate deficiency occurs in patients with psoriasis. This deficiency inversely correlates with plasma homocysteine levels and with psoriasis severity [Vanizor et al., 2003; Hild, 1969; Malerba et al., 2006; Gisondi et al., 2007]. Folic acid supplementation has been utilized to limit the toxicity of methotrexate which is used as a standard systemic therapy for severe psoriasis and rheumatoid arthritis [Prey and Paul, 2009]. Folate was further utilized in the treatment of oral ulcers from methotrexate and it has been shown to inhibit gingival hyperplasia from phenytoin use and pregnancy [Thomas and Pack, 1982; Drew et al., 1987; Barrett, 1986].

With respect to normal skin, however, there is only very little knowledge regarding the specific role of folates. A number of both *in vitro* and *in vivo* studies were recently published that now help to elucidate the function folates take over in the skin.

## UV Exposure and Cellular Folic Acid Requirements

UVA and UVB irradiation penetrate human skin to a different extent. While UVB is mostly absorbed by the epidermis a substantial amount of UVA is able to penetrate into the dermal layer. Accordingly, keratinocytes and fibroblasts are damaged by UVA and UVB inducing various mechanisms of action. Considering the above mentioned role of folic acid in DNA protection and repair on the one hand and the UV-induced photolysis of the vitamin itself on the other hand one could speculate that cellular demand for this vitamin is increased in sun-exposed skin.

In this context, our recent work investigated to which extent cultured human dermal fibroblasts (HDF) take up folic acid and whether this process is affected by UV irradiation. In this context it is important to note that folic acid represents the synthetic form of the vitamin while different chemical forms of folates occur naturally. Effects of UV exposure were determined by subjecting cultured cells to 135 mJ/cm<sup>2</sup> solar simulated irradiation (SSR). The results demonstrate that HDF were indeed able to dose-dependently take up folic acid from the cell culture medium [Knott et al., 2007]. This indicates that dermal cells make use of an external folic acid supply to balance their intracellular folate status. Even more important, compared to control cells, these cells also increased their intracellular folate levels after exposure to UV irradiation [Knott et al., 2007]. Overall, these observations demonstrated for the first time that skin cells take up extracellular folic acid and exhibit a higher demand in times of cellular stress provided that sufficient amounts of folic acid were supplied externally.

Multiple carrier-mediated processes are involved in the cellular internalization of folates in a variety of mammalian cell types. The reduced-folate carrier-1 (RFC-1) is the major transport system for folates in mammalian cells and tissues [Matherly, 2001]. This carrier serves to maintain sufficient levels of intracellular folates to support the biosynthesis of purines, pyrimidines, serine and methionine which play a central part in one-carbon transfer reactions required for normal cell metabolism [Bailey and Gregory III, 1999]. It is speculated that a decreased RFC-1 expression in human tissues contributes to disease states associated with an inadequate folate status [Whetstine et al., 2002]. As mentioned before, a large body of evidence indicates that an insufficient folate intake exhibits negative effects on a variety of physiological processes [Rampersaud et al., 2003]. Interestingly, it has been shown in this context that following UV irradiation RFC-1 expression was significantly enhanced in full-thickness skin biopsies. These effects were observed in both human epidermis and dermis with the dermal compartment displaying higher baseline levels. Even 72 hrs after UV exposure an enhanced RFC-1 gene expression was still detectable [Knott et al., 2007]. This observation suggests that the cellular up-take of folic acid in the skin is, at least in part, mediated by the RFC-1 carrier.

## Bioavailability of Folic Acid *in vivo*

Evidently, folic acid affects the physiology of skin cells. As for other tissues and organs of the human body it can be hypothesized that insufficient levels of this vitamin impair cell function. A possibility to, at least in part, compensate for such a deficit would be to topically

apply this compound. The prerequisite for increasing cutaneous folic acid levels, however, is a sufficient penetration through healthy human skin.

We addressed this issue recently in an *in vivo* study and showed that folic acid is indeed able to penetrate healthy human skin [Knott et al., 2007]. Volunteers treated one of their forearms in a home-in-use study twice daily with a folic acid-containing formulation. This special cream, containing 0.03% folic acid, largely resembled commercially available cosmetic formulations but was optimized in terms of folic acid stability. For experimental studies, synthetic folic acid was used since it is more easily absorbed than naturally occurring food folates. Specifically, it does not require enzymatic cleavage prior to absorption [Rampersaud et al., 2003] and displays an enhanced chemical stability. To determine bioavailability *in vivo*, suction blisters were induced by application of negative pressure [Südel et al., 2003] and folic acid concentration was determined in the respective suction blister fluids *ex vivo*. Interestingly, compared to untreated control areas, folic acid concentration was substantially increased after 4 week treatment with the respective test formulation. These results clearly indicate that folic acid exhibits physico-chemical properties (i.e.  $\log P = -2.63 \pm 0.85$  and a molecular weight of 441.4g) that allow for penetration through the skin barrier making this vitamin bioavailable in human skin after topical application.

## Folic Acid and DNA Repair

It is widely accepted that folic acid is crucial for DNA synthesis and repair. Studies have demonstrated that an improper folic acid status is associated with chromosomal damage and gene mutations [Everson et al., 1988; Branda et al., 1991; Branda et al., 1992; Blount, 1997; Fenech et al., 1997]. Folate deficiency impairs DNA excision repair in rat colonic mucosa [Choi et al., 1998] and is also associated with suboptimal DNA repair capacity in peripheral blood lymphocytes [Wei et al., 2003]. As described by Duthie and Hawdon DNA strand breakage and uracil misincorporation increased after lymphocytes were cultured with decreasing amounts of folic acid. While normal DNA repair processes remove the uracil, continually limited folate availability may ultimately induce double strand breakage, chromosome instability, and cancer [Reidy, 1987; MacGregor et al., 1990; Blount and Ames, 1995].

In addition, lack of proper folate supply affects methyl metabolism by depleting cellular S-adenosyl methionine (SAM) levels, causing DNA hypomethylation and inappropriate activation of proto-oncogenes [Wainfan and Poirier, 1992; Balaghi and Wagner, 1993; Pogribny et al., 1995]. Decreased DNA methylation is associated with an increased risk of some forms of cancer [Fang et al., 1997]. Together, these findings demonstrate an important role of folic acid in genomic stability and DNA repair.

Due to its central function in cellular homeostasis, sufficient folate levels are crucial specifically for cells that are highly proliferating (e.g. keratinocytes in the skin) and that are exposed to exogenous stress such as UV irradiation. Since DNA damage is considered a major contributing factor for accelerated skin aging topical agents that help to protect the DNA from exogenous insult and/or help to repair existing DNA damage are in the center of scientific attention. Interestingly, in a recent study [Burger et al., 2007] it was demonstrated that folic acid improved the DNA repair capacity also in human skin cells. Employing a so-

called host cell reactivation assay to determine cellular DNA repair capacity, Burger et al. demonstrated that folic acid supplementation increased nucleotide excision repair of cultured HDF. These data are in line with observations showing that topical application of a folic acid-containing formula protects from UV-induced DNA damage *in vivo* [Knott et al., 2008a and b]. Altogether these recent findings suggest that folic acid elicits different effects that help to protect and repair the DNA in human skin cells. Future investigations will, however, have to address this issue in more detail to corroborate the findings and to further elucidate the underlying molecular mechanisms.

## Improvement of Epidermal Re-Epithelialization and Cell Turnover

The crucial role of folic acid for cell proliferation has been established and well accepted. This is particularly evident considering the folic acid-dependent synthesis of purines/thymidine and the proliferation of lymphocytes and *lactobacillus casei*. Also, certain diseases (e.g. megaloblastic anemia) are the result of a folic acid deficiency or are treated (e.g. certain cancers) with folic acid antagonists.

With regard to the declining epidermal turnover rate in aging skin, it was speculated that folic acid has the capability to stimulate keratinocyte proliferation. This hypothesis is supported by *in vitro* data demonstrating effects on the re-epithelialization rate of skin models. In this study, organotypical EpiDerm™ models were treated with a combination of folic acid and creatine and re-epithelialization following injury was evaluated by determination of trans epithelial electric resistance (TEER) as a measure of skin barrier integrity. Creatine represents a natural body substance occurring in all vertebrates. It plays a key role in the energy homeostasis in every human cell to efficiently cope with alternating energy demands. Interestingly, the results of this study show that treatment with folic acid and creatine accelerates epithelial repair significantly after 48 hrs compared to untreated control skin models.

With regard to the *in vivo* situation, one study has been published so far that addresses the issue of epidermal turnover in more detail. Here, it was hypothesized that skin cells would benefit from a topical treatment with folic acid and creatine for several reasons. First, folic acid is essential to maintain an effective DNA protection and repair [Bailey and Gregory III, 1999]. Second, topical folic acid is readily taken up by human skin [Knott et al., 2007]. Third, creatine exerts DNA-protective effects, boosts collagen levels by enhancing cellular energy supply [Krutmann, 2001; Berneburg et al., 2005; Lenz et al., 2005] and improves the appearance of mature skin [Blatt et al., 2005].

The size of corneocytes represents a widely accepted indicator of turnover time of human epidermis. Accordingly, epidermal renewal was evaluated by measurement of corneocyte size with smaller sizes indicating improved skin regeneration [Hölzle and Plewig, 1977; Grove, 1979]. Interestingly, already after a 4 week application of the test formulation epidermal turnover was significantly improved as evidenced by smaller corneocytes derived from the treated sites in contrast to the vehicle-treated sites. Importantly, these folic acid- and creatine-mediated effects were observed at all time points investigated, thus, clearly supporting the hypothesis that folic acid and creatine are important for epidermal turnover [Knott et al. 2007].

## CONCLUSION

Increasing scientific evidence supports the notion that folic acid not only plays a crucial role for cutaneous homeostasis but also elicits a variety of beneficial effects on photo-aged human skin. Recent scientific evidence suggests that the cellular demand for folic acid is substantially increased following exogenous stress. The cellular up-take is increased and the expression of a major folate transporter, RFC-1, is significantly enhanced. Available data indicate a folic acid-mediated increased DNA repair capacity as well as beneficial effects on DNA protection and epidermal regeneration by folic acid-containing topical formulations. Based on these findings it appears that this water-soluble vitamin offers an effective treatment option for chronically sun-exposed human skin. Ongoing research is targeted on identifying the underlying molecular mechanisms that ultimately induce these clinically relevant effects.

## REFERENCES

- Bailey, LB. Folate and vitamin B12 recommended intakes and status in the United States. *Nutr. Rev.*, 2004, 62(6 Pt 2), S14-S20.
- Bailey, LB. Folate status assessment. *J. Nutr.*, 1990, 120(S11), 1508-1511.
- Bailey, LB; Gregory, JF III. Folate metabolism and requirements. *J Nutr.*, 1999, 129, 779-782.
- Bailey, LB; Rampersaud, GC; Kauwell, GPA. Folic acid supplements and fortification affect the risk for neural tube defects, vascular disease and cancer: evolving science. *J Nutr.*, 2003, 133, 1961S-1968S.
- Balaghi, M; Wagner, C. DNA methylation in folate deficiency : use of CpG methylase. *Biochem. Biophys. Res. Commun.*, 1993, 193(3), 1184-1190.
- Barrett, AP. Topical folinic acid therapy in methotrexate-induced oral ulceration. *J Periodontol.*, 1986, 57(5), 318-320.
- Berneburg, M; Gremmel, T; Kurten, V; Schroeder, P; Hertel, I; von Mikecz, A et al. Creatine supplementation normalizes mutagenesis of mitochondrial DNA as well as functional consequences. *J Invest Dermatol.*, 2005, 125, 213-220.
- Blatt, T; Lenz, H; Koop, U; Jaspers, S; Weber, T; Mumment, C et al. Stimulation of skin's energy metabolism provides multiple benefits for mature human skin. *Biofactors*, 2005, 25(1-4), 179-185.
- Blount, BC. Folate deficiency causes uracil misincorporation into human DNA and chromosomal breakage: implications for cancer and neuronal damage. *Proc Natl Acad Sci USA*, 1997, 94, 3290-3295.
- Blount, BC; Ames, BN. DNA damage in folate deficiency. *Bailliere's Clinical Haematology*, 1995, 8(3), 461-478.
- Branda, RF; Eaton, JW. Skin color and nutrient photolysis: an evolutionary hypothesis. *Science*, 1978, 201, 625-626.
- Branda, RF; O'Neill, JP; Jacobson-Kram, D; Albertini, RJ. Factors influencing mutation at the hprt locus in T-lymphocytes: studies in normal women and women with benign and malignant breast cancer. *Environ. Mol. Mutagen.*, 1992, 19, 274-281.

- Branda, RF; O'Neill, JP; Sullivan, LM; Albertini, RJ. Factors influencing mutation at the hprt locus in T-lymphocytes: women treated for breast cancer. *Cancer Res.*, 1991, 51, 6603-6607.
- Burger, K; Kieser, N; Gallinat, S; Mielke, H; Knott, A; Bergemann, J. The influence of folic acid depletion on the Nucleotide Excision Repair capacity of human dermal fibroblasts measured by a modified Host Cell Reactivation Assay. *Biofactors.*, 2007, 31(3-4), 181-190.
- Choi, SW; Kim, YI; Weitzel, JN; Mason, JB. Folate depletion impairs DNA excision repair in the colon of the rat. *Gut*, 1998, 43, 93-99.
- Crandall, BF; Corson, VL; Evans, MI; Goldberg, JD; Knight, G; Salafsky, IS. American College of Medical Genetics statement on folic acid: Fortification and supplementation. *Am J Med Genet*, 1998, 78, 381.
- Daly, S; Mills, JL; Molloy, AM; Conley, M; Lee, YJ; Kirke PN. et al. Minimum effective dose of folic acid for food fortification to prevent neural-tube defects. *Lancet*, 1997, 350, 1666-1669.
- Drew, HJ; Vogel, RI; Molofsky, W; Baker, H; Frank O. Effect of folate on phenytoin hyperplasia. *J Clin Periodontol*, 1987, 14, 350-356.
- Duthie, SJ; Hawdon, A. DNA instability (strand breakage, uracil misincorporation, and defective repair) is increased by folic acid depletion in human lymphocytes in vitro. *FASEB J.*, 1998, 12, 1491-1497.
- Everson, RB; Wehr, CM; Erexon, GL; MacGregor, JT. Association of marginal folate depletion with increased human chromosome damage in vivo: demonstration by analysis of micronucleated erythrocytes. *J. Natl. Cancer Inst.*, 1988, 80, 525-529.
- Fang, JY; Xiao, SD; Zhu, SS; Yuan, JM; Qiu, DK; Jiang, SJ. Relationship of plasma folic acid and status of DNA methylation in human gastric cancer. *J. Gastroenterol.*, 1997, 32(2), 171-175.
- Fenech, MF; Dreosti, IE; Rinaldi, JR. Folate, vitamin B12, homocysteine status and chromosomal damage rate in lymphocytes of older men. *Carcinogenesis*, 1997, 18, 1329-1336.
- Gisondi, P; Fantuzzi, F; Malerba, M; Girolomoni, G. Folic acid in general medicine and dermatology. *J Dermatolog Treat.*, 2007, 18(3), 138-146.
- Grether-Beck, S; Wlaschek, M; Krutmann, J; Scharffetter-Kochanek, K. Photodamage and photoaging - prevention and treatment. *J Dtsch Dermatol Ges.*, 2005 3 Suppl 2, S19-25.
- Grove, GL. Exfoliative cytological procedures as a nonintrusive method for dermatogerontological studies. *J Invest Dermatol*, 1979, 73, 67-69.
- Hild, DH. Folate losses from the skin in exfoliative dermatitis. *Arch Intern Med.*, 1969, 123(1), 51-57.
- Hölzle, E; Plewig, GJ. Effects of dermatitis, stripping and steroids on the morphology of corneocytes. A new bioassay. *J Invest Dermatol*, 1977, 68, 350-356.
- Jablonski, NG; Chaplin, G. The evolution of human skin coloration. *J Hum Evol*, 2000, 39(1), 57-106.
- Kligman, LH. Photoaging, manifestations, prevention and treatment. *Clin Geriatr Med*, 1989, 5(1), 235-251.
- Knott, A; Koop, U; Mielke, H; Reuschlein, K; Peters, N; Muhr, GM et al.. A novel treatment option for photoaged skin. *J Cosmet Dermatol.*, 2008a, 7(1), 15-22.

- Knott, A; Koop, U; Mielke, H; Reuschlein, K; Peters, N; Muhr, G-M et al. Folic acid and creatine improve the clinical signs of aging. *SOFW Journal - Seifen Ole Fette Wachse*, 2008b, 134(8), 14-21.
- Knott, A; Mielke, H; Koop, U; Wolber, R; Burkhardt, T; Vietzke, JP et al. Folic acid: cellular uptake and penetration into human skin. *J Invest Dermatol.*, 2007, 127(10), 2463-2466.
- Krutmann, J. New developments in photoprotection of human skin. *Skin Pharmacol Appl Skin Physiol*, 2001, 14, 401-407.
- Lenz, H; Schmidt, M; Welge, V; Schlattner, U; Wallimann, T; Elsässer, HP et al. The creatine kinase system in human skin: protective effects of creatine against oxidative and UV damage in vitro and in vivo. *J Invest Dermatol*, 2005, 124(2), 443-452.
- MacGregor, JT; Schlegel, R; Wehr, CM; Alperin, P; Ames, BN. Cytogenetic damage induced by folate deficiency is enhanced by caffeine. *Proc. Natl. Acad. Sci. USA*, 1990, 7(24), 9962-9965.
- Malerba, M; Gisondi, P; Radaeli, A; Sala, R; Calzavara Pinton, PG; Girolomoni, G. Plasma homocysteine and folate levels in patients with chronic plaque psoriasis. *Br J Dermatol.*, 2006, 155(6), 1165-1169.
- Malinow, MR; Duell, PB; Hess, DL; Anderson, PH; Kruger, WD; Phillipson, BE et al. Reduction of plasma homocyst(e)ine levels by breakfast cereal fortified with folic acid in patients with coronary heart disease. *N Engl J Med*, 1998, 338, 1009-1015.
- Matherly, LH. Molecular and cellular biology of the human reduced folate carrier. *Prog Nucleic Acid Res Mol Biol*, 2001, 67, 131-162.
- Mitchell, HK; Snell, EE; Williams, RJ. The concentrations of "folic acid". *J. Am. Chem. Soc.*, 1941, 63, 2284.
- Oakley, GP Jr; Adams, MJ; Dickinson, CM. More folic acid for everyone, now. *J Nutr*, 1996, 126, 751S-755S.
- Pogribny, IP; Basnakian, AG; Miller, BJ; Lopatina, NG; Poirier, LA; James, SJ. Breaks in genomic DNA and within the p53 gene are associated with hypomethylation in livers of folate/methyl-deficient rats. *Cancer Res.*, 1995, 55(9), 1894-1901.
- Prey, S; Paul, C. Effect of folic or folinic acid supplementation on methotrexate-associated safety and efficacy in inflammatory disease: a systematic review. *Br J Dermatol.*, 2009, 160(3), 622-628.
- Rampersaud, GC; Kauwell, GPA; Bailey, LB. Folate: a key to optimizing health and reducing disease risk in the elderly. *J Am College Nutr*, 2003, 22(1), 1-8.
- Rasmussen, LB; Ovesen, L; Bulow, I; Knudsen, N; Laurberg, P; Perrild, H. Folate intake, lifestyle factors, and homocysteine concentrations in younger and older women. *Am J Clin Nutr*, 2000, 72(5), 1156-1163.
- Reidy, JA. Folate- and deoxyuridine-sensitive chromatid breakage may result from DNA repair during G2. *Mut Res*, 1987, 192(3), 217-219.
- Roe, DA. Photodegradation of carotenoids in human subjects. *Fed Proc.*, 1987, 46(5), 1886-1889.
- Scharffetter-Kochanek, K; Wlaschek, M; Brenneisen, P; Schauen, M; Blaudschun, R; Wenk, J. UV-induced reactive oxygen species in photocarcinogenesis and photoaging. *Biol Chem*, 1997, 378, 1247-1257.
- Senti, FR; Pilch, SM. Analysis of folate data from the Second National Health and Nutrition Examination Survey (NHANES II). *J. Nutr.*, 1985, 115, 1398-1402.

- Südel, KM; Venzke, K; Knußmann-Hartig, E; Moll, I; Stäb, F; Wenck, H et al. Tight control of matrix metalloproteinase-1 activity in human skin. *Photochem Photobiol*, 2003, 78(4), 840-845.
- Suh, JR; Herbig, AK; Stover, PJ. New perspectives on folate catabolism. *Annu Rev Nutr.*, 2001, 21, 255-282.
- Thamm, M; Mensink, GB; Hermann-Kunz, E. Folic acid status, *Gesundheitswesen.*, 1998, 60 Suppl 2, S87-88.
- Thomas, ME; Pack, AR. Effects of extended systemic and topical folate supplementation on gingivitis of pregnancy. *J Clin Periodontol*, 1982, 9, 275-280.
- U.S. Department of Agriculture, Agricultural Research Service. 2003. USDA National Nutrient Database for Standard Reference, Release 16. Nutrient Data Laboratory Home Page, [http://www.nal.usda.gov/fnic/cgi-bin/nut\\_search.pl](http://www.nal.usda.gov/fnic/cgi-bin/nut_search.pl).
- Vanizor Kural, B; Orem, A; Cimşit, G; Uydu, HA; Yandi, YE; Alver, A. Plasma homocysteine and its relationships with atherothrombotic markers in psoriatic patients. *Clin Chim Acta.*, 2003, 332(1-2), 23-30.
- Wainfan, E; Poirier, LA. Methyl groups in carcinogenesis: effects on DNA methylation and gene expression. *Cancer Res.*, 1992, 52(7), S2071-S2077.
- Wei, Q; Shen, H; Wang, LE; Duphorne, CM; Pillow, PC; Guo Z et al. Association between low dietary folate intake and suboptimal cellular DNA repair capacity. *Cancer Epidemiol. Biomarkers & Prevention*, 2003, 12, 963-969.
- Whetstine, JR; Flatley, RM; Matherley, LH. The human reduced folate carrier gene is ubiquitously and differentially expressed in normal human tissues: identification of seven non-coding exons and characterization of a novel promoter. *Biochem J*, 2002, 367, 629-640.
- Yaar, M; Gilchrest, BA. Photoageing: mechanism, prevention and therapy. *Br J Dermatol.*, 2007, 157(5), 874-887.

***Chapter 11***

**TRANSCRIPTIONAL CHANGES IN ENERGY  
METABOLISM AND PROTEIN SYNTHESIS  
PREDOMINATE IN THE EARLY PHASE AFTER  
PHOTODYNAMIC THERAPY**

***Yuji Morimoto, Kouji Matsumura, Yoshinori Nakagishi  
and Satoko Kawauchi***

National Defense Medical College, Tokorozawa, Japan.

**ABSTRACT**

The mechanism of the cytotoxic effect of photodynamic therapy (PDT) with respect to gene profile has not been fully elucidated. We used DNA microarrays to analyze the time courses of transcriptional responses of lung cancer cells (RERF) at 0, 30, 60, 120 and 240 min after PDT using a water-soluble photosensitizer (ATX-S10•Na(II)). Apoptotic cell death was prominent and loss of ~ 40% of cells was seen at 120 min and 240 min after PDT using a 670-nm laser. Approximately 1300 genes in 10K tested genes responded to PDT with a more than 1.5-fold induction rate. Most of the up-regulated genes (~ 700) were revealed to be closely related to energy metabolism and protein synthesis. Immediately after PDT, genes related to activities of ATP synthase and NADH dehydrogenase were significantly up-regulated. In addition, genes related to translation in protein synthesis, ribosomal proteins and proteasome were overexpressed both at 0 min and 240 min after PDT. Expression levels of heat shock protein-related genes gradually increased over a period of 240 minutes. Further characterization of the PDT- induced gene expression profiles obtained here may lead to identification of novel biomarkers and shed light on the cytotoxic mechanism of PDT.

## INTRODUCTION

Photodynamic therapy (PDT), a treatment modality that uses a photosensitizing drug activated by light, is proving effective for various oncologic and nononcologic applications. PDT is based on optical activation of a photosensitizer, resulting in the localized formation of radicals and reactive oxygen species, primarily singlet oxygen, which cause apoptotic or necrotic cell death. In the early phase after PDT(up to a few hours), cellular components that was damaged by the reactive oxygen species resulted in triggering of a variety of signal transduction pathways and thus leading to significant changes in expressions of heterogeneous genes [1]. Activation of heat-shock-related genes [1] [2], cell-cycle-related genes [3] and early response genes[4] has been found. Cellular responses to PDT are indeed complex and can involve a substantial portion of the eukaryotic genomes. Hence, to clarify the mechanism of PDT, simultaneous observation of changes in expression of a large number of genes is required. In addition, systemic study of expressions at successive time points is important because an enhanced transcriptional response of a gene can affect expressions of many genes. Thus, time course analysis is a powerful method for elucidating functional correlations among genes.

Therefore, we studied time course patterns of early transcriptional responses of a large number of genes in PDT-treated cells. To investigate the transcriptional responses of global genes, we used oligonucleotide microarrays containing over 10,000 genes. The results of this study provided insights into the death and protective responses of cells treated by PDT as well as the relationships among gene expressions.

## MATERIALS AND METHODS

### Photosensitizer

ATX-S10·Na(II) [13,17-bis (1-carboxypropionyl) carbamoylethyl-8-etheny-2-hydroxy-3-hydroxyiminoethylidene-2,7,12,18-tetraethyl porphyrin sodium] (Photochemical Company, Okayama, Japan), a second-generation hydrophilic chlorine photosensitizer with an absorption maximum at 670 nm [5], was used with a concentration of 12 µg/mL, at which PDT induced 90% cytotoxicity under the irradiation conditions described below.

### Cell Culture

RERF-LC-AI cells, human lung squamous carcinoma cells (RCB0444, RIKEN BRC, Tsukuba, Ibaraki, Japan), were grown in modified Eagle's medium (MEM) containing 10% FBS, 10,000-U/mL crystalline penicillin G potassium and 100 µg/mL streptomycin sulfate at 37°C and 5% CO<sub>2</sub>. Cells were treated with ATX-S10·Na(II) for 24 h. The medium was then replaced by a fresh medium without the photosensitizer just before light irradiation.

## Laser Irradiation and Experimental Procedure

A continuous wave diode laser emitting 668 nm (PDT ALD-1, Hamamatsu Photonics, Shizuoka, Japan) was used for the light source. Irradiation intensity and cumulative fluence were set at 50 mW/cm<sup>2</sup> and 40 J/cm<sup>2</sup>, respectively, corresponding to the irradiation period of 800 s. The cells were incubated for 0, 30, 60, 120 and 240 minutes after the end of laser irradiation.

## Cell Viability Assay

Cell viability was determined by an MTT [3-(4,5-dimethylthiazol-2-yl)-2,5-diphenyltetrazolium bromide] assay in which light absorption (570 nm) of formazan generated from a photochemical reaction between reagents and cells was recorded by a microplate reader (Model V max, Molecular Devices, Sunnyvale, CA). Cell viability was defined as the ratio of optical densities of treated cells to those of untreated cells, which served as a control.

## Analysis of Apoptosis

Apoptosis was determined by the morphological analysis using DNA staining. Cells were fixed with 4% formaldehyde for 1h and stained with Hoechst 33342 (1 µM) (Dojindo, Kumamoto, Japan) for 30 min, followed by an observation using a fluorescence microscope (ECLIPSE TE 2000, Nikon). Randomly selected 100 fields per dish were automatically scanned using a XYZ stage controller (Scope pro, Roper, Japan). Total cell number and number of apoptotic cells in each field were automatically counted by image analysis software (Image-Pro, Roper). Cells showing chromatin aggregation were considered as apoptotic cell death.

## Microarray Procedures

Gene expression analysis was performed using AceGene Human Oligo Chip 30K subset A (Hitachi Software Engineering, Yokohama, Japan). On the glass microarray slide, 10K human genes were arrayed. Most of the genes were from ORFs with known functions (gene description and location on microarrays available at the following website: [http://hitachisoft.jp/products/lifescience/acegene/human30k/search\\_30k/human30k\\_oligo\\_annotation/index.html](http://hitachisoft.jp/products/lifescience/acegene/human30k/search_30k/human30k_oligo_annotation/index.html)).

Cells in 60-mm plates were harvested immediately after the end of laser exposure (0 m), or at 30, 60, 120 or 240 minutes after the laser irradiation. Total RNA was prepared using a Qiagen RNeasy system (Qiagen, Tokyo, Japan). Total RNA at each time point (0, 30, 60, 120 and 240 minutes after irradiation) was extracted from a mixture of 10 samples, each of which was obtained from a different culture plate on a different date. Antisense RNA (aRNA) was

purified from total RNA and then labeled with amino allyl UTP using a MessageAmp aRNA kit (Applied Biosystems/Ambion, Austin, TX).

Five micrograms of amino allyl UTP-labeled aRNA was labeled by coupling of Cy3 or Cy5 mono-reactive dye (GE Healthcare Bio-Sciences, Tokyo, Japan). aRNA fractions from PDT-untreated (photosensitizer (-) and light irradiation (-) control) samples coupled with Cy3 were used as a common reference in all pairs of hybridization. aRNA from PDT-treated samples coupled with Cy5 were used as test samples. After fragmentation, both groups of Cy dye-labeled samples were simultaneously hybridized at 45°C onto a glass microarray for 16 h. The microarray slide was serially washed in 2× SSC (sodium citrate-sodium chloride) - 0.1% SDS (sodium dodecyl sulfate), 2× SSC, and 1× SSC at 30°C.

By swapping the fluorescent dyes, another series of hybridization at each time point (0, 30, 60, 120 and 240 minutes after irradiation) was carried out to obtain the best data from a limited number of microarrays.

## Data Analysis

Microarray slides were scanned with a microarray scanner (ScanArray™ Express, PerkinElmer, Boston, MA). Scanned images were then processed to obtain signal intensity from each channel with a quantitative microarray analysis application program (QuantArray, GSI Lumonics, Boston, MA). After background correction, signal ratio for each channel on each slide was calculated, and the average of two signal ratios, one of which was obtained by swapping Cy dyes, was used for further analyses. Initial comparisons were then performed using GeneSpring software package Agilent Technologies, Santa Clara, CA). A gene expression matrix for clustering was generated (filter: more than 1.5-fold change for at least one of the tested time points). Gene tree clustering with standard correlation was applied, and the results were visualized.

Apart from clustering, expression analysis for determination of biological theme was carried out using the public domain Expression Analysis Systemic Explore (EASE) program [6] (<http://david.abcc.ncifcrf.gov/ease/ease.jsp>). A list of genes of which expressions (signal ratios) were more than 1.5 fold or less than 0.67 fold was loaded into EASE as input genes, and a list of all genes assayed was loaded as gene identifiers. All gene categories then appeared ranked by over-representation with p-values. Significant ( $p < 0.05$ ) over-represented categories are deemed ‘biological themes’ of the gene list.

## Statistical Analysis

Data obtained from cell viability assays and apoptotic analysis are presented as means ± standard deviation (SD) and were analyzed by a one-way factorial ANOVA. Games-Howell’s post-hoc test was used for multiple comparisons (SPSS, SPSS Japan, Tokyo, Japan). P-values  $< 0.05$  were considered statistically significant.

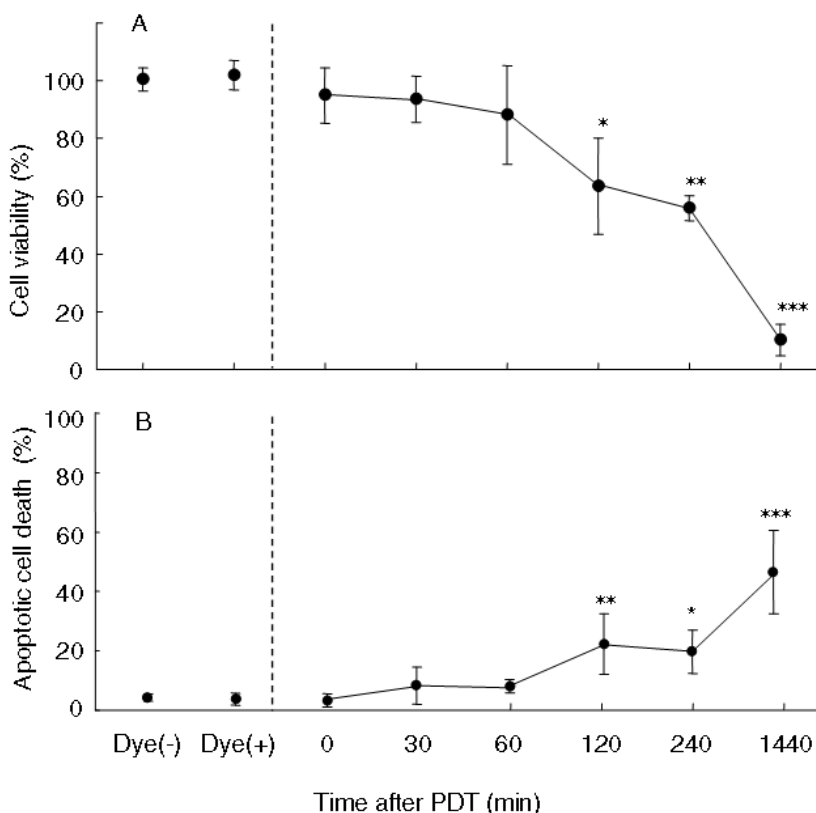


Figure 1. Cell viability (*A*) and population of apoptotic cell death (*B*) after PDT. Apoptosis was expressed as the percentage of apoptotic cells in a field. \*P < 0.05, \*\*P < 0.01, \*\*\*P < 0.0001, n = 5 in each group.

**Table 1. List of number of genes that were overexpressed or underexpressed by more than 1.5 fold at each time point.**

	Over -expressed	Under-expressed
0 min	287	199
30 min	129	95
60 min	175	183
120 min	137	62
240 min	454	390
Expressed at either time point	678	606

## RESULTS

### Cell Viability (Figure 1A)

In cells treated with PDT, significant change in viability was not seen up to 60 min after PDT. However, at 120 min after PDT, treated cells showed a significant decrease in viability.

A further decrease was seen in cells at 1440 min after PDT. These results showed that PDT using ATX-S10·Na(II) reduced number of viable RERF cells within 120 min after PDT, thus indicating induction of cell death in the early phase after PDT.

## Apoptosis (Figure 1B)

Apoptotic cells were confirmed even at 30 min after PDT (~ 8%), but a significant increase in apoptotic cells was seen at 120 min after PDT (~20%). The time course of apoptotic cell death was closely correlated with the time course of cell viability: an increase in apoptotic cells was synchronized with a decrease in viable cells.

## Single Time Point Analysis (Table 1)

Using the 1.5-fold criterion at each single time point, 1284 of ten thousand genes met the selection criteria: 678 genes showed upregulation and 606 genes showed downregulation.

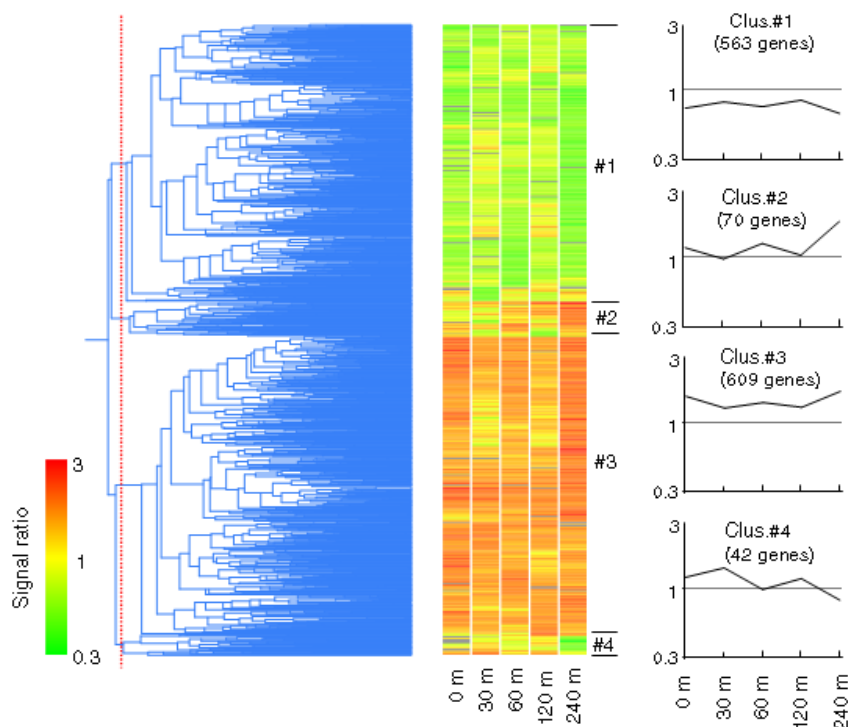
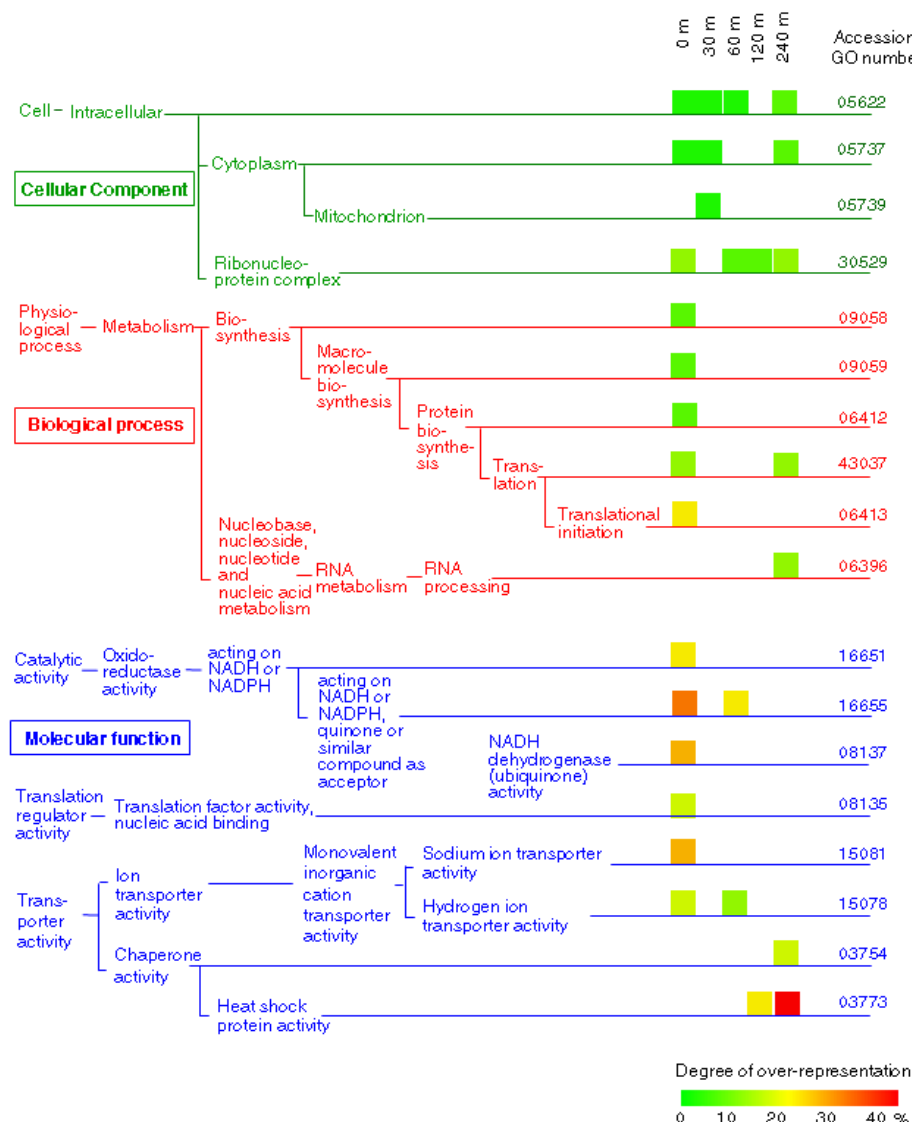


Figure 2. A hierarchical clustering map of gene expression observed for PDT-treated cells using a gene tree clustering algorithm. Four characteristic subclusters were observed with a 15% similarity coefficient (red dashed line). The small graph for each subcluster represents a trend of average expression of the genes belonging to each subcluster.



Over-representation (%) =

$$\frac{\text{Number of altered genes that belong to the biological category in a group}}{\text{Number of total genes that belong to the biological category in a microarray}} \times 100$$

For example, an over-representation of 27% in *Translational initiation* seen in 0 min group is obtained as follows:

$$\frac{\text{Number of altered genes that belong to the category } \textit{Translational initiation} \text{ in 0 min group}}{\text{Number of total genes that belong to the category } \textit{Translational initiation} \text{ in AceGene Human Oligo Chip 30K subset A}} \times 100 \\ = 100 \times 13 / 48$$

Each accession number of the Gene Ontology consortium is indicated on the right side of each graph.

Figure 3. Over-represented biological themes related to PDT. Degree of over-representation in each group or subcluster was calculated as noted above:

## Gene Expression Clustering Analysis (Figure 2)

Analysis using a gene tree clustering algorithm with standard correlation resulted in a hierarchical clustering map of the 1284 genes that met the selection criteria. Four characteristic subclusters of genes were classified at similarity coefficient of 0.15 (red dashed line in Figure 2). In subcluster #1, expression intensities of most of the genes were less than 1 at any time point. The genes classified into subcluster #2 showed little change during the first half of the time course and showed overexpression during the second half of the time course. Genes in subcluster #3 showed upregulation at all time points with biphasic peaks at 0 min and 240 min after PDT. Genes in subcluster #4 showed transient overexpression at 30 min after PDT.

## Patterns of Gene Expression of Different Functional Categories at a Single Time Point and at Multiple time Points (Figure 3)

To further examine the global similarity of gene expression patterns, each of the datasets was annotated by using an EASE program, which can hierarchically group genes into meaningful biological categories. EASE uses the three systems of the Gene Ontology (GO) Consortium Classifications as default categorization systems. EASE calculates overrepresentation with respect to the total number of genes assayed and annotated within each system to allow for side-by-side comparisons of categories from categorization systems with varying levels of annotation. In this study, we examined genes using EASE for 10 groups of genes of which expression was  $>1.5$  at a single time point [10 groups = (a group of up-regulated genes and a group of down-regulated genes)  $\times$  5 time points]. Examination using EASE revealed significant over-representation was seen in 18 biological categories.

Immediately after PDT (0 min), genes in 14 categories were significantly up-regulated. At this time point, overexpression was seen in 20 – 30% of the genes related to the function of NADH (GO: 16651, 16655 and 08137) and in ~ 25% of the genes related to the activity of sodium ion transporters (GO: 15081). Immediate overexpression was also seen in 10 – 20 % of the genes controlling protein translation (GO: 43037, 06413 and 08135), in 5 - 10% of genes related to ribonucleoprotein complex (GO: 30529) and in 1- 5% of genes related to biosynthesis (GO: 09058, 09059 and 06412). Some parts of these genes that were up-regulated immediately after PDT were up-regulated at 30, 60, 120 or 240 min after PDT. In contrast, EASE analysis revealed the existence of a unique gene category in which genes showed no overexpression immediately after PDT but showed an increase in expression with elapse of time: these genes were categorized as heat shock-related genes (GO:03773).

## Analysis of Heat Shock-Related Gene Expression (Table 2)

Since the heat shock-related genes showed remarkably high over-representation (~ 40%), the genes were further analyzed. Table 2 shows all of the heat shock-related genes that were mounted on the microarray chip used, and the genes depicted with bold letters showed an increase in expression with elapse of time. Genes of heat shock protein (hsp) tended to be up-

regulated with increase in molecular weight (MW) of the proteins that the genes encode. Probability of upregulation of the genes encoding hsp was 0.13 (2/16) when the MW of the encoded protein was 40 kDa or less, whereas the probability was 0.75 (9/12) when the MW of the encoded protein was > 40 kDa.

## DISCUSSION

Analysis of the time courses of expressions of genes in the present study revealed that several hundred genes were up-regulated or down-regulated in the early phase after PDT.

The main categories of the early up-regulated genes in this study were energy, translation, and protein synthesis/modulation. Interestingly, most of these categories coincided with categories of genes that have been reported to be early up-regulated soon after ionizing radiation [7]. Stress originating from PDT is different from that originating from ionizing radiation; however, there might be a common mechanism for gene regulation. The other remarkable finding in the present study was the behavior of hsp-related genes, which were gradually up-regulated 60 min after PDT and showed a peak at 240 min after PDT.

### Energy

Most of the up-regulated genes belonging to the categories of *catalytic activity* (GO: 16651 and 16655) and *NADH dehydrogenase* (GO: 08137) encode proteins related to NADH dehydrogenase (*NDUFA6*, *NDUFAB1*, *NDUFB3*, *NDUFB6*, *NDUFC2*, *NDUFS4*, *NDUFS* and *NQO1*). In addition, most of the up-regulated genes belonging to the category of *ion transporter activity* (GO: 15081 and 15078) encode the above-stated NADH dehydrogenase-related proteins and proteins constituting proton (H<sup>+</sup>) transporters on F<sub>0</sub>F<sub>1</sub> – ATPase complex (*ATP5B*, *ATP5E*, *ATP5J* and *ATP6AP2*). These results suggest that PDT using ATX-S10•NA(II) immediately alters mitochondrial function, especially that related to H<sup>+</sup> and NADH. This implication agrees with the description of the mechanism in many reports on PDT using other photosensitizers. Salet et al. [8] reported that PDT stimulates NADH respiration, suggesting H<sup>+</sup> leakage via the mitochondrial inner membrane. PDT-treated cells also show a decrease in NADH or an enhancement of NADH oxidation [9], probably due to the photoinduced electron abstraction [10].

One plausible reason for the immediate upregulation of genes related to mitochondrial function in PDT-treated cells is a protective response against cell death induced by stress acting on the cells. Since injured mitochondria require ATP for their recovery[11], it is quite natural that the genes related to ATP production in mitochondria are up-regulated. Another plausible reason for the immediate upregulation of genes related to mitochondrial function is the induction of an apoptotic signaling pathway for the effectual execution of cell death. When ATP is depleted, subsequent apoptosis is significantly blocked [12]. Thus, a high level of ATP is required for apoptotic signal transduction.

**Table 2. List of heat shock-related genes mounted on AceGene Human Oligo Chip 30K subset A. The genes depicted with bold letters showed an increase in expression level with time.**

Classification	Symbol	Gene Name
hsp 10	HSPE1	heat shock 10kD protein 1 (chaperonin 10)
hsp 27	HSPB1	heat shock 27kD protein 1
<b>hsp 40</b>	<b>DNAJA1</b>	<b>DnaJ (Hsp40) homolog, subfamily A, member 1</b>
hsp 40	DNAJA2	member 2
hsp 40	DNAJA3	member 3
hsp 40	DNAJA4	member 4
hsp 40	DNAJB1	DnaJ (Hsp40) homolog, subfamily B, member 1
hsp 40	DNAJB2	member 2
hsp 40	DNAJB4	member 4
hsp 40	DNAJB5	member 5
hsp 40	DNAJB6	member 6
hsp 40	DNAJB11	member 11
hsp 40	DNAJB12	member 12
hsp 40	DNAJC3	DnaJ (Hsp40) homolog, subfamily C, member 3
hsp 40	DNAJC6	member 6
<b>hsp 60</b>	<b>HSPD1</b>	<b>heat shock 60kD protein 1 (chaperonin)</b>
<b>hsp 70</b>	<b>HSPA1A</b>	<b>heat shock 70kD protein 1A</b>
<b>hsp 70</b>	<b>HSPA1L</b>	<b>heat shock 70kD protein 1-like</b>
<b>hsp 70</b>	<b>HSPA2</b>	<b>heat shock 70kD protein 2</b>
hsp 70	HSPA6	heat shock 70kD protein 6 (HSP70B)
<b>hsp 70</b>	<b>HSPA8</b>	<b>heat shock 70kD protein 8</b>
hsp 70	LOC51182	likely ortholog of mouse heat shock protein, 70 kDa 4
hsp 75	TRAP1	heat shock protein 75
<b>hsp 90</b>	<b>HSPCA</b>	<b>heat shock 90kD protein 1, alpha</b>
<b>hsp 90</b>	<b>HSPCB</b>	<b>heat shock 90kD protein 1, beta</b>
<b>hsp 105</b>	<b>HSP105B</b>	<b>heat shock 105kD</b>
<b>hsp 110</b>	<b>APG-1</b>	<b>heat shock protein (hsp110 family)</b>
hsf	HSF1	heat shock transcription factor 1
hsf	HSF2	heat shock transcription factor 2
hsf	HSF2BP	heat shock transcription factor 2 binding protein
hsf	HSF4	heat shock transcription factor 4

## Translation Regulator in Protein Synthesis

Some of the genes encoding translation regulator proteins in protein synthesis (GO: 43037, 06413 and 08135: *EEF1A2*, *EEF2*, *EIF1A*, *EIF2B3*, *EIF3S2*, *EIF3S3*, *EIF4A2*, *EIF4G2*, *EIF5* and *MTIF2*) were up-regulated immediately after PDT. Translation regulators in protein synthesis are known to be induced by exposure to various stresses such as ionizing radiation, UV and oxidative stress. Oxidative stress, such as H<sub>2</sub>O<sub>2</sub>, enhances phosphorylation

of eukaryotic translation initiation factors (eIFs), causing inhibition of protein synthesis [13]. In addition, eukaryotic translation elongation factors (eEFs) are overexpressed when cells are exposed to oxidative stress [14]. UV induces overexpression of genes related to eIF1A, 2 $\beta$ , 3 $\gamma$  and eIF3 (subunit 6) [15]. When cells are arrested at G<sub>2</sub> phase of the cell cycle in response to UV, EIF4A is up-regulated [16]. The existence of those stress-inducible eIFs-related genes suggest that modulation of translation initiation occurs during cellular stress and the emergence of those genes may represent an important adaptive response to geotaxis as well as endoplasmic reticulum stress [17].

## Protein Synthesis/Modulation

Several genes encoding ribosomal proteins and proteasome were overexpressed in the present study (GO: 09058: *RPL10A*, *RPL22*, *RPL4*, *RPL5*, *RPL6*, *RPL8*, *RPS13*, *RPS6* and *PSMA1*, *PSMB3*, *PSMB7* and *PSMD7*). Oxidative stress has been reported to increase expression levels of ribosomal protein-related genes, including *RPL13*[16], *RPL4* [18], *RPL19*, *RPL 21*, *RPL 31*, *RPL 34*, *RPL35*, *RPL 35A*, *RPS 15A*, *RPS23*, *RPS 27* and *RPS 29* [15].

Proteasome is a member of the complex enzyme systems that regulate the turnover of cellular proteins. The enzyme digests proteins in a reaction driven by ATP hydrolysis. Our study showed upregulation of genes encoding proteasome subunit proteins. This result suggests that PDT induces protein degradation. Significant increases in the expression levels of genes involved in proteasome-mediated degradation have also been seen in cells exposed to UV [19].

## Heat Shock Protein

The present results showed that hsp genes tended to be up-regulated with an increase in molecular weight of the proteins that the genes encode: Most of the genes encoding hsp110, hsp105, hsp90, hsp70 and hsp60 were up-regulated in response to PDT, whereas expressions of most of the genes encoding hsp40, hsp27 and hsp10 were unchanged (Table 2).

There have been many studies on PDT in regard to heat shock protein, but most of them focused on hsp70. PDT-generated singlet oxygen is thought to induce hsp70 protein, which acts as a suppressor of apoptosis.

Various stresses acting on cells can induce overexpression of hsp90, but it is one of the most abundant constitutive proteins that exist intracellularly. The protein modulates the cell cycle and cellular proliferation by interacting with more 100 intracellular proteins for urging their exact foldings and preserving their proper functions. The upregulation of hsp90-related genes observed in the present study might therefore be a protective reaction for sustaining the cell cycle and cellular proliferation.

Proteins of hsp60 and hsp10 can directly promote the proteolytic maturation of caspase-3 [20]. Since Hanlon et al. showed that hsp60 induction is significantly greater in PDT-resistant cells [21], it is likely that the stress protein is profoundly related to protection of cells against PDT.

Protein of hsp40 transports certain proteins into the mitochondria and endoplasmic reticulum. It is a positive cochaperone of hsp70, having a critical regulatory function in the Hsc70 ATPase cycle [22]. Protein of hsp40 thus reinforces hsp70 function. Most of the hsp40-related genes were not overexpressed in the present study. This is probably because hsp40 is a constitutive protein, thus not being induced.

Protein of hsp27 may play an important role in mediating the adaptive response to PDT-induced oxidative stress [2]. In addition, small hsp proteins, such as hsp27, can allow cancerous cells to escape from immunosurveillance mediated by death ligands and can render these cells resistant to therapy [23]. On the other hand, several cell lines did not show an increase in hsp27 after PDT [24]. Thus, the function of hsp27 protein in PDT is not clear.

Augmentation of hsp synthesis is tightly regulated by stress-inducible heat shock factors (hsf), which are part of a transcriptional signaling cascade with both positive (e.g., hsp) and negative (e.g., proinflammatory cytokines) properties. Among heat shock factors, hsf1 plays a major role in heat shock response in mammals. However, it has been shown that expression of hsf1 in mammals is not regulated by stress [25], which supports our results.

## CONCLUSION

The time course of transcriptional responses of lung cancer cells (RERF) in the early phase after PDT (0 – 240 min) using a water-soluble photosensitizer (ATX-S10•Na(II)) was analyzed. In 10K tested genes, approximately 1300 genes responded to PDT. Transcriptional changes seen immediately after PDT (0 min) predominated in energy metabolism and protein synthesis, while expression levels of heat shock protein-related genes gradually increased over a period of 240 minutes.

## ACKNOWLEDGMENTS

We would like to acknowledge the generous gift of ATX-S10•NA(II) from Dr. Isao Sakata (Photochemical Co., Okayama, Japan) and the loan of the diode laser device, model PDT ALD-1, from Hamamatsu Photonics Co.(Hamamatsu, Japan). We also thank Dr. Makoto Kikuchi for useful discussion.

## REFERENCES

- [1] Luna, MC; et al. Photodynamic therapy-mediated oxidative stress as a molecular switch for the temporal expression of genes ligated to the human heat shock promoter. *Cancer Res.*, 2000, 60, 1637-44.
- [2] Wang, HP; et al. Up-regulation of Hsp27 plays a role in the resistance of human colon carcinoma HT29 cells to photooxidative stress. *Photochem Photobiol.*, 2002, 76, 98-104.

- [3] Verwanger, T; et al. Expression kinetics of the (proto) oncogenes c-myc and bcl-2 following photodynamic treatment of normal and transformed human fibroblasts with 5-aminolaevulinic acid-stimulated endogenous protoporphyrin IX. *J Photochem Photobiol B.*, 1998, 45, 131-5.
- [4] Luna, MC; et al. Photodynamic therapy mediated induction of early response genes. *Cancer Res.*, 1994, 54, 1374-80.
- [5] Mori, M; et al. Photodynamic therapy for experimental tumors using ATX-S10(Na), a hydrophilic chlorin photosensitizer, and diode laser. *Jpn J Cancer Res.*, 2000, 91, 753-9.
- [6] Hosack, DA; et al. Identifying biological themes within lists of genes with EASE. *Genome Biol.*, 2003, 4, R70.
- [7] Otomo, T; et al. Microarray Analysis of Temporal Gene Responses to Ionizing Radiation in Two Glioblastoma Cell Lines: Up-regulation of DNA Repair Genes. *J Radiat Res (Tokyo)*. 2004, 45, 53-60.
- [8] Salet, C; et al. Effects of photodynamic action on respiration in nonphosphorylating mitochondria. *Arch Biochem Biophys.*, 1998, 358, 257-63.
- [9] Kirveliene, V; et al. Fluence-rate-dependent photosensitized oxidation of NADH. *J Photochem Photobiol B.*, 1993, 21, 53-60.
- [10] Davila, J; et al. Photosensitized oxidation of biomaterials and related model compounds. *Photochem Photobiol.*, 1989, 50, 29-35.
- [11] Kirveliene, V; et al. Post-exposure processes in Temoporfin-photosensitized cells in vitro: reliance on energy metabolism. *J Photochem Photobiol B.*, 1997, 41, 173-80.
- [12] Eguchi, Y; et al. Intracellular ATP levels determine cell death fate by apoptosis or necrosis. *Cancer Res.*, 1997, 57, 1835-40.
- [13] Brostrom, CO; et al. Regulation of translational initiation during cellular responses to stress. *Prog Nucleic Acid Res Mol Biol.*, 1998, 58, 79-125.
- [14] Chen, E; et al. Rapid up-regulation of peptide elongation factor EF-1alpha protein levels is an immediate early event during oxidative stress-induced apoptosis. *Exp Cell Res.*, 2000, 259, 140-8.
- [15] Koch-Paiz, CA; et al. Functional genomics of UV radiation responses in human cells. *Mutat Res.*, 2004, 549, 65-78.
- [16] Sasaki, Y; et al. Identification of genes highly expressed in G2-arrested Chinese hamster ovary cells by differential display analysis. *J Clin Lab Anal.*, 2000, 14, 314-9.
- [17] Sheikh, MS; et al. Cloning and characterization of a human genotoxic and endoplasmic reticulum stress-inducible cDNA that encodes translation initiation factor 1(eIF1(A121/SUI1)). *J Biol Chem.*, 1999, 274, 16487-93.
- [18] Ammendola, R; et al. Differentially expressed mRNAs as a consequence of oxidative stress in intact cells. *FEBS Lett.*, 1995, 371, 209-13.
- [19] Sesto, A; et al. Analysis of the ultraviolet B response in primary human keratinocytes using oligonucleotide microarrays. *Proc Natl Acad Sci, USA*. 2002, 99, 2965-70.
- [20] Garrido, C; et al. Heat shock proteins: endogenous modulators of apoptotic cell death. *Biochem Biophys Res Commun.*, 2001, 286, 433-42.
- [21] Hanlon, JG; et al. Induction of Hsp60 by Photofrin-mediated photodynamic therapy. *J Photochem Photobiol B.*, 2001, 64, 55-61.
- [22] Minami, Y; et al. Regulation of the heat-shock protein 70 reaction cycle by the mammalian DnaJ homolog, Hsp40. *J Biol Chem.*, 1996, 271, 19617-24.

- [23] Arrigo, AP. sHsp as novel regulators of programmed cell death and tumorigenicity. *Pathol Biol (Paris)*. 2000, 48, 280-8.
- [24] Nonaka, M; et al. Inhibitory effect of heat shock protein 70 on apoptosis induced by photodynamic therapy in vitro. *Photochem Photobiol.*, 2004, 79, 94-8.
- [25] Cotto, JJ; et al. Stress-induced activation of the heat-shock response: cell and molecular biology of heat-shock factors. *Biochem Soc Symp.*, 1999, 64, 105-18.

## ***Chapter 12***

# **THE ORIENTAL HORNET *VESPA ORIENTALIS* (HYMENOPTERA: VESPINAE) CUTICULAR YELLOW STRIPE AS AN ORGANIC SOLAR CELL: A HYPOTHESIS**

***Marian Plotkin<sup>1</sup>\**, Stanislav Volynchik<sup>1</sup>, Reuben Hiller<sup>1</sup>,  
David J. Bergman<sup>2</sup> and Jacob S. Ishay<sup>1</sup>**

<sup>1</sup>Department of Physiology and Pharmacology, Sackler Faculty of Medicine Tel-Aviv University, Ramat Aviv 69978, Israel.

<sup>2</sup>School of Physics and Astronomy, Raymond and Beverly Sackler Faculty of Exact Sciences Tel-Aviv University, Ramat Aviv 69978, Israel.

## **ABSTRACT**

Many animals such as insects, reptiles, amphibians and marine vertebrates and invertebrates are endowed with bright colors and contrasting patterns intended to warn other animals that they are venomous and such is the case also insofar as the brown yellow coloration of the Oriental hornet. The present work, however, suggests that in the Oriental hornet this is not the only purpose of these bright pigments. The Oriental hornet *Vespa orientalis* (Hymenoptera, Vespinae) correlates its flight activity with the insolation. The Oriental hornet cuticle bears yellow-colored stripes composed of yellow granules. The yellow granule contains xanthopterin. This array of yellow granules maximizes the ability of the extensively conjugated xanthopterin to absorb a wide range of visible light extending up to UV light. Photovoltaic properties of yellow cuticle evince that the potential difference between darkness and UV illumination is sufficient for ATP production from ADP. This unique photovoltaic behavior of yellow cuticle suggests that it may act as an organic solar cell.

---

\* Corresponding author: E mail: marianpl@post.tau.ac.il; Phone: 972-3-6409138; Fax: 972-3-6409113.

**Keywords:** Organic solar cell; Oriental hornet *Vespa orientalis*; cuticle; Xanthopterin; Pigment granule.

## INTRODUCTION

The Oriental hornet is a colorful insect [1] whose body is covered mostly with a brown cuticle but also bears yellow-colored stripes on its head and gaster (Figure 1a). The yellow cuticular component is a unique structure of about 45 $\mu\text{m}$  in thickness which is bordered on the one side by an exo-endocuticle 20-25 $\mu\text{m}$  thick, and on the other side- by a thin layer of hypo-cuticle (1.5 $\mu\text{m}$  in thickness)(Figure 1b). The yellow stripe is comprised of overlying lamellae of yellow granules (Figure 1c), with each granule barrel-shaped and arranged transversely (Figure 1d). The yellow color of the granules stems from the presence in them of xanthopterin [2]. Unlike the larvae or the hibernating queen, the adult worker hornets lack a fat body. As known, the fat body is the organ in charge of metabolic processes in the insect body, thus analogous in function to the liver in vertebrates. Our studies of enzymatic activity in the oriental hornet have revealed liver-like functions in the cuticular layer of yellow granules, and also that solar irradiation stimulates and produces a change in the metabolic activities of the hornet [3].

The yellow granules begin to be produced about two days prior to eclosion of the pupa, and the process continues up to about three days post eclosion [4]. During the first three days post eclosion, the nascent hornets partly participate in various tasks inside the nest, like thermoregulation of the brood and feeding of the larvae, but they do not emerge from the dark nest. In fact, exposure of these hornets to light triggers in them a photophobic response, causing them to seek shelter in the darkest spots available. It is only after the layer of yellow granules reaches full maturation, i.e., the granules fitting into densely-packed lamellae (Figure 1c), that the hornets emerge from the nest and are exposed to insolation. The most intensive hornet activity is digging out soil and small stones so as to enlarge the nest. The dug debris is then carried out orally by the digger hornets who fly out of the nest and deposit their load in the outside vicinity. The Oriental hornet coordinates its extra-nest activities with the insolation, that is, with rise in the solar radiation, it increases its activity, namely, enhanced rate of flight outside the nest, and vice versa, with diminished irradiation its activity declines [5]. For many years now, we have been engaged in studying electric properties pertaining to hornets. Thus, we measured the photoconductive [6], thermoelectric [7] and thermoconductive properties [8] in hornet cuticle. Additionally, electrical capacitance was also investigated [9], and a theoretical model was suggested for these properties [10]. All the above-mentioned tests and measurement were performed on the cuticle of intact hornets. In the present paper we focus on assessing hornet yellow stripes only, and evincing their photoenergetic contribution, which will enable to characterize and understand the role played by the yellow granules present in these cuticular stripes. In the present study, we provide micromorphological and biophysical data that explain this phenomenon.

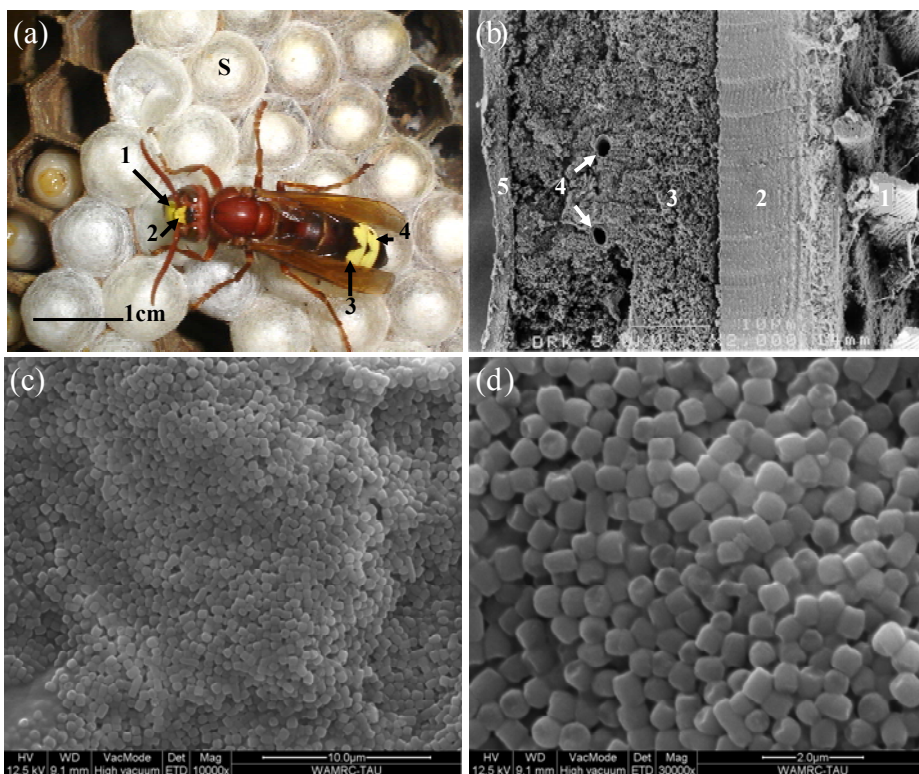


Figure 1. Micromorphological structure of the yellow stripe.

(a) Photo showing adult hornet (more than 3 days post eclosion) resting on a stretch of silk caps (s). The brown colored hornet contains yellow colored regions on the clypeus (1) and frons (2) and on the 3<sup>rd</sup> and 4<sup>th</sup> gastral segments (3 & 4). The yellow stripe on the ventral aspect of the 3<sup>rd</sup> gastral segment is not shown in picture. Bar= 1cm.(b) Cross – section through the cuticle of an adult hornet containing yellow granules. Shown are: the hairs extruding from the exocuticle (1); the exocuticle proper and the endocuticle (2), and beneath the latter, the layer of yellow granules (3); within the layer of yellow granules, tracheae are discernible (4), and underneath the hypocuticle (5). Bar= 10μm. (c) Cross-section through the layer of yellow granules shows the granules to be densely-packed. Bar= 10μm.(d) On greater magnification, one can see the barrel-like shape of the granules and their arrangement, for the most part, in transverse orientation. Bar= 2μm.

## MATERIALS AND METHODS

### Preparation for Scanning Electron Microscope (SEM)

Specimens were prepared according to the TAO (tannic acid/arginine/osmium tetroxide) non-coating technique, involving immersion of the samples in a mixture of arginine-HCl, glycine, sucrose and sodium glutamate [2%, 16h, 20°C], rinsing (3X) in distilled water and further immersion in a mixture of tannic acid and guanidine-HCl [2%, 8h, 20°C], following which the samples were carefully rinsed (3X) in distilled water. The tissues were next fixed

by immersion in an OsO<sub>4</sub> solution in distilled water [2%, 8h, 20°C], followed by rinsing (3X) in distilled water, as previously described [11]. Dehydration with ethanol was now followed by critical point drying (CPD) in liquid CO<sub>2</sub>. Observations were carried out with a JEOL FE-SEM, type 630IF, operated at 2-3 kV (see Figure 1b).

## Preparation for Environmental Scanning Electron Microscope (ESEM)

Yellow stripes were excised from adult hornets (more than 3 days post eclosion), and these stripes were viewed via the Quanta 200 FEG environmental scanning electron microscope (ESEM) (See Figure 1c, d) The samples were imaged with the secondary electron large-field detector (LFM) in low vacuum mode of 70Pa as previously described [4].

## Absorption Analysis of Cuticular Segment

During the active season, extending from June to October, we collected from the field brood-bearing combs and adult worker hornets (more than 3 days post eclosion) as previously described [12]. In our laboratory, the collected hornets were separated into six age-groups, namely, three age-groups of pupae at various developmental stages prior to eclosion (72-48 hrs, 48-24 hrs, and 24-0 hrs) and three age-groups of newly eclosed imagines aged 0-24 hrs, 24-48 hrs and 48-72 hrs.

To this end, a special cuvette was designed which enabled use of a spectrophotometer to assess the absorption in a piece of intact cuticle [2]. The absorption was measured on the yellow stripes from the dorsal part of the gaster (segments 3 and 4) and a third stripe from the ventral aspect of the gaster. The pieces were measured again after scraping off the yellow granules. (See Figure 2).

## Measurement of the Response of Yellow Stripes to UV Light

Adult worker hornets (more than 3 days post eclosion, judging by their dark-brown body color) were collected and anesthetized. Subsequently the three afore-mentioned yellow stripes were excised out, leaving only cuticle comprised of an exo-endocuticle, a layer of yellow granules and the hypocuticle. We now placed a small drop of silver paint (silver in Methyl Iso butyl Ketone) upon the exocuticle as an anchoring point for the positive electrode, and another drop on the reverse side of the stripe (the hypocuticle) as an anchoring point for the negative electrode. The electrodes, in turn, were connected to an electrometer Kietly 617 that measured the voltage. The cuticle was now placed in a box which enabled exposure of the cuticle to full darkness or, alternatively, to illumination by a UV lamp.

The yellow stripe was thus exposed to UV illumination from a distance of 10cm ( $\lambda=366\text{nm}$ : 1.2 mw/cm<sup>2</sup>, Minuvis, Desaga, Heidelberg). We used UV light because in earlier studies [5, 13] we found good correlation between UV of solar source and hornet activity. We now measured the voltage response under conditions of illumination and darkness.

## RESULTS

Assessment of the absorbance in the three yellow stripes (segments 3 and 4 from the dorsal aspect and segment 3 from the ventral aspect of the gaster), during various stages of hornet development, yielded similar results. The absorbance steadily increased with increasing age of the hornet to attain a maximum ranging between 250-380nm at about three days post eclosion (Figure 2a, c and e).

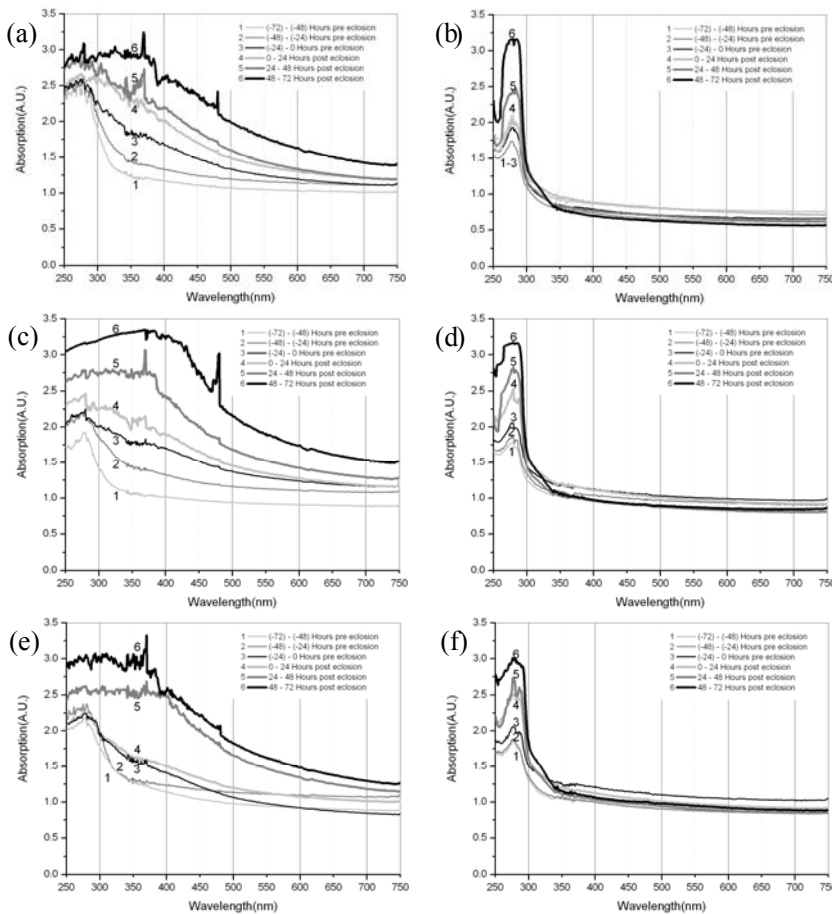


Figure 2. Absorbance by the yellow stripe at various developmental stages of the hornet.

(a) The absorbance by the yellow stripe excised from the dorsal aspect of the third gastral segment. (b) The absorbance by the yellow stripe excised from the dorsal aspect of the third gastral segment, but now after scraping off all the yellow granules, leaving behind only the upper layer of the endo- and exocuticle. (c) The absorbance by yellow stripe obtained from the dorsal aspect of the fourth gastral segment. (d) The absorbance by the yellow stripe obtained from the dorsal aspect of the fourth gastral segment but now after scraping off all the yellow granules, leaving behind only the upper layer of the endo- and exocuticle. (e) The absorbance by yellow stripe obtained from the ventral aspect of the third gastral segment. (f) The absorbance by yellow stripe obtained from the ventral aspect of the third gastral segment, but now after scraping off all the yellow granules, leaving behind only the upper layer of the endo- and exocuticle.

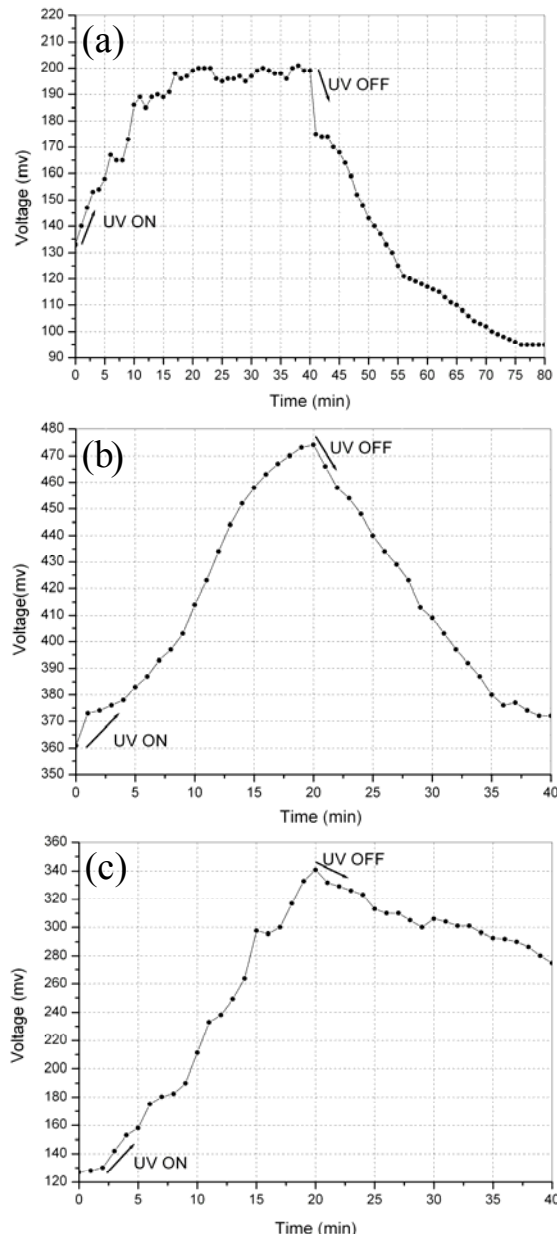


Figure 3. Three typical results obtained from measurement of the voltage across the yellow stripe. (a) Illumination of the yellow stripe for about 40 minutes reveals that already after 20 minutes of illumination the potentials differential mostly attained maximum. Upon cessation of the illumination there is a steep drop in the differential which tempers within 20 minutes. The maximal potential differential between the maxima of illumination and darkness was 104mv. (b) The yellow stripe here was illuminated for about 20 minutes before shutting off the illumination. The maximal potential differential between illumination and darkness was 113mv. (c) Here, too, the yellow stripe was illuminated for about 20 minutes before shutting off the illumination. The maximal potentials differential between illumination and darkness increases up to 214mv, and in this case, the rate of potentials discharge was slower.

Measurement of the absorbance after the removal of the yellow granules shows that the remaining layers of the endo and exocuticle are translucent to the passage of all wavelengths within the visible range and up to 290nm in all the studied age-groups. Absorbance of 250-300nm steadily increased with increasing age of the hornet and attained a maximum about three days post eclosion (Figure 2b,d, and f).

Measurement of the voltage (Figure 3) revealed similar behavior in all the studied stripes, with the hypocuticle showing negative potential with respect to the positive exocuticle. In response to illumination of the yellow stripe, the difference in potentials between light and darkness increases up to 214 milivolts (Figure 3c). Whereas at the end of the illumination and placement of the stripe in darkness caused a drop in the potential.

## CONCLUSION

The worker hornets emerge from the nest and expose themselves to insolation only after full maturation of their cuticle (i.e. 3 days post eclosion) and this because the maximum absorption of the cuticle is achieved 3 days post eclosion. The brown color of the Oriental hornet is attributed to the absorption of melanin which protects the hornet from solar irradiation [2]. The absorption in the yellow stripes is due to the presence in them of yellow pigment granules. This is clearly evinced upon removal of the yellow granules and measuring the absorbance in the remaining layers of the endo and exocuticle we observed that the cuticle was now translucent to the passage of all wavelengths within the visible range and up to 290nm in all the studied age-groups (Figure 2b,d, and f). Interestingly, removal of the yellow granules yielded a peak absorbance of 250-300nm, such as is associated with the presence of the aromatic amino acids making up the protein in the cuticle [14]. This leads us to conclude that the quantity of proteins in the cuticle becomes increasingly greater with cuticular maturation. The full role of these proteins in the Oriental hornet is unclear and will be addressed in future studies. Still, we found that if we deducted the contribution of these proteins to the overall absorption spectrum, most of the absorption occurred between 300-500nm, which is consistent with the absorption of xanthopterin, such as was extracted from the yellow granules in a previous study [2].

It is xanthopterin which lends the granules their coloration. Xanthopterin is found in high concentrations in arthropods [15-18] and lower vertebrates [19]. The creation of pigment cells in vertebrates has been extensively studied [20-22] and the prevailing opinion is that they are formed by the migration of cells from the neural crest of the developing embryo. Pteridines were studied extensively in the wings of pierid butterflies [23] where the pigment granules are located in the extracellular framework of the scales.

In hymenopteran insects such as the Oriental hornet very little is known about pteridine biosynthesis. In this instance, the granules are probably created by the endoplasmic reticulum which, in the hornets, develops as rows of microtubules, and these give rise to bladders that house the pigment cells until their maturation [4]. Xanthopterin is an extensively conjugated compound. The granules housing the xanthopterin are barrel-shaped and tightly packed, so as to increase the effective surface area available for absorption. This effect here is similar to that obtained by the nanoparticles in a dye-sensitized solar cell [24].

The primary method whereby crustaceans harden their cuticle is calcification i.e., the deposition of calcium salts on the organic matrix. It was long ago theorized by Digby [25] that there seems to be a diffusion potential across the crustacean cuticle with the inside negative with respect to the outside and the electrons moving through the semiconductive materials inside the cuticle. The Oriental hornet displays a similar phenomenon, in that there is a potential differential in the yellow stripe between the negative hypocuticle and the positive exocuticle. We note that upon exposure to UV illumination the potential differential increases whereas in the dark the differential decreases. However, although this repeated itself in all three studied gastral yellow stripes of the same worker hornet and even between one worker to another. The differences between the stripes were both in the rate of response as well as in the sum difference of potential between the positive exocuticle and the negative hypocuticle. The discrepancies here stemmed from three main reasons, namely: 1) Each measured worker hornet differed in age from its mate. In this regard, we need to remind that absorption by the cuticle is age-dependent, and in the adult workers there is drop in the absorbance capacity, owing to the fact that on prolonged light exposure during the active season, the yellow granules are progressively photodamaged. 2) Hemolymph streams in the spaces between the yellow granules. To examine the yellow stripe, we detach it from the hornet proper and thereby cause stoppage of the flow of hemolymph and its drying which, in turn, causes change in the measured results. 3) In its natural state the yellow stripe is oval in shape. However, for purpose of examination we need to stretch it, an even though the stripe is still resilient we inevitably induce minute cracks in the stripe, such as could affect the uniformity of the results. The three mentioned drawbacks diminish the ability of the yellow stripe to develop maximal energy, as is enabled in its natural environment when it is part of a living hornet. Even so, we were able to record a difference of potentials increases up to 214mv during the passage from darkness to light. To assess the biologic contribution of these findings, we compared them to prevalent photosynthesis systems. In our case the energy at a wavelength of 386nm was 3.18ev, whereas in photosynthesis systems with absorbance at 670nm or more, the energy of the primary electron was 1.83ev (in Photosystem II). Thus in a worker hornet, the initial energy excess obtained was higher by 70% than that in the mentioned photosynthetic process. A primary excess of 1.2 ev has been recorded in marine photosynthetic microbes which utilize wavelengths of up to 1000nm [26]. The synthesis of ADP from ATP requires 7.3Kcal/mol [27], while the passage of two electrons requires a potential cascade of 0.158ev. It is acceptable that in photosynthetic systems, the overall efficiency is lower when the excess in the photovoltaic gradient is utilized to compensate for the efficiency losses in the course of the process. In the present case, the obtained potentials differential is typical for the membranal potential in excitable tissue.

## ACKNOWLEDGMENTS

We thank the Israeli Ministry of Immigrant Absorption for their generous support of Dr. Stanislav Volynchik.

## REFERENCES

- [1] Spradbery, J. P. (1973). *Wasps*: An Account of the Biology and Natural History of Solitary and Social wasps. Sidgwick and Jackson, London.
- [2] Plotkin, M., Volynchik, S., Ermakov, N. Y., Benyamin, A., Boiko, Y., Bergman, D. J. & Ishay, J. S. (2009). Xanthopterin in the Oriental Hornet (*Vespa orientalis*): Light Absorbance is Increased with Maturation of Yellow Pigment Granules. *Photochem. Photobiol.*, 85, 955-961.
- [3] Plotkin, M., Volynchik, S., Itzhaky, D., Lis, M., Bergman, D. J. & Ishay, J. S. (2009). Some Liver Functions in the Oriental Hornet (*Vespa orientalis*) are Performed in its Cuticle: Exposure to UV light Influences these Activities. *Comp. Biochem. Physiol. Part A*, 153, 131-135.
- [4] Plotkin, M., Volynchik, S., Barkay, Z., Bergman, D. J. & Ishay, J. S. (2009). Micromorphology and Maturation of the Yellow Granules in the Hornet Gastral Cuticle. *Zool. Res.*, 30, 65-73.
- [5] Volynchik, S., Plotkin, M., Bergman, D. J. & Ishay J. S. (2008). Hornet flight activity and its correlation with UVB radiation, temperature and relative humidity. *Photochem. Photobiol.*, 84, 81-85.
- [6] Ishay, J. S. & Croitoru, N. (1978). Photoelectric properties of the yellow 'strips' of social wasps. *Experientia*, 34, 340-342.
- [7] Shimony, T. B. & Ishay, J. S. (1981). Thermoelectric (Seebeck) effect on the cuticle of social wasps. *J. Theor. Biol.*, 92, 497-503.
- [8] Rosenzweig, E., Fuchs, C. & Ishay, J. S. (1985). Electrical resistance of hornet cuticle: changes induced by Xanthines- a statistical model. *Physiol. Chem. Phys. Med. NMR*, 17, 435-449.
- [9] Shimony, (Benshalom) T. & Ishay, J. S. (1984). Electrical capacitance in hornet integument: frequency, light and temperature dependence; possible p-n junction effects. *Physiol. Chem. Phys. Med. NMR*, 16, 333-349.
- [10] Ben-Shalom, A., Eshed, C., Benshalom-Shimony, T. & Ishay, J. S. (1988). A theoretical model of electrical properties of the Oriental hornet cuticle. *Physiol. Chem. Phys. Med. NMR*, 20, 227-239.
- [11] Jongebloed, W. L. & Kalicharan, D. (1994). Tannic acid /arginine/ osmium tetroxide fixation of rat tissue by the microwave procedure. *Beitr. Elektronenmikroskop Direktabb. Oberfl.*, 27, 243-252.
- [12] Ishay, J. S. (1964). Observations sur la biologie de la Guêpe orientale *Vespa orientalis* en Israël. *Insect. Soc.*, XI, 193-206.
- [13] Ishay, J. S. & Kirshboim, S. (2000). Ultraviolet B light stimulates hornet activities- a review. *Semicond. Sci. Technol.*, 15, 704-723.
- [14] Willis, J. H. (1999). Cuticular proteins in insects and crustaceans. *Amer. Zool.*, 39, 600-609.
- [15] Kleinholtz, L. H. (1959). Purines and pteridines from the reflecting pigment of the arthropod retina. *Biol. Bull.*, (Woods Hole, Mass.), 116, 125-135.
- [16] Zynar, E. S. & Nicol, J. A. C. (1971). Ocular reflecting pigments of some Malacostraca. *J. Exp. Mar. Biol. Ecol.*, 6, 235-248.

- 
- [17] Veron, J .E. N., O'Farrell, A. F. & Dixon, B. (1974). The fine structure of Odonata chromatophores. *Tissue & Cell*, *6*, 613-626.
  - [18] Schliwa, M. & Euteneuer, U. (1979). Hybrid pigment organelles in an invertebrate. *Cell Tissue Res.*, *196*, 541-543.
  - [19] Le Guyader, S. & Jesuthasan, S. (2002). Analysis of xanthophore and pterinosome biogenesis in zebrafish using methylene blue and pteridine autofluorescence. *Pigment Cell Res.*, *15*, 27-31.
  - [20] Bagnara, J. T., Matsumoto, J., Ferris, W., Frast, S. K., Turner, W. A. Jr., Tchen, T. T. & Taylor, J. D. (1979). *Common origin of pigment cells*. *Science*, *203*, 410-415.
  - [21] Bronner-Fraser, M. (1994). Neural crest cell formation and migration in the developing embryo. *FASEB J.*, *8*, 699-706.
  - [22] Le Douarin, N. (1982). *The Neural Crest*. Cambridge University Press, London.
  - [23] Wijnen, B., Leertouwer, H. L. & Stavenga, D. G. (2007). Colors and pterin pigmentation of pierid butterfly wings. *J. Insect. Physiol.*, *53*, 1206-1217.
  - [24] O'Regan, B. & Grätzel, M. (1991). A low-cost, high-efficiency solar cell based on dye-sensitized colloidal TiO<sub>2</sub> films. *Nature*, *353*, 737-740.
  - [25] Digby, P. S. B. (1965). Semi-conduction and electrode processes in biological material. I. Crustacea and certain soft-bodied forms. *Proc. Roy. Soc. London Ser. B.*, *161*, 504-525.
  - [26] Green, B. R. & Parson, W. W. (eds) (2003). *Light-Harvesting Antennas in Photosynthesis* Kluwer Academic Publishers, Dordrecht, The Netherlands.
  - [27] Lehninger, A. L., Nelson D. L. & Cox, M. M. (2000). *Principles of Biochemistry*. 2nd ed., Worth Publishers Inc. New York, 558-560.

## ***Chapter 13***

# **COMMENTARY: APPLICATION OF IMAGING MASS SPECTROMETRY TO PHOTOBIOLOGY**

***Takahiro Hayasaka<sup>1</sup>, Takayuki Naito<sup>2</sup>, and Mitsutoshi Setou<sup>1,\*</sup>***

<sup>1</sup>Department of Molecular Anatomy, Molecular Imaging Frontier Research Center, Hamamatsu University School of Medicine, 1-20-1 Handayama, Higashi-ku, Hamamatsu, Shizuoka 431-3192, Japan.

<sup>2</sup>Molecular Neuroscience Unit, Okinawa Institute of Science and Technology (OIST) Promotion Corporation, 12-2 Suzaki, Uruma, Okinawa 904-2234, Japan

## **ABSTRACT**

Within the field of photobiology, the mechanism of phototransduction has been a subject of intense investigation. Phototransduction is regulated by the light-sensitive interaction among visual pigment-coupled receptor proteins, such as rhodopsin, in the retina. There are some reports that the conformation of rhodopsin is influenced by the composition of phospholipids in the lipid bilayer membrane. Very recently, we reported the distribution of retinal phospholipids based on *in situ* analysis with vacuum type imaging mass spectrometry. However, there has been no *in situ* analysis of retinal phospholipids under natural conditions with atmospheric pressure. We recently developed an atmospheric pressure matrix-assisted laser desorption/ionization (AP-MALDI)-based imaging mass spectrometry (IMS) system. This system enables us to perform structural analyses using a tandem mass spectrometer, as well as to visualize phospholipids and peptides with high spatial resolution in frozen sections. In the present study, we used the AP-MALDI-based IMS system to visualize and identify phospholipids in mouse retinal sections. From a spectrum obtained by raster-scanned analysis of the sections, peaks with high intensities were analyzed by tandem mass spectrometry (MS/MS) analysis. As a result, six diacyl-phosphatidylcholine (PC) species, i.e., PC (16:0/16:0), PC (16:0/18:1), PC (16:0/22:6), PC (18:0/18:0), PC (18:0/18:1), and PC (18:0/22:6), were identified. The ion images revealed different distributions on the retinal

---

\* Corresponding author: Department of Molecular Anatomy, Hamamatsu University School of Medicine, 1-20-1 Handayama, Higashi-ku, Hamamatsu, Shizuoka 431-3192, Japan, Tel: (+81) 53 435 2292, Fax: (+81) 53 435 2292, E-mail: setou@hama-med.ac.jp.

sections: PC (16:0/18:1), PC (18:0/18:0), and PC (18:0/18:1) were distributed in the inner plexiform, PC (16:0/16:0) in the inner plexiform layer, inner segment and outer segment, and both PC (16:0/22:6) and PC (18:0/22:6) in the inner and outer segments. The AP-MALDI-based IMS system demonstrated a zonal distribution of PC species on the retinal sections. Therefore, this approach may be useful for analyzing the phototransduction mechanism through phospholipids and the association of phospholipids in such diseases.

## INTRODUCTION

In the field of photobiology, the retina has been one of the most frequently studied organs. In the retina, phototransduction is regulated by the light-sensitive interaction among visual pigment-coupled receptor proteins, such as rhodopsin [1]. Numerous researchers have studied the rhodopsin and phospholipid molecular species around the retina as an experimental model of neural transmission [2, 3]. The membrane protein rhodopsin changes its conformation into an active form, metarhodopsin II, when it absorbs a photon, and the relationship between this form and the lipid bilayer membrane anchoring rhodopsin has been studied. Botelho et al. have used plasmon-waveguide resonance to demonstrate the conformational change in rhodopsin corresponding to a light stimulus in a lipid bilayer membrane formed with phosphatidylcholine (PC) and phosphatidylethanolamine [4]. Alves et al. have discovered that the conformation of rhodopsin does not change in the dark, but rather is dependent on a light stimulus [5]. Thus, these authors considered that the structure of rhodopsin changes in correspondence with the composition of phospholipids comprising the lipid bilayer as well as in reaction to a light stimulus. However, the distribution of phospholipids in the inner segment and outer segment, where rhodopsin actually exists, has not been analyzed *in situ* until recently due to technical limitations.

The neuronal retina is an ordered laminar tissue comprised of three cellular layers and two synaptic layers with a total width of about 200 µm (Figure 1), and each of the layers has a homogenous distribution of biomolecules. The most posterior cellular layer is the ganglion cell layer (Figure 1(a)), which is comprised of retinal ganglion cells (RGC), which project to the brain, and amacrine cells, which are inhibitory interneurons. The center cellular layer is the inner nuclear layer (INL; Figure 1(c)), which is comprised of horizontal cell, amacrine cells and glutamatergic interneurons termed bipolar cells. The most outer cellular layers are termed the photoreceptor layer and the outer nuclear layer (ONL). The photoreceptor layer is further segregated into inner segments (IS; Figure 1(f)) and outer segments (OS; Figure 1(g)). In the outside, there is the pigment epithelium (PE; Figure 1(h)). And the outer nuclear layer (Figure 1(e)) is comprised of the cell bodies of the photoreceptor cells, with the inner and outer segments being extensions of the cell bodies. There are also two synaptic layers. The outer plexiform layer (OPL; Figure 1(d)) contains synapses between photoreceptors and bipolar cell dendrites. The inner plexiform layer (IPL; Figure 1(b)) contains synapses between bipolar axons, amacrine cells and RGC dendrites. It is further divided into 5 layers that are functionally distinct.

In the techniques of metabolomics, proteomics, and transcriptomics, there is an important problem in regard to the loss of distributional information for the biomolecules of interest due to the homogenization sample preparation. In the method used to visualize the distribution of proteins in a living organism, antibodies and green fluorescent proteins (GFPs) are used to

label a target protein for observation with a microscope. The antibodies cannot identify detailed structural differences, such as the fatty acids in phospholipids and the post-translational changes in proteins. GFPs cannot also label phospholipids. Recently, imaging mass spectrometry (IMS) has been used to directly identify the distribution of all the detected molecules, such as phospholipids [6-10], proteins [11] and glycolipids [6, 9]. Many IMS systems adopt the matrix-assisted laser desorption/ionization (MALDI) technique for the ionization at the surface of tissue sections. The ionized biomolecules are measured by time-of-flight (TOF). In IMS measurement, the tissue surface is scanned with the laser. From all measurement points, the spectra are obtained. An arbitrary peak is selected and the signal intensity is compared among all measurement points. The relative value of the signal intensity at each measurement point is highlighted by special software to construct an ion image of the biomolecules. In particular, the combination of quadrupole ion trap (QIT) and tandem mass spectrometry has advantages for the molecular identification of analytes from a complex mixture on the tissue surface.

In parallel with other groups, our research team has advanced the development of IMS. A large number of signals can now be detected from a tissue section due to the recent improvements [6, 12, 13] in a pretreatment technique that greatly improves the detection sensitivity as well as the development of approaches for processing and analyzing the IMS data [14]. Thus, IMS has been applied for imaging of biological samples, such as the organs of various animals [7, 8, 13, 15] human pathological samples [16] and Scrapper-knockout mice [17] for various purposes, including the study of drug distributions.

Very recently, we developed a mass spectrometry imager with higher spatial resolution than the naked eye that combines an atmospheric pressure matrix-assisted laser desorption/ionization (AP-MALDI) with a QIT-time-of-flight (TOF) analyzer named the “Mass Microscope” [18]. In the chamber, the tissue sections can be observed microscopically with a CCD camera (magnification,  $\times 1.25$ ,  $\times 2.5$ ,  $\times 5$ ,  $\times 10$ ,  $\times 20$ , and  $\times 40$ ; Olympus Corporation, Tokyo, Japan). To illuminate the sample, one of two types of illuminators is

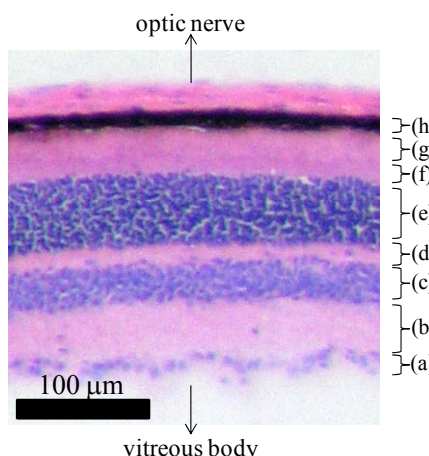


Figure 1. Optical image of a retinal section. The individual layers of this section from a mouse eye are delineated by hematoxylin and eosin staining: (a) ganglion cell layer, (b) inner plexiform layer, (c) inner nuclear layer, (d) outer plexiform layer, (e) outer nuclear layer, (f) inner segment, (g) outer segment, and (h) pigment epithelium.

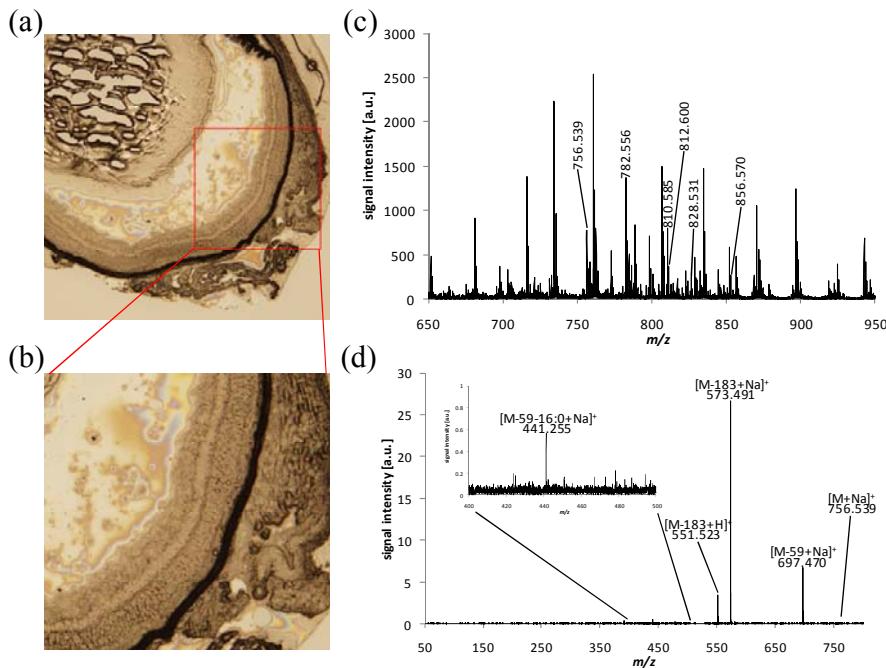


Figure 2. MS and MS/MS analyses of the mouse retina section. From the mouse eye section (a), an area of the retina (b) was chosen and analyzed. The mass spectrum obtained from a mouse retinal section and averaged from all measurement points (c). Six peaks were identified with MS/MS analyses and the values at  $m/z$  were indicated over each peak in the mass spectrum. The representative product-ion spectrum from  $m/z$  756.539 is shown (d).

chosen: a transmitted light illuminator or a reflected light illuminator, depending on the sample type and the purpose of the observations. Foci and observation points are controlled by type and the purpose of the observations. Foci and observation points are controlled by using a joystick to control an XYZ stage (Kohzu Precision, Kanagawa, Japan) on which the sample is mounted.

In this commentary, we will describe the application of AP-MALDI-based IMS to the analysis of mouse retina sections. The eyeballs enucleated from eight-week-old male C57BL/6J mice were immediately frozen in liquid nitrogen-cooled isopentane. The frozen sections of the mouse eyeballs were cut to a thickness of 10  $\mu\text{m}$  using a cryostat (CRYOCUT CM 1950; Leica Microsystems, Wetzler, Germany). Sections were thaw-mounted onto an indium-tin-oxide (ITO)-coated glass slide (Bruker Daltonics, Bremen, Germany). The sections were placed in a polycarbonate tube and stored at  $-80^\circ\text{C}$  until their analysis. An optimum cutting temperature (OCT) polymer was used only to fix each eyeball onto a support stand and was not used for embedding the eyeball, because the residual polymer on the sections might have degraded the mass spectra. The sections were thawed in their tubes at room temperature for 20 min. A thin matrix layer was applied to the surface by a 0.2-mm nozzle caliber airbrush (Procon Boy FWA Platinum; Mr. Hobby, Tokyo, Japan). A 2,5-dihydroxybenzoic acid (DHB) matrix solution (50 mg/mL in 70% methanol/0.1% TFA, 1 ml) was sprayed onto the surface of each section. After drying, the ITO glass slide was attached to an MS target plate. An electrical image of each section on the MS target plate was obtained by a flatbed scanner.

All analyses were performed in positive-ion mode with a AP-MALDI-QIT-TOF-type mass spectrometer (Shimadzu Corporation, Kyoto, Japan) equipped with a 355 nm Nd:YAG laser. In this experiment, the data acquisition and processing were controlled by LCMS Solution and MMS softwares (Shimadzu Corporation). Each raster scan was performed in square regions of 1,000  $\mu\text{m}$  x 1,000  $\mu\text{m}$  with a measurement pitch of 10  $\mu\text{m}$  automatically, giving a total of 10,000 data points (Figure 2(a) and (b)). Laser irradiation consisted of 200 shots in each spot. The construction of the ion image was performed using BioMap software. The ion images were normalized based on total ion current by the function of MMS software. Phospholipid species were identified as molecular species using tandem mass spectrometry (MS/MS) analyses. The serial sections were used for the raster scan and MS/MS analyses. The database on the Metabolite MS Search website (<http://www.hmdb.ca/labm/jsp/mlims/MSDbParent.jsp>) was used to help identify the biomolecules.

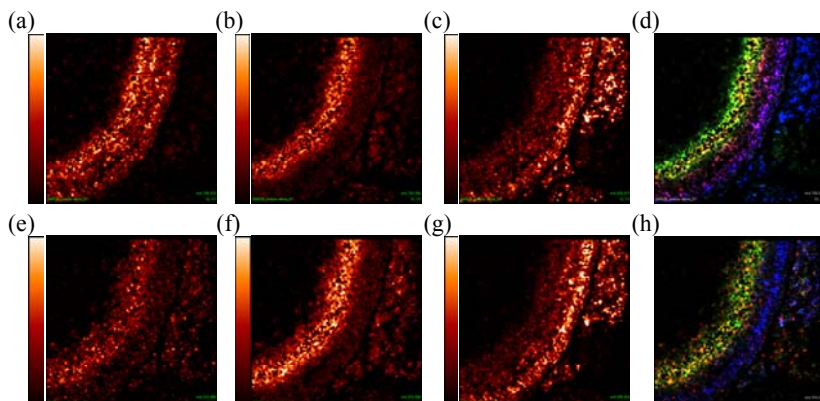


Figure 3. Ion images from six peaks and the merged ion images. The ion images at  $m/z$  756.539 (a),  $m/z$  782.556 (b), and  $m/z$  828.531 (c) were constructed and merged (d). In the same way, the ion images at  $m/z$  812.600 (e),  $m/z$  810.585 (f), and  $m/z$  856.570 (g) were constructed and merged (h).

After spraying a DHB matrix solution onto a mouse retinal section, the mass spectrum was obtained by a raster scan with our IMS system. The representative mass spectrum was accumulated and all profiles obtained from a single raster scan were accumulated (Figure 2(c)). The spectrum was obtained in the range of  $m/z$  650 to  $m/z$  950, in which many peaks representing phospholipids were detected. Several peaks were identified with MS/MS analyses. The product-ion spectra from six peaks were obtained by MS/MS analyses of mouse retinal sections, and a representative spectrum is shown in Figure 2(d). In the product-ion spectrum of  $m/z$  756.539, the fragment peaks at  $m/z$  697.470,  $m/z$  573.491, and  $m/z$  551.523 corresponded to NLs of 59 Daltons (Da) and 183 Da from the precursor ion and an NL of 22 Da from  $m/z$  573.491, indicating that the precursor ion was sodium-adducted. The NLs of 59 Da and 183 Da are known to represent trimethylamine and choline headgroup, respectively, which are part of the PC species and have been detected by MS/MS analysis of alkali-metal adducted PC species [19]. IMS measurement has also been used to identify PC species with alkali adducts [20]. The Metabolite MS Search database helped us to identify this PC, and then the PC of  $m/z$  756.539 was identified as  $[\text{PC}(\text{diacyl-32:0}) + \text{Na}]^+$ . Moreover, MS/MS analyses using our IMS system were able to detect the NL of fatty acid from PC species. The fragment peak at  $m/z$  441.255 is the NL of fatty acid (16:0) and trimethylamine from the

precursor ion of  $m/z$  756.539. The NL of fatty acids from alkali-metal, such as lithium, -adducted PC species has been reported by ESI/MS/MS analysis [19]. Therefore, [PC (diacyl-32:0) + Na] $^+$  can be identified in detail as [PC (16:0/16:0) + Na] $^+$ . In the same way, the other peaks,  $m/z$  782.556,  $m/z$  828.531,  $m/z$  812.600,  $m/z$  810.585, and  $m/z$  856.570, are identified as [PC (16:0/18:1) + Na] $^+$ , [PC (16:0/22:6) + Na] $^+$ , [PC (18:0/18:0) + Na] $^+$ , [PC (18:0/18:1) + Na] $^+$ , and [PC (18:0/22:6) + Na] $^+$ .

The ion images were constructed from six peaks identified by MS/MS analyses. We used the software package BioMap. The ion image are highlighted in correspondence with the signal intensity for each measurement point. As a result, the ion image for PC (16:0/16:0) (Figure 3(a)) was strongly highlighted in the IPL, the IS and the OS. The detailed distribution was clearly shown in the mouse retina section because our AP-MALDI-based IMS system enabled us to perform high resolution IMS measurement. The resolution was 10  $\mu\text{m}$ . In the commercial instrument, the resolution is over 20  $\mu\text{m}$ . Three ion images of PC (16:0/18:1) (Figure 3(b)), PC (18:0/18:0) (Figure 3(e)), and PC (18:0/18:1) (Figure 3(f)) were distributed in the IPL. Two ion images of PC (16:0/22:6) (Figure 3(c)) and PC (18:0/22:6) (Figure 3(g)) were distributed in the IS and OS. The ion images from PC species including 16:0 or 18:0 at sn-1 were merged (Figure 3(d) and (h)). The merged image revealed the specific zonal distribution of PC species in the mouse retina section. It can be seen that four or more zones are distributed across the merged image, including the overlapping area among PC species. In particular, the accuracy of the MALDI-based IMS experiment was demonstrated by the finding that PC species with DHA (22:6) were distributed in the IS and OS, where rhodopsin is richly present, and the PE, because it is known that PC with DHA are bound to rhodopsin [21]. In addition, DHA plays an important role in the development of visual function [22] and in promoting survival [23] and inhibiting apoptosis [24] of photoreceptors. In addition, polyunsaturated fatty acids, such as DHA, are a major target of lipid peroxidation, which contributes to several diseases, such as age-related macular degeneration [25], diabetic retinopathy [26], and Smith-Lemli-Opitz syndrome [27]. Our IMS system is expected to be useful for analyzing the phototransduction mechanism through phospholipids and the association of phospholipids in such diseases.

## REFERENCES

- [1] Menon, S. T., Han, M. & Sakmar, T. P. (2001). Rhodopsin: structural basis of molecular physiology. *Physiol Rev*, *81*, 1659-1688.
- [2] Kihara, A. H., Santos, T. O., Paschon, V., Matos, R. J. & Britto, L. R. (2008). Lack of photoreceptor signaling alters the expression of specific synaptic proteins in the retina. *Neuroscience*, *151*, 995-1005.
- [3] Grishanin, R. N., Yang, H., Liu, X., Donohue-Rolfe, K., Nune, G. C., Zang, K., Xu, B., Duncan, J. L., Lavail, M. M., Copenhagen, D. R. & Reichardt, L. F. (2008). Retinal TrkB receptors regulate neural development in the inner, but not outer, retina. *Mol Cell Neurosci*, *38*, 431-443.
- [4] Botelho, A. V., Gibson, N. J., Thurmond, R. L., Wang, Y. & Brown, M. F. (2002). Conformational energetics of rhodopsin modulated by nonlamellar-forming lipids. *Biochemistry*, *41*, 6354-6368.

- [5] Alves, I. D., Salgado, G. F., Salamon, Z., Brown, M. F., Tollin, G. & Hruby, V. J. (2005). Phosphatidylethanolamine enhances rhodopsin photoactivation and transducin binding in a solid supported lipid bilayer as determined using plasmon-waveguide resonance spectroscopy. *Biophys J*, 88, 198-210.
- [6] Hayasaka, T., Goto-Inoue, N., Sugiura, Y., Zaima, N., Nakanishi, H., Ohishi, K., Nakanishi, S., Naito, T., Taguchi, R. & Setou, M. (2008). Matrix-assisted laser desorption/ionization quadrupole ion trap time-of-flight (MALDI-QIT-TOF)-based imaging mass spectrometry reveals a layered distribution of phospholipid molecular species in the mouse retina. *Rapid Commun Mass Spectrom*, 22, 3415-3426.
- [7] Hayasaka, T., Goto-Inoue, N., Zaima, N., Kimura, Y. & Setou, M. (2009). Organ-specific distributions of lysophosphatidylcholine and triacylglycerol in mouse embryo. *Lipids*, 44, 837-848.
- [8] Shimma, S., Sugiura, Y., Hayasaka, T., Zaima, N., Matsumoto, M. & Setou, M. (2008). Mass imaging and identification of biomolecules with MALDI-QIT-TOF-based system. *Anal Chem*, 80, 878-885.
- [9] Goto-Inoue, N., Hayasaka, T., Taki, T., Gonzalez, T. V. & Setou, M. (2009). A new lipidomics approach by thin-layer chromatography-blot-matrix-assisted laser desorption/ionization imaging mass spectrometry for analyzing detailed patterns of phospholipid molecular species. *J Chromatogr A*,
- [10] Sugiura, Y., Konishi, Y., Zaima, N., Kajihara, S., Nakanishi, H., Taguchi, R., Setou, M. (2009). Visualization of the cell-selective distribution of PUFA-containing phosphatidylcholines in mouse brain by imaging mass spectrometry. *J Lipid Res*,
- [11] Burnum, K. E., Tranguch, S., Mi, D., Daikoku, T., Dey, S. K. & Caprioli, R. M. (2008). Imaging mass spectrometry reveals unique protein profiles during embryo implantation. *Endocrinology*, 149, 3274-3278.
- [12] Shimma, S., Furuta, M., Ichimura, K., Yoshida, Y. & Setou, M. (2006). A novel approach to in situ proteome analysis using a chemical inkjet printing technology and MALDI-QIT-TOF tandem mass spectrometer. *Surf Int Anal*, 38, 1712-1714.
- [13] Ikegami, K., Heier, R. L., Taruishi, M., Takagi, H., Mukai, M., Shimma, S., Taira, S., Hatanaka, K., Morone, N., Yao, I., Campbell, P. K., Yuasa, S., Janke, C., Macgregor, G. R. & Setou, M. (2007). Loss of alpha-tubulin polyglutamylation in ROSA22 mice is associated with abnormal targeting of KIF1A and modulated synaptic function. *Proc Natl Acad Sci U S A*, 104, 3213-3218.
- [14] Zaima, N., Matsuyama, Y. & Setou, M. (2009). Principal component analysis of direct matrix-assisted laser desorption/ionization mass spectrometric data related to metabolites of fatty liver. *J Oleo Sci*, 58, 267-273.
- [15] Zaima, N., Hayasaka, T., Goto-Inoue, N. & Setou, M. (2009). Imaging of metabolites by MALDI mass spectrometry. *J Oleo Sci*, 58, 415-419.
- [16] Shimma, S. & Setou, M. (2007). Mass microscopy to reveal distinct localization of heme B ( $m/z$  616) in colon cancer liver metastasis. *J Mass Spectrom Soc Jpn*, 55, 145-148.
- [17] Yao, I., Sugiura, Y., Matsumoto, M. & Setou, M. (2008). In situ proteomics with imaging mass spectrometry and principal component analysis in the Scrapper-knockout mouse brain. *Proteomics*, 8, 3692-3701.
- [18] Harada, T., Yuba-Kubo, A., Sugiura, Y., Zaima, N., Hayasaka, T., Goto-Inoue, N., Wakui, M., Suematsu, M., Takeshita, K., Ogawa, K., Yoshida, T. & Setou, M. (in

- press) Visualization of Volatile Substances in Different Organelles with an Atmospheric-Pressure Mass Microscope. *Anal Chem*,
- [19] Hsu, F. F. & Turk, J. (2003). Electrospray ionization/tandem quadrupole mass spectrometric studies on phosphatidylcholines: the fragmentation processes. *J Am Soc Mass Spectrom*, *14*, 352-363.
- [20] Woods, A. S. & Jackson, S. N. (2006). Brain tissue lipidomics: direct probing using matrix-assisted laser desorption/ionization mass spectrometry. *Aaps J*, *8*, E391-395.
- [21] Aveldano, M. I. (1988). Phospholipid species containing long and very long polyenoic fatty acids remain with rhodopsin after hexane extraction of photoreceptor membranes. *Biochemistry*, *27*, 1229-1239.
- [22] Alessandri, J. M., Goustard, B., Guesnet, P. & Durand, G. (1998). Docosahexaenoic acid concentrations in retinal phospholipids of piglets fed an infant formula enriched with long-chain polyunsaturated fatty acids: effects of egg phospholipids and fish oils with different ratios of eicosapentaenoic acid to docosahexaenoic acid. *Am J Clin Nutr*, *67*, 377-385.
- [23] Rotstein, N. P., Aveldano, M. I., Barrantes, F. J. & Politi, L. E. (1996). Docosahexaenoic acid is required for the survival of rat retinal photoreceptors in vitro. *J Neurochem*, *66*, 1851-1859.
- [24] Rotstein, N. P., Aveldano, M. I., Barrantes, F. J., Roccamo, A. M. & Politi, L. E. (1997). Apoptosis of retinal photoreceptors during development in vitro: protective effect of docosahexaenoic acid. *J Neurochem*, *69*, 504-513.
- [25] Suzuki, M., Kamei, M., Itabe, H., Yoneda, K., Bando, H., Kume, N. & Tano, Y. (2007). Oxidized phospholipids in the macula increase with age and in eyes with age-related macular degeneration. *Mol Vis*, *13*, 772-778.
- [26] Pan, H. Z., Zhang, H., Chang, D., Li, H. & Sui, H. (2008). The change of oxidative stress products in diabetes mellitus and diabetic retinopathy. *Br J Ophthalmol*, *92*, 548-551.
- [27] Ford, D. A., Monda, J. K., Brush, R. S., Anderson, R. E., Richards, M. J. & Fliesler, S. J. (2008). Lipidomic analysis of the retina in a rat model of Smith-Lemli-Opitz syndrome: alterations in docosahexaenoic acid content of phospholipid molecular species. *J Neurochem*, *105*, 1032-1047.

***Chapter 14***

# **COORDINATIVE AND DYNAMIC REGULATION OF TRANSLATION AND TRANSCRIPTION BY NITRIC OXIDE AND SUPEROXIDE UPON ULTRAVIOLET LIGHT IRRADIATION**

***Shiyong Wu and Oliver L. Carpenter***

Department of Chemistry and Biochemistry, Edison Biotechnology Institute,  
Ohio University, Athens, Ohio 45701.

## **ABSTRACT**

Exposure to ultraviolet light (UV) leads to a rapid elevation of nitric oxide ( $\text{NO}^\bullet$ ) and superoxide ( $\text{O}_2^{\cdot-}$ ) in irradiated cells.  $\text{NO}^\bullet$  competes with superoxide dismutase (SOD) for  $\text{O}_2^{\cdot-}$  to form peroxynitrite ( $\text{ONOO}^-$ ), which increases the oxidative stress and reduces  $\text{NO}^\bullet$  bioavailability. The balance between  $\text{NO}^\bullet$  and  $\text{ONOO}^-$  plays significant roles in regulation of gene expression at both the translational and transcriptional levels. In mammalian cells, three nitric oxide synthases (NOS) – neuronal NOS (nNOS, NOS1), inducible NOS (iNOS, NOS2) and endothelial NOS (eNOS, NOS3) catalyze L-arginine (L-Arg) to generate  $\text{NO}^\bullet$  in response to UV-irradiation. Depending on the type of cells and physical properties of the irradiation, the patterns of  $\text{NO}^\bullet$  and  $\text{ONOO}^-$  productions can be very dynamic. The production of  $\text{NO}^\bullet$  and  $\text{ONOO}^-$  leads to the phosphorylation of the alpha subunit of the eukaryotic initiation factor 2alpha (eIF2 $\alpha$ ) by two eIF2 $\alpha$  kinases (EIF2AK) - the dsRNA-dependent protein kinase-like endoplasmic reticulum (ER) kinase (PERK, EIF2AK3) and the general control nonderepressible protein kinase 2 (GCN2, EIF2AK4). The activation of EIF2AKs and phosphorylation of eIF2 $\alpha$  inhibit global protein synthesis, which leads to the activation of transcription factor - nuclear factor kappa-light-chain-enhancer of activated B cells (NF- $\kappa$ B). Additionally, production of  $\text{NO}^\bullet$  and  $\text{ONOO}^-$  generates oxidative and nitrosative stresses that induce signaling pathways that further modulate transcriptional activation. The combined effect of translational and transcriptional regulation ultimately determines aspects of cell physiology, such as growth and death.

## PART I. THE DYNAMICS AND MECHANISMS FOR GENERATION OF NO<sup>•</sup>, O<sub>2</sub><sup>•-</sup> AND ONOO<sup>-</sup> BY UV RADIATION (UVR)

### Introduction

UVR is divided into three categories: UVA (400-320 nm); UVB (320-280 nm) and UVC (280-100 nm). While all three categories of UVR have been shown to be capable of inducing the production of NO<sup>•</sup> and O<sub>2</sub><sup>•-</sup> in cells, the mechanisms and dynamics in the generation of these molecules could be very different depending on the wavelength, dose and dose-rate of UVR. UVA and UVB exist in solar light that reaches the earth's surface and are used for studying UV-related skin damage [1-4] and photo relaxation [5]. UVC is a germicidal light that is often used for studying DNA damage [6]. Due to the properties of electromagnetic radiation, the UV dose and dose rate used in generation of NO<sup>•</sup> vary between categories of UV light. The efficiency for UV-induced NO<sup>•</sup> production appears more correlated to dose rate and energy of photons than to total dose received by cells. Based on Planck's Equation:

$$E = \frac{hc}{\lambda} \quad (h: \text{Planck's constant}; c: \text{speed of light}; \lambda: \text{wavelength}),$$

energy per photon ranges from 3.10-3.87 eV for UVA, 3.87-4.43 eV for UVB and 4.43-12.4 eV for UVC. Much more total energy of UVA is needed to induce NO<sup>•</sup> production than the total energy of UVB or UVC that is needed. Common experimental dose values for UVA can range between 1000 and 40,000 mJ/cm<sup>2</sup> while UVB can range from 5-200 mJ/cm<sup>2</sup> and UVC 1-10 mJ/cm<sup>2</sup> [7-11].

### The Dynamics of NO<sup>•</sup> Production after UV-Irradiation

NO<sup>•</sup> generation upon treatment with UVR also varies between time points and cell type. An increase in NO<sup>•</sup> release can be observed almost immediately following ultraviolet A, B or C irradiation [5,9,12]. NO<sup>•</sup> is released at an initial rate of 0.117 nM per sec in endothelial cells at 5 sec after UVA-irradiation [5]. An increase of [NO<sup>•</sup>] is recorded at 20 sec and reached a peak at 40 sec in keratinocytes after UVB-irradiation (30 mJ/cm<sup>2</sup>) [13]. The UVB-induced elevation of NO<sup>•</sup> is dose-dependent in a range of 0-100 mJ/cm<sup>2</sup> [2]. UVC also induces NO<sup>•</sup> release from microvessels isolated from rat skin by approximately 35% or 55% within 5 or 10 min respectively [9]. NO<sup>•</sup> generation continues to increase in a time-dependent fashion within the first 2 hours post irradiation leading to a 3-fold maximum increase [1,2,14-16]. Maximal prolonged NO<sup>•</sup> generation occurs between 17 and 48 hours post irradiation based on cell type and can range from 1.5-fold to 3-fold [3,17]. However, by 6 hours post irradiation, NO<sup>•</sup> generation has returned to near basal levels [3,4]. Varying dose rates are required to elicit similar responses within various cells lines. Human keratinocytes exhibit a maximal NO<sup>•</sup> release of 3-fold with a treatment of 120 mJ/cm<sup>2</sup> UVB while human endothelium cells require only 60 mJ/cm<sup>2</sup> UVB to generate a similar NO<sup>•</sup> release. Treatments over these thresholds result in similar decreases in generation of NO<sup>•</sup> within both cell lines [1,15].

## The Mechanisms for UV-Induced Elevation of NO<sup>•</sup>

The initial release of NO<sup>•</sup> upon treatment with UVR has been found to be dependent on the activation of constitutive NOS (cNOS) and on photosensitive storage molecules of NO<sup>•</sup> [1,14,18-20]. The UVR-induced production of NO<sup>•</sup> is dependent on Ca<sup>2+</sup>/calmodulin and purified eNOS produces 3 times more NO<sup>•</sup> after UVR treatment. However, inhibition of NOS is not able to totally prevent NO<sup>•</sup> production indicating the existence of other sources for NO<sup>•</sup> production [1,2]. High performance liquid chromatography analysis of S-nitrosoglutathione (GSNO) stores within mouse aortic tissues post irradiation have shown a significant decrease in concentration after UVR, correlating with an increase in NO<sup>•</sup> levels and photorelaxation. These tissues also exhibit an increase in GSNO concentration when cells are treated with a solution containing 2 mM NO<sup>•</sup>. However, diabetic tissues with no detectable levels of GSNO still exhibit relaxation when exposed to UVR, suggesting a role for other S-nitrosothiols or other NO<sup>•</sup> storage molecules [19]. Additionally, small molecules, such as *N*<sup>G</sup>-nitro-L-arginine (L-NA) and NaNO<sub>2</sub> have also exhibited the ability to increase photorelaxation within rabbit corpus cavernosum. These molecules, when in solution, were shown to release NO<sup>•</sup> upon stimulation with UVA [18]. Another study utilizing UVA found that nitrite stores give a low level of NO<sup>•</sup> release while S-nitrosothiols are the predominant storage species for NO<sup>•</sup> release. This study also found that nitrates and nitrogen-bound S-nitroso compounds had little to no effect on NO<sup>•</sup> release [20]. The prolonged elevation of NO<sup>•</sup> is associated with an increase in expression and activation of both cNOS and iNOS [1,2,14,15,21,22]. Control of iNOS expression is the result of both transcriptional and translational regulation following irradiation [3,17].

## The Generation of O<sub>2</sub><sup>•-</sup> By UVR

In addition to the generation of NO<sup>•</sup> following UVR exposure, O<sub>2</sub><sup>•-</sup> is also generated from several potential sources in cells including water photolysis, NAD(P)H oxidase, cNOS and xanthine oxidase (XO) [12,23-27]. XO is one of the major sources for O<sub>2</sub><sup>•-</sup> generation in irradiated cells. Ultraviolet radiation stimulates XO, which converts hypoxanthine to xanthine and is responsible for the production of O<sub>2</sub><sup>•-</sup> as a byproduct. O<sub>2</sub><sup>•-</sup> generation following UVR treatment is dependent on dose and can result in a 5 to 15-fold increase upon treatment with 100 mJ/cm<sup>2</sup> UVB depending on cell type [14-16]. Release of O<sub>2</sub><sup>•-</sup> has been shown to directly correlate in a near one-to-one fashion with XO activation. Additionally, inhibitors of XO, such as allopurinol and oxypurinol, are capable of decreasing O<sub>2</sub><sup>•-</sup> release between 50% and 80%, which implicates XO as the major source of O<sub>2</sub><sup>•-</sup> in response to UVR [15,16,25]. Another potential effective generator of O<sub>2</sub><sup>•-</sup> is uncoupled cNOS [27]. UVR-activated NOS generates NO<sup>•</sup> from L-arginine (L-Arg). Since [L-Arg] is low in cells, rapid consumption of L-Arg results in a L-Arg depletion, which leads to cNOS uncoupling and increased production of O<sub>2</sub><sup>•-</sup> [13,27,28].

## The Formation of ONOO<sup>-</sup> upon UVR

NO<sup>•</sup> is able to compete with SOD for O<sub>2</sub><sup>•-</sup> to form ONOO<sup>-</sup>, which is a powerful oxidant [23]. The reaction rate for NO<sup>•</sup> and O<sub>2</sub><sup>•-</sup> to form ONOO<sup>-</sup> is approximately  $7 \times 10^9 \text{ M}^{-1} \text{ sec}^{-1}$  [29]. ONOO<sup>-</sup> formation rate is controlled by the diffusion rates of its reactants, thus as NO<sup>•</sup> and O<sub>2</sub><sup>•-</sup> generation increases in response to time point and UVR dose, ONOO<sup>-</sup> generation increases concurrently [1,14-16]. Within keratinocytes, ONOO<sup>-</sup> formation reaches a level of 6-fold that of the control within 60 minutes with a treatment of 20 mJ/cm<sup>2</sup> and a maximum of an 8 to 9-fold increase in response to a UVB dose of 200 mJ/cm<sup>2</sup> [1,14]. Rabbit brain synaptosomes show a linear generation of ONOO<sup>-</sup> in response to UVB with a 7-fold increase observed at a dose of 100 mJ/cm<sup>2</sup> [16]. ONOO<sup>-</sup> can peroxidize lipid membranes, which results in a decrease in membrane fluidity. This decrease in fluidity has been observed in keratinocytes to correlate with a prolonged activity in a particulate form of NOS. The change in fluidity of the NOS microenvironment as an effect of lipid peroxidation results in continuation of NOS activation and therefore NO<sup>•</sup> release after the initial UV response, thus serving as a positive feedback mechanism [14]. However, a study utilizing hairless mice has shown lipid peroxidation levels to decrease in response to UVB over a 6-24 hours time period. This observation has been proposed to be an effect of systemic factors not observed within cell cultures, such as release of prostaglandin, histamine and cytokines during the inflammatory response to UVR [3].

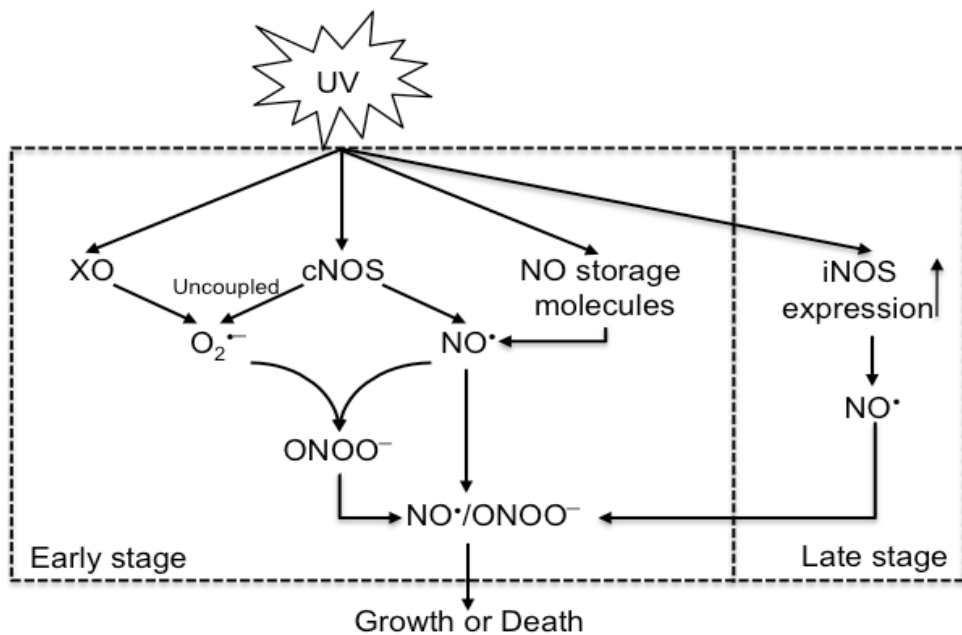
## The Roles of NO<sup>•</sup>/ONOO<sup>-</sup> in Regulation of Apoptosis upon UV Irradiation

The release of NO<sup>•</sup> after UVR has been shown to be capable of pro- or anti-apoptotic effects. However, the mechanism of NO<sup>•</sup>-mediated regulation of apoptosis upon UV irradiation is still under elucidation. An elevation in [NO<sup>•</sup>] has predominately been shown to protect cells from UV-induced apoptosis [30-33]. NO<sup>•</sup> prevents UV-induced apoptosis by inhibiting the phosphorylation of Ser46 of p53 and impairs its nuclear import [34,35]. NO<sup>•</sup> also inhibits apoptosis by various mechanisms including S-nitrosylation of caspases and transglutaminase (tTG) [36]. The level and duration of NO<sup>•</sup> elevation is a critical factor in determination of its role in regulation of apoptosis. Low doses and pretreatment with NO<sup>•</sup> have been shown to attenuate apoptosis. Low-level treatment of macrophages with NO<sup>•</sup> leads to increased levels of COX-2 expression, which resulted in an increase in cell survival [37,38]. Additionally, early transient activation of JNK in cardiac myocytes has been shown to decrease apoptosis in response to oxidative stress [37]. However, high and prolonged levels of NO<sup>•</sup> are generally observed with the pro-apoptotic activation of JNK [39,40], which leads to activation of caspase-3 and modulation of apoptosis-associated proteins, such as Bcl-2, leading to increased levels of apoptosis [41]. Another factor that determines the pro- or anti-apoptotic role of NO<sup>•</sup> is the level of O<sub>2</sub><sup>•-</sup> present [11]. O<sub>2</sub><sup>•-</sup> reacts with NO<sup>•</sup> to form ONOO<sup>-</sup>. In the presence of high level of O<sub>2</sub><sup>•-</sup>, the bioavailability of NO<sup>•</sup> is reduced with the elevation of ONOO<sup>-</sup>, which is more reactive than NO<sup>•</sup> and O<sub>2</sub><sup>•-</sup> and induces oxidative protein modifications including oxidation or nitration of various amino acid residues such as methionine, cysteine, tryptophan, and tyrosine [42-45]. An elevation of ONOO<sup>-</sup> has been shown to promote apoptosis [46-48]. Treating cells with an ONOO<sup>-</sup> generator Sin-1 induced

ER-stress and apoptosis [49].  $\text{ONOO}^-$  can also promote apoptosis by activating the MAPK signaling cascade and deactivating Akt signaling pathways [50].

## Conclusion

UVA, B and C light are able to immediately induce an elevation of  $\text{NO}^\bullet$ . The release of NO appears in two stages. In the early stage (within 6 hours post-UVR),  $\text{NO}^\bullet$  is generated from L-Arg via activation of cNOS and from photosensitive NO $^\bullet$  storage molecules, such as GSNO. In the late stage (6-24 hours post-UVR), most  $\text{NO}^\bullet$  is generated by iNOS due to an increase in its expression level and activity. UV irradiation also induces an immediate production of  $\text{O}_2^\bullet^-$  from XO and uncoupled cNOS *et al.*  $\text{NO}^\bullet$  rapidly reacts with  $\text{O}_2^\bullet^-$  to form  $\text{ONOO}^-$ , which induces oxidative and nitrosative stresses.  $\text{ONOO}^-$  can also induce cNOS uncoupling, resulting in an increase in the production of  $\text{O}_2^\bullet^-$ . The ratio of  $\text{NO}^\bullet/\text{ONOO}^-$  has a significant impact in determination of growth or death rates within irradiated cells. As the bioavailability of  $\text{NO}^\bullet$  decreases, the ratio of  $\text{NO}^\bullet/\text{ONOO}^-$  lowers and cell death rates increase due to the activation of apoptotic cascades. However, this process can be interrupted by late stage production of  $\text{NO}^\bullet$ , which increases the ratio of  $\text{NO}^\bullet/\text{ONOO}^-$  (Fig. 1).



Nitric oxide synthase-mediated regulation of translation and transcription after UVR

Figure 1. A model for  $\text{NO}^\bullet/\text{ONOO}^-$ -mediated cell growth and death upon UV irradiation.

## PART II. NITRIC OXIDE SYNTHASE-MEDIATED REGULATION OF TRANSLATION AND TRANSCRIPTION AFTER UVR

### Introduction

Eukaryotic initiation factor 2 regulates translation by forming an eIF2•GTP•Met-tRNA<sub>i</sub> ternary complex, which promotes the binding of Met-tRNA<sub>i</sub> to the 40S ribosome-mRNA complex at the expense of hydrolyzation of GTP to GDP. In order to restart the initiation cycle, the guanine exchange factor eIF2B refreshes the eIF2-GDP to eIF2-GTP [51]. Phosphorylation on Ser51 of eIF2 $\alpha$  stabilizes the eIF2-GDP-eIF2B complex preventing GDP-GTP exchange, thus halting the translational initiation process [52-54]. Environmental stimuli inhibit initiation of protein synthesis by activating one or more EIF2AKs. Four protein kinases are known to phosphorylate Ser51 in eIF2 $\alpha$  in response to different stress stimuli: (1) the heme-regulated inhibitor kinase (HRI, EIF2AK1) that responds to heme deprivation [55]; (2) the dsRNA-dependent protein kinase (PKR, EIF2AK2) that is activated by dsRNA produced during viral infection [56]; (3) PERK that responds to the accumulation of unfolded proteins in the ER as well as glucose depletion [57,58]; and (4) GCN2 that responds to amino acid depletion [59]. Previous studies demonstrated that PERK and GCN2 could mediate translational inhibition in response to UV irradiation [60-62]. The UV-induced activation of PERK and GCN2 also leads to NF- $\kappa$ B activation via the eIF2 $\alpha$  phosphorylation pathway [63-65].

### Nitric Oxide Synthase-Mediated Phosphorylation of eIF2 $\alpha$ upon UVR

Recently, NOS has been shown to play a key role in coordinating the activation of both PERK and GCN2 upon UVB-irradiation [28]. The UVB-activated NOS produces NO $^{\bullet}$ , which reacts with O<sub>2</sub> $^{-}$  to form ONOO $^{-}$  and activate PERK. NO $^{\bullet}$  and ONOO $^{-}$  have been shown to directly or indirectly induce endoplasmic reticulum (ER)-stress and unfolding protein response (UPR), which are the key inducers for PERK activation. NO $^{\bullet}$  inhibits the sarcoendoplasmic reticulum pump Ca<sup>2+</sup> ATPase 1 (SERCA 1) by a direct interaction with the pump resulting in a decrease in Ca<sup>2+</sup> uptake in the ER [66,67]. NO $^{\bullet}$  production is also associated with the down regulation of SERCA mRNA synthesis, which leads to the depletion of Ca<sup>2+</sup> stores resulting in ER stress [68]. ONOO $^{-}$  has also been implicated in the direct inhibition of the SERCA isoform 2b [69]. Depletion of Ca<sup>2+</sup> stores results in improper protein folding which activates the unfolded protein response (UPR) [70]. Additionally, NO $^{\bullet}$  also mediates cytokine-induced UPR. Inhibition of NO $^{\bullet}$  production reduces IL-1-induced elevation and slicing of Xbp-1 mRNA [71], which is an indicator of the elevation of the UPR and ER-stress [72,73]. The UPR consists of the activation of several proteins involved in proper ER protein folding as well as specific kinases to help moderate function. PERK is one such kinase activated by the UPR and ER-stress [57,74]. Once activated, PERK phosphorylates eIF2 $\alpha$  at serine 51, which globally inhibits protein translation. This helps alleviate the level of unfolded protein in the ER by reducing the level of newly synthesized protein that enters the ER for post-translational modification [28,60,63,74]. Treatment with

the NOS inhibitor N<sup>G</sup>-Methyl-L-Arginine (LNMMA) or the GSH precursor N-Acetyl-L-Cysteine (LNAC) reduces the level of eIF2 $\alpha$  phosphorylation upon UVB-irradiation suggesting the role of NO $^\bullet$  and ONOO $^-$  in UVB-induced activation of PERK [28].

While elevation of NO $^\bullet$  and ONOO $^-$  induces PERK activation, the consumption of L-Arg by NOS during NO $^\bullet$  production leads to L-Arg depletion and GCN2 activation. L-Arg is the only substrate for NOS mediated NO $^\bullet$  synthesis. Upon activation of NOS, cellular L-Arg levels begin to deplete as it is converted to NO $^\bullet$  and L-Citrulline. This depletion can eventually lead to L-Arg starvation [75]. In order to alleviate the demand for L-Arg in translation, L-Arg sensitive GCN2 phosphorylates eIF2 $\alpha$  leading to inhibition of protein synthesis [75]. Additionally, depletion of L-Arg leads to NOS uncoupling and the generation of O<sub>2</sub> $^\bullet^-$ , which can then react with NO $^\bullet$  to generate ONOO $^-$  resulting in further oxidative and ER stress culminating in additional PERK activation. Supplementation with L-Arg has demonstrated the ability to decrease eIF2 phosphorylation, however this addition could subsequently allow for an increase in NO $^\bullet$  and thereafter PERK activation [28]. In UVB-irradiated mouse embryonic fibroblast (MEF) cells, treatment with the NOS inhibitor LNMMA or supplementation with L-Arg significantly reduces phosphorylation of eIF2 $\alpha$  compared to untreated UV irradiated cells. Treatment with LNAC to scavenge O<sub>2</sub> $^\bullet^-$  shows a significant decrease in eIF2 $\alpha$  phosphorylation, indicating the importance of oxidative stress. Additionally, knockouts of PERK or GCN2 reduce or eliminate the increase of eIF2 $\alpha$  phosphorylation after UVB-irradiation [28]. Combined, UVB-induced activation of PERK and GCN2 plays a significant role in regulating the phosphorylation of eIF2 $\alpha$ .

## Phosphorylation of eIF2 $\alpha$ -Mediated NF- $\kappa$ B Activation in the Early Phase of UVR

UV-induced activation of NF- $\kappa$ B is a postponed and prolonged process. In the late phase (12-24 hours post-UV) [76,77], an inhibitor of NF- $\kappa$ B (I $\kappa$ B) kinase (IKK) is activated and phosphorylates I $\kappa$ B $\alpha$  at Ser32 and Ser36 [78,79], which leads to its dissociation from the NF- $\kappa$ B and rapid degradation through the polyubiquitin-dependent proteasomal pathway [80]. The removal of I $\kappa$ B exposes a nuclear localization signal on NF- $\kappa$ B that allows it to be shuttled into the nucleus and activate target genes [81-83]. However, this canonical pathway is not applicable to UV-induced early phase (within 12 hours) activation of NF- $\kappa$ B [76,77,84]. During this time UVR does not induce IKK activation nor N-terminal serine phosphorylation of I $\kappa$ B $\alpha$  [77]. However, while IKK activation is not detected above the basal level after UV-irradiation, IKK activity is still required as the IKK-targeted serine phosphorylation sites on I $\kappa$ B $\alpha$  are critical for UV-induced NF- $\kappa$ B activation [85].

The early phase activation of NF- $\kappa$ B after UVR is mediated via an eIF2 $\alpha$  phosphorylation and translational inhibition signaling pathway [63,64]. In this pathway, translational inhibition due to the phosphorylation of eIF2 $\alpha$  results in a decreased I $\kappa$ B synthesis. Reduced expression of I $\kappa$ B in combination with its short half-life decrease total I $\kappa$ B, which allows NF- $\kappa$ B to exist in the uninhibited state and translocate to the nucleus where it carries out its function. The activation of eIF2 $\alpha$  kinases, PERK and GCN2, regulate the early phase activation of NF- $\kappa$ B. Accordingly, when a PERK or GCN2 knockout cell line

was used in studies, the UV-induced eIF2 $\alpha$  phosphorylation and NF- $\kappa$ B activation was significantly inhibited [63,64]. Analysis of NF- $\kappa$ B activation in a MEF cell line containing an eIF2 $\alpha$  mutant in which serine 51 was mutated to alanine (MEF<sup>A/A</sup>) showed similar inhibition of NF- $\kappa$ B [65].

While IKK activation and I $\kappa$ B degradation do occur in the late phase of UVR, a recent study suggests that this may not be the cause of NF- $\kappa$ B activation [86]. The reason is that the activation of NF- $\kappa$ B in the MEF<sup>A/A</sup> cell line is independent of I $\kappa$ B depletion during the late phase of UVR [63,86]. Further studies indicate that neither ubiquitination nor proteasomal degradation have detectable contributions to late-phase UV-induced I $\kappa$ B $\alpha$  depletion. Phosphorylation of Ser536 of NF- $\kappa$ B (p65), which is a direct target of activated IKK [87,88], is not induced after UVR. However, phosphorylation levels of Ser276 of NF- $\kappa$ B (p65), which is targeted by mitogen and stress activated protein kinases (MSK) in the nucleus [89] and protein kinase A (PKA) in the cytosol [90-92], have been shown to be dramatically increased in the nucleus, but not in cytosol. These results lead to a hypothesis that UV-induced late-phase activation of NF- $\kappa$ B is mediated by the MSK signaling pathway [86,89].

## Potential Roles of NO $^\bullet$ and O<sub>2</sub> $^{\bullet-}$ in Direct Mediation of Transcription Activation upon UVR

The UV-induced activation of MSKs and their downstream transcription activators are potentially mediated by the elevation of NO $^\bullet$  in combination with oxidative stress. NO $^\bullet$  generated from NOS has been shown to activate MSKs by activation of a 38 kDa MAPK (p38) and extracellular signal-related kinases (ERK) [93,94]. Activation of MSK via p38 is mediated by stress generated by NO $^\bullet$  and oxidative stress that activates MEK3 and MEK6, the upstream kinases responsible for the phosphorylation of p38. Once activated, p38 translocates to the nucleus where it activates MSK via phosphorylation [95]. Additionally ERKs are also responsible for the activation of MSK. Activation of ERKs involve surface receptors such as tyrosine kinase and G protein coupled receptors. These receptors elicit Ras and Raf activation, which in turn activates the kinases MEK1 and MEK2 upstream of ERK. Activated ERK then translocates to the nucleus and phosphorylates MSK [95].

MSKs are responsible for the regulation of transcription factors as well as for remodeling of the chromatin structure [94]. MSKs regulate transcriptional regulation by activation of the transcription factors cAMP response element binding protein (CREB) and NF- $\kappa$ B [38,94]. MSKs, along with ribosomal S6 kinase 2 (RSK2), are the key kinases responsible for the activation of CREB, which mediates transcriptional regulation of a number of genes involved in the inflammation process. Upon activation, MSK targets CREB for phosphorylation on Ser133 conferring to it full transcriptional activation [94]. MSKs are also responsible for the activation of the transcription factor NF- $\kappa$ B via a non-canonical pathway. Activation of NF- $\kappa$ B via MSK1 is reliant upon the phosphorylation of NF- $\kappa$ B on serine 276 of the p65 subunit [89,94].

In addition to direct regulation of transcription by the activation of transcription factors, MSKs are also involved in the remodeling of chromatin; further adding to its role in transcriptional regulation. MSKs are capable of phosphorylating histone 3 (H3) at Ser10 and

Ser28 [94,96,97]. Both isoforms 1 and 2 of MSK have been shown to phosphorylate H3, however MSK2 has been observed to play a more crucial role in H3 modification [94]. Phosphorylation of either of these sites on H3 results in a change in conformational, as well as a change in charge on the molecule; both of which play important roles in chromatin binding [94,97]. In this way, MSK is capable of regulating transcription by direct activation of transcription factors as well as modifying the availability of genes for transcription.

## UV-Induced and NO<sup>•</sup>-Mediated Translational Regulation and Apoptosis

NOS mediates the UV-induced phosphorylation of eIF2 $\alpha$  through activation of both PERK and GCN2 [28]. Phosphorylation of eIF2 $\alpha$  plays roles in regulation of apoptosis due to various stimuli. MEF cells with a GCN2 knockout ( $MEF^{GCN2^{-/-}}$ ) are more susceptible to UV-induced apoptosis [64,98], which is similar to the  $MEF^{A/A}$  cells in which the phosphorylation site, Ser51, of eIF2 $\alpha$  is replaced with a non-phosphorylatable Ala (Ser51Ala) [98]. Additionally, PARP expression in  $MEF^{A/A}$  cells is reduced without being cleaved after UVR. In contrast, PARP is cleaved without a significant decrease in parental PARP in  $MEF^{S/S}$  cells after treatment with UVR. It appears that inhibition of eIF2 $\alpha$  phosphorylation sensitizes MEF cells to apoptosis by reducing PARP via a caspase independent signaling pathway [99]. In contrast to  $MEF^{GCN2^{-/-}}$  and  $MEF^{A/A}$  cells, cells with a PERK knockout or cells transfected with a dominant negative PERK are less sensitive to UV-induced apoptosis. Overexpression of wild-type PERK also sensitizes cells to UV-induced apoptosis without directly inducing cell death [98]. It is known that activation of PERK could be involved in pro- or anti-apoptotic cell death. PERK activation promotes reperfusion-induced apoptosis of brain cells by inducing the synthesis of ATF4, which transcriptionally up-regulates CHOP expression [100-102]. However, PERK activation can also protect pancreatic beta cells from ER-stress induced apoptosis [103,104]. PERK activation appears to play a pro-apoptotic role in regulation of UV-induced apoptosis.

## Conclusion

UV-induced NOS activation and NO<sup>•</sup> production mediates both translational and transcriptional regulation of gene expression. UVR induced NOS activation results in a rapid generation of NO<sup>•</sup> from L-Arg. The consumption of L-Arg leads to a shortage of the amino acid, which activates GCN2 and induces cNOS uncoupling. Uncoupled cNOS produces O<sub>2</sub><sup>•-</sup>, which is also generated by XO *et al* upon UV irradiation. In combination with NO<sup>•</sup> production, increased levels of O<sub>2</sub><sup>•-</sup> lead to an elevation in ONOO<sup>-</sup>, which generates oxidative/nitrosative stress and activates PERK. Activated PERK and GCN2 catalyze the phosphorylation of eIF2 $\alpha$  which subsequently inhibits protein synthesis. During the early phase response to irradiation, UV-induced translational inhibition leads to a reduction in I $\kappa$ B followed by NF- $\kappa$ B activation. The release of NO<sup>•</sup> upon UV irradiation also induces transcriptional activation of multiple signaling pathways. Induction of the MSK signaling pathway leads to the activation of NF- $\kappa$ B during the late phase response to UV irradiation. NO<sup>•</sup>, in combination with oxidative stress, activates p38 MAPK and ERK which

phosphorylate MSK. Subsequently, activated MSK can then phosphorylate Ser276 on NF- $\kappa$ B, resulting in activation of NF- $\kappa$ B in a mechanism independent of IKK-mediated reduction of I $\kappa$ B (Fig. 2). In this fashion, NOS-mediated activation of EIF2AKs, phosphorylation of eIF2 $\alpha$  and activation of NF- $\kappa$ B coordinately regulate apoptotic cell death in response to UV irradiation.

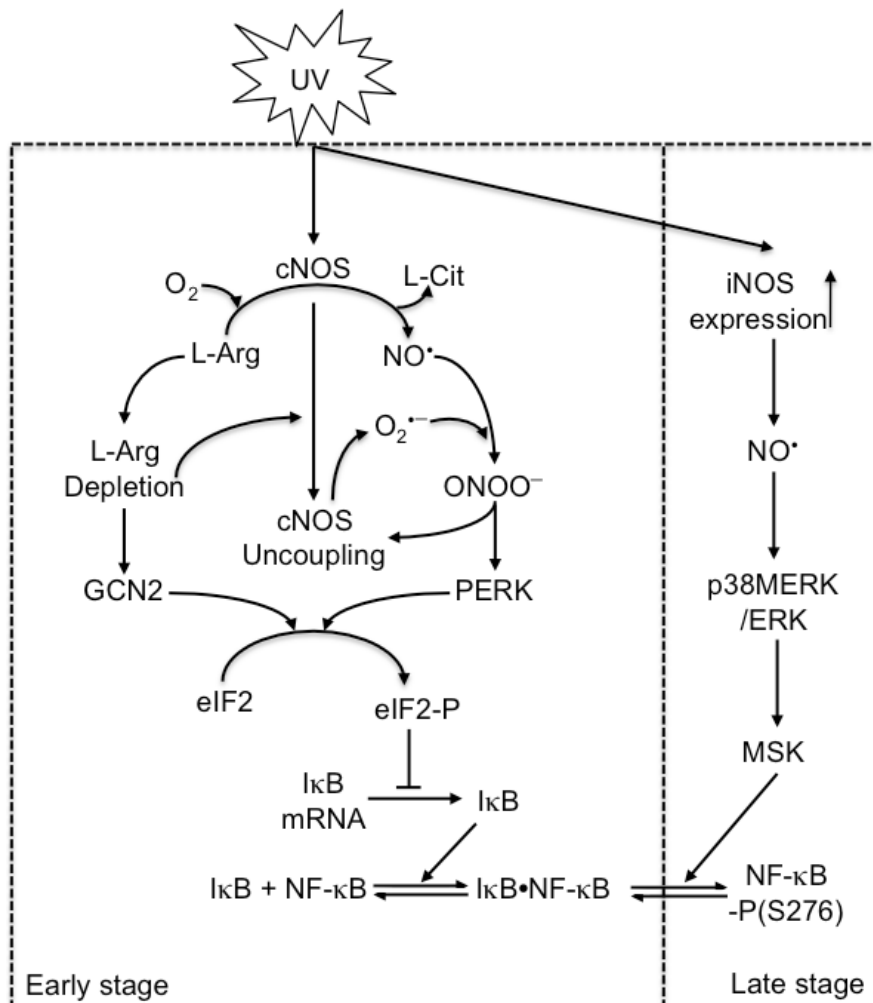


Figure 2. A model for UVR-induced and NOS-mediated eIF2 $\alpha$  phosphorylation and NF- $\kappa$ B activation.

## REFERENCES

- [1] Deliconstantinos, G; Villiotou, V; Stavrides, JC. Alterations of nitric oxide synthase and xanthine oxidase activities of human keratinocytes by ultraviolet B radiation.

- Potential role for peroxynitrite in skin inflammation. *Biochem Pharmacol*, 1996, 51(12), 1727-1738.
- [2] Deliconstantinos, G; Villiotou, V; Stravrides, JC. Release by ultraviolet B (u.v.B) radiation of nitric oxide (NO) from human keratinocytes: a potential role for nitric oxide in erythema production. *Br J Pharmacol*, 1995, 114(6), 1257-1265.
  - [3] Gonzalez Maglio, DH; Paz, ML; Ferrari, A; et al. Skin damage and mitochondrial dysfunction after acute ultraviolet B irradiation: relationship with nitric oxide production. *Photodermat Photoimmunol Photomed*, 2005, 21(6), 311-317.
  - [4] Paz, ML; Gonzalez Maglio, DH; Weill, FS; Bustamante, J; Leoni, J. Mitochondrial dysfunction and cellular stress progression after ultraviolet B irradiation in human keratinocytes. *Photodermat Photoimmunol Photomed*, 2008, 24(3), 115-122.
  - [5] Kubaszewski, E; Peters, A; McClain, S; Bohr, D; Malinski, T. Light-activated release of nitric oxide from vascular smooth muscle of normotensive and hypertensive rats. *Biochem Biophys Res Commun*, 1994, 200(1), 213-218.
  - [6] Cadet, J; Sage, E; Douki, T. Ultraviolet radiation-mediated damage to cellular DNA. *Mutat Res*, 2005, 571(1-2), 3-17.
  - [7] Cejkova, J; Ardan, T; Cejka, C; Kovaceva, J; Zidek, Z. Irradiation of the rabbit cornea with UVB rays stimulates the expression of nitric oxide synthases-generated nitric oxide and the formation of cytotoxic nitrogen-related oxidants. *Histol Histopathol*, 2005, 20(2), 467-473.
  - [8] Combes, A; McTiernan, C; Brooks, SS; Feldman, AM. UV light synergistically enhances the cardiotoxic effects of interleukin 1beta through peroxynitrite formation. *J Card Fail*, 2001, 7(2), 165-175.
  - [9] Fotiou, S; Fotiou, D; Deliconstantinos, G. Formation of heme-iron complexes with nitric oxide (NO) and peroxynitrite (ONOO-) after ultraviolet radiation as a protective mechanism in rat skin. *In Vivo*, 2009, 23(2), 281-286.
  - [10] Villiotou, V; Deliconstantinos, G. Nitric oxide, peroxynitrite and nitroso-compounds formation by ultraviolet A (UVA) irradiated human squamous cell carcinoma: potential role of nitric oxide in cancer prognosis. *Anticancer Res*, 1995, 15(3), 931-942.
  - [11] Weller, R; Billiar, T; Vodovotz, Y. Pro- and anti-apoptotic effects of nitric oxide in irradiated keratinocytes: the role of superoxide. *Skin Pharmacol Appl Skin Physiol*, 2002, 15(5), 348-352.
  - [12] Aitken, GR; Henderson, JR; Chang, SC; McNeil, CJ; Birch-Machin, MA. Direct monitoring of UV-induced free radical generation in HaCaT keratinocytes. *Clin Exp Dermatol*, 2007, 32(6), 722-727.
  - [13] Wu S, Wang L, Jacoby AM, Kasinski K, Kubant R, and Malinski T. Ultraviolet B Light-Induced Nitric Oxide/Peroxynitrite Imbalance in Keratinocytes – Implication in Apoptosis and Necrosis. *Photochem Photobiol*, 2010, In Press.
  - [14] Deliconstantinos, G; Villiotou, V; Stavrides, JC. Increase of particulate nitric oxide synthase activity and peroxynitrite synthesis in UVB-irradiated keratinocyte membranes. *Biochem J*, 1996, 320, ( Pt 3), 997-1003.
  - [15] Deliconstantinos, G; Villiotou, V; Stavrides, JC. Nitric oxide and peroxynitrite released by ultraviolet B-irradiated human endothelial cells are possibly involved in skin erythema and inflammation. *Exp Physiol*, 1996, 81(6), 1021-1033.

- [16] Deliconstantinos, G; Villiotou, V. NO synthase and xanthine oxidase activities of rabbit brain synaptosomes: peroxynitrite formation as a causative factor of neurotoxicity. *Neurochem Res*, 1996, 21(1), 51-56.
- [17] Seo, SJ; Choi, HG; Chung, HJ; Hong, CK. Time course of expression of mRNA of inducible nitric oxide synthase and generation of nitric oxide by ultraviolet B in keratinocyte cell lines. *Br J Dermatol*, 2002, 147(4), 655-662.
- [18] Buyukafsar, K; Levent, A; Un, I; Ark, M; Arikan, O; Ozveren, E. Mediation of nitric oxide from photosensitive stores in the photorelaxation of the rabbit corpus cavernosum. *Eur J Pharmacol*, 2003, 459(2-3), 263-267.
- [19] Ng, ES; Cheng, ZJ; Ellis, A. et al. Nitrosothiol stores in vascular tissue: modulation by ultraviolet light, acetylcholine and ionomycin. *Eur J Pharmacol*, 2007, 560(2-3), 183-192.
- [20] Paunel, AN; Dejam, A; Thelen, S; et al. Enzyme-independent nitric oxide formation during UVA challenge of human skin: characterization, molecular sources, and mechanisms. *Free Radic Biol Med*, 2005, 38(5), 606-615.
- [21] Chen, YC; Shen, SC; Lee, WR; Lin, HY; Ko, CH; Lee, TJ. Nitric oxide and prostaglandin E2 participate in lipopolysaccharide/interferon-gamma-induced heme oxygenase 1 and prevent RAW264.7 macrophages from UV-irradiation-induced cell death. *J Cell Biochem*, 2002, 86(2), 331-339.
- [22] Kim, JH; Hong, Y; Shim, CS. Mechanism of UV light-induced photorelaxation in isolated rat aorta. *J Vet Sci*, 2000, 1(2), 81-86.
- [23] Kalinowski, L; Malinski, T. Endothelial NADH/NADPH-dependent enzymatic sources of superoxide production: relationship to endothelial dysfunction. *Acta Biochim Pol*, 2004, 51(2), 459-469.
- [24] McCord, JM; Fridovich, I. Production of O<sub>2</sub><sup>-</sup> in photolyzed water demonstrated through the use of superoxide dismutase. *Photochem Photobiol*, 1973, 17(2), 115-121.
- [25] Koncz, P; Szanda, G; Rajki, A; Spat, A. Reactive oxygen species, Ca<sup>2+</sup> signaling and mitochondrial NAD(P)H level in adrenal glomerulosa cells. *Cell Calcium*, 2006, 40(4), 347-357.
- [26] Linetsky, M; James, HL; Ortwerth, BJ. The generation of superoxide anion by the UVA irradiation of human lens proteins. *Exp Eye Res*, 1996, 63(1), 67-74.
- [27] Huk, I; Nanobashvili, J; Neumayer, C; et al. L-arginine treatment alters the kinetics of nitric oxide and superoxide release and reduces ischemia/reperfusion injury in skeletal muscle. *Circulation*, 1997, 96(2), 667-675.
- [28] Lu, W; Laszlo, CF; Miao, Z; Chen, H; Wu, S. The Role of Nitric-oxide Synthase in the Regulation of UVB Light-induced Phosphorylation of the {alpha} Subunit of Eukaryotic Initiation Factor 2. *J Biol Chem*, 2009, 284(36), 24281-24288.
- [29] Padmaja, S; Huie, RE. The reaction of nitric oxide with organic peroxy radicals. *Biochem Biophys Res Commun*, 1993, 195(2), 539-544.
- [30] Lee, SC; Lee, JW; Jung, JE; et al. Protective role of nitric oxide-mediated inflammatory response against lipid peroxidation in ultraviolet B-irradiated skin. *Br J Dermatol*, 2000, 142(4), 653-659.
- [31] Suschek, CV; Krischel, V; Bruch-Gerharz, D; et al. Nitric oxide fully protects against UVA-induced apoptosis in tight correlation with Bcl-2 up-regulation. *J Biol Chem*, 1999, 274(10), 6130-6137.

- [32] Weller, R; Schwentker, A; Billiar, TR; Vodovotz, Y. Autologous nitric oxide protects mouse and human keratinocytes from ultraviolet B radiation-induced apoptosis. *Am J Physiol Cell Physiol*, 2003, 284(5), C1140-1148.
- [33] Yamaoka, J; Kawana, S; Miyachi, Y. Nitric oxide inhibits ultraviolet B-induced murine keratinocyte apoptosis by regulating apoptotic signaling cascades. *Free Radic Res*, 2004, 38(9), 943-950.
- [34] Fukunaga-Takenaka, R; Fukunaga, K; Tatemichi, M; Ohshima, H. Nitric oxide prevents UV-induced phosphorylation of the p53 tumor-suppressor protein at serine 46, a possible role in inhibition of apoptosis. *Biochem Biophys Res Commun*, 2003, 308(4), 966-974.
- [35] Schneiderhan, N; Budde, A; Zhang, Y; Brune, B. Nitric oxide induces phosphorylation of p53 and impairs nuclear export. *Oncogene*, 2003, 22(19), 2857-2868.
- [36] Melino, G; Bernassola, F; Knight, RA; Corasaniti, MT; Nistico, G; Finazzi-Agro, A. S-nitrosylation regulates apoptosis. *Nature*, 1997, 388(6641), 432-433.
- [37] Andreka, P; Zang, J; Dougherty, C; Slepak, TI; Webster, KA; Bishopric, NH. Cytoprotection by Jun kinase during nitric oxide-induced cardiac myocyte apoptosis. *Circ Res*, 2001, 88(3), 305-312.
- [38] von Knethen, A; Callsen, D; Brune, B. NF-kappa, B. AP-1 activation by nitric oxide attenuated apoptotic cell death in RAW 264.7 macrophages. *Mol Biol Cell*, 1999, 10(2), 361-372.
- [39] Chung, HT; Pae, HO; Choi, BM; Billiar, TR; Kim, YM. Nitric oxide as a bioregulator of apoptosis. *Biochem Biophys Res Commun*, 2001, 282(5), 1075-1079.
- [40] Zhang, X; Msc, Moilanen, E; et al. Regulation of eosinophil apoptosis by nitric oxide: Role of c-Jun-N-terminal kinase and signal transducer and activator of transcription 5. *J Allergy Clin Immunol*, 2003, 112(1), 93-101.
- [41] Li, L; Feng, Z; Porter, AG. JNK-dependent phosphorylation of c-Jun on serine 63 mediates nitric oxide-induced apoptosis of neuroblastoma cells. *J Biol Chem*, 2004, 279(6), 4058-4065.
- [42] Kuhn, DM; Aretha, CW; Geddes, TJ. Peroxynitrite inactivation of tyrosine hydroxylase: mediation by sulfhydryl oxidation, not tyrosine nitration. *J Neurosci*, 1999, 19(23), 10289-10294.
- [43] Perrin, D; Koppenol, WH. The quantitative oxidation of methionine to methionine sulfoxide by peroxy nitrite. *Arch Biochem Biophys*, 2000, 377(2), 266-272.
- [44] Tien, M; Berlett, BS; Levine, RL; Chock, PB; Stadtman, ER. Peroxynitrite-mediated modification of proteins at physiological carbon dioxide concentration: pH dependence of carbonyl formation, tyrosine nitration, and methionine oxidation. *Proc Natl Acad Sci, U S A*, 1999, 96(14), 7809-7814.
- [45] Zhang, H; Joseph, J; Feix, J; Hogg, N; Kalyanaraman, B. Nitration and oxidation of a hydrophobic tyrosine probe by peroxy nitrite in membranes: comparison with nitration and oxidation of tyrosine by peroxy nitrite in aqueous solution. *Biochemistry*, 2001, 40(25), 7675-7686.
- [46] Sandoval, M; Ronzio, RA; Muanza, DN; Clark, DA; Miller, MJ. Peroxynitrite-induced apoptosis in epithelial (T84) and macrophage (RAW 264.7) cell lines: effect of legume-derived polyphenols (phytolens). *Nitric Oxide*, 1997, 1(6), 476-483.
- [47] Brune, B; von Knethen, A; Sandau, KB. Nitric oxide, (NO): an effector of apoptosis. *Cell Death Differ*, 1999, 6(10), 969-975.

- [48] Dimmeler, S; Zeiher, AM. Nitric oxide and apoptosis: another paradigm for the double-edged role of nitric oxide. *Nitric Oxide*, 1997, 1(4), 275-281.
- [49] Dickhout, JG; Hossain, GS; Pozza, LM; Zhou, J; Lhotak, S; Austin, RC. Peroxynitrite causes endoplasmic reticulum stress and apoptosis in human vascular endothelium: implications in atherogenesis. *Arterioscler Thromb Vasc Biol*, 2005, 25(12), 2623-2629.
- [50] Shacka, JJ; Sahawneh, MA; Gonzalez, JD; Ye, YZ; D'Alessandro, TL; Estevez, AG. Two distinct signaling pathways regulate peroxynitrite-induced apoptosis in PC12 cells. *Cell Death Differ*, 2006, 13(9), 1506-1514.
- [51] Price, NT; Welsh, GI; Proud, CG. Phosphorylation of only serine-51 in protein synthesis initiation factor-2 is associated with inhibition of peptide-chain initiation in reticulocyte lysates. *Biochem Biophys Res Commun*, 1991, 176(3), 993-999.
- [52] Kimball, SR. Eukaryotic initiation factor eIF2. *Int J Biochem Cell Biol*, 1999, 31(1), 25-29.
- [53] Pain, VM. Initiation of protein synthesis in eukaryotic cells. *Eur J Biochem*, 1996, 236(3), 747-771.
- [54] Sudhakar, A; Ramachandran, A; Ghosh, S; Hasnain, SE; Kaufman, RJ; Ramaiah, KV. Phosphorylation of serine 51 in initiation factor 2 alpha (eIF2 alpha) promotes complex formation between eIF2 alpha(P) and eIF2B and causes inhibition in the guanine nucleotide exchange activity of eIF2B. *Biochemistry*, 2000, 39(42), 12929-12938.
- [55] Ranu, RS. Regulation of protein synthesis in rabbit reticulocyte lysates: the hemeregulated protein kinase (HRI) and double stranded RNA induced protein kinase (dRI) phosphorylate the same site(s) on initiation factor eIF-2. *Biochem Biophys Res Commun*, 1979, 91(4), 1437-1444.
- [56] Kaufman, RJ. The Double-stranded RNA-activated Protein Kinase PKR. In: N; Sonenberg, JWB; Hershey, MB; Mathews, (Eds.), *Translational Control of Gene Expression*. Cold Spring Harbor, New York: CSHL Press, 2000, 503-528.
- [57] Harding, HP; Zhang, Y; Bertolotti, A; Zeng, H; Ron, D. Perk is essential for translational regulation and cell survival during the unfolded protein response. *Mol Cell*, 2000, 5(5), 897-904.
- [58] Fernandez, J; Bode, B; Koromilas, A; et al. Translation mediated by the internal ribosome entry site of the cat-1 mRNA is regulated by glucose availability in a PERK kinase-dependent manner. *J Biol Chem*, 2002, 277(14), 11780-11787.
- [59] Sood, R; Porter, AC; Olsen, DA; Cavener, DR; Wek, RC. A mammalian homologue of GCN2 protein kinase important for translational control by phosphorylation of eukaryotic initiation factor-2alpha. *Genetics*, 2000, 154(2), 787-801.
- [60] Wu, S; Hu, Y; Wang, JL; Chatterjee, M; Shi, Y; Kaufman, RJ. Ultraviolet light inhibits translation through activation of the unfolded protein response kinase PERK in the lumen of the endoplasmic reticulum. *J Biol Chem*, 2002, 277(20), 18077-18083.
- [61] Deng, J; Harding, HP; Raught, B; et al. Activation of GCN2 in UV-irradiated cells inhibits translation. *Curr Biol*, 2002, 12(15), 1279-1286.
- [62] Marbach, I; Licht, R; Frohnmeyer, H; Engelberg, D. Gcn2 mediates Gcn4 activation in response to glucose stimulation or UV radiation not via GCN4 translation. *J Biol Chem*, 2001, 276(20), 16944-16951.
- [63] Wu, S; Tan, M; Hu, Y; Wang, JL; Scheuner, D; Kaufman, RJ. Ultraviolet light activates NFkappaB through translational inhibition of IkappaBalphalpha synthesis. *J Biol Chem*, 2004, 279(33), 34898-34902.

- [64] Jiang, HY; Wek, RC. GCN2 phosphorylation of eIF2alpha activates NF-kappaB in response to UV irradiation. *Biochem J*, 2005, 385(Pt 2), 371-380.
- [65] Deng, J; Lu, PD; Zhang, Y; et al. Translational repression mediates activation of nuclear factor kappa B by phosphorylated translation initiation factor 2. *Mol Cell Biol*, 2004, 24(23), 10161-10168.
- [66] Ishii, T; Sunami, O; Saitoh, N; Nishio, H; Takeuchi, T; Hata, F. Inhibition of skeletal muscle sarcoplasmic reticulum Ca<sup>2+</sup>-ATPase by nitric oxide. *FEBS Lett*, 1998, 440(1-2), 218-222.
- [67] Povreau, S; Jacquemond, V. Nitric oxide synthase inhibition affects sarcoplasmic reticulum Ca<sup>2+</sup> release in skeletal muscle fibres from mouse. *J Physiol*, 2005, 567(Pt 3), 815-828.
- [68] Cardozo, AK; Ortis, F; Storling, J; et al. Cytokines downregulate the sarcoendoplasmic reticulum pump Ca<sup>2+</sup> ATPase 2b and deplete endoplasmic reticulum Ca<sup>2+</sup>, leading to induction of endoplasmic reticulum stress in pancreatic beta-cells. *Diabetes*, 2005, 54(2), 452-461.
- [69] Grover, AK; Kwan, CY; Samson, SE. Effects of peroxynitrite on sarco/endoplasmic reticulum Ca<sup>2+</sup> pump isoforms SERCA2b and SERCA3a. *Am J Physiol Cell Physiol*, 2003, 285(6), C1537-1543.
- [70] Kaufman, RJ. Stress signaling from the lumen of the endoplasmic reticulum: coordination of gene transcriptional and translational controls. *Genes Dev*, 1999, 13(10), 1211-1233.
- [71] Chambers, KT; Unverferth, JA; Weber, SM; Wek, RC; Urano, F; Corbett, JA. The role of nitric oxide and the unfolded protein response in cytokine-induced beta-cell death. *Diabetes*, 2008, 57(1), 124-132.
- [72] Iwawaki, T; Akai, R; Kohno, K; Miura, M. A transgenic mouse model for monitoring endoplasmic reticulum stress. *Nat Med*, 2004, 10(1), 98-102.
- [73] Shen, X; Ellis, RE; Lee, K; et al. Complementary signaling pathways regulate the unfolded protein response and are required for *C. elegans* development. *Cell*, 2001, 107(7), 893-903.
- [74] Harding, HP; Zhang, Y; Ron, D. Protein translation and folding are coupled by an endoplasmic-reticulum-resident kinase. *Nature*, 1999, 397(6716), 271-274.
- [75] Lee, J; Ryu, H; Ferrante, RJ; Morris, SM; Jr., Ratan, RR. Translational control of inducible nitric oxide synthase expression by arginine can explain the arginine paradox. *Proc Natl Acad Sci, U S A*, 2003, 100(8), 4843-4848.
- [76] Li, N; Karin, M. Ionizing radiation and short wavelength UV activate NF-kappaB through two distinct mechanisms. *Proc Natl Acad Sci, U S A*, 1998, 95(22), 13012-13017.
- [77] Bender, K; Gottlicher, M; Whiteside, S; Rahmsdorf, HJ; Herrlich, P. Sequential DNA damage-independent and -dependent activation of NF- kappaB by UV. *Embo J*, 1998, 17(17), 5170-5181.
- [78] Chen, Z; Hagler, J; Palombella, VJ; et al. Signal-induced site-specific phosphorylation targets I kappa B alpha to the ubiquitin-proteasome pathway. *Genes Dev*, 1995, 9(13), 1586-1597.
- [79] Chen, ZJ; Parent, L; Maniatis, T. Site-specific phosphorylation of IkappaBalphalpha by a novel ubiquitination-dependent protein kinase activity. *Cell*, 1996, 84(6), 853-862.

- [80] Karin, M; Ben-Neriah, Y. Phosphorylation meets ubiquitination: the control of NF-[kappa]B activity. *Annu Rev Immunol*, 2000, 18, 621-663.
- [81] Mercurio, F; Zhu, H; Murray, BW; et al. IKK-1 and IKK-2: cytokine-activated IkappaB kinases essential for NF- kappaB activation [see comments]. *Science*, 1997, 278(5339), 860-866.
- [82] DiDonato, JA; Hayakawa, M; Rothwarf, DM; Zandi, E; Karin, M. A cytokine-responsive IkappaB kinase that activates the transcription factor NF-kappaB [see comments]. *Nature*, 1997, 388(6642), 548-554.
- [83] Zandi, E; Chen, Y; Karin, M. Direct phosphorylation of Ikappa B by IKKalpha and IKKbeta: discrimination between free and NF-kappaB-bound substrate. *Science*, 1998, 281(5381), 1360-1363.
- [84] Raine, DA; Jeffrey, IW; Clemens, MJ. Inhibition of the double-stranded RNA-dependent protein kinase PKR by mammalian ribosomes. *FEBS Lett*, 1998, 436(3), 343-348.
- [85] Huang, TT; Feinberg, SL; Suryanarayanan, S; Miyamoto, S. The zinc finger domain of NEMO is selectively required for NF-kappa B activation by UV radiation and topoisomerase inhibitors. *Mol Cell Biol*, 2002, 22(16), 5813-5825.
- [86] Laszlo, CF; Wu, S. Mechanism of UV-induced IkappaBalpalpha-independent activation of NF-kappaB. *Photochem Photobiol*, 2008, 84(6), 1564-1568.
- [87] Okazaki, T; Sakon, S; Sasazuki, T; et al. Phosphorylation of serine 276 is essential for p65 NF-kappaB subunit-dependent cellular responses. *Biochem Biophys Res Commun*, 2003, 300(4), 807-812.
- [88] Sakurai, H; Chiba, H; Miyoshi, H; Sugita, T; Toriumi, W. IkappaB kinases phosphorylate NF-kappaB p65 subunit on serine 536 in the transactivation domain. *J Biol Chem*, 1999, 274(43), 30353-30356.
- [89] Vermeulen, L; De Wilde, G; Van Damme, P; Vanden Berghe, W; Haegeman, G. Transcriptional activation of the NF-kappaB p65 subunit by mitogen- and stress-activated protein kinase-1 (MSK1). *EMBO J*, 2003, 22(6), 1313-1324.
- [90] Zhong, H; May, MJ; Jimi, E; Ghosh, S. The phosphorylation status of nuclear NF-kappa B determines its association with CBP/p300 or HDAC-1. *Mol Cell*, 2002, 9(3), 625-636.
- [91] Zhong, H; SuYang, H; Erdjument-Bromage, H; Tempst, P; Ghosh, S. The transcriptional activity of NF-kappaB is regulated by the IkappaB-associated PKAc subunit through a cyclic AMP-independent mechanism. *Cell*, 1997, 89(3), 413-424.
- [92] Zhong, H; Voll, RE; Ghosh, S. Phosphorylation of NF-kappa B p65 by PKA stimulates transcriptional activity by promoting a novel bivalent interaction with the coactivator CBP/p300. *Mol Cell*, 1998, 1(5), 661-671.
- [93] Lander, HM; Jacobina, AT; Davis, RJ; Tauras, JM. Differential activation of mitogen-activated protein kinases by nitric oxide-related species. *J Biol Chem*, 1996, 271(33), 19705-19709.
- [94] Vermeulen, L; Berghe, WV; Beck, IM; De Bosscher, K; Haegeman, G. The versatile role of MSKs in transcriptional regulation. *Trends Biochem Sci*, 2009, 34(6), 311-318.
- [95] Roux, PP; Blenis, J. ERK and p38 MAPK-activated protein kinases: a family of protein kinases with diverse biological functions. *Microbiol Mol Biol Rev*, 2004, 68(2), 320-344.

- [96] Zhong, S; Zhang, Y; Jansen, C; Goto, H; Inagaki, M; Dong, Z. MAP kinases mediate UVB-induced phosphorylation of histone H3 at serine 28. *J Biol Chem*, 2001, 276(16), 12932-12937.
- [97] Kouzarides, T. Chromatin modifications and their function. *Cell*, 2007, 128(4), 693-705.
- [98] Parker, SH; Parker, TA; George, KS; Wu, S. The roles of translation initiation regulation in ultraviolet light-induced apoptosis. *Mol Cell Biochem*, 2006, 293(1-2), 173-181.
- [99] Yun, SJ; Lee, DJ; Kim, MO; et al. Reduction but not cleavage of poly(ADP-ribose) polymerase during stress-mediated cell death in the rat hippocampus. *Neuroreport*, 2003, 14(7), 935-939.
- [100] Kumar, R; Krause, GS; Yoshida, H; Mori, K; DeGracia, DJ. Dysfunction of the unfolded protein response during global brain ischemia and reperfusion. *J Cereb Blood Flow Metab*, 2003, 23(4), 462-471.
- [101] DeGracia, DJ; Kumar, R; Owen, CR; Krause, GS; White, BC. Molecular pathways of protein synthesis inhibition during brain reperfusion: implications for neuronal survival or death. *J Cereb Blood Flow Metab*, 2002, 22(2), 127-141.
- [102] Jiang, HY; Wek, RC. Phosphorylation of the {alpha}-Subunit of the Eukaryotic Initiation Factor-2 (eIF2{alpha}) Reduces Protein Synthesis and Enhances Apoptosis in Response to Proteasome Inhibition. *J Biol Chem*, 2005, 280(14), 14189-14202.
- [103] Harding, HP; Zeng, H; Zhang, Y; et al. Diabetes mellitus and exocrine pancreatic dysfunction in perk-/- mice reveals a role for translational control in secretory cell survival. *Mol Cell*, 2001, 7(6), 1153-1163.
- [104] Oyadomari, S; Araki, E; Mori, M. Endoplasmic reticulum stress-mediated apoptosis in pancreatic beta-cells. *Apoptosis*, 2002, 7(4), 335-345.



***Chapter 15***

## **PHOTODYNAMIC THERAPY WITH PRESERVED IMMUNE SYSTEM – EXPECTATION FOR TREATMENT FOR LOCALIZED BACTERIAL INFECTION**

***Yuji Morimoto, Masamitsu Tanaka and Manabu Kinoshita***

National Defense Medical College, Tokorozawa, Japan.

### **PERSPECTIVE**

Bacterial infections in orthopedics are resistant to conservative therapies, and patients must therefore undergo invasive treatments and prolonged administration of antibiotics, resulting in a significant decrease in quality of life. A novel strategy for overcoming the current status is therefore needed.

Photodynamic therapy (PDT), a therapeutic modality for proliferating diseases combined with tumor-seeking photosensitizers and low-powered laser irradiation, achieves a successful outcome in clinical use. Photosensitizers are activated by light, resulting in the generation of radical oxygen species (ROSs) such as singlet oxygen, which damage proliferative tissue [1].

There have been some reports on therapeutic applications of PDT for bacterial infections, especially for infections with multi-drug-resistant bacteria [2]. Favorable results of PDT using cultured bacteria *in vitro* have been described in most reports; however, good results *in vivo* have only been described in a few reports [3]. The ineffectiveness is thought to be due to the difficulty in drug delivery of photosensitizers into bacteria in the infectious lesion [4]. However, we have another point of view: immunological competence can play a key role, determining the feasibility of PDT for localized infection.

We showed that PDT for a murine MRSA (methicillin-resistant *Staphylococcus aureus*) arthritis model damages phagocytes such as neutrophils in the lesion, resulting in progression rather than subsidence of the localized infection [5]. Further detailed investigation of PDT parameters (e.g., dye concentration, administration route and light fluence) provided preliminary results indicating that PDT with optimized parameters exerted an *in vivo* therapeutic effect without damaging phagocytes in the lesion.

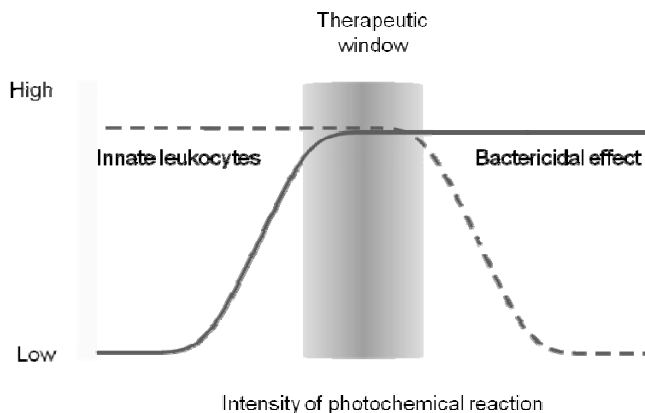


Figure 1. Presumed kinetics of photodynamic responses in local infectious lesion.

We propose a hypothesis shown in Figure 1 as kinetics of PDT for localized infection in orthopedics. In this model, there are two major photodynamic-induced responses that are regulated by the degree of photochemical reaction, and the therapeutic effect is determined by the summation of the two responses. Many previous studies have indicated that an increased photochemical reaction corresponds to an increased bactericidal action by photodynamically reacted ROSs [6]. On the other hand, the results of our preliminary analysis suggest that innate leukocytes such as neutrophils are also injured and are decreased by an increase in the degree of photochemical reaction. Hence, PDT accompanied by intensified photochemical action induces a decrease in the number of bacteria and also a decrease in the number of innate leukocytes in the lesion, resulting in decreased phagocytosis. In the post PDT phase, the attenuated phagocytic action allows a proliferation of residual bacteria even at a trace level since the growth speed of bacteria is generally (doubling time of ~0.5 h) much faster than that of human cells (doubling time of ~24 h), thus exaggerating infection.

Therefore, for the accomplishment of a therapeutic effect on localized infection by PDT, it is important to optimize the degree of photochemical action so as to maximize bactericidal effects and to minimize the loss of innate leukocytes (therapeutic window in Figure 1). In conclusion, consideration of the photodynamic actions on both bacteria and the immune system is important for the success of PDT for localized infection.

## REFERENCES

- [1] Dougherty, TJ; et al. Photodynamic therapy. *J Natl Cancer Inst.*, 1998, 90, 889-905.
- [2] Jori, G; et al. Photodynamic therapy in the treatment of microbial infections: basic principles and perspective applications. *Lasers Surg Med.*, 2006, 38, 468-81.
- [3] Bisland, SK; et al. Pre-clinical in vitro and in vivo studies to examine the potential use of photodynamic therapy in the treatment of osteomyelitis. *Photochem Photobiol Sci.*, 2006, 5, 31-8.
- [4] Lambrechts, SA; et al. Photodynamic therapy for *Staphylococcus aureus* infected burn wounds in mice. *Photochem Photobiol Sci.*, 2005, 4, 503-9.

- [5] Tanaka, M; et al. Influence of intraarticular neutrophils on the effects of photodynamic therapy for murine MRSA arthritis. *Photochem Photobiol.*, In press.
- [6] Hamblin, MR; et al. Photodynamic therapy: a new antimicrobial approach to infectious disease? *Photochem Photobiol Sci.*, 2004, 3, 436-50.



# INDEX

## A

- absorption spectra, 116, 117, 120, 150, 152, 165, 182  
acceptor, viii, ix, x, 70, 73, 74, 75, 77, 85, 88, 115, 123, 128, 134  
acceptors, 86  
accessibility, 99  
accidents, 27  
accommodation, 9, 22  
accounting, 11  
accuracy, 79, 248  
acetate, 160, 173  
acetic acid, 162  
acetone, 96, 162  
acetylcholine, 262  
achievement, 24  
acoustic, 38  
actinic keratosis, 44, 210  
activation, xiii, 49, 63, 71, 123, 135, 154, 183, 185, 189, 213, 220, 232, 251, 253, 254, 255, 256, 257, 258, 259, 260, 263, 264, 265, 266  
activators, 258  
active site, 126  
acute, 41, 43, 48, 97, 210, 261  
acylation, 173  
adaptation, 15, 172, 178  
ADC, 79, 81  
additives, 100  
adducts, 247  
adenine, 154  
adenylyl cyclase, 187, 189  
administration, xiii, 156, 269  
adolescence, 44  
adolescent behavior, 42  
adolescent female, 65  
adolescents, 40, 54, 55, 56, 60, 61, 65, 66  
ADP, xii, 233, 240, 267  
adult, 40, 41, 42, 43, 45, 46, 47, 49, 50, 51, 56, 66, 202, 234, 235, 236, 240  
adulthood, 41, 42, 43, 45, 47, 48, 59  
adults, 40, 41, 42, 45, 48, 50, 51, 52, 53, 55, 57, 65, 202, 211  
African American, 65  
Ag, 149, 151, 152  
age, viii, 39, 41, 42, 43, 44, 45, 46, 51, 52, 53, 54, 56, 57, 58, 60, 61, 63, 64, 65, 210, 211, 236, 237, 239, 240, 248, 250  
ageing, 92, 97, 98, 110  
agent, 107, 141, 143, 145, 146, 152, 157  
agents, 46, 47, 50, 53, 100, 112, 138, 139, 141, 142, 143, 145, 148, 149, 151, 152, 153, 211, 213  
age-related macular degeneration, 248, 250  
aggregates, 121, 132  
aggregation, 120, 121, 132, 221  
aging, viii, xii, 39, 40, 41, 46, 61, 107, 109, 153, 209, 210, 213, 214, 217  
aging process, 41  
agonist, 191  
air, 42, 52  
alanine, 71, 96, 258  
alcohol, 119, 121, 122, 149  
alcohols, 158  
aldehydes, 93  
algae, 126  
algorithm, 33, 224, 226  
alkali, 247  
allele, viii, ix, 69, 70, 71, 72, 73, 74, 75, 76, 81, 83, 86  
alleles, viii, 69, 71, 76, 77, 81, 85, 86  
allergy, 155  
allogeneic, 47, 62  
allopurinol, 253  
alloys, 158

- alpha, xiii, 61, 62, 63, 106, 156, 186, 190, 228, 249, 251, 262, 264, 265, 267  
 alpha-tocopherol, 156  
 alternative, viii, 48, 69, 75, 78  
 alternative hypothesis, 48  
 alters, 47, 48, 61, 205, 227, 248, 262  
 amelioration, 102  
 American Academy of Pediatrics (AAP), 52, 55, 57  
 amide, 96  
 amino, ix, x, 91, 92, 93, 100, 106, 107, 108, 109, 112, 118, 160, 166, 174, 179, 181, 183, 185, 186, 189, 190, 196, 199, 206, 211, 222, 239, 254, 256, 259  
 amino acid, ix, x, 91, 92, 93, 106, 107, 108, 109, 112, 118, 160, 166, 174, 179, 181, 183, 185, 186, 189, 190, 196, 199, 206, 211, 239, 254, 256, 259  
 amino acids, 92, 93, 106, 107, 108, 160, 181, 190, 196, 199, 206, 239  
 amphibians, xii, 233  
 amplitude, viii, 1, 2, 10, 15, 18, 21, 25, 29, 30, 33, 79, 81, 82, 183, 185, 189  
 anaemia, 70  
 analog, 49, 79  
 anatase, 151  
 anatomy, 100  
 anemia, 211, 214  
 animal models, viii, 39, 41, 45, 47, 49, 54  
 animal studies, 47  
 animals, vii, x, xii, 1, 2, 48, 137, 179, 180, 181, 186, 189, 191, 233, 245  
 annealing, 74, 88  
 annotation, 221, 226  
 ANOVA, 200, 222  
 antagonists, 214  
 Antarctic, 165, 176, 177, 178, 206  
 antenna, ix, 115, 119, 122, 125  
 anthropogenic, 206  
 anti-apoptotic, 254, 259, 261  
 anti-apoptotic role, 254  
 antibiotics, xiii, 269  
 antigen, 46, 48, 61, 70  
 antigen-presenting cell, 46  
 antimony, 154  
 antioxidant, x, 49, 97, 110, 137, 141, 145, 152, 196, 203, 210  
 anti-tumor, 48, 211  
 aorta, 262  
 apoptosis, 47, 49, 55, 59, 227, 229, 231, 232, 248, 254, 259, 262, 263, 264, 267  
 apoptotic, 219, 220, 221, 222, 223, 224, 227, 231, 254, 255, 259, 260, 263  
 apoptotic cells, 221, 223, 224  
 aqueous solution, 108, 151, 152, 155, 263  
 aqueous solutions, 155  
 aqueous suspension, 158  
*Arabidopsis thaliana*, 130  
 ARF, 62  
 Argentina, 205, 206  
 arginine, xiii, 71, 95, 96, 235, 241, 251, 253, 262, 265  
 aromatic rings, 93  
 arrest, 62  
 arthritis, 269, 271  
 arthropod, 186, 241  
 arthropods, 180, 187, 239  
 ascorbic, 111, 196, 199  
 ascorbic acid, 111, 196, 199  
 Asia, 111  
 asparagines, 94  
 assessment, 74, 101, 215  
 assessment techniques, 101  
 assumptions, 2, 4, 19  
 atherogenesis, 264  
 atherosclerotic, 218  
 atmosphere, 160, 171, 174, 176  
 atmospheric pressure, xii, 161, 243, 245  
 atoms, 95, 105, 121  
 atopic dermatitis, 50, 64  
 ATP, xii, 124, 219, 227, 229, 231, 233, 240  
 ATPase, 227, 230, 256, 265  
 attachment, 122, 123  
 attitudes, 56  
 Australia, 42, 43, 44, 45, 56, 57, 58, 60, 203  
 autofluorescence, 242  
 autoimmune diseases, 71  
 automation, 72  
 autoxidation, 145, 146  
 autosomal recessive, 149  
 availability, 204, 213, 259, 264  
 averaging, 25, 30, 34, 78  
 avoidance, 41, 42, 52, 203  
 axons, 244

## B

- B cells, xiii, 48, 251  
 B vitamins, 143  
 babies, 50, 63  
 back, 40, 54, 185  
 backscattering, 4  
 bacteria, 148, 269, 270  
 bacterial, 269  
 bacterial infection, 269  
 barley, 129, 130, 132, 134  
 barrier, xi, 49, 50, 51, 52, 63, 64, 209, 210, 213, 214  
 barriers, 56

- basal cell carcinoma, 41, 44, 55, 57  
basal layer, 44, 49, 62  
base pair, 70, 75, 85  
bcl-2, 231, 254, 262  
beams, 9  
beef, 110  
behavior, xii, 42, 56, 202, 205, 227, 233, 239  
behavioral change, 56  
beneficial effect, 215  
benefits, 52, 66, 215  
benign, 43, 59, 215  
beta cell, 259  
beta-carotene, 156  
beverages, 111  
bias, 78  
bifurcation, 124  
bilirubin, 40, 52, 53, 66, 67  
biliverdin, 53  
binding, 75, 112, 130, 154, 190, 191, 228, 249, 256, 258, 259  
bioassay, 216  
bioavailability, xiii, 213, 251, 254, 255  
biochemistry, 107, 174, 175  
biogenesis, 134, 242  
biological consequences, 112  
biological processes, 61  
biological systems, 33, 92, 101  
biomacromolecules, 139, 140, 145  
biomarkers, xii, 106, 175, 219  
biomass, 207  
biomaterials, x, 101, 137, 231  
biometry, 44  
biomolecule, 140, 158  
biomolecules, x, 137, 138, 139, 140, 143, 148, 149, 151, 152, 161, 178, 244, 247, 249  
biophysics, 1, 19  
biopolymers, 108  
biopsies, 212  
biosphere, 115, 160  
biosynthesis, ix, 65, 115, 116, 117, 118, 119, 120, 123, 124, 125, 126, 127, 128, 129, 131, 133, 135, 178, 212, 226, 239  
biosynthetic pathways, 125  
biotechnology, 156  
biotic, 196, 197  
bipolar, 244  
bipolar cells, 244  
birth, 50, 51, 52, 53, 65  
birth weight, 53, 65  
bleaching, 97, 100, 112, 131, 183, 184  
blindness, 98  
blood, 38, 53, 54, 66, 213  
blood flow, 38, 54  
body mass, 52  
body weight, 65  
Bohr, 261  
bonds, x, 95, 97, 109, 159, 172, 173  
bone density, 65  
bone mass, 65  
bovine, 108, 110, 182, 183, 184, 185, 190  
brain, vii, 1, 2, 19, 26, 33, 37, 192, 193, 244, 249, 254, 259, 262, 267  
brain structure, 37  
branching, 125  
breakdown, 78, 96, 98  
breakfast, 217  
breast cancer, 215, 216  
broad spectrum, 52  
broadband, 24, 33  
buffer, 146, 147, 150, 151  
burn, 44, 45, 270  
burning, 44, 55  
by-products, 93
- C**
- Ca<sup>2+</sup>, 253, 256, 262, 265  
calcium, 240  
caliber, 246  
calmodulin, 253  
cAMP, 187, 188, 189, 191, 258  
cancer, xii, 40, 42, 45, 58, 63, 139, 140, 145, 146, 149, 154, 156, 213, 215, 216, 219, 230, 249, 261  
cancer cells, xii, 219, 230  
cancerous cells, 148, 230  
capacitance, 50, 234, 241  
capillary, 3, 40, 72, 73  
caps, 235  
carbon, xi, 95, 96, 173, 175, 176, 195, 196, 197, 201, 204, 205, 211, 212, 263  
carbon dioxide, 176, 263  
carbonyl, 95  
carbonyl groups, 95, 97, 104, 109  
carboxylic, 160, 173, 190  
carcinogenesis, x, 48, 63, 92, 97, 137, 138, 139, 143, 147, 149, 151, 153, 210, 218  
carcinogenic, 47, 48, 138, 139, 153  
carcinogenicity, 140  
carcinogens, 47, 60, 149, 156  
carcinoma, 41, 55, 57, 97, 154, 220, 230, 261  
carcinomas, 44  
cardiac myocytes, 254  
carnosine, 108  
carotene, 145, 156  
carotenoids, 122, 126, 162, 196, 199, 217  
carrier, 125, 212, 217, 218

- case study, 43  
 caseins, 99  
 caspase, 229, 254, 259  
 caspases, 254  
 catabolism, 218  
 catalase, 149, 150, 152  
 catalyst, 149, 152, 158  
 catalytic activity, x, 137, 148, 152, 158, 227  
 cataract, 110  
 cataracts, 98  
 catechol, 145  
 categorization, 226  
 cation, 139, 186  
 Caucasian, 43, 45, 51, 57  
 CD8+, 71  
 cDNA, 187, 188, 231  
 cell body, 49  
 cell culture, viii, 39, 41, 45, 54, 212, 254  
 cell cycle, 62, 229  
 cell death, xii, 219, 220, 221, 223, 224, 227, 231, 232, 255, 259, 260, 262, 263, 265, 267  
 cell differentiation, 188  
 cell growth, 47, 210, 255  
 cell line, 154, 230, 252, 257, 258, 262, 263  
 cell lines, 154, 230, 252, 262, 263  
 cell membranes, 40, 171, 180  
 cell metabolism, xi, 209, 212  
 cellular homeostasis, 213  
 Cellular response, 220  
 cereals, 100, 211  
 CFD, 81  
 chain scission, 95, 96  
 channels, 16, 33, 187, 189, 192  
 chemical agents, 49  
 chemical properties, 213  
 chemical reactions, 16, 17, 24, 25  
 chemical stability, 213  
 chemiluminescence, viii, 69, 72  
 chemokines, 47  
 chemoprevention, 140, 141, 147, 149  
 chemopreventive agents, 142, 148, 149, 151  
 childbearing, 211  
 childhood, 40, 41, 42, 43, 44, 45, 47, 54, 56, 57, 58, 59, 60  
 children, 40, 41, 42, 43, 44, 45, 49, 51, 52, 54, 55, 56, 57, 59, 60, 61, 65, 66, 67  
 Chl, 117, 118, 120, 124, 126, 134, 200  
 chloride, 222  
 chlorine, 220  
 chlorophyll, ix, 115, 116, 117, 118, 119, 120, 122, 123, 124, 125, 126, 127, 128, 129, 130, 131, 132, 133, 134, 135, 162, 176, 200, 202, 204  
 chloroplast, 132  
 cholestasis, 53  
 chromatid, 217  
 chromatin, 221, 258, 267  
 chromatography, 119, 123, 174, 249  
 chromatophore, 16  
 chromosome, 70, 213, 216  
 cilia, 180  
 ciliate, 205  
 circadian, xi, 137, 180, 188, 189  
 circadian rhythm, 137  
 circular dichroism, 121, 122, 123, 130  
 citrus, 211  
 cladocerans, 195, 197, 199, 201, 202  
 classes, 99  
 classical, 16, 101  
 classification, xi, 179, 189  
 cleavage, 92, 93, 95, 96, 99, 213, 267  
 clinical trial, viii, 39, 41, 45, 53  
 clinical trials, viii, 39, 41, 45, 53  
 clinically significant, 53  
 cloning, 188  
 closure, 186  
 clouds, 40  
 clustering, 222, 224, 226  
 clusters, 187  
 c-myc, 231  
 cNOS, 253, 255, 259  
 Co, 52, 230  
 CO<sub>2</sub>, 161, 174, 220, 236  
 coastal zone, 197  
 coding, 70, 191, 218  
 codon, ix, 70, 76, 77, 86  
 codons, 75, 76, 81, 86  
 coffee, 113  
 coherence, 4, 16, 18, 23, 24, 25, 26, 29, 30, 33, 34  
 cohort, 50  
 coil, 109  
 collagen, 40, 50, 56, 92, 94, 95, 97, 107, 109, 210, 214  
 colon, 216, 230, 249  
 colon cancer, 249  
 colors, xii, 72, 84, 233  
 combined effect, xiii, 251  
 communities, xi, 178, 195, 201  
 community, xi, 195, 196, 202, 205  
 compatibility, viii, 69  
 compensation, 27  
 competence, 269  
 complexity, 66, 118  
 complications, 44, 53  
 components, ix, 2, 3, 4, 5, 10, 14, 18, 30, 31, 46, 72, 75, 88, 89, 101, 115, 161, 192, 220  
 composition, xii, 15, 100, 118, 123, 205, 243, 244

- compound eye, 180  
compounds, x, 47, 49, 98, 106, 137, 139, 143, 146, 149, 150, 152, 159, 160, 161, 162, 163, 165, 166, 167, 170, 171, 172, 173, 175, 176, 177, 178, 204, 231, 261  
concentration, xi, 5, 6, 51, 52, 53, 75, 76, 77, 82, 88, 125, 126, 146, 147, 150, 151, 186, 195, 196, 197, 200, 201, 213, 220, 253, 263, 269  
conception, 27  
concordance, 33  
conductance, 191  
conduction, 242  
conductivity, 202, 206  
conductor, 148  
configuration, 80  
conjugated bilirubin, 52  
conjugation, 26, 27, 53  
connective tissue, 50, 64, 97  
conservation, 206  
constraints, 176  
construction, 116, 247  
consumers, 99  
consumption, 253, 257, 259  
contaminant, 77, 88  
control, ix, xiii, 10, 41, 42, 44, 54, 57, 58, 59, 91, 101, 133, 137, 147, 204, 212, 213, 214, 218, 221, 222, 246, 251, 254, 264, 265, 266, 267  
control group, 54  
controlled trials, 53  
conversion, 16, 62, 99, 120, 128, 129, 131  
copepods, xi, 195, 197, 201  
copper, 53, 154, 156  
corn, 129  
cornea, vii, 1, 7, 20, 98, 261  
coronary heart disease, 217  
correlation, 4, 26, 33, 34, 95, 97, 99, 100, 222, 226, 236, 241, 262  
correlations, 220  
cortex, 2, 15, 18, 19, 26, 33, 34, 97, 163  
cortical neurons, 37  
couples, 186, 190  
coupling, 122, 222  
covering, 72  
cows, 111  
COX-2, 254  
CPD, 236  
creatine, 214, 217  
creatine kinase, 217  
CREB, 258  
critical period, 42, 58  
crosslinking, 96, 97, 99, 100, 102, 109  
crustaceans, 197, 204, 205, 240, 241  
crystal structure, 182  
crystal structures, 182  
crystalline, 10, 11, 29, 121, 220  
culture, viii, 39, 41, 47, 54, 109, 212, 221  
current limit, 104  
cuticle, xii, 97, 100, 102, 112, 233, 234, 235, 236, 239, 240, 241  
cyanobacteria, 161, 176, 178  
cycles, 125, 127, 161  
cyclic AMP, 266  
cysteine, 93, 95, 98, 102, 108, 112, 254, 257  
cysteine residues, 102  
cysteine-rich protein, 112  
cystine, 92, 95, 109, 172  
cytokine, 256, 265, 266  
cytokines, 46, 47, 230, 254  
cytoplasm, 5, 149  
cytosine, 148  
cytosol, 258  
cytotoxic, xii, 219, 261  
cytotoxicity, 158, 220
- D**
- dairy industry, 99  
dairy products, 99  
data analysis, 75, 86  
database, 247  
DCA, 202  
death, xii, xiii, 53, 219, 220, 221, 223, 224, 227, 230, 231, 232, 251, 255, 259, 260, 262, 263, 265, 267  
death rate, 255  
deaths, 42  
decay, ix, 70, 75, 76, 78, 81, 82, 83, 84, 85, 87, 88, 102, 117, 121, 147, 148, 191  
decay times, 75, 87  
decomposition, x, 112, 137, 149, 151, 152, 156, 158  
defects, 211, 215, 216  
deficiency, 52, 60, 65, 149, 206, 211, 213, 214, 215, 217  
deficit, 212  
deformation, 158  
degradation, ix, 91, 92, 94, 98, 99, 100, 102, 104, 109, 210, 229, 257, 258  
degradation mechanism, ix, 91  
degrading, 210  
dehydrogenase, xii, 119, 130, 219, 227  
dehydrogenases, 119, 121  
delivery, 80, 269  
denaturation, 72, 76, 96  
dendrites, 46, 244  
dendritic cell, 46, 47, 48, 49, 55, 60, 61, 62  
denitrification, 176  
density, 43, 46, 48, 50, 60, 65, 66, 80

- deoxyribonucleic acid, 55  
 Department of Agriculture, 211, 218  
 deposition, 240  
 deprivation, 256  
 derivatives, 53, 93, 96, 100, 106, 145, 146, 147, 150,  
     152, 153, 160, 166, 167, 170, 171, 173, 174  
 dermatitis, 50, 216  
 dermatologists, 52  
 dermatology, 211, 216  
 dermatosis, 67  
 dermis, 40, 55, 56, 97, 109, 210, 212  
 desert, 161, 176  
 desorption, xii, 101, 243, 245, 249, 250  
 destruction, 40, 122, 126  
 detection, viii, 69, 72, 73, 74, 75, 76, 78, 80, 88, 107,  
     111, 112, 245  
 detergents, 100  
 developmental change, 55  
 diabetes, viii, 70, 71, 250  
 diabetes mellitus, viii, 70, 250  
 diabetic retinopathy, 248, 250  
 diacylglycerol, 186  
 diaphragm, 7  
 diet, 49, 211  
 dietary, 211, 218  
 differentiation, 45, 46, 47, 55, 63, 71, 188  
 diffraction, 4, 7, 11, 17, 18, 22, 26, 30, 34, 35  
 diffuse reflectance, 50, 52  
 diffusion, 50, 73, 98, 105, 147, 240, 254  
 diffusion rates, 254  
 digestion, 71, 102, 104, 105, 111  
 dihydroxyphenylalanine, 109  
 dimer, 121, 143, 155  
 dimeric, 119  
 diode laser, 221, 230, 231  
 dipole, 73  
 dipole moment, 73  
 direct action, 49, 62  
 discipline, 101  
 discrimination, 71, 72, 266  
 disease gene, 71  
 diseases, xiii, 70, 214, 269  
 disorder, 67  
 dispersion, 24, 151  
 displacement, x, 15, 179, 183, 189, 191  
 dissociation, 257  
 distilled water, 235  
 distortions, 2  
 distribution, viii, xii, 1, 2, 5, 11, 12, 18, 25, 28, 31,  
     34, 46, 50, 51, 75, 79, 81, 82, 88, 162, 163, 164,  
     176, 205, 207, 243, 244, 248, 249  
 disulfide, 92, 95, 97, 109, 111  
 disulfide bonds, 95, 109  
 divergence, 3, 123  
 diversity, xi, 179, 180, 192  
 DNA damage, x, 49, 52, 55, 59, 62, 137, 138, 139,  
     140, 143, 145, 146, 151, 153, 154, 155, 156, 158,  
     213, 215, 252, 265  
 DNA lesions, 153  
 DNA ligase, 72  
 DNA repair, xi, 45, 49, 60, 61, 154, 209, 213, 215,  
     217, 218  
 DNA sequencing, viii, 69  
 Docosahexaenoic, 250  
 docosahexaenoic acid, 250  
 dominance, 202, 206  
 donor, viii, ix, 70, 73, 75, 77, 84, 85, 86, 88, 115,  
     118, 120, 122, 211  
 donors, 46, 60, 86  
 dosage, 67  
 down-regulated genes, 226  
 drug delivery, 269  
 drug-resistant, 269  
 drugs, x, 54, 137, 139, 141, 149, 152  
 drying, 236, 240, 246  
 duplication, 191  
 duration, viii, 1, 3, 30, 43, 51, 58, 78, 118, 254  
 dyeing, 97  
 dyes, 35, 73, 74, 222
- E**
- ears, 60  
 earth, 92, 139, 174, 252  
 ecological, 178  
 ecology, 178, 206, 207  
 ecosystems, xi, 177, 178, 195, 196, 206, 207  
 egg, 101, 112, 250  
 eicosapentaenoic acid, 250  
 elasticity, 109, 210  
 elastin, 40, 50, 92  
 elderly, 66, 217  
 election, viii, 69  
 electric potential, 2, 18, 26, 34  
 electrical properties, 241  
 electrodes, 236  
 electromagnetic, 24, 252  
 electromagnetic wave, 24  
 electron, x, 40, 92, 93, 115, 121, 128, 134, 137, 138,  
     139, 140, 141, 143, 144, 146, 147, 152, 153, 154,  
     156, 157, 172, 174, 227, 236, 240  
 electrons, 123, 172, 240  
 electrophoresis, 72, 73, 105, 111  
 electrophysiological study, 188  
 elongation, 229, 231  
 embryo, 239, 242, 249

- emission, viii, 9, 10, 22, 69, 73, 75, 76, 79, 80, 81, 83, 112, 131  
emission source, 22  
encephalopathy, 53  
encoding, 187, 227, 228, 229  
endoplasmic reticulum, xiii, 229, 230, 231, 239, 251, 256, 264, 265  
endothelial cell, 46, 252, 261  
endothelial cells, 46, 252, 261  
endothelial dysfunction, 262  
endothelium, 252, 264  
energy, viii, xii, 3, 40, 53, 70, 73, 74, 92, 94, 108, 118, 120, 121, 122, 126, 138, 139, 140, 141, 142, 144, 147, 150, 160, 196, 214, 215, 219, 227, 230, 231, 240, 252  
energy supply, 214  
energy transfer, viii, 70, 92, 94, 108, 120, 122, 126, 139, 140, 141, 147  
environment, 47, 48, 50, 54, 99, 172, 175, 240  
environmental conditions, 50  
environmental factors, xi, 209  
enzymatic, ix, 71, 72, 91, 92, 102, 123, 133, 161, 213, 234, 262  
enzymatic activity, ix, 91, 234  
enzymes, 71, 75, 100, 106, 119, 154, 188  
Epi, 218  
epidemiologic studies, 41, 43, 58  
epidemiology, 58, 60  
epidermis, 40, 44, 48, 50, 51, 59, 97, 109, 210, 212, 214  
epithelium, 2, 21, 32, 244, 245  
EPR, 121  
erythematous, 53  
erythrocyte, 149  
erythrocytes, 216  
*Escherichia coli*, 106, 130  
ESI, 101, 103, 248  
ESR, 133  
ester, x, 159, 160, 173  
ester bonds, x, 159, 173  
esterification, 122, 123, 124, 127, 160  
estrogen, 65  
ethanol, 163, 236  
ethers, 158, 176  
ethnicity, 43  
eukaryote, 177  
eukaryotic cell, 264  
evolution, x, 27, 126, 131, 172, 174, 175, 178, 179, 180, 183, 185, 189, 191, 192, 210, 216  
excision, 46, 213, 214, 216  
excitation, 36, 73, 74, 75, 76, 77, 78, 80, 88, 122, 126, 138, 141, 147, 191  
execution, 33, 227  
exocrine, 267  
exons, 218  
experimental condition, 73, 147, 151  
explosions, 175  
external influences, 51, 210  
extinction, 163, 165, 166, 167, 169, 170, 172, 175  
extracellular matrix, 40, 50  
extraction, 104, 105, 250  
eye, vii, viii, ix, 1, 7, 9, 10, 15, 17, 18, 19, 20, 22, 23, 26, 27, 28, 34, 35, 36, 37, 91, 92, 98, 106, 107, 180, 192, 245, 246  
eye movement, 34, 36  
eyeball, 246  
eyes, 19, 42, 43, 54, 180, 186, 190, 192, 193, 250
- F**
- factorial, 48, 222  
family, 42, 54, 119, 191, 228, 266  
family history, 54  
fat, 99, 234  
fatty acids, 245, 248, 250  
fauna, 175, 203  
FDA, 211  
feedback, 254  
feeding, 111, 234  
females, 65  
fetus, 50  
fiber, 3  
fibers, 4, 18, 22, 35, 40, 50, 56, 109  
fibrils, 40  
fibroblast, 257  
fibroblasts, 46, 157, 212, 216, 231  
filament, 97  
film, 24  
films, 242  
filters, 80, 98, 101, 142, 143, 154, 157  
filtration, 14, 119, 206  
fish, 111, 197, 200, 250  
fish oil, 250  
fixation, 36, 117, 161, 241  
flavor, 110, 111  
flight, xii, 233, 234, 241, 245, 249  
flow, 38, 54, 79, 240  
fluctuations, 15, 27, 78, 201  
fluid, 5, 54, 61  
fluorescence decay, ix, 70, 75, 76, 77, 78, 81, 82, 83, 86, 88, 89, 121  
fluorimeter, 72  
fluorogenic, 85  
fluorophores, 73, 75, 76, 88, 99  
focusing, 10, 11, 26, 55, 122, 134

- folate, xi, 209, 210, 211, 212, 213, 215, 216, 217, 218  
 folding, 256, 265  
 folic acid, xii, 143, 144, 145, 155, 156, 209, 210, 211, 212, 213, 214, 215, 216, 217  
 food, ix, xi, 91, 92, 98, 100, 111, 149, 152, 205, 209, 211, 213, 216  
 Food and Drug Administration (FDA), 211  
 foodstuffs, 98, 100  
 forecasting, 87  
 formaldehyde, 96, 221  
 fortification, 215, 216  
 fossil, 160, 178  
 Fourier, 10, 19, 20, 21, 22, 23, 31, 33, 50, 163  
 Fourier analysis, 19, 22  
 Fourier transformation, 10, 19, 20, 31, 33  
 fovea, 8  
 fractionation, 102, 122  
 fragmentation, 222, 250  
 France, 39  
 free energy, 143  
 free radical, 46, 92, 93, 112, 133, 145, 154, 155, 261  
 free radicals, 46, 92, 112, 133  
 freeze-dried, 110  
 freezing, 161, 162  
 freshwater, 176, 203, 204, 205, 206  
 Friedmann, 162, 165, 176  
 fruits, 211  
 FTIR, x, 159, 163, 167  
 functional analysis, 64  
 functional architecture, 36  
 functional changes, 172  
 fungi, 173, 177, 178  
 fungus, 177  
*Fusarium*, 177  
 fusion, 130
- G**
- G protein, x, 179, 182, 183, 185, 186, 187, 189, 191, 258  
 ganglion, xi, 180, 188, 189, 192, 244, 245  
 gas, 102, 147  
 gastric, 216  
 GDP, 256  
 gel, 72, 75, 111, 113, 119, 162  
 gene, viii, ix, xiii, 46, 55, 61, 62, 63, 69, 70, 75, 85, 86, 130, 146, 153, 190, 191, 212, 213, 217, 218, 219, 220, 221, 222, 224, 226, 227, 251, 259, 265  
 gene expression, xii, xiii, 61, 63, 212, 218, 219, 220, 222, 224, 226, 251, 259  
 generation, ix, 32, 40, 47, 53, 72, 81, 91, 95, 97, 112, 138, 140, 145, 148, 152, 153, 154, 156, 158, 186, 207, 220, 252, 253, 254, 257, 259, 261, 262, 269  
 genes, viii, xii, 46, 69, 70, 74, 112, 119, 188, 219, 220, 221, 222, 223, 224, 226, 227, 228, 229, 230, 231, 257, 258, 259  
 genome, viii, 69, 70, 153  
 genomes, 70, 220  
 genomic, viii, 69, 72, 74, 88, 213, 217  
 genomics, 231  
 genotoxic, 231  
 genotype, 71, 74  
 geotaxis, 229  
 germination, 175  
 gestation, 54, 211  
 gestational age, 53, 65  
 gift, 76, 230  
 gingival, 211  
 gingivitis, 218  
 girls, 65  
 glass, 30, 101, 138, 221, 222, 246  
 glial, 3  
 glial cells, 3  
 glucose, 65, 157, 256, 264  
 glucose tolerance, 65  
 glutamate, 235  
 glutamatergic, 244  
 glutamic acid, 143, 181  
 glutamine, 95  
 glycation, 98, 110  
 glycerol, 117  
 glycine, 100, 235  
 glycolipids, 245  
 goals, 92, 104, 105  
 gold, 149, 158  
 GPA, 215, 217  
 GPCR, 182  
 G-protein, x, 179, 181, 185, 187, 188, 190  
 gracilis, 199  
 grain, 211  
 grains, 211  
 grants, 190  
 granules, xii, 233, 234, 235, 236, 237, 239, 240  
 graph, 224, 225  
 grasses, 161  
 green fluorescent protein, 244  
 greening, 117, 124, 126, 127, 128, 129, 132, 134  
 grids, 22  
 groups, x, 26, 41, 45, 51, 95, 97, 100, 104, 109, 119, 159, 172, 182, 183, 184, 218, 222, 226, 236, 239, 245  
 growth, xiii, 47, 49, 55, 63, 100, 132, 175, 202, 210, 211, 251, 255, 270

growth factor, 47, 55, 63  
growth factors, 47, 55  
guanine, 139, 146, 148, 153, 154, 157, 256, 264  
guidelines, 53

**H**

**H<sub>2</sub>**, 126, 163  
**habitat**, 162, 207  
**hair follicle**, 49, 112  
**half-life**, 257  
**handling**, 4, 50, 98  
**harm**, 210  
**harmonic oscillations**, 33  
**harvesting**, ix, 115, 119, 120, 125, 128, 132  
**health**, 41, 65, 217  
**health effects**, 41  
**heart**, 156, 217  
**heart disease**, 156  
**heat**, xii, 40, 53, 54, 100, 124, 134, 141, 219, 220, 226, 228, 229, 230, 231, 232  
**heat shock protein**, xii, 100, 219, 226, 228, 229, 230, 232  
**heating**, 76, 123, 124  
**height**, 6  
**helix**, 109, 181, 183  
**hematopoiesis**, 156  
**heme**, 249, 256, 261, 262  
**heme oxygenase**, 262  
**hemisphere**, 197  
**hemoglobin**, 40, 52  
**hemolymph**, 240  
**hepatocarcinogenesis**, 156  
**hepatocyte**, 63  
**hepatocyte growth factor**, 63  
**herbicide**, 157  
**heterodimer**, 71  
**heterogeneity**, 8  
**heterogeneous**, 119, 220  
**heterotrophic**, 126, 160, 161  
**heuristic**, 10  
**hexane**, 157, 250  
**high resolution**, 248  
**high-frequency**, 15, 18  
**high-performance liquid chromatography**, 147  
**hip**, 226  
**hippocampus**, 267  
**histamine**, 254  
**histidine**, 93, 94, 96, 98, 99, 108  
**histogram**, 78  
**histological**, 192  
**histone**, 258, 267  
**HLA**, viii, ix, 69, 70, 71, 75, 76, 77, 86, 89  
**Hoechst**, 221  
**holistic**, 101  
**hologram**, 18, 19, 22, 23, 27, 30, 31, 32  
**holograms**, viii, 2, 19, 22, 23, 31, 32, 33  
**homeostasis**, xii, 61, 209, 210, 214, 215  
**hominids**, 210  
**HOMO**, 143, 150, 156, 157  
**homocysteine**, 211, 216, 217, 218  
**homogenous**, 11, 149, 244  
**homolog**, 228, 231  
**hormone**, 47, 65  
**host**, 214  
**housing**, 239  
**HPLC**, 76  
**hue**, 37  
**human development**, 17  
**human genome**, viii, 69, 70  
**Human Genome Project**, 70, 73  
**human leukocyte antigen**, 70  
**human papilloma virus**, 44  
**human subjects**, 217  
**humans**, 47, 49, 55, 137, 148  
**humic acid**, 197, 202  
**humidity**, 64, 162, 241  
**hybrid**, ix, 70, 74, 75  
**hybridization**, 71, 73, 74, 75, 81, 84, 87, 188, 222  
**hybrids**, 82, 86  
**hydration**, 40, 50, 51, 54, 64, 67  
**hydride**, 122  
**hydro**, 220, 231  
**hydrocarbon**, 177  
**hydrocarbon media**, 177  
**hydrogen**, ix, 92, 93, 95, 107, 112, 115, 116, 118, 120, 121, 122, 123, 139, 154, 156, 158  
**hydrogen abstraction**, 92  
**hydrogen atoms**, 95, 121  
**hydrogen peroxide**, 93, 112, 139, 154, 156, 158  
**hydrogenation**, ix, 115  
**hydrology**, 206  
**hydrolysis**, 99, 111, 229  
**hydroperoxides**, 92  
**hydrophilic**, 220, 231  
**hydrophilicity**, 50  
**hydrophobic**, 122, 263  
**hydroquinone**, 157, 158  
**hydroxyl**, ix, 91, 92, 93, 95, 96, 100, 104, 107, 109, 139, 160  
**hydroxylation**, 94, 95, 107, 108, 155  
**hydroxyproline**, 95  
**hygiene**, 36  
**hyperbilirubinemia**, 52, 53  
**hyperglycemia**, 157  
**hyperplasia**, 211, 216

- hypersensitivity, 61, 62  
 hypertensive, 261  
 hypomethylation, 213, 217  
 hypothesis, 4, 9, 15, 48, 180, 189, 210, 214, 215, 258, 270
- I**
- IARC, 58, 153  
 identification, ix, xii, 70, 71, 73, 104, 108, 112, 118, 130, 175, 178, 218, 219, 245, 249  
 identity, 73, 186  
 IL-1, 46, 47, 256  
 illumination, xii, 36, 116, 117, 118, 120, 121, 123, 124, 127, 134, 233, 236, 238, 239, 240  
 image analysis, 221  
 images, xiii, 3, 5, 6, 11, 13, 14, 15, 16, 17, 19, 25, 26, 28, 31, 36, 38, 222, 243, 247, 248  
 imaging, xii, 18, 36, 37, 38, 243, 245, 249  
 immersion, 235  
 immigrants, 45  
 immune function, 40, 61  
 immune reaction, 46  
 immune response, 46, 47, 48, 71  
 immune system, 45, 46, 47, 56, 61, 62, 270  
 immunity, 33, 41, 45, 48  
 immunogenicity, 98  
 immunohistochemical, 187, 188  
 immunohistochemistry, 188  
 immunological, 60, 269  
 immunomodulatory, 46, 47, 49  
 immunosuppression, 42, 44, 45, 47, 48, 49, 55, 60, 62  
 immunosurveillance, 62, 230  
 implementation, 73, 128  
 IMS, xii, 243, 245, 246, 247, 248  
 in situ, xii, 89, 131, 163, 164, 188, 207, 243, 244, 249  
 in situ hybridization, 188  
 in vitro, xii, 46, 47, 93, 106, 128, 130, 131, 142, 154, 188, 209, 210, 211, 214, 216, 217, 231, 232, 250, 269, 270  
 in vivo, xii, 4, 45, 50, 51, 63, 64, 106, 107, 110, 117, 120, 131, 132, 142, 154, 209, 210, 211, 212, 213, 214, 216, 217, 269, 270  
 inactivation, 106, 161, 263  
 inactive, 118, 120, 125  
 incidence, viii, xi, 39, 57, 58, 59, 139, 143, 145, 156, 209, 211  
 indication, 102  
 indicators, 206  
 indices, 2, 9, 14, 17  
 indium, 246
- induction, xii, 48, 62, 138, 139, 153, 156, 219, 224, 227, 229, 231, 265  
 industry, 99  
 ineffectiveness, 269  
 inelastic, 39  
 inert, 102  
 infancy, 41, 43, 45, 47, 50, 63  
 infants, 40, 41, 42, 43, 44, 45, 50, 51, 52, 53, 54, 55, 58, 60, 61, 64, 65, 66  
 infection, 44, 46, 256, 269, 270  
 infections, xiii, 269, 270  
 infectious, 60, 269, 270, 271  
 infectious disease, 60, 271  
 infectious diseases, 60  
 infinite, 9  
 inflammation, 41, 46, 258, 261  
 inflammatory, 47, 48, 60, 210, 217, 254, 262  
 inflammatory disease, 217  
 inflammatory mediators, 48  
 inflammatory response, 48, 254, 262  
 information processing, 26, 34  
 information systems, 37  
 infrared, 50, 163  
 infrared spectroscopy, 50  
 inherited, 149  
 inhibition, 143, 229, 253, 256, 257, 259, 263, 264, 265, 267  
 inhibitor, 67, 256, 257  
 inhibitors, 253, 266  
 inhibitory, 145, 146, 152, 244  
 inhibitory effect, 145, 146, 152  
 initiation, xiii, 225, 229, 231, 251, 256, 264, 265, 267  
 injury, 60, 63, 107, 214, 262  
 inorganic, x, 72, 137, 138, 148, 149, 151, 152, 154, 196  
 iNOS, xiii, 251, 253, 255  
 inositol, 186  
 insects, xii, 180, 233, 239, 241  
 insight, 158  
 instabilities, 79  
 instability, 213, 216  
 instruments, 51  
 insulin, viii, 70  
 insults, 100  
 integration, 122  
 integrity, 51, 95, 97, 101, 214  
 integument, 241  
 interaction, xii, 22, 101, 113, 120, 121, 122, 140, 146, 153, 154, 190, 243, 244, 256, 266  
 interactions, 3, 40, 120, 192, 196, 205  
 interference, 18, 19, 22, 28, 29, 34, 87  
 interferon, 262

interleukin, 261  
 intermolecular, 122, 126, 160  
 internal ribosome entry site, 264  
 internalization, 212  
 interneurons, 244  
 interrelations, 118  
 interval, 62, 76, 78, 86, 143  
 intervention, 55, 65, 156  
 intrinsic, 78, 210  
 invasive, xiii, 44, 50, 269  
 inversion, 26  
 invertebrates, xii, 180, 182, 188, 233  
 ion channels, 192  
 ion transport, 226, 227  
 ionization, xii, 113, 150, 157, 243, 245, 249, 250  
 ionization potentials, 150  
 ionizing radiation, 227, 228  
 ions, 102, 140, 156  
 iridium, 158  
 iron, 111, 261  
 ischemia, 262, 267  
 isoforms, 259, 265  
 isolation, 113, 129  
 isomerization, 183  
 isomers, 66  
 isopentane, 246  
 isotope, 104  
 ITO, 246  
 IVH, 111

**J**

jaundice, viii, 39, 41, 52, 53, 54, 55, 66, 67  
 jellyfish, xi, 179, 186, 189, 191, 192  
 JNK, 254, 263

**K**

$K^+$ , 192  
 kappa, xiii, 251, 263, 265, 266  
 kappa B, 265, 266  
 keratin, 40, 97, 109  
 keratinocyte, 46, 49, 55, 62, 214, 261, 262, 263  
 keratinocytes, 44, 45, 47, 49, 60, 61, 109, 212, 213,  
   231, 252, 254, 260, 261, 263  
 kernicterus, 53  
 kidney, 47  
 kinase, xiii, 251, 256, 257, 258, 263, 264, 265, 266  
 kinase activity, 265  
 kinases, xiii, 191, 251, 256, 257, 258, 266, 267  
 kindergarten children, 59  
 kinetics, 117, 131, 158, 231, 262, 270

knockout, 192, 245, 249, 257, 259  
 Krebs cycle, 100

**L**

labeling, 81, 85, 113, 183  
 lactating, 211  
 lactobacillus, 214  
 lactoglobulin, 99  
 lakes, 196, 197, 199, 200, 201, 202, 203, 204, 205,  
   206, 207  
 lamellae, 234  
 laminar, 244  
 Langerhans cells, 46, 55, 62, 63  
 larvae, 234  
 laser, xii, xiii, 2, 3, 78, 80, 88, 101, 112, 219, 221,  
   230, 231, 243, 245, 247, 249, 250, 269  
 lasers, 16  
 latency, 63  
 leaf blades, 127  
 leakage, 227  
 legume, 263  
 lens, vii, ix, 1, 7, 8, 10, 11, 17, 20, 21, 29, 91, 92, 98,  
   106, 107, 110, 180, 187, 262  
 lenses, 108, 109  
 lesions, 43, 44  
 leukocyte, 70  
 leukocytes, 270  
 lichen, x, 159, 160, 161, 162, 163, 165, 166, 167,  
   169, 170, 172, 173, 174, 175, 176, 177, 178

life cycle, 202  
 lifestyle, 65, 211, 217  
 life-threatening, 44  
 lifetime, ix, 42, 43, 44, 64, 70, 76, 78, 83, 84, 86, 87,  
   88, 132, 139, 147, 152  
 ligand, 75, 182  
 ligands, 75, 230  
 light emitting diode, 54  
 light scattering, 3, 4, 8, 11, 35, 36, 40, 50  
 light transmission, 98  
 light-induced, 99, 134, 262  
 limitation, 74, 87, 104, 205, 206  
 limitations, 45, 104, 244  
 linear, 11, 13, 17, 19, 25, 33, 121, 254  
 linkage, 120, 160, 181, 182, 187, 188, 192  
 links, 43  
 lipid, xii, 50, 64, 93, 99, 111, 140, 155, 243, 244,  
   248, 249, 254, 262  
 lipid oxidation, 93, 99, 111  
 lipid peroxidation, 155, 248, 254, 262  
 lipidomics, 249, 250  
 lipids, 50, 93, 111, 132, 248  
 lipopolysaccharide, 262

- lipoproteins, 171  
 liquid chromatography, 102, 147, 253  
 liquid nitrogen, 117, 133, 246  
 lithium, 248  
 liver, 47, 53, 211, 234, 249  
 localization, 64, 154, 157, 249, 257  
 location, ix, 54, 71, 91, 101, 102, 104, 105, 153, 163, 221  
 locus, viii, 69, 70, 215, 216  
 long-distance, 66  
 longitudinal study, 51  
 losses, 216, 240  
 low birthweight, 66  
 low molecular weight, x, 137  
 low temperatures, 120, 161  
 low-level, 45  
 low-power, xiii, 269  
 low-temperature, 117, 118, 119, 121, 123, 125, 126  
 lumen, 264, 265  
 luminescence, 153  
 lung, xii, 156, 219, 220, 230  
 lung cancer, xii, 156, 219, 230  
 lying, 139  
 lymph, 48, 61, 62  
 lymph node, 48, 61, 62  
 lymphatic, 46  
 lymphocyte, 62  
 lymphocytes, 213, 214, 215, 216  
 lysine, 95, 96, 98, 181, 182  
 lysosomes, 5
- M**
- machinery, 116, 160  
 machines, 72  
 macromolecules, 210  
 macrophages, 46, 47, 254, 262, 263  
 macular degeneration, 248, 250  
 magnetic, 75, 132, 163  
 maintenance, 47, 115, 126  
 maize, 131  
 major histocompatibility complex, viii, 69  
 malignancy, 42  
 malignant, 41, 42, 43, 44, 49, 55, 57, 58, 59, 60, 62, 140, 153, 158, 215  
 malignant cells, 158  
 malignant melanoma, 41, 42, 49, 55, 57, 58, 59, 60, 62, 153  
 maltose, 130  
 mammalian, 181  
 mammalian cells, xiii, 187, 193, 212, 251  
 mammals, 49, 187, 188, 211, 230  
 manifold, 123
- MAPK, 255, 258, 259, 266  
 mapping, 101  
 market, 98  
 Mars, 171  
 Martian, 172  
 mass spectrometry, xii, 101, 112, 113, 243, 245, 247, 249, 250  
 mast cells, 46, 47  
 maternal, 211  
 matrix, vii, xii, 1, 17, 40, 50, 97, 100, 101, 210, 218, 222, 240, 243, 245, 246, 247, 249, 250  
 matrix metalloproteinase, 218  
 maturation, 47, 50, 62, 64, 229, 234, 239  
 maturation process, 50  
 Mb, 27  
 MCA, 79, 81  
 measurement, 15, 30, 45, 51, 75, 78, 79, 109, 151, 153, 162, 214, 234, 238, 245, 246, 247, 248  
 measures, 42, 52, 79  
 meat, 99, 106, 111  
 mechanical properties, 95, 97  
 media, 9, 10, 18, 26, 27, 28, 102, 112, 147, 177  
 mediation, 263  
 mediators, 48  
 medications, 211  
 medulla, 160, 163  
 MEF, 257, 258, 259  
 melanin, 40, 41, 49, 50, 52, 59, 65, 97, 210, 239  
 melanocytes, 49  
 melanogenesis, 52, 55, 63, 65, 210  
 melanoma, viii, 39, 40, 41, 42, 43, 44, 48, 49, 54, 55, 57, 58, 59, 60, 61, 62, 63  
 melanosomes, 49  
 membranes, 125, 126, 130, 134, 140, 161, 190, 250, 254, 261, 263  
 memory, x, 19, 79, 115  
 men, 44, 216  
 mesh node, 10  
 mesophyll, 127  
 messengers, 181, 185  
 metabolic, 234  
 metabolism, xi, xii, 209, 210, 211, 212, 213, 215, 219, 230, 231  
 metabolites, 161, 163, 169, 170, 171, 172, 249  
 metabolomics, 244  
 metal ions, 140  
 metal nanoparticles, 149, 150, 151, 152, 158  
 metal oxide, 148  
 metalloproteinases, 210  
 metallothionein, 63  
 metals, 148, 149, 151, 158  
 metaphor, 19  
 metastasis, 44, 249

- metastasizes, 44  
metastatic, 62  
meteorites, 173, 178  
methanol, 163, 246  
methicillin-resistant, 269  
methionine, 95, 99, 108, 212, 213, 254, 263  
methylation, 213, 215, 216, 218  
methylene, 53, 150, 151, 152, 157, 242  
metric, 115  
MHC, viii, 69, 70  
mice, 47, 48, 49, 60, 61, 62, 63, 153, 156, 192, 245, 246, 249, 254, 267, 270  
microarray, 221, 222, 226  
microbes, 178, 240  
microbial, 270  
microdialysis, 61  
microenvironment, 45, 46, 48, 55, 254  
micrograms, 222  
microorganisms, 161, 176, 178  
microscope, 80, 163, 221, 236, 245  
microscopy, 4, 50, 109, 163, 166, 176, 249  
microtubules, 239  
microwave, 241  
migrants, 42, 58  
migration, 55, 198, 201, 206, 239, 242  
milk, 99, 106, 111  
mimicking, 81  
Ministry of Education, 190  
mirror, 37, 87  
mitochondria, 4, 5, 100, 111, 140, 227, 230, 231  
mitochondrial, 215, 227, 261, 262  
mitochondrial DNA, 215  
mitogen, 258, 266  
mitogen-activated protein kinase, 266  
mixing, 76, 199, 207  
ML, 60, 261  
MMS, 247  
modality, xiii, 220, 269  
model system, 121, 128  
modeling, 5, 37  
models, viii, 19, 22, 23, 27, 37, 39, 41, 45, 47, 48, 49, 55, 177, 178, 214  
modulation, 46, 60, 64, 134, 227, 229, 254, 262  
moieties, 93, 95, 96  
moisture, 97, 99  
molecular biology, 232  
molecular mechanisms, 214, 215  
molecular oxygen, 92, 95, 139, 140, 141, 146, 149, 154, 155  
molecular structure, 128  
molecular weight, x, 53, 137, 213, 227, 229  
molecules, x, 16, 24, 25, 40, 46, 49, 50, 70, 73, 74, 80, 81, 82, 83, 96, 116, 120, 121, 122, 124, 131, 137, 141, 145, 180, 188, 245, 252, 253, 255  
Møller, 111  
monochromatic light, 11  
monocytes, 46  
monomeric, 121  
Moon, 61  
morphological, viii, 1, 2, 5, 15, 180, 221  
morphology, 46, 51, 64, 163, 186, 189, 216  
mortality, 196, 198, 200, 201, 203  
mothers, 50, 51  
motion, 2  
mountain environments, 172  
mouse, xiii, 48, 49, 55, 60, 62, 63, 228, 243, 245, 246, 247, 248, 249, 253, 257, 263, 265  
mouse model, 48, 60  
movement, 15, 18  
mRNA, 256, 262, 264  
MRSA, 269, 271  
mucosa, 213  
multidimensional, 112  
multiplication, 33  
multiplicity, 140  
multiplier, 30  
murine models, 47  
muscle, 111  
mutagen, 157, 196  
mutagenesis, 62, 130, 153, 215  
mutagenic, 138, 139  
mutant, 59, 126, 129, 131, 132, 134, 183, 258  
mutant cells, 126  
mutant proteins, 183  
mutants, 134  
mutation, 44, 66, 70, 139, 146, 157, 215, 216  
mutations, 43, 44, 47, 48, 49, 59, 70, 139, 157, 171, 213  
mw, 236  
myocyte, 263

**N**

- NAD, 253, 262  
NADH, xii, 219, 226, 227, 231, 262  
nanomaterials, 148  
nanoparticles, 149, 150, 151, 152, 158, 239  
NASA, 162, 174  
National Academy of Sciences, 107, 108, 175  
native protein conformation, 96  
natural, ix, xi, xii, 2, 19, 22, 28, 29, 50, 55, 56, 88, 91, 100, 106, 112, 117, 124, 127, 138, 145, 156, 195, 196, 197, 199, 200, 201, 202, 204, 207, 210, 214, 227, 240, 243

- natural environment, 240  
 Nd, 80, 247  
 necrosis, 231  
 necrotic cell death, 220  
 neonatal, viii, 39, 41, 46, 47, 48, 49, 50, 52, 53, 54,  
   55, 61, 62, 64, 66, 67  
 neonate, 63  
 neonates, 46, 48, 53, 63, 65, 66, 67  
 neoplasm, 44  
 neoplasms, 43  
 neoplastic, 55  
 nerve, 2, 3, 4, 7, 11, 14, 15, 16, 17, 18, 20, 22, 24  
 nerve cells, 2, 3, 7, 16, 17, 18, 20  
 nerve fibers, 18, 22  
 nerves, 26  
 nervous system, 19  
 network, ix, 33, 40, 61, 110, 115, 116, 128, 196  
 neural crest, 239  
 neural development, 248  
 neural network, 33  
 neuroblastoma, 263  
 neuronal survival, 267  
 neurons, 15, 19  
 neuropeptides, 46  
 neurophysiology, 3, 16  
 neurotoxicity, 153, 262  
 neutrophil, 48  
 neutrophils, 269, 270, 271  
 nevus, 43, 54, 55, 57, 59, 67  
 Newton, 178  
 Ni, 192  
 Nielsen, 111  
 NIR, x, 159  
 nitrates, 253  
 nitric oxide (NO), xiii, 107, 251, 252, 253, 254, 255,  
   256, 257, 258, 259, 260, 261, 262, 263, 264, 265,  
   266  
 nitric oxide synthase, xiii, 251, 260, 261, 262, 265  
 nitrogen, 93, 107, 117, 133, 161, 175, 176, 246, 253,  
   261  
 nitrogen fixation, 161  
 nitrosative stress, xiii, 106, 251, 255, 259  
 nitroso compounds, 253  
 NMR, x, 107, 159, 167, 241  
 NO synthase, 262  
 noble metals, 148, 149, 151  
 nodes, 48  
 noise, 12, 15, 17, 27, 31, 33, 37, 72, 79  
 non-invasive, 45, 50, 51, 55  
 non-uniform, 6, 15, 16, 26, 38  
 non-uniformity, 6  
 normal, 12, 15, 16, 17, 25, 36, 45, 50, 52, 56, 64,  
   108, 126, 128, 129, 154, 210, 211, 212, 213, 215,  
   218, 231  
 normal conditions, 15  
 normal development, 211  
 NOS, xiii, 251, 253, 254, 256, 257, 258, 259, 260  
 NOS3, xiii, 251  
 novel biomarkers, xii, 219  
 novel materials, 138, 152  
 N-terminal, 102, 257, 263  
 nuclear, xiii, 75, 163, 244, 245, 251, 254, 257, 263,  
   265, 266  
 nuclear magnetic resonance, 75, 163  
 nuclei, 40  
 nucleic acid, 71, 74, 160  
 nucleolus, 4  
 nucleosides, 147  
 nucleotides, 72, 86, 87, 187  
 nucleus, 4, 5, 36, 149, 257, 258  
 nursery school, 43  
 nutraceuticals, 107  
 nutrient, 205, 206, 215  
 nutrients, 197  
 nutrition, ix, 65, 91, 143  
 nystagmus, 15
- O**
- oat, 112  
 observations, 173, 175, 188, 197, 202, 212, 214, 246  
 oceans, 175  
 OCT, 35, 246  
 octopus, 190  
 oil, 101, 161  
 olfactory, 187, 189, 193  
 oligonucleotides, ix, 70, 72, 74, 75, 76, 77, 81, 83,  
   84, 86  
 oncogene, 46, 74, 263  
 oncogenes, 213, 231  
 oncology, 71  
 opacification, ix, 91, 92  
 ophthalmic, 21  
 opsin, 180, 181, 182, 183, 187, 188, 191, 192, 193  
 optic nerve, 2, 18, 34  
 optical, vii, viii, 1, 3, 4, 7, 8, 9, 10, 17, 18, 20, 22, 23,  
   24, 26, 27, 28, 30, 35, 37, 40, 55, 100, 133, 220,  
   221  
 optical fiber, 4, 35  
 optical properties, 3, 40, 55  
 optics, 18, 23, 24, 26, 27, 36, 37, 51  
 oral, 52, 66, 211, 215  
 organ, viii, 70, 191, 234  
 organelle, 5, 35

- organelles, 4, 5, 40, 171, 242  
organic, x, xi, xii, 137, 138, 142, 144, 145, 148, 149, 151, 154, 155, 176, 195, 196, 197, 201, 204, 205, 233, 240, 262  
organic compounds, 142, 197  
organism, viii, 39, 196, 244  
orientation, 126, 235  
orthogonal functions, 19  
oscillation, 16  
oscillations, vii, 1, 3, 16, 17, 18, 23, 25, 27, 31, 33, 34, 161, 174  
osmium, 235, 241  
osteomyelitis, 270  
ovary, 231  
overload, 3  
oxidants, 261  
oxidation products, 93, 98, 103, 108, 110, 112  
oxidative, ix, xiii, 46, 91, 93, 95, 96, 98, 99, 100, 102, 104, 105, 106, 107, 110, 111, 113, 139, 140, 141, 145, 148, 149, 151, 152, 153, 156, 217, 228, 230, 231, 250, 251, 254, 255, 257, 258, 259  
oxidative agents, 141, 149  
oxidative damage, ix, 46, 91, 93, 95, 98, 104, 106, 110, 113, 148, 156  
oxidative stress, xiii, 106, 107, 139, 140, 153, 228, 230, 231, 250, 251, 254, 257, 258, 259  
oxide, xiii, 148, 246, 251, 255, 256, 261, 262, 263, 264, 265  
oxygen, ix, x, 91, 92, 93, 95, 99, 104, 106, 107, 108, 110, 111, 112, 137, 138, 139, 140, 141, 146, 149, 151, 153, 154, 155, 156, 158, 160, 174, 176, 203, 217, 220, 229, 262, 269  
ozone, ix, xi, 91, 92, 160, 161, 162, 163, 164, 165, 172, 173, 174, 176, 178, 195, 196, 204
- P**
- p38, 258, 259, 266  
p53, 59, 70, 146, 153, 217, 254, 263  
packaging, 98, 111  
paints, 101  
pairing, 86  
palladium, 149, 158  
pancreatic, 259, 265, 267  
paradox, 265  
paradoxical, 27  
parameter, viii, 1, 7, 8, 9, 30, 104  
parathyroid, 65  
parathyroid hormone, 65  
parents, 43, 57, 59  
Parietal, 192  
Parkinson, 153  
PARP, 259  
particles, x, 137, 148, 149, 151, 158  
pathogenesis, 59  
pathogenic, viii, 69  
pathogens, 46, 71  
pathology, 108  
pathways, ix, 58, 62, 73, 91, 93, 94, 96, 115, 123, 125, 127, 128, 160, 220, 267  
patients, xiii, 64, 71, 211, 217, 218, 269  
PC12 cells, 264  
PCR, 71, 72, 73, 74  
pediatric, 42  
peers, 45  
penicillin, 220  
peptide, 71, 74, 93, 95, 96, 98, 101, 102, 103, 104, 105, 109, 231, 264  
peptide chain, 96  
peptides, xiii, 99, 102, 104, 105, 107, 108, 110, 113, 243  
perception, 15, 16, 17, 18, 19, 20, 22, 27, 36, 97, 99  
perinatal, 50  
peripheral blood, 54, 213  
peripheral blood lymphocytes, 213  
permeability, 48  
permit, 210  
peroxidation, 155, 248, 254, 262  
peroxide, 196  
peroxiredoxins, 46  
peroxynitrite, xiii, 93, 96, 107, 251, 261, 262, 263, 264, 265  
personal computers, 9  
personal history, 42  
perturbation, 109  
petroleum, 116  
pH, 50, 64, 146, 147, 149, 150, 151, 263  
pH values, 50  
phage, 157  
phagocytic, 270  
phagocytosis, 270  
pharmaceutical, 98  
pharmaceuticals, ix, 91, 98, 110  
pharmacogenomics, 70, 71  
pharmacological, 187  
phase conjugation, 26  
phase shifts, 6, 7, 24, 31, 33  
phenol, 122  
phenolic, x, 111, 159, 160, 162, 172, 173, 176, 178  
phenolic acid, 160, 162, 173  
phenolic acids, 160, 162  
phenolic compounds, x, 159, 173, 176, 178  
phenotype, 59, 70  
phenotypic, 70  
phenylalanine, 93, 94, 108  
phenytoin, 211, 216

- philosophers, 27  
 phosphate, 143, 146, 147, 150, 151  
 phosphatidylcholine, xiii, 243, 244  
 phosphatidylethanolamine, 244  
 phosphodiesterase, 186  
 phospholipase C, 186, 190  
 phospholipids, xii, 243, 244, 245, 247, 248, 250  
 phosphorus, 154  
 phosphorylates, 256, 257, 258  
 phosphorylation, xiii, 228, 251, 254, 256, 257, 258, 259, 260, 262, 263, 264, 265, 266, 267  
 photobleaching, 100, 101  
 photocatalysis, 152, 157  
 photocatalysts, 158  
 photochemical, ix, x, 16, 18, 33, 53, 96, 115, 116, 117, 118, 120, 121, 125, 127, 128, 129, 137, 138, 140, 143, 152, 155, 156, 221, 270  
 photodegradation, 92, 93, 95, 98, 99, 100, 104, 106, 108, 126, 155  
 photodynamic therapy, xiii, 154, 220, 230, 231, 269, 270, 271  
 photo-excitation, 92  
 photoinduced electron transfer, 146, 156  
 photolysis, 36, 106, 108, 155, 210, 212, 215, 253  
 photon, ix, 39, 70, 75, 78, 80, 244, 252  
 photons, ix, 70, 78, 80, 140, 148, 252  
 photooxidation, 157  
 photoreceptor, x, 2, 3, 7, 8, 13, 14, 15, 16, 17, 18, 20, 22, 23, 24, 25, 27, 28, 179, 180, 181, 185, 186, 187, 188, 189, 190, 191, 192, 193, 244, 248, 250  
 photoreceptor cells, x, 23, 179, 180, 181, 185, 186, 187, 188, 189, 191, 192, 244  
 photoreceptors, vii, xi, 1, 2, 3, 5, 7, 11, 15, 16, 17, 18, 20, 21, 22, 23, 24, 25, 26, 30, 33, 34, 35, 179, 186, 187, 188, 189, 190, 191, 192, 193, 244, 248, 250  
 photoresponse, 186  
 photosensitivity, 193  
 photosynthesis, ix, 66, 115, 119, 123, 128, 129, 131, 138, 207, 240  
 photosynthetic, 115, 116, 119, 131, 160, 178, 240  
 photosynthetic systems, 240  
 photosystem, 126, 134, 240  
 phototransduction, x, xii, 179, 180, 181, 185, 186, 187, 188, 189, 190, 192, 193, 243, 244, 248  
 phototransformation, 124, 131, 132, 133  
 photovoltaic, xii, 233, 240  
 phylogenetic, 182  
 phylogenetic tree, 182  
 physical and mechanical properties, 97  
 physical mechanisms, 4, 24  
 physical properties, xiii, 251  
 physicists, 20  
 physicochemical, 112  
 physico-chemical properties, 213  
 physics, 1, 26, 203, 204  
 physiological, 15, 37, 133, 180, 202, 206, 212, 263  
 physiologists, 19, 22  
 physiology, vii, xiii, 1, 19, 63, 174, 190, 212, 248, 251  
 phytoplankton, 176, 206  
 pig, 130  
 pigment epithelium, 244, 245  
 pigments, x, xii, 53, 120, 123, 132, 160, 161, 166, 172, 179, 180, 183, 184, 185, 186, 187, 188, 189, 190, 192, 233, 241  
 pineal, 183, 191  
*Pisum sativum*, 130  
 placebo, 53  
 plague, 62, 79  
 planetary, 161, 173, 175, 176, 177, 178  
 planets, x, 159, 160, 171, 175, 178  
 plankton, 203  
 plants, ix, 106, 112, 115, 120, 124, 125, 128, 129, 131, 132, 134, 145, 152, 164, 171, 176, 178  
 plaque, 217  
 plasma, 211, 216, 217  
 platforms, 71  
 platinum, 149, 158  
 play, ix, xi, xii, 42, 46, 47, 49, 54, 57, 71, 91, 95, 96, 123, 209, 210, 212, 230, 256, 259, 269  
 plurality, 39  
 PNA, 71  
 point mutation, 70  
 poisoning, 158  
 polarization, 4, 25, 35, 73  
 polarized light, 73  
 pollution, 52  
 poly(ADP-ribose) polymerase, 267  
 polycarbonate, 246  
 polymer, 74, 88, 149, 151, 176, 246  
 polymerase, 72, 267  
 polymers, 88, 158  
 polymorphism, viii, 69, 71, 74, 86  
 polymorphisms, 70, 71, 86, 89  
 polypeptides, 130  
 polyphenols, 263  
 polyunsaturated fatty acids, 248, 250  
 pools, 119  
 population, viii, xi, 42, 43, 44, 69, 70, 138, 195, 196, 200, 202, 223  
 population growth, 202  
 porphyria, 53  
 porphyrins, 53, 126  
 positive feedback, 254  
 postpartum, 51

- post-translational, 102, 112, 245, 256  
post-translational modifications, 102  
potassium, 220  
powder, 149, 158  
precipitation, 162  
prediction, viii, 69, 71, 130  
pre-existing, 42  
pregnancy, 211, 218  
pregnant, 211  
pregnant women, 211  
premature infant, 63, 67  
preschool, 44  
preschool children, 44  
preschoolers, 43  
press, 37, 202, 250, 271  
pressure, xii, 111, 161, 213, 243, 245  
preterm infants, 54, 64, 67  
prevention, x, 47, 57, 60, 63, 137, 147, 148, 156, 216, 218  
preventive, x, 137, 141, 143, 145, 146, 147, 152  
primary care, 52  
primary products, 36  
primary visual cortex, 36  
primate, 36  
principal component analysis, 249  
printing, 249  
probability, 227  
probe, viii, ix, 70, 71, 72, 73, 74, 75, 76, 77, 81, 82, 83, 84, 85, 86, 87, 88, 263  
product performance, 100  
production, xii, xiii, 46, 47, 49, 52, 64, 67, 79, 92, 93, 95, 98, 107, 115, 116, 118, 119, 121, 123, 124, 125, 131, 227, 233, 251, 252, 253, 255, 256, 257, 259, 261, 262  
productivity, 115, 203, 204  
prognosis, 42, 261  
program, 10, 11, 222, 226  
proinflammatory, 230  
proliferation, 45, 46, 48, 49, 55, 63, 214, 229, 270  
promoter, 218, 230  
propagation, 20, 40  
prophylactic, 53  
prostaglandin, 254, 262  
prostaglandins, 46  
proteasome, 229, 267  
protection, 3, 16, 41, 50, 52, 55, 56, 57, 58, 59, 97, 137, 138, 141, 142, 143, 145, 148, 153, 154, 155, 160, 197, 199, 200, 202, 204, 210, 212, 214, 215, 229  
protective clothing, 52  
protective mechanisms, 98  
protective role, 46  
protein analysis, 101  
protein folding, 256  
protein kinases, 256, 258, 266  
protein oxidation, 97, 99, 101, 108, 110, 111, 112  
protein structure, 99, 111  
protein synthesis, xii, xiii, 219, 227, 228, 230, 251, 256, 257, 259, 264, 267  
proteome, 113, 249  
proteomics, 101, 104, 105, 106, 112, 113, 244, 249  
protocol, 82, 89, 175  
protocols, 98, 105, 202  
proto-oncogene, 213  
PSI, 126  
psoriasis, 139, 211, 217  
psoriatic, 218  
psychophysiology, 3, 13  
puberty, 54  
public, 41, 57, 70, 222  
public domain, 222  
public health, 41  
PUFA, 249  
pulse, 78, 80  
pulsed laser, 16  
pulses, 78, 80, 81  
pupa, 234  
pupae, 236  
pupil, 4, 7, 8, 9, 11, 12, 13, 14, 15, 16, 17, 18, 22, 32  
purification, viii, 69, 70, 81, 102, 104, 129, 190  
purines, 160, 211, 212, 214  
Purkinje, 22  
P-value, 222  
PVP, 149, 151, 152  
pyrimidine, 47, 49, 138, 139, 155  
pyrophosphate, 72  
pyrrole, 121

## Q

- quadrupole, 245, 249, 250  
quality of life, xiii, 269  
quanta, 3  
quantum, 2, 16, 74, 76, 80, 88, 124  
quasi-periodic, 11  
questionnaire, 44  
quinone, 145

## R

- radiation damage, 165, 196, 199  
radio, 26  
rain forest, 206  
Raman, 51, 108, 175  
Raman spectra, 51

- random, 3, 5, 6, 15, 18, 21, 23, 25, 29, 30, 31  
range, viii, ix, xii, 5, 6, 28, 36, 51, 53, 69, 81, 82, 91, 92, 93, 94, 100, 102, 104, 117, 166, 233, 239, 247, 252  
rat, 64, 106, 109, 157, 213, 216, 241, 250, 252, 261, 262, 267  
rats, 157, 217, 261  
RAW, 263  
RDA, 211  
reactants, 254  
reaction center, 120, 123, 124, 125, 128, 134  
reaction rate, 147, 154, 254  
reaction time, 30  
reactive nitrogen, 93, 107  
reactive oxygen species (ROS), ix, 91, 92, 93, 95, 96, 97, 100, 104, 107, 137, 138, 139, 141, 145, 146, 148, 149, 151, 152  
reactivity, 93, 108, 110  
reading, 62  
reagents, 221  
real time, 73  
reality, 30  
reception, 10, 17, 180  
receptor sites, 16  
receptors, 15, 182, 190, 248, 258  
recognition, viii, 36, 69, 70, 71, 72, 86, 157, 175  
reconstruction, 15, 20, 27, 28, 29, 31, 75  
recovery, 207, 227  
recreational, 42, 44  
redistribution, 3  
redox, 95, 101, 104, 107, 109, 105, 106, 112, 122, 145, 149, 157  
reductases, 119  
refraction index, 5  
refractive index, 5, 34  
refractive indices, 2, 9  
refractory, 5, 7, 17  
regeneration, xii, 125, 127, 134, 158, 209, 214, 215  
Registry, 59  
regular, 3, 17, 22, 23, 32, 59  
regulation, xiii, 61, 128, 227, 230, 231, 251, 253, 254, 255, 256, 258, 259, 262, 264, 266, 267  
regulations, 211  
regulators, 206, 228, 232  
rejection, 70  
relationship, 37, 42, 43, 44, 55, 57, 108, 156, 176, 184, 185, 244, 261, 262  
relationships, 218, 220  
relaxation, 24, 252, 253  
relevance, 54, 109, 112, 210  
reliability, 17  
remodeling, 258  
repair, xi, 45, 47, 49, 55, 60, 61, 154, 157, 209, 210, 212, 213, 214, 215, 216, 217, 218  
reperfusion, 259, 262, 267  
repetitions, 78  
replication, 45  
repression, 265  
reproductive age, 65  
reptiles, xii, 233  
residuals, 84, 87, 88  
residues, 92, 93, 94, 95, 96, 98, 99, 100, 102, 104, 106, 107, 108, 130, 146, 148, 172, 254  
resistance, ix, x, 60, 70, 71, 123, 159, 165, 172, 173, 214, 230, 241  
resolution, ix, xiii, 7, 13, 15, 17, 51, 70, 75, 76, 78, 81, 121, 243, 245, 248  
resource availability, 196  
resources, 204  
respiration, 227, 231  
responsiveness, 52  
restriction enzyme, 71, 75  
retail, 98, 99  
retention, 25, 48, 97, 99, 100  
reticulum, xiii, 229, 230, 231, 239, 251, 256, 264, 265, 267  
retina, vii, xii, 1, 2, 3, 4, 7, 8, 9, 10, 14, 15, 16, 17, 18, 19, 21, 22, 23, 24, 25, 26, 27, 30, 32, 33, 34, 35, 36, 37, 182, 183, 187, 191, 241, 243, 244, 246, 248, 249, 250  
retinol, 35, 156  
rheumatoid arthritis, 211  
rhodium, 149  
rhodopsin, x, xii, 34, 179, 180, 181, 182, 183, 184, 185, 186, 188, 189, 190, 191, 243, 244, 248, 249, 250  
riboflavin, 99, 111, 145, 146, 147, 150, 155, 156, 157  
ribose, 267  
ribosomal, xii, 219, 229, 258  
ribosome, 256, 264  
ribosomes, 266  
rickets, 61, 65  
rigidity, 109  
rings, 121  
risk, 40, 42, 43, 44, 45, 48, 49, 54, 55, 57, 58, 59, 67, 71, 75, 148, 211, 213, 215, 217  
risk factors, 42, 44, 54, 59  
risks, viii, 39, 41, 42, 45, 52, 61, 153  
RNA, 221, 222, 264, 266  
rods, 184, 186, 187, 191  
room temperature, 76, 124, 125, 246

**S**

- safety, 141, 148, 158, 217  
saline, 143, 203  
salts, 240  
sample, 71, 75, 77, 78, 81, 82, 84, 86, 88, 101, 102, 105, 143, 149, 150, 151, 244, 245, 246  
saturation, 37  
scatter, 51, 63  
scattering, 2, 3, 4, 5, 7, 8, 9, 11, 14, 15, 16, 17, 18, 23, 26, 28, 33, 34, 35, 36, 38, 39, 40, 50, 148  
scavenger, 145, 152, 158  
Schiff, 181, 182, 190  
Schiff base, 181, 182, 190  
Schmid, 192  
school, 43, 56, 57, 179  
sclera, 52  
SDS, 222  
sea level, 161, 171  
seafood, 99  
search, 71, 176, 218, 221  
searching, 102, 105  
seed, 121, 132  
seedlings, 116, 125, 129, 134  
seeds, 132  
selectivity, 140, 157  
self-focusing, 26  
SEM, 235, 236  
semiconductor, 148  
senescence, 55  
senile, 108  
sensitivity, ix, 22, 48, 49, 55, 70, 73, 206, 245  
sensitization, 53, 155  
sensors, 162, 163, 164  
sensory systems, 192  
separation, 73, 75  
sequelae, 53  
sequencing, viii, 11, 69, 72, 73  
series, 72, 222  
serine, 71, 212, 256, 257, 258, 263, 264, 266, 267  
serum, 53, 66, 108  
serum albumin, 108  
severity, 42, 43, 44, 99, 211  
sex, 45, 56, 64  
shape, 9, 10, 11, 15, 17, 53, 83, 191, 235, 240  
shares, 189  
shelter, 234  
shikimic, 160, 165  
shock, xii, 100, 124, 134, 219, 220, 226, 228, 229, 230, 231, 232  
short period, 15, 16  
shortage, 259  
short-term, 48, 120, 123, 202  
siblings, 71  
sickle cell, 70  
sign, 4, 33  
signal transducer and activator of transcription 5, 263  
signal transduction, 191, 220, 227  
signaling, xi, xiii, 55, 179, 187, 189, 191, 227, 230, 248, 251, 255, 257, 258, 259, 262, 263, 264, 265  
signaling pathway, xiii, 55, 227, 251, 255, 257, 258, 259, 264, 265  
signaling pathways, xiii, 55, 251, 255, 259, 264, 265  
signalling, 61  
signals, x, 19, 25, 31, 33, 34, 36, 72, 78, 80, 81, 179, 190, 245  
signal-to-noise ratio, 72, 79  
signs, 33, 51, 217  
silica, 162  
silk, 100, 112, 235  
silver, 149, 158, 236  
similarity, xi, 19, 86, 179, 187, 189, 224, 226  
simulations, 35  
single nucleotide polymorphism, 70  
SIS, 45, 46, 47, 55, 56  
sites, ix, 16, 43, 48, 52, 61, 70, 71, 95, 98, 107, 140, 214, 257, 259  
skeletal muscle, 262, 265  
skin cancer, 40, 42, 44, 45, 48, 49, 55, 57, 60, 61, 138  
skin conductance, 51  
skin diseases, viii, 39, 139  
smokers, 156  
smoking, 211  
smooth muscle, 261  
smoothing, 13  
SNP, 71, 72, 73, 74, 76, 77  
SNPs, 70, 71, 72  
SOD, xiii, 251, 254  
sodium, 146, 147, 150, 151, 220, 222, 226, 235, 247  
software, 10, 102, 112, 163, 221, 222, 245, 247, 248  
soil, 161, 162, 234  
solar cell, xii, 233, 234, 239, 242  
solar system, 175  
solid state, 98  
solid-state, 110  
sols, 149  
solubility, 99  
solvent, 162  
solvents, 132  
somatic mutations, 43, 70  
SPA, 89  
space-time, 37  
spatial, xiii, 2, 13, 14, 18, 19, 20, 24, 26, 27, 31, 33, 34, 243, 245  
spatial frequency, 13, 19, 31

- specificity, 72, 126, 130, 155  
 spectral analysis, 20  
 spectrophotometric, 104  
 spectrophotometry, 133, 163  
 spectroscopy, 2, 50, 52, 89, 112, 117, 119, 121, 123,  
     129, 132, 133, 163, 191, 249  
 spectrum, xiii, 10, 11, 19, 20, 21, 22, 23, 31, 44, 52,  
     53, 64, 73, 76, 88, 116, 117, 129, 163, 165, 166,  
     167, 171, 173, 187, 239, 243, 246, 247  
 speed, 2, 3, 9, 23, 24, 25, 26, 33, 99, 252, 270  
 speed of light, 9, 24, 25, 252  
 SPF, 42, 142, 143, 154  
 spinach, 211  
 SPSS, 162, 222  
 squamous cell carcinoma, 41, 44, 56, 261  
 stability, 26, 71, 98, 100, 111, 213  
 stabilization, vii, 1, 15, 16  
 stabilize, 181, 182  
 stable states, 183  
 stages, x, 16, 115, 116, 117, 121, 124, 128, 129, 132,  
     133, 202, 236, 237, 255  
 standard deviation, 81, 84, 88, 222  
*Staphylococcus aureus*, 269, 270  
 stars, x, 159, 160, 171, 173, 175, 176, 178  
 starvation, 257  
 statistics, 41, 58  
 steady state, 50  
 Stefin A, 46  
 steroid, 62, 63  
 steroids, 216  
 stimulus, 244  
 stochastic, 27, 37  
 stock, 76  
 storage, 98, 110, 111, 112, 253, 255  
 strategies, 101, 102, 105, 160, 171, 172, 173, 177,  
     196, 200, 201  
 stratosphere, ix, 91, 92  
 streams, 240  
 strength, 101  
 streptavidin, 104  
 stress, xiii, 106, 107, 111, 139, 140, 153, 178, 212,  
     213, 215, 227, 228, 229, 230, 231, 250, 251, 255,  
     256, 257, 258, 259, 261, 264, 265, 266, 267  
 stromal, 126  
 structural changes, 99, 122, 183  
 structural modifications, 99, 108  
 structural protein, 95, 97  
 subcellular, 154  
 subgroups, x, 179, 189  
 substances, x, xi, 129, 159, 162, 163, 170, 172, 173,  
     174, 176, 178, 195, 196, 197, 199, 202  
 substitution, 86  
 substrates, ix, 91, 92, 93, 96  
 subtraction, 82  
 sucrose, 235  
 sugars, 162  
 sulfate, 220, 222  
 sulfur, 93, 95, 97  
 summer, 43, 51, 196, 198  
 Sun, 57, 58, 59, 60, 110, 154, 155, 190, 210  
 sun protection factor (SPF), 142  
 sunlight, 42, 43, 44, 45, 52, 54, 58, 60, 61, 98, 99,  
     143, 157  
 sunscreens, 143, 144, 148, 155, 158  
 superimposition, 9  
 superoxide, xiii, 92, 93, 100, 107, 112, 139, 156,  
     158, 251, 261, 262  
 superoxide dismutase, xiii, 100, 251, 262  
 supplements, 215  
 supply, xi, 175, 209, 212, 213  
 suppression, 45, 48, 55, 123  
 suppressor, 62, 70, 146, 153, 229, 263  
 surface area, 41, 50, 53, 239  
 survival, 47, 178, 205, 248, 250, 254, 264, 267  
 susceptibility, viii, ix, 48, 58, 60, 70, 71  
 symbiosis, 175  
 symmetry, 4, 9  
 synapse, 24  
 synapses, 3, 18, 24, 244  
 synchronous, 78  
 syndrome, 53, 66, 67, 248, 250  
 synthesis, xii, xiii, 46, 52, 55, 61, 66, 72, 115, 121,  
     123, 126, 128, 130, 132, 138, 153, 157, 172, 178,  
     196, 202, 210, 211, 213, 214, 219, 227, 228, 230,  
     240, 251, 256, 257, 259, 261, 264, 267
- T**
- T cells, 47, 48, 60, 61, 71  
 T lymphocytes, 46, 61, 71  
 tandem mass spectrometry, xiii, 243, 245, 247  
 tannic acid, 241  
 targets, 55, 62, 74, 76, 86, 180, 258, 265  
 tau, 233  
 temperate rain forest, 206  
 temperature, 71, 76, 117, 118, 119, 120, 121, 122,  
     123, 124, 125, 126, 133, 147, 158, 161, 162, 205,  
     241, 246  
 temperature dependence, 120, 241  
 template molecules, 74  
 temporal, 2, 4, 23, 24, 25, 26, 29, 30, 33, 34, 75, 76,  
     78, 79, 80, 230  
 temporal distribution, 26, 79  
 tendon, 109  
 ternary complex, 120, 121, 128, 256  
 tetroxide, 235, 241

- textbooks, 183  
textile, 100, 101  
textiles, 100  
thawing, 161  
therapy, x, xii, xiii, 53, 67, 110, 137, 139, 140, 154, 211, 215, 218, 219, 220, 230, 231, 232, 269, 270, 271  
thermal energy, 147  
thermal stability, 71  
thiobarbituric acid, 110  
threats, 205  
three-dimensional, 6, 11, 26, 32  
three-dimensional space, 26  
threonine, 95  
threshold, 44, 52, 79, 81  
threshold level, 79  
thresholds, 252  
thymidine, 211, 214  
thymine, 143, 148, 155, 171  
thymus, 147  
time resolution, 79, 81  
tissue, viii, xi, 4, 39, 40, 44, 46, 47, 48, 50, 53, 64, 69, 97, 110, 140, 166, 209, 240, 241, 244, 245, 250, 262, 269  
tissue homeostasis, xi, 209  
titanium, x, 137, 148, 157, 158  
titanium dioxide, x, 137, 148, 158  
t-lymphocytes, 215, 216  
tocopherol, 156  
toddlers, 43, 52, 55, 59, 66  
tolerance, xi, 46, 48, 61, 63, 65, 195, 201, 207  
toluene, 162  
total energy, 252  
toxic, 149, 151  
toxic effect, 151  
toxicity, 53, 98, 211  
tracking, ix, 91, 102, 104  
traits, 70, 124  
trajectory, 10, 27, 28  
transcription, xiii, 228, 251, 255, 256, 258, 263, 266  
transcription factor, xiii, 228, 251, 258, 266  
transcription factors, 258  
transcriptional, xii, xiii, 219, 220, 230, 251, 253, 258, 259, 265, 266  
transcriptomics, 244  
transducer, 263  
transducin, x, 179, 181, 186, 189, 249  
transduction, 191, 192  
transfer, viii, x, 26, 70, 73, 75, 92, 94, 108, 120, 121, 122, 126, 131, 132, 133, 137, 138, 139, 140, 141, 143, 144, 146, 147, 152, 153, 154, 157, 212  
transformation, 2, 10, 16, 19, 20, 27, 31, 33, 35, 44, 49, 55, 117, 125, 126, 127, 129, 131, 133, 134, 155  
transformations, 16, 17, 18, 19, 21, 119, 127, 129  
transgenic, 47, 48, 55, 62, 63, 265  
transgenic mice, 47, 48, 62, 63  
transgenic mouse, 48, 55, 265  
transglutaminase, 254  
transition, 73, 109, 158, 201  
transition metal, 158  
transitions, 16, 172, 173  
translation, xii, 219, 226, 227, 228, 231, 255, 256, 257, 264, 265, 267  
translational, xiii, 107, 231, 251, 253, 256, 257, 259, 264, 265, 267  
transmembrane, 181, 190  
transmission, 10, 98, 244  
transparency, 24, 140, 196, 197  
transparent, xi, 3, 5, 40, 195  
transport, 49, 56, 212  
transversion mutation, 157  
tremor, 2, 15, 25, 36, 37  
triggers, 16, 78, 183, 234  
trimethylamine, 247  
trout, 111  
trypsin, 102  
tryptophan, 92, 93, 94, 98, 99, 100, 103, 106, 107, 108, 109, 110, 112, 172, 254  
tumor, xiii, 48, 55, 62, 70, 139, 146, 153, 211, 263, 269  
tumorigenesis, 70  
tumors, 47, 156, 231  
tumour, 62  
turbulent, 28  
turnover, xi, 50, 209, 211, 214, 229  
two-dimensional, 11, 175  
two-way, 200  
type II diabetes, 70  
tyrosine, 92, 93, 94, 96, 106, 108, 112, 121, 172, 191, 254, 258, 263  
tyrosine hydroxylase, 263  
tyrosyl radical, 96  
tyrosyl radicals, 96

**U**

- U.S. Department of Agriculture, 211, 218  
ubiquitin, 265  
ulceration, 215  
ultrasound, 37, 38  
ultraviolet B, x, 63, 137, 231, 260, 261, 262, 263  
ultraviolet irradiation, 109  
ultraviolet light, xiii, 41, 251, 262, 267

unconjugated bilirubin, 53  
 unfolded, 256, 264, 265, 267  
 unfolded protein response, 256, 264, 265, 267  
 uniform, 5, 10, 15, 16, 17, 26, 38, 202  
 universe, 19  
 urine, 46, 53  
 USDA, 218  
 UV absorption, 92  
 UV exposure, 56, 59, 61, 97, 100, 109, 206, 212  
 UV irradiation, xii, 96, 155, 209, 210, 212, 213, 254, 255, 256, 259, 265  
 UV light, xii, 142, 206, 210, 233, 236, 241, 252, 261, 262  
 UV spectrum, 163, 165, 166, 167, 171, 173  
 UVA irradiation, 103, 139, 148, 152, 155, 262  
 UV-irradiation, xiii, 251, 257, 262

## V

vacuum, xii, 172, 175, 236, 243  
 validation, 101, 105, 207  
 valine, 71, 96  
 values, ix, 5, 6, 7, 10, 22, 24, 32, 50, 51, 70, 74, 75, 81, 84, 86, 150, 161, 162, 163, 164, 165, 166, 167, 171, 198, 222, 246, 252  
 variability, ix, 56, 70, 205  
 variables, 21  
 variation, 34, 58, 60, 86, 104, 108, 178, 200  
 vascular disease, 215  
 vasculature, 40  
 vegetables, 211  
 vegetation, 197  
 versatility, 73  
 vertebrates, xi, xii, 180, 182, 187, 188, 189, 214, 233, 234, 239  
 vibration, 24  
 viral infection, 256  
 virus, 44  
 virus infection, 44  
 viscosity, 147  
 visible, x, xii, 50, 137, 139, 140, 141, 145, 147, 152, 179, 181, 183, 189, 206, 210, 233, 239  
 vision, vii, 1, 2, 3, 4, 12, 13, 15, 16, 19, 20, 22, 23, 32, 34, 36, 37, 191  
 visual area, 36  
 visual perception, vii, 1, 2, 3, 4, 15, 16, 17, 19, 22, 23, 27, 34, 36  
 vitamin A, 99, 145, 156  
 vitamin B1, 215, 216  
 vitamin B12, 215, 216  
 vitamin D, 46, 47, 49, 52, 55, 61, 62, 63, 65, 66, 138, 153, 210

vitamin D, 46, 61, 65, 66  
 vitamin D deficiency, 52, 61, 65, 66  
 vitamin D receptor, 47  
 vitamin E, 145, 156  
 vitamins, x, 137, 143, 145  
 voiding, 197  
 vulnerability, 51, 165, 166, 197

## W

water, xi, xii, 5, 50, 51, 54, 56, 67, 76, 98, 105, 139, 141, 147, 149, 151, 195, 196, 197, 199, 200, 201, 202, 206, 207, 210, 215, 219, 230, 235, 253, 262  
 water absorption, 51  
 water desorption, 51  
 water-soluble, xii, 149, 151, 210, 215, 219, 230  
 waveguide, 244, 249  
 wavelengths, xi, 7, 31, 53, 73, 88, 92, 122, 165, 167, 170, 195, 196, 239, 240

weakness, 74  
 weight ratio, 41  
 wheat, 134  
 women, 41, 42, 58, 65, 211, 215, 216, 217  
 wool, 100, 102, 103, 107, 108, 109, 110, 112  
 workers, 240  
 World Health Organization, 58

## X

xanthones, 160, 161  
 xeroderma pigmentosum, 42, 44  
 X-ray diffraction, 75

## Y

yeast, 211  
 yield, 73, 79, 80, 92, 100, 122, 124  
 young adults, 57  
 young women, 41  
 younger children, 54

## Z

zebrafish, 242  
 zinc, x, 137, 148, 158, 266  
 zinc oxide, x, 137, 148, 158  
 ZnO, 148, 152  
 zooplankton, xi, 195, 197, 199, 201, 202, 203, 204, 205, 206